# ANNUAL REPORTS ON NMR SPECTROSCOPY

## Volume 12

# ANNUAL REPORTS ON

# NMR SPECTROSCOPY

This Page Intentionally Left Blank

# ANNUAL REPORTS ON

# NMR SPECTROSCOPY

Edited by

## G. A. WEBB

*Department of Chemistry, University of Surrey, Guildford, Surrey, England*

**VOLUME 12**

1982

# LIST OF CONTRIBUTORS

C. A. FYFE, *Department of Chemistry, University of Guelph, Guelph, Ontario, Canada N1G 2W1.*

JOZEF KOWALEWSKI, *Department of Physical Chemistry, Arrhenius Laboratory, University of Stockholm, S-106 91 Stockholm, Sweden.*

B. E. MANN, *Department of Chemistry, University of Sheffield, Sheffield S3 7HF, U.K.*

ALLEN R. SIEDLE, *3M Central Research Laboratories, St. Paul, Minnesota 55101, U.S.A.*

R. E. WASYLISHEN, *Department of Chemistry, University of Winnipeg, Winnipeg, Manitoba, Canada R3B 2E9. (Present address: Department of Chemistry, Dalhousie University, Halifax, Nova Scotia B3H 4H6, Canada.)*

This Page Intentionally Left Blank

# PREFACE

This volume consists of authoritative accounts of four different areas of NMR spectroscopy. The appropriate literature surveys were completed in 1981.

Each of these reports covers aspects of NMR which have not been previously reviewed as such in this series. Professors Wasylishen and Fyfe present a comprehensive account of the rapidly growing area of high resolution solid state NMR studies. This is followed by a valuable contribution from Dr Kowalewski on theoretical aspects of spin–spin couplings. Dr Siedle covers recent aspects of boron NMR while dynamic NMR in inorganic and organometallic chemistry is dealt with by Dr Mann.

It is a great pleasure for me to record my appreciation of the diligence shown by these contributors in the preparation of their reports.

University of Surrey                                     G. A. Webb
Guildford, Surrey                                  September, 1981
England

This Page Intentionally Left Blank

# CONTENTS

# High-Resolution NMR of Solids

## R. E. WASYLISHEN and C. A. FYFE

# Calculations of Nuclear Spin–Spin Couplings

## JOZEF KOWALEWSKI

CONTENTS

# Boron-11 NMR Spectroscopy

## ALLEN R. SIEDLE

# Dynamic NMR Spectroscopy in Inorganic and Organometallic Chemistry

## B. E. MANN

# High-resolution NMR of Solids

## R. E. WASYLISHEN* AND C. A. FYFE

*Department of Chemistry, University of Guelph, Guelph, Ontario,
Canada, N1G 2W1*

## I. INTRODUCTION

With the development of multinuclear FT NMR spectrometers, and the cross-polarization (CP) and magic angle sample spinning (MASS) tech-

---

* Present address: Department of Chemistry, Dalhousie University, Halifax, Nova Scotia B3H 4H6, Canada.

niques, there has been considerable recent interest in high-resolution NMR studies of solids. There are several obvious advantages to studying solids. For exampie, one can study materials that are relatively insoluble (shales, coals, zeolites, etc.). Solid-state NMR provides an opportunity to study systems in the absence of intermolecular exchange (individual species). In addition, solid-state NMR allows one to investigate the nature of the solid state and provides a bridge between X-ray data and solution NMR studies.

Techniques used to obtain high-resolution NMR spectra of solids and a variety of applications of these techniques have been reviewed.[1-20] The purpose of the present report is to provide an update of the earlier reviews. It is written from the viewpoint of experimental chemists, and is therefore presented using terminology familiar to chemists. The reader is assumed to be conversant with high-resolution NMR of liquids[21-26] and basic pulse NMR techniques.[27-30] [For some other recent reviews see p. 287.]

In order to understand some of the problems that one must deal with in order to obtain high-resolution NMR spectra of solids it is necessary first to consider the important interactions that a nuclear spin encounters in a solid (Section II). Many of these interactions are averaged by rapid molecular motion in solution, so most experimental chemists are generally not concerned with them. Experimental techniques used to obtain high-resolution solid-state spectra are discussed in Section III. In order to be effective these techniques must either remove or average various nuclear spin interactions in the solid state. Section IV deals with applications of high-resolution NMR. Specific applications are discussed according to the particular nucleus observed. High-resolution NMR studies of abundant spins ($^1$H and $^{19}$F) are not discussed here.

## II. NUCLEAR SPIN INTERACTIONS IN SOLIDS

A typical nuclear spin Hamiltonian is exemplified by

$$H = H_Z + H_{rf}(t) + H_Q + H_D + H_{CS} + H_{other} \tag{1}$$

The first two terms describe "external" interactions of the spins with the static and the rf fields, both of which are controlled by the experimenter. The remaining terms depend upon the fundamental characteristics of the nucleus under observation and its environment. Below we consider each term for a hypothetical two-spin system I and S; more detailed discussions are available in the monographs by Mehring,[1] Haeberlen,[2] and Andrew.[3]

### A. The Zeeman term ($H_Z$)

The Zeeman term results from the interaction of the nuclear magnetic moment, $\mu_t$, of nucleus t with the applied static field, $B_0$. Hence, the

operator $H_Z$ can be written as

$$H_Z = -\sum_t \vec{\mu}_t \cdot \vec{B}_0 = -\sum_t \gamma_t \hbar \vec{B}_0 \cdot \vec{I}_t \tag{2}$$

where $\vec{I}_t$ is a spin operator and $\gamma_t$ is the magnetogyric ratio of nucleus t. The applied field is generally chosen to lie along the z-direction. From the general properties of spin angular momentum, $\hat{H}_Z$ for a two-spin system can be written as

$$\hat{H}_Z = -\gamma_1 \hbar B_0 \vec{I}_z - \gamma_s \hbar B_0 \vec{S}_z \tag{3}$$

where $\vec{I}_z$ and $\vec{S}_z$ represent the components of the nuclear spin in the z-direction. For an applied field, $B_0$, of 2·349 tesla, values of the Zeeman interaction (in MHz) are given in Table 1 for some of the common nuclei discussed in this review.

TABLE 1

NMR properties of the important nuclei discussed in this review.

| Isotope | Natural abundance | Spin | Magnetogyric ratio $\gamma$ ($10^7$ rad $T^{-1}$ $s^{-1}$) | Quadrupole moment $Q$ ($10^{-28}$ $m^2$) | NMR frequency (MHz) |
|---|---|---|---|---|---|
| $^1$H | 99·985 | 1/2 | 26·7510 | | 100·000 |
| $^2$H | 0·015 | 1 | 4·1064 | $2·86 \times 10^{-3}$ | 15·351 |
| $^{13}$C | 1.108 | 1/2 | 6·7263 | | 25·145 |
| $^{14}$N | 99·635 | 1 | 1·9324 | $1·93 \times 10^{-2}$ | 7·224 |
| $^{15}$N | 0·365 | 1/2 | −2·7107 | | 10·138 |
| $^{19}$F | 100·000 | 1/2 | 25·1665 | | 94·094 |
| $^{29}$Si | 4·70 | 1/2 | −5·3141 | | 19·867 |
| $^{31}$P | 100·000 | 1/2 | 10·829 | | 40·481 |
| $^{63}$Cu | 69·09 | 3/2 | 7·0904 | −0·211 | 26·606 |
| $^{65}$Cu | 30·91 | 3/2 | 7·5958 | −0·195 | 28·394 |
| $^{111}$Cd | 12·86 | 1/2 | −5·6699 | | 21·209 |
| $^{113}$Cd | 12·34 | 1/2 | −5·9330 | | 22·193 |
| $^{117}$Sn | 7·67 | 1/2 | −9·5303 | | 35·626 |
| $^{119}$Sn | 8·68 | 1/2 | −9·9707 | | 37·291 |
| $^{195}$Pt | 33·7 | 1/2 | 5·7505 | | 21·414 |
| $^{199}$Hg | 16·86 | 1/2 | 4·7690 | | 17·91 |

## B. The radio frequency term ($H_{rf}$)

In NMR spectroscopy transitions between energy levels are generally induced by an applied rf field, $B_{rf}$, which is applied perpendicularly to the static field direction,

$$B_{rf} = B_1 \cos \omega t \tag{4}$$

where $B_1$ is the amplitude and $\omega = 2\pi\nu$ is the frequency. Assuming that $B_{rf}$ is the applied field along the x-direction, then

$$H_{rf} = -\gamma_i \hbar \vec{B}_{rf} \cdot \vec{I}_x(i) \tag{5}$$

From time-dependent perturbation theory the probability, $P_{mm'}$, of a transition per unit time between two states, $m$ and $m'$, is

$$P_{mm'} = \gamma^2 B_1^2 |\langle m|\vec{I}_x|m'\rangle|^2 \, \delta(\nu_{mm'} - \nu) \tag{6}$$

where $\langle m|\vec{I}_x|m'\rangle$ is zero unless $m = m' \pm 1$ and $\delta(\nu_{mm'} - \nu)$ is the Dirac delta function. The frequency, $\nu_{mm'}$, corresponding to the energy differences between $m$ and $m'$ is given by

$$\nu_{mm'} = \frac{\gamma B_0}{2\pi} |m' - m| \tag{7}$$

Note that only the Zeeman interaction has been considered; other interactions discussed below slightly modify the resonance frequency given in equation (7).

## C. The quadrupolar term ($H_Q$)

This interaction is important only in the case where the nucleus has a spin $I > 1/2$ (Table 1) and hence a quadrupole moment $eQ$. For a single spin $I$,

$$H_Q = \vec{I} \cdot \hat{Q} \cdot \vec{I} \tag{8}$$

where $\hat{Q} = [eQ/2I(2I-1)h]\hat{V}$ and $\hat{V}$ is the electric field gradient tensor at the nuclear site. The trace of $\hat{V}$ is zero, and $V_{ij} = V_{ji}$ thus $\{V_{ij}\}$ has five independent elements, three of which specify the orientation and two that indicate the magnitude and shape of the field gradient. In the principal axis frame of $V_{ij}$, in which $\{V_{ij}\}$ is diagonal, equation (8) becomes

$$H_Q = \frac{e^2 qQ}{4I(2I-1)}[3I_z^2 - I^2 + \eta(I_x^2 - I_y^2)] \tag{9}$$

where the magnitude and shape of the field gradient are specified by $eq = V_{zz}(|V_{zz}| \gg |V_{xx}| > |V_{yy}|)$ and $\eta$, the asymmetry parameter, is defined as $(V_{xx} - V_{yy})/V_{zz}$. Two limiting cases are generally discussed, $H_Z \gg H_Q$ (the so-called high-field case) and $H_Z \ll H_Q$ (low-field case). For $H_Z \approx H_Q$ calculations of an energy level diagram are tedious. The nuclear quadrupole coupling constant, $e^2 Qq/h$, is symbolized by $\chi$.

In the high-field case (e.g. $^2$H) the quadrupolar Hamiltonian serves as a perturbation on the larger Zeeman interaction. Using perturbation theory

to the first order, the energy shifts for the $I = 1$ system are given by

$$\Delta E_Q = \frac{h\nu_Q}{4}(3\cos^2\theta - 1 + \eta\cos 2\phi\sin^2\theta)(m^2 - 2/3) \qquad (10)$$

where $\nu_Q = (3/2)\chi$ and $\theta$ and $\phi$ are the standard polar angles which specify the orientation of the principal axis of the electric field gradient in the laboratory frame of reference. For $\eta = 0$,

$$\Delta E_Q = \frac{h\nu_Q}{4}(3\cos^2\theta - 1)(m^2 - 2/3) \qquad (11)$$

where $\theta$ is the angle between $B_0$ and the principal axis of the field gradient. An energy level diagram for this situation is shown in Fig. 1. For a single
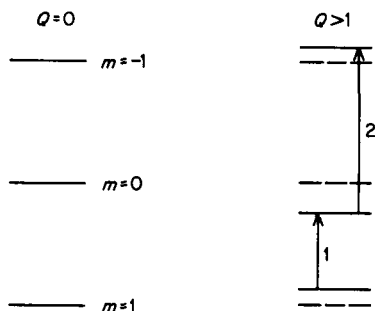


FIG. 1. Energy levels for a spin $I = 1$ nucleus in a large magnetic field and an axially symmetric electric field gradient. Each transition is shifted by $|h\nu_Q/4(3\cos^2\theta - 1)|$ relative to its position in the absence of an electric field gradient.

crystal, the NMR spectrum for a spin $I = 1$ nucleus interacting with an axially symmetric electric field gradient is a doublet of separation $\Delta\nu$, where

$$\Delta\nu = (3/4)\chi(3\cos^2\theta - 1) \qquad (12)$$

Note that the two lines of the doublet coalesce when the angle between the electric field gradient and the applied field, $B_0$, approaches 54°44′8″ (the "magic angle" where $\cos^2\theta = 1/3$). This is a general result regardless of the value of $I$.

For a powder sample, one must average equation (12) over all possible values of $\theta$. The resulting powder pattern for an axially symmetric electric field gradient is shown in Fig. 2. The central doublet separation is $(3/4)\chi$, corresponding to $\theta = 90°$ in equation (12). The outer features just below the base line are separated by $(3/2)\chi$ and correspond to $\theta = 0°$ and 180° in equation (12).
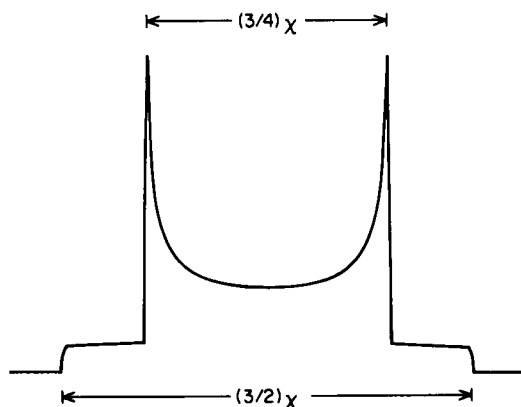
FIG. 2. NMR spectrum for a powder sample of $I = 1$ spins with an axially symmetric electric field gradient.

Typical quadrupole coupling constants for $^2$H in carbon–deuterium bonds are 150–200 kHz. Nitrogen-14 quadrupole coupling constants are generally much larger, ranging from 0 to 5 MHz. Experimental aspects and values of nuclear quadrupole coupling constants are discussed and tabulated in several texts.[25,31–34]

### D. The dipole–dipole term ($H_D$)

For a substance containing two different magnetic species, I and S, of magnetogyric ratios $\gamma_I$ and $\gamma_S$,

$$H_D = H_{II} + H_{SS} + H_{IS} \tag{13}$$

In the discussion that follows we are particularly interested in the last term of equation (13), $H_{IS}$, which for two isolated spins I and S may be written as

$$H_{IS} = \frac{\gamma_I \gamma_S}{r^3} \hbar^2 \vec{I} \cdot \hat{D} \cdot \vec{S} \tag{14}$$

where $r$ is the distance between the two spins I and S, which have components $(I_x, I_y, I_z)$ and $(S_x, S_y, S_z)$, and $\hat{D}$ is the dipolar coupling tensor. In the Cartesian coordinate system,

$$\hat{D} = \frac{1}{r^2} \begin{bmatrix} (r^2 - 3x^2) & -3xy & -3xz \\ -3xy & (r^2 - 3y^2) & -3yz \\ -3xz & -3yz & (r^2 - 3z^2) \end{bmatrix} \tag{15}$$
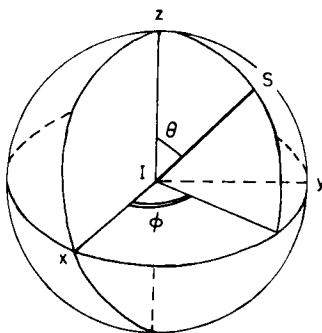
FIG. 3. Axis system and polar coordinates for I–S dipolar coupling.

The trace of $\hat{D}$ is clearly zero, also it is axially symmetric; $D_{12} = D_{21}$, $D_{13} = D_{31}$, and $D_{23} = D_{32}$. In the principal axis system, $r$ lies along the z-axis, all off-diagonal elements are zero, and

$$\hat{D} = \frac{1}{r^2}\begin{bmatrix} 1 & 0 & 0 \\ 0 & 1 & 0 \\ 0 & 0 & -2 \end{bmatrix} \tag{16}$$

It is useful to transform equation (14) to spherical polar coordinates (Fig. 3). In this coordinate system equation (14) may be decomposed into six terms as follows:

$$H_{IS} = \frac{\gamma_I \gamma_S}{r^3}\hbar^2(A + B + C + D + E + F) \tag{17}$$

where $A = \vec{I}_z\vec{S}_z(1 - 3\cos^2\theta_{IS})$ and expressions for the other terms can be found in a number of standard texts.[1-3] Only the $A$ term commutes with the Zeeman operator, hence this is the only term that we need to consider in calculating an energy level diagram (to the first order) for an isolated two-spin system. Operating on the product functions $|\alpha\alpha\rangle$, $|\alpha\beta\rangle$, $|\beta\alpha\rangle$, and $|\beta\beta\rangle$ with $H_Z + H_{IS}^D$ it is trivial to show that two transitions are allowed for spin I and two for spin S. Thus for the case of two isolated spins, I and S, in a single crystal the two lines are separated by

$$\frac{\gamma_I \gamma_S}{r^3}\hbar^2(1 - 3\cos^2\theta_{IS}) \tag{18}$$

For a powder sample one must average over all possible orientations; a line shape analogous to that shown in Fig. 2 is obtained. Typical $^{13}C-^{1}H$ dipolar interactions are 10–40 kHz.[35]

Expressions for $H_{II}$ and $H_{SS}$ in equation (13) are analogous to those given for $H_{IS}$ in equation (17). For like spins the $B$ terms in equation (17) also commute with the Zeeman Hamiltonian and must be considered in calculating the energy level diagram. For a two-spin homonuclear dipolar interaction between spin number one and spin number two,

$$A = (1 - 3\cos^2\theta)\vec{I}_{1z}\vec{I}_{2z} \tag{19}$$

$$B = -(1/4)(1 - 3\cos^2\theta)(I_1^+I_2^- + I_1^-I_2^+) \tag{20}$$

where $I^+$ and $I^-$ are the shift operators, $I^+ = \vec{I}_x + i\vec{I}_y$ and $I^- = \vec{I}_x - i\vec{I}_y$. $I^+|\alpha\rangle = 0$, $I^+|\beta\rangle = |\alpha\rangle$, $I^-|\alpha\rangle = |\beta\rangle$, and $I^-|\beta\rangle = 0$. Note that the $A$ term does not shift the nuclear spin quantum numbers $m_1$ and $m_2$ but that $B$ alters both nuclear spins by $\pm 1$. The term $B$ is sometimes referred to as the "flip-flop" or exchange term and is particularly important because it provides an efficient path for the spin–lattice relaxation of abundant spins. Note that for a two-spin homonuclear system two transitions separated by

$$(3/2)\frac{\gamma_I^2}{r^3}\hbar^2(1 - 3\cos^2\theta) \tag{21}$$

are allowed. For more complex systems it is often impossible to explicitly calculate the energy level diagram and the resulting frequency spectrum. In such cases it is possible however to use the van Vleck method of moments. Excellent discussions of this procedure are available elsewhere.[12,22,27]

### E. The chemical shielding term ($H_{CS}$)

It is well known that electrons modify the field experienced by a nucleus. The shielding produced at a particular nuclear site may be described by the Hamiltonian

$$H_{CS} = \hbar\gamma\vec{I} \cdot \hat{\sigma} \cdot \vec{B} \tag{22}$$

where $\hat{\sigma}$ is a dimensionless tensor of rank two called the chemical shielding tensor. In large static magnetic fields $\hat{\sigma}$ is symmetric and six quantities are required to specify it. It is always possible to find an axis system (called the principal axis system) in which all off-diagonal elements are zero, thus one can describe $\sigma$ in terms of three principal values, $\sigma_{11}, \sigma_{22}, \sigma_{33}$, and three angles which specify the orientation of the principal axis system. Experimentally it is possible to obtain $\sigma_{11}$, $\sigma_{22}$, and $\sigma_{33}$ for a spin 1/2 system directly from a powder pattern provided that dipolar interactions are small or eliminated. Theoretical powder patterns for a general shielding tensor ($\sigma_{11} = \sigma_{22} \neq \sigma_{33}$) are shown in Fig. 4. In reporting principal components of the chemical shielding tensor we use the convention $\sigma_{11} < \sigma_{22} <$
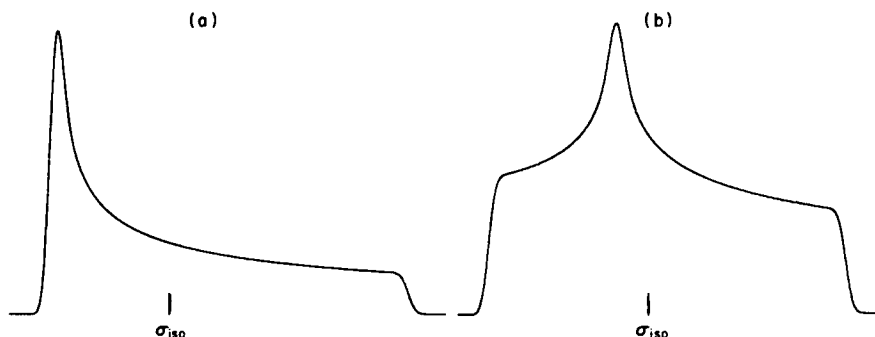
FIG. 4. Chemical shielding powder pattern: (a) axially symmetric ($\sigma_{11} = \sigma_{22} \neq \sigma_{33}$); (b) arbitrary second-rank tensor ($\sigma_{11} \neq \sigma_{22} \neq \sigma_{33}$).

$\sigma_{33}$. For an axially symmetric shielding tensor one can define the chemical shielding anisotropy, $\Delta\sigma$, as

$$\Delta\sigma = \sigma_{\parallel} - \sigma_{\perp} \qquad (23)$$

where $\sigma_{\parallel}$ is along the symmetry axis. For non-symmetric shielding tensors the definition of $\Delta\sigma$ is ambiguous. Some workers have defined $\Delta\sigma = \sigma_{11} - (1/2)(\sigma_{22} + \sigma_{33})$ while others have defined $\Delta\sigma = \sigma_{33} - (1/2)(\sigma_{11} + \sigma_{22})$.

Single-crystal studies are generally required in order to establish the orientation of the principal axis with respect to the molecular axes. An excellent discussion of the experimental procedure has been given by Veeman[36] and by Weil et al.[37]

Theoretical[38-40] and experimental[1,9,36,40] shielding tensors and anisotropies have been summarized. The general review by Appleman and Dailey is highly recommended.[40]

### F. Other interactions and summary

Other interactions include the indirect electron-coupled spin–spin interaction

$$H_J = \hbar\vec{I} \cdot \hat{J}_{IS} \cdot \vec{S} \qquad (24)$$

where $\hat{J}_{IS}$ is a second rank tensor (not necessarily traceless); also included is the spin–rotation interaction, $H_{SR}$, where

$$H_{SR} = \hbar\vec{I} \cdot \hat{C} \cdot \vec{J} \qquad (25)$$

$H_{SR}$ represents the couplings of the nuclear spins with the magnetic moment produced by the angular momentum of the molecule. The spin–rotation

constant $\hat{C}$ is a second rank tensor whose trace is non-zero. In solids $H_{SR}$ is generally unimportant and hence is neglected in the discussion that follows.

It is interesting to point out that, with the exception of $H_D$ and $H_J$, all the terms in equation (1) represent the sums of single-spin Hamiltonians; the latter two terms couple, in principle, every spin of the sample with all the others.

In the above discussion we have used Cartesian tensors to represent the various interactions. Often it is more convenient to use irreducible tensors. These permit one to write the spin Hamiltonians, $H_\lambda$, for the different couplings, $\lambda$, in a common form

$$H_\lambda = C^\lambda \sum_{l=0}^{2} \sum_{m=-l}^{l} (-1)^m T^\lambda_{l,m} R^\lambda_{l,-m} \qquad (26)$$

where $C^\lambda$ is a constant specific to each interaction, $T^\lambda_{l,m}$ are spin products built out of two vectors, and $R^\lambda_{l,-m}$ are coupling tensors. (See references 1 and 9 for excellent discussions of irreducible tensors.) Another convenient way of expressing the magnetic dipolar and quadrupolar Hamiltonians has been discussed by Pettitt.[41]

In liquids, where molecules are generally undergoing rapid "isotropic" reorientation, the second rank tensor interactions discussed above are averaged. Under these conditions the electric field gradient tensor, $\hat{V}$, and the dipolar coupling tensor, $\hat{D}$, vanish because their traces are zero. The isotropic average of the shielding tensor, $\hat{\sigma}$, is $(1/3) \text{Tr}\{\sigma_{ii}\}$, i.e.

$$\sigma_{iso} = (1/3)(\sigma_{11} + \sigma_{22} + \sigma_{33}) \qquad (27)$$

Similarly the isotropic indirect spin–spin coupling is $(1/3)\text{Tr}\{J_{ii}\}$. Thus under conditions of rapid isotropic reorientation the Hamiltonian describing the "internal" interactions of our two-spin system reduces to the familiar high-resolution Hamiltonian, $H$, used to describe the NMR spectra obtained in liquids, i.e.

$$H = -\hbar\gamma_I B_0(1-\sigma_I)\vec{I}_z - \hbar\gamma_S B_0(1-\sigma_S)\vec{S}_z + hJ_{IS}\vec{I} \cdot \vec{S} \qquad (28)$$

If the object of an NMR experiment is to obtain a high-resolution spectrum on a rigid sample (e.g. powdered solid) then one must develop and apply techniques that reduce the effective internal Hamiltonian to one approaching that given in equation (28). For a spin 1/2 species, S, this implies that one must reduce all of the dipolar interactions with a given S nucleus to essentially zero. Also the chemical shielding and indirect spin–spin coupling interactions must somehow be completely averaged.

[Some further recent references to theoretical aspects of the technique are included in the list on p. 287.]

# III. EXPERIMENTAL TECHNIQUES USED TO OBTAIN HIGH-RESOLUTION NMR SPECTRA OF SOLIDS

In this section we present a brief qualitative description of the experimental techniques that have been used to observe some dilute spins, S, in the presence of abundant spins, I (generally $^1$H or $^{19}$F). By dilute we mean a system where homonuclear S-spin dipolar interactions are quite small, e.g. 1 kHz. This condition is satisfied for $^{13}$C in almost any carbon-containing molecule since the natural abundance of $^{13}$C is only 1·1%. Similarly it generally applies for any spin 1/2 nucleus with the exception of $^1$H and $^{19}$F. Even in the case of $^{31}$P (natural abundance 100%), $^{31}$P–$^{31}$P dipolar interactions are generally less than 1 kHz unless the phosphorus atoms are chemically bonded to one another. In the discussion that follows, both I and S will be assumed to have spin 1/2 unless otherwise stated.

## A. High-power decoupling and cross-polarization (CP)

By applying a strong rf field to the I-spins in a pulsed or continuous fashion, the I–S dipolar interaction is removed. Qualitatively the rf irradiation forces the I-spins to change their spin states rapidly compared with the I–S dipolar interaction, and thus "decouples" them from the S-spins. Decoupling is a coherent averaging of the I–S dipolar interaction in spin space as opposed to the incoherent averaging process that occurs due to random motion in liquids. In some ways it is analogous to the proton decoupling used in NMR studies of liquids except that much larger decoupling fields are required. Typically I-spin decoupling fields of 40 kHz or more are required to eliminate I–S dipolar interactions. Because of the heating that results from rf fields of this magnitude they are generally not left on continuously for more than 200 ms.

Continuous I-spin decoupling is generally more effective than pulsed decoupling; also, as one might expect, on-resonance decoupling is more effective than off-resonance decoupling. Spin decoupling dynamics are discussed in the original literature[42,43] and in Section 4.4 of the monograph by Mehring.[1]

In addition to removing the I–S dipolar coupling, the I-spin decoupling field, $B_{1,I}$, can also be used to enhance the sensitivity of a dilute spin, S, by a cross-polarization (CP) technique. The object of this technique is to transfer polarization from the more abundant I species, which in thermodynamic language has a high heat capacity, to the S system which has a small heat capacity (Fig. 5). Recall that exchange of Zeeman energy is not normally permitted by the I–S dipolar interaction (i.e. the I and S systems are "insulated" from each other). Polarization transfer can be accomplished in more than one way;[1,44–48] the most common technique is to allow both
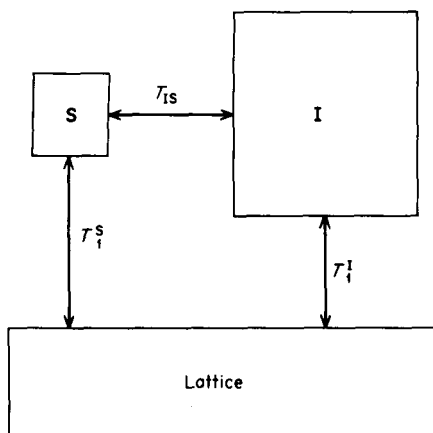
FIG. 5. Thermodynamic picture of I and S reservoirs.

the I and S spins to precess in their respective rotating frames at some common frequency,

$$\gamma_I B_{1,I} = \gamma_S B_{1,S} \tag{29}$$

Under this condition, known as the Hartmann–Hahn condition, the Zeeman levels in the rotating frame are matched and effective coupling between the I and S spins occurs via the dipolar interaction.

Experimentally, one possible sequence of events for establishing contact between the I and S spin systems and observing the S spins is summarized below and in Fig. 6:

(1) Establish I-spin polarization in the static field $B_0$.

(2) Spin-lock the I-spin magnetization along $B_{1,I}$.

(3) Establish I–S contact with a Hartmann–Hahn match by applying an rf field $B_{1,S}$ to the S-spins for some time $t_c$.

(4) Turn off $B_{1,S}$ and record the S-spin FID.

(5) Turn off $B_{1,I}$ and repeat the sequence.

Two important questions are: (i) What parameters govern $T_{IS}^{-1}$, the cross-relaxation rate, and hence the efficiency of "communication" between the I and S spin systems? (ii) What is the gain in sensitivity realized in using a CP procedure such as that outlined in Fig. 6?

The rate of CP is related to a number of parameters, the most important being the I–S second moment ($T_{IS}^{-1} \propto M_2^{IS}$). Thus in a $^{13}$C NMR experiment one would expect a non-protonated $^{13}$C nucleus to cross-polarize much more slowly than a methylene carbon. Since experimentally observed second moments depend on molecular motion, one might, for example, expect the carbon of a rapidly reorientating methyl group to cross-polarize
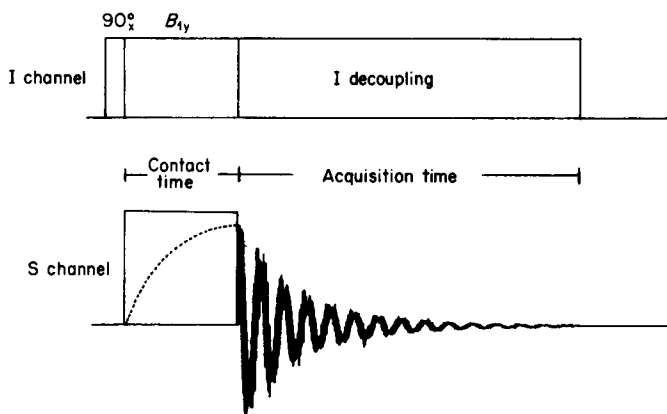
FIG. 6. Cross-polarization timing diagram.

at a rate quite different from that of a carbon associated with a rigid methyl group (this is indeed observed). Typical $^1$H–$^{13}$C CP times, $T_{CH}$, vary between $10^{-4}$ and $10^{-2}$ s. The dynamics of cross-relaxation are discussed by Demco, Tegenfeldt and Waugh[49] and summarized by Mehring.[1]

The S-spin magnetization established in the rotating frame after a single CP contact with Hartmann–Hahn matching, compared with that observable in the applied static field $B_0$ after $5 \times T_{IS}$, is approximately $(\gamma_I/\gamma_S)$.[48] This ratio is 4 (16 in time) for $S \equiv {}^{13}C$ and $I \equiv {}^1H$. If the I-spin magnetization decays slowly in the rotating frame (i.e. if the $T_{1\rho}{}^I$ is long) then it is possible to repeat the contact and observe steps 3 and 4 above before re-establishing I-spin polarization (step 1). Although a further gain in sensitivity can be achieved by this procedure it is generally not used in practice because it requires the $B_{1,I}$ field to be on for excessive lengths of time.

A further important advantage of the CP technique is that it allows one to use recycle times of the order of $T_1{}^I$ instead of $T_1{}^S$. In practice, $T_1{}^S$ is generally much longer than $T_1{}^I$, so in a given time period one can accumulate many more FIDs using the CP technique than with conventional $\pi/2$ S-spin pulses.

As already mentioned, there are a number of variations in the procedure mentioned above for establishing CP. These techniques are discussed by Pines et al.[48] and by Mehring.[1]

Specifications for a CP spectrometer have been presented.[10,14,15,18,48,50] Pulse programmers,[51–54] probes,[55] and receivers[56] are discussed in a number of recent references. Readers interested in building a spectrometer should consult the above references and recent issues of journals such as Review of Scientific Instruments and Journal of Magnetic Resonance. [Further recent references are in the list on p. 287.]

## B. Magic angle sample spinning (MASS)

### 1. Influence of rapid sample spinning on Hamiltonians

The first technique used to reduce dipolar interactions was proposed independently by Lowe[57] and by Andrew *et al.*[58] It involves physically spinning the sample about an axis that is approximately 54°44′8″ with respect to the applied static field $B_0$ (Fig. 7). If the rate of sample spinning
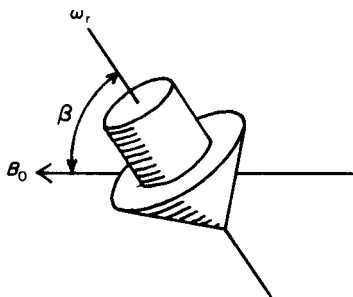


FIG. 7. Orientation of field and spinning axis vectors for magic angle sample spinning experiment.

is large compared with the dipolar interaction, the time-averaged dipolar Hamiltonian is scaled by $1/2(3 \cos^2 \beta - 1)$. In high-resolution S-spin NMR with high-power I-spin decoupling, MASS is useful in reducing dipolar interactions between S-spins and other dilute spins (including other S-spin homonuclear interactions). Such interactions are usually small ($<0.5$ kHz) and readily averaged to zero by MASS. An exception occurs when the S-spin is dipolar coupled to a quadrupolar nucleus (Section IV.A.2).

One of the most important results of MASS is that it reduces the chemical shielding powder pattern to the isotropic value provided that the rate of spinning, $\nu_r$, is comparable to the shielding anisotropy in frequency units. Therefore, under high-power I-spin decoupling and MASS, one observes a single peak for each chemically distinct S-spin at its respective Larmor precession frequency. For nucleus t (an S-spin),

$$\nu_t = \frac{\gamma_S}{2\pi} B_0 (1 - \sigma_t)$$  (30)

where all the symbols have their usual meanings. It is customary to express the relative shielding of nuclei in terms of their chemical shifts. Both IUPAC and ASTM have recommended that the chemical shift, $\delta_t$, should be reported on a dimensionless scale and defined as

$$\delta_t = \frac{\nu_t - \nu_R}{\nu_R} \times 10^6 = \frac{\sigma_R - \sigma_t}{1 - \sigma_R} \times 10^6 \approx (\sigma_R - \sigma_t) \times 10^6$$  (31)

where R refers to a reference standard. Ideally it would be desirable to reference all isotropic chemical shifts with respect to that of the bare nucleus (an absolute scale). Although considerable progress has been made in establishing absolute chemical shift scales,[59–62] theoretical and experimental problems still exist, and experimentalists generally prefer to use reference standards. Tetramethylsilane is the accepted reference in $^1H$, $^{13}C$, and $^{29}Si$ NMR; both nitromethane and anhydrous liquid ammonia have been used to reference $^{15}N$ chemical shifts. Phosphoric acid (85%) is generally used to reference $^{31}P$ chemical shifts. In contrast to solution NMR studies it is often necessary to use external references for solids, hence measured chemical shifts should in principle be corrected for bulk susceptibility differences. In practice these corrections are generally estimated to be less than 1 ppm (for $^{13}C$) and hence are often ignored.

If nucleus t is scalar coupled to some other nucleus k, one observes a splitting, $J_{tk} = (1/3) \operatorname{Tr} \hat{J}$, in the MASS NMR spectrum of t. Here $J_{tk}$ is the isotropic scalar coupling which corresponds to that measured in solution studies.

In general, MASS reduces the magnitude of all symmetric second-rank tensor interactions to one-third of their trace provided that the rate of rotation is comparable to the interaction energy in frequency units.[3,4,63]

## 2. MASS combined with high-power decoupling and CP

The effect of MASS on the $^{31}P$ NMR spectrum of triphenylphosphine is illustrated in Fig. 8. The spectra were obtained with high-power proton decoupling and CP. The relatively sharp peak observed with MASS has an isotropic chemical shift of $-7.2$ ppm, which is within the range of $^{31}P$ NMR chemical shifts ($-5.4$ to $-8.0$ ppm) observed for triphenylphosphine in solution studies.[64] Despite the increased S/N ratio and resolution obtained with high-power decoupling CP/MASS, one also loses information. Heteronuclear dipolar interactions and hence potential structural information are lost with dipolar decoupling. The principal values of the chemical shielding tensor are averaged by MASS. Ideally one would like to have available experimental techniques that would allow one to obtain high-resolution NMR spectra and yet retrieve the dipolar and anisotropic shielding information. Significant progress has been made in extracting anisotropic chemical shielding information from NMR spectra with spinning; work in this area is summarized below. Recently progress has been made in obtaining chemical shift resolved dipolar spectra.[6,35,65–71]

(a) *Recovering shielding anisotropies from high-resolution solid-state spectra.* Three different techniques have been suggested for obtaining chemical shielding anisotropies (CSA) from the high-resolution NMR spectra of solids: (1) slow magic angle sample spinning, SMASS;[77–82] (2)
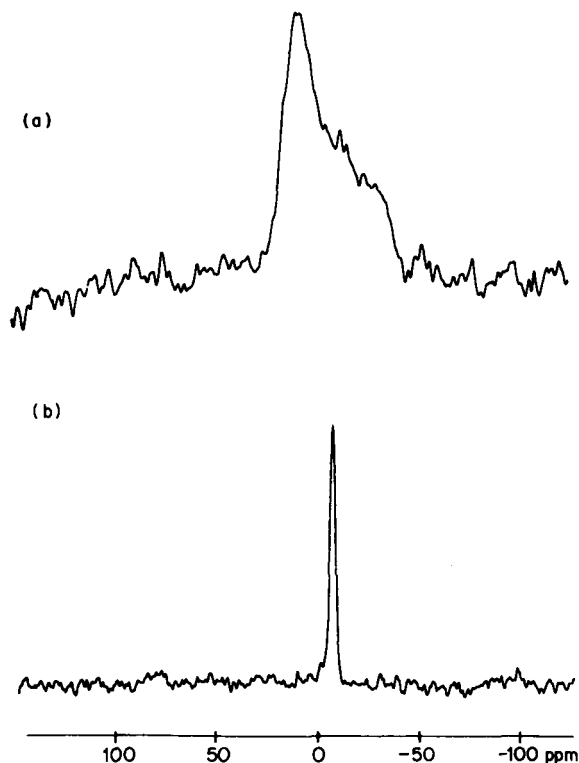
FIG. 8. $^{31}$P NMR spectra (34 MHz) of triphenylphosphine, Ph₃P: (a) with MASS; (b) without MASS. Spectra were obtained with high-power $^1$H decoupling and CP.

off-magic angle sample spinning, OMASS;[77,78,83,84] and (3) rotation synchronized rf pulse techniques.[84]

When the sample spinning speed is reduced so that $\nu_{rot}$ is less than the CSA,[77-82] the isotropic peak is flanked by spinning sidebands spaced at the spinning frequency (Fig. 9). Herzfeld and Berger[82] have recently developed a convenient graphical procedure for extracting the principal components of the chemical shielding tensor from the intensities of the spinning sidebands. The method is easy to apply and in principle requires the analysis of a single SMASS spectrum. We have found, however, that two or three spectra obtained with SMASS at different spinning frequencies are required for reliable estimates of the principal components of $\hat{\sigma}$.

Rapid but off-magic angle sample spinning results in a scaled powder pattern which can also be analysed to obtain the principal components of individual chemical shielding tensors.[77,78,83] The OMASS technique has recently been used to obtain shielding anisotropies of the carboxy and
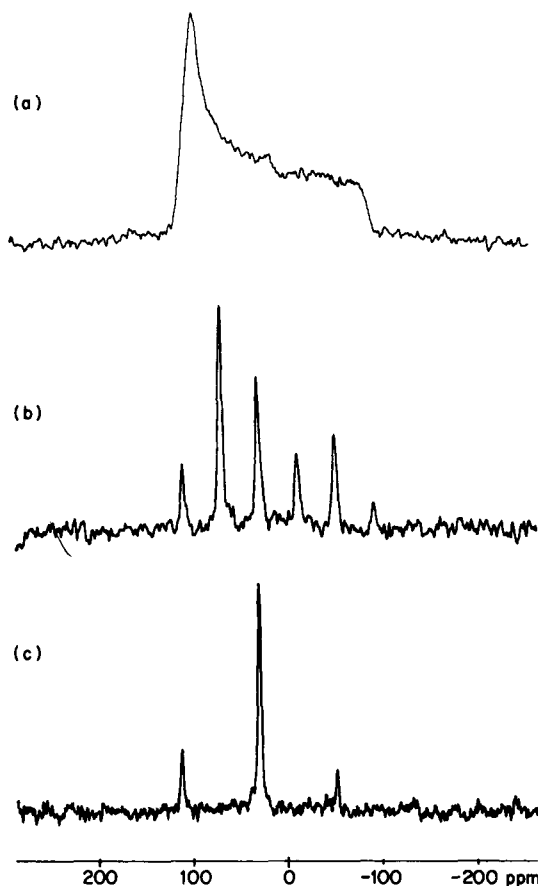
FIG. 9. Solid-state $^{31}$P NMR spectra of triphenylphosphine oxide, Ph$_3$P=O (34 MHz): (a) stationary sample; (b) slow MASS, $\nu_{rot} = 1\cdot5$ kHz; (c) MASS, $\nu_{rot} = 3\cdot0$ kHz.

methylene carbons in poly(ethylene terephthalate),[84] and to separate the tensor components of the methylene resonance in *cis*-1,4-polybutadiene.[72]

An elegant general technique for recovering shielding anisotropies from high-resolution NMR spectra has been described by Lippmaa *et al.*[77] Unfortunately this technique is time-consuming and there are a number of practical problems in employing it.[78]

(b) *Useful pulse sequences.* Here we mention a few pulse techniques which can be used in high-resolution NMR studies of solids to improve the S/N ratio, aid in spectral assignments, and measure relaxation times.

As already mentioned, the recycle time used in CP experiments depends on $T_1^I$ and not $T_1^S$. If $T_{1\rho}^I$ is long compared with the mixing time plus the

FIG. 10. CP in solids with flip-back of I-spin magnetization: (a) Pulse timing for the cross-polarization experiment with flip-back; (b) I-channel irradiation for the phase-alternated version of the flip-back experiment.

acquisition time for observation of the S-spin FID (time $t_1$ in Fig. 10, typically 50–100 ms) then a substantial fraction of I-spin pola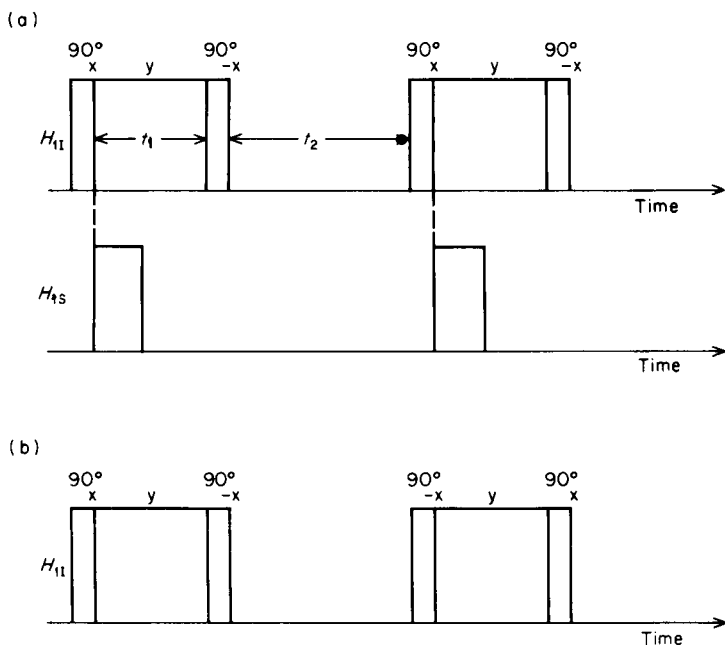rization remains at the end of the observation period. Tegenfeldt and Haeberlen[85] have suggested that a 90° pulse reversed in phase with respect to the initial preparation pulse, $90^\circ_{\bar{x}}$, be applied at the end of the spin-locking pulse (i.e. at the end of the observation period). The I-magnetization remaining at time $t_1$ is thus flipped back along the static field, $B_0$, before the spin-locking sequence is repeated. The S/N ratio obtained using this procedure has been compared to that obtained using a single- and multiple-contact sequence. The conclusion is that the introduction of the flip-back pulse will never decrease the S/N ratio compared with the standard single-contact experiment. The most undesirable situation arises when $T_{1\rho}{}^I$ is very short (much less than $T_{IS}$) and $T_1{}^I$ is long.

Opella and Frey[86] have employed the pulse sequence sketched in Fig. 11 to selectively suppress $^{13}C$ NMR signals from carbons with directly bonded protons. During the delay period magnetization decays most rapidly for carbon nuclei which are strongly dipolar coupled to protons. Since the $^{13}C-^{1}H$ dipolar interaction depends on $r_{CH}{}^{-3}$, one can easily adjust the
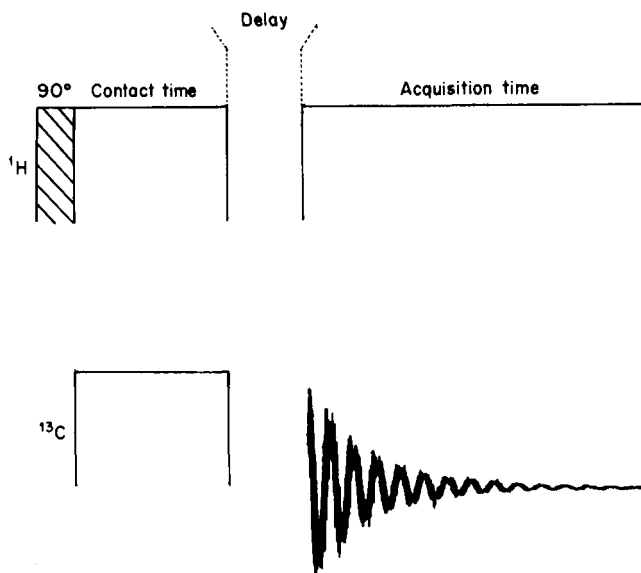
FIG. 11. Pulse sequence used to suppress signals from protonated carbons in solids.

delay so that protonated carbons are completely suppressed relative to non-protonated ones. The technique is illustrated for compound 1 in Fig. 12. Note that rapid internal motion of the methyl groups can significantly reduce the local dipolar field, hence $^{13}$C signals from methyl carbons are generally not suppressed in these experiments.



(1)
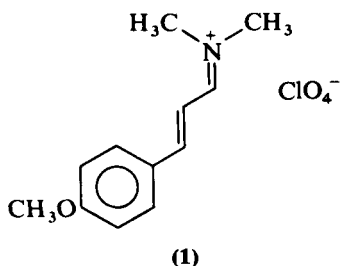
A number of pulse sequences have been devised to measure relaxation times in high-resolution CP experiments on solids.[87-92] An inversion-recovery experiment for the measurement of $T_1$ has been described,[87] measurement of $T_2$ has been discussed,[88] and experiments designed to measure $T_{1\rho}^{I}$, $T_{1\rho}^{S}$, $T_{1D}^{I}$, $T_{IS}$, etc. have been presented.[17,89-92]

|  | | | |
|---|---|---|---|
| 200 | 100 | 0 | ppm |
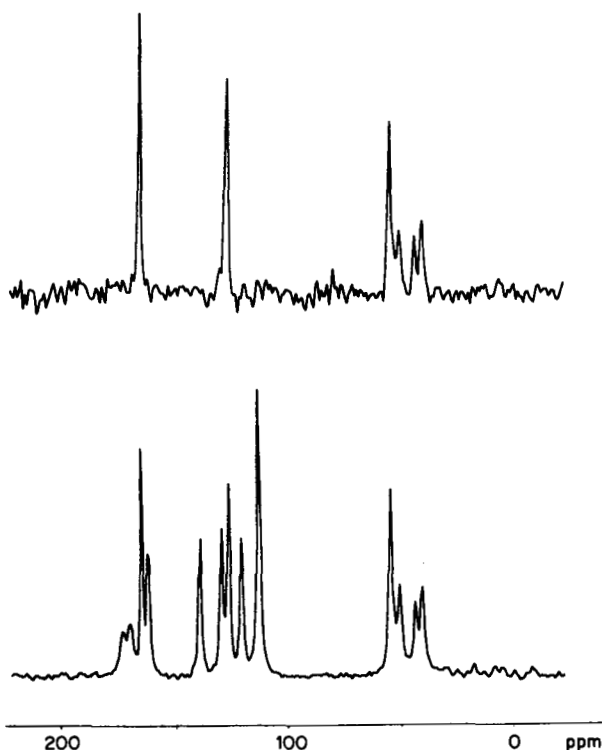
FIG. 12. $^{13}$C CP/MASS spectra (22·6 MHz) illustrating the selection of non-protonated carbons in compound **1** using the pulse sequence illustrated in Fig. 11.

## 3. Experimental aspects of MASS; spinner design

Most of the rotors that have been reported in the literature are modifications of either the conical spinner[58] (Fig. 13) or the cylindrical spinner;[57] the general features of these two systems have been reviewed.[10]



(a)                    (b)
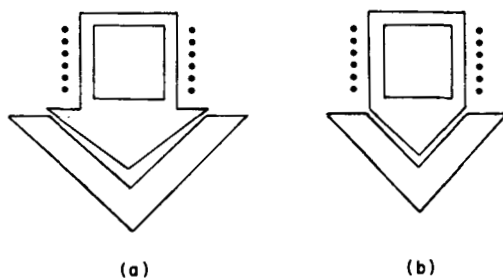
FIG. 13. Schematic representation of magic-angle spinning systems: (a) Andrew–Beams; (b) bullet.

No attempt is made here to critically evaluate the spinner systems mentioned below.

Bartuska and Maciel[93] have described a bullet-shaped rotor which uses an Andrew-type stator (Fig. 13). Reliable spinning at 1·5–3·5 kHz is achieved with this system.[93] The relative merits of the bullet system compared with the conventional Andrew spinner are discussed in detail.[93] Zilm et al.[94] have designed a high-speed magic angle spinner for electromagnets which is capable of rotation rates of up to 15 kHz. The spinner design is that of Andrew. A convenient quick-change sample spinning apparatus for superconducting magnet systems has been described.[95] The sample chamber holds approximately 300 mg of a typical organic material. The fluted rotors spin at rates of 3·5 kHz with air pressures of 40 psi. Fyfe, Mossbruger and Yannoni[96] have described a spinning apparatus that is convenient for variable temperature studies (Fig. 14). This system routinely spins at 3–
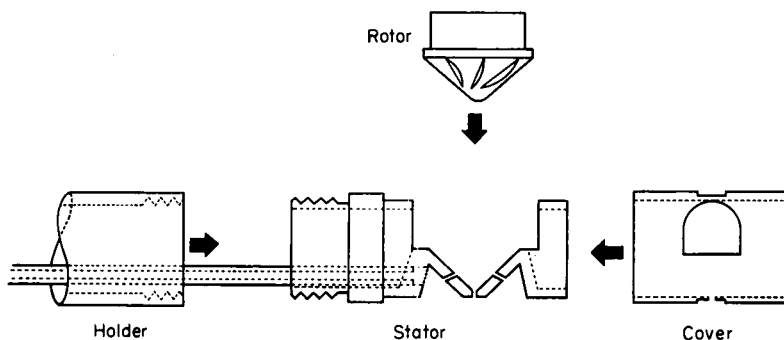


FIG. 14. A spinner system suitable for variable temperature MASS studies.

4 kHz at liquid nitrogen temperature with helium as the propellant gas. A cylindrical rotor has been reported.[73,97,98] This system has a number of advantages and can be used for variable temperature operation. A high-speed cylindrical spinner (~7 kHz) has recently been reported.[99] The rotor is supported by two air bearings.

Spinners may be constructed from a number of materials, including Kel-F (polytrifluorochloroethylene), Delrin (polymethylene oxide), Teflon, poly(methyl methacrylate), boron nitride,[100] and aluminium oxide. Kel-F and Delrin appear to be the most commonly used materials. Delrin is stronger and easier to work with than Kel-F but gives rise to a strong $^{13}$C NMR signal at $\delta = 89·5$ ppm.[94]

A simple method for measuring spinning frequency in MASS experiments has been reported.[101]

## IV. APPLICATIONS OF HIGH-RESOLUTION SOLID-STATE NMR STUDIES

Most of the high-resolution solid-state NMR studies on dilute spins have been carried out on $^{13}$C, so we begin this section by dealing with this nucleus. Most of the techniques that have been used to obtain and assign high-resolution solid-state $^{13}$C NMR spectra are, in principle, applicable to any other dilute spin 1/2 nucleus. In addition, the problems and limitations observed in $^{13}$C NMR studies apply to other spin 1/2 isotopes. Our discussion of $^{13}$C NMR is followed by a summary of applications involving $^{29}$Si, $^{31}$P, $^{113}$Cd, and some other nuclei of the spin 1/2 and quadrupolar varieties. Applications of high-resolution $^{1}$H and $^{19}$F solid-state NMR are not presented here. Excellent discussions are provided elsewhere.[2,6,102–105]

### A. Carbon-13

After a general introduction to $^{13}$C NMR, specific applications are discussed. For convenience, these applications are discussed as they apply to relatively small molecular solids, synthetic macromolecules, and natural macromolecules. [For further recent references see p. 287.]

### 1. Introduction

The low natural abundance of $^{13}$C (1·1%) and its relatively small gyromagnetic ratio presented a challenge to early NMR spectroscopists interested in the characteristics of this nucleus. However, the development of double resonance and FT techniques in the late 1960s led to an explosion of activity in $^{13}$C NMR studies of solutions. In 1972, two books devoted entirely to $^{13}$C NMR appeared which summarized this early work.[106,107] Also in 1972, Pines, Gibby and Waugh[108] described the proton-enhanced dilute spin NMR technique and applied it to observe the $^{13}$C spectrum of solid adamantane. This report was quickly followed by a full paper[48] describing the technique, the necessary instrumentation, and several experimental results. Later in 1973, $^{13}$C double-resonance FT NMR experiments in solids were reported.[109] Below we outline some of the general characteristics of $^{13}$C NMR.

(a) *Chemical shifts.* The range of $^{13}$C chemical shifts is typically 250 ppm. Carbons with four neighbours ("sp$^3$ carbons") are generally highly shielded ($\delta = 0$–80 ppm) while those with three neighbours ("sp$^2$ carbons") are generally least shielded ($\delta = 100$–220 ppm). Carbons with two neighbours ("sp carbons") generally have intermediate chemical shifts ($\delta = 70$–130 ppm). Electronegative substituents (e.g. F, Cl, O) tend to deshield a given carbon. Detailed discussions of substituent effects on $^{13}$C chemical shifts are given elsewhere.[110]

Carbon CSA values range from approximately 0 to 400 ppm. Extensive tables of the principal components of $^{13}C$ chemical shielding tensors have been compiled.[1,9,36,40,111] Representative data from the recent literature are collected in Table 2.

TABLE 2

Components of carbon-13 chemical shielding tensors.

| Compound | | $\sigma_{11}$ | $\sigma_{22}$ | $\sigma_{33}$ | Ref. |
|---|---|---|---|---|---|
| n-Eicosane (n-$C_{20}H_{42}$) | $CH_3$ | $166 \cdot 7 \pm 2 \cdot 0$ | $171 \cdot 2 \pm 2 \cdot 0$ | $189 \cdot 8 \pm 2$ | |
| | $CH_2$ | $156 \cdot 0 \pm 2 \cdot 5$ | $163 \cdot 1 \pm 2 \cdot 5$ | $178 \cdot 0 \pm 2 \cdot 5$ | |
| | $CH_2$ | $142 \cdot 6 \pm 2 \cdot 0$ | $154 \cdot 6 \pm 2 \cdot 0$ | $175 \cdot 6 \pm 2 \cdot 0$ | 112 |
| Ethylene | | $238 \pm 2$ | $126 \pm 2$ | $29 \pm 2$ | 113, 114 |
| Acetylene | | 150 | 150 | $-90 \pm 5$ | 114 |
| Benzene | | $-88 \cdot 2$ | $-12 \cdot 0$ | $127 \cdot 7$ | 69 |
| Ferrocene | | 34 | 34 | 110 | 115 |
| Carbon monoxide | | $-122$ | $-122$ | 244 | 116 |
| $Rh_6(CO)_{16}$ CO bridged | | $-102$ | $-296$ | $-296$ | 117, 118 |
| CO terminal | | 80 | $-305$ | $-315$ | |
| L-Alanine | $CH_3$ | $98 \cdot 2$ | $107 \cdot 1$ | $120 \cdot 2$ | 119 |
| | CH | $63 \cdot 4$ | $72 \cdot 0$ | $97 \cdot 2$ | |
| | COOH | $-114 \cdot 4$ | $-55 \cdot 0$ | $-21 \cdot 8$ | |
| $Mg(OCH_3)_2$ | | $-74$ | $-74$ | 10 | 120 |

Isotropic $^{13}C$ chemical shifts, measured in the solid state with MASS, are generally within a few ppm of those observed in solution studies.[121] In the solid, however, one often observes chemical shift non-equivalence which would generally not be observable in solution. For example, the solid-state $^{13}C$ spectrum of p-diacetylbenzene (2) shows four peaks in the



(2)
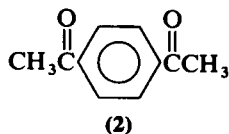
aromatic region (Fig. 15). In solution, rapid internal rotation about the carbonyl carbon to aromatic carbon bond renders all four protonated aromatic carbons equivalent at room temperature.

Additional peaks in the solid state can also arise because of crystallographic effects. For example, Balimann et al.[18] report two equally intense peaks separated by 2·9 ppm in the methyl region of the $^{13}C$ spectrum of 2,4-dinitrotoluene. Subsequent X-ray data have confirmed that there are
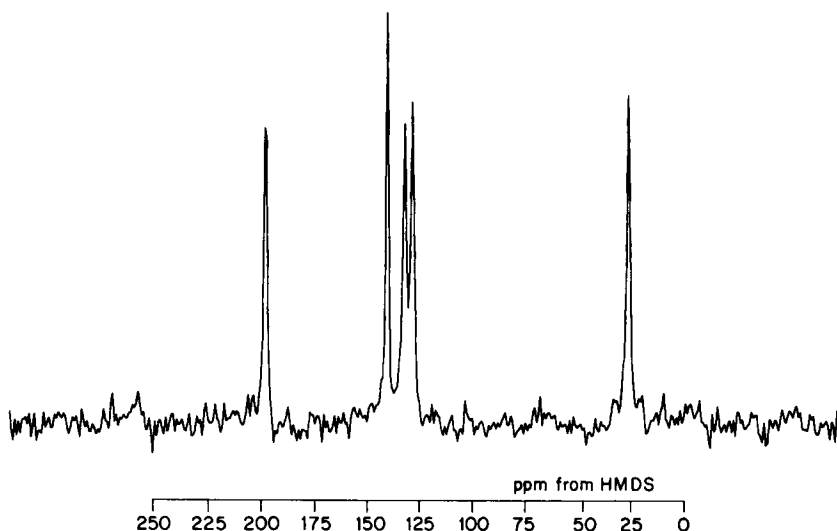
FIG. 15. CP/MASS $^{13}$C NMR spectrum of p-diacetylbenzene (2) (22·6 MHz).

two non-equivalent molecules per unit cell.[122] Examples of crystallographic effects on $^{31}$P NMR spectra are discussed in the following Section C.

(b) *Scalar coupling*. One-bond spin–spin couplings to protons, $^1J(^{13}C–^1H)$, vary from approximately 115 to 320 Hz. Because high-power $^1H$ decoupling is generally necessary to remove $^1H–^{13}C$ dipolar interactions in solids, scalar coupling information to protons is lost in the study of solids. Coupling to other spin 1/2 nuclei should generally be observable, particularly to spin 1/2 metal nuclei that are known to exhibit large scalar couplings to carbon, e.g. $^{113}Cd$, $^{119}Sn$, $^{183}W$, $^{195}Pt$, $^{199}Hg$, $^{205}Tl$, and $^{207}Pb$. Recently the following scalar couplings have been observed in solid-state $^{13}$C NMR: $^1J(^{31}P–^{13}C) = 54$ Hz in Me$_3$PS;[18] $^1J(^{199}Hg–^{13}C) = 2820$ Hz in $(CF_3)_2Hg$;[123] $^1J(^{207}Tl–^{13}C) = 5215$ Hz in an aromatic system containing a Tl–C bond.[18] Solution values are not known for the latter compound but the $^{13}$C coupling to $^{31}$P in Me$_3$PS is 56·1 Hz in solution.[124] For $(CF_3)_2Hg$, $^1J(^{199}Hg–^{13}C)$ is 2950 Hz in dimethoxyethane, 3225 Hz in pyridine, and 2088 Hz in chloroform.[125]

(c) *Resolution in the $^{13}C$ NMR spectra of solids*. The $^{13}$C linewidths observed in high-resolution solid-state NMR studies are at least one to two orders of magnitude larger than those observed in solution. What are the factors that limit the resolution attainable in solids with high-power decoupling and magic angle spinning? This question has been dealt with in detail.[17,126] Line broadening mechanisms are divided into those that produce a distribution of resonance frequencies (inhomogeneous broadening) and those that derive from relaxation effects and result in homogeneous

broadening. Two general types of solids are discussed: non-crystalline glassy materials, e.g. a glassy polymer below $T_g$, and rigid crystalline solids. Generally the glassy solids exhibit linewidths of 30–120 Hz at 1·41 tesla while rigid, crystalline materials typically have linewidths of 3–12 Hz. The mechanisms for line broadening and their typical, or maximum, linewidth contribution in the MASS experiment are summarized in Table 3. The dependence of linewidth on the applied static field ($B_0$), decoupling field ($B_1$, $\nu_{1H}$), rotor spinning frequency ($\nu_{rot}$), temperature ($T$), and sample orientation are indicated. If the linewidth has a simple power law dependence on a variable the exponent is given; otherwise, the notation w, m, and s is used to indicate weak, medium, or strong dependence. Two numbers with a slash between them indicate power law behaviour in two limits. The data in Table 3 are based on a sound analysis of the mechanisms that can contribute to linewidths, and extensive experimental data. Strong $^{13}C$–$^{13}C$ dipolar interactions or dipole–dipole coupling to nuclei other than protons are not considered by VanderHart et al.[126] but are considered elsewhere.[19,81,127] We discuss the effect of a dipolar coupling to a quadrupolar nucleus in the following Section 2.

For glassy materials, the lack of a fixed single conformation results in a dispersion of chemical shifts and makes a significant contribution to the observed linewidths. As an example of this type of broadening the authors[126] point out that in linear polyethylene the non-crystalline carbons ($\nu_{\frac{1}{2}} = 14 \pm 4$ Hz) are shifted by 2·36 ppm to low frequency because they can participate in both *gauche* and *trans* bonds whereas the crystalline carbons ($\nu_{\frac{1}{2}} \approx 1·0 \pm 0·6$ Hz) are confined to the *trans* conformation.

At the frequency of proton decoupling, $\nu_{1H} = \gamma_H B_{1H}/2\pi$, molecular motion provides an efficient pathway for transverse relaxation and hence $^{13}C$ line broadening. In practice this mechanism appears to be most important for methyl groups in glasses.[126] Also, random motional modulation of the CSA can make a contribution to $\nu_{\frac{1}{2}}$.[128] VanderHart et al.[126] conclude that for glasses at 1·4 T this mechanism is not generally the dominant one for line broadening; however, at high fields its effects can be significant.

For crystalline organic solids, all mechanisms with the exception of insufficient decoupler power (IDP) depend at least linearly on $B_0$ (Table 3). Since IDP is usually negligible, the maximum resolution attainable for these types of solids is unlikely to improve at higher static fields. If the resolution at the lower field is limited by the stability or homogeneity of $B_0$ higher fields may result in improved resolution.

## 2. Relatively small molecular solids

(a) *Orientationally disordered solids.* A number of approximately spherically shaped molecules have one or more solid phases in which the molecules are rotationally disordered.[12,129] Adamantane, $C_{10}H_{16}$, is a classic example

## TABLE 3

### Size and dependence of carbon-13 line broadening in organic solids.[a]

| Source of broadening | Size of broadening[b] | $B_0$ | $\nu_{1H}$ | $\nu_{rot}$ | $T$ | Orient. | Misc. |
|---|---|---|---|---|---|---|---|
| *Glasses* | | | | | | | |
| Conformational inequivalence | 2–6 ppm | 1 | 0 | 0 | m | 0 | |
| Packing effects | | 1 | 0 | 0 | m | ? | |
|   bond distortion | ? | | | | | | |
|   variation in local susceptibility | 0·5–2 ppm | | | | | | |
| Motional modulation of the C–H coupling | 4 kHz max. | 0 | −2/0 | 0 | s | w | $M_{CH}^{(2)}$ |
| Motional modulation of the resonance frequency via chemical shift anisotropy | 200 Hz max. at 15 MHz | 2/0 | 0 | −2/0 | s | w | $\Delta\sigma^2$ |
| | 1 kHz max. at 50 MHz | | | | | | |
| *Crystalline solids* | | | | | | | |
| Magic angle mis-setting | 2·47% of non-spinning linewidth per degree | 1 | 0 | 0 | m | s | $\Delta\sigma$ |
| Rotor instability | ≤0·3 ppm | (1) | 0 | ? | 0 | 0 | |
| Anisotropic bulk magnetic susceptibility | 1 ppm max. | 1 | 0 | 0 | 0 | m | $\Delta\chi_v$ |
| Off-resonance proton irradiation | | 2 | −2 | m | m | m | $M_{CH}^{(2)}, \tau_D$ |
|   $\Delta\sigma_H$ | 0·1–12 Hz | | | | | | |
|   distribution of $\bar{\sigma}_H$ | 1–60 Hz | | | | | | |
| Insufficient decoupling power | Sudden onset for decoupling fields much below 40 kHz | 0 | m | 0 | m | m | $M_{CH}^{(2)}$ |

[a] For power law dependence, the exponent or range of exponents is given. Temperature ($T$) dependence is weak (w), medium (m), or strong (s). Orient. refers to whether there is a change in broadening resulting from the use of an oriented (e.g. a single crystal) as opposed to a powder sample.

[b] Broadening in Hz or ppm; a broadening linear in $B_0$ is defined to leave the resolution in ppm independent of $B_0$.

of such a molecule. It has a high melting point, 542 K, and a solid II → solid I phase transition at 208·6 K ($\Delta S = 1 \cdot 95 R$).[130] The high-temperature phase (solid I) has a face-centred cubic structure while the low-temperature phase (solid II) is tetragonal. In solid I, molecular reorientation is rapid enough to effectively average intramolecular dipolar interactions among the protons and carbons to zero. Proton,[131] $^2$H,[132] and $^{13}$C[132] relaxation times and quasielastic incoherent neutron scattering data[133] have been used to obtain the temperature dependence of rotational jump times for adamantane ($\tau_2 \approx 15$ ps at 300 K).

Because of its relatively narrow $^{13}$C resonance ($\nu_{\frac{1}{2}} \approx 40$ Hz) in the absence of MASS, adamantane has proven to be an important model compound in the development of high-resolution $^{13}$C NMR of solids. Here we briefly outline the studies carried out on adamantane in chronological order. As already mentioned, the first $^{13}$C–$^1$H CP experiments were performed on adamantane.[108] The dependence of CP times on $B_{1C}$ in adamantane was first investigated by Pines and Shattuck.[134] A plot of $T_{IS}^{-1}$ vs. $B_1$ is found to be exponential, $T_{IS}^{-1} \propto \exp(-\gamma B_1 \tau_{SD})$, with $\tau_{SD} \approx 140$ μs.

Adamantane was first used to investigate the dynamics of spin decoupling in $^{13}$C–$\{^1$H$\}$ experiments.[42] By considering only intermolecular $^{13}$C–$^1$H dipolar interactions, a $^{13}$C linewidth of 2105 Hz is calculated. This is approximately twice the actual $^{13}$C linewidth observed in the absence of $^1$H decoupling. The line narrowing is attributed to "self-decoupling" caused by the I–I coupling. The same phenomenon was observed in AgF by Abragam and Winter[135] who realized that the $^{109}$Ag–$^{19}$F interaction in AgF is influenced by the flip-flop motion of the fluorine spins. Detailed discussions of these interactions are given elsewhere.[1,43]

The influence of MASS on rates of polarization transfer from abundant to rare spins has been investigated.[136] For adamantane, MASS significantly modifies the rate of polarization transfer from $^1$H to $^{13}$C spins in the CP experiment. However, in solids where the spin speed is much less than that required to remove the dipolar coupling among abundant spins (e.g. $^1$H), the influence of MASS on polarization transfer is not dramatic regardless of the nature of the static dipolar coupling between rare and abundant spins.

Garroway[137] has shown that $^{13}$C–$^{13}$C intermolecular dipolar interactions are responsible for the 40 Hz linewidth observed for adamantane in the absence of MASS. Slow sample spinning (25 Hz) at the magic angle is sufficient to narrow the $^{13}$C linewidth to 6 Hz, the estimated field inhomogeneity. In a separate paper, Garroway[138] has investigated the mechanism for adamantane proton-relaxation in the rotating frame.

Recently, Rothwell and Waugh[139] have produced an expression for the spin–spin relaxation time, $T_2$, for an S-spin dipolar coupled to an unlike I-spin under conditions of random isotropic rotational motion and I-spin

rf decoupling:

$$\frac{1}{T_2} = (4/15) \frac{\gamma_I^2 \gamma_S^2 \hbar^2}{r^6} I(I+1) \frac{\tau_c}{1+\omega_1^2 \tau_c^2} \tag{32}$$

For rotational correlation times such that $\tau_c \omega_1 = 1$, $T_2^{-1}$ clearly takes a maximum value. For typical laboratory proton decoupling fields, linewidths of several hundred Hz can result when $\tau_c = \omega_{1,H}^{-1}$. Rotational correlation times for the solid II phase of adamantane are relatively long, approximately $10^{-6}$ s at 150 K, hence the technique of Rothwell and Waugh is ideal for motions on this time scale. They have demonstrated that the $^{13}$C linewidths are a maximum at approximately 153 K and are substantially sharper 25° above or below this temperature as predicted by equation (32). Between temperatures of approximately 173 and 195 K the linewidth of the methylene carbon is 1·71 times that of the methine carbon. [It is interesting to note that, in the solid I phase, $T_1(^{13}CH)/T_1(^{13}CH_2)$ is observed to be 1·72.[132]] This same analysis was applied to hexamethylbenzene and hexamethylethane. In each case activation energies and inverse frequency factors calculated assuming an Arrhenius behaviour are in good agreement with earlier proton data.

Finally it is worth mentioning that adamantane is used in several laboratories as a standard in adjusting rf fields in order to establish the Hartmann–Hahn condition.

Carbon-13 NMR data have been reported for several other "globular" solids in the rotationally disordered plastic crystalline phase: pivalic acid;[140-143] norbornadiene;[144] camphor;[145] camphene;[146] succinonitrile;[147] carbon tetrabromide;[148] neopentane;[149] tris(hydroxymethyl)-aminomethane;[150] triethylenediamine;[151] bicyclo[3.3.1]nonan-9-one;[152] hexamethylethane;[153] 1-vinyl-o-carborane.[154] The aim of many of these studies has been to use measured $^{13}$C spin–lattice relaxation times to characterize molecular motion in the solid phase. Because molecular motion in the plastic phase is generally isotropic and rapid enough to average intramolecular dipolar interactions, "high-resolution" spectra ($\nu_{\frac{1}{2}} \approx$ 1–4 ppm) can usually be obtained with relatively low $^1$H decoupling fields and without MASS. For example, the $^{13}$C spectrum of solid bicyclo[3.3.1]nonan-9-one at 315 K (approximately 115° below its melting point) is shown in Fig. 16. This spectrum was obtained on a commercial $^{13}$C NMR spectrometer ($\omega_{1H}/2\pi \approx 4$ kHz) without MASS. In this case the spectral resolution is sufficient to allow the measurement of the $^{13}$C $T_1$ values of each of the chemically shifted resonances and, at least in principle, allows one to learn something about the anisotropy of the rotational motion.[152] It should be pointed out however that the NMR spectra of quadrupolar nuclei (e.g. $^2$H and $^{14}$N) are expected to be much more sensitive to anisotropic motion than are $^1$H decoupled $^{13}$C NMR spectra.[155]
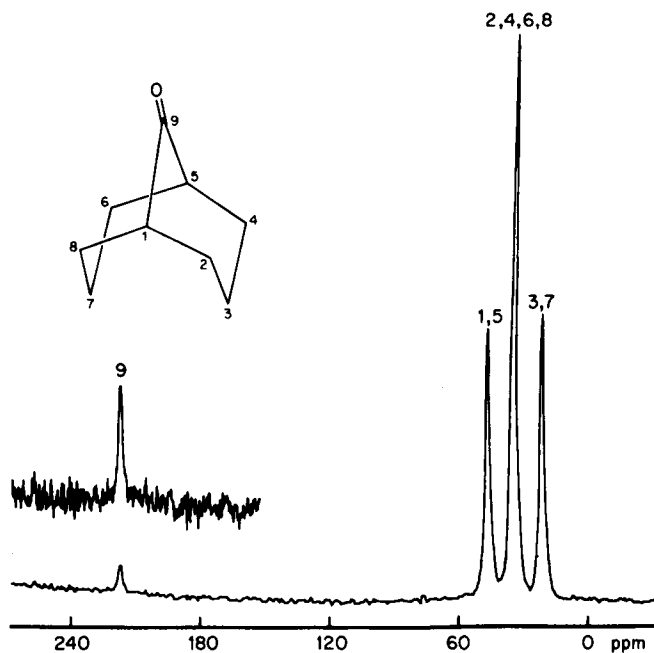
FIG. 16. $^{13}$C NMR spectrum of bicyclo[3.3.1]nonan-9-one at 315 K (22·6 MHz).

A number of salts of the general structure $M^+XY^-$ exhibit orientationally disordered solid phases. Recently $^{13}$C and $^{14}$N spin–lattice times of two such salts, NaCN and KCN, have been reported.[156]

(b) *Fluxional molecules; variable temperature* $^{13}$C *NMR studies.* Variable temperature $^{13}$C NMR has proved to be a powerful technique for the study of fluxional molecules in solution. In the case of solids the variable temperature study of tetracarbonylbis(cyclooctatetraene)triruthenium(0) (3) demonstrates the potential of the technique. The room temperature $^{13}$C NMR spectrum of 3 shows only three peaks at $\delta = 64·1$, 200·7, and
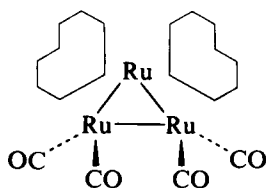


(3)

213·9 ppm from TMS. The observation of a single peak ($\delta = 64 \cdot 1$ ppm) assigned to the 16 ring carbons of the non-planar cyclooctatetraene ring[157] indicates a rapid exchange process on the NMR time scale at 27°C. At −180°C, motion of the cyclooctatetraene ring system is relatively slow and at least 6 peaks between $\delta = 40$ and 90 ppm are resolved. X-ray diffraction data are generally insensitive to dynamic processes measured in the solid state such as the one measured for 3. Carbon-13 measurements over a range of temperatures on 3 and related molecules may provide information on the mechanism of exchange.

Wemmer et al.[158] have recently demonstrated that one can obtain information concerning exchange mechanisms from $^{13}$C NMR line shapes in the absence of MASS. For permethylferrocene, comparison of the theoretical and experimental line shapes indicates that cyclopentadiene ring reorientation (4) occurs via jumps between symmetry-related orienta-
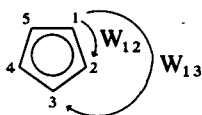


(4)

tions, with jumps of $2\pi/5(72°)$ highly favoured over $4\pi/5(144°)$ jumps ($W_{12}/W_{13} > 10$). The activation energy for the jump process is 13·5 kJ mol$^{-1}$. This value of $E_a$ is in excellent agreement with that measured from an analysis of the zeroth order spinning sidebands under MASS.[128]

Miller and Yannoni[159] have recently reported the high-resolution $^{13}$C NMR spectrum of semibullvalene (5) at −110°C and −155°C. Five chemically shifted peaks are observed in this temperature range, indicating that the rate of the rearrangement shown for 5 is slow, $<400$ s$^{-1}$. In contrast,



(5)

the rearrangement proceeds extremely rapidly in solution (the rate constant is $2 \cdot 2 \times 10^{-5}$ s$^{-1}$ at −110°C). The large difference in rate constants is surprising since the arrangement apparently involves little geometric distortion.

Temperature dependent $^{13}$C NMR spectra have also been observed for several other molecules that are generally not regarded as fluxional. For example, the room temperature spectrum of naphthazarin B (6) consists

(6)
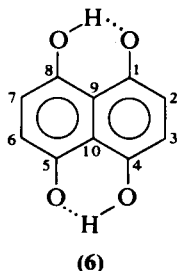
of three peaks both in solution and in the solid state.[160] The high frequency peak is assigned to $C_1$, $C_4$, $C_5$, and $C_8$, and the low frequency peak to $C_9$ and $C_{10}$. At $-160°C$ at least 5 peaks are observed; the low frequency line ($C_9$, $C_{10}$) remains unchanged, while the two high frequency absorptions observed at $25°C$ are each split into two lines. The nature of the exchange process is currently under investigation.[161]

(c) *Carbonium ions.* Preliminary indications are that high-resolution solid-state $^{13}C$ NMR is an important technique for the study of reactive chemical intermediates, such as carbonium ions. The first CP/MASS spectra of such species were reported by Lyerla *et al.*[162] The $^{13}C$ chemical shift measured for both diethoxycarbonium hexachloroantimonate (Fig. 17) and heptamethylbenzenonium ion in the solid state are within 6 ppm of the values observed in solution studies.

Recently Myhre and Yannoni[163] have reported the high-resolution $^{13}C$ NMR spectra of the reactive s-butyl cation (7) in the solid state. The cation

$$CH_3\overset{+}{C}HCH_2CH_3 \rightleftharpoons CH_3CH_2\overset{+}{C}HCH_3$$

(7)
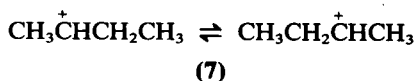
was prepared at $< -85°C$ from a mixture of $SbF_5$ and 2-chlorobutane. The $^{13}C$ spectrum obtained at $-85°C$ with both $^1H$ and $^{19}F$ decoupling shows two principal peaks, one at $\delta = 22$ ppm ($C_1$ and $C_4$) and the other ($C_2$ and $C_3$) at $\delta = 170$ ppm. The $^{13}C$ label is scrambled among all four carbon positions. A resonance at $\delta = 48$ ppm is assigned to the methyl carbons of the t-butyl cation which apparently results from the rearrangement of the s-butyl cation. No convincing evidence is found for a "static" s-butyl cation at temperatures as low as $-190°C$.

(d) *Nitrogen-containing molecules; the influence of $^{14}N$.* Carbon-13 resonances assigned to carbon nuclei directly bonded to $^{14}N$ ($I = 1$) often show interesting splittings.[18,19,119,164–167] For example, at applied fields of $2·1$ T, the $C_\alpha$ resonance of amino acids generally shows broadened asymmetric doublets (splitting $\sim100$ Hz).[164] Such splittings are not observed in the MASS $^{13}C$ NMR spectra of compounds where $^{14}N$ is replaced with $^{15}N$ ($I = 1/2$) or in compounds where the $^{14}N$ quadrupolar coupling constant
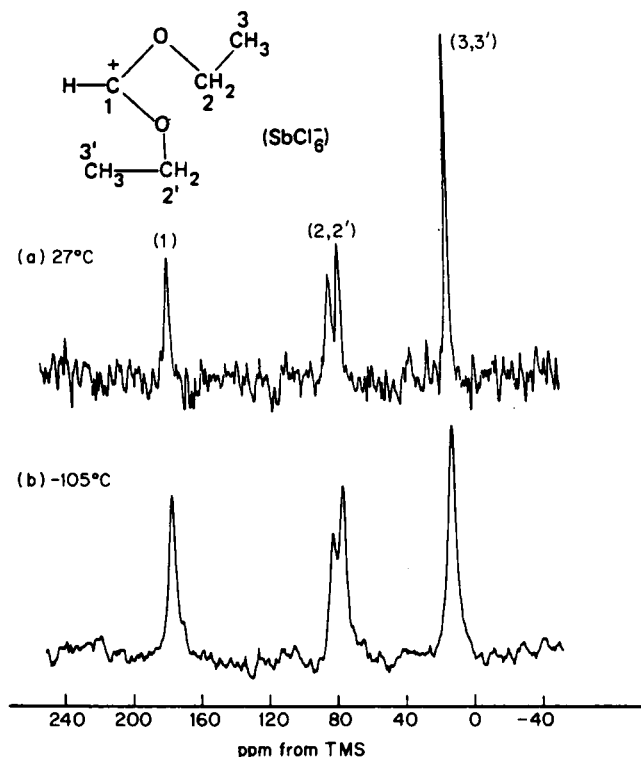
FIG. 17. $^{13}$C NMR spectrum of diethoxycarbonium hexachloroantimonate.[162]

is small.[165] They result from rather small $^{13}$C–$^{14}$N dipolar interactions which are not averaged by MASS. In applied fields where the nitrogen Zeeman interaction, $H_Z$, is not large compared with the quadrupolar interaction, $H_Q$, the axis of quantization of the $^{14}$N spin is tilted away from $B_0$. Under these conditions, the $^{13}$C–$^{14}$N dipolar interaction contains angular dependent terms other than $(1–3\cos^2\theta_{IS})$.

Typical $^{14}$N quadrupolar interactions, $\chi$, are of the order of 1–4 MHz, while $^{14}$N Zeeman interactions are 4·3 and 14·5 MHz at $B_0$ values of 1·4 and 4·7 T, respectively. Theoretical line shapes for a $^{13}$C nucleus dipolar coupled to a $^{14}$N nucleus where $H_Q(^{14}\text{N})$ is comparable to $H_Z(^{14}\text{N})$ have been presented.[166] Hexem et al.[166] have simulated MASS $^{13}$C spectra for the $C_\alpha$ resonance in glycine assuming $\chi = 1·18$ MHz ($\eta = 0·54$), $r_{CN} = 1·49$ Å, and $\nu(^{14}\text{N}) \approx 10·87$ MHz. The calculated $^{13}$C spectrum appears as the sum of three first-order quadrupole powder patterns. Two of these powder patterns are essentially superimposed and well separated from the third. With a 20 Hz line broadening the fine structure in the powder patterns

is lost and two broad peaks of relative intensity $2:1$ are calculated in agreement with experiment. The calculated peak–peak separation increases with: (a) a decrease in the $^{14}N$–$^{13}C$ bond length (i.e. an increase in the $^{14}N$–$^{13}C$ dipolar interaction); (b) a decrease in $B_0$; (c) an increase in the $^{14}N$ quadrupolar coupling constant.

A general treatment of quadrupole effects in MASS NMR spectra has been presented.[167] Theoretical spectra for a spin 1/2 nucleus coupled to a spin 1 nucleus, as a function of the ratio of the spin 1 Zeeman frequency, $Z$, to the nuclear quadrupolar coupling constant, $\chi$, are shown in Fig. 18. The axes of symmetry of the dipolar and quadrupolar interaction tensors coincide. The horizontal scale is in fractions of the dipolar coupling constant,
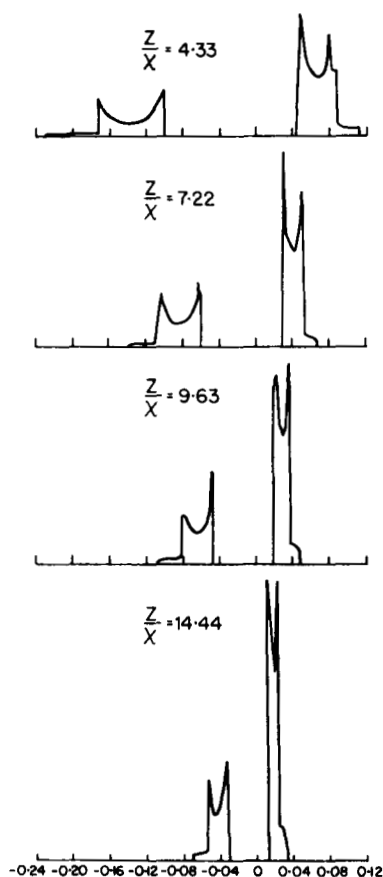


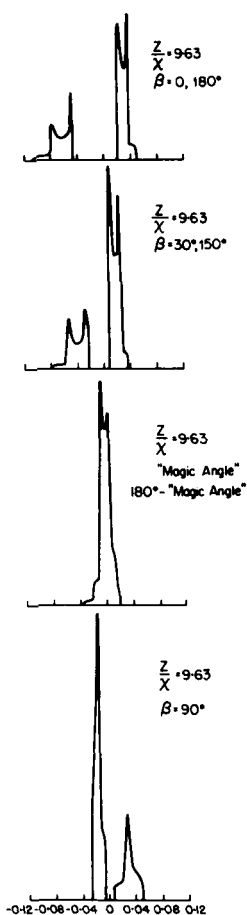FIG. 18. Theoretical spectra for a spin 1/2 nucleus coupled to a spin 1 nucleus as a function of $Z/\chi$.

FIG. 19. Theoretical spectra for a spin 1/2 nucleus coupled to a spin 1 nucleus as a function of $\beta$.

$D = \hbar\gamma_I\gamma_S/r_{IS}^3$. Theoretical spectra, as a function of the angle $\beta$ between the unique principal axes of the dipolar and axially symmetric quadrupolar interactions, are shown in Fig. 19. The appearance of the spectra depends critically on the mutual orientation of the dipolar and quadrupolar interaction tensors. Calculated spectra are also found to be very dependent on the orientation of the spinning axis with respect to $B_0$. For the case of a spin 1/2 nucleus dipolar coupled to a quadrupolar nucleus of spin 3/2, the spectra are calculated to be more complex.

The influence of quadrupolar relaxation on spin 1/2 line shapes has not been considered theoretically but it is known experimentally that self-

decoupling probably accounts for the relatively sharp lines that one often observes for a $^{13}$C nucleus directly bonded to Cl.

In both of the above papers scalar coupling between the spin 1/2 and quadrupolar nucleus is ignored. Although this generally is a good approximation for $^{14}$N–$^{13}$C, such couplings must be considered for $^{63}$Cu–$^{31}$P interactions (Section C below).

While the splittings discussed here may appear to be a nuisance they can in fact be useful in making $^{13}$C spectral assignments[18,19] (see e.g. Fig. 12). Also, they may be used to obtain accurate $^{14}$N–$^{13}$C bond lengths if the orientation and magnitude of the nuclear quadrupole coupling constant are known. Conversely, if $r_{CN}$ is known it may be possible to obtain information about the nature of the quadrupole coupling constant.

(e) *Surface adsorbed species; catalysis studies.* Most $^{13}$C NMR investigations of adsorbed species have involved the study of relatively mobile rapidly diffusing adsorbates.[169,170] Spectra from such species, e.g. olefins adsorbed on synthetic zeolites,[171,172] are generally relatively sharp and can be obtained using conventional high-resolution FT NMR spectrometers. An interesting early application of $^{13}$C NMR in this area is that by Michel *et al.*[171] who demonstrated that it is possible to monitor isomerization and polymerization of n-butene on CaNaY type zeolites. More recent applications are described in references 173 and 174.

With the development of CP techniques, $^{13}$C NMR can be used to study more rigid systems where motional narrowing is not complete. Measurement of $^{13}$C CSA patterns in such systems can provide order parameters and information regarding the nature of surfaces and interfaces.[175–177] The sensitivity of $^{13}$C line shapes to the nature of the motion that an anchored phenyl group may undergo is illustrated in Fig. 20. Analysis of proton decoupled spectra of phenyl groups chemically bound to silica gel and alumina indicates that motions which tend to keep the plane of the phenyl group parallel to the substrate surface are preferred.[176]

Carbon-13 NMR and infrared spectroscopy have been used to characterize the adsorbed states of carbon monoxide on Rh dispersed on $Al_2O_3$.[117,118] Carbon monoxide is believed to be associated with such surfaces in one of three ways (**8–10**). Combining $T_1$ and chemical shift data, the $^{13}$CO distributions (**8**:**9**:**10**) for a freshly prepared 2·2% Rh on $Al_2O_3$ sample are found to be 34:44:22. It is expected that variable temperature carbon-13 $T_1$
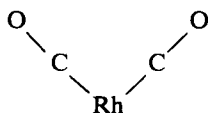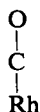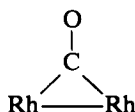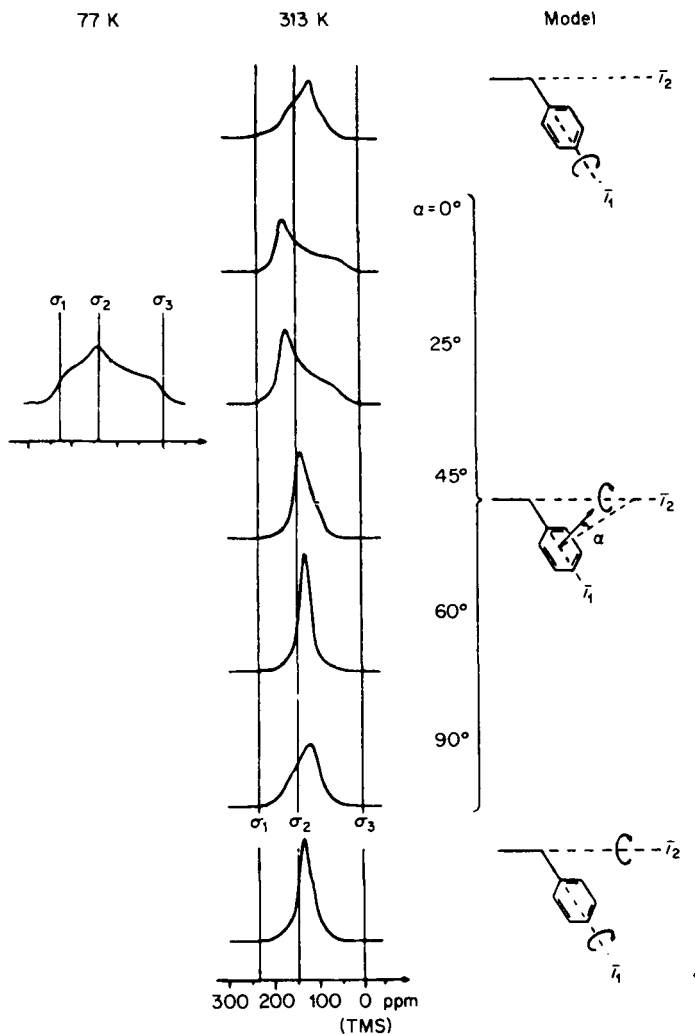


(8)          (9)          (10)

FIG. 20. Calculated proton-decoupled $^{13}$C NMR lineshapes of an anchored phenyl group. The calculations are based on different models for the molecular reorientation motion (see original ref. 176 for details). All phenyl carbons were assumed to have the same principal values of the chemical shielding tensor. Lorentzian broadening = 20 ppm, peak to peak.

data with MASS will be useful in characterizing the motions of CO at these different sites.

Gay has recently used $^{13}$C NMR to study chemisorption of methanol on MgO.[120] It is found that adsorption to give coverages of less than about half a monolayer produces a rigidly bound methoxide-like species ($\Delta\sigma =$

$\sigma_\parallel - \sigma_\perp = 63 \pm 2$ ppm). Higher coverages are reported to produce an isotropically rotating methanol species ($\delta = 49 \pm 2$ ppm) in addition to the rigidly bound species.

Quantitative analysis of chemisorbed molecules is, in principle, also possible. See the section on coals that follows for a discussion of potential problems in using the CP/MASS techniques in quantitative analysis.

CNDO and PCILO calculations of $^{13}$C chemical shifts of sorbed molecules have recently been reported by Deininger et al.[178]

A collection of papers and references dealing with $^{13}$C NMR studies of adsorbed species and catalysts can be found in a recently published text[174] which is highly recommended. Additionally, NMR studies of molecules physisorbed on homogeneous surfaces have recently been reviewed.[179]

(f) *Model and biological membranes.* The principles and techniques used to study relatively rigid molecules on surfaces can also be used to study "anisotropic" systems such as liquid crystals, and model and biological membranes. For example, Cornell and coworkers have used the proton-enhanced natural-abundance $^{13}$C NMR spectra of phospholipid bilayers to study the acyl chain order[181] and dynamics of carbonyl groups.[180] Spectra of the carbonyl region of dimyristoyl phosphatidylcholine (DMPC) dispersed with water indicate a superposition of two individual resonances which are assigned to the carbonyls of the $\gamma$ and $\beta$ chains. Residual carbonyl shielding anisotropies of $-25 \pm 2$ and $-5 \pm 2$ ppm indicate that one chain is more disordered than the other. A model for the motion of these groups, consistent with these data, is suggested.

In a related study, proton $T_{1\rho}$ and cross-relaxation times, $T_{CH}$, obtained from variable contact proton-enhanced $^{13}$C NMR spectra are used to monitor lipid mobility in a hydrated dispersion of DMPC. In these experiments the intensity of the $^{13}$C methylene resonances is assumed[182] to be governed by an equation of the form

$$I \propto \exp(-t_c/T_1{}^H)[1 - \exp(-t_c/T_{CH})] \qquad (33)$$

where $t_c$ is the contact or mixing time, $T_{1\rho}{}^{-1}$ is assumed to monitor motion in the vicinity of $\omega_1$, while $T_{CH}$ values provide a measure of the residual dipolar interaction (increases in $T_{CH}$ are associated with increased reorientational freedom). Using this approach, added amounts of cholesterol or gramicidin A are found to restrict the motion of the hydrocarbon chain relative to pure DMPC dispersions. The results obtained for myelin and chloroplast membranes are discussed.

The effect of the bilayer phase transition on the carbonyl $^{13}$C CSA has been investigated,[183] and a study of the lecithin gel to liquid crystalline transition has been reported.[184]

In summary, it appears that proton-enhanced $^{13}$C NMR can be useful in studying membrane systems. Such studies should complement more

traditional $^2$H NMR studies and allow some information to be gained when $^2$H labelling is not feasible.

(g) *Miscellaneous studies.* The sensitivity of $^{13}$C chemical shifts to subtle changes in molecular conformation is nicely illustrated in a $^{13}$C NMR study of 1,3,5-trimethoxybenzene.[185] The three protonated ring carbons are chemically non-equivalent in the solid state. Single-crystal X-ray analysis indicates that the benzene rings and the three oxygen atoms are planar, with the three methoxy carbons displaced by $-0.071$, $0.003$, and $0.192$ Å, respectively. The non-equivalence in the NMR spectrum is not resolved for the three non-protonated aromatic resonances or the three methyl carbon resonances.

Hill *et al.*[186] have demonstrated that optical purity differences can influence high-resolution solid-state $^{13}$C NMR spectra. The *l*, *dl*, and *meso* forms of tartaric acid each show unique spectra in the solid state.

High-resolution $^{13}$C NMR spectra of solid vitamin C (**11**) and other ascorbates have been discussed.[187,188] In *l*-ascorbic acid[188] the splitting of the $C_3$, $C_4$, and $C_6$ resonances is attributed to two crystallographically independent ions which are distorted differentially in the solid state.
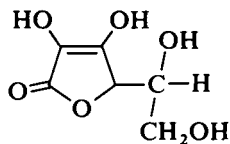


(**11**)

The MASS/CP technique has been used to characterize cholesterol and bilirubin pigment composition of human gallstones.[189] The cholesterol stones are found to be similar to each other whereas the bilirubin pigment stones exhibit more variation in spectral features.

High-power $^1$H decoupled $^{13}$C NMR spectra of methanol enclathrated in hydroquinone have been studied.[190,191] The $^{13}$C CSA of enclathrated methanol is $20.6 \pm 1$ ppm at room temperature (rigid-lattice value is $63 \pm 3$ ppm[192]).

One of the most exciting applications of two-dimensional (2-D) NMR is illustrated in a recent publication.[70] The 2-D technique, which separates chemical shift and dipolar interactions, is applied to samples spinning at the magic angle. Projection of the resulting rotational sideband spectra on to one axis yields a normal shielding anisotropy spinning pattern while a Pake pattern, free of shielding anisotropy effects, results on the other 2-D axis. In principle, these spectra permit a determination of the relative orientations of the chemical shielding and dipolar interactions as well as

the principal values of these two tensors. Previously this information was available only from 2-D NMR experiments on single crystals.[35,71]

### 3. Synthetic macromolecules

The first combined application of the MASS and CP techniques involved a $^{13}$C NMR study of several polymers.[193] In order to demonstrate the potential of CP/MASS, $^{13}$C NMR spectra of polysulphone, wood, and ivory obtained with and without MASS were compared with spectra obtained in solution. Since this initial report,[193] several papers have appeared describing applications of CP/MASS $^{13}$C NMR in polymer science. This work has been extensively reviewed.[10,14,15] The reviews by Lyerla[14,15] cover the literature up to early 1979 while that of Schaefer and Stejskal[10] deals with work appearing before 1978. Applications of rotating frame relaxation times, $T_{1\rho}$, have been reviewed.[89-91] Fleming et al.[194] have recently discussed applications of variable temperature MASS $^{13}$C NMR studies of solid polymers. The most recent reviews dealing with applications of high-resolution NMR in solid polymers are by Schaefer and coworkers[16] and by Garroway and coworkers.[17] Most of the material discussed in the latter reviews[16,17] is work carried out in the authors' respective laboratories. Here we only mention papers appearing in the 1980 and 1981 literature.

As well as providing structural information, high-resolution $^{13}$C NMR studies of solid polymers can also yield dynamic information. The dynamic information may, in principle, be obtained from rotating frame relaxation times, $T_{1\rho}(H)$ and $T_{1\rho}(C)$ which are particularly effective in probing motions in the mid-kilohertz frequency range. For many solid synthetic polymers, main-chain or side-chain motions lie in this frequency range and are thus amenable to study by $T_{1\rho}$ measurements.

The interpretation of $^{13}$C $T_{1\rho}$ data is complicated because both $^{13}$C–$^{1}$H spin–spin interactions and rotating frame spin–lattice processes may contribute to the value of $T_{1\rho}$. Since only the spin–lattice processes provide information on motional processes, it has been necessary to devise experiments that isolate the relative contributions of the two mechanisms. Such experiments have been devised and summarized.[16] In one approach, the average value of the polarization transfer in an adiabatic demagnetization rotating frame experiment, $\langle T_{IS}(\text{ADRF})\rangle^{-1}$, provides a measure of the spin–spin contribution to $\langle T_{1\rho}(C)\rangle$ for carbon. Therefore, if the ratio $\langle T_{1\rho}(C)\rangle/\langle T_{IS}(\text{ADRF})\rangle$ is close to zero, $\langle T_{1\rho}(C)\rangle$ is determined by spin–lattice processes; if it is close to unity, spin–spin interactions dominate $\langle T_{1\rho}(C)\rangle$. Qualitatively it appears that spin–spin processes are most likely to be a problem for protonated carbons in rigid polymers. Examples where spin–spin processes are important include crystalline polyoxymethylene,[89] crystalline polyethylene,[195] and crystalline poly(ethylene terephthalate). In

glassy polymers,[196] where strong static $^1H$–$^1H$ dipolar interactions are relatively small, $T_{1\rho}(C)$ is dominated by motional processes. Examples of the latter situation include polycarbonate[197] and poly(ethylene terephthalates).[196] $T_{1\rho}$ values for the protonated main-chain carbons of polycarbonate indicate the presence of a broad distribution of high-frequency motions at room temperature. This molecular motion in the solid state is thought to be responsible for the high impact strength of glassy polycarbonate. Studies of $T_{1\rho}(C)$ data in modified polycarbonates lend support to the hypothesis that the impact strength of thin films is related to microscopic motion.

Veeman et al. have carried out extensive carbon spin–lattice relaxation ($T_1$ and $T_{1\rho}$) measurements on polyoxymethylene,[198,199] Delrin, and poly(methyl methacrylates).[199] The single $^{13}C$ peak observed in Delrin is found to have two components, one amorphous the other crystalline. Carbon-13 $T_1$, $T_{1\rho}$, and NOE data measured at 45 MHz and at room temperature with $\nu_{1C} = 25$ kHz are shown in Table 4. The differences in

TABLE 4

Carbon-13 spin–lattice relaxation and NOE data for
polyoxymethylene.[a]

|  | Amorphous | Crystalline |
| --- | --- | --- |
| $T_{1\rho}$ | 17·5 ms | 3–0·6 ms[b] |
| $T_1$ | 0·75 s | 15 s |
| NOE | 1·7 | 1·3 |

[a] $\nu_{0c} = 45$ MHz; $\nu_{1c} = 25$ kHz.
[b] 3 ms without MASS, 0·6 ms with MASS at 5·6 kHz.

$^{13}C$ $T_1$ and $T_{1\rho}$ for the two components result from differences in the molecular mobility in the two phases. Motion in the amorphous phase is relatively fast ($\tau \approx 10^{-9}$ s) while that in the crystalline phase is much slower. Problems in interpreting the $T_{1\rho}(C)$ values of the crystalline component [note that $T_{1\rho}(C)$ for this component depends on the rate of MASS] are discussed by the authors.

Proton spin diffusion effectively averages local differences in proton relaxation times, so direct measurement of $^1H$ $T_{1\rho}$ values in polyoxymethylene does not distinguish between the amorphous and crystalline regions. Veeman and Menger[199] show, however, that when the effects of spin diffusion are eliminated by strong off-resonance decoupling, differences in $^1H$ $T_{1\rho}$ values for the crystalline and amorphous regions can be measured via $^{13}C$ NMR spectroscopy.

Schaefer and coworkers[200,201] have used carbon resolved $^1$H $T_{1\rho}$ data to study polymer blends[201] and the nature of the interface between phases in a blend of polystyrene and a polystyrene–polybutadiene block copolymer.[200] Values of $T_{1\rho}$ for protons attached to chemically shifted carbons are measured by tracking the carbon magnetization as a function of the contact time, $t_c$, in a matched single contact CP experiment. For long contact times ($t_c \gg T_{CH}$) the carbon magnetization, $M_C(t)$, can be approximated by equation (34). Thus $T_{1\rho}{}^H$ can be obtained from a semilog plot of $M_C(t)$ versus $t_c$. Proton $T_{1\rho}$ data measured in this way are strongly dependent on proton–proton spin diffusion, thus $T_{1\rho}{}^H$ values provide a measure of spin diffusion rates between different chemical species.

$$M_C(t) = M_{C,0}[\exp(t_c/T_{1\rho}{}^H)](1 - T_{CH}/T_{1\rho}{}^H) \tag{34}$$

Schaefer et al.[202] have recently measured $^1$H local dipolar fields (local proton linewidths) using solid-state $^{13}$C NMR. The proton dipolar order established by a two-pulse (Jeener Broekaert) sequence as a function of pulse spacing, $t$, is monitored by a carbon rf pulse. For poly-($\alpha$-methylstyrene) proton local fields of 7 and 10 kHz are calculated for the aromatic and methylene protons respectively. Values of the individual proton local fields should be useful in evaluating the spin–spin contribution to carbon $T_{1\rho}$ results.

Carbon-13 relaxation data for highly mobile liquid-like polymers have been discussed.[203,204] Two recent papers dealing with $^{13}$C relaxation in such systems include one on semicrystalline polymers[205] and one dealing with molecular motion in natural rubber.[206]

Annealing-induced changes in the orientation and mobility of the non-crystalline region of drawn linear polyethylene have been studied.[207] A $(180°–10\,s–90°–10\,s)_x$ pulse sequence is used to isolate the non-crystalline component of the $^{13}$C NMR signal. The relative merits of the techniques for monitoring changes in orientation and mobility are discussed.

A nice example of the conformational information available from high-resolution $^{13}$C NMR is provided in a recent study of polypropene.[208] On the basis of X-ray diffraction data, the conformation of syndiotactic polypropene is thought to be an involuted helix containing two equally probable but distinct methylene sites.[209] This structure is supported by the $^{13}$C NMR spectrum which shows two peaks in the methylene region separated by $8·7 \pm 0·5$ ppm. The internal methylene groups are shielded by two gauche $\gamma$ carbons. The $^{13}$C NMR spectrum of isotactic polypropene shows only three resonances due to the methyl, methylene, and methine carbons, an observation that is consistent with some X-ray diffraction data.[210]

Fyfe et al.[211] have used high-resolution $^{13}$C NMR to investigate the structure of cured phenolic resins prepared under alkaline and acidic conditions. The $^{13}$C NMR spectra are found to give a direct measure of

the nature and the extent of the crosslinking. The technique of Opella,[86] which selectively suppresses protonated carbons, is used to investigate the pattern and degree of substitution in the phenol ring.

Fleming *et al.*[212] have demonstrated that well resolved ^{13}C spectra can be obtained for solid fluoropolymers by MASS and [13]C{[19]F} dipolar decoupling. Decoupling fields of at least 70 kHz are necessary to effectively remove [19]F–[13]C dipolar interactions in poly(tetrafluoroethylene) and poly(chlorotrifluoroethylene) (PCTFE). Although two peaks are observed in the ^{13}C spectrum of PCTFE at 48°C, the high-field *C*FCl resonance broadens and "disappears" at low temperature. This differential broadening is attributed to residual ^{13}C–Cl dipolar interactions which are not averaged to zero by MASS.

## 4. *Natural macromolecules*

(a) *Biopolymers.* High-resolution solid-state ^{13}C NMR spectra (37·74 MHz) of a protein were first reported by Opella *et al.*[213] The protein studied was the major coat protein which consists of 50 amino acid residues. Six of these amino acid residues are aromatic (3 Phe, 2 Tyr, and 1 Try), and contain a total of 10 non-protonated carbons. Carbon-13 spectra of isolated fd coat proteins, fd virus (90% by weight coat protein), and detergent solubilized fd coat protein are obtained by selectively suppressing ^{13}C resonances due to carbons with directly bonded protons. Except for the broader resonances observed for the solid samples, the spectra of the non-protonated aromatic resonances are essentially the same. The single carbon resonance assigned to $C_\gamma$ of Try 26 appears at a slightly higher frequency.* Opella *et al.*[213] point out that the solid-state spectra of proteins can be obtained in less time than solution spectra, and that in some cases resolution is sufficient to distinguish different types of aromatic carbons.

Carbon-13 NMR spectra of crystalline human carbonyl haemoglobin A (HbAcO) have recently been reported.[214] The solid-state spectra obtained at 15·1 MHz are essentially equivalent to those obtained in solution. A resonance assigned to haem bound [13]CO appears at approximately $\delta = 206·7$ ppm in both the crystalline and solution samples, indicating that the structure of HbAcO, especially in the bound CO region, is the same in both states.

Carbon-13 NMR spectra (45 MHz) of tobacco mosaic virus have been obtained.[215] Using a pulse sequence that suppresses carbons with long $T_1$ and short $T_{1\rho}$ values it is possible to selectively observe spectra arising from the more mobile part of the virus.

---

* It is interesting to note that Opella *et al.*[19] report significant chemical shift differences between solution and powder samples of amino acids and linear peptides. For cyclic peptides, however, differences in solid and solution spectra are negligible.

It has recently been suggested that the protein content of solid organic materials (e.g. plant seeds etc.) can be monitored using CP/MASS $^{13}$C NMR.[216] Peaks arising from the carbonyl resonances of the proteins ($\delta \approx$ 175 ppm) in these samples are well separated from other peaks (e.g. carbohydrates), and integration of these resonances relative to others is claimed to provide a measure of protein content.

Torchia and coworkers[217] have demonstrated that $^{13}$C/$^{1}$H double resonance can be used to monitor the amounts of sickle haemoglobin polymer in erythrocytes. They have also used proton-enhanced $^{13}$C spectra to characterize the molecular motion of foetal enamel proteins[218] and collagen backbone motion in fibrils.[219]

High-power double resonance studies (without MASS) of fibrous proteins, proteoglycans, and model membranes have been reviewed.[11] Lyerla[14,15] has reviewed $^{13}$C NMR studies of solid biopolymers; in addition a very recent article on NMR of biopolymers[19] is highly recommended.
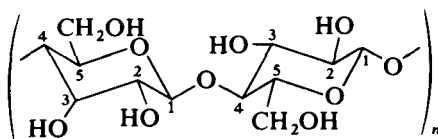


(12)

(b) *Polysaccharides; wood and humic acid.* Cellulose (12) a $\beta$-1,4 polymer of anhydroglucose, can be prepared in at least four different polymorphic forms.[220] Cellulose occurs in nature predominantly in a lattice type characterized as cellulose I or native cellulose. The process of mercerization or generation produces another polymorph known as cellulose II. Vibrational spectroscopy suggests that the extended molecular chains of polymorphs I and II have different conformations.[221] The CP/MASS $^{13}$C NMR spectra of polymorphs I and II have been presented.[222] The $C_1$ resonance of both forms, and the $C_4$ resonance of II, are split indicating the presence of two types of glycosidic linkage. The $^{13}$C NMR spectrum of an amorphous sample prepared by regeneration from DMSO–paraformaldehyde is distinct. The peaks are broadened and the $C_4$ and $C_6$ resonances are shifted to low frequency relative to their position in crystalline samples of I and II. The $^{13}$C NMR spectrum of native I (Whatman CF-1) is similar to that of highly crystalline cellulose I but broad shoulders on the $C_4$ and $C_6$ resonances indicate the presence of some amorphous cellulose. Earl and VanderHart[223] have presented spectra of crystalline cellulose I. On the basis of extensive $T_{1C}$, $T_{2C}$, and linewidth measurements they conclude that the glucose units are in two magnetically inequivalent environments. They also suggest that there exist two types of glucose monomer, one of

which allows more freedom of motion or easier access to labile protons than the other. Although a clear $1:1$ "doublet" splitting is observable in the $C_1$ resonance at all fields and a similar splitting in $C_4$ at higher fields,[224] recent high-field CP/MASS spectra[224,74] have not revealed clear doublet splitting for $C_1$ of cellulose I as originally reported, and the structure of this polymorph is not yet entirely clear. A spectrum of cellulose II is shown in Fig. 21.[224]
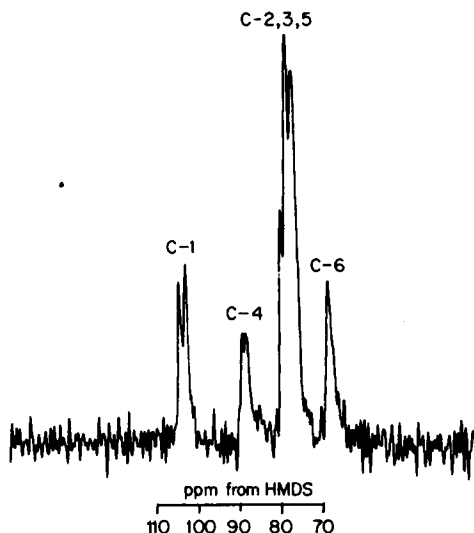


FIG. 21.  CP/MASS $^{13}$C NMR spectrum of cellulose II (22·6 MHz).

The application of CP/MASS $^{13}$C NMR for studying the primary structure of polysaccharides has been reported.[225] Spectra of three insoluble polysaccharides, viz. xanthan gum, its octadecylamide, and [$N$-(3-fluorophenyl)methyl]chitosan, are presented and assigned.

Schaefer and Stejskal[193] have reported that CP/MASS $^{13}$C spectra of wood are sufficiently resolved to identify peaks associated with the major components—celluloses, hemicelluloses, and lignin. In addition, it is possible to distinguish between different woods, for example maple and pine. A high-resolution $^{13}$C NMR spectrum of poplar chips is shown in Fig. 22.[226] More recently Hatcher et al.[227] have reported the results of NMR studies on ancient buried wood.

High-resolution solid-state $^{13}$C NMR has been used to characterize humic substances (complex macromolecular compounds) found in sediments and soils.[228] Hatcher and coworkers[229] have shown that quantifiable distinctions between structural features of aquatic and terrestrial humic substances are possible. It is suggested that aliphatic carbons of the humic substances
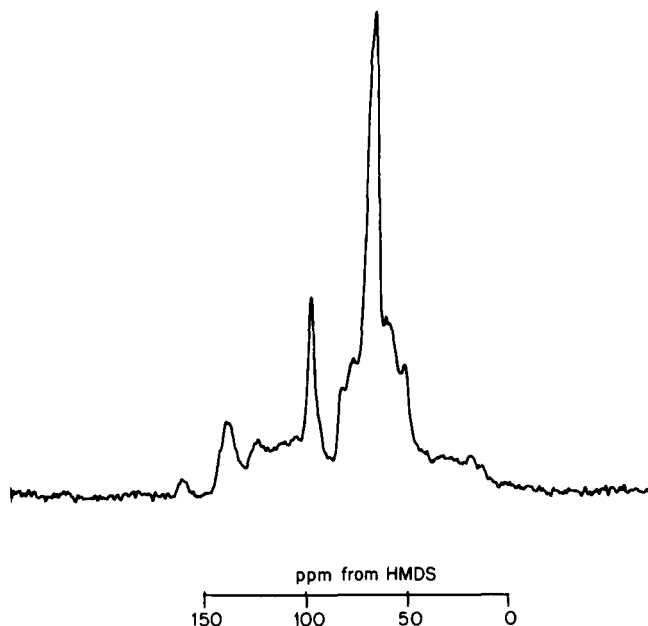
ppm from HMDS

150    100    50    0

FIG. 22. CP/MASS $^{13}$C NMR spectrum of poplar wood chips (22·6 MHz).

originate from lipid-like materials. CP $^{13}$C NMR studies (75 MHz) of whole soils and CP/MASS $^{13}$C NMR spectra of humic soil and a brown coal have been reported.[230,231] Soil organic material shows considerable variation— from highly aliphatic to moderately aromatic. The brown coal sample is thought to be a modified lignin.

(c) *Coals.* In recent years there has been considerable interest in the analysis and characterization of coal.[111,232] This interest stems in part from the desire to find efficient ways of converting coals into more environmentally acceptable fuels.

Coal is a sedimentary "organic" rock made up of a heterogeneous mixture of organic compounds and minerals.[232] The organic part of coal is thought to consist of complex macromolecular hydrocarbons containing oxygen, nitrogen, sulphur, and traces of other elements. The most common minerals in coal are kaolinite (an aluminium silicate hydrate), pyrite ($FeS_2$), and calcite ($CaCO_3$).

Coals are often classified by their rank. This may be defined as the extent to which the organic material has matured during geological time. Types of coal in ascending order of rank are: peat, soft brown coal, lignite, sub-bituminous coal, high volatile bituminous coal, medium volatile bituminous coal, low volatile bituminous coal, semi-anthracite, anthracite,

meta-anthracite, coal, graphite. The maturation or coalification process, metamorphism, depends on several factors including the depth of burial, pressure, and temperature. As the rank of the coal increases the carbon content increases (from approximately 60% in peat to 100% in graphite), and recognizable plant structure decreases (free cellulose is found only in peat).

Petrakis and Grandy[232] have presented a good introduction to coal analysis, characterization, and petrography. Peat and its organic chemistry have been discussed in a similar introductory article.[233] Applications of high-resolution NMR to the study of fossil fuels have been previously reviewed.[234-237] In this section we concentrate on reviewing some of the problems associated with determining $f_a'$, the fraction of aromatic carbons in fossil fuel samples. Also, some of the detailed structural information available from recent high-resolution $^{13}C$ NMR studies is mentioned.

The first combined application of the CP and MASS techniques to the study of coal was reported in 1977.[238] Carbon-13 spectra of anthracite, lignite, algal coal, kerogen, and a raw oil shale sample were presented and discussed. The $^{13}C$ CP/MASS spectrum of the anthracite sample shows only one broad slightly skewed resonance which is assigned to aromatic carbons. In contrast the $^{13}C$ spectrum of lignite shows two broad but well resolved resonances assigned to aromatic and aliphatic carbons from which the apparent carbon fraction in the aromatic region, $f_a'$, is estimated to be 72%. Figure 23 shows a "typical" $^{13}C$ NMR spectrum of a lignite sample.[239]
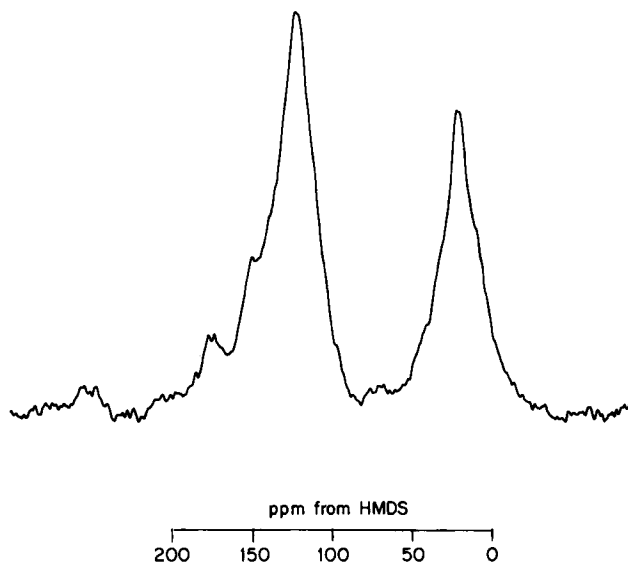


FIG. 23. CP/MASS $^{13}C$ NMR spectrum of lignite A (Estevan, Saskatchewan) (22·6 MHz).

During the past few years several other papers have appeared in the literature that describe the application of high-resolution solid-state $^{13}C$ NMR to determine $f_a'$ values in fossil fuels.[240–253] One of the main problems in determining accurate values of $f_a'$ is that some particular types of carbons in the sample may be essentially isolated from protons and not as effectively cross-polarized as others. Under these conditions $f_a'$ depends on the cross-polarization time, $t_c$ (see specific examples below). For an accurate measurement of $f_a'$ using the CP experiment one requires a uniform distribution of protons throughout the sample and an approximately uniform distance between all carbons and protons.[251]

This problem has been recognized and dealt with in a variety of ways. Often $f_a'$ values obtained on representative samples by varying both $t_c$ and the pulse repetition rate are compared with those measured using high-power decoupling (without CP). Taking the $f_a'$ values obtained without CP as being the "correct" values, contact and pulse delays which give an optimum value of the S/N ratio and reliability are selected and used in all subsequent measurements. In a recent study of a large number of coal samples of varying rank, Miknis and coworkers[249] found that contact times of 1 ms and pulse delays of 4 s appear to give an optimum S/N ratio and reliability. Sample aromaticities are found to increase with increasing rank.

Other workers[242,253] have suggested minimum $t_c$ values of 3–6 ms for coals. On the basis of an extensive study of the influence of $t_c$ on $f_a'$, Dudley and Fyfe[239] have found that the optimum value of $t_c$ is very sample-dependent. Also, they find that $^{13}C$ relaxation times in fossil fuels are often relatively short (52 s) because of the presence of paramagnetic species, and conclude that 90° pulse experiments (high-power decoupling without CP) with pulse repetition times of $5 T_1$ should be used whenever possible.

Recently Taki et al.[250] have reported that, in spin-counting measurements of the $^{13}C$ content of coals of different rank, more than 95% of the carbons are observed in anthracites while as little as 50–60% are observed in some lower rank coals. For the latter samples it is necessary to assume that the structural distribution of the detected and undetected $^{13}C$ spins are identical, if $f_a'$ values from CP/MASS $^{13}C$ NMR data are accurate.

Another potential problem is that, if a sample contains inorganic carbonates, olefins, or carbonyl carbons, it is possible that carbons from these moieties contribute to signals in the aromatic region.[237,249,253] Recently, Murphy et al.[251] have reported first and second moments of the aromatic and aliphatic $^{13}C$ NMR absorptions of coals varying in rank between lignites and anthracites. Such measurements are expected to reflect the homogeneity of shieldings of the carbons in coals. For the lignites and sub-bituminous coals three absorptions are resolved; the high-frequency peak ($\delta = 177$ ppm with respect to TMS) represents 3–6% of the total carbons and is assigned to the carbonyl carbons of quinones, carboxylic

acids, and their derivatives. Shoulders observed on the high-frequency side of the aromatic bands of highly volatile bituminous, sub-bituminous, and lignite coals ($\delta = 160$ ppm) are assigned to aromatic carbons attached to hydroxy, alkoxy, or aryloxy groups. These shoulders are less pronounced in the higher-rank coals since these contain less oxygen. High-, medium-, and low-volatile bituminous coals show only two absorptions, the aromatic and aliphatic peaks. On the basis of $f_a'$ values measured using $t_c = 1\cdot5$ ms and moment analyses the following conclusions are reached in this study.[251] (1) In general, the aromatic fraction, $f_a'$, increases with increasing rank (%C). (2) In general, the second moments (dispersiveness) of the $^{13}C$ aromatic absorptions decrease with increasing rank. Thus, with increasing age, the aromatic species of the coal become more homogeneous. (3) The first and second moments of the aliphatic absorptions show little correlation with rank. This result led the authors to suggest that the processes that convert aliphatic functionalities into aromatic functionalities during maturation must occur randomly.

Spinning sidebands from the aromatic resonances can be significant, particularly at higher applied fields. In such cases the low-frequency sideband can be buried under the aliphatic absorption and hence distort the apparent values of $f_a'$.[235] Corrections for spinning sidebands should obviously be made if reliable quantitative data are required. It is important to note that artifacts in the spectra can arise from absorptions due to materials present in the sample rotors.[245,247]

One can improve the spectral detail of fossil fuels by selectively suppressing a particular type of carbon on the basis of differences in $^{13}C-^{1}H$ dipole–dipole couplings and differences in the intrinsic spin–spin relaxation time, $T_2$. Applications of these techniques have been described.[249,252]

More work on model systems is required before it will be possible to assess the full potential of $^{13}C$ NMR in the study of fossil fuels. At the present time, it appears that the determination of $f_a'$ by CP/MASS $^{13}C$ NMR is at least semi-quantitative (accurate to within $\pm10\%$).[251]

## B. Silicon-29

Silicon-29 has a natural abundance of $4\cdot7\%$ and a magnetic moment of approximately 20% that of the proton. Although $^{29}Si$ has an NMR receptivity $2\cdot1$ times that of $^{13}C$, solution studies have been impeded by long $^{29}Si$ relaxation times, and a negative nuclear Overhauser enhancement. Dipole–dipole ($^{29}Si-^{1}H$) relaxation is particularly inefficient because of relatively large Si–H separations. Fortunately this problem of long relaxation times is generally avoided in studies of solids by using CP techniques.

Silicon-29 chemical shifts cover a range of approximately 400 ppm. Tetramethylsilane is the accepted reference. Substituent effects on $^{29}Si$

chemical shifts have been investigated and discussed by many investigators. $p\pi$–$d\pi$ interactions have often been invoked to rationalize trends in $^{29}$Si shielding which differ from those observed for $^{13}$C. Semi-empirical MO calculations of $^{29}$Si shielding constants reproduce qualitatively some of the trends observed in $^{29}$Si NMR. Detailed discussions of such calculations, empirical correlations between $^{29}$Si and various parameters such as Hammett $\sigma$ constants, substituent electronegativity, etc. have appeared elsewhere[254–256] and are not presented here.

Results of the first $^{29}$Si NMR study on solid silicon compounds which used CP techniques were reported[257] in 1972. Values of the $^{29}$Si shielding constants measured at $-186°C$ are given in Table 5. In general the $^{29}$Si shielding anisotropies are relatively small. As noted previously for $^{13}$C shifts, average $^{29}$Si shieldings do not change appreciably on sample melting. In some cases, it appears that the crystal symmetry is responsible for deviations of the shielding tensor from axial symmetry. For example, in an isolated $CH_3Si(OCH_3)_3$ molecule one would expect an axially symmetric shielding tensor; however, in the solid $\sigma_{11}$ and $\sigma_{22}$ differ by 12 ppm.

## TABLE 5

**Silicon-29 chemical shielding parameters in organosilicon compounds.[a]**

| Compound | $\sigma_{11}$ | $\sigma_{22}$ | $\sigma_{33}$ | $\Delta\sigma^b$ | $\bar{\sigma}^c$ | $\sigma_i{}^d$ |
|---|---|---|---|---|---|---|
| $(CH_3)_4Si$ | 0 | 0 | 0 | 0 | 0 | 0 |
| $(CH_3)_3SiOCH_3$ | −33 | −31 | 8 |  | −19 | −17 |
| $(CH_3)_2Si(OCH_3)_2$ | −12 | −12 | 35 | 47 | 4 | 2·5 |
| $CH_3Si(OCH_3)_3$ | 23 | 35 | 68 |  | 42 | 41·5 |
| $Si(OCH_3)_4$ | 80 | 80 | 80 | 0 | 80 | 79·5 |
| $[(CH_3)_3Si]_3CH$ | −8 | 4 | 18 |  | 5 |  |
| $(CH_3)_3SiC_6H_5$ | −2 | 4 | 29 |  | 10 | 4·5 |
| $[(CH_3)_3Si]_2O$ | −16 | −8 | 14 |  | −3 | −4 |
| $[(CH_3)_2SiO]_3$ | −8 | 0 | 62 |  | 18 | $10^e$ |
| $[(CH_3)_2SiO]_4$ | 4 | 4 | 53 | 49 | 20 | 20 |

$^a$ All values are in ppm ($\pm3$) relative to solid TMS; positive values are to low frequency of TMS.
$^b$ $\Delta\sigma = \sigma_\parallel - \sigma_\perp$ for axially symmetric shielding tensors.
$^c$ $\bar{\sigma} = (1/3)(\sigma_{11} + \sigma_{22} + \sigma_{33})$.
$^d$ $\sigma_i$ is the isotropic shift in the neat liquid referred to liquid TMS.
$^e$ Solution in benzene.

Recently $^{29}$Si shielding anisotropies have been reported for two solid silicates,[258] one containing the $Si_2O_7{}^{6-}$ anion and the other the $Si_8O_{20}{}^{8-}$ anion. On the basis of the observed shielding anisotropies and estimated geometries about the Si atoms in these anions, the authors conclude that

the most shielded direction corresponds to the shortest Si–O bond. Also, it is suggested that the direction of highest $\pi$-bond character coincides with the direction of maximum shielding of the Si nucleus. Clearly further experiments, including single-crystal studies, are required to investigate the generality of these suggested trends. [259] Si shielding anisotropies for a few other organosilicon compounds have been reported by Lippmaa et al.[259] [For further recent references see the list on p. 287.]

High-resolution solid-state ^{29}Si NMR studies appear to have considerable potential in studying systems of practical importance. For example, solid-state ^{29}Si NMR has been used to study the surface of silica gel, silica attached species, and aluminosilicates including zeolites. Below we outline the results of these studies.

High-resolution ^{29}Si NMR provides a powerful technique for studying the surface of silica gel. Only silicon atoms near the surface are expected to be effectively cross-polarized by protons and hence observable in reasonable experimental times. Si atoms buried below the surface are expected to have exceedingly long relaxation times making their observation difficult. The [29]Si CP/MASS spectrum of silica gel SG-2 has been reported (Fig. 24).[260] The three resonances have been assigned on the basis of [29]Si chemical shifts reported in earlier studies on silicate-water glass solutions.[261] Assignments made on the basis of solution studies are supported by the [29]Si–[1]H CP times, $T$(Si–H), given in Table 6.
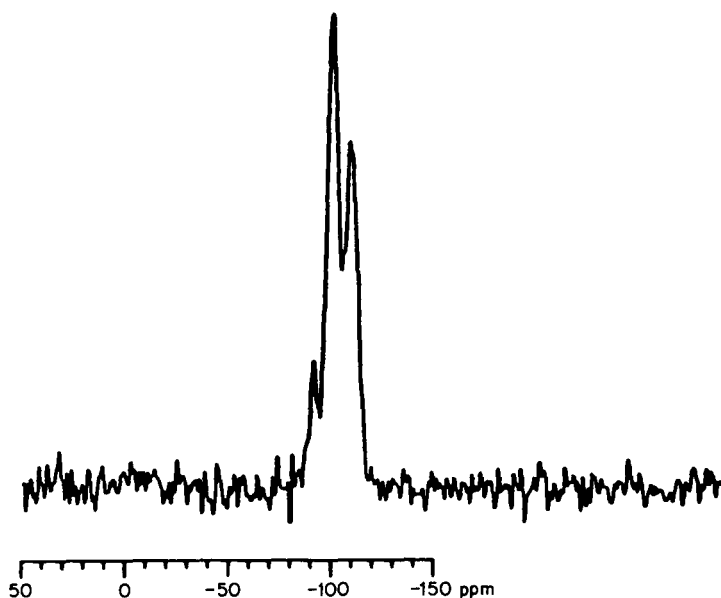


FIG. 24. CP/MASS ^{29}Si NMR spectrum of silica gel SG-2 (11·88 MHz);[264] 1014 scans, 20 ms contact times, 1 s repetitions.

## TABLE 6

### Summary of cross-polarization relaxation results on silica gel.

| Structural type[a] | $\delta_{Si}$[b] | $T_{SiH}$[c] (ms) | $T_{1\rho H}$[d] (ms) | $M_{\alpha e}$[e] |
|---|---|---|---|---|
| $(HO)_2Si^*(OSi\equiv)_2$ | $-90\cdot6$ | $2\cdot3\pm0\cdot2$ | $20\cdot3\pm1\cdot4$ | $6\cdot3\pm0\cdot2$ |
| $HOSi^*(OSi\equiv)_3$ | $-99\cdot8$ | $2\cdot9\pm0\cdot1$ | $22\cdot1\pm0\cdot8$ | $21\cdot7\pm0\cdot4$ |
| $Si^*(OSi\equiv)_4$ | $-109\cdot3$ | $12\cdot7\pm1\cdot7$[f] | $21$[g] | $18\cdot8\pm0\cdot5$ |

[a] The silicon nucleus of interest is indicated by an asterisk.

[b] Chemical shifts in ppm with respect to liquid $Me_4Si$; higher numbers correspond to lower shieldings.

[c] $^{29}Si-^1H$ cross-polarization relaxation time in milliseconds.

[d] Proton spin–lattice relaxation time in the rotating frame in milliseconds.

[e] Magnitude of the maximum available magnetization in arbitrary, relative units.

[f] As the cross-polarization time for $^*Si(OSi\equiv)_4$ is rather large, an accurate measure requires that the radio frequency fields be extremely well matched over the entire sample; hence, the value 12·7 ms should be considered qualitative.

[g] This value was chosen as an average of the other two $T_{1\rho H}$ values and used as a constraint on the least-squares analysis for this peak. In an unconstrained analysis the value $33\pm9$ was obtained for $T_{1\rho H}$; the corresponding $T_{SiH}$ and $M_{\alpha e}$ values were $9\cdot0\pm2\cdot1$ ms and $13\cdot9\pm1\cdot7$, respectively.

$^{29}Si$ and $^{13}C$ CP/MASS spectra of four different silica-attached species have also been assigned,[262] complementing earlier work on $^{13}C$ spectra of surface-attached species.[177] The $^{29}Si$ NMR spectrum of a sample prepared by the reaction of $(CH_3)_3SiCl$ with silica gel consists of three peaks. One at $-15\cdot4$ ppm (high frequency with respect to TMS) is assigned to the $Si(CH_3)_3$ group in a silica-attached species of the type $\equiv SiO-^*Si(CH_3)_3$. Two peaks at approximately 100 and 109 ppm are observed in all $^{29}Si$ spectra and are assigned to $HO^*Si(OSi\equiv)_3$ and $Si^*(OSi\equiv)_4$ respectively.[260] A sample prepared from the silylating agent $(CH_3O)_3SiCH_2CH_2CH_2SH$ shows a large peak at 56·6 ppm which is assigned to the $Si_\alpha$ atoms shown in structure **13**. The $^{29}Si$ spectrum of a species presumed to have structure **14** shows a resonance at $-12\cdot7$ ppm.

$$\equiv Si-O$$
$$O-Si_\alpha CH_2CH_2CH_2SH$$
$$\equiv Si \quad OCH_3$$

**(13)**

$$-O-Si-CH_2CH_2CH_2NH_3^+ \quad CH_3 \quad CH_3$$

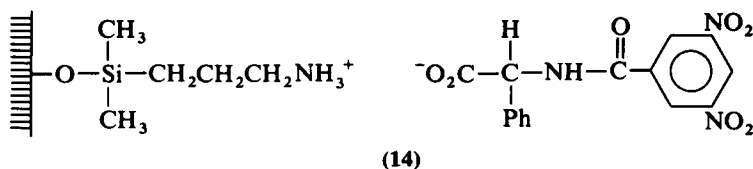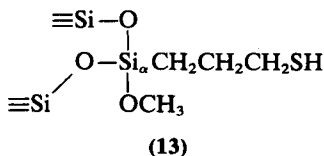$$^-O_2C-C-NH-C-\langle NO_2, NO_2 \rangle \quad H \quad O \quad Ph$$

**(14)**

# TABLE 7

Silicon-29 isotropic shifts (ppm from Me₄Si) in solid silicates.

| Compound | Type of Si–O tetrahedra | $Q^0$ single tetrahedra | $Q^1$ end group | $Q^2$ middle group | $Q^3$ branching site | $Q^4$ crosslinking group |
|---|---|---|---|---|---|---|
| NaH₃SiO₄ | single | −66·4 | | | | |
| Na₂H₂SiO₄·5H₂O | single | −67·8 | | | | |
| CaNaHSiO₄ | single | −73·5 | | | | |
| (CaOH)CaHSiO₄ | single | −72·5 | | | | |
| Zn₄(OH)₂[Si₂O₇]·H₂O (hemimorphite) | double | | −77·9 | | | |
| Ca₆(OH)₆[Si₂O₇] | double | | −82·6 | | | |
| K₄H₄[Si₄O₁₂] | cyclotetra | | | −87·5 | | |
| Ca₂(OH)₂[SiO₃] (hillebrandite) | single chain | | | −86·3 | | |
| Ca₄(OH)₂[Si₃O₉] (foshagite) | single chain | | | −86·5 | | |
| Ca₃[Si₃O₉] (wollastonite) | single chain | | | −88·0 | | |
| Ca₂NaH[Si₃O₉] (pectolite) | single chain | | | −86·3 | | |
| Ca₆(OH)₂[Si₆O₁₇] (xonotlite) | double chain | | | −86·8 | −97·8 | |
| Mg₃(OH)₂[Si₄O₁₀] (talc) | layer | | | | −98·1 | |
| (Me₄N)₈[Si₈O₂₀] | double 4-ring | | | | −99·3 | |
| (Et₄N)₆[Si₆O₁₅] | double 3-ring | | | | −90·4 | |
| SiO₂ (low quartz) | 3-D spiral, 6-rings | | | | | −107·4 |
| (low cristobalite) | | | | | | −109·9 |

# TABLE 8

Silicon-29 isotropic shifts (ppm from Me$_4$Si) in solid aluminosilicates.

| Compound | Al/Si ratio in lattice | Q$^3\cdots$Al$^a$ | | Q$^4$ | | | | |
|---|---|---|---|---|---|---|---|---|
| | | 1 Al$^b$ | 0 Al | 4 Al | 3 Al | 2 Al | 1 Al | 0 Al |
| Al$_2$(OH)$_2$[Si$_4$O$_{10}$] (pyrophyllite) | | | −91·5 −95·0 | | | | | |
| KAl$_2$(OH)$_2$[AlSi$_3$O$_{10}$] (muscovite) | 1/3 | −84·6$^c$ −86·7$^c$ | | | | | | |
| SiO$_2$ (low quartz) | | | | | | | | −107·4 |
| Na[AlSi$_3$O$_8$] (albite) | 1/3 | | | | | −92·5 | −96·7 −104·2 | |
| K[AlSi$_3$O$_8$] (orthoclase) | 1/3 | | | | | −95$^c$ | −98$^c$ −101$^c$ | |
| K[AlSi$_3$O$_8$] (adular) | 1/3 | | | | | −95$^c$ | −98·2$^c$ −100·5$^c$ | |
| K[AlSi$_3$O$_8$] (sanidine) | 1/3 | | | | | −95·7$^c$ | −96·8$^c$ −100·9$^c$ | |
| Na$_2$[Al$_2$Si$_3$O$_{10}$]·2H$_2$O (natrolite) | 2/3 | | | | −87·7 | −95·4 | | |
| KNa$_3$[AlSiO$_4$]$_4$ (nepheline) | 1/1 | | | −84·6 | −88·4$^d$ | | | |
| Ca[Al$_2$Si$_2$O$_8$] (anorthite) | 1/1 | | | −83·1$^c$ | | | | |

$^a$ Six-coordinated aluminium.
$^b$ Four-coordinated aluminium.
$^c$ Broadened lines.
$^d$ Signal of low intensity.

Finally the spectrum of a commercially available stationary phase known as Spherisorb $C_{18}$ has resonance peaks at 64·9, 54·7, and −16·0 ppm. These peaks are assigned to Si atoms at the silica surface in which (a) three ≡Si–O– groups and a carbon of the alkyl group, (b) two ≡Si–O– groups, an OH group, and an alkyl group, and (c) one ≡Si–O– group and three alkyl groups are attached.

Lippmaa and coworkers[263] have recently reported the results of CP/MASS $^{29}$Si NMR studies on solid silicates and aluminosilicates. The results obtained at 39·74 MHz using a Bruker CXP-200/300 spectrometer are given in Tables 7 and 8. The linewidths are usually 1–2 ppm. Recycle times of only 1–2 s are used for many of the samples; however, some samples, particularly those without protons, require recycle times of up to 30 s.

The total range of $^{29}$Si chemical shifts observed in the silicates is approximately 60 ppm. The shifts appear to fall into distinct ranges depending upon the nature of the silicon–oxygen tetrahedra. Increasing condensation from the single to double tetrahedra, to chains and cyclic layered structures, and finally to three-dimensional frameworks leads to low-frequency shifts. Similar trends are observed in solution studies. The effect of replacing Si by Al on neighbouring $^{29}$Si chemical shifts is illustrated in Table 8[259] and Fig. 25. Going from quartz (zero Al neighbours) to nepheline or anorthite (a central Si atom joined through oxygen bridges to four Al atoms and vice versa), a high-frequency shift of approximately 23 ppm is observed. Because the $^{29}$Si chemical shifts fall into five distinct ranges depending on whether a given $SiO_4^{4-}$ tetrahedron is linked, via oxygen bridges, to four, three, two, one, or zero $AlO_4^{5-}$ tetrahedra, and are essentially independent of the cation, high-resolution solid-state $^{29}$Si NMR offers a powerful technique for studying the ordering of Si and Al in solid aluminosilicates (feldspars, feldspathoids, and zeolites). Previously, the detailed distribution of Si and Al in these important compounds[264] has been difficult to determine experimentally because of the similar X-ray scattering properties of Si and Al, and the difficulty in preparing single crystals of adequate size and quality.

From $^{29}$Si data, Engelhardt et al.[75,265] concluded that in zeolite Linde A, which is very important commercially, the ordering is Si(3Al) contrary to what had been previously thought.[264] This means that in this zeolite, which has Si/Al = 1·0, each Si atom is linked, via oxygen bridges, to *three* Al atoms and *one* other Si atom and vice versa. Thus some Al–O–Al bonding must exist in this zeolite, and Loewenstein's rule,[266] which states that aluminium atoms cannot occupy neighbouring tetrahedral sites, is violated. A new structure for Linde A that is consistent with the $^{29}$Si NMR results has been recently suggested.[76]

It is interesting to point out that in zeolites X and Y, which have the same building blocks (sodalite cages) as Linde A but only differently joined,
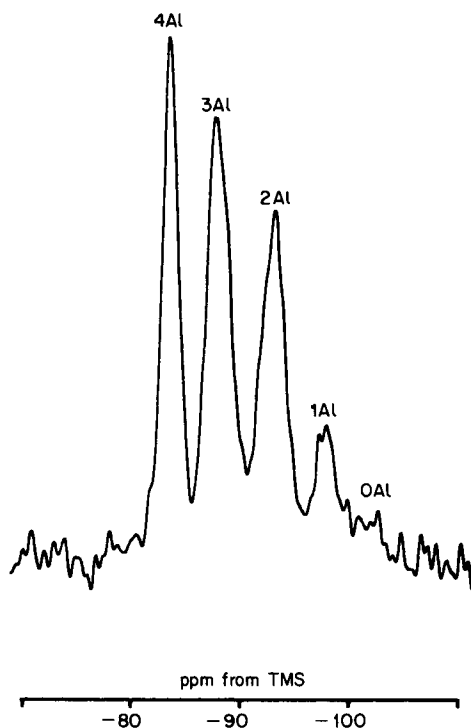
FIG. 25. MASS $^{29}$Si NMR spectrum of the zeolite analcite (79·46 MHz).

Ramdas et al.[267] have found that Loewenstein's rule is obeyed for Si/Al = 1·0–3·0. However, these conclusions were based on the chemical shift of a single peak, using the previously determined shift ranges for the assignment of the coordination around silicon, and are ambiguous. Recent investigations[268] of zeolite ZK-4, which has the zeolite A structure but with Si/Al > 1, gave $^{29}$Si NMR spectra that clearly showed five peaks and confirmed the Si(4Al) ordering in zeolite A, the shift of the Si(4Al) peak being outside the previously determined range for this coordination. Care must obviously be taken in situations where only single peaks are observed.

Klinowski et al.[269] have also used $^{29}$Si NMR to study a new material, a silicate analogue of zeolite Y. This is prepared by replacing the Al in the structure by Si using a solid-state method. The four peaks in the $^{29}$Si NMR spectrum of zeolite Y collapse to a single extremely sharp Si(OSi)$_4$ peak at −107·4 ppm which corresponds exactly to the chemical shift of silicon in pure quartz.[263]

The structure of silicate anions in tetraethylammonium silicates and their aqueous solutions has been examined using $^{29}$Si–$^{1}$H CP/MASS techniques.[270] For two crystalline TEA/Si silicates with molar ratios of 0·67 and 1·26, chemical shielding anisotropies, $\sigma_\perp - \sigma_\parallel$, of 60 and 110 ppm respectively are reported.

Recently $^{29}$Si CP/MASS NMR spectra for two plasma-deposited amorphous silicon–hydrogen films have been reported.[271] The spectra show the gross features expected from the vibrational spectra assignment of the polysilane local environments in one of the films. The lack of significant line narrowing on MASS is taken as evidence for a range of chemical shifts for Si in these films ($\nu_\frac{1}{2} \approx 50·8$ ppm with MASS and 81·5 ppm without MASS).

## C. Phosphorus-31

Phosphorus-31 has a natural abundance of 100% and a relatively large magnetic moment making it a particularly sensitive nucleus for NMR studies. Several monographs and reviews on $^{31}$P NMR are available.[272-279] Some of these deal specifically with biochemical applications of $^{31}$P NMR,[278] some with organometallic[279] and transition metal phosphine complexes,[277] while others are more general. [For further references see p. 287.]
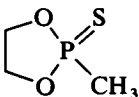
### 1. Chemical shifts

The most common reference in $^{31}$P NMR studies is 85% phosphoric acid, $H_3PO_4$. $^{31}$P chemical shifts range from approximately 250 ppm on the high-frequency side to 460 ppm on the low-frequency side of $H_3PO_4$, a total range of approximately 700 ppm. Phosphorus chemical shifts have been empirically related to a number of variables including oxidation state, bond angles, electronegativity of substituents, and $\pi$-bonding character of the substituents. Generally P(v) compounds have a relatively small chemical shift range, $\delta = 100$ ppm to $\delta = -50$ ppm compared with P(iii) compounds which have shifts over the full range. Some additivity relationships seem to work reasonably well in the absence of $\pi$-bonding but a discussion of these is outside the scope of this review.

Chemical shielding anisotropies range from a few ppm in free phosphorus to 200 ppm or more in phosphine oxides. Mehring[1] and Appleman and Dailey[40] have compiled tables summarizing early measurements of CSA. In Table 9 we present some of the more recent results. Recently, *ab initio* calculations of the $^{31}$P magnetic shielding tensor in the phosphate group have been reported.[294]

## TABLE 9

Principal values of phosphorus-31 shielding constants[a] and chemical shielding anisotropies, $\Delta\sigma$.[b]

| Compound | $\sigma_{11}$ | $\sigma_{22}$ | $\sigma_{33}$ | $\Delta\sigma$ | $\bar{\sigma}$ | Ref. |
|---|---|---|---|---|---|---|
| $KH_2PO_4$ | −16·6 | −1·1 | 1·1 | 15 | −6·2 | 280 |
| $P_4$ | | | | −405 | | 281 |
| $Ba(C_2H_5PO_4)_2$ | | | | −60 | | 282 |
| $Ca_{10}(OH)_2(PO_4)_6$ (calcium hydroxyapatite) | −19 | −4 | 15 | | −2·8 | 283 |
| $CaHPO_4 \cdot 2H_2O$ (brushite) | −70 | 12 | 53 | | −1·7 | 283 |
| $Ca(H_2PO_4)_2 \cdot H_2O$ | −49 | 1 | 48 | | 0·0 | 283 |
| | −59 | 7 | 66 | | 4·6 | |
| 5'-AMP (Na salt) | −78 | 29 | 29 | −107 | −7 | 284 |
| 5'-AMP (free acid) | −77 | −8 | 83 | | −1 | 284 |
| Poly A | −89 | −24 | 110 | | −1 | 284 |
| Dipalmitoylphosphatidyl choline (DPPE) | −81 | −20 | 105 | | 1·3 | 285 |
| Dipalmitoyllecithin (DPL) | −131·0 | 34·5 | 97·6 | | 0·4 | 286 |
| DNA | −85 | −25 | 109 | | −0·3 | 284, 287 |
| $P(CH_3)_3$ | | | | ±8 | | 289 |
| $P(C_6H_5)_3$ | | | | 23 | | 289, 290 |
| $OP(CH_3)_3$ | | | | 174 | | 289 |
| $OP(C_6H_5)_3$ | | | | 280 | | 289, 290 |
| $SP(CH_3)_3$ | | | | 112 | | 289 |
| $SP(C_6H_5)_3$ | | | | 112 | | 289 |
| $Na_5P_3O_{10}$ | | | | 182 | | 291 |
| $OPF_3$ | | | | 278 | | 292 |
| (structure) | −13 | 109 | 243 | | 113 | 293 |

[a] All values of shielding constants are given in ppm relative to 85% $H_3PO_4$, taking low frequency as positive. Note that positive $\bar{\sigma}$ values correspond to negative values of the chemical shift, $\delta$.

[b] $\Delta\sigma = \sigma_{\parallel} - \sigma_{\perp}$ where $\sigma_{\parallel}$ is along the symmetry axis.

### 2. Scalar coupling

Scalar coupling constants, $^nJ(^{31}P-X)$, can be very useful in characterizing phosphorus compounds.[272-279] Typical one-bond scalar couplings to some spin 1/2 transition metals are: $^1J(W-P)$, 200–500 Hz;[295] $^1J(Rh-P)$, 80–150 Hz;[295] $^1J(Pt-P)$, 1200–5000 Hz.[279,295] These couplings are generally relatively easy to resolve in CP/MASS experiments and can be very useful in identifying geometric isomers in the solid state. Splittings of $^{31}P$ spectra due to quadrupolar nuclei such as $^{63}Cu$ and $^{65}Cu$ in the solid state are difficult to interpret.

## 3. Applications

A number of early high-resolution $^{31}$P NMR experiments were carried out on solids without high-power proton decoupling or CP.[296-301] Such solids generally do not contain protons (e.g. phosphides etc.) hence MASS alone is sufficient to effectively eliminate weak dipolar interactions and average any CSA. One interesting example is the $^{31}$P NMR spectrum of phosphorus pentachloride.[298] The spectrum obtained with MASS gives two well resolved lines at 91 ppm and −281 ppm with respect to external $H_3PO_4$. The high-frequency resonance is assigned to $[PCl_4]^+$ while the low-frequency resonance results from $[PCl_6]^-$. In carbon disulphide solution, $PCl_5$ gives rise to a single resonance at −80 ppm and is thus thought to exist as a molecular compound instead of an ion pair. Most of these early applications of MASS have been reviewed.[4,63]

$^{31}$P NMR studies have been carried out on a number of orientationally disordered $^{31}$P-containing solids (plastic crystals). For $P_4S_3$ a high-resolution $AX_3$ spectrum is observed at 420 K, over 25° below its melting point, without any line-narrowing techniques.[302] The spectrum is consistent with the known structure of $P_4S_3$ (15).[303]
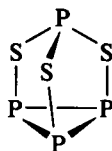


(15)

Detailed line-shape[304] and relaxation[305] studies have been carried out on white phosphorus, $P_4$. In the plastic phase (196–317 K) a single sharp symmetric line is observed indicating rapid molecular motion, while at the lowest temperature studied (4·2 K) an axially symmetric powder pattern is observed with $\Delta\sigma = \sigma_\parallel - \sigma_\perp = -405 \pm 10$ ppm. Between 80 K and 120 K line-shape analysis indicates molecular jump rates that are within an order of magnitude of $\Delta\omega = 2\pi\nu\Delta\sigma$ (234 kHz in the study of Spiess et al.[304]). $^{31}$P relaxation studies of the reorientation of $PH_3$ and $PD_3$ in the liquid and plastic crystalline phases have been reported.[306] Proton and $^{31}$P spin–lattice times have been measured for solid trimethyl phosphate, $(CH_3O)_3P{=}O$, between 77 and 305 K.[307]

$^{31}$P NMR without CP or MASS has been used to identify $PF_6^-$ ions in a graphite intercalation compound[308] resulting from the reaction (35). A possible side-reaction of the graphite fluorination, reaction (36), can be

$$NO_2PF_6 + nC \;\rightarrow\; NO_2(\text{gas}) + C_n{}^+PF_6^- \tag{35}$$

$$C_n{}^+PF_6^- \;\rightarrow\; C_nF + PF_5 \tag{36}$$
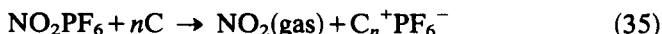
postulated without any change in stoichiometry. No evidence for the presence of $PF_5$ is obtained, and furthermore, dominance of reaction (36) would give no mechanism for the enhanced conductivity of the graphite intercalation compound. The relatively sharp $^{31}P$ resonances [$\delta = 128$ ppm, $^1J(^{31}P-^{19}F) = 708 \pm 20$ Hz] result from rapid tumbling and translational diffusion of the $PF_6^-$ ion.

Using MASS Andrew et al.[291] have observed two chemically shifted resonances in the $^{31}P$ spectrum of $Na_5P_3O_{10}$, a linear triphosphate. Chemical shift differences in aqueous solution and the solid ($\delta_{solution} - \delta_{solid}$) are too large to be accounted for in terms of bulk susceptibility differences, and the authors suggest that the low-frequency shifts observed in solution are due to an effective increase in coordination number of the phosphorus by water.

Calcium phosphates occur naturally in bone and teeth and are particularly difficult to characterize. Recently, Rothwell et al.[283] have examined the utility of $^{31}P$ CP/MASS to characterize a variety of calcium phosphates including hydroxyapatite, $Ca_{10}(OH)_2(PO_4)_6$, and some of its non-stoichiometric forms. Spectra were obtained on a superconducting wide-bore magnet operating at $4\cdot0$ T ($^{31}P = 68\cdot42$ MHz). Samples ($\sim0\cdot3$ cm$^3$) were packed and spun at $1-2\cdot5$ kHz using a Beams-type rotor. As in solution, the isotropic $^{31}P$ chemical shifts tend to move to low frequency upon protonation of the phosphate group. Although the total isotropic $^{31}P$ chemical shift difference between $PO_4^{3-}$ and $H_3PO_4$ is only 6 ppm in solution, variations in CSA are much larger on protonation of phosphate (Table 9). Several of the calcium phosphates give rise to two or more incompletely resolved peaks. By varying the CP times it is often possible to selectively enhance the intensity of one of the peaks relative to the others. Also, the relative intensities of spinning sidebands are used to facilitate peak assignments. Samples of calcium hydroxyapatite show large variations in $^{31}P$ $T_1$ values, from about 90 s in human enamel to anywhere between 1 and 22 s in synthetic samples. For samples with long $^{31}P$ $T_1$ values, CP offers significant sensitivity advantages over simple 90° pulses. Low-temperature $^{31}P$ experiments provide evidence for molecular motion of the $HPO_4^{2-}$ ion in the hydroxyapatite lattice, even at $-180°C$. Proton and $^2H$ MASS experiments are suggested to further characterize proton motion in these compounds. The authors conclude that increased resolution would be advantageous, particularly in preliminary studies of amorphous calcium phosphates where $^{31}P$ resonances are broader than those observed in the crystalline calcium phosphates.

Herzfeld et al.[309] have used $^{31}P$ MASS NMR to study the relative concentration of $^{31}P$ as hydroxyapatite and brushite ($CaHPO_4 \cdot 2H_2O$) as a function of tissue maturation. On the basis of the large spinning sidebands observed in young bone tissue from chicks 17 days embryonic, it is

concluded that brushite is the most probable initial mineral phase in bone. Brushite is known to exhibit a large CSA compared with hydroxyapatite (Table 9). In more mature bone, the lack of spinning sidebands suggests that apatite is the dominant calcium phosphate phase. These conclusions are supported by a comparison of spectra from the biological samples with those obtained from samples prepared from different mixtures of synthetic brushite and apatite.

The CP and MASS techniques have been used to obtain high-resolution $^{31}P$ NMR spectra of a number of solid triphenylphosphine transition metal complexes.[310] The $^{31}P$ spectrum of Wilkinson's catalyst, $RhCl(PPh_3)_3$ (**16**),

$$\begin{array}{c} Cl \\ | \\ P_A - Rh - P_B \\ | \\ P_X \end{array}$$

(**16**)
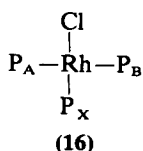
shows a typical ABX pattern. The P atoms *trans* to one another are non-equivalent in the solid state, consistent with the X-ray structure, and constitute the AB portion $[\Delta\delta_{AB} = 7.4\ ppm,\ ^2J(P_A-P_B) = 365\ Hz]$ of the spectrum. The phosphorus *trans* to Cl is 50·2 ppm to high frequency of external $H_3PO_4$ and about 22 ppm to high frequency of the centre of the AB multiplet; it shows one resolvable splitting, $^1J(^{103}Rh-P_X) = 185\ Hz$. The rhodium also couples to $P_A$ and $P_B$, $^1J(Rh-P_A) \approx\ ^1J(Rh-P_B) \approx 139\ Hz$.

The $^{31}P$ NMR spectra for two copper–phosphine complexes, $(Ph_3P)_2CuNO_3$ and $(Ph_3P)_3CuCl$, are also reported. The spectra of both complexes show large splittings of the order of 1 kHz due to coupling with $^{63}Cu$ (69·1% natural abundance) and $^{65}Cu$ (30·9%) both of which have a spin of 3/2. The splittings are complex and not simply equal to $^1J(Cu-P)$ because the copper nuclear quadrupolar coupling constants are comparable in energy to the Cu Zeeman interactions; thus Cu–P dipolar and $J$ tensor interactions are not averaged by spinning at the magic angle.

A $^{31}P$ spectrum of the gold cluster $[Au_9(PPh_3)_8][NO_3]_3$ is presented in the communication by Diesveld *et al.*;[310] two resonances at 48·0 and 68·7 ppm are observed. Without a crystal structure it is not possible to decide whether the two lines result from non-equivalent P sites within one molecule or two crystallographically non-equivalent molecules per unit cell.

Phosphorus-31 CP/MASS NMR spectra of six different Rh(I) diphosphine catalysts and their corresponding ligands have been investigated.[311] Chemical shifts and scalar couplings, $^1J(Rh-P)$, measured in the solid state are compared with the corresponding data obtained in solution (Tables 10 and 11). Solid-state spectra are obtained on a JEOL FX-60Q ($^{31}P = 24.22$ MHz) spectrometer and a home-built multinuclear CP/MASS spectrometer based on a Varian HR-60 magnet. The samples are packed in

## TABLE 10

**Phosphorus-31 data of diphosphine ligands.**

| Ligand | Solution,[a] $\delta_P$ (ppm)[b] | Solid, $\delta_P$ (ppm) |
|---|---|---|
| diphos[c] | −11·9 | −12.5 |
| BPPM[d] | −7·3, −21·9 | −14·8, −21·7 |
| diPAMP[e] | −21·0 | −25·6 |
| chiraphos[f] | −8·7 | −11·9, −14·0 |
| prophos[g] | 2·3, −20·0 | −4·5, −27·3 |
| | $(J_{P-P} = 20·4)$ | |

[a] The solvent was DCCl$_3$.
[b] Chemical shifts are given with respect to 85% H$_3$PO$_4$.
[c] diphos = 1,2-ethanediylbis(diphenylphosphine).
[d] BPPM = (2S,4S)-N-t-butoxycarbonyl-4-diphenylphosphine-2-diphenylphosphinomethylpyrrolidine.
[e] diPAMP = (R,R)1,2-ethanediylbis-(o-methoxyphenylphosphine).
[f] chiraphos = (S,S,)-2,3-butanediylbis(diphenylphosphine).
[g] prophos = (R)-1,2-bis(diphenylphosphino)propane.

## TABLE 11

**Phosphorus-31 data of rhodium(i) diphosphine catalysts.**

| Catalyst | Solution[a] $\delta_P$ (ppm)[b] | Solution[a] $J_{Rh-P}$ (Hz) | Solid $\delta_P$ (ppm) | Solid $J_{Rh-P}$ (Hz) |
|---|---|---|---|---|
| [Rh(cod)diphos]$^+$ClO$_4^{-e}$ | 58·3 | 132·1 | 56·8 | 126 |
| [Rh(cod)BPPM]$^+$ClO$_4^-$ | 43·6[c] | 146·4 | 38·9, 12·7 | [d] |
| | | $(J_{P-P} = 36)$ | | |
| | 43·4[c] | 144·8 | | |
| | | $(J_{P-P} = 37)$ | | |
| | 14·7 | 139·5 | | |
| [Rh(cod)diPAMP]$^+$ClO$_4^-$ | 52·3 | 150·9 | 51·6, 45·8 | 138, 145 |
| [Rh(nbd)chiraphos]$^+$ClO$_4^{-f}$ | 59·2 | 154·0 | 62·2, 61·4 | ~107, ~133 |
| [Rh(cod)chiraphos]$^+$ClO$_4^-$ | 56·6 | 146·2 | 57·6, 54·6 | ~117, ~125 |
| [Rh(nbd)prophos]$^+$ClO$_4^-$ | 62·2 | 156 | 64·0 | 162 |
| | | $(J_{P-P}) = 33$ | | |
| | 43·6 | 155 | 43·4 | 124 |
| | | $(J_{P-P}) = 34$ | | |

[a] The solvent was either DCCl$_3$ (first and last compounds in table) or acetone-d$_6$ (remaining compounds).
[b] Chemical shifts given with respect to 85% H$_3$PO$_4$.
[c] Assumed to represent two conformational forms of the –CH$_2$P(C$_6$H$_5$)$_2$ phosphorus.
[d] Not observable. [e] cod = cyclooctadiene. [f] nbd = norbornadiene.

10 mm or 13 mm (diameter) bullet rotors and spun at the magic angle at speeds of about 2·5 kHz. The $^{31}$P chemical shifts of the solid ligands are similar to those measured in chloroform solutions. One of the ligands, chiraphos (17), shows a single $^{31}$P resonance (−8·7 ppm) in solution but



Ph$_2$P          PPh$_2$

(17)
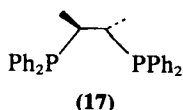
two peaks in the solid state. On binding to Rh(I), the $^{31}$P peaks of the diphosphine ligands shift to high frequency by approximately 50–80 ppm. Although the chemical shifts and couplings in solution and in the solid state are generally comparable, diphosphine complexes that give rise to chemically equivalent $^{31}$P resonances in solution often yield two chemically shifted $^{31}$P peaks in the solid state. It is suggested that the degree of phosphorus non-equivalence is related to the distance between the rhodium atom and the site of chirality in the ligand.

In a more recent study, $^{31}$P solid-state NMR spectra of several phosphorus(III) ligands and their Ni(II), Pd(II), and Pt(I) complexes have been examined.[312,313] Phosphorus-31 spectra of Pt(II) complexes of the general structure PtCl$_2$(PR$_3$)$_2$ are particularly interesting because they exhibit scalar coupling to $^{195}$Pt (33·8% natural abundance) which may be used to differentiate between square planar *cis* and *trans* isomers. Spectra for two such complexes are shown in Fig. 26. As observed in solution studies,
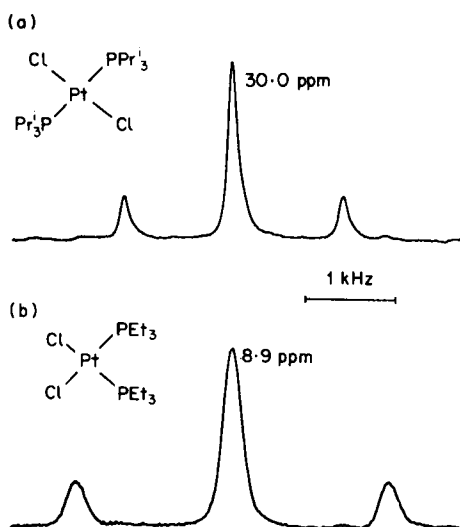


FIG. 26. CP/MASS $^{31}$P NMR spectra (34 MHz): (a) *trans*-[PtCl$_2$(PPr$^i$$_3$)$_2$]; (b) *cis*-[PtCl$_2$(PEt$_3$)$_2$].

$^{1}J(^{195}Pt-^{31}P)$ is ~3500 Hz for the *cis* arrangement and ~2500 Hz for the *trans* isomer. The relative merits of two different preparative routes [equations (37) and (38)] to phosphine-linked immobilized transition metal complexes on silica and glass surfaces were evaluated. Although condensation of *cis*-[PtCl$_2$(Ph$_2$PCH$_2$CH$_2$Si(OEt)$_3$)$_2$] with silica gel [equation (37)] leads to the desired product (Fig. 27), route (38) is less successful. $^{31}$P



FIG. 27. CP/MASS $^{31}$P NMR spectra (34 MHz) of *cis*-{PtCl$_2$[Ph$_2$PCH$_2$CH$_2$Si(OEt)$_3$]$_2$}: (a) polycrystalline solid; (b) after immobilization on silica gel.

NMR spectra indicate that condensation of the linking ligand, (EtO)$_3$Si(CH$_2$)$_2$PPh$_2$, with silica gel and with high surface area glass beads results in two chemically distinct phosphorus-containing species on the surface. Although one of these, believed to be a P(v) species, can be removed by reduction, reaction of the surface-immobilized phosphine with PtCl$_2$(NCPh)$_2$ leads to unidentified products. These preliminary studies indicate that high-resolution $^{31}$P NMR will be a powerful technique in characterizing surface-immobilized phosphorus-containing species and have far-reaching effects in the study of polymer-supported transition metal catalysts.

$$[ML_n] + (EtO)_3Si(CH_2)_2PPh_2 \rightarrow (EtO)_3Si(CH_2)_2\overset{\overset{\displaystyle Ph}{|}}{\underset{\underset{\displaystyle Ph}{|}}{P}}-ML_{n-1}$$

$$\downarrow \text{\small(Si)}-OH \qquad (37)$$

$$\text{\small(Si)}-O\overset{|}{\underset{|}{Si}}(CH_2)_2\overset{\overset{\displaystyle Ph}{|}}{\underset{\underset{\displaystyle Ph}{|}}{P}}-ML_{n-1}$$

$$\text{\small(Si)}-OH + (EtO)_3Si(CH_2)_2PPh_2 \rightarrow \text{\small(Si)}-O\overset{|}{\underset{|}{Si}}(CH_2)_2PPh_2$$

$$\downarrow ML_n \qquad (38)$$

$$\text{\small(Si)}-O\overset{|}{\underset{|}{Si}}(CH_2)_2\overset{\overset{\displaystyle Ph}{|}}{\underset{\underset{\displaystyle Ph}{|}}{P}}-ML_{n-1}$$
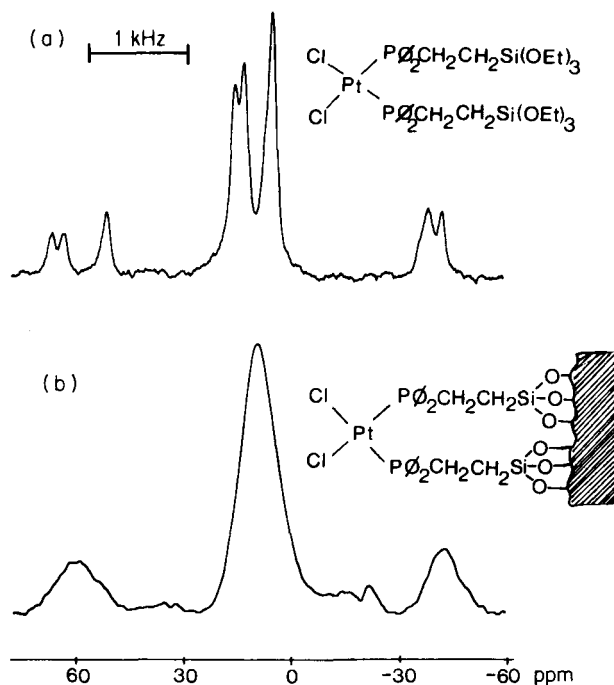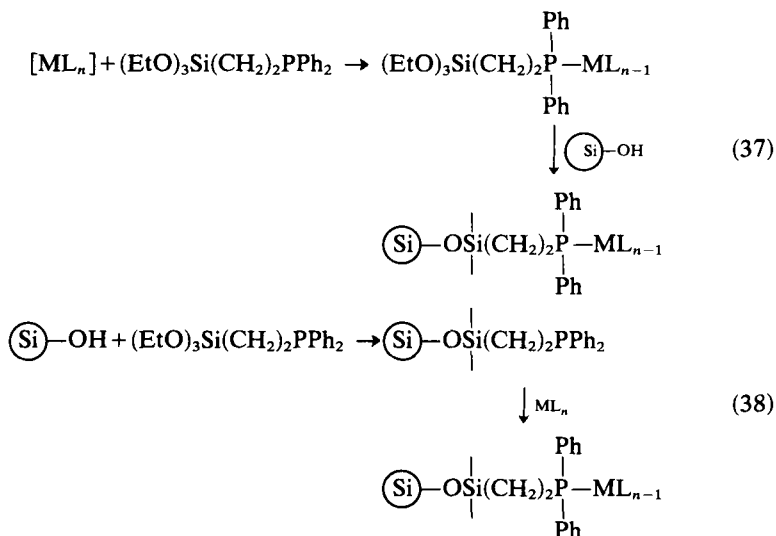
## D. Cadmium-113

High-resolution cadmium NMR studies can be carried out on either $^{111}Cd$ ($I = 1/2$, 12·8% natural abundance, $\gamma = -5\cdot6699 \times 10^7$ rad $T^{-1}$ $s^{-1}$) or $^{113}Cd$ ($I = 1/2$, 12·3% natural abundance, $\gamma = -5\cdot9330 \times 10^7$ rad $T^{-1}$ $s^{-1}$). $^{113}Cd$ NMR studies are preferred because of its slightly larger magnetic moment. Solution chemical shifts cover a range of approximately 1000 ppm.[314] Solutions of $Cd(ClO_4)_2$, 0·1M or extrapolated to infinite dilution, have been the most commonly used reference in $^{113}Cd$ NMR studies. Nölle,[315] however, has used 3M $CdSO_4$ in $H_2O$ as a reference since the chemical shift is known with respect to the free $^{113}Cd$ atom.[316] Dimethylcadmium has some advantages as a reference particularly in the study of organocadmium derivatives.[314]

Nölle[315] has obtained $^{113}Cd$ spectra for powder samples of the cadmium halides and cadmium chalcogenides CdO, CdS, CdSe, CdTe and $CdCO_3$. Axially symmetric shielding tensors ($\Delta\sigma = \sigma_\parallel - \sigma_\perp$) are observed for the $^{113}Cd$ resonances in $CdCl_2$ (115 ± 8 ppm), $CdBr_2 \cdot 4H_2O$ (−127 ± 9 ppm), CdS (−54 ± 8 ppm), and CdSe (−64 ± 7 ppm), while no anisotropy in the shielding is observable for the other halides, chalcogenides, and the carbonate.

Cheung et al.[317] have utilized $^{113}Cd$–$^1H$ CP to observe CSA in three hydrated cadmium salts. The powder indicates axially symmetric shielding tensors for each compound, $Cd(OH)_2 \cdot 1\cdot12H_2O$ (−149 ± 8 ppm), $3CdSO_4 \cdot 8H_2O$ (−102 ± 8 ppm), and $Cd(NO_3)_2 \cdot 4H_2O$ (−189 ppm). The $^{113}Cd$ spectrum of the first compound is shown in Fig. 28.
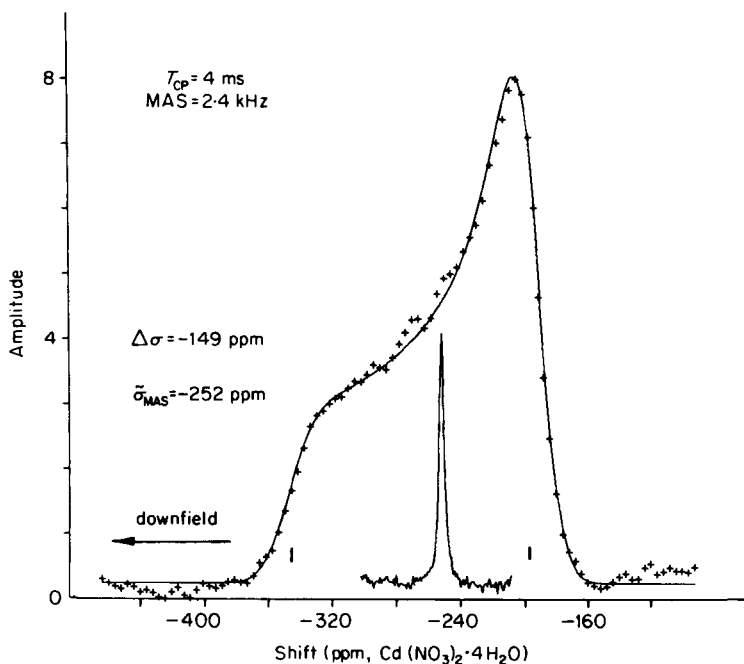
FIG. 28. CP and CP/MASS $^{113}$Cd NMR spectra of Cd(OH)$_2$·$x$H$_2$O.

CP/MASS spectra of CdCl$_2$·2·5H$_2$O show two lines of relative intensity 1:3 separated by 21 ppm.[317] This is consistent with the known structure of CdCl$_2$·2·5H$_2$O in which two types of Cd(II) of coordination number 6 are found.[318] One is surrounded by five chlorines and one water, while the other is surrounded by four chlorines and two water molecules *cis* to one another. The relative intensity of the two peaks is ascribed to the different cross-relaxation rates at each Cd site. $T_{IS}^{-1}$ is expected to be approximately proportional to the number of protons in the first coordination sphere; thus the less intense high-frequency peak is assigned to the Cd(II) ions that are bound to one water. With MASS two lines are also observed for 3CdSO$_4$·8H$_2$O, again consistent with X-ray results.[323]

Cheung et al.[317] report significant enhancements in the S/N ratio due to CP not only because $\gamma_I/\gamma_S = -4·5$ but also because one can use recycle times much less than the $^{113}$Cd relaxation times which are estimated to be well over 300 s. The $^1$H $T_1$ values however are less than 0·5 s thus allowing relatively short recycle times. Contact times of approximately 4 ms result in the optimum S/N value for the compounds studied.[317] Substantial enhancements of $^{113}$Cd signals due to CP have also been reported elsewhere.[320,321]

Ackerman et al.[320] have used the MASS and CP techniques to obtain $^{113}Cd$ chemical shifts of solid 4-coordinate (approximately tetrahedral) Cd(II) tetrahalide complexes, $CdX_4^{2-}$, where $X = Cl$, Br, or I. Using these chemical shifts as "benchmarks" together with the appropriate solution equilibrium constants, chemical shifts for the various Cd(II)–halide complexes are derived. The authors conclude that analogous use of solid-state chemical shift benchmarks for interpreting liquid solution data should see increased popularity particularly in systems complicated by ligand exchange and/or uncertainties in metal-complex structure in solution.

In a more recent study, a wide range of Cd(II) complexes with a variety of coordination patterns have been examined.[321] Representative samples are given in Table 12. The $^{113}Cd$ chemical shifts of $CdI_4^{2-}$ are to low frequency of $CdBr_4^{2-}$ which are in turn to low frequency of $CdCl_4^{2-}$. Similar trends have been observed for the central nucleus in Group IV halides,[25] and for $^{67}Zn$ in $ZnX_4^{2-}$ [322] and $^{199}Hg$ in $HgX_4^{2-}$.[323] For a given ligand atom, increases in coordination number appear to be accompanied

## TABLE 12

### Cadmium-113 chemical shifts of crystalline powdered compounds.

| Compound | | Chemical shift, $\delta$ (ppm)[a] | Attached atoms and approximate first coordination sphere |
|---|---|---|---|
| Bis(tetraethylammonium) tetrachlorocadmate | $(Et_4N)_2CdCl_4$ | 483 | 4 Cl, tetrahedral |
| Bis(tetraethylammonium) tetrabromocadmate | $(Et_4N)_2CdBr_4$ | 374 | 4 Br, tetrahedral |
| Bis(tetraethylammonium) tetraiodocadmate | $(Et_4N)_2CdI_4$ | 79 | 4 I, tetrahedral |
| Cadmium n-butylxanthate | $Cd(n-buxan)_2$ | 445 | 4 S, tetrahedral |
| Hexaamminecobalt(III) pentachlorocadmate | $[Co(NH_3)_6][CdCl_5]$ | 134 | 5 Cl, trigonal bipyramid |
| Cadmium(II) diethyldithiocarbamate | $Cd(Et_2dtc)_2$ | 377 | 5 S, tetragonal |
| Tris(ethylenediamine)cadmium(II) chloride monohydrate | $Cd(en)_3Cl_2·H_2O$ | 380 | 6 N, octahedral pyramid |
| Hexakis(imidazole)cadmium(II) nitrate | $Im_6Cd(NO_3)_2$ | 238 | 6 N, octahedral |
| Cadmium(II) maleate dihydrate | $Cd(O_2CCHCHCO_2)·2H_2O$ | 12 | 6 O, octahedral |
| | | −7 | 6 O, octahedral |
| Sodium (ethylenediaminetetraacetato)-cadmate | $Na_2Cd(EDTA)$ | 117, 107, 97 | 2 N, 4 O, octahedral |

[a] Shifts are referenced to $0·1M$ $Cd(ClO_4)_2$ in aqueous solution with $I = 4·5$.

by high-frequency $^{113}$Cd shifts. In general, the authors find that the chemical shifts measured in the solid state are substantially different from those obtained in solution. This is easily rationalized since in solution studies one is generally observing an average shift of several species in rapid equilibrium. The $^{113}$Cd spectra of some of the compounds studied, e.g. HthiCdCl$_4$·H$_2$O, Cd(en)$_3$Cl$_2$·2H$_2$O, Co(NH$_3$)$_6$CdCl$_5$, exhibit linewidths of several hundred Hz. The authors have ruled out impurities as a likely source for these large linewidths, and suggest the following possibilities: (1) small deviations from the magic angle; (2) broadening by $^{14}$N, as the dipolar interaction with a quadrupolar nucleus need not be averaged out by MASS; (3) crystal imperfections, which could give a dispersion of chemical shifts; or (4) polymorphism.

The $^{113}$Cd powder spectra obtained in the absence of MASS exhibit shielding anisotropies comparable to those reported for related compounds by other workers.[315,317] Relative shielding tensor elements with respect to isotropic averages and $\Delta\sigma$ values reported in ref. 321 are given in Table 12. It is interesting to note that small distortions of tetrahedral or octahedral symmetry are sufficient to produce significant shielding anisotropies. For example, (Me$_4$N)$_2$CdBr$_4$ has $\Delta\sigma = 33$ ppm although the spectrum of (Et$_4$N)$_2$CdBr$_4$ shows no noticeable anisotropy. Similarly, $\Delta\sigma \approx 0$ ppm for Cd(ClO$_4$)·6H$_2$O while in Cd(NH$_4$)$_2$(SO$_4$)$_2$·6H$_2$O the shielding anisotropy is 76 ppm. On the basis of a "slow-spinning" experiment the authors find a large shielding anisotropy in cadmium(II) diethyldithiocarbamate, Cd(Et$_2$dtc)$_2$. Since it appears to be impossible to obtain a satisfactory spectrum without MASS, no estimate of $\Delta\sigma$ is reported. A good estimate should be possible, however, using the results of Herzfeld and Berger.[82]

Finally, high-resolution solid-state $^{113}$Cd NMR studies may be helpful in characterizing metalloproteins that bind Cd.[324]

## E. Other nuclei

In general, the references quoted here are confined to high-resolution NMR studies of other nuclei that utilize MASS or some other line-narrowing technique. [For further references see p. 287.]

### 1. Spin 1/2 nuclei

(a) *Nitrogen-15.* The recent book of Levy and Lichter[325] provides a good introduction to high-resolution $^{15}$N NMR spectroscopy. Nitrogen-15 NMR spectra obtained using high-power $^1$H decoupling and CP were first reported by Gibby *et al.*[326] Spectra of stationary samples of (NH$_4$)$_2$SO$_4$, NH$_4$NO$_3$, and glycine were discussed.

Recently, Schaefer, Stejskal and coworkers[327] have used high-resolution $^{15}$N NMR (CP/MASS) to study nitrogen metabolism. Different parts of a

soybean plant grown on $^{15}$N-enriched fertilizer were studied during various stages of its development. The resolution was sufficient to allow the estimate of the relative concentrations of amide and amine nitrogens in the seed and pod. Peaks due to histidine ring nitrogens, arginine $NH_2$ nitrogens, and proline, alanine, $NO_3^-$, and $NH_4^+$ were also resolved.

In a similar study, the nitrate-$^{15}$N metabolism of *Neurospora crassa* was studied by MASS/CP $^{15}$N NMR.[328] Good quality spectra are obtained in 18 hours or less. Contact times of 1 ms are used indicating that cross-relaxation is very efficient. The authors conclude that the CP studies, which measure only the completely or partially immobilized components of the cell, complement conventional $^{13}$C or $^{15}$N NMR measurements which monitor the mobile components of *in vivo* cellular systems.

Protein turnover in soybean leaves[329] has been studied using $^{13}$C and $^{15}$N double labelling, together with double-cross-polarization (DCP) NMR.[330] The DCP technique allows detection of $^{15}$N–$^{13}$C pairs. Further discussion of the technique and its application in nitrogen metabolism are given in an excellent review.[16]

(b) *Tin-119.* With the exception of the $^{119}$Sn chemical shifts given for three organotin compounds, we are unaware of any other high-resolution solid-state NMR studies of other nuclei.

## 2. Quadrupolar nuclei

(a) *Hydrogen-2 (I = 1).* Pine and coworkers have successfully demonstrated two different approaches for obtaining high-resolution $^2$H NMR spectra: (1) MASS with synchronous spinning; (2) double quantum FT NMR (DQFTNMR) with MASS.[333]

In principle MASS removes first-order quadrupole broadening and CSA interactions. Because spinning rates are generally two orders of magnitude less than the quadrupolar broadening, the FID following a single pulse consists of a series of spatially induced echoes separated by $\nu_r^{-1}$. By sampling in synchronization with the rotation a "high-resolution" decay results. Using this approach Ackerman, Eckman and Pines[331,332] were able to resolve three peaks in the $^2$H NMR spectrum of perdeuteroterephthalic ester (**18**) which are assignable to the aromatic, methylene, and methyl deuterons. For a number of compounds $^2$H NMR linewidths vary between 1·5 and 3·5 ppm. The second-order quadrupolar interaction is estimated



**(18)**
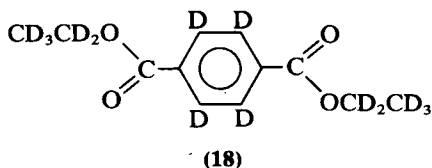
to be responsible for a line broadening of approximately 1 ppm ($\nu_0 =$ 28 MHz). Since this interaction depends on $\nu_Q^2/\nu_0$, its contribution to linewidth could be significantly reduced at higher fields. The main limitation of this first approach is associated with the MASS; an extremely stable spinner with angular fluctuations of less than a few millidegrees is required.

In the second approach, DQFTNMR,[333] the requirements on sample spinning are much less stringent. The double-quantum transitions (2-Q) are independent of the quadrupolar coupling to first order, thus the MASS serves only to remove CSA interactions which are generally less than 10 ppm. The pulse sequence used[333] to observe the double quantum spectra is illustrated in Fig. 29. For a 28% randomly deuterated ferrocene sample
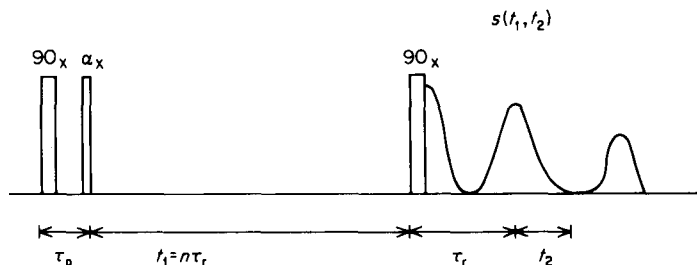


FIG. 29. Schematic representation of the pulse sequence used for double quantum NMR spectroscopy.

the linewidth of the 2-Q line is approximately 40 Hz, which is double that of the 1-Q line (the spinning axis is within $0\cdot006°$ of the magic angle). Static field inhomogeneity and susceptibility anisotropies have double their effect for 2-Q transitions since all the chemical shifts are doubled.[333] The width of the 2-Q resonance is however much less sensitive to spinner angle adjustment and stability. The second-order quadrupole perturbation shifts the deuterium resonance of the 2-Q transition by exactly twice that of the 1-Q transition.

Müller, Eckman and Pines[334] have demonstrated that single quantum $^1H-^2H$ CP leads to a substantial sensitivity gain in MASS $^2H$ NMR. The resolution is improved since it is possible to use a lower level of isotopic substitution ($^2H-^1H$ dipolar interactions are reduced). Sample spinning leads to complex CP dynamics and a broad Hartmann–Hahn matching region.[334] For large quadrupolar coupling long contact times are required. Müller[335] has demonstrated that long contact times can be avoided by off-resonance CP.

(b) *Nitrogen-14 (I = 1).* As far as we are aware all high-resolution $^{14}N$ experiments on rigid solids to date have been carried out by using single

crystals. Applications of $^{1}$H dipolar coupled $^{14}$N NMR spectra in determining accurate N–H bond lengths in amino acids and peptides have recently been reviewed.[35]

Double quantum CP has recently been examined.[336,337] The 2-Q cross-relaxation rate is predicted, and observed, to be four times that of a single quantum cross-relaxation.[336] For one particular orientation of a $(NH_4)_2SO_4$ crystal, the $^{14}$N 2-Q spectrum is a doublet of splitting 180 Hz. Correcting for the second-order quadrupolar shifts, a splitting of 126 Hz (~8 ppm) is attributed to the chemical shift difference for the two non-equivalent $NH_4^+$ sites in $(NH_4)_2SO_4$. For large quadrupole coupling constants excessively high rf fields are required to match the 2-Q Hartmann–Hahn condition. For quadrupole splittings up to 2 MHz $^{14}$N 2-Q transitions can be observed by indirect CP via dipolar order.[337]

(c) *Aluminium-27 (I = 5/2)*. High-resolution $^{27}$Al NMR spectra of polycrystalline aluminates have been studied at high field (70·4 MHz) using MASS.[338] Pulses are selectively applied to excite the central $1/2 \leftrightarrow 1/2$ transition which is not broadened by first-order quadrupole interactions.[338] Isotropic chemical shifts appear to depend mainly on the Al–O coordination. For tetrahedral sites the shifts range from 55 to 80 ppm (to low frequency of aqueous $AlCl_3$) while octahedral sites have shifts near 0 ppm. High-resolution $^{27}$Al NMR should complement the $^{29}$Si studies of zeolites discussed earlier; such studies have recently been performed at 104 MHz.[339]

(d) *Boron-11 (I = 3/2)*. Chemical shifts have been detected in a few tetrahedrally coordinated compounds in the solid state.[340]

## V. CONCLUDING REMARKS

We have attempted to outline recent applications of multinuclear high-resolution solid-state NMR. Although many of the spectra we have used in the figures are from our own work, they were chosen mainly for convenience. Near the time of completion of this review the discussions of a meeting, "Nuclear Magnetic Resonance Spectroscopy in Solids," organized by R. Richards and K. J. Packer were published (*Phil. Trans. Roy. Soc.*, 1981, *A* **299**, 477). We have referred to several of the papers in this excellent collection. The Specialist Periodical Reports on NMR, edited by G. A. Webb and published by the Royal Society of Chemistry, review solid-state NMR annually. References to the literature dealing with applications of solid-state NMR to the study of natural and synthetic macromolecules are generally found under these headings; biennial reports also appear on heterogeneous systems.

With the increasing availability of commercial spectrometers designed specifically for solid-state work, and the practical and theoretical importance of many of the systems amenable to these techniques, we expect much

more activity in this area and a renewed interest in the solid state by chemists.

## Acknowledgements

## REFERENCES

1. M. Mehring, "High Resolution NMR Spectroscopy in Solids", in *NMR Basic Principles and Progress* (ed. P. Diehl, E. Fluck and R. Kosfeld), Vol. 11, Springer Verlag, New York, 1976.
2. U. Haeberlen, *Adv. Magn. Resonance*, Suppl. 1, 1976.
3. E. R. Andrew, *Progr. NMR Spectroscopy*, 1971, **8**, 1.
4. E. R. Andrew, in *International Review of Science, Physical Chemistry*, Series 2, Vol. 4 (Magnetic Resonance) (ed. C. A. McDowell), p. 173, Butterworths, London, 1975.
5. R. G. Griffen, *Analyt. Chem.*, 1977, **49**, 951A.
6. R. W. Vaughan, *Ann. Rev. Phys. Chem.*, 1978, **29**, 397.
7. L. W. Gerven (ed.), "Nuclear Magnetic Resonance in Solids", *NATO Advanced Study Institutes Series*, Vol. B-22, Plenum Press, New York, 1974.
8. R. K. Harris and K. J. Packer, *European Spectrosc. News*, 1978, **21**, 37.
9. H. W. Spiess, "Dynamic NMR Spectroscopy", in *NMR Basic Principles and Progress* (ed. P. Diehl, E. Fluck and R. Kosfeld), Vol. 15, Springer Verlag, New York, 1978.
10. J. Schaefer and E. D. Stejskal, "High Resolution $^{13}$C NMR of Solid Polymer", in *Topics in Carbon-13 NMR Spectroscopy* (ed. G. C. Levy), Vol. 3, p. 283, Wiley-Interscience, New York, 1979.
11. D. A. Torchia and D. L. VanderHart, "High-Power Double-Resonance Studies of Fibrous Proteins, Proteoglycans, and Model Membranes", in *Topics in Carbon-13 NMR Spectroscopy* (ed. G. C. Levy), Vol. 3, p. 325, Wiley-Interscience, New York, 1979.
12. N. Boden, "NMR Studies of Plastic Crystals", in *The Plastically Crystalline State* (ed. J. N. Sherwood), p. 147, John Wiley and Sons, New York, 1979.
13. F. P. Miknis, V. J. Bartuska and G. E. Maciel, *Amer. Lab.*, 1979, Nov., 19.
14. J. R. Lyerla, "High Resolution Carbon-13 NMR Studies of Bulk Polymers", in *Contemporary Topics in Polymer Science* (ed. M. Shen), Vol. 3, p. 143, Plenum Publishing Corp., New York, 1979.
15. J. R. Lyerla, "High Resolution Nuclear Magnetic Resonance Spectroscopy of Macromolecules", to be published.
16. J. Schaefer, E. O. Stejskal, M. D. Sefcik and R. A. McKay, *Phil. Trans. Roy. Soc.*, 1981, *A299*, 475.
17. A. N. Garroway, D. L. VanderHart and W. L. Earl, *Phil. Trans. Roy. Soc.*, 1981, *A299*, 609.
18. G. E. Balimann, C. J. Groombridge, R. K. Harris, K. J. Packer, B. J. Say and S. F. Tanner, *Phil. Trans. Roy. Soc.*, 1981, *A299*, 643.

19. S. J. Opella, J. G. Hexem, M. H. Frey and T. A. Cross, *Phil. Trans. Roy. Soc.*, 1981, *A***299**, 665.
20. B. C. Gerstein, "High Resolution Nuclear Magnetic Resonance of Solids", in *Magnetic Resonance in Colloid and Interface Science* (ed. J. P. Fraissard and H. A. Resing), p. 175, Reidel Publishing Company, 1980.
21. J. A. Pople, W. G. Schneider and H. J. Bernstein, *High Resolution Nuclear Magnetic Resonance*, McGraw-Hill, New York, 1959.
22. A. Abragam, *The Principles of Nuclear Magnetism*, Oxford University Press, London, 1961.
23. J. W. Emsley, J. Feeney and L. H. Sutcliffe, *High Resolution NMR Spectroscopy*, Pergamon Press, Oxford, 1965.
24. A. Carrington and A. D. McLachlan, *Introduction to Magnetic Resonance*, Harper and Row, New York, 1967.
25. R. K. Harris and B. E. Mann (eds), *NMR and the Periodic Table*, Academic Press, London, 1978.
26. E. D. Becker, *High Resolution NMR—Theory and Chemical Applications*, 2nd Edn, Academic Press, New York, 1980.
27. C. P. Slichter, *Principles of Magnetic Resonance*, 2nd Edn, Springer, Berlin, 1978.
28. T. C. Farrar and E. D. Becker, *Pulse and Fourier Transform NMR*, Academic Press, New York, 1971.
29. D. Shaw, *Fourier Transform NMR Spectroscopy*, Elsevier, Amsterdam, 1976.
30. M. L. Martin, J.-J. Delpuech and G. S. Martin, *Practical NMR Spectroscopy*, Heyden, London, 1980.
31. H. Mantsch, H. Saitó and I. C. P. Smith, *Progr. NMR Spectroscopy*, 1977, **11**, 211.
32. J. M. Lehn and J. P. Kintzinger, in *Nitrogen NMR* (ed. M. Witanowski and G. A. Webb), p. 79, Plenum, London, 1973.
33. E. A. C. Lucken, *Nuclear Quadrupole Coupling Constants*, Academic Press, London, 1969.
34a. J. A. S. Smith (ed.), *Advances in Nuclear Quadrupole Resonance*, Heyden, London: Vol. 1, 1974; Vol. 2, 1975; Vol. 3, 1977.
34b. K. B. Dillon, "Nuclear Quadrupole Resonance Spectroscopy", in *Spectroscopic Properties of Inorganic and Organometallic Compounds*, Specialist Periodical Reports (ed. D. M. Adams and E. A. V. Ebsworth), p. 159, Royal Society of Chemistry, London, 1980.
35. R. G. Griffin, G. Bodenhausen, R. A. Haberkorn, T. H. Huang, M. Munowitz, R. Osredkar, D. J. Ruben, R. E. Stark and H. van Willigen, *Phil. Trans. Roy. Soc.*, 1981, *A***299**, 475.
36. W. S. Veeman, *Phil. Trans. Roy. Soc.*, 1981, *A***299**, 475.
37. J. A. Weil, T. Buch and J. E. Clapp, *Adv. Magn. Resonance*, 1973, **6**, 183.
38. R. Ditchfield and P. D. Ellis, "Theory of $^{13}$C Chemical Shifts", in *Topics in Carbon-13 NMR Spectroscopy* (ed. G. C. Levy), Vol. 1, p. 1, Wiley-Interscience, New York, 1974.
39. K. A. K. Ebraheem and G. A. Webb, *Progr. NMR Spectroscopy*, 1977, **11**, 149.
40. B. R. Appleman and B. P. Dailey, *Adv. Magn. Resonance*, 1974, **7**, 231.
41. B. A. Pettitt, *J. Magn. Resonance*, 1979, **34**, 247.
42. G. Sinning, M. Mehring and A. Pines, *Chem. Phys. Lett.*, 1976, **43**, 382.
43. M. Mehring and G. Sinning, *Phys. Rev. (B)*, 1977, **15**, 2519.
44. S. R. Hartmann and E. L. Hahn, *Bull. Amer. Phys. Soc.*, 1960, **5**, 498.
45. S. R. Hartmann and E. L. Hahn, *Phys. Rev.*, 1962, **128**, 2042.
46. F. M. Lurie and C. P. Slichter, *Phys. Rev. (A)*, 1964, **133**, 1108.
47. H. E. Bleich and A. G. Redfield, *J. Chem. Phys.*, 1977, **67**, 5040.
48. A. Pines, M. G. Gibby and J. S. Waugh, *J. Chem. Phys.*, 1973, **59**, 569.
49. D. E. Demco, J. Tegenfeldt and J. S. Waugh, *Phys. Rev. (B)*, 1975, **11**, 4133.

50. T. A. Cross, J. A. DiVerdi, W. B. Wise and S. J. Opella, in *NMR and Biochemistry*, p. 67, Dekker, New York, 1979.
51. J. Dart, D. P. Burum and W. K. Rhim, *Rev. Sci. Instr.*, 1980, **51**, 224.
52. D. J. Adduci and B. C. Gerstein, *Rev. Sci. Instr.*, 1979, **50**, 1403.
53. J. W. M. van Os and W. S. Veeman, *Rev. Sci. Instr.*, 1979, **50**, 445.
54. R. G. Pratt and J. L. Ackerman, *J. Magn. Resonance*, 1980, **41**, 140.
55. M. Linder, A. Höhener and R. R. Ernst, *J. Magn. Resonance*, 1979, **35**, 379.
56. M. E. Stroll, *Rev. Sci. Instr.*, 1981, **52**, 391.
57. I. J. Lowe, *Phys. Rev. Lett.*, 1959, **2**, 285.
58. E. R. Andrew, A. Bradbury and R. G. Eades, *Nature*, 1958, **182**, 1659.
59. J. Mason, *Adv. Inorg. Chem. Radiochem.*, (a) 1978, **21**, 197; (b) 1979, **22**, 199.
60. W. T. Raynes, in *Nuclear Magnetic Resonance* (ed. R. J. Abraham), Specialist Periodical Reports, Vol. 8, p. 1, Royal Society of Chemistry, London, 1979.
61. C. J. Jameson and J. Mason, in *Nuclear Magnetic Resonance* (ed. G. A. Webb), Specialist Periodical Reports, Vol. 9, p. 1, Royal Society of Chemistry, London, 1980.
62. C. J. Jameson, *Bull. Magn. Resonance*, 1980, **3**, 3.
63. E. R. Andrew, *Phil. Trans. Roy. Soc.*, 1981, *A***299**, 506.
64. G. M. Kosolapoff and L. Marer, *Organic Phosphorus Compounds*, Vol. 1, Wiley-Interscience, New York, 1972.
65. R. K. Hester, J. L. Ackerman, V. R. Cross and J. S. Waugh, *Phys. Rev. Lett.*, 1975, **34**, 993.
66. J. S. Waugh, *Proc. Nat. Acad. Sci. USA*, 1976, **73**, 1394.
67. E. F. Rybaczewski, B. L. Neff, J. S. Waugh and J. S. Sherfinski, *J. Chem. Phys.*, 1977, **67**, 1231.
68. H. van Willigen, R. G. Griffen and R. A. Haberkorn, *J. Chem. Phys.*, 1977, **67**, 5855.
69. M. Linder, A. Höhener and R. R. Ernst, *J. Chem. Phys.*, 1980, **73**, 4959.
70. M. G. Munowitz, R. G. Griffen, G. Bodenhausen and T. H. Huang, *J. Amer. Chem. Soc.*, 1981, **103**, 2529.
71. R. A. Haberkorn, R. E. Stark, H. van Willigen and R. G. Griffen, *J. Amer. Chem. Soc.*, 1981, **103**, 2534.
72. J. R. Lyerla, *Contemporary Topics in Polymer Science* (ed. M. Shen), Vol. 3, p. 191, Plenum, New York, 1979.
73. B. Schneider, D. Doskočilová, J. Babka and Z. Ružička, *J. Magn. Resonance*, 1980, **37**, 41.
74. W. L. Earl and D. L. VanderHart, *Macromolecules*, 1981, **14**, 570.
75. G. Engelhardt, U. Lohse, E. Lippmaa, M. Tarmak and M. Mägi, *Z. Anorg. Allg. Chem.*, in the press.
76. J. M. Thomas, L. A. Bursill, E. A. Lodge, A. K. Cheetham and C. A. Fyfe, *J. Chem. Soc. Chem. Commun.*, 1981, 276.
77. E. Lippmaa, M. Alla and T. Tuheim, in *Proceedings of the XIXth Congress Ampere*, p. 113, Groupement Ampere, Heidelberg/Geneva, 1976.
78. E. O. Stejskal, J. Schaefer and R. A. McKay, *J. Magn. Resonance*, 1977, **25**, 569.
79. M. Maricq and J. S. Waugh, *Chem. Phys. Lett.*, 1977, **47**, 327.
80. J. S. Waugh, M. Maricq and R. Cantor, *J. Magn. Resonance*, 1978, **29**, 183.
81. M. M. Maricq and J. S. Waugh, *J. Chem. Phys.*, 1979, **70**, 3300.
82. J. Herzfeld and A. E. Berger, *J. Chem. Phys.*, 1980, **73**, 6021.
83. R. E. Taylor, R. G. Pembleton, L. M. Ryan and B. C. Gerstein, *J. Chem. Phys.*, 1979, **71**, 4541.
84. P. D. Murphy, T. Taki, B. C. Gerstein, P. M. Henrichs and D. J. Massa, submitted for publication.
85. J. Tegenfeldt and U. Haeberlen, *J. Magn. Resonance*, 1979, **36**, 453.

86. S. J. Opella and M. H. Frey, *J. Amer. Chem. Soc.*, 1979, **101**, 5854.
87. D. A. Torchia, *J. Magn. Resonance*, 1978, **30**, 613.
88. W. L. Earl and D. L. VanderHart, *Macromolecules*, 1979, **12**, 762.
89. E. O. Stejskal, J. Schaefer and T. R. Steger, *Faraday Soc. Symp.*, 1979, **13**, 56.
90. A. N. Garroway, W. B. Moniz and H. A. Resing, *Faraday Soc. Symp.*, 1979, **13**, 63.
91. A. N. Garroway, W. B. Moniz and H. A. Resing, in *Carbon-13 NMR in Polymer Science*, Amer. Chem. Soc. Symposium Series, No. 103 (ed. W. M. Pasika), p. 67, 1979.
92. D. L. VanderHart and A. N. Garroway, *J. Chem. Phys.*, 1979, **71**, 2773.
93. V. J. Bartuska and G. E. Maciel, *J. Magn. Resonance*, 1981, **42**, 312.
94. K. W. Zilm, D. W. Alderman and D. M. Grant, *J. Magn. Resonance*, 1978, **30**, 563.
95. S. J. Opella, M. H. Frey and J. A. DiVerdi, *J. Magn. Resonance*, 1980, **37**, 165.
96. C. A. Fyfe, H. Mossbruger and C. S. Yannoni, *J. Magn. Resonance*, 1979, **36**, 61.
97. G. Balimann, M. J. S. Burgess, R. K. Harris, A. G. Oliver, K. J. Packer, B. J. Say, S. F. Tanner, R. W. Blackwell, L. W. Brown, A. Bunn, M. E. A. Cudby and J. W. Eldridge, *Chem. Phys.*, 1980, **46**, 469.
98. D. J. Burton, R. K. Harris and L. H. Merwin, *J. Magn. Resonance*, 1980, **39**, 159.
99. P. A. S. van Dijk, W. Schut, J. W. M. van Os, E. M. Menger and W. S. Veeman, *J. Phys. (E) Sci. Instr.*, 1980, **13**, 1309.
100. G. R. Hayes, R. Huis and A. D. H. Clague, *Bull. Magn. Resonance*, 1981, **2**, 120.
101. R. D. Kendrick, R. A. Wind and C. S. Yannoni, *J. Magn. Resonance*, 1980, **40**, 585.
102. P. Mansfield, *Phil. Trans. Roy. Soc.*, 1981, *A*299, 479.
103. U. Haeberlen, *Phil. Trans. Roy. Soc.*, 1981, *A*299, 497.
104. B. C. Gerstein, *Phil. Trans. Roy. Soc.*, 1981, *A*299, 521.
105. M. E. Stoll, *Phil. Trans. Roy. Soc.*, 1981, *A*299, 565.
106. J. B. Stothers, *Carbon-13 NMR Spectroscopy*, Academic Press, New York, 1972.
107. G. C. Levy and G. L. Nelson, *Carbon-13 NMR for Organic Chemists*, Wiley-Interscience, New York, 1972.
108. A. Pines, M. G. Gibby and J. S. Waugh, *J. Chem. Phys.*, 1972, **56**, 1776.
109. P. K. Grannell, P. Mansfield and M. A. B. Whitaker, *Phys. Rev. (B)*, 1973, **8**, 4149.
110. G. C. Levy, R. L. Lichter and G. L. Nelson, *Carbon-13 Nuclear Magnetic Resonance Spectroscopy*, 2nd Edn, Wiley-Interscience, New York, 1980.
111. D. E. Wemmer, A. Pines and D. D. Whitehurst, *Phil. Trans. Roy. Soc.*, 1981, *A*300, 15.
112. D. L. VanderHart, *J. Chem. Phys.*, 1976, **64**, 830.
113. K. W. Zilm, R. T. Conlin, D. M. Grant and J. Michl, *J. Amer. Chem. Soc.*, 1978, **100**, 8038.
114. K. W. Zilm, R. T. Conlin, D. M. Grant and J. Michl, *J. Amer. Chem. Soc.*, 1980, **102**, 6672.
115. D. E. Wemmer and A. Pines, *J. Amer. Chem. Soc.*, 1981, **103**, 34.
116. A. A. V. Gibson, T. A. Scott and E. Fukushima, *J. Magn. Resonance*, 1977, **27**, 29.
117. T. M. Duncan, J. T. Yates, and R. W. Vaughan, *J. Chem. Phys.*, 1979, **71**, 3129.
118. T. M. Duncan, J. T. Yates, and R. W. Vaughan, *J. Chem. Phys.*, 1980, **73**, 975.
119. A. Naito, S. Ganapathy, K. Akasaka and C. A. McDowell, *J. Chem. Phys.*, 1981, **74**, 3190.
120. I. D. Gay, *J. Phys. Chem.*, 1980, **84**, 3230.
121. E. T. Lippmaa, M. A. Alla, T. J. Pehk and G. Engelhardt, *J. Amer. Chem. Soc.*, 1978, **100**, 1929.
122. M. J. Begley, unpublished, 1980.
123. R. D. Kendrick, C. S. Yannoni, R. Aikman and R. J. Lagow, *J. Magn. Resonance*, 1980, **37**, 555.
124. W. McFarlane, *Proc. Roy. Soc.*, 1968, *A*306, 185.
125. L. A. Fedorov, A. A. Stumbrevichyute and E. I. Fedin, *Zh. Strukt. Khim.*, 1974, **15**, 1063.

126. (a) D. L. VanderHart, W. L. Earl and A. N. Garroway, *J. Magn. Resonance*, 1981, **44**, 361. (b) D. L. VanderHart, *J. Magn. Resonance*, 1981, **44**, 117.
127. E. Kundla and M. Alla, *Proc. 20th Congress Ampere* (Tallinn), p. 92, Springer Verlag, Berlin, 1979.
128. D. Suwelack, W. P. Rothwell and J. S. Waugh, *J. Chem. Phys.*, 1980, **73**, 2559.
129. N. G. Parsonage and L. A. K. Staveley, *Disorder in Crystals*, Clarendon Press, Oxford, 1978.
130. S. Chang and E. F. Westrum, *J. Phys. Chem.*, 1960, **64**, 1547.
131. H. A. Resing, *Mol. Cryst. Liq. Cryst.*, 1969, **9**, 101.
132. R. E. Wasylishen and B. A. Pettitt, *Canad. J. Chem.*, 1980, **58**, 655.
133. M. Bee, J. P. Amoureux and R. E. Lechner, *Mol. Phys.*, 1980, **40**, 617.
134. A. Pines and T. W. Shattuck, *J. Chem. Phys.*, 1974, **61**, 1255.
135. A. Abragam and J. Winter, *Compt. Rend.*, 1959, **249**, 1633.
136. E. O. Stejskal, J. Schaefer and J. S. Waugh, *J. Magn. Resonance*, 1977, **28**, 105.
137. A. N. Garroway, *J. Magn. Resonance*, 1977, **28**, 365.
138. A. N. Garroway, *J. Magn. Resonance*, 1979, **34**, 283.
139. W. P. Rothwell and J. S. Waugh, *J. Chem. Phys.*, 1981, **74**, 2721.
140. J. D. Graham and J. S. Darby, *J. Magn. Resonance*, 1976, **23**, 369.
141. L. K. Kimtys, D. W. Aksnes and T. Gramstad, *Mol. Phys.*, 1979, **38**, 993.
142. T. Hasebe, N. Nakamura and H. Chihara, *Bull. Chem. Soc. Japan*, 1980, **53**, 896.
143. L. L. Kimtys, *Mol. Cryst. Liq. Cryst. Lett.*, 1979, **56**, 83.
144. M. Alla and E. Lippmaa, *Chem. Phys. Lett.*, 1976, **37**, 260.
145. R. E. Wasylishen and M. R. Graham, *Mol. Cryst. Liq. Cryst. Lett.*, 1979, **49**, 225.
146. N. Chatterjee, *J. Magn. Resonance*, 1979, **33**, 241.
147. R. E. Wasylishen and B. A. Pettitt, *Mol. Phys.*, 1978, **36**, 1459.
148. B. A. Pettitt and R. E. Wasylishen, *Chem. Phys. Lett.*, 1979, **63**, 539.
149. B. A. Pettitt, R. E. Wasylishen, R. Y. Dong and T. P. Pitner, *Canad. J. Chem.*, 1978, **56**, 2576.
150. R. E. Wasylishen, P. F. Barron and D. M. Doddrell, *Austral. J. Chem.*, 1979, **32**, 905.
151. R. E. Wasylishen, B. A. Pettitt and R. Y. Dong, *J. Chem. Soc. Faraday II*, 1980, **76**, 571.
152. R. E. Wasylishen and K. J. Friesen, *Org. Magn. Resonance*, 1980, **13**, 343.
153. J. Virlet and D. Chesquieres, *Chem. Phys. Lett.*, 1980, **73**, 323.
154. N. E. Heimer, *Mol. Cryst. Liq. Cryst.*, 1980, **62**, 59.
155. R. E. Wasylishen, B. A. Pettitt and J. S. Lewis, *Chem. Phys. Lett.*, 1979, **67**, 459.
156. R. E. Wasylishen, B. A. Pettitt and K. R. Jeffrey, *J. Chem. Phys.*, 1981, **74**, 6022.
157. J. R. Lyerla, C. A. Fyfe and C. S. Yannoni, *J. Amer. Chem. Soc.*, 1979, **101**, 1351.
158. D. E. Wemmer, D. J. Ruben and A. Pines, *J. Amer. Chem. Soc.*, 1981, **103**, 28.
159. R. D. Miller and C. S. Yannoni, *J. Amer. Chem. Soc.*, 1980, **102**, 7396.
160. W-I. Shiau, E. N. Duesler, I. C. Paul, D. Y. Curtin, W. G. Blann and C. A. Fyfe, *J. Amer. Chem. Soc.*, 1980, **102**, 4546.
161. C. A. Fyfe and R. E. Wasylishen, to be published.
162. J. R. Lyerla, C. S. Yannoni, D. Bruck and C. A. Fyfe, *J. Amer. Chem. Soc.*, 1979, **101**, 4770.
163. P. C. Myhre and C. S. Yannoni, *J. Amer. Chem. Soc.*, 1981, **103**, 230.
164. C. J. Groombridge, R. K. Harris, K. J. Packer, B. J. Say and S. F. Tanner, *J. Chem. Soc. Chem. Commun.*, 1980, 174.
165. M. H. Frey and S. J. Opella, *J. Chem. Soc. Chem. Commun.*, 1980, 474.
166. J. G. Hexem, M. H. Frey and S. J. Opella, *J. Amer. Chem. Soc.*, 1981, **103**, 224.
167. N. Zumbulyadis, P. M. Henrichs and R. H. Young, *J. Chem. Phys.*, 1981, **75**, 1603.
168. H. W. Spiess, U. Haeberlen and H. Zimmermann, *J. Magn. Resonance*, 1977, **25**, 55.
169. D. Michel, *Surf. Sci.*, 1974, **42**, 453.

170. J. F. Kriz and I. D. Gay, *J. Phys. Chem.*, 1976, **80**, 2951.
171. D. Michel, W. Meiler and H. Pfeifer, *J. Mol. Catalysis*, 1975/76, **1**, 85.
172. E. G. Derouane, J.-P. Gilson and J. B. Nagy, *J. Mol. Catalysis*, 1981, **10**, 331.
173. H. A. Resing and C. G. Wade (eds), *Magnetic Resonance in Colloid and Interface Science*, Amer. Chem. Soc. Symposium Series, No. 34, Washington, D.C., 1976.
174. J. P. Fraissard and H. A. Resing (eds), *Magnetic Resonance in Colloid and Interface Science*, Reidel Publishing Company, 1980.
175. H. A. Resing and D. Slotfeldt-Ellingsen, *J. Magn. Resonance*, 1981, **38**, 401.
176. D. Slotfeldt-Ellingsen and H. A. Resing, *J. Phys. Chem.*, 1980, **84**, 2204.
177. H. A. Resing, D. Slotfeldt-Ellingsen, A. N. Garroway, D. C. Weber, T. J. Pinnavaia and K. Unger, in *Magnetic Resonance in Colloid and Interface Science*, p. 239, 1980.
178. D. Deininger, D. Michel and D. Heidrich, *Surf. Sci.*, 1980, **100**, 541.
179. J. Tabony, *Progr. NMR Spectroscopy*, 1980, **14**, 1.
180. B. A. Cornell, *Chem. Phys. Lett.*, 1980, **72**, 462.
181. B. A. Cornell and G. W. Francis, *J. Magn. Resonance*, 1980, **41**, 175.
182. B. A. Cornell, M. Keniry, R. G. Hiller and R. Smith, *FEBS Lett.*, 1980, **115**, 134.
183. B. A. Cornell, *Chem. and Phys. Lipids*, 1981, **28**, 69.
184. R. J. Wittebort, C. F. Schmidt and R. G. Griffin, *Biochemistry*, in the press.
185. T. R. Steger, E. O. Stejskal, R. A. McKay, B. Ray-Stults and J. Schaefer, *Tetrahedron Lett.*, 1979, 295.
186. H. D. Hill, A. P. Zens and J. Jacobus, *J. Amer. Chem. Soc.*, 1979, **101**, 7090.
187. B. Pedersen, *Bull. Magn. Resonance*, 1981, **2**, 230.
188. J. Hvoslef and B. Pedersen, *Acta Chem. Scand.*, 1979, *B***33**, 503.
189. K. W. Zilm, D. M. Grant, E. Englert, and R. C. Straight, *Biochem. Biophys. Res. Commun.*, 1980, **93**, 857.
190. J. A. Ripmeester, *Chem. Phys. Lett.*, 1980, **74**, 536.
191. J. A. Ripmeester, R. E. Hawkins and D. W. Davidson, *J. Chem. Phys.*, 1979, **71**, 1889.
192. A. Pines, M. G. Gibby and J. S. Waugh, *Chem. Phys. Lett.*, 1972, **15**, 373.
193. J. Schaefer and E. O. Stejskal, *J. Amer. Chem. Soc.*, 1976, **98**, 1031.
194. W. W. Fleming, C. A. Fyfe, R. D. Kendrick, J. R. Lyerla, H. Vanni and C. S. Yannoni, in *Polymerization Characterization by ESR and NMR* (ed. A. E. Woodward and F. A. Bovey), Amer. Chem. Soc. Series, No. 142, p. 193, 1980.
195. D. L. VanderHart and A. N. Garroway, *J. Chem. Phys.*, 1979, **71**, 2772.
196. M. D. Sefcik, J. Schaefer, E. O. Stejskal and R. A. McKay, *Macromolecules*, 1980, **13**, 1132.
197. T. R. Steger, J. Schaefer, E. O. Stejskal and R. A. McKay, *Macromolecules*, 1980, **13**, 1127.
198. W. S. Veeman, E. M. Menger, W. Ritchey and E. deBoer, *Macromolecules*, 1979, **12**, 924.
199. W. S. Veeman and E. M. Menger, *Bull. Magn. Resonance*, 1981, **2**, 77.
200. J. Schaefer, M. D. Sefcik, E. O. Stejskal and R. A. McKay, *Macromolecules*, 1981, **14**, 188.
201. E. O. Stejskal, J. Schaefer, M. D. Sefcik and R. A. McKay, *Macromolecules*, 1981, **14**, 275.
202. J. Schaefer, M. D. Sefcik, E. O. Stejskal and R. A. McKay, *Macromolecules*, 1981, **14**, 280.
203. J. Schaefer, in *Topics in* [13]*C NMR Spectroscopy* (ed. G. C. Levy), Vol. 1, p. 149, Wiley-Interscience, New York, 1974.
204. D. A. Wright, D. E. Axelson and G. C. Levy, in *Topics in* [13]*C NMR Spectroscopy* (ed. G. C. Levy), Vol. 3, p. 103, Wiley-Interscience, New York, 1979.
205. L. Mandelkern, Division of Polymer Chem., Inc., Papers presented at the Atlanta meeting, Vol. 12, p. 276, 1981.

206. O. W. Howarth, *J. Chem. Soc., Faraday II*, 1980, **76**, 1219.
207. D. L. VanderHart, *Macromolecules*, 1979, **12**, 1232.
208. A. Bunn, M. E. A. Cudby, R. K. Harris, K. J. Packer and B. J. Say, *J. Chem. Soc., Chem. Commun.*, 1981, 15.
209. H. A. Resing, D. Slotfeld-Ellingsen, A. N. Garroway, D. C. Weber, T. J. Pinnavia and K. Unger, in *Magnetic Resonance in Colloid and Interface Science* (ed. J. P. Fraissard and H. A. Resing), p. 239, Reidel Publishing Company, 1980.
210. P. Corradini, G. Natta, P. Ganis and P. A. Temussi, *J. Polymer Sci.*, 1967, **C16**, 2477.
211. C. A. Fyfe, A. Rudin and W. Tchir, *Macromolecules*, 1980, **13**, 1320.
212. W. W. Fleming, C. A. Fyfe, J. R. Lyerla, H. Vanni and C. S. Yannoni, *Macromolecules*, 1980, **13**, 460.
213. S. J. Opella, M. H. Frey and T. A. Cross, *J. Amer. Chem. Soc.*, 1979, **101**, 5856.
214. G. E. Maciel, M. P. Shatlock, R. A. Houtchens and W. S. Caughey, *J. Amer. Chem. Soc.*, 1980, **102**, 6884.
215. M. A. Hemminga, W. S. Veeman, H. W. M. Hilhorst and T. J. Schaafsma, *Bull. Magn. Resonance*, 1981, **2**, 344.
216. V. Rutar, R. Blinc and L. Ehrenberg, *J. Magn. Resonance*, 1980, **40**, 225.
217. J. W. H. Sutherland, W. Egan, A. N. Schechter and D. A. Torchia, *Biochemistry*, 1979, **18**, 1797.
218. J. D. Termine and D. A. Torchia, *Biopolymers*, 1980, **19**, 741.
219. L. W. Jelinski and D. A. Torchia, *J. Mol. Biol.*, 1979, **133**, 45.
220. R. H. Atalla and S. C. Nagel, *Science*, 1974, **185**, 522.
221. R. H. Atalla and B. E. Dimick, *Carbohydrate Res.*, 1975, **39**, C1.
222. R. H. Atalla, J. C. Gast, D. W. Sindorf, V. J. Bartuska and G. E. Maciel, *J. Amer. Chem. Soc.*, 1980, **102**, 3249.
223. W. K. Earl and D. L. VanderHart, *J. Amer. Chem. Soc.*, 1980, **102**, 3251.
224. R. L. Dudley, C. A. Fyfe and coworkers, unpublished.
225. L. D. Hall and M. Yalpani, *Carbohydrate Res.*, 1981, **91**, C1.
226. R. L. Dudley, C. A. Fyfe and coworkers, unpublished.
227. P. G. Hatcher, I. A. Breger, N. M. Szeverenyi and G. E. Maciel, *Org. Geochem.*, in the press.
228. P. G. Hatcher, R. Rowan and M. A. Mattingly, *Org. Geochem.*, 1980, **2**, 77.
229. P. G. Hatcher, D. L. VanderHart and W. L. Earl, *Org. Geochem.*, 1980, **2**, 87.
230. P. F. Barron, M. A. Wilson, J. F. Stephens, B. A. Cornell and K. R. Tate, *Nature*, 1980, **286**, 585.
231. P. F. Barron and M. A. Wilson, *Nature*, 1981, **289**, 275.
232. L. Petrakis and D. W. Grandy, *J. Chem. Educ.*, 1980, **57**, 689.
233. M. Morita, *J. Chem. Educ.*, 1980, **57**, 695.
234. H. L. Retcofsky and T. A. Link, "High Resolution $^1$H, $^2$H, and $^{13}$C NMR in Coal Research", Chapter 24 in *Analytical Methods for Coal and Coal Products* (ed. C. Karr), Vol. II, Academic Press, New York, 1978.
235. B. C. Gerstein, "Fingerprinting Solid Coals Using Pulse and Multiple Pulse Nuclear Magnetic Resonance", Chapter 51 in *Analytical Methods for Coal and Coal Products* (ed. C. Karr), Vol. III, Academic Press, New York, 1978.
236. L. Petrakis and E. Edelheit, *Appl. Spectroscopy Rev.*, 1979, **15**, 195.
237. F. P. Miknis and G. E. Maciel, "Applications of Nuclear Magnetic Resonance to Oil Shale Evaluation and Processing", from Proceedings of ANS/ACS Topical Conference on Atomic and Nuclear Methods for Fossil Energy Research, Mayaguez, Puerto Rico, Dec. 1–4, 1980, Plenum Press, to be published.
238. V. J. Bartuska, G. E. Maciel, J. Schaefer and E. O. Stejskal, *Fuel*, 1977, **56**, 354.
239. R. L. Dudley and C. A. Fyfe, unpublished results.
240. H. A. Resing, A. N. Garroway and R. N. Hazlett, *Fuel*, 1978, **57**, 450.

241. G. E. Maciel, V. J. Bartuska and F. P. Miknis, *Fuel*, 1978, **57**, 505.
242. K. W. Zilm, R. J. Pugmire, D. M. Grant, R. E. Wood and W. H. Wiser, *Fuel*, 1979, **58**, 11.
243. G. E. Maciel, V. J. Bartuska and F. P. Miknis, *Fuel*, 1979, **58**, 155.
244. G. E. Maciel, V. J. Bartuska and F. P. Miknis, *Fuel*, 1979, **58**, 391.
245. D. Vučelić, N. Juranić and D. Vitorović, *Fuel*, 1979, **58**, 759.
246. F. P. Miknis, G. E. Maciel and V. J. Bartuska, *Org. Geochem.*, 1979, **1**, 169.
247. M. T. Melchior, K. D. Rose and F. P. Miknis, *Fuel*, 1980, **59**, 594.
248. J. A. MacPhee and B. N. Nandi, *Fuel*, 1981, **60**, 169.
249. F. P. Miknis, M. Sullivan, V. J. Bartuska and G. E. Maciel, *Org. Geochem.*, 1981, **3**, 19.
250. T. Taki, T. Sogabo, P. D. Murphy and B. C. Gerstein, *Fuel*, submitted.
251. P. D. Murphy, T. J. Cassady, W. S. Trahanovsky and B. C. Gerstein, *Fuel*, submitted.
252. P. D. Murphy, T. J. Cassady and B. C. Gerstein, *Fuel*, submitted.
253. D. L. VanderHart and H. L. Retcofsky, *Fuel*, 1976, **55**, 202.
254. H. Marsmann, "$^{29}$Si NMR Spectroscopic Results", in *NMR Basic Principles and Progress*, Vol. 17, p. 65 (ed. P. Diehl, E. Fluck and R. Kosfeld), Springer Verlag, New York, 1981.
255. E. A. Williams and J. D. Cargioli, *Ann. Reports NMR Spectroscopy*, 1979, **9**, 221.
256. J. Schraml and J. M. Bellama, "$^{29}$Si Nuclear Magnetic Resonance", in *Determination of Organic Structure by Physical Methods*, Vol. 6, p. 203 (ed. F. C. Nachod, J. J. Zuckerman and E. W. Randall), Academic Press, New York, 1976.
257. M. G. Gibby, A. Pines and J. S. Waugh, *J. Amer. Chem. Soc.*, 1972, **94**, 6231.
258. A.-R. Grimmer, R. Peter, E. Fechner and G. Molgedey, *Chem. Phys. Lett.*, 1981, **77**, 331.
259. E. T. Lippmaa, A. A. Madis, T. J. Pehk and G. Engelhardt, *J. Amer. Chem. Soc.*, 1978, **100**, 1929.
260. G. E. Maciel and D. W. Sindorf, *J. Amer. Chem. Soc.*, 1980, **102**, 7607.
261. H. C. Marsmann, *Z. Naturforsch.*, 1974, *B***29**, 495.
262. G. E. Maciel, D. W. Sindorf and V. J. Bartuska, *J. Chromatogr.*, 1981, **205**, 438.
263. E. Lippmaa, M. Mägi, A. Samoson, G. Engelhardt and A.-R. Grimmer, *J. Amer. Chem. Soc.*, 1980, **102**, 4889.
264. L. V. C. Rees, *Nature*, 1980, **286**, 204.
265. G. Engelhardt, D. Kunath, A. Samoson, M. Tarmak, and M. Mägi, Workshop on Adsorption of Hydrocarbons in Zeolites, Berlin-Adlershof, 19–20 Nov., 1979.
266. W. Loewenstein, *Amer. Mineral.*, 1954, **39**, 92.
267. S. Ramdas, J. M. Thomas, J. Klinowski, C. A. Fyfe and J. S. Hartman, submitted for publication.
268. (a) J. M. Thomas, C. A. Fyfe, S. Ramdas, J. Klinowski and G. C. Gobbi, to be published. (b) M. T. Melchior, D. E. W. Vaughan, R. H. Jarman and A. J. Jacobson, *Nature*, submitted.
269. J. Klinowski, J. M. Thomas, M. Audier, S. Vasudevan, C. A. Fyfe and J. S. Hartman, *J. Chem. Soc., Chem. Commun.*, 1981, in press.
270. D. Hoebbel, G. Garzó, G. Engelhardt, R. Engelhardt, R. Ebert, E. Lippmaa and M. Alla, *Z. Anorg. Allg. Chem.*, 1980, **465**, 15.
271. J. A. Reimer, P. D. Murphy, B. C. Gerstein and J. C. Knights, *J. Chem. Phys.*, 1981, **74**, 1501.
272. M. M. Crutchfield, C. H. Dungan, J. H. Letcher, V. Mark and J. R. Van Wazer, in *Topics in Phosphorus Chemistry*, Vol. 5, p. 46 (ed. M. Grayson and E. J. Griffith), Interscience Publishing, 1967.
273. J. Nixon and A. Pidcock, *Ann. Reports NMR Spectroscopy*, 1969, **2**, 345.
274. J. R. Van Wazer, in *Determination of Organic Structures by Physical Methods* (ed. F. C. Nachod and J. J. Zuckerman), Vol. 4, p. 323, Academic Press, 1971.

275. G. Mavel, *Ann. Reports NMR Spectroscopy*, 1973, **5B**, 1.

276. J. R. Llinas, E.-J. Vincent and G. Peiffer, *Bull. Soc. Chim. France*, 1973, 3209.

277. P. S. Pregosin and R. W. Kunz, $^{31}P$ and $^{13}C$ *NMR of Transition Metal Phosphine Complexes*, Springer Verlag, Berlin, 1979.

278. I. K. O'Neill and C. P. Richards, *Ann. Reports NMR Spectroscopy*, 1980, **10A**, 133.

279. J. A. Davies, "Multinuclear Magnetic Resonance Methods in the Study of Organometallic Compounds", in *The Chemistry of the Metal-Carbon Bond* (ed. S. Patai and F. R. Hartley), Wiley-Interscience, New York, in press.

280. T. Terao and T. Hashi, *J. Phys. Soc. Japan*, 1974, **36**, 989.

281. H. W. Spiess, R. Grosescu and U. Haeberlen, *Chem. Phys.*, 1974, **6**, 226.

282. J. Herzfeld, R. G. Griffin and R. A. Haberkorn, *Biochemistry*, 1978, **17**, 2711.

283. W. P. Rothwell, J. S. Waugh and J. P. Yesinowski, *J. Amer. Chem. Soc.*, 1980, **102**, 2637.

284. T. Terao, S. Matsui and K. Akasaka, *J. Amer. Chem. Soc.*, 1977, **99**, 6136.

285. S. J. Kohler and M. P. Klein, *Biochemistry*, 1977, **16**, 519.

286. R. G. Griffin, *J. Amer. Chem. Soc.*, 1976, **98**, 851.

287. S. J. Opella, W. B. Wise and J. A. DiVerdi, *Biochemistry*, 1981, **20**, 284.

288. H. Shindo, J. D. McGhee and J. S. Cohen, *Biopolymers*, 1980, **19**, 523.

289. J. B. Robert and L. Wiesenfeld, *J. Magn. Resonance*, 1980, **38**, 357.

290. C. A. Fyfe and R. Wasylishen, unpublished results.

291. E. R. Andrew, D. J. Bryant, E. M. Cashell and B. A. Dunell, *Chem. Phys. Lett.*, 1981, **77**, 614.

292. A.-R. Grimmer, *Spectrochim. Acta*, 1978, **34A**, 941.

293. J. P. Dutasta, J. B. Robert and L. Wiesenfeld, *Chem. Phys. Lett.*, 1981, **77**, 336.

294. F. Ribas Prado, C. Giessner-Prettre, B. Pullman and J.-P. Daudey, *J. Amer. Chem. Soc.*, 1979, **101**, 1737.

295. R. G. Kidd and R. J. Goodfellow, in *NMR and the Periodic Table* (ed. R. K. Harris and B. E. Mann), p. 195, Academic Press, London, 1978.

296. E. R. Andrew and V. T. Wynn, *Proc. Roy. Soc.*, 1966, **A291**, 257.

297. H. Kessemeier and R. E. Norberg, *Phys. Rev.*, 1967, **155**, 321.

298. R. E. Andrew, A. Bradbury, R. G. Eades and G. J. Jenks, *Nature*, 1960, **188**, 1096.

299. R. E. Andrew, M. Firth, A. Jasinski and P. J. Randall, *Phys. Lett.*, 1970, **31A**, 446.

300. R. E. Andrew, S. Clough, L. F. Farnell, T. D. Gledhill and I. Roberts, *Phys. Lett.*, 1966, **19**, 6.

301. D. J. Burton, R. K. Harris and L. H. Merwin, *J. Magn. Resonance*, 1980, **39**, 159.

302. E. R. Andrew, W. S. Hinshaw and A. Jasinski, *Chem. Phys. Lett.*, 1974, **24**, 399.

303. Y. C. Leung, J. Waser, S. van Houten, A. Vos, G. A. Wiegers and E. H. Wiebenga, *Acta Cryst.*, 1957, **10**, 574.

304. H. W. Spiess, R. Grosescu and U. Haeberlen, *Chem. Phys.*, 1974, **6**, 226.

305. N. Boden and R. Folland, *Chem. Phys. Lett.*, 1971, **10**, 167.

306. N. Boden and R. Folland, *Chem. Phys. Lett.*, 1975, **32**, 127.

307. L. J. Burnet, R. M. Knowles, C. L. Rottler and S. A. Smiley, *J. Chem. Phys.*, 1978, **68**, 1988.

308. G. R. Miller, H. A. Resing, F. L. Vogel, A. Pron, T. C. Wu and D. Billaud, *J. Phys. Chem.*, 1980, **84**, 3333.

309. J. Herzfeld, A. Roufosse, R. A. Haberkorn, R. G. Griffin and M. J. Glimcher, *Phil. Trans. Roy. Soc.*, 1980, **B289**, 459.

310. J. W. Diesveld, E. M. Menger, H. T. Edzes and W. S. Veeman, *J. Amer. Chem. Soc.*, 1980, **102**, 7935.

311. G. E. Maciel, D. J. O'Donnell and R. Greaves, *Advances in Chemistry Series*, Amer. Chem. Soc., in the press.

312. L. Bemi, H. C. Clark, J. A. Davies, D. Drexler, C. A. Fyfe and R. Wasylishen, *J. Organometal. Chem.*, 1982, **224**, C9.
313. L. Bemi, H. C. Clark, J. A. Davies, C. A. Fyfe and R. E. Wasylishen, *J. Amer. Chem. Soc.*, 1982, **104**, 438.
314. R. J. Goodfellow, in *NMR and the Periodic Table* (ed. R. K. Harris and B. E. Mann), p. 261, Academic Press, London, 1978.
315. A. Nölle, *Z. Naturforsch.*, 1978, **33A**, 666.
316. H. Krüger, O. Lutz, A. Schwenk and G. Stricker, *Z. Physik*, 1974, **266**, 233.
317. T. T. P. Cheung, L. E. Worthington, P. DuBois Murphy and B. C. Gerstein, *J. Magn. Resonance*, 1980, **41**, 158.
318. P. H. Leligny and J. C. Monier, *Acta Cryst.*, 1974, **B30**, 305.
319. H. Lipson, *Proc. Roy. Soc.*, 1936, **A156**, 462.
320. J. J. H. Ackerman, T. V. Orr, V. J. Bartuska and G. E. Maciel, *J. Amer. Chem. Soc.*, 1979, **101**, 341.
321. P. G. Mennitt, M. P. Shatlock, V. J. Bartuska and G. E. Maciel, *J. Phys. Chem.*, 1981, **85**, 2087.
322. G. E. Maciel, L. Simeral and J. J. H. Ackerman, *J. Phys. Chem.*, 1977, **81**, 263.
323. G. E. Maciel, unpublished results.
324. P. Ellis, unpublished results.
325. G. C. Levy and R. L. Lichter, *Nitrogen-15 Nuclear Magnetic Resonance*, Wiley-Interscience, New York, 1979.
326. M. G. Gibby, R. G. Griffin, A. Pines and J. S. Waugh, *Chem. Phys. Lett.*, 1972, **17**, 80.
327. J. Schaefer, E. O. Stejskal and R. A. McKay, *Biochem. Biophys. Res. Commun.*, 1979, **88**, 274.
328. G. S. Jacob, J. Schaefer, E. O. Stejskal and R. A. McKay, *Biochem. Biophys. Res. Commun.*, 1980, **97**, 1176.
329. T. A. Skokut, J. E. Varner, J. Schaefer, E. O. Stejskal and R. A. McKay, *Pl. Physiol. Suppl.*, 1979, **63**, 46.
330. J. Schaefer, R. A. McKay and E. O. Stejskal, *J. Magn. Resonance*, 1979, **34**, 443.
331. J. L. Ackerman, R. Eckman and A. Pines, *Chem. Phys.*, 1979, **42**, 423.
332. R. Eckman, M. Alla and A. Pines, *J. Magn. Resonance*, 1980, **41**, 440.
333. R. Eckman, L. Muller and A. Pines, *Chem. Phys. Lett.*, 1980, **74**, 370.
334. L. Müller, R. Eckman and A. Pines, *Chem. Phys. Lett.*, 1980, **76**, 149.
335. L. Müller, *Chem. Phys.*, in press.
336. P. Brunner, M. Reinhold and R. R. Ernst, *J. Chem. Phys.*, 1980, **73**, 1086.
337. M. Reinhold, P. Brunner and R. R. Ernst, *J. Chem. Phys.*, 1981, **74**, 184.
338. D. Muller, W. Gessner, H. J. Behrens and G. Scheler, *Chem. Phys. Lett.*, 1981, **79**, 59.
339. C. A. Fyfe and coworkers, unpublished.
340. K. B. Dillon and T. C. Waddington, *Spectrochim. Acta*, 1974, **30A**, 1873.

# Calculations of Nuclear Spin–Spin Couplings

## JOZEF KOWALEWSKI

*Department of Physical Chemistry, Arrhenius Laboratory, University of Stockholm, S-106 91 Stockholm, Sweden*

## GLOSSARY OF ABBREVIATIONS

| | |
|---|---|
| AO | Atomic Orbital |
| ASO | Atomic Spin Orbital |
| APSG | Antisymmetrized Product of Separated Geminals |
| CDOE | Charge Dependent Orbital Exponents |
| CGTO | Contracted Gaussian Type Orbital |
| CHF | Coupled Hartree–Fock |
| CI | Configuration Interaction |
| CNDO | Complete Neglect of Differential Overlap |
| CVB-PT | Coupled Valence Bond Perturbation Theory |
| DPT | Double Perturbation Theory |
| EHT | Extended Hückel Theory |
| FC | Fermi Contact |
| FP-CI | Finite Perturbation–Configuration Interaction |
| FPM | Finite Perturbation Method |
| FPT | Finite Perturbation Theory |
| GTF | Gaussian Type Function |
| GTO | Gaussian Type Orbital |
| INDO | Intermediate Neglect of Differential Overlap |
| LCAO | Linear Combination of Atomic Orbitals |
| LCASO | Linear Combination of Atomic Spin Orbitals |
| MBPT | Many Body Perturbation Theory |
| MCCHF | Multiconfigurational Coupled Hartree–Fock |
| MO | Molecular Orbital |
| MOA | Maximum Overlap Approximation |
| MINDO | Modified INDO |
| NDDO | Neglect of Diatomic Differential Overlap |
| OB | Orbital (contribution to coupling constants) |
| REX | Relativistically parametrized Extended Hückel |
| SCF | Self-Consistent Field |
| SCPT | Self-Consistent Perturbation Theory |
| SD | Spin-Dipolar |
| SOPPA | Second-Order Polarization Propagator Approximation |
| SOS | Sum Over States |
| STO | Slater Type Orbital |
| TDHF | Time Dependent Hartree–Fock |
| UHF | Unrestricted Hartree–Fock |
| VB | Valence Bond |
| ZDO | Zero Differential Overlap |

# I. INTRODUCTION

Nuclear spin–spin couplings are important NMR parameters and are of considerable interest for both theoreticians and experimentalists. A great body of experimental data has been built up through the years, providing a basis for a stringent test of different theoretical approaches. Through the interplay of empirical correlations, theoretical interpretations, the

specification of more accurate empirical relationships, and so forth, spin–spin couplings have proven to be an invaluable source of experimental information about the nature of bonding and stereochemistry in solution.

The first successful theory of electron-mediated nuclear spin–spin coupling was formulated in 1953 by Ramsey[1] who also provided the first theoretical estimate of the coupling in the HD molecule. A few years later, simple computational schemes based on Ramsey's theory were suggested by McConnell[2] within the framework of the molecular orbital (MO) theory and by Karplus and Anderson[3] who used the valence bond (VB) method. In the mid-sixties Pople and Santry[4] presented a way to circumvent the most serious drawbacks of McConnell's formulation and laid the ground for one of the methods still in use today. In the late sixties, Pople and coworkers[5] established yet another milestone in the development of coupling theory by proposing the so-called FPT-INDO approach, which proved to be very useful in various fields of chemistry and biology. The development of computational methods as well as the application-oriented computational work of the period 1969–1975 has been reviewed.[6] More recent developments have been reviewed on an annual basis.[7] A brief account of the theory of nuclear spin–spin couplings can be found in a chapter by Webb.[8]

The purpose of the present review is to provide a complete follow-up of my review from 1977.[6] The structure of this review is similar to the previous one in the sense that it begins with a discussion of basic theory and computational methods. This is done in Sections II and III. What is new in these sections is an attempt to employ the SI system consistently in all equations. The layout of the following sections, which are devoted to applications, is different from that employed in 1977. The principal reason for the change is the dramatic increase in interest in couplings involving nuclei other than protons. Therefore the present review uses the nature of the coupled nuclei, rather than the number of bonds between nuclei, as the primary criterion for the section division. Section IV deals with proton–proton couplings, Section V with proton–other-nucleus couplings, Section VI with other couplings involving carbon, and Section VII with the remaining couplings. As in the 1977 review, this survey contains a "special topics" section (VIII). It closes with concluding remarks.

The nuclear spin–spin interaction energy in isotropic fluids can be written as:

$$E(NN') = hJ(NN')\mathbf{I}_N \cdot \mathbf{I}_{N'} \tag{1}$$

where $\mathbf{I}_N$ and $\mathbf{I}_{N'}$ are dimensionless nuclear spin operators and $J(NN')$ is the nuclear spin–spin coupling constant in units of hertz (Hz). Alternatively, the interaction energy can be written in terms of nuclear magnetic moments,

$\mu_N$ and $\mu_{N'}$, rather than spins:

$$E(NN') = K(NN')\mu_N \cdot \mu_{N'} \tag{2}$$

where $K(NN')$ is called the reduced coupling constant because, as opposed to $J(NN')$, it does not depend on the magnetogyric ratios, $\gamma$, of the coupled nuclei. The relation between $J(NN')$ and $K(NN')$ is:

$$K(NN') = 4\pi^2 J(NN')/h\gamma_N\gamma_{N'} \tag{3}$$

In the SI system, $K$ appears in the units $\text{m}^{-2}\,\text{kg}\,\text{s}^{-2}\,\text{A}^{-2}$. In the discussions of couplings involving a particular pair of nuclear species, the numerical values of the ordinary couplings, $J$, are used to facilitate comparison with experiments. In discussions of couplings involving different nuclear species, use of the reduced coupling is more meaningful. In these discussions numerical values of $K$ are given. To make the numbers more tractable, the units of $K$ in the text or the tables are $10^{19}\,\text{m}^{-2}\,\text{kg}\,\text{s}^{-2}\,\text{A}^{-2}$ throughout in this review. As a rule, the experimental values are quoted without giving references. In almost all cases the experimental data are taken from the theoretical papers in connection with which they are quoted, and thus the original experimental work can be traced through these. A few exceptions to this rule are made, e.g. when all experimental data quoted in a table are reported in a single paper.

This review covers the period from 1976. Since its aim is to provide a follow-up of the 1977 review, the references overlooked there are in general mentioned here. When in context, important papers from the period prior to 1976 are also quoted. This review was completed in the sping of 1981 and includes papers mentioned in *Chemical Abstracts* (or published in some major journals) before January 1, 1981. A few papers (of which I was aware at the preprint stage) that appeared after that date are also included.

## II. BASIC THEORY OF NUCLEAR SPIN–SPIN COUPLINGS

### A. Basic interactions

According to Ramsey[1] the electron-coupled interactions between the nuclear spins in molecules can be described in terms of the non-relativistic hyperfine Hamiltonian:

$$\hat{H} = \hat{H}_{1a} + \hat{H}_{1b} + \hat{H}_2 + \hat{H}_3 \tag{4}$$

The first and the second terms, which describe the interaction between the nuclear magnetic moments and the orbital motion of the electrons, are

given by the following equations:

$$\hat{H}_{1a} = \frac{\mu_0^2 e \hbar \mu_B}{(4\pi)^2} \sum_{N,N'} \gamma_N \gamma_{N'} \sum_k r_{kN}^{-3} r_{kN'}^{-3} [(\hat{\mathbf{I}}_N \cdot \hat{\mathbf{I}}_{N'})(\mathbf{r}_{kN} \cdot \mathbf{r}_{kN'}) - (\hat{\mathbf{I}}_N \cdot \mathbf{r}_{kN'})$$

$$\times (\hat{\mathbf{I}}_{N'} \cdot \mathbf{r}_{kN})] \tag{5}$$

$$\hat{H}_{1b} = \frac{\mu_0 \mu_B \hbar}{2\pi i} \sum_N \gamma_N \hat{\mathbf{I}}_N \cdot \sum_k r_{kN}^{-3} (\mathbf{r}_{kN} \times \nabla_k) \tag{6}$$

where $\mu_0$ is the permeability of the vacuum, $\mu_B$ is the Bohr magneton, and $\mathbf{r}_{kN}$ is the radius vector from electron $k$ to nucleus $N$.

The third term in equation (4) corresponds to the dipole–dipole interaction between the nuclear and the electron spins and is given in the following form:

$$\hat{H}_2 = \frac{\mu_0 \mu_B \hbar}{2\pi} \sum_N \gamma_N \sum_k [3(\hat{\mathbf{S}}_k \cdot \mathbf{r}_{kN})(\hat{\mathbf{I}}_N \cdot \mathbf{r}_{kN}) r_{kN}^{-5} - (\hat{\mathbf{S}}_k \cdot \hat{\mathbf{I}}_N) r_{kN}^{-3}] \tag{7}$$

where $\hat{\mathbf{S}}_k$ denotes the spin of electron $k$.

Finally, the Fermi contact (FC) Hamiltonian is given by:

$$\hat{H}_3 = \frac{4\mu_0 \mu_B \hbar}{3} \sum_N \gamma_N \sum_k \delta(\mathbf{r}_{kN}) \hat{\mathbf{S}}_k \cdot \hat{\mathbf{I}}_N \tag{8}$$

where $\delta(\mathbf{r}_{kN})$ is the Dirac delta function. This form of the FC interaction has been subject to some controversy.[9] A vast majority of the calculations reviewed here are however based on the contact operator as given in equation (8). Some perturbation-variation calculations for the hydrogen molecule constitute an exception however, and the relevant aspects of the problem of the functional form of the contact operator are discussed further in connection with this type of work.

The theory of Ramsey[1] is non-relativistic; it assumes that the spin and orbital angular momenta are LS coupled and that the vector potential of a nucleus, $\mathbf{A}_N$, is that of a point dipole:

$$\mathbf{A}_N = \frac{\mu_0}{4\pi} \gamma_N \hbar \frac{\hat{\mathbf{I}} \times \mathbf{r}_N}{r_N^3} \tag{9}$$

A relativistic analogue to Ramsey's theory was presented in 1977 by Pyykkö.[10] In this theory, the terms $\hat{H}_{1b}$, $\hat{H}_2$, and $\hat{H}_3$ in equation (4) are replaced by a single hyperfine Hamiltonian:

$$\hat{H}' = \frac{\mu_0}{4\pi} ec \gamma_N \hbar \frac{\boldsymbol{\alpha} \cdot \hat{\mathbf{I}} \times \mathbf{r}_N}{r_N^3} \tag{10}$$

where $\hat{H}'$ is given for one electron and one nucleus with the vector potential given by equation (9). The term $\hat{H}_{1a}$ is found in the relativistic theory as a second-order contribution from the positron-like intermediate states.

## B. Coupling mechanisms

Once the basic interactions are formulated and it is recognized that they are small compared with the molecular electrostatic Hamiltonian, different approaches of perturbation theory may be applied to the problem of calculating the nuclear spin–spin couplings. In the original formulation of Ramsey,[1] conventional second-order perturbation theory was used. The derivation appears in earlier reviews[11,12] and is omitted here. Recapitulating the results briefly one finds that the electron coupled nuclear spin–spin interaction has the following form:

$$E(NN') = h\hat{\mathbf{I}} \cdot \mathbf{J}(NN') \cdot \hat{\mathbf{I}}_{N'} \tag{11}$$

where $\mathbf{J}$ is a second-rank coupling tensor; the isotropic coupling mentioned above in equation (1) is equal to one-third of the trace of the tensor:

$$J = (1/3)(J_{xx} + J_{yy} + J_{zz}) \tag{12}$$

The isotropic coupling can, in the non-relativistic theory, be written as a sum of four distinct contributions:

$$J(NN') = J^{(1a)}(NN') + J^{(1b)}(NN') + J^{(2)}(NN') + J^{(3)}(NN') \tag{13}$$

where $J^{(1a)}(NN')$, which is called the diamagnetic orbital contribution to the coupling, is simply the expectation value of the part of $\hat{H}_{1a}$ involving N and N' for the unperturbed ground state of the molecule. The terms $J^{(1b)}(NN')$, $J^{(2)}(NN')$, and $J^{(3)}(NN')$, which are called the paramagnetic orbital or, concisely, orbital (OB), the spin-dipolar (SD), and the Fermi contact (FC) terms, correspond to the second-order corrections to the energy due to the appropriate terms in $\hat{H}_{1b}$, $\hat{H}_2$, and $\hat{H}_3$.

In partially oriented liquids, the anisotropy of the coupling tensor can be observed. Generally, the coupling tensor may consist of nine independent elements.[13] The number of these elements decreases if the molecule possesses elements of symmetry. If the internuclear axis coincides with a threefold, or higher, symmetry axis of the molecule (z-axis), the off-diagonal elements of the tensor vanish and the two diagonal elements, $J_{xx}$ and $J_{yy}$, become equal. The coupling anisotropy may then be defined as a simple (scalar) quantity:

$$\Delta J = J_{zz} - (1/2)(J_{xx} + J_{yy}) \equiv (3/2)(J_{zz} - J) \tag{14}$$

The FC term is always isotropic and does not contribute to $\Delta J$. The SD and OB terms, as well as the diamagnetic orbital term, can all contribute

to the coupling anisotropy. Further, a FC-SD cross term $\Delta J^{(2,3)}$, though vanishing for the isotropic $J$, may contribute to $\Delta J$.

The distinction of the OB and SD terms in Ramsey's theory[1] is the result of the use of LS coupling. In the relativistic theory of Pyykkö,[10] j–j coupling is used instead and the two contributions cannot be separated. The non-contact terms in both theories are however related to the non-s electrons and may as such be identified in the numerical calculations even when the relativistic theory is used. In a similar manner, the relativistic s orbital contribution may be separated. It corresponds in the non-relativistic limit to the FC contribution. It is interesting to note that Pyykkö's theory also predicts a non-vanishing mixed orbital s–p contribution to the isotropic coupling, which is absent at the non-relativistic limit. The magnitude of this term for Hg–C coupling in dimethylmercury is estimated to be ~1·7% of the total.[10]

Besides introducing the spin–orbit splitting of the p, d, ... shells, and thus requiring the use of the j–j coupling mentioned above, the relativistic effects on the electronic structure of atoms and molecules consist of the contraction of s and p shells and the relativistic self-consistent field expansion of d and f shells.[14,15] When couplings are evaluated using the Hamiltonian in equation (10), one obtains an expression containing the atomic hyperfine integrals:

$$a_{\kappa\kappa'} = \int_0^\infty (g_\kappa{}^* f_{\kappa'} + g_{\kappa'} f_\kappa{}^*)\, \mathrm{d}r \tag{15}$$

where $g$ and $f$ are the radial functions of the large and the small component of a four-spinor, and where the quantum number $\kappa$ carries information on both l and j. Owing to the relativistic contraction of the s and p shells, for heavy elements the relativistic hyperfine integrals (and the relativistically calculated couplings) are of substantially larger magnitude than their non-relativistic counterparts.

The theory proposed by Pyykkö[10] can also be used to calculate coupling anisotropies. The pure s-orbital contribution to $\Delta J$ vanishes, in analogy with the FC term of Ramsey's theory; the s–p term for the anisotropy corresponds, in the non-relativistic limit, to $\Delta J^{(2,3)}$, and the other terms to the combined and non-separable effects of $\Delta J^{(2)}$ and $\Delta J^{(1b)}$.

## III. COMPUTATIONAL METHODS

### A. Introductory remarks

This section deals with general computational procedures for calculations of nuclear spin–spin couplings in polyatomic molecules. As mentioned

above, the calculations of couplings are usually based on perturbation theory. The different approaches used can be characterized, on the one hand, by the perturbational treatment applied and, on the other hand, by the level of approximation adopted in the calculations of the wavefunctions involved. Very roughly, perturbation theory methods can be divided into two categories: the uncoupled methods, based on a straightforward expansion of the second-order energy as a sum-over-states (SOS), and the coupled methods, in which calculations seek to attain self-consistency. It should be stressed that in the extreme the two schemes can actually become identical and that some of the methods do not really fit this particular division. The uncoupled schemes are reviewed only briefly. Emphasis is thus placed on coupled schemes that have undergone important developments during the last few years.

The basic classification of the MO methods into independent electron LCAO-MO, semiempirical SCF-LCAO-MO, and non-empirical methods, used in the 1977 review,[6] still seems appropriate. Distinguishing features of the period covered by this review have been the continuing interest in the INDO method, introduction of new, more advanced semiempirical schemes (MINDO, NDDO, $X\alpha$), and, most importantly, the greatly increased use of non-empirical calculations with large basis sets. Combination of the coupled perturbation schemes and the large basis non-empirical calculations has proved to be very fruitful, not least in studies involving the role of non-contact mechanisms.

In analogy with the 1977 review,[6] the following Section B discusses the computational methods used for calculating the FC term. The increasing interest in non-contact mechanisms is reflected here by the fact that the particular aspects of the calculations of the OB and SD contributions are allocated a separate section each, i.e. Sections C and D.

A special position in this area is held by the interesting paper by Pyykkö and Wiesenfeld[16] who have applied the relativistic theory of couplings,[10] in which the division into FC, OB, and SD contributions is artificial. We shall discuss this paper in Section B.

## B. The Fermi contact term

The simplest MO theory of the FC contribution to nuclear spin–spin couplings is that proposed by McConnell.[2] In his formulation, the coupling is proportional to the square of the bond order matrix element between the valence s orbitals centred on the coupled nuclei. The method is hardly used any more but it has undoubtedly had a strong impact on subsequent developments. Pople and Santry[4] have advocated a simple SOS approach using a truncated set of excited-state wavefunctions constructed by promoting a single electron from the molecular orbital occupied in the ground

state into a virtual orbital. The resulting equation is:

$$K^{(3)}(NN') = -(16/9)\mu_0^2\mu_B^2\sum_i\sum_a({}^3\Delta E_{i\to a})^{-1}\langle i|\delta(\mathbf{r}_N)|a\rangle\langle a|\delta(\mathbf{r}_{N'})|i\rangle \quad (16)$$

The summation is carried out over the occupied MOs (i) and virtual MOs (a). Depending on the type of wavefunctions chosen, the triplet excitation energies and the matrix elements of the Dirac delta function are, in turn, given by different expressions. For the simplest sort of independent electron model, e.g. the EHT method (extended Hückel theory), the excitation energy is expressed simply as the difference between the orbital energies, $\varepsilon_a - \varepsilon_i$. At this level, it is reasonable to retain only the one-centre atomic integrals over the Dirac delta functions. This leads to the simple expression:

$$K^{(3)}(NN') = (4/9)\mu_0^2\mu_B^2 s_N^2(0)s_{N'}^2(0)\pi_{NN'} \quad (17)$$

with

$$\pi_{NN'} = -4\sum_i^{occ}\sum_a^{unocc}\frac{c_{iN}c_{aN}c_{iN'}c_{aN'}}{\varepsilon_a - \varepsilon_i} \quad (18)$$

where $s_N(0)$ is the amplitude at the origin of the valence shell s orbital associated with the nucleus N, $\pi_{NN'}$ is called the atom–atom polarizability, and $c_{iN}$ is the coefficient of the valence shell s orbital at atom N in the ith MO.

Pyykkö and Wiesenfeld[16] have extended equation (17) to make it compatible with the relativistically parametrized extended Hückel method (REX)[17] and Pyykkö's relativistic theory of couplings.[10] In REX, one constructs and diagonalizes a Hamiltonian matrix using $|lsjm\rangle$ coupled atomic orbitals as the basis. The diagonal matrix elements are identified with the atomic orbital energies from Dirac–Fock calculations, and the Slater type orbital (STO) exponents are fitted to the radial functions. The off-diagonal Hamiltonian matrix elements are calculated using the Wolfsberg–Helmholtz expression.

Pyykkö and Wiesenfeld[16] calculate the whole reduced coupling tensors. They express the nuclear spin operators as irreducible tensors and write the coupling energy:

$$E(NN') = \gamma_N\gamma_{N'}\hbar^2\sum_{\mu=-1}^{1}\sum_{\nu=-1}^{1}I_{N\mu}K_{NN'}{}^{\mu\nu}I_{N'\nu} \quad (19)$$

The $\mu\nu$ component of the coupling tensor is then given by:

$$K_{NN'}{}^{\mu\nu} = 2\sum_i^{occ}\sum_a^{unocc}\left[\sum_{t,u\in N}c_{it}^*c_{au}\langle\chi_t|(V_N^\mu)^+|\chi_u\rangle\right]$$

$$\times\left[\sum_{v,w\in N'}c_{av}^*c_{iw}\langle\chi_v|(V_{N'}^\nu)^+|\chi_w\rangle\right](\varepsilon_i - \varepsilon_a)^{-1} \quad (20)$$

The one-centre hyperfine matrix elements $\langle \chi_t | V_N^\mu | \chi_u \rangle$ are basically products of the "3j" symbols and the hyperfine integrals of equation (15). These integrals are also taken from the relativistic atomic calculations.

The REX calculations can be compared systematically to the non-relativistic calculations by replacing the relativistic atomic parameters with their non-relativistic counterparts, with both sets of parameters coming from *ab initio* atomic calculations. No other alterations are necessary.

With semiempirical SCF MO theories like CNDO or INDO, one can in principle still use equations (17) and (18). This is not strictly correct, however, because at this level the excitation energy should be decreased by subtracting the Coulomb integral (ii|aa). The one-centre integral approximation for the Dirac delta integrals is, on the other hand, consistent with the remaining approximations in the zero differential overlap (ZDO) methods.

Within the uncoupled framework, equation (16) may be refined further by allowing for various degrees of configuration interaction (CI) in the zero-order wavefunction, $\Psi^{(0)}$, and in the first-order correction to the wavefunction, $\Psi^{(1)}$. For a general case of an arbitrarily accurate $\Psi^{(0)}$ ($|0\rangle$) and an expansion of $\Psi^{(1)}$ in an arbitrary set of triplet configurations $|\mu\rangle$, the coefficient $c_{\mu,N}^{(1)}$ of the triplet configuration $\mu$ in $\Psi^{(1)}$ is given by:

$$\sum_{\mu=1}^{K} \langle \lambda | \hat{H}^{(0)} - E_0^{(0)} | \mu \rangle c_{\mu,N}^{(1)} = - \langle \lambda | \sum \delta(\mathbf{r}_{kN}) \hat{S}_{zk} | 0 \rangle \qquad (21)$$

where $\lambda = 1, \ldots, K$. The coupling is then written as:

$$K^{(3)}(NN') = (32/9)\mu_0^2 \mu_B^2 \sum_{\mu=1}^{K} c_{\mu,N}^{(1)} \langle \mu | \sum \delta(\mathbf{r}_{kN}) \hat{S}_{zk} | 0 \rangle \qquad (22)$$

Equations (21) and (22), with highly correlated $\Psi^{(0)}$ and with the $\mu$-space including all single and double replacements with respect to the ground state Hartree–Fock determinant, have been applied to the hydrogen molecule[18] and to several polyatomic molecules.[19] The latter work produces rather unsatisfactory results, in spite of the substantial computational effort involved.

During the period covered by this review, the uncoupled SOS approaches have been subject to few new developments. Probably the most important one, that involving relativistic calculations,[16] has already been mentioned. Bendazzoli and coworkers[20] have discussed the use of a Padé-type algorithm for solving the system given in equation (21). Klöpper[21] has generalized equation (16) so that it is valid for the antisymmetrized product of separated geminal (APSG) wavefunctions instead of ordinary MO wavefunctions. A theory leading to the expression for a coupling as a dot product of two abstract vectors, involving occupied and virtual molecular orbitals, has been presented.[22] Joela[23] and Zhidomirov *et al.*[24] have reported expressions for

couplings involving products of atom–atom polarizabilities rather than a single one.

A series of papers[25–27] report qualitative discussions of the importance of the correlation effects in the calculations of nuclear spin–spin couplings. Hirao and Kato[28] have compared the SOS INDO calculations of couplings between directly bonded carbons and protons and between two carbon atoms, using localized and canonical MOs. Their calculations, using the localized MOs, show closer agreement with the finite perturbation theory (FPT) method than do the corresponding conventional SOS calculations with canonical MOs. Two papers have dealt with comparisons between simple SOS calculations using approximations to equation (16) and different MO approaches. André et al.[29] calculated 99 couplings in 22 reference compounds using the standard versions of EHT, CNDO/2, and STO-3G MO procedures. They examined the linear correlations between the experimental and the theoretical results and discussed the capabilities of various methods. Some of the correlations are quite satisfactory, but none of the methods has been able to reproduce the experimental magnitudes of the couplings. Tarpø et al.[30] have tested different SOS CNDO and SOS INDO schemes and parametrizations for various one-, two-, and three-bond couplings. Among the many different computational features tested by them, one should mention the use of Slater exponents varying according to the atomic charges, and the use of the parametrization proposed by Boyd rather than the usual one. As in the work of André and coworkers,[29] linear correlations between the calculated results and the experimental data were examined. A number of papers have used the Pople–Santry method together with some kind of perturbation treatment of molecular orbitals in a series of related molecules. This type of work is reviewed below in connection with the particular type of coupling involved.

We now turn to the coupled methods. The coupled methods may further be divided into the finite perturbation and infinitesimal perturbation methods. The finite perturbation method (FPM) (the abbreviation FPT, finite perturbation theory, is also used) was originally proposed by Slater and Kirkwood[31] and adapted to the problem of nuclear spin–spin couplings by Pople and coworkers.[5] As proposed by Pople et al.,[5] the FPT is presented as a way to perform the coupled Hartree–Fock (CHF) calculations. Generally speaking, with CHF the Hartree–Fock equations for the molecular orbitals are solved in the presence of a perturbation. In the case of FPT the perturbation is finite; in the case of nuclear spin–spin couplings it involves an unnaturally large nuclear magnetic moment. Following the original work, it is convenient to continue the discussion in terms of the reduced coupling $K(NN')$.

Consider a molecule with two nuclear magnetic moments, $\mu_N$ and $\mu_{N'}$, directed along the z-axis. In the presence of the FC interaction alone, the

Hamiltonian for the molecule may be written as:

$$\hat{H} = \hat{H}_0 + \mu_N \hat{H}_N + \mu_{N'} \hat{H}_{N'} \tag{23}$$

where

$$\hat{H}_N = (4/3)\mu_0\mu_B \sum_k \delta(\mathbf{r}_{kN})\hat{S}_{zk} \tag{24}$$

From the power expansion of the energy in the presence of the two magnetic moments, the expression for the reduced coupling may be written as:

$$K^{(3)}(NN') = \left[\frac{\partial^2 E(\mu_N, \mu_{N'})}{\partial\mu_N\partial\mu_{N'}}\right]_{\mu_N=\mu_{N'}=0} \tag{25}$$

Using the Feynman–Hellmann theorem, proved[5] to be valid for the SCF functions used in the case at hand, the second derivative of energy may be set equal to the first derivative of the expectation value of $\hat{H}_N$ with respect to $\mu_{N'}$, evaluated in the presence of $\mu_{N'}$:

$$K^{(3)}(NN') = \left[\frac{\partial}{\partial\mu_{N'}}\langle\Psi(\mu_{N'})|\hat{H}_N|\Psi(\mu_{N'})\rangle\right]_{\mu_{N'}=0} \tag{26}$$

Thus, calculation of $K(NN')$ requires calculation of the wavefunction in the presence of one of the nuclear magnetic moments, $\mu_{N'}$. Subsequent calculation of the expectation value of $\hat{H}_N$ and its derivative is much simpler and can be done easily for any number of magnetic nuclei in a molecule.

In the FPT,[5] $\Psi(\mu_{N'})$ is computed as an unrestricted SCF-LCAO-MO wavefunction. This is necessary because the presence of $\mu_{N'}\hat{H}_{N'}$ (the matrix elements of which enter the Fock matrix with a different sign for the $\alpha$ and $\beta$ electrons) induces a non-vanishing spin-density in the molecule. The spin-density matrix $\rho$ may be defined as the difference between the first-order density matrices associated with the $\alpha$ and $\beta$ electron spins:

$$\rho = \mathbf{P}^\alpha - \mathbf{P}^\beta \tag{27}$$

Now, the expectation value of $\hat{H}_N$ appearing in equation (26) may be written in terms of $\rho$:

$$\langle\Psi(\mu_{N'})|\hat{H}_N|\Psi(\mu_{N'})\rangle = \frac{2\mu_0\mu_B}{3}\sum_{\lambda,\nu}\rho_{\lambda\nu}(\mu_{N'})\langle\lambda|\delta(\mathbf{r}_N)|\nu\rangle \tag{28}$$

where $\lambda$ and $\nu$ denote the atomic orbitals. The $\mu_{N'}$ dependence of the right-hand side of equation (28) is limited to the spin-density matrix. Derivation with respect to $\mu_{N'}$ gives the reduced coupling:

$$K^{(3)}(NN') = \frac{2\mu_0\mu_B}{3}\sum_{\lambda,\nu}\langle\lambda|\delta(\mathbf{r}_N)|\nu\rangle\left[\frac{\partial}{\partial\mu_{N'}}\rho_{\lambda\nu}(\mu_{N'})\right]_{\mu_{N'}=0} \tag{29}$$

which is generally valid for any type of SCF-LCAO-MO procedure. Pople and associates then introduce a number of approximations consistent with the semiempirical CNDO and INDO methods, and calculate the derivative using the method of finite differences. They arrive at:

$$K^{(3)}(NN') = \frac{4\mu_0^2\mu_B^2}{9} s_N^2(0)s_{N'}^2(0)\frac{\rho_{s_N s_N}(h_{N'})}{h_{N'}}$$  (30)

where $h_{N'}$ is the quantity actually added to or subtracted from the diagonal matrix elements of the Hartree–Fock operator.

Equation (30) has been applied recently together with other semiempirical ZDO procedures. Dewar and coworkers[32] and Pandey and Chandra[33] report MINDO/3 calculations for a large number of couplings involving carbon, hydrogen, nitrogen, and fluorine, and find no improvement over INDO calculations. Mehrotra et al.[34] and Solkan and Leonidov[35] have reported similar calculations using the NDDO method. They have examined only a few cases, and again there is no evident advantage over INDO.

Contreras et al.[36] have investigated the effects of small alterations in the original INDO parameters (bonding parameters, electronegativities, Slater exponents) on couplings in model compounds, calculated using the FPT INDO method. Some of the couplings are found to be very sensitive to some of the parameter changes. Similar ideas of modifying the INDO parameters in order to reproduce better a particular effect have been reported.[37] More recently, Facelli and Contreras[38] have investigated the effect of including polarization functions (2p orbitals on hydrogens) in the basis set used in the INDO calculations. Different couplings show a different sensitivity towards this extension of the basis set.

As a method for performing coupled Hartree–Fock calculations, the FPT scheme is not particularly efficient and the infinitesimal self-consistent perturbation methods are preferable. However, the FPT has the advantage of being compatible with computational schemes beyond the Hartree–Fock approximation. Peinel and Klöpper[39] have proposed the application of the FPT scheme together with APSG wavefunctions. More important are applications allowing for different types of configuration interaction, suggested[40] for the study of another second-order property, static polarizability. Finite perturbation configuration interaction (FP-CI) calculations of nuclear spin–spin couplings were proposed by Kowalewski and coworkers.[41] There is one principal difference between the FPT calculations at the Hartree–Fock and truncated CI levels of approximation: the equivalence of equations (25) and (26) at the Hartree–Fock level is based on the Feynman–Hellmann theorem. This theorem is not valid for truncated CI wavefunctions[40,41] (unless both the orbitals and CI coefficients are simultaneously optimized, as in the multiconfigurational SCF procedures), and

the two expressions in general do not lead to the same result. In the case of the parallel component of the polarizability in the hydrogen fluoride molecule, Werner and Meyer[40] find that the two values differ by 2% and suggest that the first derivative of an expectation value should give the more reliable result. No such tests have been performed for the computation of couplings. Kowalewski et al.[41] worked with equation (25) because it is simpler to implement. Another reason for this choice is that, while the polarizability may be phenomenologically defined either in terms of the second derivative of energy or in terms of the first derivative of the induced dipole moment, the coupling is phenomenologically defined only in terms of energy. Kowalewski et al.[41] note the symmetry properties of the energies computed in the presence of a perturbation and approximate equation (25) by:

$$K(NN') = [E(\lambda_N, \lambda_{N'}) - E(\lambda_N, -\lambda_{N'})]/2\lambda_N\lambda_{N'} \qquad (31)$$

where $\lambda_N$ and $\lambda_{N'}$ are the artificially large values of the nuclear magnetic moments, typically $10^4$–$10^5$ times larger than the real ones. It is worth noting that equation (31) conforms nicely to the phenomenological definition of the coupling as a quantity that is proportional to the energy difference between the parallel and the antiparallel orientations of the nuclear spins for two spin-1/2 nuclei.

Calculations performed according to equation (31) are carried out in two steps. First, the unrestricted Hartree–Fock (UHF) calculations of the total energy and the molecular orbitals are performed. At this stage, the CHF value for the coupling can be computed. In the second step, the perturbed orbitals are used as an input to a UHF-based CI program and different correlation energy estimates are computed. The most accurate method used is the full variational calculation involving all single and double replacements with respect to the reference UHF determinant. Also possibilities of using simpler approaches are investigated. In subsequent reports[42–44] the full variational calculations and simple (and computationally cheap) second-order estimates have been found to be most useful. A more detailed discussion of the results is presented below but it should be mentioned at this stage that the correlation effects are found to be very important for the quantitative interpretation of couplings.

As mentioned above, the CHF values of couplings can be obtained more efficiently using the infinitesimal coupled Hartree–Fock methods. A general presentation of the CHF method has been given.[45] The formulation most often used in the calculations of nuclear spin–spin couplings is the self-consistent perturbation theory (SCPT) method of Blizzard and Santry.[46]

As in FPT, equation (29) is also the basic expression in the SCPT procedure. The derivative of the spin-density matrix is, however, evaluated in a different way, i.e. from the first-order correction to the molecular

orbitals. Let $c_i^{(0)}$ be a column vector representing the ith occupied MO in the space spanned by the atomic orbital basis, and $c_i^{(1)}$ a column vector representing the first-order correction to $c_i^{(0)}$ due to the perturbation $\mu_{N'}\hat{H}_{N'}$ [compare equations (23) and (24)]. Using standard second-order perturbation theory with

$$\mathbf{F}^{(0)}c_i^{(0)} = \varepsilon_i c_i^{(0)} \tag{32}$$

as the zero-order equation, the expression for $c_i^{(1)}$ becomes:

$$c_i^{(1)} = \left[\sum_a (\varepsilon_a - \varepsilon_i)^{-1} c_a^{(0)} \tilde{c}_a^{(0)}\right] \mathbf{F}^{(1)} c_i^{(0)} \tag{33}$$

where $\mathbf{F}^{(0)}$ is the Fock matrix in the absence of a perturbation and $\mathbf{F}^{(1)}$ is the first-order correction to the Fock matrix. The correction $\mathbf{F}^{(1)}$ depends on the first-order correction to the density matrices for the $\alpha$ and $\beta$ electrons, defined in the following way:

$$P_{\lambda\nu}^{\alpha(1)} \equiv \left(\frac{\partial P_{\lambda\mu}^{\alpha}}{\partial \mu_{N'}}\right)_{\mu_{N'}=0} = \sum_i (c_{i\lambda}^{(0)} c_{i\nu}^{(1)} + c_{i\lambda}^{(1)} c_{i\nu}^{(0)}) \tag{34}$$

Owing to the dependence of $\mathbf{F}^{(1)}$ on $\mathbf{P}^{(1)}$, equation (33), which gives the first-order correction to the orbitals, must be solved iteratively. When convergence is achieved, equation (34) gives the sought-after value of the derivative of the spin-density matrix. From the symmetry of the operator $\hat{H}_{N'}$, we have:

$$\mathbf{P}^{\alpha(1)} = -\mathbf{P}^{\beta(1)} \tag{35}$$

and

$$\left(\frac{\partial \rho_{\lambda\nu}}{\partial \mu_{N'}}\right)_{\mu_{N'}=0} = 2P_{\lambda\nu}^{\alpha(1)} \tag{36}$$

Further, Blizzard and Santry[46] have introduced the INDO approximation with the same assumptions about the integrals as those of Pople et al.[5] In practice, they find it more convenient to set the $s_N s_N$ element of the one-electron part of $\mathbf{F}^{(1)}$, which is identical to $\hat{H}_N$, as defined in equation (24), equal to unity instead of $2\mu_0\mu_B s_N^2(0)/3$. The resulting first-order density matrix element is then multiplied by $2\mu_0\mu_B s_N^2(0)/3$. The final expression for the reduced coupling becomes:

$$K^{(3)}(NN') = 2P_{s_N s_N}^{\alpha(1)} \frac{4\mu_0^2 \mu_B^2}{9} s_N^2(0) s_{N'}^2(0) \tag{37}$$

The advantage of the SCPT method compared to FPT Hartree–Fock calculations is twofold. First, the SCPT method replaces the tedious and

sometimes slow-to-converge UHF scheme with a series of matrix multiplications. Second, the disadvantage associated with the numerical calculation of derivatives, i.e. limited precision, is also avoided.

The SCPT method was for the first time applied at the non-empirical level by Ditchfield and Snyder.[47] A similar approach has been used more recently by Guest et al.[48,49] who have improved the computational procedure by using damping factors and level shifters. These authors point out that the CHF theory may be unsuitable for systems that show UHF instabilities in the ground state, e.g. some multiply bonded systems. Lazzeretti[50,51] has compared the CHF method with uncoupled methods and with the geometric approximation based on the first two terms of the double perturbation expansion.

Two interesting new method developments took place during 1980. Albertsen et al.[52] derived the multiconfigurational coupled Hartree–Fock (MCCHF) equations for the FC contribution to couplings. The method has so far been applied only to diatomic molecules (HD and HF) but it is general in principle. A way has been suggested[53] to generalize the self-consistent perturbation theory, as sketched above, to the configuration interaction level of accuracy. The method has not yet been used to calculate nuclear spin–spin couplings.

The quality of a non-empirical calculation is determined, to a degree comparable to the choice of the perturbation approach, by the choice of the basis set. It was noticed several years ago that the non-empirical CHF calculations of couplings using the minimal basis set are unsuccessful.[54] This early observation has probably delayed the development of non-empirical CHF (and related) calculations. In the more recent work mentioned above,[41–44,48–51] larger basis sets of Gaussian type functions (GTF) have been used, and the results have turned out to agree much better with experiment. In some of these papers[41,43,48–50] the effects of basis set variation have also been investigated. The general picture that arises is that the basis set requirements vary for different types of coupling and for different chemical situations. For certain "easy" problems, like the variation of the vicinal couplings in ethane with the dihedral angle[42] or the substituent effects on one-bond carbon–proton couplings,[44] the use of a rather small double-zeta basis has proved to be sufficient. A more detailed discussion of this problem is given in connection with the discussion of particular couplings.

One more basis set related problem should be mentioned in this methodological section. It has been pointed out[55] that the s-type GTFs may be unsuitable for calculating the FC contribution to couplings because they do not satisfy the cusp condition, i.e. they do not behave properly at the origin. These authors suggest a way to improve the situation but stress that their method does not remove the principal difficulties involved in

calculating the value of a wavefunction at the site of a nucleus. An alternative way of circumventing the cusp problem in molecular calculations has been proposed.[56]

It is mentioned in the preceding Section A that the division into the uncoupled and coupled schemes is to a certain extent arbitrary and does not cover all the methods used for calculating couplings. The group of methods falling in between comprises the double perturbation theory (DPT) or many-body perturbation theory (MBPT) calculations. It was pointed out[57] in 1972 that for the case of nuclear spin–spin couplings all the important terms appearing in the CHF calculations also appear in the DPT calculations. Lazzeretti[50] has treated the first two terms in a special case of the double perturbation expansion as leading terms in an expansion converging at the CHF solution. He has found that, at least in some cases, the geometric approximation based on these two terms agrees rather well with the CHF result. According to the analysis presented by Robb and Chin,[58] who use the diagrammatic MBPT technique, the sum of the three leading terms in the MBPT expansion corresponds closely to the CHF calculation, while the higher terms correspond to the correlation effects described by a CI treatment based on the perturbed Hartree–Fock orbitals or by including the doubly and triply excited configurations in the $\mu$-space of equation (21). The methods of double perturbation theory and the results obtained using the localized MOs have been reviewed.[59] Related studies have more recently been reported;[60,61] the calculations involve the non-empirical approach. Additionally, calculations within the frameworks of the semiempirical schemes[62,63] are reported.

## C. The orbital term

As mentioned in the preceding Section B, there are really two terms in Ramsey's[1] expression for the coupling that depend on the orbital motion of the electrons. The diamagnetic term, $J^{(1a)}(NN')$, is a straightforward expectation value evaluated using the unperturbed ground state wavefunction:

$$K^{(1a)}(NN') = \frac{e^2\mu_0^2}{24m\pi^2}\langle 0| \sum_k r_{kN}^{-3}r_{kN'}^{-3}\bar{\mathbf{r}}_{kN}\cdot\mathbf{r}_{kN'}|0\rangle \tag{38}$$

Nevertheless, the diamagnetic orbital term has been calculated by only a few authors. Lee and Schulman[64] have used the Monte Carlo integration method and have reported calculations of several couplings between directly bonded nuclei. They find that the contributions from different regions of space largely cancel, leading to rather small total values. The calculated results are found to be very sensitive to the basis set, leading the authors to the conclusion that $J^{(1a)}$ is the most basis set sensitive first-order property

computed to date.[64] The method of Lee and Schulman[64] has the advantage of being applicable together with any type of ground state wavefunction. For the specific case of calculations using GTFs, Matsuoka and Aoyama[65] have derived reasonably simple expressions for the integrals in equation (38), relating them to the analytical expressions for four-centre field or overlap integrals. For one-bond couplings, the results of Matsuoka and Aoyama[65] differ rather little from the work of Lee and Schulman.[64] More interesting are the large orbital diamagnetic contributions to $^2J(HH)$ in the first-row hydrides, discussed in detail in Section IV.B.

The paramagnetic orbital term, $J^{(1b)}(NN')$, has received much more attention in the literature. The classical papers[3,4] have proposed simple expressions relating $J^{(1b)}$ to the integrals $\langle 2p_N | r_N^{-3} | 2p_N \rangle \equiv \langle r_N^{-3} \rangle$. Since no 2p orbitals are assigned to the hydrogen atoms, these models predict that the OB term vanishes for couplings involving protons. It is natural to retain this assumption in all semiempirical calculations. The recent non-empirical studies have shown, however, that this assumption can, at least in some cases, be incorrect.

In principle, most of the methods developed for the contact term can be, and have been, applied to the calculation of the OB term. Towl and Schaumburg[66] have presented calculations using the uncoupled SOS CNDO and SOS INDO schemes. Nakatsuji et al.[67] have adapted the FPT method for calculations of the OB term. The SCPT method of Blizzard and Santry[46] has been developed for all three mechanisms. Among these coupled Hartree–Fock methods, the SCPT approach has been applied most frequently and thus is presented here.

We assume, by analogy with the case of the FC term, a system with two nuclear magnetic moments in the z-direction, and write the Hamiltonian as:

$$\hat{H} = \hat{H}_0 + \mu_N \hat{H}_{N,z}{}^{OB} + \mu_{N'} \hat{H}_{N',z}{}^{OB} \tag{39}$$

where

$$\hat{H}_{N,z}{}^{OB} = \frac{\mu_0 \mu_B}{2\pi i} \sum_k r_{kN}^{-3} \left( x_{kN} \frac{\partial}{\partial y_{kN}} - y_{kN} \frac{\partial}{\partial x_{kN}} \right) = \sum_k h_N{}^{OB}(k) \tag{40}$$

The orbital contribution to the reduced coupling is also given here by the second derivative of the energy with respect to the magnetic moments of N and N':

$$K^{OB}(NN')_{zz} = \left[ \frac{\partial E(\mu_N, \mu_{N'})}{\partial \mu_N \partial \mu_{N'}} \right]_{\mu_N = \mu_{N'} = 0} = \left[ \frac{\partial}{\partial \mu_{N'}} \langle \Psi(\mu_{N'}) | \hat{H}_{N,z}{}^{OB} | \Psi(\mu_{N'}) \rangle \right]_{\mu_{N'} = 0} \tag{41}$$

where the second equality is the result of the Feynman–Hellmann theorem. The derivative in equation (41) is calculated from the first-order perturbation correction $c_j^{(1)}$ to the molecular orbital coefficients $c_j$. The basic

equation of the SCPT for the OB term has the same form as equation (33), with the first-order correction to the Fock matrix, $F_{\lambda\nu}^{(1)}$, given by:

$$F_{\lambda\nu}^{(1)} = \langle \lambda | h_{N'}^{OB} | \nu \rangle + \sum_{\sigma\tau} P_{\sigma\tau}^{(1)}[(\lambda\nu|\sigma\tau) - (1/2)(\lambda\tau|\sigma\nu)] \tag{42}$$

where $(\lambda\nu|\sigma\tau)$ and $(\lambda\tau|\sigma\nu)$ denote standard two-electron integrals and $P_{\sigma\tau}^{(1)}$ is the first-order correction to the density matrix:

$$P_{\sigma\tau}^{(1)} = \left(\frac{\partial P_{\sigma\tau}}{\partial \mu_{N'}}\right)_{\mu_{N'}=0} = i2 \sum_{j}^{occ} (c_{\sigma j}^{(0)} c_{\tau j}^{(1)} - c_{\sigma j}^{(1)} c_{\tau j}^{(0)}) \tag{43}$$

Note that in this case the perturbation is spin-free and that the $F_{\lambda\nu}^{(1)}$ matrix elements are purely imaginary. Consequently, the perturbed molecular orbitals remain identical for the $\alpha$ and $\beta$ spins but are composed of a real (unperturbed) part $c_{\sigma j}^{(0)}$ and an imaginary part $ic_{\sigma j}^{(1)}$.

Equation (33) is now solved iteratively until self-consistency in $\mathbf{c}^{(1)}$ or $\mathbf{P}^{(1)}$ is obtained. The orbital contribution to $K(NN')$, due to the magnetic moments in the z-direction, is then given by:

$$K^{OB}(NN')_{zz} = \sum_{\lambda\nu} P_{\lambda\nu}^{(1)}\langle \lambda | h_N^{OB} | \nu \rangle \tag{44}$$

which is analogous to equation (29) for the FC contribution.

If we now introduce the usual INDO-type approximations (minimal basis set of valence shell s and p orbitals; only one-centre integrals retained) and redefine the one-electron part of equation (42) to be equal to unity for $\lambda = x_{N'}$ and $\nu = y_{N'}$, equation (44) becomes:

$$K^{OB}(NN')_{zz} = 2P_{x_{N'}y_{N'}}^{(1)}\frac{\mu_0^2\mu_B^2}{4\pi^2}\langle r_N^{-3}\rangle\langle r_{N'}^{-3}\rangle \tag{45}$$

where $x_{N'}$ denotes a valence shell $p_x$ orbital on atom N'.

In fact, the interaction leading to the orbital contribution to the coupling is anisotropic and calculations must be repeated for the nuclear magnetic moments in the x- and y-directions. Equations analogous to equations (44) and (45) are obtained after a suitable permutation of $x$, $y$, and $z$ in equation (40). The isotropic part of $K^{OB}(NN')$ is then obtained as an average of $K^{OB}(NN')_{xx}$, $K^{OB}(NN')_{yy}$, and $K^{OB}(NN')_{zz}$.

After the redefinition of $\langle \lambda | h_{N'}^{OB} | \nu \rangle$ mentioned above, the integral $\langle r_N^{-3}\rangle$ is factored out from the expression for $K^{OB}(NN')$. By analogy with the parameter $s_N^2(0)$ in the case of the FC term, $\langle r_N^{-3}\rangle$ may either be obtained from atomic calculations or treated as an adjustable parameter. The latter procedure seems to be used more frequently.

During the last few years SCPT INDO calculations of the OB term for couplings between two first-row atoms have become usual. There is however

a certain sense of ambiguity about the results, because the adjusted $\langle r_N^{-3} \rangle$ values are usually much larger than what would correspond to the STO exponents used in the INDO calculations. Further, for the classical benchmark for calculations of the OB term, the one-bond coupling between carbon and fluorine in fluoromethane, the semiempirical[67] and non-empirical[47] calculations predict opposite signs.

Several non-empirical coupled Hartree–Fock calculations of the OB term have appeared since 1978.[43,48-51,68,69] The most important single conclusion arising from these studies is that the OB term is definitely non-negligible for several couplings involving protons. It has been reported[48] that the experimentally observed variation in the geminal proton couplings in the series water—ammonia—methane arises mainly from the variation in the OB term. A more detailed discussion of these calculations is given in connection with particular types of couplings in the following sections. A few more aspects should however be mentioned here. Guest and co-workers[48,49] and Lazzeretti[50] have studied the basis set dependence of the orbital term. It is found that the proton–proton couplings of the first-row hydrides are very basis set sensitive while the proton–first-row atom couplings display greater stability with respect to the basis set.[48,50] The OB contribution to the one-bond proton–second-row atom coupling in the second-row hydrides has also been found to be rather insensitive to the basis set.[49] Finally, Lazzeretti[50] has found that the double perturbation expansion of the orbital contribution to both $^2J(HH)$ and $^1J(OH)$ in the water molecule is much more well-behaved than the similar expansion of the contact term, and that the geometric approximation to the CHF response may be quite successful for this mechanism.

### D. The spin-dipolar term

The spin-dipolar contribution to nuclear spin–spin couplings, $J^{(2)}$ or $J^{SD}$, is similar to the OB term in the sense that similar integrals over atomic orbitals are involved. In semiempirical formulations the only integral retained is again $\langle r_N^{-3} \rangle$. Using the same type of argument as for the OB term, Pople and Santry[4] have predicted the SD term to vanish if one of the coupled nuclei is a proton.

The development of the theory of the SD term parallels closely the development of the theory for the OB term. Thus, Towl and Schaumburg[66] have introduced the SOS CNDO and SOS INDO calculations of $J^{SD}$. Nakatsuji and coworkers[67] have used the FPT in connection with semiempirical ZDO procedures. The SCPT method for $J^{SD}$ has been formulated at the INDO level[46] and for non-empirical calculations.[47] In order to focus on the similarities and differences between the calculations of $J^{OB}$ and $J^{SD}$, the SCPT formulation of $J^{SD}$, based on the paper of Blizzard and Santry,[46] is presented here.

For the nuclear magnetic moments in the z-direction, the Hamiltonian for the SD interaction may be written in a form similar to equations (23) or (39), with:

$$\hat{H} = \hat{H}_0 + \mu_N \hat{H}_{N,z}{}^{SD} + \mu_{N'} \hat{H}_{N',z}{}^{SD} \tag{46}$$

$$\hat{H}_{N,z}{}^{SD} = \frac{\mu_0 \mu_B}{2\pi} \sum_k r_{kN}{}^{-5} [3x_{kN} z_{kN} \hat{S}_{xk} + 3y_{kN} z_{kN} \hat{S}_{yk} + (3z_{kN}{}^2 - r_{kN}{}^2)\hat{S}_{zk}]$$

$$= \sum_k [h_{xz,N}{}^{SD}(k) + h_{yz,N}{}^{SD}(k) + h_{zz,N}{}^{SD}(k)] \tag{47}$$

The form of the Hamiltonian in equations (46) and (47) makes the SD term more complicated to handle than the other two second-order terms. Since $\hat{H}_{N,z}{}^{SD}$ contains $\hat{S}_x$ and $\hat{S}_y$ it will therefore mix the $\alpha$ and $\beta$ spin orbitals and, at the same time, introduce both the real and the imaginary perturbation to the wavefunction. These features require a modification both of the basis set to be used and of the SCF procedure. The molecular orbitals are expressed as linear combinations of atomic spin-orbitals (LCASO), which doubles the size of the atomic basis set. The Hartree–Fock equations become:

$$\begin{pmatrix} F^{\alpha\alpha} & F^{\alpha\beta} \\ F^{\beta\alpha} & F^{\beta\beta} \end{pmatrix} \begin{pmatrix} c^{\alpha\alpha} & c^{\alpha\beta} \\ c^{\beta\alpha} & c^{\beta\beta} \end{pmatrix} = \begin{pmatrix} c^{\alpha\alpha} & c^{\alpha\beta} \\ c^{\beta\alpha} & c^{\beta\beta} \end{pmatrix} \begin{pmatrix} E^{\alpha} & 0 \\ 0 & E^{\beta} \end{pmatrix} \tag{48}$$

where $F^{\alpha\alpha}$ and $F^{\beta\beta}$ are the Fock matrices, corresponding to those encountered in the usual unrestricted Hartree–Fock theory, and $F^{\alpha\beta}$ and $F^{\beta\alpha}$ are the terms mixing the $\alpha$ and $\beta$ character of the MOs. The MO space is divided, arbitrarily at this stage, into two subspaces in which the $\alpha$ spin ASOs have the coefficients $c^{\alpha\alpha}$ and $c^{\alpha\beta}$ respectively; $E^{\alpha}$ and $E^{\beta}$ form together the diagonal eigenvalue matrix. Now, the division of the MO space becomes less arbitrary if we consider the unperturbed case. The unperturbed Fock matrix is block-diagonal:

$$F^{\alpha\beta(0)} = F^{\beta\alpha(0)} = 0 \tag{49}$$

The unperturbed MOs are pure spin orbitals and the coefficient matrix is therefore also block-diagonal. It is then natural to define the two MO subspaces as corresponding to the $\alpha$ and $\beta$ spin MOs in the unperturbed case. Then $\mathbf{c}_j{}^{\alpha\beta}$ corresponds to the $\beta$ spin contribution induced by the perturbation into the j-th $\alpha$ spin MO. Clearly, we can write:

$$c^{\alpha\beta(0)} = c^{\beta\alpha(0)} = 0 \tag{50}$$

If we substitute equations (49) and (50) into (48), perform the standard perturbation expansion, and collect first-order terms, we find that the contributions from each of the four submatrices, $F^{\sigma\alpha}$, $F^{\alpha\beta}$, $F^{\beta\alpha}$, and $F^{\beta\beta}$,

can be solved separately. Denoting, for brevity, $F^{\alpha\alpha(0)}$, $c^{\alpha\alpha(0)}$, and $E^{\alpha(0)}$ as $F$, $c$, and $E$, we get:

$$Fc^{\alpha\alpha(1)} + F^{\alpha\alpha(1)}c = c^{\alpha\alpha(1)}E + cE^{\alpha(1)} \tag{51}$$

and

$$F^{\beta\alpha(1)}c + Fc^{\beta\alpha(1)} = c^{\beta\alpha(1)}E \tag{52}$$

These are the equations to be solved for $\mathbf{c}^{(1)}$ using equation (33) with the appropriate $\mathbf{F}^{(1)}$.

To solve equation (51) we only need to consider the $h_{zz,N}$ term of equations (46) and (47). The $h_{xz,N}$ and $h_{yz,N}$ terms enter equation (52), but it can be shown that they can nevertheless be treated separately, since they lead to real and imaginary perturbations of the MOs respectively. The final expression for the zz-component of the SD part of the coupling tensor becomes:

$$K^{SD}(NN')_{zz} = 2\sum_{\lambda\nu} [M_{\lambda\nu}^{(1)}\langle\lambda|h_{zz,N}^{SD}|\nu\rangle + Q_{\lambda\nu}^{(1)}\langle\lambda|h_{xz,N}^{SD}|\nu\rangle$$
$$+ R_{\lambda\nu}^{(1)}\langle\lambda|h_{yz,N}^{SD}|\nu\rangle] \tag{53}$$

Equation (53) is analogous to equations (29) and (44). The various first-order density matrices entering equation (53) are:

$$M_{\lambda\nu}^{(1)} = \sum_{j}^{\alpha\,occ} (c_{\lambda j}^{\alpha\alpha(1)}c_{\nu j} + c_{\lambda j}c_{\nu j}^{\alpha\alpha(1)}) \tag{54}$$

$$Q_{\lambda\nu}^{(1)} = \sum_{j}^{\alpha\,occ} (\mathrm{Re}\,c_{\lambda j}^{\alpha\beta(1)}\,c_{\nu j} + c_{\lambda j}\,\mathrm{Re}\,c_{\nu j}^{\alpha\beta(1)}) \tag{55}$$

$$R_{\lambda\nu}^{(1)} = \sum_{j}^{\alpha\,occ} (\mathrm{Im}\,c_{\lambda j}^{\alpha\beta(1)}c_{\nu j} + c_{\lambda j}\,\mathrm{Im}\,c_{\nu j}^{\alpha\beta(1)}) \tag{56}$$

The matrix elements of the perturbing Hamiltonian in equation (53) are:

$$\langle\lambda|h_{xz,N}^{SD}|\nu\rangle = \frac{3\mu_0\mu_B}{4\pi}\langle\lambda|r_N^{-5}x_N z_N|\nu\rangle \tag{57}$$

$$\langle\lambda|h_{yz,N}^{SD}|\nu\rangle = \frac{3\mu_0\mu_B}{4\pi}\langle\lambda|r_N^{-5}y_N z_N|\nu\rangle \tag{58}$$

$$\langle\lambda|h_{zz,N}^{SD}|\nu\rangle = \frac{\mu_0\mu_B}{4\pi}\langle\lambda|r_N^{-5}(3z_N^2 - r_N^2)|\nu\rangle \tag{59}$$

At the INDO level and after a redefinition of $\mathbf{F}^{(1)}$ [analogous to that leading to equations (37) and (45)], equation (53) simplifies considerably and

becomes:

$$K^{SD}(NN')_{zz} = \frac{\mu_0^2 \mu_B^2}{20\pi^2} [2M_{z_{N'}z_{N'}}{}^{(1)} - M_{x_{N'}x_{N'}}{}^{(1)} - M_{y_{N'}y_{N'}}{}^{(1)} + 3Q_{x_{N'}z_{N'}}{}^{(1)}$$

$$+ 3R_{y_{N'}z_{N'}}{}^{(1)}]\langle r_N^{-3}\rangle\langle r_{N'}^{-3}\rangle \tag{60}$$

As is the case for calculations of the OB term, it is necessary to repeat the whole calculation two more times with the perturbing magnetic moments in the x- and y-directions, and to take the average over the three directions to obtain the final SD contribution to the isotropic $K(NN')$.

The non-empirical coupled Hartree–Fock calculations of the SD contributions to couplings following closely the original formulations[46,47] are reported by Guest and coworkers.[48,49] Lazzeretti[50,51] has compared the CHF calculations with uncoupled schemes and the geometrical approximation to the CHF response. In the case of the SD mechanism, the geometric approximation seems to be useful only for certain types of couplings. Lazzeretti and Zanasi[70] have also investigated the possibility of making calculations of the SD term more efficient by making use of molecular symmetry. Lee and Schulman[71] have published a somewhat different formulation of the coupled Hartree–Fock theory for the SD term and have applied it to perform calculations for several molecules. These authors also note that the CHF calculations for systems with multiple bonds (ethene, ethyne, hydrogen cyanide) lead to very large values of $K^{SD}(NN')$. Their analysis shows that the CHF method fails for these systems. The reason for this failure, which was anticipated,[48] may be traced to triplet instabilities. Lee and Schulman[71] have also discussed different possibilities of circumventing this problem. A general conclusion from the non-empirical calculations mentioned above is that the SD term is usually small. On the other hand, Robb and Chin[58] have reported non-empirical MBPT calculations of the SD contribution to several couplings involving fluorine and have found them to be very large in some cases.

## IV. PROTON–PROTON COUPLINGS

### A. The hydrogen molecule

The first case to be discussed in this section on proton–proton couplings is really the case of a proton–deuteron coupling. The experimental coupling $^1J(HD) = 42\cdot94 \pm 0\cdot1$ Hz has been obtained for the HD species of molecular hydrogen,[72] and it has become a tradition among theoreticians to quote the results of calculations (independent of the isotopic species with the possible exception of vibrational corrections) for this particular combination of magnetogyric ratios. For comparison with the proton–proton couplings,

$J(HH)$, in the following sections, one should simply multiply $J(HD)$ by a factor of $\gamma_H/\gamma_D = 6\cdot514$.

The 1977 review[6] presented a detailed discussion of the different methods used to calculate the FC contribution to the coupling in the HD molecule. This discussion is not repeated here. Basically, the methods proposed by different authors may be classified as either using a more or less conventional perturbation theory or applying a variation-perturbation scheme. The distinguishing feature of the latter category, compared to the former, is that the first-order correction to the wavefunction is sought beyond the concepts of orbital and configuration.

During the period prior to 1976, the most sophisticated calculations for the hydrogen molecule involved configuration interaction methods,[18,73] many-body perturbation theory,[74,75] and the Green's function approach.[76] All these lines of development have more recently been followed by similar studies. Selected results are collected in Table 1. Kowalewski et al.[41] have compared the FP-CI and SOS-CI methods and found that both approaches are completely equivalent if full CI is performed. Bendazzoli et al.[77] (entry

## TABLE 1

**Calculated Fermi contact contribution to the coupling constant in the HD molecule at the interatomic distance of $1\cdot4$ a.u.**

|    | Method | Author and reference | Basis set | $J(HD)$ (Hz) |
|----|--------|----------------------|-----------|--------------|
| 1. | approx. CI | Meyer[73] | 55 CGTO | 42·4 |
| 2. | CI | Kowalewski et al.[18] | 40 CGTO | 43·3 |
| 3. | CI | Kowalewski (unpublished) | 50 GTO | 38·8 |
| 4. | CI | Bendazzoli et al.[77] | 24 CGTO | 39·0 |
| 5. | MBPT, Hartree potential | Schulman and Kaufman[74] | 62 GTO | 38·1 |
| 6. | MBPT, bare nucleus potential | Schulman and Kaufman[75] | 84 GTO | 49·0 |
| 7. | MBPT, Hartree–Fock potential | Schulman and Lee[78] | 62 GTO | 37·0 |
| 8. | MBPT, Hartree–Fock potential | Itagaki and Saika[79] | 86 GTO | 38·0 |
| 9. | SOPPA | Oddershede et al.[76] | 28 STO | 47·0 |
| 10. | SOPPA | Oddershede et al.[80] | 46 STO | 48·7 |
| 11. | CVB-PT | Kirtman and Kirtley[82] | 74 GTO | 42·3 |
| 12. | CHF | Kirtman and Kirtley[82] | 62 GTO | 50·9 |
| 13. | CHF | Schulman and Lee[78] | 50 GTO | 51·0 |
| 14. | CHF | Oddershede et al.[80] | 46 STO | 59·5 |
| 15. | CHF | Albertsen et al.[52] | 44 STO | 70·0 |
| 16. | MCCHF | Albertsen et al.[52] | 44 STO | 56·3 |
| 17. | Experiment | Benoit and Piejus[72] | | 42·9 ± 0·1 |
| 18. | Suggested | Schulman and Lee[83] | | 40·95 |

4) have compared different methods of generating configurations to be included in the CI. With full CI, they report results similar to those obtained by Kowalewski et al.[18] (entries 2 and 3). The differences between entries 2, 3, and 4 in the table reflect the basis set sensitivity of the results, present even when very large basis sets are used. Schulman and Lee[78] and Itagaki and Saika[79] have reported MBPT calculations using the Hartree–Fock potential (entries 7 and 8). The convergence of the MBPT treatment with this particular potential is slow. The zero-order and first-order terms reported in the three papers[74,78,79] agree closely with each other and are $J_0 = 12$ Hz and $J_1 = 9$ Hz. Schulman and Lee[78] have also calculated contributions from selected second-order diagrams which give another 15·2 Hz. Itagaki and Saika[79] have proceeded in a somewhat different way and include selected second-, third-, and higher-order corrections. In addition they apply the selective geometric approximation (starting with $J_3$) and energy denominator shifting. The final results of the two papers are close to each other.[78,79] Oddershede et al.[80] have reported new calculations using the second-order polarization propagator (SOPPA) and a large STO basis set (entry 10).

Kirtman and coworkers[81,82] have suggested that the valence bond (VB) method should be more suitable than the Hartree–Fock molecular orbital theory for calculating nuclear spin–spin couplings. In the first paper of the series[81] the uncoupled valence bond "distinguishable electron" model is described and tested for the simple screening approximation. In the second paper[82] a fully coupled valence bond perturbation theory (CVB-PT) of nuclear spin–spin coupling in HD is presented. The calculations are performed using large basis sets,[74,75] and the results (entry 11) agree very well with experimental data. Kirtman and Kirtley[82] have reported CHF calculations with the same 10s5p1d basis set (entry 12). The coupled Hartree–Fock calculations for HD are not really interesting by themselves but may provide a good reference for evaluating the CHF method for larger molecules. Therefore, some other CHF results are listed in Table 1 (entries 13, 14, and 15). Albertsen et al.[52] have reported CHF and multi-configurational CHF (using up to four configurations) calculations with a large STO basis set (entry 16). Table 1 contains, for comparison, the experimental value of $J(HD)$ (entry 17) and the suggested "accurate" value of the FC term at the equilibrium internuclear separation (entry 18, discussion below).[83]

The variation perturbation calculations of the coupling in HD, and problems related to such calculations, have drawn continued attention. Pyykkö[84] criticized some of the approaches in use, and his criticism has been answered.[86] Delpuech et al.[86] have reported calculations with the Gregson, Hall and Reese operator, instead of the usual Dirac delta function, using the minimization of the self-coupling energy as the variational

criterion. The problems involved with possible variational criteria have been discussed.[87-89] Rayez-Meaume and coworkers[90,91] have continued the effort to solve the problems caused by the Dirac delta function, by using a transformation suggested originally by Vladimiroff and Dougherty.[92] In the two papers[90,91] the interest is centred on the convergence properties. A common feature of the perturbation-variation calculations is still the simplicity of the unperturbed wavefunctions used.

The non-contact contributions to the coupling in the HD molecule have been calculated and reported in a series of papers.[64,78,83] The results are collected in Table 2. The $J^{(1a)}$ value quoted in the table has been calculated

## TABLE 2

**Non-contact contributions to the coupling constant in HD, and vibrational corrections to the Fermi contact term.**

| Type of term | Author and reference | Value (Hz) |
|---|---|---|
| Orbital diamagnetic, $J^{(1a)}$ | Lee and Schulman[64] | $-0.37$ |
| Orbital paramagnetic, $J^{(1b)}$ | Schulman and Lee[78] | $0.78$ |
| Spin-dipolar, $J^{(2)}$ | Schulman and Lee[83] | $0.48$ |
| Total non-contact, estimated | Schulman and Lee[83] | $0.61$ |
| Vibrational correction | Kowalewski et al.[18] | $0.22$ |
| Vibrational correction | Schulman and Lee[83] | $1.39$ |
| Vibrational correction | Facelli et al.[94] | $1.3$ |

using the Monte Carlo integration technique[64] and the accurate Kolos–Roothaan wavefunctions; $J^{(1a)}$ in the HD molecule has also been calculated by Matsuoka and Aoyama,[65] and $J^{(1b)}$ and $J^{(2)}$ have been calculated using the coupled Hartree–Fock method.[78,83] The sum of the three contributions is $0.89$ Hz, or about 2% of the experimental value. Schulman and Lee[83] consider this value to be overestimated and have suggested that the total non-contact contribution is closer to $0.6$ Hz.

Neglect of the non-contact terms is one error source in the calculations collected in Table 1. Another reason why discrepancies can arise between a calculation performed at the experimental equilibrium geometry ($R_e = 1.401$ a.u.) and the experimental value can be the neglect of vibrational corrections. The experimental value is a Boltzmann average over the thermally populated vibration-rotational states, vN:

$J(\text{HD})(T)$

$$= \frac{\langle J \rangle_{00} + 3\langle J \rangle_{01} \exp(E_{00} - E_{01})/kT + 5\langle J \rangle_{02} \exp(E_{00} - E_{02})/kT + \cdots}{1 + 3 \exp(E_{00} - E_{01})/kT + 5 \exp(E_{00} - E_{02})/kT + \cdots}$$

$$\tag{61}$$

Schulman and Lee[83] have estimated the averages $\langle J \rangle_{vN}$ in the following way. They take the $J(HD)$ value calculated[18] for different interatomic distances, and McLaurin-expand it in terms of a dimensionless parameter $\xi = (R - R_e)/R_e$:

$$J(\xi) = J(0) + \left(\frac{\mathrm{d}J}{\mathrm{d}\xi}\right)_0 \xi + (1/2)\left(\frac{\mathrm{d}^2 J}{\mathrm{d}\xi^2}\right)_0 \xi^2 + \cdots \qquad (62)$$

The average value of $J(HD)$ for any vibration-rotational state may then be written:

$$\langle J \rangle_{vN} = J(0) + \left(\frac{\mathrm{d}J}{\mathrm{d}\xi}\right)_0 \langle \xi \rangle_{vN} + (1/2)\left(\frac{\mathrm{d}^2 J}{\mathrm{d}\xi^2}\right)_0 \langle \xi^2 \rangle_{vN} + \cdots \qquad (63)$$

$\langle \xi \rangle_{vN}$ and $\langle \xi^2 \rangle_{vN}$ can be derived from the vibrational analysis data. Such results have been tabulated.[93] The vibrational correction obtained by Schulman and Lee[83] using this procedure is given in Table 2. Facelli and coworkers[94] have also used the data of Kowalewski et al.[18] and carried out the averaging using an approach very similar to that of equations (62) and (63). They calculate the average values of $\xi$ and $\xi^2$ using three different methods. In the most accurate calculation, Facelli and coworkers[94] have applied the method[95] where $\langle \xi \rangle$ and $\langle \xi^2 \rangle$ are calculated as averages over the ground state wavefunctions for the Morse potential. This result is also listed in Table 2. The work of Schulman and Lee[83] and Facelli et al.[94] shows that the original estimate of the vibrational correction made at our laboratory[18] (see Table 2) was not accurate.

Before concluding this section on the calculations for the hydrogen molecule, one should also mention that the coupling of HD has been used, with varying degrees of success, as a benchmark for judging the accuracy of different molecular orbital schemes, e.g. NDDO,[34] INDO,[36,38,94] MINDO/3,[33] and LCAO-SCF-X$\alpha$.[96]

## B. Geminal and vicinal proton-proton couplings

The geminal and vicinal proton-proton couplings are grouped together in this section not so much because of their similarities but rather for the practical reason that they often are reported in the same papers. The basic outline of this section is the following. It begins with a review of calculations of geminal proton couplings in simple hydrides, $XH_n$. Next we deal with the few papers covering geminal couplings in a $XH_2$ group, where X is not a carbon atom. We proceed with the papers reporting non-empirical calculations of other geminal and vicinal proton couplings. Finally we turn to more application-oriented semiempirical work on organic molecules, using the type of chemical system as the criterion for grouping different papers.

A problem that might appear simple at first glance, but for which we have not yet reached a satisfactory degree of understanding, is the variation of the geminal proton–proton coupling in the series methane—ammonia—water. Experimentally the magnitude of the negative coupling decreases along the series. Prior to 1978 no calculations were able to reproduce this trend. The most accurate of the earlier investigations, using the large CI treatment of the contact term, predicts almost no variation along the series.[19] In 1978 Guest and coworkers[48] reported large basis set non-empirical CHF calculations. The CHF values of the contact term show very little variation in this study (see Table 3). However, Guest et al.[48] also

## TABLE 3

Geminal proton coupling constants (Hz) in the first- and second-row hydrides.

| | Coupled Hartree–Fock[a] | | | | $J^{(1a)}$ | Correl. contr. to $J^{FC}$ [b] | Total calc. | Exp. |
|---|---|---|---|---|---|---|---|---|
| | $J^{FC}$ | $J^{OB}$ | $J^{SD}$ | total | | | | |
| $H_2O$ | −23·8 | 7·1 | 1·4 | −15·3 | −6·4[d] | 11·7 | −10·0 | −7·2 |
| $NH_3$ | −24·3 | 4·7 | 0·8 | −18·8 | −4·0[d] | 12·1 | −10·7 | −10·4 |
| $CH_4$ | −25·4 | 2·7 | 0·4 | −22·3 | −2·4[d] | 11·8 | −12·9 | −12·4 |
| $H_2S$ | −19·7 ($-16·0^c$) | 1·6 | 0·2 | −17·9 | | 5·0 | −12·9 | |
| $PH_3$ | −22·2 ($-19·8^c$) | 0·9 | 0·2 | −21·1 | | 7·6 | −13·5 | −13·4 |
| $SiH_4$ | −2·5 ($-1·4^c$) | 1·0 | 0·1 | −1·4 | | 2·3 | +0·9 | +2·75 |
| $AlH_3$ | $32·0^c$ | | | | | | | |

   [a] Ref. 48, basis set $\langle 5,3,1/3,1 \rangle$, for the first-row hydrides; ref. 43, basis set $\langle 6,5,1/3,1 \rangle$, for the second-row hydrides.
   [b] Ref. 41 for the first-row hydrides; ref. 43 for the second-row hydrides.
   [c] Ref. 49, basis set $\langle 10,6,1/4,1 \rangle$.
   [d] Ref. 65, basis set $\langle 4,2/2 \rangle$.

computed the non-contact terms. They found, in contrast to the qualitative ideas, that the OB and SD terms are not only significant but are responsible for the variation in the series of molecules (see Table 3). We can see in the table that, after including all three mechanisms, the CHF results reproduce the experimental trend, even though the calculated values are shifted by about 8–10 Hz compared to the experimental results. This shift can, to a large extent, be explained as being due to correlation effects. These effects had already been anticipated to be important for geminal couplings.[6] Table 3 also contains the results of the work of Kowalewski et al.[41] who calculated the correlation contributions to the couplings for the

first-row hydrides using the FP-CI method. The CI results are an improve-
ment compared with the CHF level, but the agreement between the best
calculated and experimental values[41] is still not too impressive. The most
recent (but certainly not the last) important contribution to the discussion
of $^2J$(HH) in the first-row hydrides is presented[65] (the paper contains minor
errors in the results for ammonia; the value quoted in Table 3 is the correct
one). After adding the $J^{(1a)}$ values to the sum of the CHF results and the
correlation contributions to the FC term, the agreement with the experi-
mental data becomes very good for $CH_4$ and $NH_3$, but not for $H_2O$. The
calculations[65] were performed with a small basis set; it would be very
interesting to see the effect of increasing the size of the set.

The papers[41,48] mentioned above also contain studies of basis set depen-
dence. The results of a large investigation of basis set effects on the CHF
(and more approximate) calculations have also been reported[50] for the case
of the water molecule. The results are in excellent agreement with the data
of Table 3. The non-empirical SOS and CHF calculations of the contact
contribution to $^2J$(HH) in $H_2O$ have been compared[97] using only rather
limited basis sets. The non-contact contributions to the same coupling
constant have been computed at the *ab initio* level.[68,71] The geminal proton
couplings in simple first-row hydrides have also been calculated using
semiempirical methods.[29,30,32–34,38,63]

An interesting study of the effects of vibrational averaging on the calcu-
lated $^2J$(HH) in ammonia has been reported.[98] The SCPT INDO calcula-
tions agree very well with the earlier non-empirical work[99] for $^2J$(HH)
expressed as a function of the totally symmetric ($A_1$) normal coordinate.
It is also found[98] that the vibrational correction from the E modes outweighs
the $A_1$ mode correction. The total correction is predicted to be negative
and equal to 9% of the equilibrium geometry value.

Two papers have recently dealt with geminal proton couplings in the
second-row hydrides. Guest and Overill[49] have reported CHF calculations
of $J^{FD}$, $J^{OB}$, and $J^{SD}$ for the series $H_2S$—$PH_3$—$SiH_4$—$AlH_3$, including an
investigation of the basis set dependence. Kowalewski and coworkers[43]
have performed similar calculations for $H_2S$, $PH_3$, and $SiH_4$, though with
less extensive basis set variation, and include the correlation contribution
to the FC term. The results are presented in Table 3. Both sets of results
are quoted for the FC term; the non-contact terms calculated in both papers
turn out to be exactly the same. It is interesting to note that the trend
displayed by the geminal proton couplings in the second-row hydrides is
notably different from the trend in the first-row hydrides, and that the
calculations are very successful in reproducing the large change in $^2J$(HH)
between silane and phosphine. In $PH_3$ and $H_2S$ both the correlation effects
and the non-contact terms are less important than in $NH_3$ and $H_2O$. In
terms of absolute values, the same is also true for the pair methane—silane.

However, the CHF calculation of the contact term in $SiH_4$ yields a small negative coupling which becomes positive (in agreement with experiment) first after a correction has been made for other mechanisms and correlation.

Since the previous survey[6] some new papers have appeared that deal with geminal proton couplings in systems, other than simple hydrides, where the coupled protons are bonded to an atom other than carbon. Laaksonen and Kowalewski[44] have reported non-empirical CHF and FP-CI calculations for $^2J(HNH)$ in aminomethane. Purcell and Martin[100] have calculated $^2J(HBH)$ in the $BH_3 \cdot CO$ adduct using the FPT INDO method, and the SOS EHT method has been used[101] to calculate $^2J(HPH)$ in methylphosphine.

Non-empirical calculations of geminal couplings $^2J(HCH)$ and vicinal couplings $^3J(HCXH)$ in substituted methanes have been reported by several authors. Barbier and coworkers[60] have calculated the FC contribution to geminal couplings in the series of $CH_3X$ compounds with $X = H$, $CH_3$, $NH_2$, OH, and F, and in propane using the DPT method and the minimal basis set (see Table 4). It can be seen that the positive shift in the coupling

## TABLE 4

Geminal proton coupling constants, $^2J(HCH)$ (Hz), in methane derivatives, $CH_3X$, calculated by non-empirical methods.

| X | $CHF^a$ | $FP\text{–}CI^a$ | CHF Fermi contact | CHF FC+OB+SD | $MBPT^d$ | $DPT^e$ | Experiment |
|---|---------|------------------|-------------------|--------------|----------|---------|------------|
| H | −31·2 | −17·2 | $−25·4^b$ | $−22·3^b$ | −25·0 | −10·2 | −12·4 |
| $CH_3$ | −30·9 | −15·7 | | | −10·0 | −16·2 | |
| $NH_2{}^f$ | −28·4 | −14·4 | | | | −8·4 | |
| $OH^f$ | −28·4 | −14·2 | $−23·9^c$ | $−21·0^c$ | | −7·6 | −10·8 |
| F | −27·8 | −13·9 | | | | −6·5 | −9·6 |

[a] Ref. 44, double zeta basis, Fermi contact only.
[b] Ref. 48, ⟨5,3,1/3,1⟩ basis.
[c] Ref. 51, ⟨5,3,1/3,1⟩ basis.
[d] Ref. 58, Fermi contact only.
[e] Ref. 60, minimal basis, Fermi contact only.
[f] Average value.

value caused by the electronegative substituent in the $\alpha$-position, predicted by the classical Pople–Bothner-By rules,[102] is reproduced by the calculations. Both Barbier et al.[60] and Robb and Chin[58] have predicted large differences between the geminal proton coupling in methane and ethane, which appears astonishing (no experimental data are available for ethane).

Robb and Chin[58] have also reported calculations of geminal couplings in ethene and difluoromethane, and of vicinal couplings in ethene and ethane.

Lazzeretti[51] has reported the CHF and more approximate calculations for methanol using a large Gaussian basis set and including the FC as well as the OB and the SD mechanisms. His calculated average $^2J$(HH) is listed in Table 4. A comparison with a similar calculation for methane[48] shows that the effect of substitution is reproduced within a few tenths of a hertz. Lazzeretti[51] also calculated the vicinal proton coupling in methanol at four values of the dihedral HCOH angle ($\phi$). The FC term itself, and the sum of $J^{FC}$ and $J^{OB}$, are found to follow, roughly, a $\cos^2 \phi$ curve. The orbital term alone shows another type of angular variation, with extreme values of $-0.5$ Hz and $+3.9$ Hz.

Laaksonen and coworkers have reported calculations of vicinal couplings in ethane,[42] and of all possible couplings in the series of substituted methanes $CH_3X$ with $X = CH_3$, $NH_2$, OH, and F.[44] The calculated geminal proton couplings are given in Table 4. The general trend is similar to the results of Barbier et al.[60] but the difference between methane and ethane is reduced. In the case of ethane, aminomethane, and methanol, the authors have reported extensive studies of the dependence of $^2J$(HH) and $^3J$(HCXH) on rotation around the C–X bond.

Laaksonen and Kowalewski[44] have found that, at the CHF level, the geminal proton couplings in the methyl groups of methanol and aminomethane show a variation of about 5–6 Hz when the substituent is rotated around the C–X bond. The size of this variation, as well as the magnitude of the calculated coupling, is reduced after including the correlation correction. The shape of the *ab initio* calculated $^2J$(HH) curves in methanol is similar to those obtained in the FPT INDO study.[103] The plot of $^2J$(HH) in aminomethane versus the rotation angle is shown in Fig. 1.

The large variation of the vicinal proton–proton couplings in ethane with the dihedral HCCH' angle ($\phi$) has been known for a long time. In fact, the prediction of this conformational dependence probably constitutes the most important successful application of the early theoretical methods. Using the valence bond theory for a six-electron fragment, Karplus[3b] derived the following relation between the vicinal coupling in ethane and the angle $\phi$:

$$^3J(\mathrm{HH}) = \begin{cases} 8.5 \cos^2 \phi - 0.28 & 0 < \phi < 90° \\ 9.5 \cos^2 \phi - 0.28 & 90° < \phi < 180° \end{cases} \tag{64}$$

Later, Karplus[104] modified equation (64) and obtained:

$$^3J(\mathrm{HH}) = A + B \cos \phi + C \cos 2\phi \tag{65}$$

Equation (65), known as the Karplus relation, is widely used by theoreticians as well as by experimentalists. Laaksonen and coworkers have
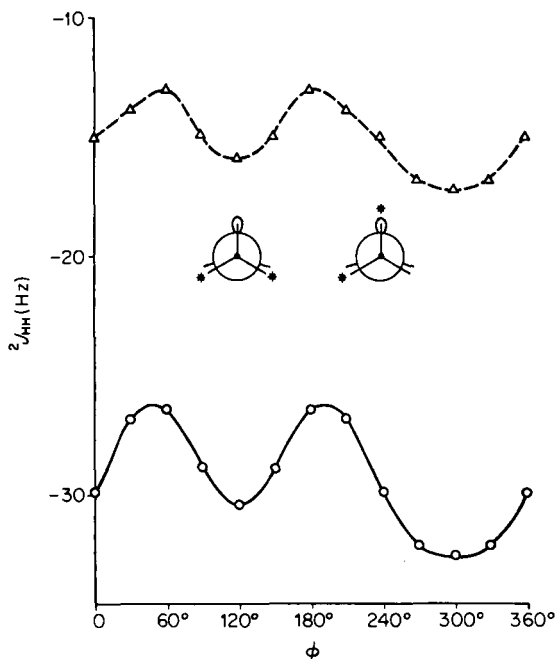
FIG. 1. The dependence of $^2J$(HH) in aminomethane on the dihedral HCN-lone pair angle (O, CHF; △, approximate FP-CI). Two of the conformations are depicted in the figure. (Laaksonen and Kowalewski[44])

found it to be an excellent representation of the vicinal couplings in ethane[42,44] (see Fig. 2) and in methanol.[44] For aminomethane, CHF and FP-CI curves of the vicinal proton coupling vs. $\phi$ are found[44] to be somewhat asymmetric with respect to 180°.

Lee and Schulman[68,69,71] have reported CHF calculations of the OB and the SD contributions to geminal and vicinal proton couplings in several molecules. Simple SOS calculations of the FC term (using the STO-3G basis set) in many small molecules have been reported.[29]

It is noteworthy that no non-empirical CHF calculations have been reported for the FC and SD contributions to couplings in ethene. The reason is not lack of interest but rather the fact that ethene exhibits, at least under certain circumstances, UHF instability. This problem has been discussed for the case of the contact mechanism[48] and for the SD mechanism.[71] In contrast, the OB term is easy to compute and has been reported.[68]

Among semiempirical calculations of geminal and vicinal couplings the series of extensive FPT INDO investigations[103,105,106] still holds the central position. The newer work is therefore reviewed rather briefly. Table 5
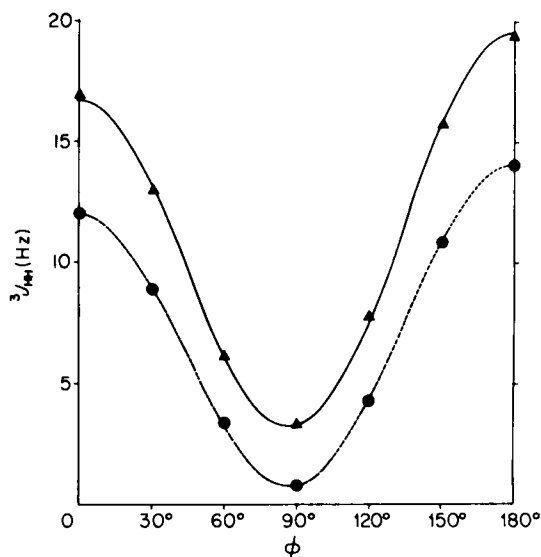
FIG. 2. Least-squares fit of the calculated vicinal proton–proton coupling constant in ethane to the Karplus equation [equation (65)]. The triangles and the solid line correspond to the CHF calculations, the circles and the broken line to the FP-CI results. (Laaksonen, Kowalewski and Siegbahn[42])

# TABLE 5

**Selected geminal and vicinal coupling constants calculated using the finite perturbation method with the CNDO/2, INDO, MINDO/3, and NDDO approximations; the entries are ordered according to increasing experimental value.**

|  | Coupling | CNDO/ 2[a] | INDO[a] | INDO with 2p on H[b] | MINDO/ 3[c] | NDDO[d] | Exp. |
|---|---|---|---|---|---|---|---|
| $CH_4$ | $^2J(HH)$ | 1·2 | −6·1 | −7·9 | −5·6 | −10·9 | −12·4 |
| $CH_3F$ | $^2J(HH)$ |  | −1·9[e] | −4·2 | 10·7[g] | −13·3 | −9·6 |
| $H_2O$ | $^2J(HH)$ | 1·3 | −8·1 | −4·5 | −6·6 | −5·4 | −7·2 |
| $C_2H_4$ | $^2J(HH)$ | 8·5 | 3·2 | 1·1 | 3·2 |  | 2·5 |
| $C_6H_6$ | $^3J(HH)$ | 7·6 | 8·2 | 9·2 | 23·9 |  | 7·5 |
| $C_2H_6$ | $^3J(HH)_{av}$ | 6·8 | 8·4 |  | 6·0[g] | 3·2 | 8·0 |
| $C_2H_2$ | $^3J(HH)$ | 6·6 | 11·0 |  | 42·1 | 15·4 | 9·6 |
| $C_2H_4$ | $^3J(HH)_{cis}$ | 8·0 | 9·3 | 12·4 | 8·8 |  | 11·7 |
| $C_2H_3F$ | $^3J(HH)_{trans}$ |  | 20·7[f] |  | 42·8 |  | 12·8 |
| $C_2H_4$ | $^3J(HH)_{trans}$ | 19·5 | 25·2 | 27·5 | 47·9 |  | 19·1 |

[a] Ref. 5c, unless otherwise stated.    [b] Ref. 38.    [c] Ref. 32, unless otherwise stated.    [d] Ref. 34.    [e] Ref. 103.    [f] Ref. 105.    [g] Ref. 33.

contains a selection of typical geminal and vicinal couplings[5,103,105] com-
pared with more recent data obtained from INDO with 2p orbitals on
hydrogens,[38] MINDO,[32,33] and NDDO[34] work. By and large, the MINDO
and NDDO schemes do not seem to provide any advantage compared to
INDO, and including the 2p orbitals on hydrogens in this scheme gives a
minor improvement only. Among other method-oriented semiempirical
studies one should mention the papers by André et al.,[29] Tarpø et al.,[30]
Archirel and Barbier,[63] and Karafiloglou.[107]

Several authors have reported more application-oriented calculations of
geminal and vicinal proton–proton couplings. Ohkubo and coworkers[108,109]
have performed SOS INDO calculations for some small hydroxycarbonium
ions. Laatikainen et al.[110] have reported FPT INDO and SOS INDO
calculations of $^3J(HCOH)$ and $^3J(HCCH)$ in several alcohols. Jaworski
and coworkers[111] have studied $^3J(HCCH)$ in ethanol and ionized ethanol
as a function of the dihedral angles HCCH and HOCC. Aminova and
Samitov[112] have reported SOS EHT calculations of various couplings in
methanol and aminomethane as functions of the molecular conformation.
Elguero et al.[113] have carried out FPT INDO calculations of $^3J(HH)$ in
formylhydrazine (1) as a function of the dihedral HNNH angle.

$$\begin{array}{c} H \\ \diagdown \\ H \diagup \end{array} N - N \begin{array}{c} \diagup CHO \\ \diagdown H \end{array}$$

(1)
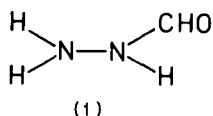
Safiullin and coworkers[101,114,115] have presented SOS EHT calculations
of $^2J(HCH)$ and $^3J(HCPH)$ in methylphosphine and other phosphorus-
organic compounds. The three-bond proton–proton coupling in methyl-
phosphine, calculated as a function of the HCPH dihedral angle, has been
found to behave similarly to the corresponding $^3J(HCNH)$ in
aminomethane. Iwayanagi and coworkers[116] have also used the EHT
method; the systems under consideration are some mercury-organic com-
pounds.

Steiger et al.[117] have performed various SOS INDO and CNDO
calculations, including and excluding the d orbitals in the atomic basis
set and the Coulomb integrals in the energy denominators, for a series of
monosubstituted ethenes. Using the FPT INDO approach, Mamaev and
coworkers[118-121] have investigated the dependence of couplings in
butadiene, its methyl derivatives, and cyclopropane on small changes in
bond length and bond angle. Rummens and collaborators[122,123] have
studied, in a similar fashion, the proton–proton couplings in ethene, pro-
pene, butene, and 3-methylbutene. Lemarié and Braillon[124] have presented
a discussion of the coupling mechanism in penta-1,4-diene, based on FPT

CNDO and FPT INDO calculations. The work dealing with the particular problem of separation of couplings into $\sigma$ and $\pi$ contributions is dealt with in the following Section C.

Concern with the couplings in cyclic systems has steered the research of numerous authors. Rabideau et al.[125] have calculated, using FPT INDO, $^3J(\mathrm{HH})$ in flat cyclohexa-1,4-diene for different assumed geometries. Schreurs and coworkers[37] have reported FPT INDO and CNDO calculations for cyclopent-2-enone (2) and cyclohex-2-enone (3). The CNDO and INDO parameters are calibrated from calculations for some smaller molecules. The related system cyclopent-3-enone (4) has also been studied.[126]



(2)               (3)               (4)
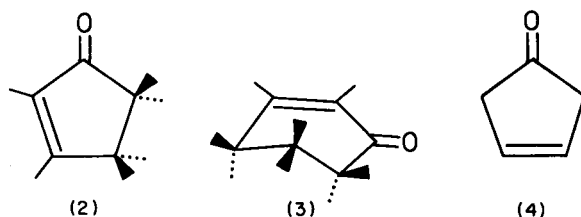
Bicyclic hydrocarbon systems have been studied[23,127] using the INDO approximation. An interesting study of vicinal proton couplings in norbornane (5) and norbornene (6) has been presented.[128] Experimentally, $^3J_{exo,exo}$ is larger than $^3J_{endo,endo}$ in 5, while the two couplings are almost equal in 6. The mechanistic reasons for this observation are discussed within the framework of FPT INDO calculations with certain interactions deleted.



exo

endo

(5)               (6)
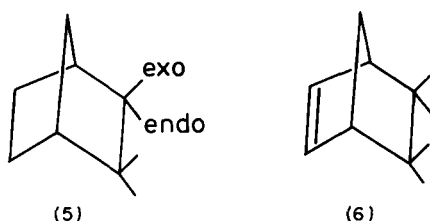
Calculations of vicinal proton couplings in benzene derivatives and aromatic hydrocarbons have been reported in three papers. Ernst and coworkers[129] have calculated vicinal couplings in aniline and nitrobenzene, using the SCPT INDO method. Long and Memory[130] have reported FPT INDO calculations for benzene, naphthalene, anthracene, phenanthrene, biphenyl, and pyrene. Günther and coworkers[131] have investigated the effect of small angle deformations on the couplings in benzene. They worked

with SOS CNDO/2 and FPT INDO calculations, and sought correlations between $^3J$(HH) and the $\pi$-bond order in planar cyclic $\pi$-systems.

Several papers have recently dealt with heterocyclic systems, mainly in relation to conformational analysis. Benassi et al.[132] have reported an interesting study of couplings in dioxolane (7), using the FPT INDO and SOS EHT methods. Their calculations are performed for several conformations. Dioxolane is a system with a low barrier to pseudorotation. Because of this, the value of the coupling for comparison with experiments has to be an average:

$$\langle J \rangle = \sum_i J_i \exp(-\Delta E_i/RT) \Big/ \sum_i \exp(-\Delta E_i/RT) \tag{66}$$

where $\Delta E_i$ is the energy of conformation i relative to the most stable conformation. Benassi et al. find that the $^2J$(HH) values at positions 2 and 4 of 7, obtained using equation (66), are consistent with experimental findings only if the energies are calculated non-empirically (with the 4-31G basis set) and the couplings calculated with the EHT method. The trends in the vicinal coupling can be reproduced by both FPT INDO and SOS EHT calculations, provided that *ab initio* energies are used.[132]
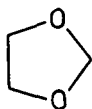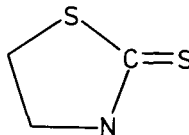


(7)                                    (8)

Using the FPT INDO method, Chanon and collaborators[133,134] calculated geminal and vicinal couplings for different conformations of the thiazolidine 8 and its derivatives; the same method has been used[135] for a study of the couplings in glycals. Samitov and coworkers[136] have reported SOS EHT calculations for phosphorus-containing heterocyclic compounds. Jokisaari and Rahkamaa[137] have performed FPT INDO calculations of vicinal couplings in pyrrole. Finally, Burmistrov and Mamaev[138] have reported an SOS INDO study of couplings in porphin dication.

## C. Long-range proton–proton couplings

There is a tendency in the literature, especially in connection with couplings involving nuclei other than protons, to call all couplings through more than one bond long-range couplings. In this review, however, "long-range" is reserved for couplings through four or more bonds.

No non-empirical calculations of the FC contribution to long-range proton–proton couplings have been reported. On the other hand, Lee and

Schulman have calculated the $OB^{69}$ and the $SD^{71}$ contributions to the four-bond proton–proton couplings in bicyclopentane (9); $^4J^{OB}(HH) = 0.87$, $0.73$, and $-0.64$ Hz for the *exo–exo*, *endo–exo*, and *endo–endo* couplings respectively, and the $^4J^{SD}(HH)$ are very small.



(9)
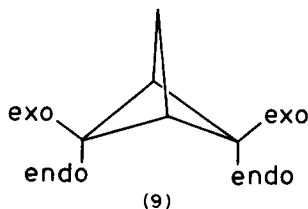
Turning to the semiempirical method-oriented work, we should note that double perturbation calculations[63] have confirmed the empirical W-rule (the long-range couplings are large for coupling paths having a zig-zag or W-like shape). Two papers have concentrated on the theory of separation of the $\sigma$ and $\pi$ contributions to the FC term. Vysotskii and Luzanov[139] have formulated a theory of the $\pi$-electron contribution to couplings based on the concept of atom–atom polarizability. Yoshida[140] has worked within the framework of the FPT and the INDO approximation. The $\pi$ contribution to coupling in this approach can be obtained by comparing a full calculation with a calculation involving only the $\sigma$ part:

$$J^\pi = J^{\text{total}} - J^\sigma \qquad (67)$$

Earlier it was suggested that, if $J^{\text{total}}$ is calculated using the FPT INDO approach, $J^\sigma$ could be obtained by CNDO/2,[5] or by special FPT INDO calculations with the $\sigma$–$\pi$ exchange integrals deleted.[141] Yoshida[140] has suggested that $J^\sigma$ should rather be calculated by constraining the $\pi$-electron spin density to zero; he has reported the comparisons of the three approaches for hydrocarbons as well as for systems containing heteroatoms.

Since the previous review,[6] numerous papers have appeared that deal with application-oriented calculations of long-range proton couplings. The methods chosen have usually been FPT INDO or SCPT INDO. Therefore, in the rest of this section, it is assumed implicitly that the underlying computational scheme is one of those, unless specified otherwise. The calculations are reviewed following the philosophy of the previous survey,[6] i.e. using the chemical nature of the bonding path as the basic criterion for classification; the nomenclature of Barfield and Chakrabarti[142] is employed.

We start with molecules containing only single bonds. Schulman and Venanzi[127] have reported calculations of long-range proton–proton couplings in bicyclobutane and methylbicyclobutane. The HCCCH couplings

in these systems may be called propanic. Santoro[135] has reported calcula-
tions for glycals (10) in different configurations and conformations. Note
that in 10 the propanic coupling, $^4J(H_3H_5)$, is not the only long-range
coupling; other types of long-range couplings (see below) occur. Benassi
and coworkers[132] have studied similar $^4J(HH)$ couplings (but with a
heteroatom in the coupling path) in dioxolane (7) and its derivatives. They
used the SOS EHT scheme, which they find to be superior to the FPT
INDO approach in the case of geminal and vicinal couplings (preceding
Section B). Ohkubo and coworkers[108,109] have reported SOS INDO calcula-
tions for systems possessing partial double-bond character along the coup-
ling path, e.g. protonated formic acid (11).

(10)                    (11)
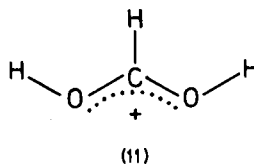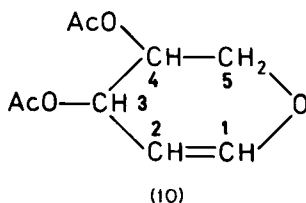
The four-bond couplings in the fragment 12 are called allylic. Allylic
couplings have been reviewed.[143] The five-bond couplings in 13 are called
homoallylic. Rummens and coworkers[122,123] have studied allylic and

(12)                    (13)
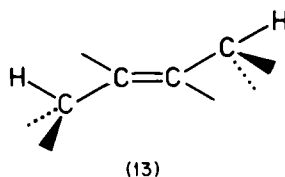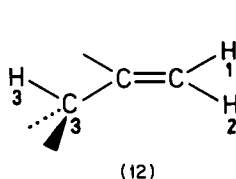
homoallylic couplings in propene, but-2-ene, and related systems as a
function of geometry parameters. Barfield and Abia[144] have reported
calculations for cyclobutene (14) and related systems. Here the couplings
between protons 3 (3′) and 4 (4′) are transmitted along a dual path, vicinal
as well as homoallylic. Rabideau and coworkers[125] and Marshall et al.[145]
have studied the homoallylic couplings in cyclohexa-1,4-diene (15). This

(14)                    (15)
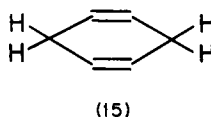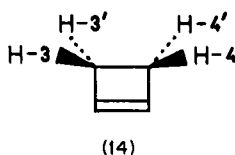
compound actually contains two identical homoallylic coupling paths which apparently[145] lead to a very large calculated $^5J(HH)$ value, much more than twice that obtained for the single path in but-2-ene.[146] Marshall *et al.*[145] have suggested a negative through-space contribution to the axial–axial $^5J(HH)$ in the non-planar form of **15**. Cyclopent-3-enone (**4**) contains two coupling paths, one of which is homoallylic.[126]

Schaefer and coworkers[147] have presented a paper in which the possibility of the occurrence of a negative long-range coupling under conditions of spatial proximity of the coupled protons has been investigated. In this study they examine five-bond and six-bond couplings in the methylhydrazone **16** as a function of two dihedral angles ($NNC_4H$ and $C_1NNC_4$). The calculations predict a negative $^5J(HH)$ only for certain, energetically unfavourable, conformations, contrary to the results obtained from measurements. In the same paper, calculations for methyl vinyl ether (**17**) and anisole (**18**) are reported. The agreement with experimental data appears satisfactory for these cases. Five-bond and six-bond couplings in ethyl vinyl ether have also been reported.[148]



(16)                    (17)                    (18)
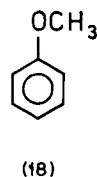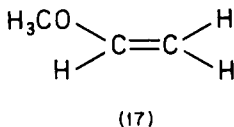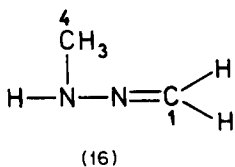
Turning to couplings in butadiene and its methyl derivatives, it can be noted that several of the papers mentioned earlier in connection with vicinal couplings also include calculations of long-range couplings.[118–120,124] A similar study for these systems has been reported.[149] Mstislavsky and coworkers[150] have investigated long-range proton couplings in methyl derivatives of cyclopentadiene, including some conformational dependences. Runge[151] has reported an experimental study of couplings in substituted allenes, where he sought correlations between $^4J(HH)$ and various quantum-chemical indices, e.g. the *ab initio* calculated overlap populations.

Intra-ring couplings in aromatic compounds have been reported for aniline and nitrobenzene[129] and for pyrrole.[137] Long and Memory[130] have calculated a variety of intra-ring as well as inter-ring couplings in benzene and several polycyclic aromatic hydrocarbons. They have noted that it may in some cases be important to use actual rather than standard geometries if comparisons between couplings of similar magnitude are the aim of the investigation. Burmistrov and Mamaev[138] have calculated, using the SOS CNDO/2 method, various long-range couplings in porphin dication.

Several Canadian researchers have, during the period since the previous review, continued their interesting work on long-range couplings between substituent protons and ring protons in substituted aromatic and heterocyclic compounds. In most cases they have reported both FPT INDO and FPT CNDO/2 calculations. The "J-method" for studies of rotation barriers in substituted benzenes and related compounds has recently been reviewed.[152]

Schaefer and coworkers[153] have investigated the five-bond couplings between the OH proton and the ring protons in phenol. The effect of association on this coupling has been studied by performing calculations for the systems 19 and 20. The calculations have been found to be consistent with the monomer–dimer model. In another paper Schaefer et al.[154] have studied the long-range substituent-to-ring coupling in α-fluorotoluene as a function of the rotation angle between the $CH_2F$ group and the ring. The results obtained for this system are similar to those for toluene.[155]
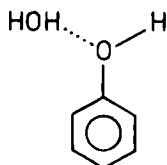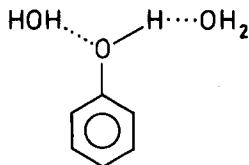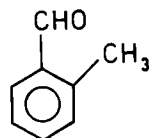


Parr and Schaefer[156] have studied phenylcyclopropane and have reported calculations of $^6J(HH)$ between the para proton and the α proton in the three-membered ring. Parr[157] has reported calculations of couplings between $PH_2$ protons and the ring protons in phenylphosphine. The results of the calculations are displayed in Fig. 3. An extension of this type of study is the work[158] on coupling between the proton in the CHO group and protons in the $CH_3$ group of 2-methylbenzaldehyde (21).

Parr and coworkers[159] have reported calculations for 2-vinylfuran, two of its derivatives, and 2-vinylthiophene in the cis (22) and trans (23) con-



a: X = O  Y = H
b:    O    NO₂
c:    O    CHO
d:    S    H
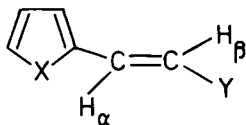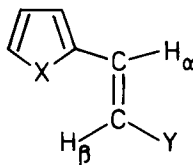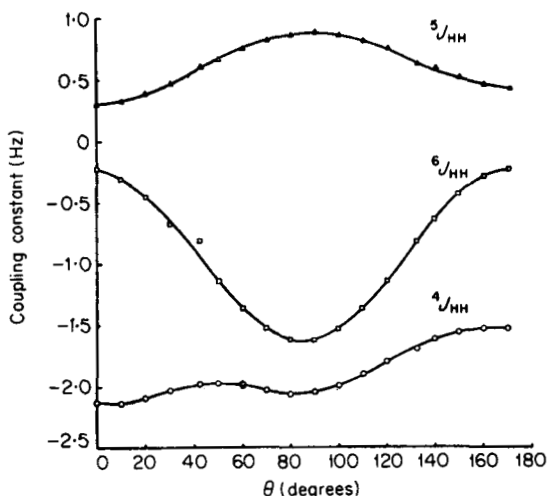
FIG. 3. FPT INDO computed long-range proton–proton coupling constants between side-chain and ring protons in phenylphosphine, as a function of the dihedral angle between the side-chain proton and the plane of the aromatic ring. (Parr[157])

formations, as well as the case for which the vinyl group is perpendicular to the ring plane. As in the case of styrene,[160] the authors claim the CNDO/2 results to be more reliable, at least for some of the substituent-to-ring couplings. Finally, Danchura and collaborators[161] have performed CNDO and INDO calculations of couplings between the $\alpha$ proton in the substituent and the ring protons in pyridinecarboxaldehyde oximes (24 and 25). As in the above-mentioned work on vinylfurans and vinylthiophene,[159] also this investigation covers three conformations (*syn*, *anti*, and perpendicular).

(24)

(25)
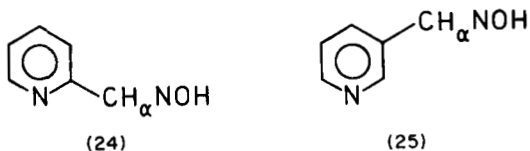
## V. PROTON–OTHER NUCLEUS COUPLINGS

### A. General trends in one-bond couplings in simple hydrides

In this section we review papers dealing with trends in one-bond couplings in simple hydrides, $XH_n$, as a function of the heavy atom X. In such discussions it is mandatory to work in terms of the reduced coupling,

$K$(XH), rather than $J$(XH). The conversion factors, $f_{NN'}$, between $K$(NN') (in the units $10^{19}\,m^{-2}\,kg\,s^{-2}\,A^{-2}$) and $J$(NN') (in the units Hz) are listed for easy reference in Table 6 for several pairs of nuclei.

## TABLE 6

The conversion factor, $f_{NN'}$, between the reduced coupling constant $K$(NN') ($10^{19}\,m^{-2}\,kg\,s^{-2}\,A^{-2}$) and the ordinary coupling constant $J$(NN') (Hz) for several pairs of nuclei.

| N | N' | $f_{NN'}$ | N | N' | $f_{NN'}$ |
|---|---|---|---|---|---|
| $^1H$ | $^1H$ | 12·01 | $^{13}C$ | $^{13}C$ | 0·759 |
| $^1H$ | $^{11}B$ | 3·85 | $^{13}C$ | $^{15}N$ | −0·306 |
| $^1H$ | $^{13}C$ | 3·02 | $^{13}C$ | $^{17}O$ | −0·409 |
| $^1H$ | $^{15}N$ | −1·22 | $^{13}C$ | $^{19}F$ | 2·84 |
| $^1H$ | $^{17}O$ | −1·63 | $^{15}N$ | $^{15}N$ | 0·123 |
| $^1H$ | $^{19}F$ | 11·30 | $^{15}N$ | $^{17}O$ | 0·165 |
| $^1H$ | $^{27}Al$ | 3·13 | $^{15}N$ | $^{19}F$ | −1·14 |
| $^1H$ | $^{29}Si$ | −2·39 | $^{17}O$ | $^{17}O$ | 0·221 |
| $^1H$ | $^{31}P$ | 4·86 | $^{17}O$ | $^{19}F$ | −1·53 |
| $^1H$ | $^{33}S$ | 0·921 | $^{19}F$ | $^{19}F$ | 10·63 |
| $^1H$ | $^{35}Cl$ | 1·18 | $^{13}C$ | $^{29}Si$ | −0·600 |
|  |  |  | $^{13}C$ | $^{31}P$ | 1·22 |

The classical papers in the field of "around the periodic table" correlations were published in the late sixties and early seventies.[162,163] During recent years the subject has been treated in a more quantitative fashion by several authors. In four papers[41,43,48,49] the one-bond couplings in the first- and second-row hydrides have been computed using the non-empirical coupled Hartree–Fock and finite perturbation-configuration interaction methods. A combination of these advanced schemes and large basis sets has led to results in good agreement with experiments (see Tables 7 and 8).

It is interesting to compare the behaviour of the couplings in the first- and the second-row hydrides. In both rows the importance of the orbital paramagnetic term increases rapidly when moving towards the right in the periodic table. The SD term is always small however; in fact it is practically negligible. The same is true for the orbital diamagnetic term, which has been reported only for the first-row hydrides.[64,65] The FC term calculated at the CHF level is almost constant in the first-row hydrides, as is the correlation contribution to the coupling. For the second-row hydrides the situation is different. The CHF values increase strongly between HCl and $SiH_4$ (or $AlH_3$), and the correlation contribution exhibits a trend of its own. In fact the correlation contribution for HCl has a different sign from

## TABLE 7

One-bond reduced coupling constants ($10^{19}$ m$^{-2}$ kg s$^{-2}$ A$^{-2}$) in the first-row hydrides; the contracted basis set is $\langle 5,3,1/3,1 \rangle$ unless stated otherwise.

| | Guest et al.[48] | | | | Kowalewski et al.[41] | | | |
| --- | --- | --- | --- | --- | --- | --- | --- | --- |
| | $^1K^{FC}$ | $^1K^{OB}$ | $^1K^{SD}$ | $^1K^{total}$ | $^1K^{FC}$, CHF | $^1K^{FC}$, FP–CI | $^1K^{total\ a}$ | Exp. |
| HF | 42·3[b] | 17·4[b] | −0·9[b] | 58·8[b] | 41·9[c] | 30·7[c] | 47·2[c] | 46·9 |
| $H_2O$ | 48·8 | 7·5 | −0·4 | 55·8 | 51·3 | 40·2 | 48·1 | 48 |
| $NH_3$ | 57·5 | 2·4 | −0·2 | 59·7 | 56·2 | 43·9 | 46·1 | 50 |
| $CH_4$ | 48·2 | 0·5 | −0·1 | 48·6 | 49·0 | 37·7 | 38·1 | 41·3 |

[a] FP–CI value of $^1K^{FC}$ from ref. 41 plus CHF values of non-contact terms from ref. 48.
[b] Basis set $\langle 11,8,3/7,3 \rangle$.
[c] Basis set $\langle 8,4,2/4,2 \rangle$.

## TABLE 8

One-bond reduced coupling constants ($10^{19}$ m$^{-2}$ kg s$^{-2}$ A$^{-2}$) in the second-row hydrides.

| | Guest and Overill[a] | | | | Kowalewski et al.[b] | | | |
| --- | --- | --- | --- | --- | --- | --- | --- | --- |
| | $^1K^{FC}$ | $^1K^{OB}$ | $^1K^{SD}$ | $^1K^{total}$ | $^1K^{FC}$, CHF | $^1K^{FC}$, FP–CI | $^1K^{total\ c}$ | Exp. |
| HCl | 15·4 | 12·0 | 0·0 | 27·4 | 7·4 | 12·4 | 23·1 | 32[d] |
| $H_2S$ | 36·3 | 4·5 | −0·3 | 40·5 | 33·0 | 27·7 | 31·7 | |
| $PH_3$ | 45·6 | 0·9 | −0·4 | 46·1 | 45·7 | 34·1 | 34·6 | 37·8 |
| $SiH_4$ | 93·8 | −0·2 | −0·1 | 93·5 | 98·7 | 80·0 | 79·7 | 84·9 |
| $AlH_3$ | 96·6 | −0·5 | 0·0 | 96·1 | | | | |

[a] Ref. 49, CHF, basis set $\langle 10,6,1/4,1 \rangle$ for $PH_3$, $SiH_4$ and $AlH_3$, $\langle 10,6,2/4,2 \rangle$ for HCl and $H_2S$.
[b] Ref. 43, basis set $\langle 6,5,1/3,1 \rangle$ for $H_2S$, $PH_3$, and $SiH_4$, $\langle 6,5,2/3,1 \rangle$ for HCl.
[c] $^1K^{FC}$(FP–CI) plus CHF values of non-contact terms; the non-contact terms in refs. 43 and 49 are practically identical.
[d] Sign unknown.

that for the other molecules. In consequence, the total value of the calcu-lated reduced coupling increases between the first and the second row in Group IV but decreases in Groups V, VI, and VII.

Guest, Kowalewski, and coworkers[41,43,48,49] have also investigated the basis set dependence of calculated couplings. For the FC term in both the first- and the second-row hydrides, the basis set sensitivity is weak in Groups IV and V of the periodic table, increases in Group VI, and becomes

finally very dramatic in Group VII. Some results of calculations of $^1K^{FC}$ for the HF and HCl molecules using different basis sets are shown in Table 9. The corresponding non-contact terms show only a weak basis-set dependence.

TABLE 9

The basis set dependence of the CHF calculations of the Fermi contact contribution to the coupling constants in hydrogen fluoride and hydrogen chloride.

| Hydrogen fluoride[48] | | | Hydrogen chloride[49] | | |
|---|---|---|---|---|---|
| Primitive basis | Contracted basis | $^1K^{FC}$ | Primitive basis | Contracted basis | $^1K^{FC}$ |
| (9,5/4) | ⟨9,5/4⟩ | 20·0 | (10,6/5) | ⟨10,6/5⟩ | −12·5 |
| (10,6/5) | ⟨10,6/5⟩ | 24·9 | (11,7/5) | ⟨11,7/5⟩ | −3·3 |
| (10,6,2/5,1) | ⟨10,6,2/5,1⟩ | 35·9 | (13,10/7) | ⟨10,6/4⟩ | −2·4 |
| (11,8,2/7,2) | ⟨11,8,2/7,2⟩ | 39·9 | (13,10,1/6,1) | ⟨10,6,1/4,1⟩ | +13·1 |
| (15,12,3/10,3) | ⟨11,8,3/7,3⟩ | 42·3 | (13,10,2/6,2) | ⟨10,6,2/4,2⟩ | +15·4 |

Pyykkö and Wiesenfeld[16] have reported calculations for the hydrides of Groups IV–VII using the REX formulation of Pyykkö's theory of spin–spin coupling.[10] Comparison with the non-relativistic extended Hückel values (Fig. 4) provides an estimate of the role of relativity. The calculations predict that the couplings will decrease strongly when going from Group IV to Group VII in all rows of the periodic table except the first one. In Group IV the coupling is predicted to increase with an increase in the atomic number of the central atom, while the opposite trend is predicted for all other groups. Recall that the same trend has been obtained in the non-empirical calculations mentioned above. Pyykkö and Wiesenfeld[16] state that the difference between the Group IV hydrides and the other compounds lies in the absence of lone pairs in the former. In confirmation of this proposal the authors report a large negative coupling in $PbH_3^-$. Both of the above-mentioned trends are obtained in the relativistic as well as in the non-relativistic EHT calculations. Relativity, however, is shown to enhance the effects greatly.

For Group IV hydrides, a reasonable approximation to the relativistic calculations may be obtained by applying simple multiplicative corrections.[164] This approach cannot be applied, however, for Groups V–VII, where full relativistic calculations are necessary for the heavy elements. Finally, Pyykkö and Wiesenfeld[16] also report that the s-orbital term, corresponding to the non-relativistic FC contribution, invariably dominates $^1K(XH)$. In view of the results of recent non-empirical calculations,

| C | N | O | F |
|---|---|---|---|
| 23·2 | 32 | 36·6 | 33 |
| 41·3 | 50 | 48 | 46·9 |
| **Si** | **P** | **S** | **Cl** |
| 53·1 | 30 | 28·5 | 8 |
| 84·9 | 37·8 | | 32 |
| **Ge** | **As** | **Se** | **Br** |
| 142·4 | 36 | 2·6 | −69 |
| | (41) | (14·1) | (−47) |
| 232 | ±45 | 28·4 | ±19 |
| **Sn** | **Sb** | **Te** | **I** |
| 289 | 5 | −98 | −223 |
| (219) | (40) | (−16) | (−128) |
| 430 | | ±15·5 | |
| **Pb** | **Bi** | | |
| 844 | −572 | | |
| (373) | (19) | | |
| 938 | | | |

FIG. 4. Reduced coupling constants between directly bonded atoms, $^1K(HX)$, in simple hydrides in relation to the periodic table. The uppermost value is the calculated REX value. The number in parentheses is the non-relativistic EHT value (when different from the relativistic one). The lowermost number is the experimental value. (The calculated results are from Pyykkö and Wiesenfeld.[16])

especially for HF and HCl,[41,43,48,49] this conclusion may prove to be an artifact of the simple computational scheme employed and may not reflect a real trend. Before leaving this section one should also mention the work on EHT calculations for several simple hydrides of the first-, second-, and third-row atoms.[165]

## B. Couplings between Group IV elements and protons

The theory of couplings involving $^{13}C$ was reviewed a few years ago.[166] Further, the theoretical as well as the experimental aspects of two-bond carbon–proton couplings are the subject of a review by Ewing.[167]

Carbon–proton couplings have been the subject of several non-empirical studies. Kowalewski et al.[41] and Guest and coworkers[48] have reported accurate calculations for methane (see Table 7). The data quoted in Table 7 as well as other calculations[51,64,65,68,69,71] clearly demonstrate that the

non-contact terms are not important for C–H couplings. Laaksonen and Kowalewski[44] have calculated one-bond and two-bond carbon–proton couplings in substituted methanes, using the CHF and FP-CI methods. These authors also investigated the conformational dependence of $^1J(CH)$ and $^2J(CH)$. Lazzeretti[51] has reported CHF calculations of one-bond and two-bond carbon–proton couplings in methanol. Barbier *et al.*[60] have performed double perturbation theory calculations of $^2J(CH)$ in ethane and propane.

Turning to the area of semiempirical calculations, the extensive FPT INDO study of $^1J(CH)$ by Maciel *et al.*[168] still holds a central position. An extensive compilation of SOS INDO results obtained using a special parametrization has recently been provided.[169] Several of the method-oriented papers mentioned earlier also contain semiempirical calculations of $^1J(CH)$ and $^2J(CH)$.[16,28–30,32–35,38,63,107,165]

The results of several non-empirical and semiempirical calculations of $^1J(CH)$ in substituted methanes, ethene, and ethyne are gathered in Table 10. For the series of substituted methanes, the non-empirical methods, as well as FPT INDO calculations, are capable of reproducing the effect of electronegative substituents. It is rather remarkable how close the results of the non-empirical finite perturbation-variational CI and the FPT INDO calculations are to each other. No non-empirical CHF type results are available for ethene or ethyne, for the reasons discussed earlier. We can note that all semiempirical approaches reported in Table 10 are successful in reproducing the experimental trend in the series $CH_3CH_3 - CH_2CH_2 - CHCH$. In fact, it has been shown[170] that the trend of increasing $^1J(CH)$ in this series can be explained without performing any calculations. A simple argument taking into account only two electrons in the bonding MO (constructed as a linear combination of a hybrid orbital on carbon and a 1s orbital on the hydrogen atom) leads to the simple relationship:

$$^1J(CH) \propto \% \text{ s character in the carbon hybrid} \qquad (68)$$

This simple model has been put into more quantitative terms by several authors.[e.g.171,172] The results of Van Alsenoy and coworkers,[171] who used the localized INDO MOs obtained with the charge-dependent atomic-orbital exponents (CDOE) technique, are in Table 10.

The couplings between carbon and a proton separated by two bonds have proved to be much more difficult to study theoretically. Results of different calculations of $^2J(CH)$ in ethane, ethene, and ethyne are in Table 11. The FPT method at the CNDO/2, INDO, and MINDO/3 levels of approximation gives results bearing no relationship to the experimental data. The SOS INDO calculations[66] (as well as SOS CNDO, not quoted in the table) are in fact the most successful among the semiempirical studies.

## TABLE 10

Calculated one-bond carbon–proton coupling constants, $^1J(CH)$ (Hz), in substituted methanes, ethene, and ethyne.

| | Ab initio | | | | Semiempirical | | | | | | |
|---|---|---|---|---|---|---|---|---|---|---|---|
| | CHF[a] | CHF[b] | FP-CI[c] | FP-CI[d] | FPT INDO[e] | FPT MINDO/3[f] | EHT[g] | REX[h] | CDOE/ INDO[i] | SOS INDO[j] | Experimental |
| CH$_4$ | 150·7 | 148·0 | 109·6 | 120·1 | 122·9 | 104·3 | 63·4 | 70·1 | | 120·9 | 125·0 |
| CH$_3$CH$_3$ | 157·9 | | 111·4 | 121·0 | 122·1 | 99·2 | 77 | 68·9 | 124·0 | 124·3 | 124·9 |
| CH$_3$NH$_2$ [k] | 161·7 | | 116·2 | | 129·9 | 108·9 | 72 | | 138·2 | 136·4 | 133·0 |
| CH$_3$OH[k] | 169·5 | 172·5 | 121·4 | | 135·3 | | 71·6 | | | 152·4 | 141·0 |
| CH$_3$F | 177·8 | | 128·2 | 136·6 | 140·1 | 122·3 | | | 160·1 | 171·4 | 149·1 |
| C$_2$H$_4$ | | | | | 156·7 | 132·9 | | 83·7 | 161·6 | 171·8 | 156·4 |
| C$_2$H$_2$ | | | | | 232·7 | 191·4 | | 133 | 242·9 | 286·4 | 248·7 |

$^a$ Ref. 44, basis set $\langle 4,2/2\rangle$.  $^b$ Refs 41 and 51, basis set $\langle 5,3,1/3,1\rangle$.  $^c$ Ref. 44, approximate CI.  $^d$ Ref. 44, variational CI.  $^e$ Refs 5 and 168.  $^f$ Ref. 32.  $^g$ Ref. 112.  $^h$ Ref. 16.  $^i$ Ref. 171.  $^j$ Ref. 169.  $^k$ Average value.

## TABLE 11

Calculated two-bond carbon–proton coupling constants, $^2J(CH)$ (Hz), in ethane, ethene, and ethyne.

| | Ab initio | | Semiempirical | | | | |
|---|---|---|---|---|---|---|---|
| | CHF[a] | FP-CI[a] | FPT CNDO/2[b] | FPT INDO[b] | FPT MINDO/3[c] | SOS INDO[d] | Experimental[e] |
| C$_2$H$_6$ | −16·4 | −5·6 | −2·56 | −7·20 | −4·98 | −1·66 | −4·5 |
| C$_2$H$_4$ | | | −3·85 | −11·57 | −22·6 | −1·27 | −2·4 |
| C$_2$H$_2$ | | | 5·51 | 2·52 | −2·91 | 7·46 | +49·3 |

$^a$ Ref. 44.  $^b$ Ref. 5.  $^c$ Ref. 33.  $^d$ Ref. 66.  $^e$ Ref. 173.

The *ab initio* CHF and FP-CI calculations for ethane[44] show that correlation effects in $^2J(CH)$ are even more important than in $^2J(HH)$, which might explain the failure of the semiempirical FPT methods.

We now turn to the more application-oriented papers on carbon–proton couplings. By analogy with the philosophy of Section IV.B, the chemical nature of the compounds under investigation is the primary criterion for the organization of the discussion. We start with saturated aliphatic hydrocarbons and their derivatives, and proceed via the unsaturated hydrocarbons to the alicyclic hydrocarbons and related systems. Finally, calculations for aromatic and heterocyclic molecules are reviewed. As in the case of proton–proton couplings, the FPT INDO procedure has been the most widely used method of calculating carbon–proton couplings. Unless otherwise specified, the FPT INDO (or SCPT INDO) method is implicitly assumed to be that used in the papers reviewed in the rest of this section.

Sergeyev and Solkan[174] have reported calculations of $^1J(CH)$ in methane as a function of the carbon–hydrogen distance. They predict a non-linear variation in $^1J(CH)$ within the range from 109·7 to 141·7 Hz for the carbon–hydrogen distance varying between 1·013 and 1·173 Å. Pachler and Pachter[175] have presented calculations of $^1J(CH)$ in ethane and ethyl cation as a function of the dihedral HCCH angle. In ethane they find $^1J(CH)$ to be essentially constant, while the coupling in the cation is predicted to vary over a range of about 12 Hz. Meille and coworkers[176] have performed SOS CNDO/2 calculations of $^1J(CH)$ in chloroform as a function of the HCCl angle, and used the data for the interpretation of the variation of the coupling upon complexation of chloroform with hexamethylphosphoric triamide.

Several papers have appeared that deal with carbon–proton couplings in alcohols and related systems. Laatikainen *et al.*[110] have reported FPT INDO and SOS INDO calculations of $^2J(CH)$ and $^3J(CH)$ for various conformations of methanol, ethanol, propan-2-ol, t-butanol, and acetylacetone. Aminova and Samitov[112] have studied $^1J(CH)$ and $^2J(CH)$ in methanol and aminomethane as a function of the dihedral HCXH angle, using the EHT approach. Schwarcz and coworkers[177] have investigated the two-bond carbon–proton couplings in ethanol and ethane-1,1-diol using the SOS CNDO/2 approach. Cyr *et al.*[178] have reported calculations of $^2J(CH)$ for propane-1,1,2-triol and butane-2,3-diol. In both of these papers[177,178] the calculated couplings are found to be sensitive functions of the degree of torsion around the C–C bond containing the coupled nucleus, which is in agreement with the experimental data for carbohydrates.

Wasylishen and coworkers[179] have studied $^1J(CH)$, $^2J(CH)$, and $^3J(CH)$ in propanes substituted in the 2-position (**26**). Their calculated $^1J(C_2H)$ data are very similar to the values of the corresponding couplings in

$$CH_3 \diagdown \atop 1 \quad {CH_3 \atop 3} \diagup \atop CHX \atop 2$$
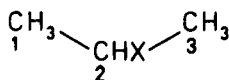
(26)

substituted methanes, while the $^1J(C_1H)$ results are rather insensitive to substitutions. They find that the $^2J(C_2H)$ values are much less sensitive to substitution than the $^2J(C_1H)$ data. The calculated $^3J(CH)$ values are found to be only weakly dependent on X, with the single exception of X = Li. All these trends are in agreement with experimental data.

The three-bond (vicinal) carbon–proton couplings in propane and sub-stituted propanes have been studied extensively.[180] Similar work has been presented more recently by Barfield[181] who explains the calculated changes in $^3J(CH)$ caused by substitution in position-2 in terms of the symmetry of MOs entering the SOS expression, arguing along lines similar to those expounded by Pople and Bothner-By[102] for geminal proton couplings. Further, Barfield[181] has investigated the effects of non-bonded interactions by selectively deleting the corresponding Fock matrix elements in the FPT INDO procedure.

Concentrating on the role of a methyl substituent (or another carbon substituent) in propane, butane, and larger hydrocarbons, Barfield and coworkers[182,183] have shown that substituents on the $\gamma$-carbon ($C_3$ in the nomenclature of 26) decrease the magnitude of the vicinal coupling between $^{13}C$ in position-1 and the proton oriented *trans* to it. Also this $\gamma$-substituent effect has been analysed in terms of non-bonded interactions by deleting selected Fock matrix elements.[183]

Ohkubo and coworkers[108,109] have calculated $^1J(CH)$ in some protonated carbonyl compounds using the SOS INDO method. Cheremisin and Schastnev[184] have reported SOS INDO calculations (using their own special parametrization[169]) of $^1J(CH)$ for classical and non-classical structures of several aliphatic and alicyclic carbonium ions. London et al.[185] have performed calculations of couplings between the carbonyl carbon and protons in aspartic acid and glutamic acid, including the conformational dependences. One- and two-bond carbon–proton couplings in organophos-phorus compounds have been calculated by Safiullin et al.[101,114,115] using the EHT method, and by Albright and Schweizer.[186] Albright and Free-man[187] have calculated $^1J(CH)$ in some diazo compounds. Boyd et al.[188] have calculated directly bonded carbon–proton couplings in N-methyl-enemethylamine N-oxide. Iwayanagi et al.[116] have applied the EHT pro-cedure to calculate some $^1J(CH)$ data in organomercuric compounds.

Several of the papers mentioned earlier on proton–proton couplings in unsaturated systems also presented calculations of carbon–proton

coupling.[37,117,120] Aydin and collaborators[189] have reported SOS CNDO calculations of $^2J$(CH) in ethene. The dependence of carbon–proton couplings in butadiene and cyclopropane on small changes in bond length has been studied.[190] Runge and Kosbahn[191] have studied correlations between $^1J$(CH) in substituted ethenes and products of bond orders squared and charge-corrected orbital amplitudes at the sites of nuclei. The authors also report some SOS CNDO calculations. Runge[192] has sought correlations between $^1J$(CH) in allenes and the STO-3G calculated overlap populations.

The vicinal and long-range carbon–proton couplings in alicyclic compounds have been studied.[182,183,193] The couplings between the starred carbon and the proton in position X in the bicyclic alkanes **27–30** are
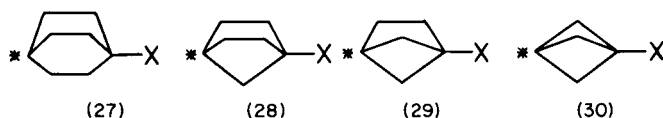


coupling.[37,117,120] shown to provide an interesting example of the non-additivity of different coupling paths, which is explained in terms of the non-bonded interactions between the bridgehead carbons. Table 12 summarizes the calculated couplings and the changes in them caused by deleting the non-bonded interactions between the bridgehead carbons. Also the corresponding couplings between the starred carbon and the carbonyl carbon in the case of X = COOH are quoted in the table.

TABLE 12

Calculated carbon–proton and carbon–carbon coupling constants (Hz) between C* and X in compounds 27–30, and the changes in them caused by deleting the non-bonded interactions between bridgehead carbons.[193]

| Compound | $J$(CH) | $\Delta J$(CH) | $J$(CC) | $\Delta J$(CC) |
|---|---|---|---|---|
| **27** | 0·36 | −0·47 | 0·20 | −0·12 |
| **28** | 8·56 | −3·46 | 5·17 | −1·63 |
| **29** | 13·75 | −7·53 | 8·42 | −3·91 |
| **30** | 17·55 | −30·12 | 11·87 | −17·31 |

Carbon–proton couplings in cyclohexane have been studied.[194] Bicyclic compounds have been investigated by Joela[23] who uses his own theoretical formulation, by Schulman and Venanzi,[127] and by Figeys and coworkers[195] who relate $^1J$(CH) to the percentage of s-character in the carbon hybrid orbital involved in the carbon–hydrogen bond.

Carbon–proton couplings in benzene, calculated using several different methods, are listed in Table 13. As might be expected, all the semiempirical

## TABLE 13

Carbon–proton coupling constants in benzene calculated using different semiempirical methods.

| | FPT CNDO/2[a] | FPT INDO[a] | FPT INDO with 2p on H[b] | FPT MINDO/3[c] | FPT NDDO[d] | SOS CNDO[e] | Experimental[f] |
|---|---|---|---|---|---|---|---|
| $^1J(CH)$ | 116·0 | 140·3 | 151·5 | 134·1 | 158·4 | 57·13 | 157·5 |
| $^2J(CH)$ | −0·17 | −4·94 | −4·37 | −14·07 | | 0·51 | 1·0 |
| $^3J(CH)$ | 5·51 | 9·40 | 9·69 | 23·23 | 6·8 | 2·45 | 7·4 |
| $^4J(CH)$ | −0·06 | −2·27 | −2·71 | −14·94 | | 0·04 | −1·1 |

[a] Ref. 5.  [b] Ref. 38.  [c] Ref. 33.  [d] Ref. 35.  [e] Ref. 197.  [f] Ref. 196.

FPT methods have difficulties with $^2J(CH)$; only SOS INDO[197] predicts the correct sign for this coupling. Two papers[35,198] dealing with the CHF NDDO calculations for benzene and cyclopentadiene unfortunately do not report the $^2J(CH)$ or $^4J(CH)$ values. Couplings between ring carbons and ring protons in substituted benzenes have been reported.[199–202]

Since the last survey,[6] some papers have appeared that deal with couplings between substituent protons and ring carbons in benzene derivatives. Ernst et al.[201] have studied the case of toluene, and Parr[157] has reported calculations for phenylphosphine. Äyräs et al.[203] have performed SOS INDO calculations for salicylaldehyde. Hansen and coworkers[204] have reported SOS INDO calculations of couplings between the carbonyl carbon and ring protons in aromatic carbonyl compounds. Granger and Mangras[205] have reported calculations for naphthalene, and Long and Memory[130] have studied benzene, naphthalene, and four other benzenoid hydrocarbons. Braun et al.[206] have studied $^1J(CH)$, $^2J(CH)$, and $^3J(CH)$ in azulene (31) and aceheptylene (32). The calculated $^1J(CH)$ and $^2J(CH)$ values do not reproduce the experimental pattern, while the calculations of $^3J(CH)$ are more successful.



(31)                    (32)
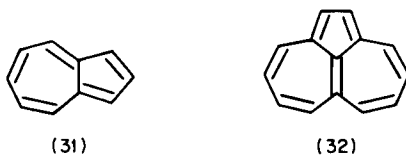
Some of the papers reporting carbon–proton couplings in heterocyclic compounds have already been mentioned in connection with the discussion of proton–proton couplings.[137,138] Carbon–proton couplings in unsaturated

five-membered rings containing two heteroatoms have been reported.[207-209] Wamsler et al.[210] have calculated $J(CH)$ couplings in pyridine N-oxide using the SOS CNDO/2 approach. Seel and Günther[211] have reported SOS CNDO/2 and FPT INDO calculations of carbon–proton couplings in pyridine and the pyridinium ion. The calculated protonation-induced changes in the couplings fail to reproduce the experimental data.

Couplings between protons and other Group IV elements have drawn some attention in the recent literature. Some studies, dealing with one-bond couplings, are already mentioned in the preceding Section A.[16,43,49] The theoretical aspects of proton–Group IV element couplings have been briefly discussed in a review.[212]

Couplings between directly bonded silicon and protons are similar to their carbon–proton counterparts in that both types of coupling may quite successfully be related to hybridization. For silicon compounds, the quantitative relationship between $^1J(SiH)$ and the percentage of s-character in the silicon hybrid orbital participating in the Si–H bond has been given.[213,214] Beer and Grinter[215] have reported FPT INDO calculations of $^1J(SiH)$ in several substituted silanes. Some of the calculations of Kovacevic et al.[213] and Beer and Grinter[215] are compared with each other and with experimental data in Table 14. It can be seen there that the simple hybridization approach works quite well.

TABLE 14

Some coupling constants, $^1J(SiH)$ (Hz), between directly bonded $^{29}Si$ and protons calculated using the maximum overlap approximation (MOA) approach and the FPT INDO method; note that the magnetogyric ratio for $^{29}Si$ is negative.

|                      | MOA[a]  | FPT INDO[b] | Experimental |
|----------------------|---------|-------------|--------------|
| $SiH_4$              |         | −215        | −202·5       |
| $SiH_3CH_3$          | −191·4  | −215        | −194·3       |
| $SiH_2(CH_3)_2$      | −186·8  | −213        | −188·6       |
| $SiH(CH_3)_3$        | −182·1  | −210        | −184·0       |
| $SiH_3SiH_3$         | −197·7  | −199        | −198·2       |

[a] Ref. 213, equation 13.    [b] Ref. 215, parameter set III.

Beer and Grinter[215] have also calculated some two-bond silicon–proton couplings. For these, the calculations predict that the sign will be the opposite of that of $^1J(SiH)$, which seems to agree with the experimental results. A positive $^2J(SiH)$ in tetramethylsilane has also been reported by Barbieri et al.[165] who used the EHT method. Finally, EHT calculations for $^1J(SnH)$ and $^2J(SnH)$ in organostannanes have been presented.[216]

## C. Couplings between protons and Group V elements

Some of the calculations for simple Group V hydrides ($NH_3$, $PH_3$, etc.) have been mentioned in Section A.[16,41,43,48,49,165] In this section other calculations of $J(NH)$ and $J(PH)$ are reviewed, in that order.

Laaksonen and Kowalewski[44] have calculated $^1J(NH)$ and $^2J(NH)$ in aminomethane using the non-empirical CHF and FP-CI methods. In this molecule, $^1J(NH)$ is found to be rather insensitive to the rotation of the methyl group relative to the amine moiety. On the other hand, $^2J(NH)$ is found to vary very significantly with conformation (see Fig. 5). It is worth mentioning that a curve of virtually identical shape, but scaled up relative to Fig. 5, was reported earlier by Wasylishen and Schaefer[217] who applied the FPT INDO method to a variety of nitrogen–proton couplings. Calculations for different conformations of aminomethane have also been reported.[112]

Solomon and Schulman[98] have reported CHF INDO calculations of $^1J(NH)$ in ammonia as a function of the six internal degrees of freedom. Vibrational corrections to the coupling, calculated using two different procedures, have been found to reduce the equilibrium geometry value of $^1J(NH)$ by about 15%.
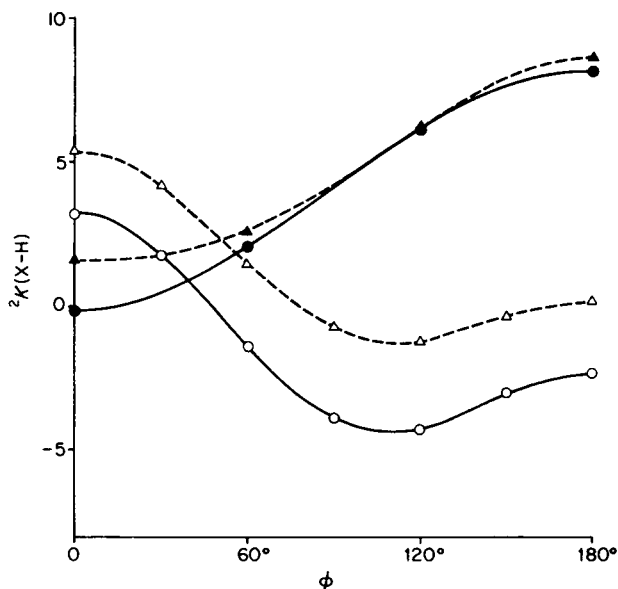


FIG. 5. The dependence of $^2K(XH)$ in aminomethane ($X = N$) and methanol ($X = O$) on the rotation around the C–X bond. The dihedral angle $\phi$ is defined as HCN-lone pair in aminomethane (○, CHF; △, FP-CI) and as HCOH in methanol (●, CHF; ▲, FP-CI). (Laaksonen and Kowalewski[44])

Other workers dealing with calculations of nitrogen–proton couplings have been satisfied to report values for single geometries of selected molecules. Barbieri et al.[165] have applied the EHT method to calculations for $NH_3$, $NH_4^+$, and $N(CH_3)_4^+$. Tarpø and coworkers[30] have applied several different SOS INDO and SOS CNDO schemes to calculations of $^1J(NH)$ in the ammonium ion, pyrrole, pyridazine, and formamide. Dewar et al.[32] have reported FPT MINDO/3 calculations for dimethylformamide, aminomethane, protonated hydrogen cyanide, and protonated acetonitrile. London and coworkers[218] have applied the CHF INDO approach to calculate couplings in 1-methylguanidine. Boyd et al.[188] have reported FPT INDO calculations of $^2J(NH)$ and $^3J(NH)$ in N-methylenemethylamine N-oxide as well as in model aldimines, ketimines, oxaziridines, and nitrones. Lichter and collaborators[219] have studied couplings in ethyl diazoacetate using the CHF method and the INDO approximation. The same method has also been applied for the calculation of $J(NH)$ in pyrrole[137] and for calculations of $J(NH)$ in aniline and nitrobenzene.[129] The results of these calculations are shown in Table 15. Finally, Wamsler and coworkers[210] have reported SOS CNDO calculations for pyridine N-oxide, and Kuroda et al.[220] have calculated $^1J(NH)$ in 4-aminoazobenzene.

TABLE 15

Calculated (FPT INDO) and experimental reduced coupling constants $K(XH)$ and $K(XC)$ (X = N or P) in nitrobenzene, aniline, and phenylphospine.

| Coupling constant | Nitrobenzene[129] (X = N) | | Aniline[129] (X = N) | | Phenylphosphine[157] (X = P) | |
|---|---|---|---|---|---|---|
| | calc. | exp. | calc. | exp. | calc. | exp. |
| $^1J(XH)$ | | | $48.8^a$ | $64.7^a$ | −38.7 | 40.5 |
| $^3J(XH)$ | 3.94 | 1.59 | 2.22 | 1.59 | −0.40 | 1.48 |
| $^4J(XH)$ | 1.16 | 0.68 | 0.86 | 0.39 | 0.15 | 0.32 |
| $^5J(XH)$ | 0.89 | 0.24 | −0.11 | ±0.01 | −0.30 | 0.14 |
| $^1J(XC)$ | 95.6 | 47.6 | 49.0 | 37.5 | −94.9 | −6.69 |
| $^2J(XC)$ | −10.9 | 5.46 | 1.14 | 8.76 | 5.57 | 12.8 |
| $^3J(XC)$ | 17.0 | 7.59 | 3.20 | 4.22 | −5.13 | 4.85 |
| $^4J(XC)$ | −4.22 | ±1.97 | 5.10 | ±0.88 | 4.98 | |

$^a$ Ref. 217.

Proton–phosphorus couplings have attracted considerable interest during the last few years. Non-empirical (STO-3G) double perturbation calculations of phosphorus–proton couplings in phosphine, the phosphonium ion, dimethyl phosphate, and ethyl phosphate have been reported.[61] The calculations for $PH_3$ and $PH_4^+$ yield values about 50% lower than those obtained

experimentally. The calculations for dimethyl phosphate predict a positive three-bond coupling $J$(POCH) in the *trans* arrangement, contrary to earlier FPT INDO calculations.[221] The $^3J$(POCH) coupling obtained from non-empirical calculations displays a dihedral POCH angle dependence similar to what has been predicted earlier for other types of three-bond coupling.[103,180,217]

An extensive set of FPT CNDO/2 calculations of phosphorus–proton couplings in 46 compounds has been reported.[222] The calculations are performed with and without d orbitals in the basis set. Generally, the differences between these two sets of data are found to be small. The predictions of $^1J$(PH) are quite successful for the phosphonium ions (at least for the few cases where experimental data are available). On the other hand, the wrong sign is obtained for $^1J$(PH) in phosphines. In phosphine oxides and related compounds, the sign of the calculated $^1J$(PH) is correct but the trends are somewhat erratic. With the exception of the phosphines, the calculated $^1J$(PH) correlates very well with the square of the s-orbital bond order, $P_{s_Ps_H}{}^2$. Also the effects of some geometrical variations on $^1J$(PH) are reported. The calculations[222] of $^2J$(PH) are in general in poor agreement with experiment, which might be expected by analogy with the difficulties generally encountered in applying the FPT CNDO scheme to calculate geminal couplings. Albright[222] has also studied the dependence of the three-bond phosphorus–proton coupling in the ethylphosphonium cation (**33**) and in ethylidenephosphorane (**34**) on the dihedral PCCH angles and reports typical Karplus-type behaviour. Gray and Albright[223,224]

$$CH_3\!\!-\!\!CH_2\!\!-\!\!PH_3^+ \qquad\qquad CH_3\!\!-\!\!CH\!\!=\!\!PH_3$$
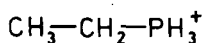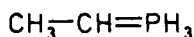
<div align="center">(33)            (34)</div>

have reported similar FPT CNDO/2 calculations for compounds containing phosphorus–nitrogen bonds.

Beer and Grinter[215] have reported FPT INDO calculations of $^1J$(PH) and $^2J$(PH) in a series of model compounds using three different parametrizations. According to these authors, the one-bond coupling in the phosphine molecule proves to be a difficult case also at the INDO level; the calculated value is much too low. The effect of electronegative substituents turns out to be another difficult problem. Otherwise, the calculation of both $^1J$(PH) and $^2J$(PH) is quite successful. Beer and Grinter[215] agree with the conclusion of Albright[222] that d orbitals are not important for calculations of couplings in phosphorus compounds.

Safiullin and coworkers[101] have performed EHT calculations for methylphosphine and obtained values of $^1J$(PH) in good agreement with experimental data. The two-bond coupling $^2J$(PH) is calculated as a function of the angle of rotation of the $PH_2$ group relative to the methyl group. EHT

calculations of phosphorus–proton couplings in $(CH_3)_2PO$, $(CH_3)_2POOH$, $CH_3POCl_2$, $H_3PO_4$, $CH_3PH_2$, and $(CH_3)_3P$ have been reported.[114,115] Several cases of stereochemical dependence are investigated. The value of $^2J(PH)$ in trimethylphosphine has been calculated using the EHT method.[165] Further, calculations of $^1J(PH)$ and $^2J(PH)$ in $OPR_2H$ and $OPR_2CH_3$ type compounds have been presented.[225] Kunz[226] has reported EHT calculations of $^1J(PH)$ in the $HPR_3{}^+$ system as a function of the electronegativity of R, simulated by the variation of the valence shell ionization potential.

Parr[157] has reported calculations of various phosphorus–proton couplings in phenylphosphine and its $P$-halogenated derivatives. The results of calculations for the parent compound are compared with the data for aniline in Table 15. It can be seen in the table that three out of four of the calculated P–H couplings have the wrong sign.

### D. Fluorine–proton couplings

Fluorine couplings in general, including the couplings between fluorine nuclei and protons, are the subject of a review.[227] The obvious model system for performing calculations of fluorine–proton couplings is the hydrogen fluoride molecule. The results of various calculations reported for this molecule are put together in Table 16. The results collected leave no doubt about the difficulties involved in calculations for the HF molecule. The semiempirical methods, with the exception of the EHT method,[16] yield the wrong sign (entries 13–17). The simple SOS approach, compared[97] to the FP Hartree–Fock calculation, gives a $^1J(FH)$ value close to zero (entry 6). The time dependent Hartree–Fock and SOPPA calculations[80] using a basis set of 33 STOs (entries 1 and 3) give values that are much too large. Surprisingly, augmentation of this already large basis with further STOs causes a dramatic change in the SOPPA value (entry 2). The CHF calculations,[52] which also use a large STO basis set, produce still another value of $^1J(FH)$ (entry 4). Correcting for correlation effects, by means of the MC CHF procedure (entry 5), increases the calculated coupling, i.e. has the effect opposite to the SOPPA correction.

A more consistent set of data, providing grounds for some optimism regarding the possibility of quantitative interpretation of the coupling in the HF molecule, has been obtained with large scale calculations using Gaussian type orbitals. Guest et al.[48] have tested the convergence of $^1J(FH)$ (both the contact and the non-contact terms) with respect to the basis-set size (see Table 9 and entry 8 in Table 16). The FC term converges slowly but without major irregularities. The non-contact terms are large and converge quite easily. The non-contact terms have also been reported by Lee and Schulman[64,68,71] (entries 11 and 12 in Table 16) and agree rather well with the findings of Guest et al.[48] The orbital diamagnetic contribution

## TABLE 16

**Calculated proton–fluorine coupling constants, $J$(HF) (Hz), in hydrogen fluoride.**

|     | Method | Author and reference | Basis set | Fermi contact | Other |
|-----|--------|----------------------|-----------|---------------|-------|
| 1.  | SOPPA | Oddershede et al.[80] | 33 STO | 724 | |
| 2.  | SOPPA | Oddershede et al.[80] | 44 STO | 291 | |
| 3.  | TDHF | Oddershede et al.[80] | 33 STO | 955 | |
| 4.  | CHF | Albertsen et al.[52] | 38 STO | 229 | |
| 5.  | MCCHF | Albertsen et al.[52] | 38 STO | 301 | |
| 6.  | SOS | Fukui et al.[97] | 12 CGTO | 3·4 | |
| 7.  | CHF | Fukui et al.[97,228] | 12 CGTO | 295 | |
| 8.  | CHF | Guest et al.[48] | 69 CGTO | 478 | 187 |
| 9.  | CHF | Kowalewski et al.[41] | 42 CGTO | 473 | |
| 10. | FP-CI | Kowalewski et al.[41] | 42 CGTO | 347 | |
| 11. | CHF | Lee and Schulman[68,71] | 6-31 G | | 172 |
| 12. | Monte Carlo integr. | Lee and Schulman[64] | 32 STO | | −8·1[a] |
| 13. | FP-X$\alpha$ | Fukui[96] | | −1360 | |
| 14. | FPT MINDO/3 | Pandey and Chandra[33] | | −228 | |
| 15. | FPT INDO | Facelli et al.[94] | | −140 | |
| 16. | FPT INDO with 2p on H | Facelli and Contreras[38] | | −31·7 | |
| 17. | REX | Pyykkö and Wiesenfeld[16] | | 373 | 0 |
| 18. | Experiment | Muenter and Klemperer[229] | | 530 | |

[a] The diamagnetic orbital term only.

to $^1J$(FH) has very recently been reported by Matsuoka and Aoyama.[65] The calculations by Kowalewski et al.[41] (entries 9 and 10) confirm the results[48] at the CHF level and give an estimate of the correlation effects. We can also note that the sum of the FP-CI result for the contact term (entry 10), the CHF results for the non-contact terms (entry 8), and the Monte Carlo integration result for the diamagnetic orbital contribution (entry 12) is within a few Hz of the experimental value. Though rather impressive, this agreement may to some extent be fortuitous, since it does not take into account vibrational corrections, discussed[94] in connection with simpler calculations.

A favourite model system for performing calculations of $^2J$(FH) is fluoromethane. Some calculations for this system are listed in Table 17. Even here the semiempirical methods perform poorly, while the non-empirical calculations yield results in reasonable agreement with experiment. Tarpø et al.[30] and Pandey and Chandra[33] have also reported calculations of other geminal and vicinal proton–fluorine couplings.

## TABLE 17

**Calculated and experimental proton–fluorine coupling constant in fluoromethane.**

| Author and reference | Method | $^2J(\text{HF})$ |
|---|---|---|
| Laaksonen and Kowalewski[44] | *Ab initio*, CHF | $73\cdot5^a$ |
| Laaksonen and Kowalewski[44] | *Ab initio*, FP-CI | $57\cdot6^a$ |
| Ditchfield and Snyder[47] | *Ab initio*, CHF | $66\cdot6^b$ |
| Pople *et al.*[5] | FPT INDO | $4\cdot7^a$ |
| Facelli and Contreras[38] | FPT INDO with 2p on H | $23\cdot6^a$ |
| Pandey and Chandra[33] | FPT MINDO/3 | $-5\cdot2^a$ |
| Tarpø *et al.*[30] | SOS INDO | $12\cdot3^a$ |
| Frankiss[230] | Experiment | $46\cdot4$ |

$^a$ Fermi contact only.   $^b$ FC(58·5)+OB(12·3)+SD(−4·2).

The long-range proton–fluorine couplings in fluorine-containing benzene derivatives have recently been the subject of several investigations. One particular aspect of the problem, the "through space" or "proximity" mechanism, which refers to the transmission of the coupling between nuclei close to each other in space but separated formally by several chemical bonds, has been reviewed.[231] FPT INDO calculations investigating the "though space" couplings between fluorine and protons have during recent years been reported for α-fluorotoluene,[154] 2-fluorobenzyl alcohol (35),[232] 2-methylbenzoyl fluoride (36),[158,233] 2-methylbenzenesulphonyl fluoride



(35)          (36)          (37)          (38)
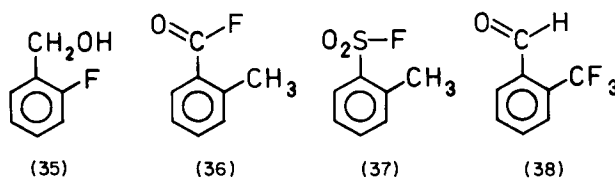
(37),[234] and 2-trifluoromethylbenzaldehyde (38).[158] The calculations predict very large negative couplings between proximate H and F nuclei separated by five bonds,[158,232,233] which is in disagreement with experimental data for **38**. Conformational dependences of more usual long-range proton–fluorine couplings in 3-fluorotoluene[235] and phenyldifluorophosphine[157] have also been reported.

### E. Other couplings involving protons

The oxygen–proton coupling in the water molecule has been calculated using numerous non-empirical[41,48,50,68,71,97] and semiempirical[16,165] approaches. Non-empirical calculations of proton–oxygen couplings,

$^1J$(OH) and $^2J$(OH), in methanol have been reported.[44,51] The plot of $^2K$(OH) in this molecule versus the dihedral HCOH angle[44] is shown in Fig. 5. Calculations of three-bond oxygen–proton couplings in several phosphorus compounds have also been performed.[114,115]

Couplings involving $^{11}$B have been reported[30] for $BH_4{}^+$ using various SOS INDO and CNDO procedures, for BH using the $X\alpha$ method,[96] and for the $BH_3 \cdot CO$ adduct using the FPT INDO method.[100] Solkan and coworkers[236] have presented FPT INDO calculations of $^2J$(BH) and $^3J$(BH) for a series of compounds of the type 39. Their calculations of $^3J$(BH),

$$\begin{array}{c} \diagdown \\ \diagup \end{array} C=C \begin{array}{c} \diagup \\ \diagdown \end{array} B(OH)_2$$

(39)
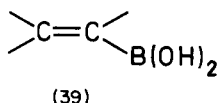
but not $^2J$(BH), turn out to agree reasonably well with the experimental data, conforming to the pattern cited above in Sections B and C. Kroner and Wrackmayer[237] have studied the correlation between experimental $^1J$(BH) in several compounds and the squared bond orders between the s orbitals on the boron and hydrogen atoms, calculated using the non-empirical (STO-3G) and semiempirical (CNDO/2) procedures.

Some of the calculations of couplings between protons and more "odd" nuclei are mentioned above in Section A.[16,43,49,165] Before leaving the subject, mention should be made of the calculation of $^1J$(LiH) in the LiH molecule,[96] and two papers dealing with proton–mercury couplings.[116,238]

## VI. CARBON COUPLINGS

### A. General trends in one-bond couplings between carbon and other nuclei in the periodic table

Laaksonen and Kowalewski[44] have reported non-empirical CHF and FP-CI calculations of $^1K$(CX) for the series of methyl-substituted simple hydrides $CH_3XH_n$, where X = C, N, O, F. The trend found in the series (see Table 18) is remarkably different from the trend in $^1K$(XH) in simple hydrides (Table 7). While $^1K$(XH) in the series HF—$H_2O$—$NH_3$—$CH_4$ is roughly constant, the calculated one-bond couplings between carbon and the same nuclei X vary very dramatically, in agreement with experiment. Applying the ideas of Gutowsky and coworkers,[162,163] the trend in the $CH_3XH_n$ series can be explained in terms of the increasing importance of the core polarization mechanism. In hydrides, or at least in hydrogen fluoride, this mechanism seems to be overriden by the substantial ionic

## TABLE 18

Reduced one-bond coupling constants $^1K(CX)$ ($10^{19}$ m$^{-2}$ kg s$^{-2}$ A$^{-2}$) in some methyl-substituted hydrides.

| | Fermi contact | | | Other mechanisms, | |
| | CHF[a] | FP-CI[a] | Semiemp.[b] | CHF | Experimental |
|---|---|---|---|---|---|
| $CH_3CH_3$ | 79·7 | 43·2 | 54·6 | 1·6[c] | 45·6 |
| $CN_3NH_2$ | 37·9 | 10·8 | 15·0 | | 14·7 |
| $CH_3OH$ | −47·7 | −56·5 | −52·2 | 8·7[d] | |
| $CH_3F$ | −114·0 | −101·6 | −83·5 | 18·3[e] | −57·0 |

[a] Ref. 44.    [b] Ref. 239.    [c] Refs. 68 and 71.    [d] Ref. 51.    [e] Ref. 47.

character of the bond. It should also be noted that the opposite behaviour of $^1K(CX)$ and $^1K(XH)$ is limited to the FC term, while the non-contact contributions in both series behave in a similar way, i.e. they increase upon going from X = C to X = F (note however that the non-contact terms quoted in Table 18 have been obtained using different basis sets for different molecules and are not strictly comparable).

Spin–spin couplings between $^{13}C$ and the first-row nuclei are the subject of a review.[239] In this review are presented some otherwise unpublished results of (unspecified) calculations for the series $CH_3XH_n$, X = Li to F. The results for X = C to F are included in Table 18 for comparison.

Pyykkö and Wiesenfeld[16] have reported a REX study of the systematic variations of $^1K(CX)$ within the columns of the periodic table, i.e. in the series $X(CH_3)_4$ (X = C, Sn, Pb), $CH_3XH$ (X = O, S, Se, Te), $X(CH_3)_2$ (X = O, S, Se, Te). The trends in $^1K(CX)$ within both Group IV and Group VI compounds parallel the trends in $^1K(XH)$ shown in Fig. 4. It should be pointed out, however, that one serious discrepancy arises between the work of Pyykkö and Wiesenfeld[16] and the non-empirical studies:[44,51] the reported value of $^1K(CO)$ in methanol is positive in REX but negative in the *ab initio* work.

A general discussion of one-bond couplings $^1K(CX)$ has been presented by Gutowsky and coworkers,[162,163] and more recently by Shustorovich[240] who uses a generalization of the Pople–Santry theory.[4]

### B. Carbon–carbon and carbon–other Group IV element couplings

Besides the review by Wasylishen[239] mentioned in the preceding section, the carbon–carbon couplings (or more specifically, couplings through two or more bonds) have been reviewed by Hansen.[241] Couplings between carbon and heavier Group IV elements have also been discussed.[212]

Carbon–carbon couplings have been subject to several non-empirical calculations for model systems. The work by Laaksonen and Kowalewski[44] on ethane has been mentioned in the preceding section. Jansen and co-workers[242] have applied the non-empirical version of the scanning MO method to compute the C–C couplings in ethane, ethene, and ethyne. The same series of compounds was studied earlier by Barbier *et al.*[243] who used a simple SOS approach and included the contact as well as non-contact terms. The non-contact terms in ethane, ethene, ethyne and a few other molecules have been reported.[68,69,71] Also many of the previously mentioned method-oriented papers dealing with semiempirical schemes contain some calculations of carbon–carbon couplings.[16,28–30,32,33]

Results of some of the non-empirical and semiempirical calculations are shown in Table 19. Several interesting comments can be made about the data in this table. None of the schemes presented has any trouble reproducing the general trend of the couplings, which increase rapidly with increasing s-orbital contribution to the carbon-carbon $\sigma$ bond. By analogy with the C–H coupling, the trend in the coupling between directly bonded carbons in simple hydrocarbons may in fact be explained without actually performing calculations. A Muller–Pritchard[170] type theory for $^1J(CC)$ has been given;[244] it is found that the coupling is proportional to the product of s-characters of the bonding hybrids of the two coupled carbons. These simple hybridization ideas have found confirmation in non-empirical work.[242] It should be stressed, however, that arguments of this type are valid only for the FC mechanism.

The role of the non-contact mechanisms in $^1J(CC)$ has been the subject of some controversy, as may be inferred from Table 19. All authors seem to agree that both the OB and SD terms in ethane are quite small. For ethene, on the other hand, both non-contact terms are usually found to be rather large and of opposite sign, with the negative OB term prevailing. The magnitudes of the individual OB and SD terms predicted by different methods vary widely, as does their sum (see Table 19). For ethyne, there seems to be general agreement that the SD and OB terms are both quite large and positive. Also for this molecule, various calculations predict a strongly varying total non-contact contribution to the coupling. For the OB term, non-empirical CHF calculations[68] give undoubtedly the most reliable values, 0·2, −9·7, and 15·3 Hz for $C_2H_6$, $C_2H_4$, and $C_2H_2$ respectively. The SD term is more problematical since it cannot be computed using the usual non-empirical CHF methods for ethene and ethyne.[71]

Carbon–carbon couplings are the first type of coupling encountered in this review for which the semiempirical methods also predict non-vanishing non-contact terms. In discussions dealing with such calculations one should start by recognizing one general consideration that can lead to some

## TABLE 19

**One-bond carbon–carbon coupling constants (Hz) in the series $C_2H_6$, $C_2H_4$, and $C_2H_2$.**

| Author and reference | Method | $C_2H_6$ | | $C_2H_4$ | | $C_2H_2$ | |
|---|---|---|---|---|---|---|---|
| | | Contact | Non-contact | Contact | Non-contact | Contact | Non-contact |
| Jansen et al.[242] | Non-empirical, scanning MO | 19·7 | | 53·9 | | 149 | |
| Barbier et al.[243] | Non-empirical, SOS | 17·4 | 0·6 | 69·2 | −1·2 | 190·7 | 2·2 |
| Lee and Schulman[68,71] | Non-empirical, CHF[a] | | 1·2 | | −7·4 | | 19·7 |
| Pople et al.[5] | FPT INDO | 41·5 | | 82·1 | | 163·8 | |
| Blizzard and Santry[46] | SCPT INDO | 35·6 | −2·2 | 70·6 | −14·7 | 140·8 | 31·9 |
| Pandey and Chandra[33] | FPT MINDO/3 | 29·9 | 0·2 | 72·3 | 2·5 | 84·0 | 87·5 |
| Hirao and Kato[28] | SOS INDO, Loc. MO | 27·2 | −1·1 | 71·6 | −2·7 | 141·1 | 3·6 |
| Pyykkö and Wiesenfeld[16] | REX | 22·2 | 0·2 | 60·2 | −9·6 | 116·7 | 15·6 |
| | Experiment | 34·6 | | 67·6 | | 171·5 | |

[a] Approximate expression for the spin-dipolar term has been used.

confusion. The total calculated coupling can be written:[46]

$$J(NN') = a_{NN'}j^{FC}(NN') + b_{NN'}[j^{OB}(NN') + j^{SD}(NN')] \qquad (69)$$

where $j^{FC}(NN')$, $j^{OB}(NN')$, $j^{SD}(NN')$ denote the density matrix dependent parts of equations (37), (45), and (60), while $a_{NN'}$ and $b_{NN'}$ denote the integral products:

$$a_{NN'} = s_N^2(0)s_{N'}^2(0) \qquad (70)$$

$$b_{NN'} = \langle r_N^{-3} \rangle \langle r_{N'}^{-3} \rangle \qquad (71)$$

Now, these integral products can be assigned theoretical values based on atomic calculations or can be used as adjustable parameters to be determined by least-squares fitting of the calculated to the experimental data. If the latter approach is chosen, the parameter values will obviously depend on the experimental data set used. The same problem exists also, at least in principle, for couplings involving protons, where $a_{NN'}$ has to be assigned some value. It appears however that the differences between the $a_{HX}$ values suggested by different authors are not very large. On the other hand, the integral parameters suggested for the case of carbon–carbon couplings vary over quite a wide range. This is illustrated by Table 20, where several of

## TABLE 20

Some $a_{NN'}$ and $b_{NN'}$ integral parameters (atomic units) suggested for the semiempirical calculations of carbon–carbon coupling constants.

| Parametrization | $a_{CC}$ | $b_{CC}$ |
|---|---|---|
| Atomic calc.[a] | 7·656 | 2·863 |
| FPT INDO[b] | 16·255 | |
| SCPT INDO[c] | 13·978 | 8·290 |
| SCPT MINDO/3[d] | 12·585 | 3·590 |
| SCPT INDO, $^1J_{CC}$ only[e] | 13·503 | 5·072 |
| SOS INDO, $^2J_{CC}$ only[f] | 29·146 | 16·208 |
| SOS INDO, $^3J_{CC}$ only[f] | 29·025 | 5·66 |

[a] As quoted in refs 46 and 245.   [b] Ref. 5.   [c] Ref. 46.   [d] Ref. 33.   [e] Ref. 245.   [f] Ref. 246.

the proposed parameter sets are compared with each other. It can be noted that all sets of fitted parameters are larger than the parameters obtained from atomic calculations, in some cases almost by an order of magnitude.

The parameters suggested by Tun Khin and Webb have been obtained in two papers[245,246] presenting extensive studies of carbon–carbon couplings in a variety of bonding situations. The first of the papers[245] contains results

of SCPT INDO calculations of more than 70 one-bond carbon–carbon couplings. In contrast to the classical paper by Maciel *et al.*,[247] Tun Khin and Webb also include the non-contact terms. In the second paper[246] they compare the SCPT INDO and SOS INDO methods applied to a large number of two-, three-, and four-bond carbon–carbon couplings. They find that the SCPT method usually predicts a negative $^2J(CC)$ while most of the attempts to determine the sign experimentally yield a positive sign. The SOS approach is in this respect more successful. They also find the SOS approach to be more satisfactory for $^3J(CC)$.[246] In the vast majority of cases the FC term turns out to be dominant.

We turn now to the more application-oriented papers studying either trends in a particular series of compounds or conformational dependences in model systems. We begin with couplings in aliphatic and alicyclic compounds and proceed to aromatic and heterocyclic systems. Within each group the discussion begins with one-bond couplings and continues with couplings between nuclei separated by several bonds. In most papers the authors have chosen either the SCPT INDO approach (often including the contact as well as the non-contact terms) or the FPT INDO method (usually including only the contact contribution). If no additional comment is made, reference to the FPT INDO method implicitly means that non-contact terms have been neglected.

Kamienska-Trela[248] has reported SCPT INDO calculations of $^1J(CC)$ in acetylene and carbon–carbon couplings in diacetylene (butadiyne). She reproduced the experimentally observed fact that $^1J(CC)$ between carbons 1 and 2 in diacetylene is larger than in acetylene, which is attributed to the FC mechanism. Albright and Schweizer[186] have reported FPT INDO calculations of $^1J(CC)$ in ethane and in ethyllithium. Schulman and Venanzi[127] have performed CHF INDO calculations of $J(CC)$ in bicyclobutane and 1-methylbicyclobutane, including the non-contact terms. They reproduce the negative value of the one-bond coupling between the carbons participating in the central bond. Other couplings calculated by them show good agreement with experiment. Stöcker and Klessinger[249] have investigated $^1J(CC)$ in *cis* and *trans* disubstituted cyclopropanes using the FPT INDO approach. They find that the couplings between the substituted carbon atoms are larger when the substituents are *trans* to each other. These authors have also studied the dependence of $^1J(CC)$ in disubstituted ethanes on the dihedral XCCY angle. London and coworkers[185] have reported FPT INDO calculations of various carbon–carbon couplings in aspartic acid and glutamic acid, including conformational dependence.

Vicinal (three-bond) carbon–carbon couplings have attracted considerable attention that has resulted in several interesting papers. Barfield and coworkers[250] have reported FPT INDO calculations for butane, 1-fluorobutane, 1-cyanobutane, methylcyclohexane, and methyladamantane.

They relate $^3J(CC)$ to different proton–proton couplings by means of the bond orders of valence bond theory. They have also investigated the role of "rear lobes". In a series of more recent papers[181–183,193] Barfield and collaborators have continued the FPT INDO studies of the effects of non-bonded interactions ($\gamma$-substituent effect, bridgehead interactions) on a variety of vicinal carbon–carbon couplings. In order to clarify the mechanisms, the authors delete certain interactions from the INDO calculations. The results[181,250] strongly indicate that no simple Karplus-type relationship exists for $^3J(CC)$. Some of the results for $J(CC)$ in compounds of varying ring size are shown in Table 12.

The dependence of $^3J(CC)$ in butan-1-ol on two dihedral angles, $\phi$ (CCCC) and $\phi'$ (OCCC), has been studied[251] by the FPT INDO method. For $\phi$ larger than 60° it is found that $^3J(CC)$ is almost independent of $\phi'$. For small values of $\phi$ the variation of $^3J(CC)$ with $\phi'$ is found to be substantial. Wray[252] has studied $^3J(CC)$ in numerous butane derivatives, cyclic hydrocarbons, and carboxylic acids. He used the SCPT INDO method and studied the role of non-contact terms. Both the OB and the SD terms are invariably found to be negligible. The calculations reproduce the experimental trends.

Carbon–carbon couplings in substituted benzenes have been the subject of two large SCPT INDO investigations.[253,254] Both of these investigations include the contact as well as non-contact mechanisms, and both groups find that, given the coupled pair of atoms, the couplings fall within rather narrow limits, irrespective of the substituents. Both papers agree also on the observation that the FC term seems to dominate, but differ (because of adopting different integral parameters $b_{CC}$) on the estimates of the absolute values of the non-contact terms. The calculations are reasonably successful in reproducing the experimental data for $^1J(CC)$, less successful for $^3J(CC)$, and fail completely for $^2J(CC)$. A similar pattern with respect to the consistency with experiment has also been noted in FPT INDO investigations on larger aromatic hydrocarbons,[130] and in work on exo-methylene benzocycloalkanes.[255]

Hansen and coworkers[204] have reported SOS INDO calculations (including the FC, OB, and SD mechanisms) of couplings between the carbonyl carbon and the ring carbons in aromatic carbonyl compounds. They obtain the pattern of $^1J(CC) \gg ^3J(CC) > ^2J(CC) > ^4J(CC)$, in agreement with experiment. They find that the OB term is important for two-bond couplings. The same authors have applied the same method to calculations of $J(CC)$ in naphthalene[256] and find poor agreement with experiment. Wasylishen and Pettitt[257] have applied the FPT INDO method to calculate couplings between the substituent carbon and the ring carbons in benzyl cyanide.

The couplings between an exocyclic carbon and ring carbons have also been studied[258,259] by the FPT INDO method. In the work on benzoic acid

and phenylacetic acid (40),[258] the authors note the inadequacy of the CHF INDO method for calculations of geminal carbon–carbon couplings. In the case of phenylacetic acid, the authors studied some cases of conformation dependence and discussed the results in terms of $\sigma$ and $\pi$ mechanisms. In their paper covering cis-crotonaldehyde (41) and o-cyanotoluene (42), Marshall and coworkers[259] studied the mechanism by which various carbon–carbon couplings occur by deleting certain overlap integrals.
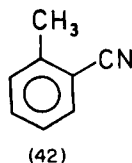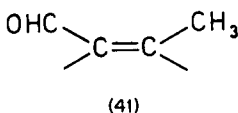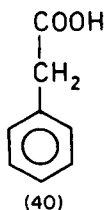


Two of the papers dealing with $J(CC)$ in heterocyclic compounds[137,210] have been mentioned earlier in connection with other types of couplings. Further, London[260] has reported calculations of $^3J(CC)$ in methylimidazole as a function of the protonation site and solvent interactions.

Finally, some papers dealing with couplings between carbon and heavier Group IV elements should be mentioned. Two papers have examined one-bond silicon–carbon couplings. Summerhays and Deprez[261] have reported FPT INDO calculations of $^1J(SiC)$ in a series of trimethylsilyl compounds, $(CH_3)_3SiX$. In general they achieve good agreement between calculation and experiment. The authors claim that in some cases improvement can be expected upon including the d orbitals on silicon in the basis set. They also report correlations between calculated couplings and parameters related to hybridization. More recently[262] calculations of contact and non-contact contributions to $^1J(SiC)$ in a variety of compounds using three different parameter sets[215] in the CHF INDO calculations have been reported. The FC term is found to be predominant and agreement with experiment is good. It may be worth mentioning that the calculations[262] yield a value for $^1K(SiC)$ in $CH_3SiH_3$ of about $90 \times 10^{19}$ $m^{-2}$ kg s$^{-2}$ A$^{-2}$ (no experimental value for this compound is available), while the corresponding $^1K(CC)$ in ethane is only about half as large. Couplings between carbon and tin and between carbon and lead have been reported.[16]

## C. Couplings between carbon and Group V elements

Non-empirical calculations of carbon–nitrogen and carbon–phosphorus couplings are scarce. Laaksonen and Kowalewski[44] have reported CHF and FP-CI calculations for the FC term in aminomethane. Giessner-Prettre

and Pullman[61] have performed DPT calculations (using the STO-3G basis set) for the contact contribution to $^2J(PC)$ and $^3J(PC)$ in dimethyl phosphate and ethyl phosphate. Lee and Schulman[68] have calculated the OB contribution to several nitrogen couplings, e.g. in HCN $^1J^{OB}(CN) = -5.2$ Hz, in $CH_3CN$  $^1J^{OB}(CN) = -4.4$ Hz and  $^2J^{OB}(CN) = 0.4$ Hz, in $CH_3NC$ $^1J^{OB}(CN) = -1.2$ Hz (double bond) and $^1J^{OB}(CN) = 0.4$ Hz (single bond). These values are of interest in the discussion of different semiempirical results.

Semiempirical calculations of carbon–nitrogen couplings, scarce in the first half of the nineteen-seventies, started to flourish in the second half of the decade as a consequence of the greatly increased availability of experimental data. In two papers quoted previously in this review, the FC contribution to CN couplings is reported.[32,47] A general review of carbon–nitrogen couplings has been published.[239] Several papers dedicated to the semiempirical methodology of calculating carbon–nitrogen couplings have appeared recently. Four papers have been devoted to the applicability of the SCPT INDO method.[263–266] Schulman[267] has investigated the capabilities of MINDO/3, and Tun Khin and Webb[268] have reported extensive tests of the SOS INDO approach.

One of the problems dealt with in the above-mentioned calculations has been the evaluation of the relative importance of the FC, OB, and SD mechanisms. As in the case of carbon–carbon couplings, the semiempirical calculations of $J(NC)$ require knowledge of the integral parameters $a_{CN}$ and $b_{CN}$. Schulman and Venanzi[263,264] were the first to report that it was not possible to find unique $a_{CN}$ and $b_{CN}$ parameters that fit all types of coupling. Instead, they suggested a "normal set" for $^1J(NC)$ in molecules with single carbon–nitrogen bonds and another set for the triply bonded situations. Such an approach has no strict motivation; nevertheless, it has been followed subsequently by other authors.[265,266] In the SOS INDO work done by Tun Khin and Webb[268] a single set of $a_{CN}$ and $b_{CN}$ is used; however, no nitriles or related systems are included in the study. The $a_{CN}$ and $b_{CN}$ values suggested by different authors are collected in Table 21. We can note that the "normal sets" obtained by the three groups working with the SCPT INDO method differ somewhat, owing to differences in the sets of experimental data included in the fitting procedure. The differences are larger for the triple-bond set, where experimental data are much more scarce and some sign controversies still remain unsettled. We can further note that, as is also the case for carbon–carbon couplings, the $a_{CN}$ and $b_{CN}$ values suggested on the grounds of SOS INDO calculations are larger than the SCPT INDO based parameters.

Table 22 contains a comparison of the results of different semiempirical calculations for $^1J(NC)$ in aminomethane, acetonitrile, and pyridine. The first observation is that the SCPT MINDO/3 method (using the integral

## TABLE 21

Some $a_{NN'}$ and $b_{NN'}$ integral parameters (atomic units) suggested for the semiempirical calculations of carbon–nitrogen coupling constants.

|                         | Single bonds |          | Multiple bonds |          |
|-------------------------|--------------|----------|----------------|----------|
|                         | $a_{CN}$     | $b_{CN}$ | $a_{CN}$       | $b_{CN}$ |
| Atomic SCF[a]           | 13·199       | 5·247    |                |          |
| SCPT INDO[b]            | 13·79        | 1·77     | 17·08          | 15·34    |
| SCPT INDO[c]            | 14·480       | 2·446    | 10·444         | 17·664   |
| SCPT INDO[d]            | 13·654       | 4·490    | 3·730          | 13·428   |
| SOS INDO[e]             | 35·167       | 4·980    |                |          |

[a] As quoted in refs 265 and 268. [b] Ref. 263. [c] Ref. 265. [d] Ref. 266. [e] Ref. 268.

parameters $a_{CN}$ and $b_{CN}$ from INDO calculations) works very unsatisfactorily.[267] For aminomethane, all other available calculations agree quite well. The three SCPT INDO calculations agree rather well with each other, and also with experimental data for acetonitrile. However, it is somewhat disturbing to see that the $b_{CN}$ parameter yielding this agreement with experiment is about three times larger than the atomic SCF value. Further, the SCPT INDO OB term is highly overestimated compared to the *ab initio* calculations.[68] Thus, it might be over-optimistic to consider the interpretation of $^1J(NC)$ in acetonitrile as being settled. In the case of pyridine the SOS INDO and the SCPT INDO methods agree in predicting the dominance of the OB term.

Wasylishen[269] has studied one-bond nitrogen–carbon coupling in amines and some other compounds. He used the FPT INDO method, limited to the FC term; as in the case of carbon–carbon couplings, the reference to FPT INDO implies that the non-contact terms are not included. Wasylishen finds a positive value for $^1J(^{15}N–^{13}C)$, corresponding to a negative reduced coupling $^1K(NC)$, in the three-membered ring compounds aziridine (**43**) and oxaziridine (**44**). Certain similarities between the variation of $^1J(NC)$ and $^1J(NH)$ under the influence of nitrogen hybridization changes are also noted.
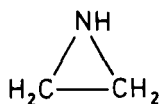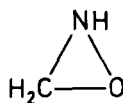


(43)                    (44)

# TABLE 22

Selected results of calculations of carbon-13–nitrogen-15 coupling constants, $^1J$(NC) (Hz), using different methods; note that for the $^{13}C^{15}N$ case $J$ and $K$ have opposite signs.

| Method | CH$_3$NH$_2$ | | | | CH$_3$CN | | | | Pyridine | | | |
|---|---|---|---|---|---|---|---|---|---|---|---|---|
| | FC | OB | SD | total | FC | OB | SD | total | FC | OB | SD | total |
| *Ab initio*, CHF | −11·6[a] | | | | | 4·4[b] | | | | | | |
| *Ab initio*, FP-CI | −3·3[a] | | | | | | | | | | | |
| SCPT INDO[c] | −2·7 | 0·2 | −0·1 | −2·6 | 3·7 | −7·9 | −12·7 | −16·8 | −0·7 | 1·6 | −0·3 | 0·6 |
| SCPT INDO[d] | −2·3 | 0·4 | −0·2 | −2·1 | 2·3 | −9·3 | −15·0 | −21·9 | | | | |
| SCPT INDO[e] | −4·5 | 0·5 | −0·2 | −4·2 | 0·8 | −6·9 | −11·2 | −17·2 | | | | |
| SCPT MINDO[f] | +3·0 | 0·4 | −0·7 | +2·7 | 22·1[g] | −20·3 | −36·3 | −34·5 | −3·7 | 0·0 | −2·1 | −5·8 |
| SOS INDO[h] | | | | | | | | | 0·0 | 2·6 | −0·1 | 2·5 |
| Experiment | | | | −4·5 | | | | −17·5 | | | | 0·6 |

[a] Ref. 44.  [b] Ref. 68.  [c] Ref. 263.  [d] Ref. 265.  [e] Ref. 266.  [f] Ref. 267.  [g] Computed for HCN.  [h] Ref. 268.

Berger and Roberts[270] have reported FPT INDO calculations for different carbon–nitrogen couplings in 1-aminopropane at various conformations and for quinuclidine (**45**). In the latter case they predict $^1J$(NC) and $^3J$(NC) to be of the same order of magnitude, in agreement with experiment. Carbon–nitrogen couplings in azaadamantane (**46**) have been calculated[271] by the FPT INDO method.
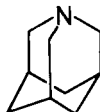


(45)                                         (46)

Axenrod and coworkers[272] have reported SOS INDO calculations of the FC, OB, and SD mechanisms for $^1J$(NC) in a series of ring-substituted anilines and anilinium ions. The FC term is found to dominate these couplings. They only reproduce some of the experimentally established trends. Ernst *et al.*[129] have calculated carbon–nitrogen couplings in aniline and nitrobenzene, including the contact as well as the non-contact terms (see Table 15). The agreement of their results with experiment is not impressive, however, in particular for $^nJ$(NC) with even $n$.

London and coworkers[218] have reported calculations of $^1J$(NC) in 1-methylguanidine and urea. Berger[273] has performed FPT INDO calculations of $^1J$(NC), $^2J$(NC), and $^3J$(NC) in propionic acid N-ethylamide and its O-protonated derivative; they are able to reproduce experimentally established changes following O-protonation. Boyd *et al.*[188] have used the FPT INDO method to calculate $^1J$(NC) in N-methylenemethylamine N-oxide. Kuroda *et al.*[220] have used the SCPT INDO method to calculate several $^1J$(NC) data in 4-aminoazobenzene (**47**).
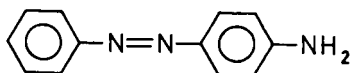


(47)

FPT INDO calculations[274] of one-, two-, and three-bond carbon–nitrogen couplings in oximes show rather poor agreement with experiment. Similar calculations, also with poor results, were reported later.[275,276] In the latter paper the authors point out that the couplings are very sensitive to small changes in geometry.

Carbon–nitrogen couplings in diazo compounds have been studied.[187,219] Runge and Firl[277] have compared, using the SOS CNDO method and

including all mechanisms, the one-bond carbon–nitrogen coupling in diazomethane with the corresponding carbon–carbon coupling in 1,1-dimethylallene.

Carbon–nitrogen couplings in heterocyclic compounds have been reported in several of the papers dealing with carbon–nitrogen coupling in general,[263–268] as well as in some other papers. Galasso[278] has reported SCPT INDO calculations (including the non-contact contributions) for pyridine, pyridinium cation, and pyridine N-oxide. Pyridine N-oxide has also attracted the attention of Wamsler et al.[210] who have applied the SOS INDO approach. Alei and coworkers[279] have used the SCPT INDO approach and calculated various carbon–nitrogen couplings in imidazole, several methylated imidazoles, and some protonated species.

We turn now to carbon–phosphorus couplings. Two papers have dealt with the problem in general and contain comparisons of various carbon–phosphorus couplings in a large number of different compounds. Albright[222] has used the FPT CNDO approach for the FC term and has reported calculations for 46 molecules. He finds that the inclusion of d orbitals centred on phosphorus in the calculations is of some importance. His calculations of $J(PC)$ follow some of the characteristics of the calculations of phosphorus–proton couplings; see Section V.C. In particular, the phosphines turn out to represent a particularly difficult set of cases. Beer and Grinter[262] have studied $^1J(PC)$ in a series of eleven compounds using the FPT INDO method and including the non-contact terms. Their calculations are unsuccessful in reproducing the experimental data. The calculations indicate that the non-contact terms may be important, especially for the compounds of trivalent phosphorus. They do not include the d orbitals on phosphorus but nevertheless argue that it is unlikely that the inclusion of these orbitals alone could significantly improve the results.

A smaller sample of phosphorus compounds has been investigated[114,115] by means of the EHT method employing the FC term only. In another paper[280] the role of the non-contact terms has been studied for $^1J(PC)$ in $CH_3PH_2$, $(CH_3)_2PH$, $(CH_3)_3PO$, and $CH_3POCl_2$. The authors use both the SOS CNDO and EHT methods and find that the non-contact terms are much smaller than the FC contribution. They explain this in terms of the smallness of $\langle r_P^{-3} \rangle$ for the phosphorus valence 3p orbital as compared to the corresponding integral involving 2p orbitals in the first-row atoms.

Calculations of carbon–phosphorus couplings have also been reported in numerous, more application-oriented papers. Safiullin and coworkers[101] have performed EHT calculations of $^1J(PC)$ in methylphosphine. Albright and Schweizer[186] have calculated $^1J(PC)$ in $H_3P{=}CH_2$, $(H_3P{-}CH_3)^+$, and $(H_3P{-}CH_2Li)^+$ using the FPT CNDO method, limiting their interest to the FC term. The same method has been applied[281] to a series of organophosphoranes, $(CH_3O)_2P(O)CH_2X$.
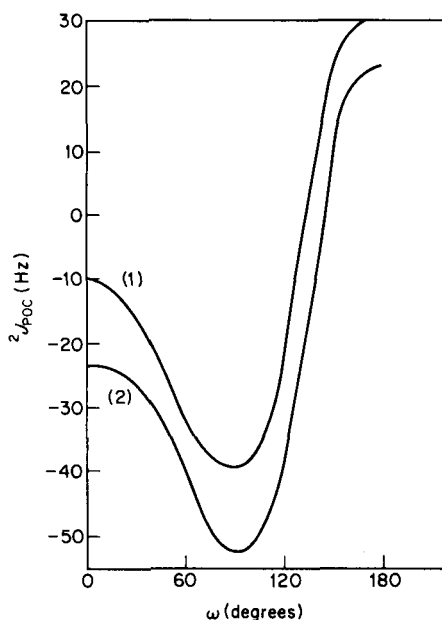
FIG. 6. FPT INDO calculated variation of $^2J$(PC) in ethyl phosphate as a function of the angle $\omega$: (1) $\phi = 180°$; (2) $\phi = 0°$. (Giessner-Prettre and Pullman[221])

$^1J$(PC), $^2J$(PC), and $^3J$(PC) in ethyl phosphate (**48**) and some other compounds have been studied[221] using the FPT INDO method. For ethyl phosphate an extensive study of conformational dependence of $^2J$(PC) and $^3J$(PC) is reported. The curves obtained for $^2J$(PC) as a function of the angle $\omega$ resemble closely the Karplus-type shapes well known for $^3J$(HH) and other couplings (see Fig. 6). Calculations of $^2J$(PC) have been reported in a non-empirical study[61] in which the form (but not the magnitude) of the angular variation of the coupling is confirmed.
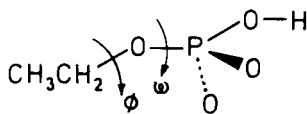


(48)                                    (49)

Pyykkö and Wiesenfeld[16] have calculated $^1J$(PC) in the series $(CH_3)_3PX$, with X = nothing, O, S, Se, Te. Their calculations predict the wrong sign for trimethylphosphine (another example of the difficulties presented by phosphines!), while the calculations for the rest of the series agree reasonably well with experiment.

Two papers[282,283] report the results of FPT INDO calculations for phospha-aromatic compounds, e.g. phosphorin (**49**) and related systems. The

results show that the non-contact mechanisms are significant. In fact, $^1J$(PC) in **49** is dominated by the OB term, while the FC and SD terms almost cancel each other. This is in analogy with the case of $^1J$(NC) in pyridine. For some $^2J$(PC) and $^3J$(PC) couplings the calculations predict the dominance of the SD term. The agreement with experiment is, in general, found to be satisfactory.[282] Inclusion of the d orbitals on phosphorus is shown to be less important.[283]

Parr[157] has reported FPT INDO (contact only) calculations of phosphorus–carbon couplings in phenylphosphine. These results are compared with experiment and with the results for the corresponding nitrogen compound (aniline) in Table 15. As can be seen in this table, the FPT INDO method is not successful for this set of couplings.

### D. Fluorine–carbon couplings

The fluorine–carbon coupling in fluoromethane is another "classical case" and is a favourite model for testing different theoretical approaches. The results of some non-empirical[44,47] and semiempirical[5,30,33,46] calculations of $^1J$(FC) in $CH_3F$ are summarized in Table 23. We can see that the two

TABLE 23

Carbon–fluorine coupling constants, $^1J$(FC) (Hz), in fluoromethane calculated using different methods.

| Author and reference | Method | FC | OB | SD | Total |
|---|---|---|---|---|---|
| Laaksonen and Kowalewski[44] | FP-CI | −288·5 | | | −288·5 |
| Laaksonen and Kowalewski[44] | CHF | −323·8 | | | −323·8 |
| Ditchfield and Snyder[47] | CHF | −149·5 | +32·4 | +19·6 | −97·5 |
| Blizzard and Santry[46] | CHF INDO | −168·7 | −65·0 | +31·0 | −202·7 |
| Pople et al.[5] | FPT INDO | −237·2 | | | −237·2 |
| Pandey and Chandra[33] | CHF MINDO/3 | −129·8 | 202·5 | 503·9 | 576·2 |
| Tarpø et al.[30] | SOS INDO | | | | −229·4 |
| Frankiss[230] | Experiment | | | | −157·5 |

non-empirical CHF calculations fall on either side of the experimental value, and that the correlation effects are rather small. The work of Ditchfield and Snyder[47] is particularly interesting because it also contains the calculation of the non-contact terms. It is noteworthy that semiempirical CHF calculations predict values of the non-contact terms that differ greatly from the non-empirical results. All the methods predict a negative contact contribution, in agreement with the core polarization mechanism.[162,163] The papers for which results are in Table 23, and which report semiempirical calculations for fluoromethane, present similar calculations for other

molecules. Among the earlier more methodological work on carbon–fluorine couplings one should mention the papers by Maciel et al.[247] (FPT INDO, FC term only) and by Towl and Schaumburg[66] (SOS CNDO and SOS INDO, all mechanisms).

Carbon–fluorine couplings have been reviewed.[227,239] Calculations of $J$(FC) have been reported in several application-oriented papers. Wray[284] has applied the SCPT INDO method, including the non-contact mechanisms, to the problem of calculating the angular dependence of three- and four-bond carbon–fluorine couplings. His calculations for fluoropropane predict $^3J$(FC) to be positive, with a sign opposite to that of $^1J$(FC), and dominated by the FC term. His calculated $^3J$(FC) shows a dependence on the dihedral CCCF angle similar to that found for $^3J$(HH) and $^3J$(FH). Wray[284] has reported calculations for 1-fluoro-2-hydroxypropane and for some fluorinated ethers and pyran derivatives. His calculations explain numerous experimental observations. Barfield and coworkers[183] have also studied $^3J$(FC) in fluoropropane and its derivatives. The authors limit their interest to the FC term and investigate the effects of methyl substitution and ring formation on $^3J$(FC) in a *trans* arrangement. They find that the methyl substituent $\gamma$ to the coupled carbon has a larger effect than a similar substituent in the $\alpha$ or $\beta$ position, in analogy with the case of C–C and C–H couplings.

Several papers have recently discussed $J$(FC) data in fluorinated aromatic compounds. Some of the results for fluorobenzene are listed in Table 24. We can see in this table that the two CHF INDO results[278,285] agree well for the contact term; the difference may be due to the slightly different parametrizations and geometries adopted in the two studies. When the non-contact terms are included[278] the calculated $^1J$(FC), $^3J$(FC), and $^4J$(FC) values agree better with experiment.[286] The two SOS INDO calculations[287,288] differ largely in the values selected for $s_C^2(0)s_F^2(0)$ and $\langle r_C^{-3}\rangle\langle r_F^{-3}\rangle$, and consequently give different couplings. Hansen and co-workers[287] have used the theoretical atomic values[66] while Duangthai and Webb[288] have used adjusted parameter values, allowed to be different for $^1J$(FC) and $^3J$(FC). All the INDO calculations listed in Table 24 (but not the EHT work[286]) fail to give the correct positive sign for $^2J$(FC), showing once more that geminal couplings provide a difficult task for theoretical studies.

The interests of the authors of the above-mentioned papers have not been limited to fluorobenzene. Doddrell and coworkers[285] have reported calculations for fluoronaphthalenes, fluoropyridines, and fluoroquinolines. These authors present an analysis of the relationship between carbon–fluorine couplings and proton–fluorine couplings, using the valence bond Penney–Dirac bond orders. Fluoropyridines have been studied by Galasso,[278] while fluoronaphthalenes have attracted the attention of

## TABLE 24

Calculated and experimental values of $^nJ$(FC) (Hz) in fluorobenzene.

| | FPT INDO[a] contact | SCPT contact | INDO[b] total | SOS INDO[c] total | SOS contact | INDO[d] total | EHT[e] | Experiment[e] |
|---|---|---|---|---|---|---|---|---|
| $^1J$(FC) | −213·0 | −220·9 | −238·7 | −75·6 | −228·0 | −265·3 | +207 | −245·3 |
| $^2J$(FC) | −1·7 | −1·8 | −13·0 | −0·9 | | | +4·5 | +21·0 |
| $^3J$(FC) | +12·4 | +12·8 | +11·6 | 1·6 | +1·3 | +3·4 | +9·6 | +7·7 |
| $^4J$(FC) | −0·9 | −0·9 | +3·5 | 2·8 | | | −0·8 | +3·3 |

[a] Ref. 285.  [b] Ref. 278.  [c] Ref. 287.  [d] Ref. 288.  [e] Ref. 286.

Hansen et al.[287] Duangthai and Webb[288] have studied $^1J$(FC) and $^3J$(FC) in a long series of substituted fluorobenzenes. Further, Wray[289] has reported calculations of $J$(FC) in pentafluorobenzenes using the SCPT INDO method. In general he finds that the non-contact contributions are significant. As in the papers mentioned above, Wray[289] also encounters difficulties in correctly predicting $^2J$(FC). On the other hand, the substituent effects on $^3J$(FC) are reproduced rather successfully.

Carbon–fluorine couplings are discussed in some of the papers dealing with the general aspects of fluorine couplings. Work of this type is reviewed in Section VII.A.

### E. Other couplings involving carbon

Couplings between carbon and first-row atoms in general are the subject of a review.[239] The directly bonded carbon–oxygen couplings in methanol and carbon monoxide have been calculated at the ab initio level by three groups.[44,51,80] The experience of these studies is that, while the CHF and FP-CI calculations for methanol[44,51] give a positive $^1J(^{17}O^{13}C)$ value [negaTIVE $^1K$(OC)], the CHF and SOPPA calculations for CO predict the opposite sign.[80] Two-bond carbon–oxygen couplings have been calculated for several phosphorus-organic compounds.[114,115,280]

Three papers have been concerned with carbon–boron couplings. Hall and coworkers[290] have reported FPT INDO calculations of the FC term for nine organoboranes. The pattern of the calculated $^1J$(CB) data [$^1J$(CB) in $B_5H_8X$ with X = $CH_3$, $C_2H_5$, $CH(CH_3)_2$ close to 70 Hz, decreasing $^1J$(CB) along the series $B(C_2H_3)_3$—$B(C_2H_5)_3$—$B(CH_3)_3$, and the smallest $^1J$(CB) of about 30 Hz in $BH_3 \cdot CO$] is found to agree with the experimental data. No correlation is found between calculated couplings and the fractional s character in the boron–carbon bond. $^1J$(CB) in the $BH_3 \cdot CO$ adduct has also been calculated.[100] Kroner and Wrackmayer[237] have sought

correlations between $^1K(BX)$, $X = B$, C, H, and the square of the bond order matrix elements involving s orbitals.

Some papers have contained calculations or theoretically interesting discussions of carbon–metal couplings. Iwayanagi and Saito[291] have reported EHT calculations of $^1J(PtC)$ in ethene and carbonyl complexes of platinum. The difference in the magnitude of the couplings for these two cases is reproduced and the causes explained. Finally, mention should be made of the papers by Jokisaari *et al.*[292,293] discussing the experimental results for carbon–cadmium and carbon–mercury couplings in relation to the relativistic theory.[10] Carbon–thallium couplings have also been reported.[16]

## VII. OTHER COUPLINGS

### A. General trends in one-bond couplings between fluorine and other nuclei

The foundation of our understanding of trends in $^1K(FX)$ in $XF_n$ compounds as a function of the position of X in the periodic table has been laid by Gutowsky and coworkers in the papers[162,163] mentioned earlier in connection with $^1J(XH)$ and $^1J(CX)$ couplings.

Nefedov and coworkers[294,295] have presented a general discussion of $^1K(AF)$ in the $AF_n^{x-}$ compounds. They derive and analyse the Pople–Santry type formulae and find that $^1K(AF)$ should be negative for A being a main group element (with the exception of the compounds with markedly ionic AF bonds) and, most likely, positive for A being a transition metal. They establish a correlation between the "completely reduced coupling constant" (i.e. $K$ divided by the valence s-orbital densities at the coupled nuclei) and s-orbital energies for A. Further, they apply perturbation theory to explain the changes in $^1K(AF)$ when going from $AF_6^{x-}$ to $AF_5L^{x-}$, and find a relationship between the nature of A and the relative values of $^1K(AF)_{trans}$ and $^1K(AF)_{cis}$.

Shustorovich and Dobosh[240,296,297] have presented a discussion of the effects of substituents on the value of $^1K(AF)$ in substituted fluorides $AF_{3-k}L_k$, $AF_{4-k}L_k$, and $AF_{6-k}L_k$. For the planar trigonal and tetrahedral main-group fluorides, Shustorovich and Dobosh[296] show that their model predicts different types of behaviour for different elements A, depending on the relative energies of the $s_A$ and $p_F$ orbitals. They report that the substituents L can be divided into two classes, using the presence (or lack) of an s lone pair as the criterion for the classification. Thus, four different trends of $^1K(AF)$ in $AF_{4-k}L_k$, compared to $AF_4$, are predicted, all of which are in agreement with the experimental evidence. For the case of A = C or Si, the authors also report some EHT calculations confirming their

model. In a paper on octahedral substituted fluorides, Shustorovich and Dobosh[297] have discussed the trends in the series $^1K(AF)_{unsubstituted}$—$^1K(AF)_{cis}$—$^1K(AF)_{trans}$ for A being a main-group element as well as a transition metal. Also, they criticize the approach of Nefedov et al.[294,295] Shustorovich and Dobosh[297] show that, for A being a main-group element, the relation between $^1K(AF)_{cis}$ and $^1K(AF)_{trans}$ may be different, depending on the relative orbital energies of $s_A$ and $p_F$ and on the presence, or the absence, of an s lone pair on the ligand.

## B. Fluorine–fluorine and fluorine–other first-row atom couplings

Fluorine couplings have been the subject of a review.[227] The problem of the "through space" mechanism of spin–spin coupling, often interesting in the context of fluorine coupling constants, has been reviewed.[231]

The two fluorine nuclei in the $F_2$ molecule are spin–spin coupled, but the coupling cannot be observed. Calculations of this $^1J(FF)$ have been reported by Towl and Schaumburg[66] (about 2000 Hz using the SOS INDO methods) and by Jansen et al.[242] (5040 Hz using the scanning MO method). Two- and three-bond fluorine–fluorine couplings in model organic compounds have been reported[46] from the SCPT INDO approach and show that the OB term is always at least comparable to the FC term and often dominant to it. More recent work,[33] by the SCPT MINDO/3 method, confirms this prediction but the results show no resemblance whatsoever to the experimental data. Robb and Chin[58] have reported non-empirical calculations of the FC and SD contributions to $^2J(FF)$ in difluoromethane (FC, 60·6 Hz; SD, 117·8 Hz), to $^3J(FF)$ in 1,2-difluoroethane (FC, 41·6 Hz; SD, 27·2 Hz), and to $^3J(FF)$ in cis-difluoroethene (FC, −0·7 Hz; SD, 51·0 Hz).

Wray[289] has reported SCPT INDO calculations of F–F couplings in pentafluorobenzenes. For three-bond couplings his calculations predict that the FC mechanism yields the largest contribution but that the other terms are also important. In his calculations, both the FC and the total non-contact contributions are negative. For four-bond couplings, Wray[289] finds that the FC term is always negative and that the non-contact contributions are positive, with the total taking either sign. For five-bond couplings he obtains a positive sign. The overall correlation between theory and experiment for the $C_6F_5X$ systems is rather good, as can be seen in Fig. 7.

Matthews[298] has reported results from an investigation of fluorine–fluorine couplings in heptafluoroquinoline (50) and heptafluoroisoquinoline (51). He has examined the correlation between the experimental data and the corresponding carbon–carbon mutual polarizabilities and carbon–carbon $\pi$ bond orders. Schaefer and coworkers[299] have discussed the fluorine–fluorine couplings in ring-fluorinated derivatives of $C_6H_5CF_3$ and
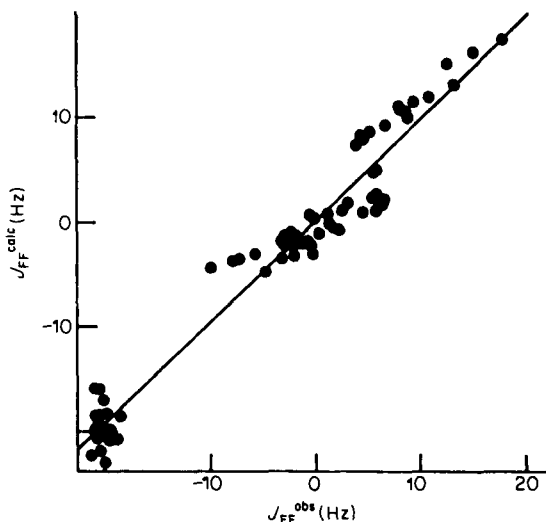
FIG. 7. Correlation of $J$(FF) calculated using the SCPT INDO method with observed data. (Wray[289])

related systems. They do not report numerical results but refer to Niemczura's M.Sc. thesis.



(50)                        (51)
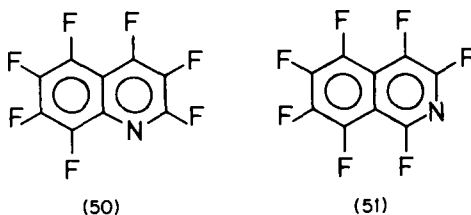
Tun Khin et al.[300] have reported SCPT INDO and SOS INDO calculations of twenty-five nitrogen–fluorine couplings through one to five bonds. As in most other work from that laboratory, the couplings are expressed by equation (69) with $a_{NF}$ and $b_{NF}$ treated as adjustable parameters. In all cases $^1J(^{19}F^{15}N)$ is found to be positive [$^1K$(FN) negative] and dominated by the FC term. They also find couplings through more than one bond to be dominated by the FC interaction; $J$(FN) data of either sign are predicted. By and large, the SCPT and the SOS treatments lead to equally satisfactory agreement with experiment. Further, the nitrogen–fluorine coupling in the $NF_3$ molecule and boron–fluorine couplings in $BF_3$ and $BF_4^-$ have been computed.[30]

## C. Phosphorus couplings

Numerous authors have shown interest in phosphorus–phosphorus coup-lings and, for obvious reasons, diphosphine $P_2H_4$ has proven to be a favourite model system. Albrand and coworkers[301] have reported simple SOS non-empirical calculations of $^1J(PP)$ for four conformations of this molecule, including the contact as well as non-contact terms. They find that the FC contribution varies between $-241 \cdot 8$ Hz (for the eclipsed confor-mation) to $+9 \cdot 6$ Hz (in the staggered conformation). The SD term is found to be almost independent of the rotation of the two $PH_2$ groups and close to 4 Hz. They report a negative value for the OB term, with a magnitude of at most 3 Hz. The shape of the curve of $^1J(PP)$ versus the rotation angle[301] (see Fig. 8) seems to be consistent with experimental data for related comounds. The same angular dependence curve has been investi-gated[283] by the FPT INDO method. The angular dependence of the coup-ling appears to be dominated by the FC term. The calculated magnitudes of the OB and, in particular, the SD contributions deviate strongly from the *ab initio* results. This might at least partly be an artifact of the large values of $\langle r_P^{-3}\rangle\langle r_P^{-3}\rangle$ adopted,[283] contrary to other proposals.[280] The total calculated $^1J(PP)$ reported as a function of the dihedral HPPH angle is included in Fig. 8. Galasso[283] has also reported calculations of $^1J(PP)$ in
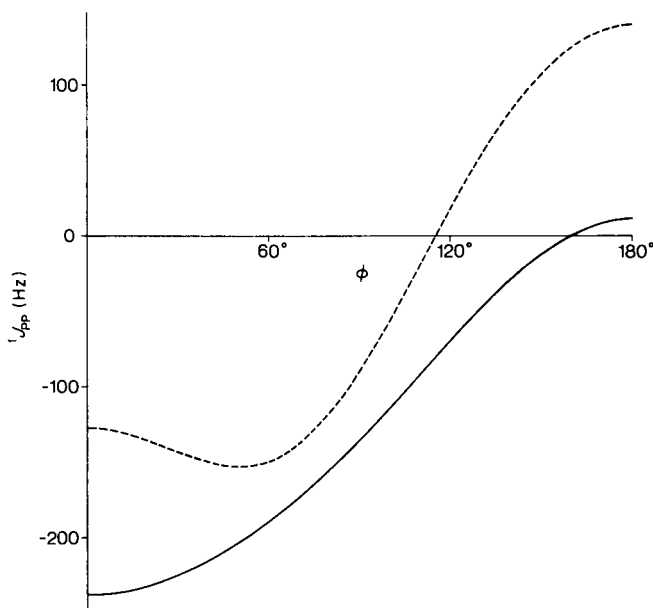


FIG. 8. Variation of the calculated $^1J(PP)$ in $P_2H_4$ as a function of the dihedral angle between the lone pairs. The solid line corresponds to the *ab initio* calculations of Albrand *et al.*,[301] the broken line to the FPT INDO (spd basis) results of Galasso.[283]

tetramethyldiphosphine, dimethyldiphosphine, and tetrafluorodiphosphine. For the latter molecule the SD mechanism is found to dominate. $^1J(PP)$ in diphosphine has been reported from the REX method,[16] the scanning MO method,[242] and the FPT CNDO/2 approach.[224] Further, calculations of $^2J(PP)$ and $^3J(PP)$ in some organophosphorus compounds have been reported.[221]

Gray and Albright[223,224] have reported FPT CNDO/2 calculations of the FC contribution to couplings between phosphorus on the one hand and nitrogen, oxygen, and sulphur on the other. In Fig. 9 their calculated $^1J(^{31}P^{15}N)$ data for aminophosphine, $PH_2NH_2$, are shown as a function of the dihedral lone pair–P–N–lone pair angle ($\phi$) for two geometries of the $NH_2$ group (pyramidal, planar trigonal). For both geometries the calculated $J$ value is positive [$K(PN)$ is negative] over the whole range of values of the dihedral angle. It should be noted that the calculated couplings for the trigonal geometry of the amino group are essentially independent of $\phi$, while a considerable variation is obtained for the pyramidal case. The figure also contains the plot of the square of the bond order term, $P^2_{s_Ns_P}$, as a function of $\phi$ (dashed–dotted line) for the case of pyramidal geometry at the nitrogen site. The two curves, $J(^{31}P^{15}N)$ and $P_{s_Ns_P}{}^2$, are parallel in the figure. The search for $J$–$P_{s_Ns_P}{}^2$ correlations does not, however, seem to be
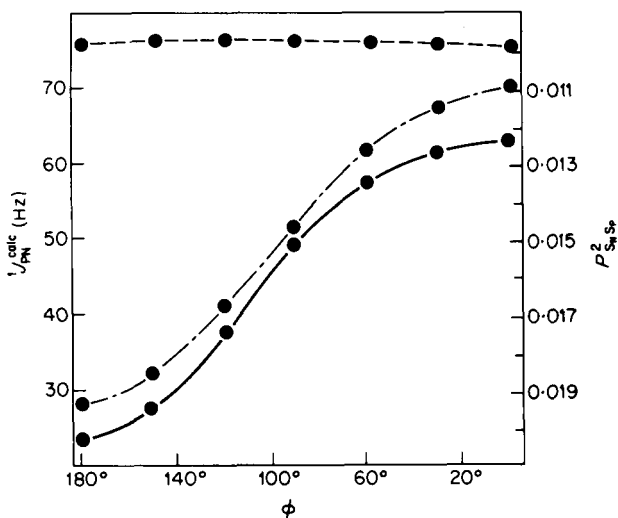


FIG. 9. The calculated P–N coupling constant in aminophosphine as a function of the dihedral angle $\phi$ between the lone pairs. The solid line refers to a pyramidal geometry at nitrogen, the dashed line to the trigonal geometry. The dashed-dotted line refers to the dependence of the phosphorus s–nitrogen s bond order squared, $P^2_{s_Ns_P}$, as a function of $\phi$ for the pyramidal geometry of nitrogen. Note that the scale of $P^2_{s_Ns_P}$ is plotted inversely. (Gray and Albright[224])

fruitful in this case because of the negative sign of the reduced coupling. The calculated values of $J(^{31}P^{17}O)$ are in general positive, corresponding to a negative $K(PO)$.[223,224] Phosphorus–oxygen couplings have also been reported,[114,115] as well as calculations of $^1J(PO)$ and $^1J(ClP)$.[280]

Pyykkö and Wiesenfeld[16] have reported REX calculations of $^1K(PX)$ in the series $(CH_3)_3P{=}X$ with $X = O$, S, Se, Te. They successfully reproduce the experimental trend of $^1K(PX)$ changing from large and positive for the case of $X = O$ to large and negative for heavier chalcogenides. Shustorovich[302] has reported a qualitative discussion of phosphorus couplings in phosphorus(III) compounds, using the perturbation extension of the Pople–Santry theory. A general discussion of phosphorus couplings, with a special stress on the charge dependence of couplings, has been given.[226]

## D. Other couplings

Schulman and coworkers[303] have reported model studies of nitrogen–nitrogen couplings using the SCPT INDO method. The authors chose hydrazine, $NH_2NH_2$, as a model system and studied the dependence of $^1J(NN)$ on the dihedral angle, $\phi$, between the lone pairs. Further, the effect of eliminating the s-hybridized lone pair is investigated by assuming one (or both) $NH_2$ moiety to be either planar or protonated. The results can be summarized by the following three points. (1) For systems with no s-hybridized lone pairs, $^1J(NN)$ is positive owing to a large and positive contribution from the FC mechanism; this is analogous to results for $^1K(NC)$ in similar systems. (2) When one s-hybridized lone pair is present, the sign of $^1J(NN)$ is negative owing to a large but negative FC contribution; this corresponds again to the case of carbon–nitrogen couplings and illustrates the concept of the one-bond lone pair effect.[263,264] For cases corresponding to points (1) and (2), the calculated coupling shows only a weak dependence on the rotation of the two $NH_2$ groups relative to each other [compare this with the results[224] for $^1J(PN)$!]. (3) In the situation involving two s-hybridized lone pairs there is a strong dihedral angle dependence (see Fig. 10), resulting in the possibility of the coupling having either sign. Schulman et al.[303] present a discussion of these particular trends in terms of the simple SOS model.

Tun Khin and Webb[304] have reported a large set of SOS INDO calculations of nitrogen–nitrogen couplings. The authors find the calculated one-bond couplings between nitrogen nuclei connected by a single bond to be (in general) negative, with the FC term constituting the major contribution. Their study of $^1J(NN)$ for the case of multiply bonded nitrogen atoms indicates that the FC and OB terms are similar in magnitude, both with a negative sign. Tun Khin and Webb[304] report also calculations of $^2J(NN)$
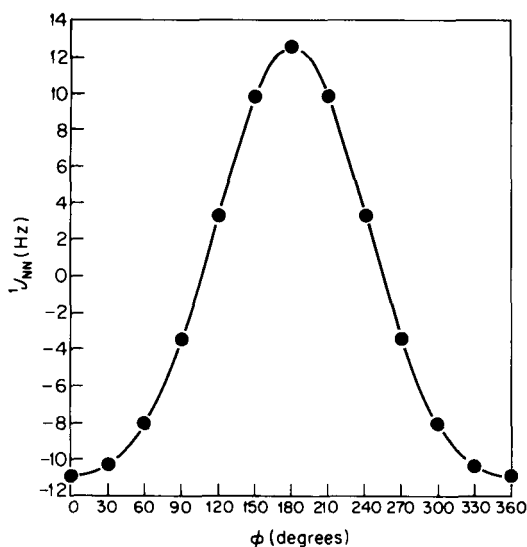
FIG. 10. $J(^{15}N^{15}N)$ of hydrazine as a function of dihedral angle $\phi$ between nitrogen lone pairs. (Schulman et al.[303])

in urea and dimethylurea. $^2J(NN)$ in urea is found to oscillate as a function of the dihedral angle between the lone pairs but to remain positive for all values of the angle. Calculations of other nitrogen–nitrogen couplings have also been reported.[219,220,242,305]

Jansen and coworkers[242] have reported calculations of the lithium–lithium coupling in the $Li_2$ molecule, and of the silicon–silicon coupling in disilane, $SiH_3SiH_3$, and in the triply bonded $Si_2H_2$ molecule. The spectral density functions for the silicon–silicon couplings in both molecules are very similar in shape. The coupling in the triply bonded system is calculated to be a factor of 3·5 larger than in disilane, which is to be compared with the factor of 4 expected from simple hybridization arguments. Homonuclear couplings between heavier Group IV elements (Si, Ge, Sn, Pb) have been calculated.[16] The same paper contains calculations of homonuclear coup-lings between heavier Group VI and VII elements and of couplings between thallium and heavier halogens. Boron–boron couplings have been corre-lated with the corresponding bond order parameters;[237] finally, oxygen–chlorine couplings have been reported.[280]

## VIII. SPECIAL TOPICS

### A. The solvent dependence of couplings

The solvent dependence of couplings is the subject of several theoretical papers published in the early nineteen-seventies and of a review article.[306]

During recent years, two papers have dealt with solvent effects on one-bond carbon–proton couplings. Kondo and coworkers[307] have presented calculations of the effects of the solvent dielectric constant on $^1J(CH)$ in acrylonitrile, difluoromethane, trifluoromethane, dichloromethane, and chloroform (trichloromethane). These authors have worked within the framework of the FPT method using either the CNDO/2 or INDO approximations and include the role of the solvent by adding to the Hamiltonian the terms corresponding to the solute–solvent interactions as described by Klopman's solvaton theory.[308,309] Their calculations predict a large increase of $^1J(CH)$ with an increasing dielectric constant; the trend as such is in agreement with experimental findings but the magnitude of the variations is overestimated. Kondo and coworkers[307] predict the functional relationship between $^1J(CH)$ and the dielectric constant $\varepsilon$ as:

$$^1J(CH) = a\left(\frac{\varepsilon - 1}{\varepsilon}\right) + b\left(\frac{\varepsilon - 1}{\varepsilon}\right)^2 + c \qquad (72)$$

A subsequent paper from the same laboratory[310] has applied the same methods to the study of the solvent dependence of $^1J(CH)$ in chlorinated ethanes. In these systems the total experimentally observed changes in $^1J(CH)$ are determined by two separate effects, the solvent-induced changes in the couplings for a given conformation and those in confomer populations. According to Watanabe and Ando[310] the former effect can be expected to be the more important of the two.

A different approach to the problem of solvent interactions has been applied by London[260] who has studied the effects of surroundings on the three-bond carbon–carbon couplings in 4-methylimidazole by explicitly including one hydrogen-bonded molecule of water or ammonia in the calculations.

## B. Anisotropy in the nuclear spin–spin coupling

The subject of the anisotropy of nuclear spin–spin couplings has gained wider interest with increasing use of the NMR of molecules dissolved in liquid crystalline solvents.[311] The theoretical work in this field during the last few years has been pursued by Pyykkö and associates, who presented the relativistic theory of the phenomenon,[10] applied it in a semiquantitative fashion,[10,292,293] and more recently also reported pertinent SOS REX calculations.[16]

As noted in Section II.B, the coupling tensor, **J** or **K**, is in general asymmetric and may contain nine independent elements. Pyykkö and Wiesenfeld[16] compute the tensor **K** in spherical form. At the end of the calculation, **K** is brought into cartesian form and split into a symmetric and an antisymmetric tensor. The symmetric tensor is then diagonalized and the antisymmetric tensor is expressed in the same coordinate system.

In cases where the axis connecting the coupled nuclei coincides with a 3-fold, or higher, symmetry axis of the molecule, the number of independent elements is reduced to two, $K_{\parallel}$ (parallel) and $K_{\perp}$ (perpendicular), and the relative anisotropy $R$ may be defined as:

$$R = (K_{\parallel} - K_{\perp})/K_{\text{isotropic}} \tag{73}$$

In the same study[16] a report is given of the anisotropies of the couplings between light elements that are in qualitative agreement with earlier work. The trends found for the variation of the relative anisotropy along the columns of the periodic table can be illustrated by the data for $^1K(XH)$ in the series $XH_4$ and $^1K(CX)$ in the series $X(CH_3)_4$, with X being the Group IV element C, Si, Ge, Sn, and Pb. The results are shown in Table 25. The

## TABLE 25

Calculated relative anisotropies, $R$, of one-bond coupling constants $^1K(XH)$ and $^1K(XC)$ in $XH_4$ and $X(CH_3)_4$ compounds, where X is a Group IV element.[16]

| X | $R(X–H)$ | | $R(X–C)$ | |
| | rel. | non-rel. | rel. | non-rel. |
|---|---|---|---|---|
| C | 0·64 | 0·64 | 0·71 | 0·71 |
| Si | 0·40 | 0·40 | | |
| Ge | 0·44 | | | |
| Sn | 0·25 | 0·34 | 1·10 | 1·05 |
| Pb | 0·61 | 0·32 | 1·16 | 0·96 |

main feature stressed is the relativistic increase of the anisotropy that makes the $R$ values for Pb–H and Pb–C couplings larger than the corresponding values for Sn–H and Sn–C couplings. The increase of the coupling anisotropy with an increase in atomic number in a column of the periodic table has been verified experimentally for $Cd(CH_3)_2$ and $Hg(CH_3)_2$.[292,293] The origin of the relativistic increase in $R$ has, for the case of $PbH_4$, been traced to one particular excitation involving MOs consisting of hydrogen 1s and lead $6p_{1/2}$ atomic orbitals.

## C. Calculations of couplings of systems of biological interest

The definition of a system of biological interest is vague, for obvious reasons. The papers reviewed in this section deal with two categories of compounds, the model systems for peptides and nucleosides.

The application of couplings to studies of conformational behaviour of peptide systems has been reviewed.[312] A fragment of the peptide chain is

(52)
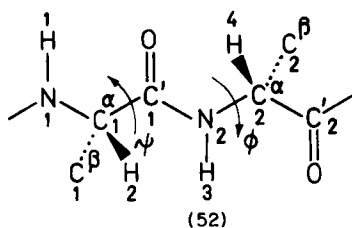
depicted in **52**. The conditions for the determination of the angle $\phi$ by measuring couplings are quite favourable because there is a pair of vicinal protons ($H_3$ and $H_4$) between which the coupling is large and strongly dependent on $\phi$. The FPT INDO calculations of the dependence of $^3J(H_3H_4)$ on $\phi$ have been presented[313] for N-methylacetamide as a model system. The use of three-bond proton–other nucleus couplings for the determination of $\phi$ has also been suggested, most recently by Mohanakrishnan and Easwaran[314] who use the Dirac vector model to calculate the coupling between $C_{1'}$ and $H_4$.

The experimental conditions for NMR determination of the angle $\psi$ are less favourable; there is no vicinal proton–proton coupling that can be used for this purpose. In the search for a substitute, some years ago Karplus and Karplus[315] suggested the use of the three-bond coupling between $N_2$ and $H_2$. Such a three-bond nitrogen–proton coupling has recently been calculated, and determined experimentally,[316] for the rigid system 2-azabicyclo[2.2.2]octan-3-one (**53**). The authors find that $^3J(NH_2)$ in **53**



(53)
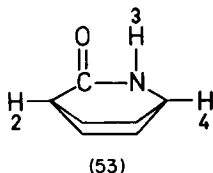
calculated by FPT INDO is similar to the corresponding calculated coupling in N-methylacetamide, but that the values greatly overestimate the experimental coupling between $^{15}N$ and $H_2$ in **53** which is only about 1·3 Hz. Kopple and coworkers[316] conclude that the optimism regarding the use of $^3J(NH)$ for determining $\psi$ is probably exaggerated. The authors have calculated several other couplings in **53**. The same model system is chosen by Aubry et al.[317] who have applied the FPT INDO method to calculate the dependence of $^3J(H_3H_4)$ and $^4J(H_2H_3)$ on the deformation of the valence angles in the molecule.

Other recent papers dealing with the calculation of angular dependence of couplings in models of peptide chains have concentrated on one- and

two-bond couplings. Gavrilov and coworkers[318] have reported FPT INDO calculations of carbon–proton couplings involving $C_{2\alpha}$ and protons $H_4$ and $H_3$ in the notation of **52**. They use $N$-methylacetamide as the model system, varying the dihedral angle corresponding to $\phi$. Both couplings are predicted to display a dependence on $\phi$, though the dependence is not as pronounced as in the case of vicinal couplings. Barfield *et al.*[319] have investigated the dependence of geminal proton–proton couplings on the $\phi$ and $\psi$ angles in peptides. The authors have applied the FPT INDO method and calculate the geminal coupling in the $CH_3$ groups in $N$-methylacetamide and in the methylene group of $N^\alpha$-acetylglycinamide (**54**) which is, at least for the



(54)
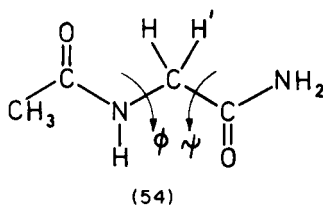
case of geminal proton couplings, a more realistic model of **52**. The calculations for **54** reflect the simultaneous effects of adjacent carbonyl and amide functions on $^2J(HH')$ but do not indicate that the two types of contribution should be additive. Barfield and coworkers suggest that the dependence of $^2J(HH')$ on $\phi$ and $\psi$ in **54** can be given as:

$$^2J(HH') = -13\cdot91 - 1\cdot55 \cos^2 \psi - 2\cdot80 \cos^4\psi + 4\cdot65 \cos^2 \phi \qquad (74)$$

Equation (74) corresponds to a total range of $J(HH')$ of about 8 Hz. Some calculations for larger model systems are also reported and the authors conclude that geminal proton couplings may provide a complement for other NMR parameters in attempts to probe the peptide conformation.[319]

Mohanakrishnan and Easwaran[320] have studied the dependence of geminal couplings on the peptide $\psi$ angle. They have concentrated on $^2J(CH)$ values corresponding in the notation of **52** to the coupling between $C_{1'}$ and $H_2$, and have applied the Dirac vector model and the Penney-Dirac bond order formulation. They find that the orientational dependence amounts to several Hz.

Selected proton–proton couplings in model compounds for nucleosides and nucleotides containing both the sugar fragment and the base fragment have been reported.[321] More recently, careful investigations of proton couplings in the sugar fragment have been performed.[322,323] The authors warn that attempts to establish the conformation about an isolated bond on the basis of experimentally determined *cisoid* vicinal couplings and a Karplus-type relationship may lead to erroneous conclusions unless the influence of the remainder of the molecule is properly taken into account.

## IX. CONCLUDING REMARKS

When I concluded the 1977 review of calculations of nuclear spin–spin couplings I stated that the picture presented by non-empirical calculations was rather gloomy and that for the semiempirical work the general outlook was much more optimistic. Further, I expressed the opinion that it would be very interesting to see the non-empirical coupled Hartree–Fock method applied both to problems where INDO performs poorly and to problems where INDO performs well.

The non-empirical coupled Hartree–Fock studies that have appeared during the last few years have indeed proved very interesting, not least because of revolutionary findings regarding the role of non-contact mechanisms in couplings involving protons. The successes of the CHF and FP-CI calculations have transformed what appeared earlier to be a gloomy situation into a satisfactory state of affairs for non-empirical calculations, and new and interesting methodological developments seem to be under way. Undoubtedly very much remains to be done, e.g. development of reliable methods that would be able to handle molecules with multiple bonds. Also, the application-oriented non-empirical calculations for systems containing two or more atoms other than hydrogen are only at the initial stage. The very recent work on the orbital diamagnetic term indicates that the role of this mechanism may be ready for reassessment, and further work is urgently needed. By and large, however, the state of the art in the field of non-empirical calculations gives many good reasons for optimism.

Turning to the assessment of the situation in the field of semiempirical work, I find that the developments of the last few years are less encouraging. The CHF INDO approach applied to proton–proton couplings retains its well deserved good reputation. Further, the CHF INDO approach has proved to be successful when applied to certain other types of coupling, e.g. $^1J(CH)$, where the agreement between the non-empirical FP-CI calculations and the FPT INDO results is striking. For the above-menioned cases, however, most of the interesting calculations for model systems had already been completed in the late sixties and early seventies, and thus most of the work presented more recently has a touch of routine. The CHF INDO method does not perform satisfactorily for many other couplings involving protons, both between directly bonded atoms, e.g. $^1J(PH)$, and in particular between atoms separated by two bonds. Attempts to apply the more sophisticated MINDO/3 scheme in connection with the finite perturbation approach have, when compared to FPT INDO, invariably led to poorer agreement with experimental couplings.

The availability of experimental data on couplings between two nuclei other than protons is increasing steadily owing to rapid developments in instrumentation. The response of theoreticians to this challenge has nòt been slow. Some of the calculations have provided good explanations of

experimental observations and have helped to increase our understanding
of the underlying mechanisms and trends. The couplings between two
nuclei other than protons can contain a non-contact contribution at the
level of approximation consistent with the INDO method. For those perfor-
ming INDO calculations of such couplings a popular approach has been
to treat the integral parameters $s_N^2(0)$ and $\langle r_N^{-3} \rangle$ as adjustable parameters.
This approach certainly has some advantages but, if the resulting parameters
deviate in an unreasonable way from the atomic values, it also introduces
the risk of dimming the general picture rather than of illuminating it.
Hopefully the relative magnitudes of the contributions from various
mechanisms will soon be established for model systems by non-empirical
calculations and the possibility of using these data for calibrating the
semiempirical methods will not be neglected.

Another development contributing towards a closing of the gap between
non-empirical calculations and semiempirical work, that I feel is very
interesting and worth encouraging, involves the application of recent
advances in the field of pseudo-potentials to calculations of nuclear spin-
spin couplings. Excluding the inner shells from the configuration interaction
part of the FP-CI treatment has proved to provide a good approximation.
In the same way, the pseudo-potential description of the inner shells may
become a reasonable way to make reliable coupled Hartree–Fock type
calculations at a lower price.

**Acknowledgements**

REFERENCES

1. N. F. Ramsey, *Phys. Rev.*, 1953, **91**, 303.
2. H. M. McConnell, *J. Chem. Phys.*, 1956, **24**, 460.
3. (a) M. Karplus and D. H. Anderson, *J. Chem. Phys.*, 1959, **30**, 6. (b) M. Karplus, *J. Chem. Phys.*, 1959, **30**, 11.
4. J. A. Pople and D. P. Santry, *Mol. Phys.*, 1964, **8**, 1.
5. J. A. Pople, J. W. McIver and N. S. Ostlund, (a) *Chem. Phys. Lett.*, 1967, **1**, 465; (b) *J. Chem. Phys.*, 1968, **49**, 2960; (c) *J. Chem. Phys.*, 1968, **49**, 2965.
6. J. Kowalewski, *Progr. NMR Spectroscopy*, 1977, **11**, 1.

7. (a) R. Grinter, *Nuclear Magnetic Resonance*, 1976, **5**, 58, The Chemical Society, London. (b) K. G. R. Pachler, *ibid.*, 1977, **6**, 1; *ibid.*, 1978, **7**, 73; *ibid.*, 1980, **9**, 49; *ibid.*, 1981, **10**, 56. (c) K. G. R. Pachler and A. A. Chalmers, *ibid.*, 1979, **8**, 63.

8. G. A. Webb, in *NMR and the Periodic Table* (ed. R. K. Harris and B. E. Mann), p. 49, Academic Press, London, 1978.

9. Selected recent papers: (a) S. M. Blinder, *Phys. Rev. (A)*, 1978, **18**, 853; (b) S. M. Blinder, *Theor. Chim. Acta*, 1979, **53**, 159; (c) T. Hannesson and S. M. Blinder, *Internat. J. Quant. Chem.*, 1979, **15**, 7; (d) H. P. Trivedi, *Mol. Phys.*, 1979, **38**, 1603; (e) J. W. Gonsalves and R. E. Moss, *Chem. Phys. Lett.*, 1979, **67**, 17; (f) S. Pick, *Theor. Chim. Acta*, 1980, **56**, 307.

10. P. Pyykkö, *Chem. Phys.*, 1977, **22**, 289.

11. M. Barfield and D. M. Grant, *Adv. Magn. Resonance*, 1965, **1**, 149.

12. J. N. Murrell, *Progr. NMR Spectroscopy*, 1971, **6**, 1.

13. A. D. Buckingham and I. Love, *J. Magn. Resonance*, 1970, **2**, 338.

14. P. Pyykkö, *Adv. Quant. Chem.*, 1978, **11**, 353.

15. P. Pyykkö and J. P. Desclaux, *Accounts Chem. Res.*, 1979, **12**, 276.

16. P. Pyykkö and L. Wiesenfeld, *Mol. Phys.*, 1981, **43**, 557.

17. L. L. Lohr and P. Pyykkö, *Chem. Phys. Lett.*, 1979, **62**, 333.

18. J. Kowalewski, B. Roos, P. Siegbahn and R. Vestin, *Chem. Phys.*, 1974, **3**, 70.

19. J. Kowalewski, B. Roos, P. Siegbahn and R. Vestin, *Chem. Phys.*, 1975, **9**, 29.

20. G. Bendazzoli, S. Evangelisti and F. Ortolani, *Internat. J. Quant. Chem.*, 1980, **18**, 1393.

21. D. Klöpper, *Acta Phys. Acad. Sci. Hung.*, 1974, **37**, 171.

22. R. Lozach and B. Braillon, *J. Chim. Phys.*, 1978, **75**, 987.

23. H. Joela, *Org. Magn. Resonance*, 1977, **9**, 338.

24. G. M. Zhidomirov, A. Yu. Shteinshneider and I. A. Abronin, *Teor. Eksp. Khim.*, 1979, **15**, 311.

25. E. Hiroike, *J. Chem. Phys.*, 1976, **65**, 4712.

26. E. Hiroike, *J. Chem. Phys.*, 1977, **67**, 1170.

27. E. Hiroike, *J. Chem. Phys.*, 1978, **68**, 5305.

28. K. Hirao and H. Kato, *Bull. Chem. Soc. Japan*, 1977, **50**, 303.

29. J. M. André, J. B. Nagy, E. G. Derouane, J. G. Fripiat and D. P. Vercauteren, *J. Magn. Resonance*, 1977, **26**, 317.

30. A. Tarpø, H. Bildsøe and K. Schaumburg, *Acta Chem. Scand.*, 1977, **A31**, 595.

31. J. C. Slater and J. G. Kirkwood, *Phys. Rev.*, 1931, **37**, 682.

32. M. J. S. Dewar, D. Landman, Sung Ho Suck and P. K. Weiner, *J. Amer. Chem. Soc.*, 1977, **99**, 3951.

33. P. K. K. Pandey and P. Chandra, *Theor. Chim. Acta*, 1978, **50**, 211.

34. P. K. Mehrotra, J. Chandrasekhar, P. T. Manoharan and S. Subramanian, *Chem. Phys. Lett.*, 1979, **68**, 219.

35. V. N. Solkan and N. B. Leonidov, *Izv. Akad. Nauk SSSR, Ser. Khim.*, 1979, 1131.

36. R. H. Contreras, A. R. Engelmann, G. E. Scuseria and J. C. Facelli, *Org. Magn. Resonance*, 1980, **13**, 137.

37. J. Schreurs, C. A. H. van Noorden-Mudde, L. J. M. van de Ven and J. W. Haan, *Org. Magn. Resonance*, 1980, **13**, 354.

38. J. C. Facelli and R. H. Contreras, *Internat. J. Quant. Chem.*, 1980, **18**, 1175.

39. G. Peinel and D. Klöpper, *Acta Phys. Acad. Sci. Hung.*, 1974, **37**, 31.

40. H.-J. Werner and W. Meyer, *Mol. Phys.*, 1976, **31**, 855.

41. J. Kowalewski, A. Laaksonen, B. Roos and P. Siegbahn, *J. Chem. Phys.*, 1979, **71**, 2896.

42. A. Laaksonen, J. Kowalewski and P. Siegbahn, *Chem. Phys. Lett.*, 1980, **69**, 109.

43. J. Kowalewski, A. Laaksonen and V. R. Saunders, *J. Chem. Phys.*, 1981, **74**, 2412.

44. A. Laaksonen and J. Kowalewski, *J. Amer. Chem. Soc.*, 1981, **103**, 5277.

45. K. Thomsen and P. Swanstrøm, *Mol. Phys.*, 1973, **26**, 735.
46. A. C. Blizzard and D. P. Santry, *J. Chem. Phys.*, 1971, **55**, 950. Erratum: *J. Chem. Phys.*, 1973, **58**, 4714.
47. R. Ditchfield and L. C. Snyder, *J. Chem. Phys.*, 1972, **56**, 5823.
48. M. F. Guest, V. R. Saunders and R. E. Overill, *Mol. Phys.*, 1978, **35**, 427.
49. M. F. Guest and R. E. Overill, *Chem. Phys. Lett.*, 1980, **73**, 612.
50. P. Lazzeretti, *Internat. J. Quant. Chem.*, 1979, **15**, 181.
51. P. Lazzeretti, *J. Chem. Phys.*, 1979, **71**, 2514.
52. P. Albertsen, P. Jørgensen and D. L. Yaeger, *Chem. Phys. Lett.*, 1980, **76**, 354.
53. G. T. Daborn, W. I. Ferguson and N. C. Handy, *Chem. Phys.*, 1980, **50**, 255.
54. N. S. Ostlund, M. D. Newton, J. W. McIver and J. A. Pople, *J. Magn. Resonance*, 1969, **1**, 298.
55. E. Yurtsever and J. Hinze, *J. Chem. Phys.*, 1978, **69**, 3431.
56. E. Steiner, *J. Chem. Soc. Faraday II*, 1980, **76**, 391.
57. C. Barbier, B. Lévy and P. Millié, *Chem. Phys. Lett.*, 1972, **17**, 122.
58. M. A. Robb and S. Chin, *Progr. Theor. Org. Chem.*, 1977, **2**, 468.
59. Y. Ellinger, B. Lévy, P. Millié and R. Subra, in *Localization and Delocalization in Quantum Chemistry*, Vol. 1 (ed. O. Chalvet *et al.*), pp. 283–326, Reidel Publishing Company, Dordrecht, Holland, 1975.
60. C. Barbier, G. Berthier, B. Lévy, P. Millié and P. Noël, *J. Chim. Phys.*, 1975, **72**, 859.
61. C. Giessner-Prettre and B. Pullman, *J. Theor. Biol.*, 1978, **72**, 751.
62. R. Lozach, *Chem. Phys. Lett.*, 1976, **42**, 93.
63. P. Archirel and C. Barbier, *J. Chim. Phys.*, 1978, **75**, 1003.
64. W. S. Lee and J. M. Schulman, *J. Chem. Phys.*, 1979, **70**, 1530.
65. O. Matsuoka and T. Aoyama, *J. Chem. Phys.*, 1980, **73**, 5718; O. Matsuoka, private communication.
66. A. D. C. Towl and K. Schaumburg, *Mol. Phys.*, 1971, **22**, 49.
67. H. Nakatsuji, K. Hirao, H. Kato and T. Yonezawa, *Chem. Phys. Lett.*, 1970, **6**, 541.
68. W. S. Lee and J. M. Schulman, *J. Amer. Chem. Soc.*, 1979, **101**, 3182.
69. W. S. Lee and J. M. Schulman, *J. Magn. Resonance*, 1979, **35**, 451.
70. P. Lazzeretti and R. Zanasi, *Internat. J. Quant. Chem.*, 1979, **15**, 645.
71. W. S. Lee and J. M. Schulman, *J. Amer. Chem. Soc.*, 1980, **102**, 5184.
72. H. Benoit and P. Piejus, *Compt. Rend.*, 1967, *B265*, 101.
73. W. Meyer, *Z. Physik*, 1969, **229**, 452.
74. J. M. Schulman and D. N. Kaufman, *J. Chem. Phys.*, 1970, **53**, 477.
75. J. M. Schulman and D. N. Kaufman, *J. Chem. Phys.*, 1972, **57**, 2328.
76. J. Oddershede, P. Jørgensen and N. H. F. Beebe, *J. Chem. Phys.*, 1975, **63**, 2996.
77. G. L. Bendazzoli, G. Fano, F. Ortolani and P. Lazzeretti, *Chem. Phys. Lett.*, 1979, **68**, 162.
78. J. M. Schulman and W. S. Lee, *J. Chem. Phys.*, 1979, **71**, 922.
79. T. Itagaki and A. Saika, *J. Chem. Phys.*, 1979, **71**, 4620.
80. J. Oddershede, P. Jørgensen and N. H. F. Beebe, *Chem. Phys.*, 1977, **25**, 451.
81. B. Kirtman, K. B. Kirtley and D. A. Hasman, *J. Chem. Phys.*, 1976, **65**, 1357.
82. B. Kirtman and K. B. Kirtley, *J. Phys. Chem.*, 1979, **83**, 1470.
83. J. M. Schulman and W. S. Lee, *J. Chem. Phys.*, 1980, **73**, 1350.
84. P. Pyykkö, *Theor. Chim. Acta*, 1975, **39**, 185.
85. W. Sänger and J. Voitländer, *Theor. Chim. Acta*, 1976, **41**, 263.
86. A. Delpuech, J. Paviot and J. Hoarau, *Theor. Chim. Acta*, 1976, **42**, 345.
87. H. P. Trivedi, *Z. Naturforsch.*, 1979, **34a**, 1158.
88. H. P. Trivedi, *Chem. Phys. Lett.*, 1980, **70**, 159.
89. H. P. Trivedi, *Z. Naturforsch.*, 1980, **35a**, 1108.

90. M. T. Rayez-Meaume and J. Hoarau, *Chem. Phys.*, 1978, **27**, 73.
91. M. T. Rayez-Meaume, F. Achard and J. Hoarau, *J. Chem. Phys.*, 1980, **72**, 3434.
92. T. Vladimiroff and T. J. Dougherty, *J. Chem. Phys.*, 1967, **47**, 1881.
93. W. T. Raynes and J. P. Riley, *Mol. Phys.*, 1974, **27**, 337.
94. J. C. Facelli, R. H. Contreras, G. E. Scuseria and A. R. Engelmann, *J. Mol. Struct.*, 1979, **57**, 299.
95. E. Ishiguro, T. Arai, M. Mizushima and M. Kotani, *Proc. Phys. Soc.*, 1952, **A65**, 178.
96. H. Fukui, *J. Chem. Phys.*, 1976, **65**, 844.
97. H. Fukui, K. Miura and N. Ishigami, *J. Chem. Phys.*, 1979, **71**, 560.
98. P. Solomon and J. M. Schulman, *J. Amer. Chem. Soc.*, 1977, **99**, 7776.
99. J. Kowalewski and B. Roos, *Chem. Phys.*, 1975, **11**, 123.
100. K. F. Purcell and R. L. Martin, *Theor. Chim. Acta*, 1974, **35**, 141.
101. R. K. Safiullin, R. M. Aminova and Yu. Yu. Samitov, *Zh. Strukt. Khim.*, 1974, **15**, 907.
102. J. A. Pople and A. A. Bothner-By, *J. Chem. Phys.*, 1965, **42**, 1339.
103. G. E. Maciel, J. W. McIver, N. S. Ostlund and J. A. Pople, *J. Amer. Chem. Soc.*, 1970, **92**, 4151.
104. M. Karplus, *J. Amer. Chem. Soc.*, 1963, **85**, 2870.
105. G. E. Maciel, J. W. McIver, N. S. Ostlund and J. A. Pople, *J. Amer. Chem. Soc.*, 1970, **92**, 4497.
106. G. E. Maciel, J. W. McIver, N. S. Ostlund and J. A. Pople, *J. Amer. Chem. Soc.*, 1970, **92**, 4506.
107. P. K. Karafiloglou, *Nouv. J. Chim.*, 1979, **3**, 151.
108. K. Ohkubo, K. Tsuchihashi, T. Yoshida and M. Okada, *Bull. Chem. Soc. Japan*, 1975, **48**, 3436.
109. K. Ohkubo, K. Tomiyoshi and T. Yoshida, *J. Mol. Struct.*, 1977, **36**, 73.
110. R. Laatikainen, S. Lötjönen and P. Äyräs, *Acta Chem. Scand.*, 1980, **A34**, 249.
111. A. Jaworski, D. Shugar and E. Darżynkiewicz, *J. Phys. Chem.*, 1976, **80**, 324.
112. R. M. Aminova and Yu. Yu. Samitov, *Zh. Strukt. Khim.*, 1974, **15**, 607.
113. J. Elguero, B. L. Johnson, J.-M. Pereillo, G. Pouzard, M. Rajzmann and E. W. Randall, *Org. Magn. Resonance*, 1977, **9**, 145.
114. R. K. Safiullin, R. M. Aminova and Yu. Yu. Samitov, *Zh. Strukt. Khim.*, 1975, **16**, 42.
115. Yu. Yu. Samitov, R. K. Safiullin, R. M. Aminova, N. D. Chuvylkin and G. M. Zhidomirov, *Phosphorus*, 1975, **5**, 151.
116. T. Iwayanagi, T. Ibusuki and Y. Saito, *J. Organometal. Chem.*, 1977, **128**, 145.
117. Th. Steiger, E. Gey and R. Radeglia, *Z. Phys. Chem.* (Leipzig), 1976, **257**, 172.
118. V. M. Mamaev and Kh. A. Orazberdiev, *Zh. Strukt. Khim.*, 1975, **16**, 896.
119. V. M. Mamaev, Kh. A. Orazberdiev and N. M. Sergeyev, *Dokl. Akad. Nauk SSSR, Ser. Khim.*, 1975, **220**, 877.
120. V. M. Mamaev and Kh. A. Orazberdiev, *Vestn. Mosk. Univ., Khim.*, 1976, **17**, 610.
121. Kh. A. Orazberdiev and V. M. Mamaev, *Vestn. Mosk. Univ., Khim.*, 1976, **17**, 476.
122. F. H. A. Rummens and L. Kaslander, *Canad. J. Chem.*, 1976, **54**, 2884.
123. F. H. A. Rummens, C. Simon, C. Coupry and N. Lumbroso-Bader, *Org. Magn. Resonance*, 1980, **13**, 33.
124. B. Lemarié and B. Braillon, *J. Magn. Resonance*, 1979, **35**, 343.
125. P. W. Rabideau, J. W. Paschal and J. L. Marshall, *J. Chem. Soc. Perkin II*, 1977, 842.
126. B. Lemarié and J. L. Ripoll, *Org. Magn. Resonance*, 1977, **10**, 169.
127. J. M. Schulman and T. J. Venanzi, *Tetrahedron Lett.*, 1976, 1461.
128. J. L. Marshall, S. R. Walter, M. Barfield, A. P. Marchand, N. W. Marchand and A. L. Segre, *Tetrahedron*, 1976, **32**, 537.
129. L. Ernst, E. Lustig and V. Wray, *J. Magn. Resonance*, 1976, **22**, 459.
130. S. A. T. Long and J. D. Memory, *J. Magn. Resonance*, 1978, **29**, 119.

131. H. Günther, H. Schmickler, M. E. Günther and D. Cremer, *Org. Magn. Resonance,* 1977, **9**, 420.
132. R. Benassi, L. Schenetti, L. Villa and V. Ferri, *Org. Magn. Resonance,* 1980, **13**, 17.
133. F. Chanon, M. Rajzmann, M. Chanon, J. Metzger and G. Pouzard, *Canad. J. Chem.,* 1980, **58**, 599.
134. F. Chanon, M. Rajzmann, M. Chanon, J. Metzger, G. Pouzard and T. Drakenberg, *Canad. J. Chem.,* 1980, **58**, 604.
135. J. Santoro, *An. Quim.,* 1978, **74**, 538.
136. Yu. Yu. Samitov, A. A. Musina, R. M. Aminova, M. A. Pudovik, A. I. Khayarov and M. D. Medvedeva, *Org. Magn. Resonance,* 1980, **13**, 163.
137. J. Jokisaari and E. Rahkamaa, *Rept. Dept. Phys. Univ. Oulu,* 1979, No. 69.
138. V. N. Burmistrov and V. M. Mamaev, *Zh. Strukt. Khim.,* 1978, **19**, 28.
139. Yu. B. Vysotskii and A. V. Luzanov, *Zh. Strukt. Khim.,* 1975, **16**, 195.
140. K. Yoshida, *Chem. Phys.,* 1977, **21**, 317.
141. M. Bacon and G. E. Maciel, *Mol. Phys.,* 1971, **21**, 257.
142. M. Barfield and B. Chakrabarti, *Chem. Rev.,* 1969, **69**, 757.
143. M. Barfield, R. J. Spear and S. Sternhell, *Chem. Rev.,* 1976, **76**, 593.
144. M. Barfield and A. A. Abia, *Org. Magn. Resonance,* 1980, **14**, 404.
145. J. L. Marshall, L. G. Faehl, C. R. McDaniel and N. D. Ledford, *J. Amer. Chem. Soc.,* 1977, **99**, 321.
146. M. Barfield and S. Sternhell, *J. Amer. Chem. Soc.,* 1972, **94**, 1905.
147. T. Schaefer, H. D. Gesser and J. B. Rowbotham, *Canad. J. Chem.,* 1976, **54**, 2235.
148. T. Schaefer and W. J. E. Parr, *Canad. J. Chem.,* 1977, **55**, 2835.
149. H. Sterk and A. Wachmann, *Z. Naturforsch.,* 1976, **31a**, 71.
150. V. I. Mstislavsky, V. A. Korenevsky, N. M. Sergeyev and V. N. Solkan, *Org. Magn. Resonance,* 1976, **8**, 368.
151. W. Runge, *Z. Naturforsch.,* 1978, **33b**, 932.
152. W. J. E. Parr and T. Schaefer, *Accounts Chem. Res.,* 1980, **13**, 400.
153. T. Schaefer, J. B. Rowbotham and K. Chum, *Canad. J. Chem.,* 1976, **54**, 3666.
154. T. Schaefer, J. B. Rowbotham, W. J. E. Parr, K. Marat and A. F. Janzen, *Canad. J. Chem.,* 1976, **54**, 1322.
155. R. Wasylishen and T. Schaefer, *Canad. J. Chem.,* 1972, **50**, 1852.
156. W. J. E. Parr and T. Schaefer, *J. Amer. Chem. Soc.,* 1977, **99**, 1033.
157. W. J. E. Parr, *J. Chem. Soc. Faraday II,* 1978, **74**, 933.
158. T. Schaefer, S. R. Salman and T. A. Wildman, *Canad. J. Chem.,* 1980, **58**, 2364.
159. W. J. E. Parr, R. E. Wasylishen and T. Schaefer, *Canad. J. Chem.,* 1976, **54**, 3216.
160. I. R. Peat and W. F. Reynolds, *Canad. J. Chem.,* 1974, **52**, 2403.
161. W. Danchura, R. E. Wasylishen, J. Delikatny and M. R. Graham, *Canad. J. Chem.,* 1979, **57**, 2135.
162. C. J. Jameson and H. S. Gutowsky, *J. Chem. Phys.,* 1969, **51**, 2790.
163. D. K. Dalling and H. S. Gutowsky, *J. Chem. Phys.,* 1971, **55**, 4959.
164. P. Pyykkö and J. Jokisaari, *Chem. Phys.,* 1975, **10**, 293.
165. G. Barbieri, R. Benassi and F. Taddei, *Gazz. Chim. Ital.,* 1975, **105**, 807.
166. P. D. Ellis and R. Ditchfield, in *Topics in Carbon-13 NMR Spectroscopy* (ed. G. C. Levy), Vol. 2, p. 433, 1976.
167. D. F. Ewing, *Ann. Rep. NMR Spectroscopy,* 1975, **6A**, 389.
168. G. E. Maciel, J. W. McIver, N. S. Ostlund and J. A. Pople, *J. Amer. Chem. Soc.,* 1970, **92**, 1.
169. A. A. Cheremisin and P. V. Schastnev, *Zh. Strukt. Khim.,* 1980, **21**, 177.
170. N. Muller and D. E. Pritchard, *J. Chem. Phys.,* 1959, **31**, 768, 1471.
171. C. Van Alsenoy, H. P. Figeys and P. Geerlings, *Theor. Chim. Acta,* 1980, **55**, 87.

172. R. Boca, *Coll. Czech. Chem. Commun.*, 1979, **44**, 3041.
173. R. M. Lynden-Bell and N. Sheppard, *Proc. Roy. Soc.*, 1962, **A269**, 385.
174. N. M. Sergeyev and V. N. Solkan, *J. Chem. Soc. Chem. Commun.*, 1975, 12.
175. K. G. R. Pachler and R. Pachter, *Org. Magn. Resonance*, 1979, **12**, 183.
176. J. P. Meille, J. C. Duplan, A. Briguet and J. Delmau, *J. Phys. Chem.*, 1978, **82**, 2029.
177. J. A. Schwarcz, N. Cyr and A. S. Perlin, *Canad. J. Chem.*, 1975, **53**, 1872.
178. N. Cyr, G. K. Hamer and A. S. Perlin, *Canad. J. Chem.*, 1978, **56**, 297.
179. R. E. Wasylishen, K. Chum and J. Bukata, *Org. Magn. Resonance*, 1977, **9**, 473.
180. R. Wasylishen and T. Schaefer, *Canad. J. Chem.*, 1972, **50**, 2710; 1973, **51**, 961.
181. M. Barfield, *J. Amer. Chem. Soc.*, 1980, **102**, 1.
182. M. Barfield, J. L. Marshall, E. D. Canada and M. R. Willcott, *J. Amer. Chem. Soc.*, 1978, **100**, 7075.
183. M. Barfield, J. L. Marshall and E. D. Canada, *J. Amer. Chem. Soc.*, 1980, **102**, 7.
184. A. A. Cheremisin and P. V. Schastnev, *Org. Magn. Resonance*, 1980, **14**, 327.
185. R. E. London, T. E. Walker, V. H. Kollman and N. A. Matwiyoff, *J. Amer. Chem. Soc.*, 1978, **100**, 3723.
186. T. A. Albright and E. E. Schweizer, *J. Org. Chem.*, 1976, **41**, 1168.
187. T. A. Albright and W. J. Freeman, *Org. Magn. Resonance*, 1977, **9**, 75.
188. D. R. Boyd, M. E. Stubbs, N. J. Thompson, H. J. C. Yeh, D. M. Jerina and R. E. Wasylishen, *Org. Magn. Resonance*, 1980, **14**, 528.
189. R. Aydin, H. Günther, J. Runsink, H. Schmickler and H. Seel, *Org. Magn. Resonance*, 1980, **13**, 210.
190. V. M. Mamaev and Kh. A. Orazberdiev, *Teor. Eksp. Khim.*, 1977, **13**, 226.
191. W. Runge and W. Kosbahn, *Ber. Bunsenges. Phys. Chem.*, 1976, **80**, 1330.
192. W. Runge, *Z. Naturforsch.*, 1979, **34b**, 118.
193. M. Barfield, S. E. Brown, E. D. Canada, N. D. Ledford, J. L. Marshall, S. R. Walter and E. Yakali, *J. Amer. Chem. Soc.*, 1980, **102**, 3355.
194. V. A. Chertkov and N. M. Sergeyev, *J. Amer. Chem. Soc.*, 1977, **99**, 6750.
195. H. P. Figeys, P. Geerlings, P. Raeymaekers, G. Van Lommen and N. Defay, *Tetrahedron*, 1975, **31**, 1731.
196. F. J. Weigert and J. D. Roberts, *J. Amer. Chem. Soc.*, 1967, **89**, 2967.
197. H. Günther, H. Seel and M.-E. Günther, *Org. Magn. Resonance*, 1978, **11**, 97.
198. V. N. Solkan and N. B. Leonidov, *Zh. Strukt. Khim.*, 1979, **20**, 1104.
199. V. A. Chertkov and N. M. Sergeyev, *J. Magn. Resonance*, 1976, **21**, 159.
200. N. M. Sergeyev, V. N. Solkan and V. A. Chertkov, *Teor. Eksp. Khim.*, 1976, **12**, 693.
201. L. Ernst, V. Wray, V. A. Chertkov and N. M. Sergeyev, *J. Magn. Resonance*, 1977, **25**, 123.
202. V. Wray, L. Ernst and E. Lustig, *J. Magn. Resonance*, 1977, **27**, 1.
203. P. Äyräs, R. Laatikainen and S. Lötjönen, *Org. Magn. Resonance*, 1980, **13**, 387.
204. P. E. Hansen, O. K. Poulsen and A. Berg, *Org. Magn. Resonance*, 1977, **9**, 649.
205. P. Granger and M. Mangras, *J. Magn. Resonance*, 1976, **22**, 405.
206. S. Braun, J. Kinkeldei and L. Walther, *Org. Magn. Resonance*, 1980, **14**, 466.
207. R. E. Wasylishen and G. Tomlinson, *Canad. J. Biochem.*, 1977, **55**, 579.
208. R. E. Wasylishen and H. M. Hutton, *Canad. J. Chem.*, 1977, **55**, 619.
209. R. Faure, J.-R. Llinas, E. J. Vincent and M. Rajzmann, *Canad. J. Chem.*, 1975, **53**, 1677.
210. T. Wamsler, J. T. Nielsen, E. J. Pedersen and K. Schaumburg, *J. Magn. Resonance*, 1978, **31**, 177.
211. H. Seel and H. Günther, *J. Amer. Chem. Soc.*, 1980, **102**, 7051.
212. R. K. Harris, J. D. Kennedy and W. McFarlane, in *NMR and the Periodic Table* (ed. R. K. Harris and B. E. Mann), p. 309, Academic Press, London, 1978.
213. K. Kovacevic, K. Krmpotic and Z. B. Maksic, *Inorg. Chem.*, 1977, **16**, 1421.

214. M. Eckert-Maksic, M. Kovacevic and Z. B. Maksic, *J. Organometal. Chem.*, 1979, **168**, 295.
215. M. D. Beer and R. Grinter, *J. Magn. Resonance*, 1977, **26**, 421.
216. G. Barbieri, R. Benassi and F. Taddei, *J. Organometal. Chem.*, 1977, **129**, 27.
217. R. E. Wasylishen and T. Schaefer, *Canad. J. Chem.*, 1972, **50**, 2989.
218. R. E. London, T. E. Walker, T. W. Whaley and N. A. Matwiyoff, *Org. Magn. Resonance*, 1977, **9**, 598.
219. R. L. Lichter, P. R. Srinivasan, A. B. Smith, R. K. Dieter, C. T. Denny and J. M. Schulman, *J. Chem. Soc. Chem. Commun.*, 1977, 366.
220. Y. Kuroda, H. Lee and A. Kuwae, *J. Phys. Chem.*, 1980, **84**, 3417.
221. C. Giessner-Prettre and B. Pullman, *J. Theor. Biol.*, 1974, **48**, 425.
222. T. A. Albright, *Org. Magn. Resonance*, 1976, **8**, 489.
223. G. A. Gray and T. A. Albright, *J. Amer. Chem. Soc.*, 1976, **98**, 3857.
224. G. A. Gray and T. A. Albright, *J. Amer. Chem. Soc.*, 1977, **99**, 3243.
225. L. I. Vinogradov, *Fosfororg. Soedin. Polim.*, 1978, **4**, 35.
226. R. W. Kunz, *Helv. Chim. Acta*, 1980, **63**, 2054.
227. J. W. Emsley, L. Phillips and V. Wray, *Progr. NMR Spectroscopy*, 1977, **10**, 85.
228. H. Fukui, A. Sanyoshi and K. Miura, *J. Chem. Phys.*, 1978, **69**, 943.
229. J. S. Muenter and W. Klemperer, *J. Chem. Phys.*, 1970, **52**, 6033.
230. S. G. Frankiss, *J. Phys. Chem.*, 1963, **67**, 752.
231. J. Hilton and L. H. Sutcliffe, *Progr. NMR Spectroscopy*, 1975, **10**, 27.
232. T. Schaefer and W. J. E. Parr, *J. Chem. Phys.*, 1976, **65**, 1197.
233. T. Schaefer, K. Chum, K. Marat and R. E. Wasylishen, *Canad. J. Chem.*, 1976, **54**, 800.
234. W. J. E. Parr and T. Schaefer, *Canad. J. Chem.*, 1976, **54**, 3564.
235. T. Schaefer, W. Danchura and W. Niemczura, *Canad. J. Chem.*, 1978, **56**, 2233.
236. V. N. Solkan, G. M. Zhidomirov, V. S. Bogdanov, A. V. Khesenikh, N. D. Chuvylkin and V. V. Negrebetskii, *Izv. Akad. Nauk SSSR, Ser. Khim.*, 1974, 2623.
237. J. Kroner and B. Wrackmayer, *J. Chem. Soc. Faraday II*, 1976, **72**, 2283.
238. H. F. Henneike, *J. Amer. Chem. Soc.*, 1972, **94**, 5945.
239. R. E. Wasylishen, *Ann. Rep. NMR Spectroscopy*, 1977, **7**, 245.
240. E. Shustorovich, *Inorg. Chem.*, 1979, **18**, 1039.
241. P. E. Hansen, *Org. Magn. Resonance*, 1978, **11**, 215.
242. H. B. Jansen, A. Meeuwis and P. Pyykkö, *Chem. Phys.*, 1979, **38**, 173.
243. C. Barbier, H. Faucher and G. Berthier, *Theor. Chim. Acta*, 1971, **21**, 105.
244. K. K. Frei and H. J. Bernstein, *J. Chem. Phys.*, 1963, **38**, 1216.
245. Tun Khin and G. A. Webb, *Org. Magn. Resonance*, 1979, **12**, 103.
246. Tun Khin and G. A. Webb, *Org. Magn. Resonance*, 1980, **13**, 148; this paper contains a summary of the results presented in Tun Khin's Ph.D. thesis, University of Surrey, 1978.
247. G. E. Maciel, J. W. McIver, N. S. Ostlund and J. A. Pople, *J. Amer. Chem. Soc.*, 1970, **92**, 11.
248. K. Kamienska-Trela, *Org. Magn. Resonance*, 1980, **14**, 398.
249. M. Stöcker and M. Klessinger, *Annalen*, 1979, 1960.
250. M. Barfield, S. A. Conn, J. L. Marshall and D. E. Miiller, *J. Amer. Chem. Soc.*, 1976, **98**, 6253.
251. J. L. Marshall, S. A. Conn and M. A. Barfield, *Org. Magn. Resonance*, 1977, **9**, 404.
252. V. Wray, *J. Amer. Chem. Soc.*, 1978, **100**, 768.
253. P. Lazzeretti, F. Taddei and R. Zanasi, *J. Amer. Chem. Soc.*, 1976, **98**, 7989.
254. V. Wray, L. Ernst, T. Lund and H. J. Jakobsen, *J. Magn. Resonance*, 1980, **40**, 55.
255. G. W. Buchanan, J. Selwyn and B. A. Dawson, *Canad. J. Chem.*, 1979, **57**, 3028.
256. P. E. Hansen, O. K. Poulsen and A. Berg, *Org. Magn. Resonance*, 1979, **12**, 43.

257. R. E. Wasylishen and B. A. Pettitt, *Canad. J. Chem.*, 1979, **57**, 1274.
258. J. L. Marshall, L. G. Faehl, A. M. Ihrig and M. Barfield, *J. Amer. Chem. Soc.*, 1976, **98**, 3406.
259. J. L. Marshall, L. G. Faehl, R. Kattner and P. E. Hansen, *Org. Magn. Resonance*, 1979, **12**, 169.
260. R. E. London, *J. Chem. Soc. Chem. Commun.*, 1978, 1070.
261. K. D. Summerhays and D. A. Deprez, *J. Organometal. Chem.*, 1976, **118**, 19.
262. M. D. Beer and R. Grinter, *J. Magn. Resonance*, 1978, **31**, 187.
263. J. M. Schulman and T. Venanzi, *J. Amer. Chem. Soc.*, 1976, **98**, 4701.
264. J. M. Schulman and T. Venanzi, *J. Amer. Chem. Soc.*, 1976, **98**, 6739.
265. Tun Khin and G. A. Webb, *Org. Magn. Resonance*, 1978, **11**, 487.
266. P. K. K. Pandey and P. Chandra, *Indian J. Chem.*, 1979, **17A**, 218.
267. J. M. Schulman, *J. Magn. Resonance*, 1977, **28**, 137.
268. Tun Khin and G. A. Webb, *Org. Magn. Resonance*, 1977, **10**, 175.
269. R. E. Wasylishen, *Canad. J. Chem.*, 1976, **54**, 833.
270. S. Berger and J. D. Roberts, *J. Amer. Chem. Soc.*, 1974, **96**, 6757.
271. S. Berger and H. Kaletsch, *Org. Magn. Resonance*, 1976, **8**, 438.
272. T. Axenrod, M. J. Wieder, Tun Khin, G. A. Webb, H. J. C. Yeh and S. Bulusu, *Org. Magn. Resonance*, 1979, **12**, 1.
273. S. Berger, *Tetrahedron*, 1978, **34**, 3133.
274. R. L. Lichter, D. E. Dorman and R. Wasylishen, *J. Amer. Chem. Soc.*, 1974, **96**, 930.
275. G. W. Buchanan and B. A. Dawson, *Canad. J. Chem.*, 1978, **56**, 2200.
276. S. Fortier, G. I. Birnbaum, G. W. Buchanan and B. A. Dawson, *Canad. J. Chem.*, 1980, **58**, 191.
277. W. Runge and J. Firl, *Z. Naturforsch.*, 1976, **31b**, 1515.
278. V. Galasso, *Org. Magn. Resonance*, 1979, **12**, 318.
279. M. Alei, L. O. Morgan, W. E. Wageman and T. W. Whaley, *J. Amer. Chem. Soc.*, 1980, **102**, 2881.
280. R. K. Safiullin, Yu. Yu. Samitov and R. M. Aminova, *Teor. Eksp. Khim.*, 1974, **10**, 828.
281. G. A. Gray, *J. Amer. Chem. Soc.*, 1971, **93**, 2132.
282. V. Galasso, *J. Magn. Resonance*, 1979, **34**, 199.
283. V. Galasso, *J. Magn. Resonance*, 1979, **36**, 181.
284. V. Wray, *J. Chem. Soc. Perkin II*, 1976, 1598.
285. D. Doddrell, M. Barfield, W. Adcock, M. Aurangzeb and D. Jordan, *J. Chem. Soc. Perkin II*, 1976, 402.
286. F. J. Weigert and J. D. Roberts, *J. Amer. Chem. Soc.*, 1971, **93**, 2361.
287. P. E. Hansen, A. Berg, H. J. Jakobsen, A. P. Manzara and J. Michl, *Org. Magn. Resonance*, 1977, **10**, 179.
288. S. Duangthai and G. A. Webb, *Org. Magn. Resonance*, 1979, **12**, 98.
289. V. Wray, *J. Chem. Soc. Perkin II*, 1978, 855.
290. L. W. Hall, D. W. Lowman, P. D. Ellis and J. D. Odom, *Inorg. Chem.*, 1975, **14**, 580.
291. T. Iwayanagi and Y. Saito, *Chem. Lett.*, 1976, **11**, 1193.
292. J. Jokisaari, K. Räisänen, L. Lajunen, A. Passoja and P. Pyykkö, *J. Magn. Resonance*, 1978, **31**, 121; Erratum: *J. Magn. Resonance*, 1979, **33**, 481.
293. J. Jokisaari, K. Räisänen, J. Kuonanoja, P. Pyykkö and L. Lajunen, *Mol. Phys.*, 1980, **39**, 715.
294. V. I. Nefedov, V. G. Yarzhemsky and V. P. Tarasov, *Koord. Khim.*, 1976, **2**, 1443.
295. V. I. Nefedov, V. G. Yarzhemsky and V. P. Tarasov, *Chem. Phys.*, 1976, **18**, 417.
296. E. Shustorovich and P. A. Dobosh, *J. Magn. Resonance*, 1980, **39**, 79.
297. E. Shustorovich and P. A. Dobosh, *J. Magn. Resonance*, 1980, **39**, 101.
298. R. S. Matthews, *Org. Magn. Resonance*, 1976, **8**, 628.

299. T. Schaefer, W. Niemczura, C.-M. Wong and K. Marat, *Canad. J. Chem.*, 1979, **57**, 807.
300. Tun Khin, S. Duangthai and G. A. Webb, *Org. Magn. Resonance*, 1980, **13**, 240.
301. J. P. Albrand, H. Faucher, D. Gagnaire and J. B. Robert, *Chem. Phys. Lett.*, 1976, **38**, 521.
302. E. Shustorovich, *Inorg. Chem.*, 1979, **18**, 2108.
303. J. M. Schulman, J. Ruggio and T. J. Venanzi, *J. Amer. Chem. Soc.*, 1977, **99**, 2045.
304. Tun Khin and G. A. Webb, *J. Magn. Resonance*, 1979, **33**, 159.
305. A. R. Farminer and G. A. Webb, *J. Mol. Struct.*, 1975, **27**, 417.
306. M. Barfield and M. Johnston, *Chem. Rev.*, 1973, **73**, 53.
307. M. Kondo, S. Watanabe and I. Ando, *Mol. Phys.*, 1979, **37**, 1521.
308. G. Klopman, *Chem. Phys. Lett.*, 1967, **1**, 200.
309. G. Klopman, *J. Amer. Chem. Soc.*, 1968, **90**, 223.
310. S. Watanabe and I. Ando, *Bull. Chem. Soc. Japan*, 1980, **53**, 1257.
311. J. W. Emsley and J. C. Lindon, *NMR Spectroscopy Using Liquid Crystal Solvents*, Pergamon Press, 1975.
312. V. F. Bystrov, *Progr. NMR Spectroscopy*, 1976, **10**, 41.
313. M. Barfield and H. L. Gearhart, *J. Amer. Chem. Soc.*, 1973, **95**, 641.
314. P. Mohanakrishnan and K. R. K. Easwaran, *Biopolymers*, 1979, **18**, 1769.
315. S. Karplus and M. Karplus, *Proc. Nat. Acad. Sci. USA*, 1972, **69**, 3204.
316. K. D. Kopple, A. Ahsan and M. Barfield, *Tetrahedron Lett.*, 1978, **38**, 519.
317. A. Aubry, C. Giessner-Prettre, M. T. Cung, M. Marraud and J. Neel, *Biopolymers*, 1974, **13**, 523.
318. Yu. D. Gavrilov, V. N. Solkan and V. F. Bystrov, *Izv. Akad. Nauk SSSR, Ser. Khim.*, 1975, 2482.
319. M. Barfield, V. J. Hruby and J.-P. Meraldi, *J. Amer. Chem. Soc.*, 1976, **98**, 1308.
320. P. Mohanakrishnan and K. R. K. Easwaran, *Org. Magn. Resonance*, 1979, **12**, 196.
321. C. Giessner-Prettre and B. Pullman, *J. Theor. Biol.*, 1973, **40**, 441; *Internat. J. Quant. Chem.* Symp. No. 7, 1973, p. 295.
322. A. Jaworski, I. Ekiel and D. Shugar, *J. Amer. Chem. Soc.*, 1978, **100**, 4357.
323. A. Jaworski and I. Ekiel, *Internat. J. Quant. Chem.*, 1979, **16**, 615.

# Boron-11 NMR Spectroscopy

## ALLEN R. SIEDLE

*3M Central Research Laboratories, St. Paul, Minnesota 55101, U.S.A.*

## I. INTRODUCTION

In the four years since the topic of $^{11}$B NMR spectroscopy was last reviewed[1] the literature has continued to proliferate, and so many new boron compounds have been reported that an updated survey seems justified. Unlike many other branches of spectroscopy, that dealing with $^{11}$B is infrequently a free-standing discipline and is used more often as a characterization tool to probe structure and reactivity in boron compounds. Nevertheless, outstanding efforts have been made to develop a deeper theoretical understanding of $^{11}$B chemical shifts and coupling constants.[2] Further, a sufficient

body of empirical data is available to at least partially deduce gross structural features of large polyboron molecules directly from measurements of chemical shifts, coupling constants, and spin–lattice relaxation times. The situation will further improve as data from high-field spectrometers become available. These instruments are now designed so that spectroscopic techniques requiring sophisticated data manipulation have become practical, examples of which are two-dimensional correlated $^1H$–$^{11}B$ NMR, multiple resonance experiments, line narrowing, and measurement of $T_1$ and $T_2$. An additional development which contributes much to the appreciation of $^{11}B$ NMR data is the increasing availability of X-ray crystallographic data, which establishes *solid state* structural details beyond cavil, although it is not necessarily true that these details will persist in solution.

In 1976 there began a change in the sign convention used for $^{11}B$ chemical shifts so that a positive sign denotes a shift at higher frequency than the $BF_3 \cdot OEt_2$ reference. Although this author does not agree that such a change is justified, it is used here throughout. Adoption of the new convention was not sudden and experimental sections of papers published in 1977–1978 especially should be examined to see how chemical shifts are expressed. Also somewhat unsettled is the numbering convention for polyhedral boron molecules, which has changed in the past and may do so again. Some readers may be puzzled that insertion of a CpCo unit into $7,8\text{-}B_9C_2H_{11}^{2-}$ generates $3,1,2\text{-}CpCoB_9C_2H_{11}$, but consultation of the original literature should reveal the numbering schemes used.

In this account, $^{11}B$ chemical shifts are expressed in ppm with respect to external $BF_3 \cdot O(C_2H_5)_2$, followed by multiplicity (the abbreviations br, s, d, t, and q refer to broad, singlet, doublet, triplet, and quartet respectively), relative area, and B–H coupling constant.

## II. SPECTROSCOPIC TECHNIQUES

Weiss and Grimes[3] have obtained linewidth and $^{11}B$ spin–lattice relaxation time ($T_1$) data at different temperatures for $B_4H_{10}$ and $B_5H_9$, and have also calculated line shapes for different values of $2\pi JT_1$ for $^{11}B$ spin coupled to $^1H$. For the B(2,4) resonances in $B_4H_{10}$, the extra breadth of the peak is found to be due principally to unresolved $^{11}B$–$^{11}B$ coupling, but for the B(1,3) resonance the "extra" linewidth contains a significant term associated with the scalar contribution to $T_2$ from B(2,4).

The collapse at $-62\,°C$ of the high-frequency quartet in the $^{11}B\{^1H\}$ NMR spectrum of $B_5H_9$ appears not to be due to thermal decoupling, i.e. a decrease in $T_1$ of the apical $^{11}B$ nucleus due to changes in $\tau_c$, because the spectra obtained at intermediate (higher) temperatures differ from those calculated. Scalar contributions to $T_2$ may again be important in this case.

The authors make the important point that the lower boron hydrides comprise complex spin systems, and that all spectral parameters must be considered in an explanation of the $^{11}$B NMR spectra.

Two-dimensional correlated NMR spectra of 2,4-$B_5C_2H_7$ have been reported. This technique appears capable of resolving overlapping $^{11}$B resonances and of correlating the resonances of individual $^{11}$B and $^{1}$H nuclei which are spin coupled to one another. An added advantage is that only $^{11}$B–$^{1}$H pairs, and not protons in organic residues, are observed.
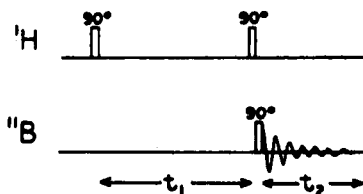


FIG. 1. Pulse sequence used in two-dimensional $^{11}$B–$^{1}$H NMR experiments.

The pulse sequence employed is shown in Fig. 1. Application of a 90° pulse to a proton population at thermal equilibrium generates transverse magnetization. After a period $t_1$ the transverse magnetization vectors, viz. the two components of a doublet, occupy different orientations in the rotating frame. Application of a second 90° pulse rotates the dephased vectors out of the x–y plane, producing corresponding vectors of different $M_z$ values. The second pulse results in a selective pumping of the spin populations of $^{11}$B nuclei scalar coupled to protons. Finally, a 90° pulse is applied to the $^{11}$B nuclei to monitor the $^{11}$B free induction decay during $t_2$. Repetition of the experiment while varying $t_1$ and $t_2$ generates a two-dimensional data matrix over $t_1$ and $t_2$. Double Fourier transformation of this matrix provides a two-dimensional spectrum with orthogonal $^{1}$H and $^{11}$B frequency axes. The two-dimensional correlated $^{11}$B–$^{1}$H NMR spectrum of 2,4-$B_5C_2H_7$ is shown in Fig. 2.

The same authors have also reported an elegant study of $^{1}$H and $^{11}$B spin–lattice relaxation times in carboranes and metallocarboranes.[4] One expects for $^{11}$B and nuclei with $I > 1/2$ that the magnitude of the quadrupolar interaction will be much larger than internuclear dipolar couplings. Thus, $T_1$ for both normal and $^{1}$H decoupled $^{11}$B spectra of 2,4-$B_5C_2H_7$ are the same within experimental error. For nuclei with $I > 1/2$, the major contribution to $T_1$ is the quadrupolar interaction caused by modulation of the tensor coupling between the nuclear spin and the electric field gradient at the nucleus by reorientation of the molecule in solution, for an axially
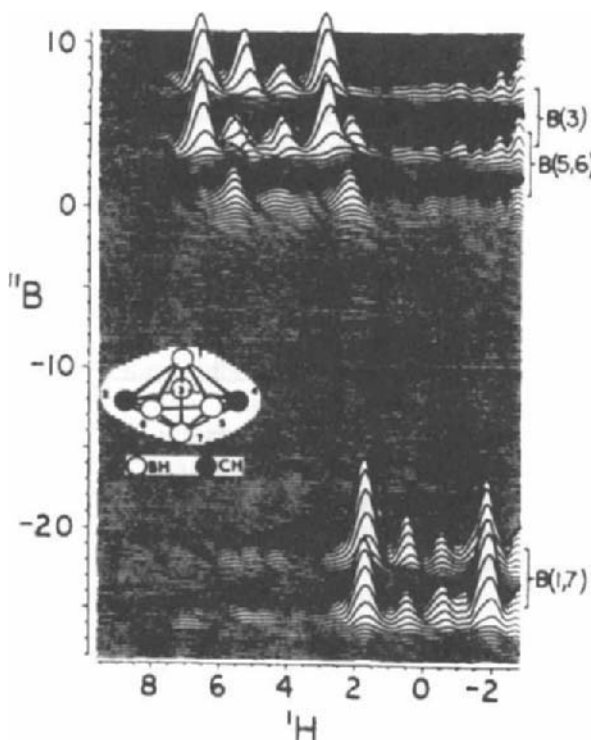
FIG. 2. Two-dimensional $^{11}\text{B}-^{1}\text{H}$ correlated NMR spectrum of 2,4-$\text{B}_5\text{C}_2\text{H}_7$. The x axis shows $^{1}\text{H}$ chemical shifts in ppm relative to $\text{Me}_4\text{Si}$ at 150 MHz. The y axis shows $^{11}\text{B}$ shifts relative to $\text{BF}_3\cdot\text{OEt}_2$ at 48 MHz.

symmetric electric field:

$$\frac{1}{T_1} = \frac{1}{T_2} = \frac{3\pi^2}{10}\left(\frac{2I+3}{I^2(2I-1)}\right)\chi^2\tau_c \quad . \tag{1}$$

where $\chi = e^2qQ/\hbar$ is the nuclear quadrupole coupling constant in hertz (dependent on the field gradient at the nucleus, $eq$), $I$ is the nuclear spin, and $\tau_c$ is the molecular correlation time which describes molecular reorientation. Therefore alterations in $T_1$ may be traced, to a good approximation, to changes in the correlation time or the nuclear quadrupole coupling constant.

$^{11}\text{B}$ spin–lattice relaxation time data have been obtained for a number of carboranes and metallocarboranes (Table 1). The data show some interesting trends. $T_1$ for 2,4-$\text{B}_5\text{C}_2\text{H}_7$ and 2,3-$\text{B}_4\text{C}_2\text{H}_8$ are longer than for the corresponding metallocarboranes in which CpCo replaces a BH unit, and these in turn have $T_1$ values which are longer then those for the

## TABLE 1

**$^{11}$B spin–lattice relaxation time data.**

| Compound | $\delta$ (ppm) | Assignment | $T_1$ (ms) |
|---|---|---|---|
| 2,4-B$_5$C$_2$H$_7$ | 12·5 | B(3) | 38·6 |
| | 9·2 | B(5,6) | 47·7 |
| | −16·4 | B(1,7) | 68·3 |
| 2,3-B$_4$C$_2$H$_8$ | −1·9* | B(4,5,6)* | 47·0 |
| | −53·0 | B(1) | 93·9 |
| CpCo-1,2,3-B$_3$C$_2$H$_7$ | 2·7 | B(4,6) | 13·9 |
| | 2·0 | B(5) | 16·0 |
| CpCo-2-Me-1,2,3-B$_4$C$_2$H$_5$ | 13·1 | B(5) or B(7) | 6·60 |
| | 8·0 | B(7) or B(5) | 5·83 |
| | 3·0 | B(4,6) | 5·91 |
| CpCo-1,2,4-B$_4$C$_2$H$_6$ | 6·7* | B(3,5,6)* | 9·70 |
| | 1·4 | B(7) | 14·7 |
| CpCo-1,4,5-B$_4$C$_2$H$_6$ | 66·7 | B(6) | 16·6 |
| | 4·1 | B(3) | 12·1 |
| | −3·7 | B(2) | 14·5 |
| | −9·6 | B(9) | 14·4 |
| | −16·4 | B(8) | 16·8 |
| | −21·0 | B(7) | 11·8 |
| (CpCo)$_2$-1,7,2,3-B$_3$C$_2$H$_5$ | 53·3 | B(5) | 4·47 |
| | 5·7 | B(4,6) | 3·19 |
| (CpCo)$_2$-1,7,2,4-B$_3$C$_2$H$_5$ | 21·2 | B(5,6) | 3·61 |
| | 12·0 | B(3) | 2·86 |
| (CpCo)$_2$-1,2,3,5-B$_3$C$_2$H$_5$ | 48·7 | B(6) | 5·60 |
| | 8·0* | B(3,7)* | 9·08 |
| (CpCo)$_2$-1,2,4,5-B$_3$C$_2$H$_5$ | 44·7 | B(3,6) | 6·39 |
| | 11·4 | B(7) | 6·64 |
| (CpCo)$_2$-1,7,5,6-B$_5$C$_2$H$_7$ | 80·3 | B(4) | 7·01 |
| | −2·9 | B(3,9) or B(2,8) | 8·00 |
| | −12·3 | B(2,8) or B(3,9) | 9·72 |

* Overlapping, non-equivalent $^{11}$B signals.

corresponding dimetallocarboranes. The order of magnitude change in $T_1$ is considered too large to be due solely to an increase in the electric field gradient due to the presence of the cobalt atom and so changes in $\tau_c$ must also be involved.

Further, $T_1$ values for apical $^{11}$B nuclei are generally longer than for those in non-apical locations. Another observation is that $T_1$ for $^1$H bound to cage carbon atoms is strongly affected by $^{11}$B decoupling, indicative of a scalar heteronuclear cross-relaxation effect. This cross-relaxation can be used with good effect to help deduce the structure of CpCo-1,4,5-B$_6$C$_2$H$_8$. No unique geometry can be inferred from the $^{11}$B NMR spectrum, and the crystal structure is unavailable.

Saturation of the [11]B peaks at $-16\cdot4$, $-9\cdot6$, $-3\cdot7$, and $-4\cdot1$ ppm changes $T_1$ for the low-frequency C–$H$ resonance, whilst saturation of the [11]B peaks at $-21\cdot0$, $-16\cdot4$, and $-3\cdot7$ ppm affects $T_1$ of the high-frequency C–$H$ signal. This implies that one carbon is directly bonded to three boron atoms, and the other carbon to four boron atoms. Further, saturation of the $-3\cdot7$ and $-16\cdot4$ ppm [11]B resonances alters the $T_1$ data for *both* C–$H$ protons. Only placement of Co in position 1 and the CH units in the 4 and 5 positions is consistent with these data. Assignments of the ^{11}B NMR spectrum can then be extracted from the $T_1$ data. The doublet at $66\cdot7$ ppm is logically due to B(6), the four-coordinate boron adjacent to cobalt. B(2) and B(8) are associated with the [11]B signals at $-3\cdot7$ and $-16\cdot4$ ppm. The former has the shorter $T_1$ value ($14\cdot5$ ms) and so it is assigned to B(2) whose environment is slightly less symmetrical than that of B(8). Similar arguments are used to assign $\delta$ $4\cdot1$ to B(3) and $\delta$ $9\cdot6$ to B(9). Saturation of the $-21\cdot0$ ppm boron resonance does not occasion a large change in the C–$H$ $T_1$ value, and this peak can be assigned to B(7).

## III. ANALYTICAL APPLICATIONS

^{11}B NMR spectroscopy has been used as an analytical tool to monitor reactions of various boron-containing compounds. Examples include the methanolysis of $Me_2NBH_3^-$,[5] electrolysis of $B_3H_8^-$ salts at copper or silver anodes in the presence of phosphine ligands,[6] a study of catalysed H/D exchange in 1,2-, 1,7-, and 1,12-$B_{10}C_2H_{12}$, 1,6-$B_8C_2H_{10}$, CpCo-3,1,2-$B_9C_2H_{11}$, CpCo-1,2,4-$B_8C_2H_{10}$, $B_{10}H_{14}$, and $Me_3NBH_3$,[7] a study of the kinetics of the diethyl ether catalysed isomerization of 1-$ClB_5H_9$ to 2-$ClB_5H_9$,[8] and an investigation of the systems $AlH_3$–$BH_3$–THF and $LiAlH_4$–$BH_3$–THF in which are formed solvated $AlH_{3-n}(BH_4)_n$ and $LiAlH_{3-n}(BH_4)_{n+1}$.[9]

## IV. ONE-BORON COMPOUNDS

Materials containing only one boron atom comprise the most heterogeneous of the classes considered in this review. The structural and compositional diversity is such that few connections can be made amongst the compounds considered in this section.

Pentaphenylborole, $Ph_5BC_4$, has been synthesized from 1,1-dibutyl-2,3,4,5-tetraphenylstannole and $PhBCl_2$. Reduction using potassium affords the dianion which forms $\pi$ complexes with transition metals. ^{11}B NMR data are given in Table 2. Although the [11]B signals are broad, it is clear that complexation and reduction produces a large increase in boron shielding. No [11]B–[195]Pt coupling is reported in $(Ph_5BC_4)Pt(C_8H_{12})$.[10]

## TABLE 2

$^{11}$B NMR data for complexes of pentaphenyl-
borole.

| Compound | $\delta^{11}$B |
|---|---|
| Ph$_5$BC$_4$ | 55 ± 5 |
| K$_2$(Ph$_5$BC$_4$) | 29 ± 2 |
| (Ph$_5$BC$_4$)Fe(CO)$_3$ | 17 ± 2 |
| (Ph$_5$BC$_4$)CoCp | 17 ± 2 |
| (Ph$_5$BC$_4$)Ni(CO)$_2$ | 24 ± 2 |
| (Ph$_5$BC$_4$)Pt(C$_8$H$_{12}$) | 16 ± 2 |

The chemistry of heterocycles containing, in addition to a boron atom, carbon, nitrogen, or sulphur, has attracted increasing attention. Many of these compounds form $\pi$ complexes with metals. $^{11}$B NMR chemical shift data for some of these compounds are collected below in linear form. 1-Me-2,5-(t-C$_4$H$_9$)$_2$-1,3,5-BN$_2$C$_2$H$_2$ has $\delta^{11}$B 26·2 ppm and the Cr(CO)$_3$ complex 26·2 ppm.[11] (1-Ph-2-Et-1-BC$_4$H$_3$)Fe(CO)$_3$ in C$_6$D$_6$ has $\delta^{11}$B 19·6.[12] $^{11}$B chemical shifts for 1-Ph-2-(t-C$_4$H$_9$)-1,2-BNC$_3$H$_6$ (46 ppm), [1-Ph-2-(t-C$_4$H$_9$)-5-Me-1,2-BNC$_3$H$_2$]$_2$Fe$_2$(CO)$_4$ (22 ± 1 ppm in THF), and 1-Ph-2-(t-C$_4$H$_9$)-5-Me-1,2-BNC$_3$H$_3$ (41 ppm) have been reported.[13] The silicon–boron heterocycle 1-Ph-4,4-Me$_2$-1,4-BSiC$_4$H$_4$ has $\delta^{11}$B 52·7 ppm and (1-Ph-4,4-Me$_4$-1,4-BSiC$_4$H$_4$)CoCp 20·9 ppm.[14] Again, complexation to a metal usually appears to shield boron atoms in heterocyclic ligands.

Chemical shift data have been reported for tetramethylethylenediamine adducts of BH$_3$ and BF$_3$,[15] and complexes of tertiary amines with 9-borabicyclo[3.3.1]nonane.[16] Exchange of Lewis bases between BBN and the BBN adducts is slow on the NMR time scale and so it is possible to observe peaks in the $^{11}$B NMR spectra that are due to complexes too unstable to isolate.

Triphenylborane and (Et$_4$N)[CpFe(CO)$_2$] form a 1:1 adduct (Et$_4$N)·[CpFe(CO)$_2$BPh$_3$], $\delta^{11}$B 28·8, which contains an iron–boron bond. In tetrahydrofuran this compound rearranges to form (Et$_4$N)Ph$_3$BH and (Et$_4$N)[Ph$_3$BC$_5$H$_4$Fe$_2$(CO)$_4$Cp] for which NMR data were not reported.[17]

Biffer and Nöth have characterized a series of trimethylsilylborates.[18] $^{11}$B NMR data for these compounds are given in Table 3. The sign of $^1J(^{29}$Si–$^{11}$B) is reported to be negative. There is an increasing Si–B coupling and a low-frequency shift of the $^{11}$B resonance with increasing silicon substitution.[18]

$^{11}$B chemical shifts for thirteen compounds of the type (2,4,6-Me$_3$Ph)$_2$BOR (R = alkyl, aryl, alkenyl, alkynyl) are reported to lie in the range 51 ± 2 ppm.[19]

## TABLE 3

### ^{11}B NMR data for trimethylsilylborates.

| Compound | $\delta^{11}$B | $J$(Si–B) | Solvent |
|----------|------------|-----------|---------|
| Li(Me$_3$BSiMe$_3$) | −28·5 | −74 | C$_6$D$_6$ |
| Li[Me$_2$B(SiMe$_3$)$_2$] | −36·1 | −61 | C$_6$H$_{14}$ |
| Li[MeB(SiMe$_3$)$_3$] | −45·3 | −53 | C$_6$D$_6$ |
| Li[B(SiMe$_3$)$_4$] | −53·4 | −48 | C$_6$D$_6$ |
| Li[(Me$_3$Si)$_2$-9-borabicyclononane] | −25·0 | −65 | THF |

[11]B (and ^{14}N) chemical shift data have been recorded for a large series of alkynylborane derivatives (Table 4). The diamagnetic anisotropy of the carbon–carbon triple bond leads to an increase in shielding relative to the corresponding alkenylboranes.[20]

Boron chemical shift data for a large series of Cr(CO)$_3$ complexes of phenylboranes and benzodiazaboroles, in which chromium is $\pi$-bonded to the carbocyclic ring, have been published.[21]

The relationships between [11]B and ^{13}C chemical shifts of three-coordinate boranes and the analogous carbonium ions are more complex than previously thought. Divergence is notable in the case of ferrocenylboranes and ferrocenylcarbonium ions, and indicates a contribution from a fulvalene-like structure in the carbocationic compound.[22] ^{13}C and ^{11}B NMR

## TABLE 4

### ^{11}B NMR data for alkynylboranes.

| Compound | $\delta^{11}$B |
|----------|------------|
| Me$_2$BC≡CMe | −71·7 |
| Et$_2$BC≡CMe | −73·2 |
| (n-Pr)$_2$BC≡CMe | −73·5 |
| C$_4$H$_8$BC≡CBC$_4$H$_8$ | −76·3 |
| PhB(−C≡CMe)$_2$ | −40·0 |
| (MeO)$_2$BC≡CH | −21·6 |
| (Me$_2$N)$_2$BC≡CH | −23·8 |
| (1,5,5-Me$_3$-1,2,6-BO$_2$C$_3$H$_3$)C≡CH | −20·9 |
| (2,5-Me$_2$-1,2,5-BN$_2$C$_2$H$_4$)C≡CH | −24·9 |
| [(Et$_2$N)$_2$B]$_2$C$_2$ | −24·0 |
| Me$_2$NB(C≡CH)$_2$ | −23·5 |
| Me$_2$NB(C≡CMe)$_2$ | −23·0 |
| Et$_2$NB(C≡CMe)$_2$ | −22·0, $^1J$($^{13}$C–$^{11}$B) = +132 |
| (PhC≡C)$_4$BLi | 31·0 |
| [Me$_2$BN(C≡CH)$_2$]$_2$ | 5·6 |

data on a series of 29 boron-substituted aromatic heterocycles (e.g. thiophene, furan, $N$-methylpyrrole) have been compiled. A roughly linear relationship between $\delta^{13}C$ in phenylcarbonium ions and $\delta^{11}B$ in the analogous borane is taken to be indicative of a mesomeric $p\pi$–$p\pi$ interaction between boron and the aromatic rings. In a series of compounds of the type $(aryl)_3B$, the $^{11}B$ chemical shifts are aryl = phenyl 68·0, 2-thienyl 47·3, 2-($N$-methylpyrrolyl) 44·3, 2-furyl 38·0 ppm. This suggests that the five-membered heterocyclic rings are better $\pi$ donors than phenyl.[23]

Signs and magnitudes of coupling constants between boron and carbon have been measured for $1\text{-}^{13}CH_3B_5H_8$, $LiBMe_4$, and $Bu_4NBPh_4$ in multiple resonance experiments. The results are collected in Table 5.[24]

## TABLE 5

**Boron coupling constants.**

|  | $1\text{-}^{13}CH_3B_5H_8$ | $LiBMe_4$ | $Bu_4NBPh_4$ |
|---|---|---|---|
| $^1J(^{11}B_1\text{-}^{11}B_2)$ | +18·9 |  | $^2J(^{13}C_3\text{-}^{11}B) = \pm 1\cdot 4$ |
| $^1J(^{13}C\text{-}^{11}B_1)$ | +73·1 | +39·8 | $^3J(^1H_2\text{-}^{11}B) = \pm 2\cdot 2$ |
| $^1J(^{13}C\text{-}^{10}B_1)$ | +24·6 | +13·1 |  |
| $\lvert^2J(^{13}C\text{-}^{11}B_2)\rvert$ | ~1–2 |  |  |
| $^2J(^{11}B_1\text{-}C\text{-}^1H)$ | −6·8 |  |  |

Partial replacement of hydride by $SiF_3^-$ occurs in the reaction of (n-$C_4H_9)_4BH_4$ with $SiF_4$ to give $BH_3SiF_3^-$ [$\delta$ 46·9, $J_{BH}$ 86, $J_{BSiF}$ 20·9] and $BH_2(SiF_3)_2^-$ [$\delta$ 55·6, $J_{BH}$ 85, $J_{BSiF}$ 24·3].[25] Halogen-substituted $BH_4^-$ derivatives have also been prepared: $(Bu_4N)HBBr_3$ ($\delta$ −13·0, $J_{BH}$ 176) and $(Bu_4N)HBCl_3$ ($\delta$ 3·1, $J_{BH}$ 158).[26]

$^{11}B$ NMR data for dihydroboron(+1) cations, and their halogenated derivatives, of the type $H_2B(phosphine)_2^+PF_6^-$ are given in Table 6. $J(^{31}P\text{-}^{11}B)$ increases as hydride is replaced by chloride.[27]

## V. DIBORANE DERIVATIVES

Bulky alkyl groups stabilize the boron–boron bond in $B_2H_4$ derivatives, and this strategy has been used in the synthesis of long sought after tetraalkyl diborane derivatives. $^{11}B$ NMR data ($CDCl_3$ as solvent) are collected in Table 7.[28]

Some $^{11}B$ NMR data have been reported for a series of related compounds. Noteworthy is the spectrum of $1,1,2\text{-}(t\text{-}C_4H_9)_3\text{-}2\text{-}Me_3SiB_2$, in which the boron bonded to two alkyl groups has $\delta$ 102·0 whilst boron

## TABLE 6

$^{11}$B NMR data for dihydroboron cations.

| Compound | $\delta^{11}$B |
|---|---|
| [(CH$_3$)$_3$NBH$_2$P(C$_6$H$_5$)$_3$]$^+$PF$_6^-$ | 29·1 ppm ($J_{PB} \approx J_{BH} \approx 92$ Hz) |
| [(CH$_3$)$_3$NBH$_2$P(CH$_3$)$_2$C$_6$H$_5$]$^+$PF$_6^-$ | 27·42 ppm ($J_{PB} \approx J_{BH} \approx 86$ Hz) |
| [(C$_6$H$_5$)$_3$PBH$_2$P(CH$_3$)$_3$]$^+$PF$_6^-$ | 51·9 ppm ($J_{PB} \approx J_{BH} \approx 100$ Hz) |
| [(C$_6$H$_5$)$_3$PBH$_2$P(CH$_3$)$_2$C$_6$H$_5$]$^+$PF$_6^-$ | 51·4 ppm ($J_{PB}, J_{BH}$ indeterminable) |
| [H$_2$B-P(C$_6$H$_5$)$_2$CH$_2$CH$_2$P(C$_6$H$_5$)$_2$]$^+$PF$_6^-$ | 51·7 ppm ($J_{PB}, J_{BH}$ indeterminable) |
| [(CH$_3$)$_3$NBHClP(C$_6$H$_5$)$_3$]$^+$PF$_6^-$ | 17·5 ppm ($J_{PB}, J_{BH}$ indeterminable) |
| [(CH$_3$)$_3$NBHClP(CH$_3$)$_2$C$_6$H$_5$]$^+$PF$_6^-$ | 18·7 ppm ($J_{PB} \approx J_{BH} \approx 121$ Hz) |
| [(CH$_3$)$_3$NBCl$_2$P(CH$_3$)$_2$C$_6$H$_5$]$^+$PF$_6^-$ | 12·1 ppm ($J_{PB} = 156\cdot6$ Hz) |
| [(C$_6$H$_5$)$_3$PBHClP(CH$_3$)$_3$]$^+$PF$_6^-$ | 34·74 ppm ($J_{PB} \approx J_{BH} \approx 104$ Hz) |
| [(C$_6$H$_5$)$_3$PBHClP(CH$_3$)$_2$C$_6$H$_5$]$^+$PF$_6^-$ | 33·8 ppm ($J_{PB}, J_{BH}$ indeterminable) |
| [(C$_6$H$_5$)$_3$PBCl$_2$P(CH$_3$)$_3$]$^+$PF$_6^-$ | 20·75 ppm ($J_{PB} = 134\cdot6$ Hz) |
| [(C$_6$H$_5$)$_3$PBCl$_2$P(CH$_3$)$_2$C$_6$H$_5$]$^+$PF$_6^-$ | 20·10 ppm ($J_{PB} = 136\cdot3$ Hz) |

## TABLE 7

$^{11}$B NMR data for alkylated diborane(4) compounds.

| Compound | $\delta$,B–OCH$_3$ (ppm) | $\delta$,B–R (ppm) |
|---|---|---|
| 1,2-(t-C$_4$H$_9$)$_2$-1,2-(MeO)$_2$B$_2$ | 64 | 106 |
| 1,1,2-(t-C$_4$H$_9$)$_3$-2-(MeO)B$_2$ | 65 | 106 |
| 1,2-(t-C$_4$H$_9$)$_2$-1,2-(neopentyl)$_2$B$_2$ |  | 103 |
| 1,1,2-(t-C$_4$H$_9$)$_3$-2-(neopentyl)B$_2$ |  | 104 |

bonded to both carbon and silicon has $\delta$ 126·9, the largest high-frequency shift yet reported for three-coordinate boron.[29]

$T_1$ and $T_2^*$ data for both $^{10}$B and $^{11}$B have been reported for tetrakis(dimethylamino)diborane(4) and are given in Table 8. Simulation of the line narrowed $^{10}$B NMR spectrum yields $^1J(^{11}B-^{10}B) \leqslant 25$ Hz and $^1J(^{11}B-^{11}B) \leqslant 75$ Hz.[30]

## TABLE 8

Boron relaxation time data for (Me$_2$N)$_4$B$_2$.

| Temp. (°C) | $^{11}$B $T_1$ | $^{11}$B $T_2^*$ | $^{10}$B $T_1$ | $^{11}$B $T_2^*$ |
|---|---|---|---|---|
| 34 | 1·9 | 1·8 | 2·7 | 2·4 |
| 100 | 5·0 | 4·1 | 7·3 | 3·9 |
| 150 | 8·8 |  |  |  |
| 200 | 11·7 | 7·5 | 17·9 | (multiplet) |

The two-boron heterocycle 2,5-$Me_2$-3,4-$Et_2$-1,3,5-$B_2SC_2$ forms a triple-decker sandwich compound with cobalt. The suggested structure features three stacked heterocycles with cobalt atoms in the two interplanar vacancies. Accordingly, the $^{11}B$ NMR spectrum contains singlets at 14 ppm for the centre ligand and at 30 ppm for the two exterior $B_2SC_2$ rings.[31]

A hydride-bridged diborohydride species, probably $K(Et_3BHBEt_3)$, is formed from $Et_3B$ and $K^+HBEt_3$ in THF. It has $\delta^{11}B$ 7·5 (cf. −13·0 ppm for $K^+HBEt_3$). This compound may be in equilibrium with its constituents; no B–H coupling data are reported.[32]

## VI. TRIBORANE DERIVATIVES

Gaines and Hildebrandt have discovered a general synthesis of transition metal complexes of $B_3H_8^-$ of the type $L_nMB_3H_8$ (L = ligand) which comprises the reaction of an organometallic carbonyl halide with $(Me_4N)B_3H_8$ in dichloromethane. Spectroscopic studies indicate that in these compounds the $B_3H_8$ unit serves as a bidentate ligand and is bonded to the metal atom through bridging hydrogen atoms. A representative suggested structure, that of $(CO)_4MnB_3H_8$, is shown in Fig. 3. The 86·7 MHz $^{11}B$ NMR spectral
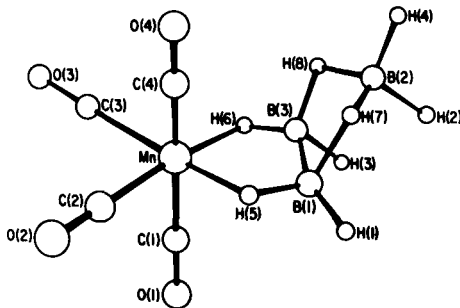


FIG. 3. Proposed structure of $(CO)_4MnB_3H_8$.

data are collected in Table 9. Typical spectra contain a high-frequency triplet of unit area which is assigned to B(2) and a "doublet" at low frequency due to B(1,3). The "doublet" exhibits considerable fine structure; some of this disappears upon decoupling the M–H–B protons but the resulting signal is still broad. Upon broad band $^1H$ decoupling, the resonance collapses to a sharp singlet, showing that the complexity is due to $^1H$–$^{11}B$ interactions. This low frequency resonance, upon $^1H$ decoupling and line narrowing, reveals a wealth of fine structure due to a combination of short- and long-range spin–spin interactions, and the spectrum has not

## TABLE 9

**86·7 MHz $^{11}$B NMR data for metal–$B_3H_8$ complexes.**

| Complex | Solvent | Temp. (°C) | Chemical shift (coupling constant) | |
|---|---|---|---|---|
| | | | B(1,3) | B(2) |
| $(CO)_4MnB_3H_8$ | $(C_2H_8)_2O$ | ambient to −40 | −42·2 (133) | +1·5 (123) |
| | $C_6D_6$ | ambient | −41·8 (134) | +2·4 |
| | $CD_2Cl_2$ | ambient | −41·9 (134, 140*) | +2·4 |
| | $CD_2Cl_2$ | −36·2 | −41·8 (127, 139*) | +1·9 |
| $(CO)_4ReB_3H_8$ | $C_6D_6$ | ambient | −43·3 (142) | +0·3 |
| | $CD_2Cl_2$ | ambient | −43·2 (132) | +0·3 |
| $(\eta^5-C_5H_5)(CO)FeB_3H_8$ | $C_6D_6$ | ambient | −42·0 (132) | +3·4 (122) |
| | $CD_2Cl_2$ | ambient | −42·5 (127, 139*) | +2·5 (125) |
| $(H)(CO)_3FeB_3H_8$ | $CD_2Cl_2$ | ambient | −42·1 (127) | +3·0 (127) |
| | $CD_2Cl_2$ | −36·2 | −42·0 (137, 142*) | +2·8 (107) |
| $(\eta^5-C_5H_5)(CO)_2MoB_3H_8$ | $C_6D_6$ | ambient | −40·7 (98, 128*) | +4·0 (112) |
| $(\eta^5-C_5H_5)(CO)_2WB_3H_8$ | $(CD_3)_2CO$ | ambient | −42·5 | −4·3 |
| $(Ph_3P)(CO)_3MnB_3H_8$ | $C_6D_6$ | ambient | −38·5, −39·9 | +1·4 |
| | $CD_2Cl_2$ | ambient | −38·3, −40·6 | +0·3 |
| $(Ph_2PCH_2CH_2PPh_2)-$ $(CO)_2MnB_3H_8$ | $C_6D_6/$ DMF | ambient | −40·6 | +3·8 |
| $(PF_3)(CO)_3MnB_3H_8$ | $C_6D_6$ | 23 | −41·6, −42·8 | +3·2, +2·2 |
| | $CD_3C_6D_5$ | 23 | −41·6, −42·8 | +2·6 |
| $(NH_3)(CO)_3MnB_3H_8$ | $C_6D_6$ | 23 | −39·2, −40·3 | +0·2 |
| | $CD_2Cl_2$ | 23 | −39·2, −40·2 | −0·2 |
| $(CO)_4MnB_3H_7Cl$ | $CD_2Cl_2$ | −36·2 | −41·3 (122, 139*) | +9·0 (122, 139*) |
| | $CD_2Cl_2$ | +23 | −41·3 (42*) | +9·4 |
| $(CO)_4MnB_3H_7Br$ | $CD_2Cl_2$ | −36·2 | −41·6 (137*) | +2·3 (98) |
| | $CD_2Cl_2$ | +23 | −41·6 (44) | +2·5 |
| | $CD_3C_6D_5$ | +23 | −41·9 | +2·7 |
| $(CO)_4MnB_3H_7I$ | $CD_3CN$ | +23 | −41·1 | −11·2 |

* Coupling constants obtained from line narrowed spectra.

yet been completely interpreted. Line narrowing enhances resolution of the high-frequency triplet but does not lead to new fine structure. Therefore the couplings $J(B_2–H_2)$ and $J(B_2–H_4)$ must be nearly identical and coupling between B(2) and the bridge protons is small.

The ferraborane $(CO)_3Fe(H)B_3H_8$ is formulated as the *mer* isomer on the basis that all nine protons have different chemical shifts in the 270 MHz $^1$H NMR spectrum. This absence of a plane of symmetry is not revealed, however, in the 86·7 MHz $^{11}$B NMR spectrum which indicates that B(1) and B(3) are equivalent over the temperature range −85 to 23 °C. It is probable that there is an accidental degeneracy of chemical shifts. In

general, increasing temperature and increasing solvent polarity increase the resolution in the $^1$H and $^{11}$B NMR spectra. Part of this may be due to effects associated with thermal decoupling and solution viscosity.

Treatment of $(CO)_4MnB_3H_8$ with a ligand L ($L = Ph_3P$, $NH_3$, and $PF_3$) produces $L(CO)_3MnB_3H_8$. In these complexes the $B_3H_8$ unit probably still behaves as a bidentate ligand but the situation is complicated by the coexistence of isomers since the $^{11}B\{^1H\}$ spectra contain more resonances than would be expected for an isomerically pure compound.

Halogenation of $(CO)_4MnB_3H_8$ with chlorine or bromine affords $(CO)_4MnB_3H_7X$ ($X = Cl$, Br). At low temperatures, the $^{11}$B NMR spectra suggest static structures in which the halogen atom occupies a terminal position on B(2), since the B(2) resonance but not those of B(1,3) shift on halogenation. An expansion of the low frequency resonance at 23 °C under conditions of line narrowing, line narrowing with Mn–H–B protons decoupled, and line narrowing with B–H and B–H–B protons decoupled is shown in Fig. 4. In sum, it is concluded that the Mn–H–B protons are static on the NMR time scale and that B(1,3) are coupled to the equivalent protons H(1–5). Even with line narrowing, fine structure in the B(2)
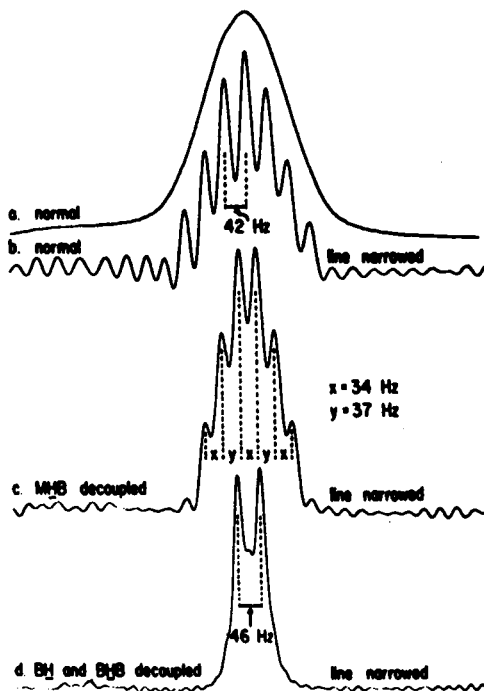


FIG. 4. $^{11}$B NMR spectrum of the B(1,3) resonance of $(CO)_4MnB_3H_7Cl$ at 23 °C.
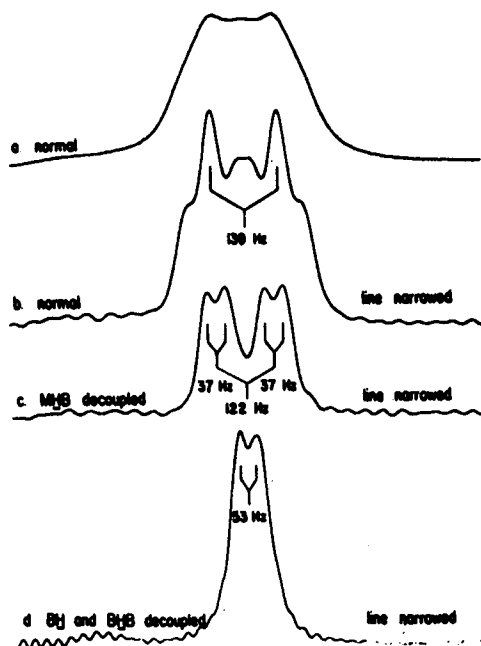
FIG. 5. ^{11}B NMR spectrum of the B(1,3) resonance in $(CO)_4MnB_3H_7Cl$ at $-36\,°C$.

resonance is not observed. An expansion of the same B(1,3) resonances under similar conditions but at $-36\,°C$ is shown in Fig. 5. At this temperature, H(1-5) are no longer equivalent. With line narrowing and decoupling of the Mn–H–B protons, a large coupling ($\sim122$ Hz) between B(1,3) and the terminal protons, H(1,3), is seen. Coupling to the bridge protons, H(4,5), is about 37 Hz, and that to the Mn–H–B protons, H(6,7), is $\sim53$ Hz. The scrambling of H(1,3), H(2), and H(4,5) is confirmed by the variable temperature ^{1}H NMR spectra. Such fluxional behaviour is the more remarkable in that it is not observed in the parent $(CO)_4MnB_3H_8$.

Photolytic or thermal decarbonylation of $(CO)_4MnB_3H_8$ affords $(CO)_3MnB_3H_8$ whose static, solid state structure is shown in Fig. 6. It demonstrates a $fac$-$B_3H_8$ unit bonded to the manganese atom by one Mn–H–B bridge to each boron atom. Two hydrogen atoms bridge B(1)–B(2) and B(2)–B(3) so that the symmetry is $C_{2v}$. However, the 86·7 MHz ^{11}B NMR spectrum of this unusual compound consists of a single resonance centred at $-47·2$ ppm down to $-80\,°C$. The ^{1}H NMR spectrum at room temperature shows two sets of resonances. One, at low frequency, has a relative area of 3 and is assigned to the Mn–H–B bridges. The single, higher
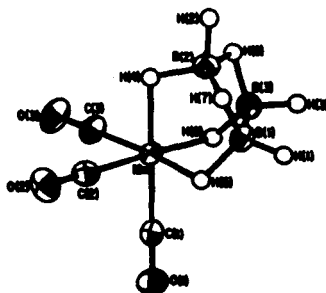
FIG. 6. Molecular structure of $(CO)_3MnB_3H_8$.

frequency, resonance of relative area 5 implies that the B–H and B–H–B protons are rapidly interconverting. This, of course, also leads to magnetic equivalence of the three boron atoms as is observed in the $^{11}$B NMR spectrum. Line narrowed $^{11}$B NMR spectra, obtained with selective decoupling at $-10\,°C$, confirm that each boron atom is coupled to a single Mn–H–B proton. When these bridge protons are decoupled, a sextet appears, so the normal spectrum is approximately a doublet ($J \approx 68$ Hz) of sextets ($J \approx 44$ Hz), although some additional fine structure is apparent.[33]

The reaction of halogens with $(CO)_3MnB_3H_8$ in the presence of aluminium chloride yields $(\mu\text{-}X)(CO)_6Mn_2B_3H_8$. The molecular structure of the dimanganoborane contains a $(CO)_3Mn\text{–}Br\text{–}Mn(CO)_3$ unit in which each manganese atom is linked to B(1,3) of a bis(bidentate) $B_3H_8$ ligand by Mn–H–B bonds (Fig. 7). The $^{11}$B NMR data for X = Cl and Br are given in Table 10;[34] these molecules appear to be static on the NMR time scale.
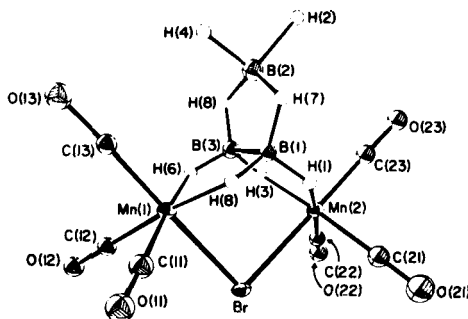


FIG. 7. Solid state structure of $(\mu\text{-}Br)(CO)_6Mn_2B_3H_8$.

The $^{11}$B NMR spectrum of $CuB_3H_8$ in dichloromethane exhibits only a very broad signal at $-7$ ppm ($W/2$ 1790 Hz).[35]

Proton decoupled $^{11}$B NMR spectra have been employed to follow the cleavage reactions of $B_5H_9$ by trimethylphosphine. Thus, $B_3H_5(PMe_3)_2$ is

## TABLE 10

$^{11}$B NMR data for $(\mu\text{-}X)(CO)_6Mn_2B_3H_8$.

|        | X = Br | X = Cl |
|--------|--------|--------|
| B(1,3) | −38·3  | −37·1  |
| B(2)   | 10·4   | 10·0   |

identified as a probable intermediate which showed broad signals at −36·5 (2B) and −39·0 (1B) ppm.[36]

Diborane and tetraborane undergo unsymmetrical cleavage by $B_2H_4(PMe_3)_2$ to give $[B_3H_6(PMe_3)_2]^+B_2H_7^-$ and $[B_3H_6(PMe_3)_2]^+B_3H_8^-$ respectively. The $^{11}$B NMR spectrum of the new triborane cation $[B_3H_6(PMe_3)_2]^+$ shows a broad singlet at −39·0 (1B) and −10·5 (2B, $J_{BP}$ 114) ppm.[37]

The novel bimetallic $CpFe(Me_5\text{-}1,3\text{-}B_3C_2)CoCp$, which likely has a triple-decker structure with iron and cobalt on opposite sides of a planar $B_3C_2$ ligand, has $\delta^{11}B$ 19·6.[38]

## VII. TETRABORANE DERIVATIVES

Kodama and coworkers have studied the cleavage of $B_4H_{10}$ by Lewis bases. The reaction with trimethylamine provides an intermediate, $B_4H_8\cdot NMe_3$. The $^{11}$B NMR spectrum of this material at 0 °C shows resonances at $\delta$ 1·1 (d, B(3), 130), −8·5 (t, B(2,4), 116), and −2·5 (d, B(1), 116).[39] A similar reaction with hexamethylenetetramine leads to $(B_4H_{10})_2\cdot(CH_2)_6N_4$, $\delta^{11}B$ −1·1 (d, B(3), 132), −9·3 (t, B(2,4), 120), and −28·5 (d, B(1), 96). Extrusion of borane yields $(B_3H_7)_2\cdot(CH_2)_4N_4$, $\delta^{11}B$ −15·2 (2B) and −24·7 (1B) in $CH_2Cl_2$.[40]

A multinuclear ($^1$H, $^{11}$B, $^{19}$F, $^{31}$P) NMR study of $B_4H_8\cdot PF_2NMe_2$ has delineated geometrical and rotational isomers. The dimethyl-aminodifluorophosphine ligand may assume an *exo* or *endo* orientation at B(1) in the butterfly-shaped tetraborane unit. The $^{11}$B NMR spectrum of this compound exhibits a triplet at −54·9 ppm with $J_{BH} \approx J_{BP} \approx 175$ Hz due to the phosphine-substituted B(1). Upon line narrowing and $^1$H decoupling, a complicated resonance is resolved into a singlet at −3·9 ppm due to B(2,4) and two quartets at 3·6 and −0·5 ppm with $J(B_1\text{-}B_3)$ 24 Hz. The two quartets are assigned to B(3) in the two geometrical isomers, and these two signals coalesce as the isomers interconvert at about 90 °C with $\Delta G^{\ddagger}$ 19 kcal mol$^{-1}$. Curiously, the chemical shifts of B(1) and B(2,4) in the two isomers appear to be essentially the same. It is of interest that the barrier

to rotation about the B–P bond in one of the isomers is found to be
7·8 kcal mol$^{-1}$.[41]

Silicon-bridged carboranes of the type $\mu$-(ClCH$_2$SiMe$_2$)-2,3-B$_4$C$_2$H$_7$
have been prepared from ClCH$_2$SiMe$_2$Cl and Na$^+$2,3-B$_4$C$_2$H$_7^-$. The silane
is considered to bridge a basal B–B edge in the pentagonal pyramidal B$_4$C$_4$
through B$_2$Si three-centre bonds since the 32 MHz $^{11}$B NMR spectra (Table
11) show a low-frequency doublet due to the apical BH unit, doublets at

## TABLE 11

**$^{11}$B NMR data for ClCH$_2$Me$_2$Si substituted carboranes and related compounds.**

| Compound | $\delta^{11}$B ($J_{BH}$) |
|---|---|
| $\mu$-(ClCH$_2$Me$_2$Si)-2,3-B$_4$C$_2$H$_7$ | −47·1 (d, B(1), 176), −2·8 (d, B(4), 124), 0·8 (dd, B(6), 164, 35), 9·1 (d, B(5), 158) |
| 5-(ClCH$_2$Me$_2$Si)-2,3-B$_4$C$_2$H$_7$ | −51·3 (d, B(1), 181), −0·5 (s, B(5)), 0·9 (dd, B(4,6), 154, ~35) |
| 4-(ClCH$_2$Me$_2$Si)-2,3-B$_4$C$_2$H$_7$ | −51·8 (d, B(1), 179), −2·2 (d, B(5,6), 148), 8·1 (s, B(4)) |
| 5-(ClMe$_2$SiCH$_2$)-2,3-B$_4$C$_2$H$_7$ | −52·1 (d, B(2), 179), −2·6 (dd, B(4,6), 148, 38), 10·5 (s, B(5)) |
| 2-ClMe$_2$SiCH$_2$-1,5-B$_3$C$_2$H$_4$ | 8·0 (d, B(3,4)), 9·4 (s, B(2)) |
| 2-ClMe$_2$SiCH$_2$-1,6-B$_4$C$_2$H$_5$ | −23·1 (d, B(4), 192), −17·3 (d, B(3,5), 188), −9·6 (s, B(2)) |

−9·1 and 2·8 ppm assigned to B(5) and B(4) respectively, and a doublet
of doublets at −0·8 ppm due to B(6) which is spin coupled to the remaining
bridge proton bonded to B(5) and B(6). Distinction between B(5) and B(6)
is made on the basis of empirical correlations which show that in related
compounds the B(5) resonance is usually broader than those of B(4,6) and
lacks resolved coupling with the bridge proton.

Isomerization reactions of $\mu$-(ClCH$_2$SiMe$_2$)B$_4$C$_2$H$_7$ lead to many new
carborane compounds. Thermal rearrangement at 60 °C involves migration
of the ClCH$_2$SiMe$_2$ group from a bridging to a terminal position and affords
5-(ClCH$_2$SiMe$_2$)B$_4$C$_2$H$_7$. The $^{11}$B NMR spectrum of this compound con-
tains a singlet in the high-frequency region, which is consistent with basal
boron substitution, and a preference for B(5) comes from the observation
of only one bridge proton resonance. A 1,2-shift of the carboranyl group
from silicon to the methylene carbon is catalysed by aluminium chloride
and yields 4-(ClMe$_2$SiCH$_2$)B$_4$C$_2$H$_7$. The $^{11}$B NMR spectrum still shows a
high-frequency singlet due to basal boron substitution, but two bridge
hydrogen peaks appear in the $^1$H spectrum, which is suggestive of transfer
of the isomerized substituent to B(4). Pyrolysis of 5-(ClCH$_2$SiMe$_2$)-2,3-
B$_4$C$_2$H$_7$ at 150 °C generates a mixture of 4- and 5-(ClMe$_2$SiCH$_2$)B$_4$C$_2$H$_7$.

The C-substituted B(5) atom is shielded relative to the unsubstituted B(4) atom. A useful trend in these compounds is noted: the degree of resolution of basal B–$H_b$ coupling is greater when the boron atom is adjacent to one than to two bridge hydrogen atoms.

Flash thermolysis of 4- or 5-($ClMe_2SiCH_2$)-2,3-$B_4C_2H_7$ at 690 °C produces *inter alia* 2-($ClMe_2SiCH_2$)-1,5-$B_3C_2H_4$ and 2-($ClMe_2SiCH_2$)-1,4-$B_4C_2H_5$.[42]

The cupraborane $(Ph_3P)_2CuB_4H_9$ has been prepared from $(Ph_3P)_3CuCl$ and $KB_5H_{12}$ or $KB_4H_9$. The 28·8 MHz $^{11}$B NMR spectrum obtained at 0 °C shows a triplet of relative area 1 at −55·2 ppm ($J_{BH}$ 98) and a broad, asymmetric resonance of area 3 at 3·2 ppm. The suggested structure of this compound features a square pyramidal cage with $BH_2$ units at the 1, 2, and 4 positions. The $(Ph_3P)Cu$ unit occupies a basal position and is simultaneously bonded to B(1,2,4). Low temperature $^{11}$B NMR spectra of this material, and of the analogous $Et_3P$ derivative, would be of interest.[43]

Tetraboron tetrachloride, $B_4Cl_4$, has $\delta^{11}$B 85 ppm at 28 MHz and over a 200 °C temperature range. The compound is electron deficient and the $^{11}$B nuclei in it are very deshielded relative to perhalogenated polyhedral borane anions and carboranes.[44]


## VIII. PENTABORANE DERIVATIVES

Hydroboration of pentaborane(9) with dimethylacetylene in the presence of $(MeC\equiv CMe)Co_2(CO)_6$ yields 2-(*cis*-but-2-enyl)$B_5H_8$, a compound not detected in uncatalysed reactions. Its $^{11}$B NMR spectrum shows peaks at $\delta$ −50·9 (d, 1B, 174), −18·6 (d, 1B, 167), −14·4 (d, 2B, 160), and 3·2 (s, 1B), consistent with B(2) substitution. Pyrolysis of the alkenylpentaborane produces *inter alia* the monocarbon carborane 2-Me-4-Et-2-$B_5CH_7$, $\delta^{11}$B −48·4 (d, B(1), 156), −4·9 (d, B(5), 172), 11·7 (s, B(4)), and 13·7 (d, B(2,6), 141).[45]

2-Benzyl- and 2-allyl-pentaborane have been reported. Respectively, these compounds have $\delta^{11}$B −52·3 (d, B(1), 173), −18·8 (d, B(4)), −14·1 (d, B(3,5), 164), 1·8 (s, B(2)); and −52·5 (d, B(1), 175), −18·8 (d, B(4), 166), −14·4 (d, B(3,5), 166), 0·5 (s, B(2)).[46]

Pentaborane adducts of bidentate Lewis bases have recently been reported. For $B_5H_9(Ph_2PC_2H_4PPh_2)$, $\delta^{11}$B −57·1 (1B), −28·8 (1B), −18·3 (3B), and for $B_5H_9(Me_2NC_2H_4NMe_2)$, $\delta^{11}$B −55·2, −12·4, −3·7, and 18·1. The sequential cleavage of $B_5H_9$ by $Me_3P$ is followed by $^{11}$B{$^1$H} NMR spectroscopy, and an unstable intermediate, $B_3H_5(PMe_3)_2$, is characterized by two broad overlapping peaks centred at −39·0 (1B) and −36·5 (2B) ppm. Cleavage of this material with hydrogen chloride leads to $BH_2Cl\cdot PMe_3$, $\delta^{11}$B −18·1 ($J_{BH}$ 115, $J_{BP}$ 85).[47]

Removal of four cage boron atoms from $6\text{-Me}_3\text{N-6-B}_9\text{C}_2\text{H}_{11}$ with methanolic potassium hydroxide affords $B_5\text{CH}_{11}\cdot\text{NMe}_3$. Its 32 MHz $^{11}$B spectrum displays peaks at $-60\cdot2$ (dd, 2B, 140, 55), $-23\cdot2$ (dd, 2B, 120, 30), and $-12\cdot4$ (t, 2B, 115) ppm. It is suggested that this compound is a structural analogue of $B_5H_{11}$ in which the hydrogen bridge between B(3) and B(4) is replaced by a $\text{CHNMe}_3$ bridge. There would also be a unique bridge hydrogen atom which tautomerizes between B(1)–B(2) and B(1)–B(5) as is considered to occur in $B_5H_{11}$.[48]

Trimethylamine and $5\text{-Cl-2,4-B}_5\text{C}_2\text{H}_6$ form a 1:1 adduct with $\delta^{11}$B $-19\cdot4$ (d, 2B), $2\cdot3$ (d, 1B), $6\cdot3$ (d, 1B), $17\cdot4$ (s, 1B). The resonances are broadened, suggesting possible *nido–closo* or neutral–ion-pair equilibria. Removal of chloride ion with $BCl_3$ generates the $\text{Me}_3\text{N}$ substituted cationic cage compound $5\text{-Me}_3\text{N-2,4-B}_5\text{C}_2\text{H}_6{}^+$, isolated as the $BCl_4{}^-$ salt, $\delta^{11}$B $-19\cdot3$ (d, B(1,7), 190), $1\cdot7$ (d, B(6), 156), $6\cdot3$ (d, B(3), 183), $10\cdot3$ ($BCl_4{}^-$), $16\cdot8$ (s, B(5)).[49]

Onak and coworkers[50] have studied the reactions of 2-[(chlorodimethyl-silyl)methyl]pentaborane(9), obtained from $B_5H_8{}^-$ and $\text{SiMe}_2(\text{CH}_2\text{Cl})\text{Cl}$. The compound initially produced contains the $\text{Me}_2\text{SiCH}_2\text{Cl}$ group in a bridging position between two basal borons, as is required by the observation of two doublets in a 4:1 ratio in the 32 MHz $^{11}$B NMR spectrum (Table 12). Diethyl ether induced rearrangement produces 2-$(\text{ClCH}_2)\text{SiMe}_2\text{B}_5\text{H}_8$, in the $^{11}$B NMR spectrum of which a singlet appears

## TABLE 12

$^{11}$B NMR data for 2-[(chlorodimethylsilyl)methyl]pentaborane derivatives.

| Compound | $\delta^{11}$B ($J_{BH}$) |
|---|---|
| $\mu$-[(ClCH$_2$)Me$_2$Si]B$_5$H$_8$ | $-45\cdot4$ (d, B(1), 174), $-9\cdot4$ (d, B(2–5), 145) |
| 2-[(ClCH$_2$)Me$_2$Si]B$_5$H$_8$ | $-49\cdot8$ (d, B(1), 173), $-13\cdot1$ (s, B(2)), $-10\cdot7$ (d, B(3,5), ~160), $-7\cdot2$ (d, B(4), ~160) |
| 1-[(ClCH$_2$)Me$_2$Si]B$_5$H$_8$ | $-58\cdot2$ (s, B(1)), $-12\cdot7$ (d, B(2–5), 169) |
| 2-[(ClMe$_2$Si)CH$_2$]B$_5$H$_8$ | $50\cdot2$ (d, B(1), 164), $-18\cdot2$ (d, B(4), 156), $-13\cdot2$ (d, B(3,5), 156), $1\cdot5$ (s, B(2)) |
| 1-[(ClMe$_2$Si)CH$_2$]B$_5$H$_8$ | $-44\cdot6$ (s, B(1)), $-13\cdot8$ (d, B(2–5), 164) |
| 1-[(Cl$_3$Si)CH$_2$]B$_5$H$_8$ | $-43\cdot1$(s, B(1)), $-11\cdot7$ (d, B(2–5), 160) |

in the high-frequency region. Rearrangement of the 2-isomer with hexamethylenetetramine results in 1-$(\text{ClCH}_2)\text{SiMe}_2\text{B}_5\text{H}_8$ which exhibits a low-frequency singlet at $-58\cdot2$ ppm. Pyrolysis of the 2-isomer causes a 1,2-shift of the pentaboranyl unit and its isomerization to form 1-[(ClMe$_2$Si)CH$_2$]B$_5$H$_8$. 2-[(ClMe$_2$Si)CH$_2$]B$_5$H$_8$ is formed from this by

hexamethylenetetramine-induced rearrangement or by aluminium chloride catalysed isomerization of $2\text{-}ClCH_2SiMe_2B_5H_8$.

Chemical shift data for a large number of methylated $2,4\text{-}B_5C_2H_7$ derivatives have been reported and are summarized in Table 13. Good agreement with shifts calculated using empirically derived substituent parameters[51] is obtained.[52]

## TABLE 13

^{11}B NMR data for $Me_x\text{-}2,4\text{-}B_5C_2H_{7-x}$ isomers.

| Compound | B(1) | B(3) | B(5) | B(6) | B(7) |
|---|---|---|---|---|---|
| $1\text{-}CH_3\text{-}2,4\text{-}C_2B_5H_6$ | 11·6 | −8·3 (183) | −4·0 (166) | −4·0 (166) | 27·1 (182) |
| $3\text{-}CH_3\text{-}2,4\text{-}C_2B_5H_6$ | 20·7 (178) | −14·1 | −4·0 (166) | −4·0 (166) | 20·7 (178) |
| $5\text{-}CH_3\text{-}2,4\text{-}C_2B_5H_6$ | 20·6 (176) | −6·8 (182) | −11·2 | −2·7 (169) | 20·6 (176) |
| $1,3\text{-}(CH_3)_2\text{-}2,4\text{-}C_2B_5H_5$ | 12·0 | −14·0 | −3·2 (167) | −3·2 (167) | 27·1 (196) |
| $1,5\text{-}(CH_3)_2\text{-}2,4\text{-}C_2B_5H_5$ | 12·0 | −7·2 (176) | −10·6 | −3·2 (167) | 27·1 (196) |
| $1,7\text{-}(CH_3)_2\text{-}2,4\text{-}C_2B_5H_5$ | 15·6–17·2 | | | | 15·6–17·2 |
| $3,5\text{-}(CH_3)_2\text{-}2,4\text{-}C_2B_5H_5$ | 20·4 (186) | −12·8 | −10·6 | −1·4 to −3·2 | 20·4 (186) |
| $5,6\text{-}(CH_3)_2\text{-}2,4\text{-}C_2B_5H_5$ | 20·4 (177) | −5·3 (177) | −9·6 | −9·6 | 20·4 (177) |
| $1,3,5\text{-}(CH_3)_3\text{-}2,4\text{-}C_2B_5H_4$ | 10·7 | −13·9 | −10·4 | −3·2 | 25·2 (176) |
| $1,3,7\text{-}(CH_3)_3\text{-}2,4\text{-}C_2B_5H_4$ | 16·9 | ~−15·3 | −3·2 | −3·2 | 16·9 |
| $1,5,6\text{-}(CH_3)_3\text{-}2,4\text{-}C_2B_5H_4$ | 10·5 | −6·9 (173) | −9·6 | −9·6 | 25·2 (175) |
| $1,5,7\text{-}(CH_3)_3\text{-}2,4\text{-}C_2B_5H_4$ | 16·9 | −10·4 | −10·4 | −3·2 | 16·9 |
| $3,5,6\text{-}(CH_3)_3\text{-}2,4\text{-}C_2B_5H_4$ | 19·2 (177) | −13·9 | −10·4 | −10·4 | 19·2 (177) |
| $1,3,5,6\text{-}(CH_3)_4\text{-}2,4\text{-}C_2B_5H_3$ | 12·6 | −11·2 | −9·3 | −9·3 | 25·4 (160) |
| $1,3,5,7\text{-}(CH_3)_4\text{-}2,4\text{-}C_2B_5H_3$ | 17·7 | −11·2 | −11·2 | 0·9 | 17·7 |
| $1,5,6,7\text{-}(CH_3)_4\text{-}2,4\text{-}C_2B_5H_3$ | 16·0 | −7·7 (180) | −9·8 | −9·8 | 16·0 |

## IX. HEXABORANE DERIVATIVES

Shore and coworkers have prepared $3\text{-}CH_3B_6H_{11}$ from $B_2H_6$ and $K(1\text{-}CH_3B_5H_7)$. Cleavage with $NH_3$ removes the $BH_2$ unit furthest from the methyl substituent; subsequent protonation then yields the alkylated boranes $3\text{-}CH_3B_5H_{10}$ and $1\text{-}CH_3B_4H_{10}$. The ^{11}B NMR data for these compounds are given in Table 14.[53]

1:1 Adducts of $B_6H_{10}$ and $PMe_3$ or $PPh_3$ have been reported. The structure of these *arachno* compounds, isoelectronic with $B_6H_{11}^-$, presumably comprises a square pyramidal array of borons with the ligand-bearing B(6) bridging the B(2–5) basal edge. B(6) can be assigned on the basis of the ~82 Hz [31]P–[11]B coupling. The low-frequency resonance of unit area is attributed to the apical B(1) boron but assignment of B(2,5) and B(3,4) seems less certain (see Table 15).[54]

## TABLE 14

### $^{11}$B NMR data for methylated boranes.

| 3-CH$_3$B$_6$H$_{11}$ | | 3-CH$_3$B$_5$H$_{10}$ | | 1-CH$_3$B$_4$H$_9$ | |
|---|---|---|---|---|---|
| B(3) | 35·2 (s) | B(3) | 20·4 (s) | B(2,4) | −4·7 (129, ~26) |
| B(6) | 20·5 (150) | B(5) | 8·8 (122) | B(1) | −2·9 (~40) |
| B(4 or 1) | 9·8 (124) | B(2) | 2·4 (127) | B(3) | −41·1 (161) |
| B(1 or 4) | 6·2 (114) | B(4) | 7·8 (179) | | |
| B(2 or 5) | −19·1 (162) | B(1) | 52·0 (142) | | |
| B(5 or 2) | −24·0 (151) | | | | |

## TABLE 15

### $^{11}$B NMR data [$\delta^{11}$B($J_{BH}$)] for phosphine–B$_6$H$_{10}$ complexes.

| Position | B$_6$H$_{10}$·PMe$_3$ | B$_6$H$_{10}$·PPh$_3$ |
|---|---|---|
| B(2,5) | −10·5 (146) | −9·1 (140) |
| B(3,4) | −23·1 (151) | 20·0 (155) |
| B(6) | −44·2 (103, $J_{BP}$ 84) | −42·3 (~100, $J_{BP}$ 80) |
| B(1) | −56·3 | −54·1 (170) |

Several anions derived from hexaborane(10) were prepared in a study which shows that the Brönsted acidities are in the order 2-BrB$_6$H$_9$ > B$_6$H$_{10}$ > 2-CH$_3$B$_6$H$_9$. $^{11}$B NMR data for the conjugate bases of these anions are collected in Table 16. The 2-BrB$_6$H$_8^-$ and 2-CH$_3$B$_6$H$_8^-$ ions are fluxional, as are their conjugate acids, owing to movement of the bridge protons or bridge magnesium atom in the case of (THF)$_2$Mg(2-CH$_3$B$_6$H$_8$)$_2$. It is noted that the basal boron signals broaden on cooling; this may be a general characteristic of pyramidal boranes containing basal B–B bonds. In 2-BrB$_6$H$_8^-$, $T_1$ for B(1) and B(3–6) are $20 \pm 2$ and $1·9 \pm 0·1$ ms respectively at −80 °C.[55]

## TABLE 16

### $^{11}$B NMR data [$\delta^{11}$B($J_{BH}$)] for hexaborane anions.

| Position | K(2-BrB$_6$H$_8$) | K(2-CH$_3$B$_6$H$_8$) (0 °C) | (THF)$_2$Mg(2-CH$_3$B$_6$H$_8$)$_2$ (22 °C) |
|---|---|---|---|
| B(1) | −48·9 (142) | −48·0 (133) | −46·5 (142) |
| B(2) | 22·5 | 32·5 | 32·7 |
| B(4,5) | 6·6 (130) | −6·1 | −4·2 |
| B(3,6) | 6·6 (130) | 18·6 | 17·7 |

Synthesis of halogenated derivatives of $B_6H_{10}$ has been reported. $IB_6H_9$, $ClB_6H_9$, and $I_2B_6H_8$ are all substituted in the basal positions as judged by the persistence of a low-frequency doublet of unit area in the $^{11}B$ NMR spectra (Table 17). A more precise location of the halogen is not feasible because the compounds are fluxional. As noted earlier, this process involves migration of the bridge protons along the basal B–B edges while terminal substituents remain fixed. A 1:1 adduct of hexaborane(10) with triisobutyl-aluminium is characterized by its $^{11}B$ NMR spectrum; this compound appears to be an unusual example of complex formation with an electron acceptor rather than an electron donor.[56]

## TABLE 17

### $^{11}B$ NMR data for halogenated hexaborane(10) compounds.

| Compound | $\delta^{11}B$ ($J_{BH}$) |
|---|---|
| $IB_6H_9$ | −48·3 (d, 1B, 159), 7·1 (d, 2B, 161), 8·5 (s, 1B), 20·2 (d, 2B, 135) |
| $ClB_6H_9$ | −48·8 (d, 1B, 160), 5·6 (d, 2B, 160), 15·9 (d, 2B, 160), 32·2 (s, 1B) |
| $I_2B_6H_8$ | −32·2 (d, 1B, 165), −3·5 (d, 1B, 160), 11·4 (s, 2B), 19·0 (d, 2B, 165) |
| $B_6H_{10}\cdot Al(i\text{-}C_4H_9)_3$ | −44·6 (d, 1B, 180), −16·4 (d, 2B, 120), −12·7 (d, 2B, 180), 8·6 (d, 1B, 140) |

Compounds of the type $R_nB_n$ can, in principle, exist either in a cyclic or a polyhedral form. Cyclo-$(Me_2N)_6B_6$ exhibits a singlet at 65 ppm in toluene solution, indicating that boron has a coordination number of 3 and that the molecule is indeed cyclic. This has been confirmed by an X-ray crystal structure analysis.[57]

## X. OCTABORANE DERIVATIVES

Dehydrogenation of $4\text{-}B_8CH_{14}$ at 350 °C provides $B_8CH_{12}$, $\delta^{11}B$ −57·9 (d, 1B, 150), −31·2 (d, 2B, 170), −16·0 (d, 2B, 150), −8·2 (d, 2B, 160), and 3·0 (d, 1B, 165). The doublets at −16·0 and −31·2 ppm exhibit a secondary splitting of about 40 Hz due to coupling with bridge protons. The $^{11}B$ NMR spectrum indicates that this carborane has a plane of symmetry but the carbon atom could be located at either the 4 or the 7 position, using the same numbering system as in the isoelectronic $B_9H_{12}^-$.[58]

## XI. NONABORANE DERIVATIVES

The 70·6 MHz $^{11}B$ NMR spectra of a large number of carbon- and B(4,7)-substituted derivatives of $2,3\text{-}B_9C_2H_{11}$ have been reported and are

collected in Tables 18 and 19. Figure 8 shows the structure of the carborane cage and the numbering scheme employed.[59]

## TABLE 18

$^{11}$B NMR data for $C$-substituted 2,3-B$_9$C$_2$H$_{11}$ derivatives.
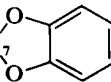
| Compound | $\delta^{11}B$ $(J_{BH})$ |
|---|---|
| 2,3-B$_9$C$_2$H$_{11}$ | $-17\cdot3$ (d, 1B, 169), $-10\cdot5$ (d, 2B, 169), $-7\cdot3$ (d, 2B, 169), $-1\cdot2$ (d, 4B, 164) |
| 2,3-Me$_2$-2,3-B$_9$C$_2$H$_9$ | $-11\cdot0$ (1B), $-10\cdot5$ (2B), $-6\cdot8$ (d, 2B, 169), $-2\cdot9$ (d, 4B, 169) |
| 2,3-Et$_2$-2,3-B$_9$C$_2$H$_9$ | $-14\cdot1$ (1B), $-12\cdot6$ (2B), $-7\cdot7$ (2B), $-4\cdot9$ (4B) |
| 2,3-Ph$_2$-2,3-B$_9$C$_2$H$_9$ | $-11\cdot8$ (1B), $-10\cdot3$ (2B), $-6\cdot6$ (2B), $-4\cdot5$ (4B) |
| 2-Et-3-Me-2,3-B$_9$C$_2$H$_9$ | $-13\cdot0$ (1B), $-11\cdot7$ (2B), $-8\cdot4$ (1B), $-7\cdot1$ (1B), $-4\cdot6$ (2B), $-4\cdot0$ (2B) |

## TABLE 19
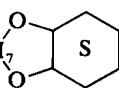
$^{11}$B NMR data for 4,7-(ORO)-2,3-B$_9$C$_2$H$_7$ compounds.

1  (CH$_3$C)$_2$B$_9$H$_7$(OH)$_2$     2  (CH$_3$C)$_2$B$_9$H$_7$⟨O O⟩     3  (CH$_3$C)$_2$B$_9$H$_7$⟨O O-benzene⟩

4  (CH$_3$C)$_2$B$_9$H$_7$⟨O O⟩     5  (CH$_3$C)$_2$B$_9$H$_7$⟨O O - S⟩

| | B(4,7) | B(1) | B(8,9) | B(11) | B(5,6) | B(10) |
|---|---|---|---|---|---|---|
| 1. | 18·6 | $-0\cdot9$ (190) | $-3\cdot4$ (169) | $-9\cdot4$ (146) | $-21\cdot3$ (162) | $-22\cdot6$ (137) |
| 2. | 16·3 | $-1\cdot8$ (161) | $-4\cdot2$ (168) | $-11\cdot6$ (144) | $\sim\!-23\cdot1$ | |
| 3. | 14·5 | $-0\cdot3$ (177) | $-4\cdot7$ (163) | $-11\cdot1$ (151) | $\sim\!-21\cdot5$ | |
| 4. | 19·5 | $\sim\!-1\cdot2$ | $\sim\!-3\cdot7$ | $-12\cdot1$ (142) | $-23\cdot3$ (161) | $-26\cdot6$ (142) |
| 5. | 14·9 | $-2\cdot9$ (171) | $-5\cdot3$ (166) | $-12\cdot4$ (149) | $\sim\!-24\cdot1$ | |

The $^{11}$B NMR spectrum of the parent 2,3-B$_9$C$_2$H$_{11}$ contains four doublets of relative areas $4:2:2:1$ (reading from high to low frequency). That of area 4 must be due to the chemically equivalent B(4,5,6,7), and the doublet of unit area is attributed to B(1). The doublet of area 2 at $-7\cdot3$ ppm is assigned to B(8,9) and the resonance at $-10\cdot5$ ppm to B(10,11) because in the $^{11}$B NMR spectrum of 2-Et-3-Me-2,3-B$_9$C$_2$H$_9$, in which the mirror plane of symmetry passing through B(10) and B(11) is lost, the higher-frequency doublet is split into two doublets each of unit area.

The $^{11}$B NMR spectra of 4,7-(OH)$_2$-2,3-Me$_2$-2,3-B$_9$C$_2$H$_7$ and its condensation products with glycols, 4,7-(ORO)-2,3-Me$_2$-2,3-B$_9$C$_2$H$_7$, are
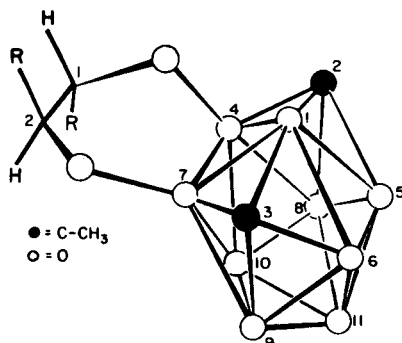
FIG. 8. Structure and numbering scheme for $4,7\text{-}(ORO)\text{-}2,3\text{-}Me_2\text{-}2,3\text{-}B_9C_2H_7$.

quite different from that of the parent carborane and extend over a larger range of chemical shifts. Assignment of the spectra of these compounds is achieved by clever use of isotopically and chemically labelled derivatives.

Deuterium exchange catalysed by $(Ph_3P)_2Rh(H)\text{-}3,1,2\text{-}B_9C_2H_{11}$ between $D_2$ and $4,7\text{-}(1,2\text{-}C_6H_4O_2)\text{-}2,3\text{-}Me_2\text{-}2,3\text{-}B_9C_2H_7$ affords $4,7\text{-}(1,2\text{-}C_6H_4O_2)\text{-}2,3\text{-}Me_2\text{-}2,3\text{-}B_9C_2H_3D_4$ in which the doublets centred at $-21\cdot5$, $-11\cdot1$, and $-4\cdot7$ ppm collapse to singlets. The $^{11}B$ NMR spectrum of $10\text{-}Br\text{-}4,7\text{-}(OH)_2\text{-}2,3\text{-}Me_2\text{-}2,3\text{-}B_9C_2H_6$, in which the halogen substituent is located at $B(10)$ by an X-ray structure analysis, has $\delta^{11}B$ $-21\cdot4$ (d, 2B, 161), $-14\cdot8$ (s, 1B), $-7\cdot5$ (d, 1B, 119), $-3\cdot4$ (d, 2B, 156), $1\cdot5$ (d, 1B, 126), and $16\cdot1$ (s, 2B) ppm. Inspection of this spectrum allows assignment of the $-22\cdot6$ ppm doublet in the parent hydroxylated carborane to $B(10)$. Further assignments are made in the following way.

Reduction and hydrolysis of $4,7\text{-}(1,6\text{-}C_6H_4O_2)\text{-}2,3\text{-}Me_2\text{-}2,3\text{-}B_9C_2H_7$ involves displacement by hydride of the unique $B(1)$ atom to the side of the cage containing the dioxyphenyl group.[60] When this reaction is applied to $4,7\text{-}(1,2\text{-}C_6H_4O_3)\text{-}2,3\text{-}Me_2\text{-}2,3\text{-}B_9C_2H_3D_4$, there is formed $3,4\text{-}(C_6H_4O_2)\text{-}1,2,5,6\text{-}D_4\text{-}7,9\text{-}Me_2\text{-}7,9\text{-}B_9C_2H_4^-$. It has $\delta^{11}B$ $-42\cdot0$ (s), $-32$ (s), $-25\cdot6$ (br q), $-6\cdot0$ (s), $3\cdot7$ (s), and $0\cdot2$ (d), and is a derivative of $7,9\text{-}B_9C_2H_{12}^-$ with the dioxyphenyl group attached to $B(3,4)$. Placement of the deuterium labels in the 1, 2, 5, and 6 positions follows then from the previous assignment of the $^{11}B$ NMR spectrum of $7,9\text{-}B_9C_2H_{12}^-$.[61]

On the basis of this suggested mechanism for the cage opening reaction, the doublet of area 2 at $-21\cdot5$ ppm in $4,7\text{-}(1,2\text{-}C_6H_4O_2)\text{-}2,3\text{-}Me_2\text{-}2,3\text{-}B_9C_2H_7$ is assigned to $B(5,6)$. Further assignments extracted from these data are $\delta$ $-11\cdot1$ $(B_{11})$, $-0\cdot3$ $(B_1)$, and $-4\cdot7$ $(B_{8,9})$. Relative to $2,3\text{-}Me_2\text{-}2,3\text{-}B_9C_2H_9$, oxygen substitution deshields $B(4,7)$ along with the adjacent $B(1)$ and $B(6,9)$ positions. The $B(5,6)$ resonances move to higher frequency, possibly owing to an antipodal deshielding effect.

Pyrolysis of $Tl_2MeB_9C_2H_{10}$ generates thallium metal and $(TlMeB_9C_2H_{10})_2$ whose 80·6 MHz $^{11}$B NMR spectrum in THF contains eight doublets, at −37 (144), −33·4 (112), −22·0 (152), −18·7 (112), −17·8 (128), −13·5 (138), −11·1 (128), and −10·3 (128) ppm. The suggested static structure is shown in Fig. 9. Coupling with possibly tautomerizing bridge hydrogen atoms may account for the fine structure on the −33·4 ppm doublet.[62]
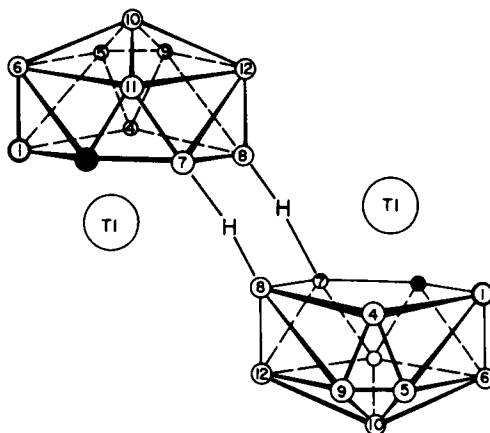


FIG. 9. Proposed static structure of $(TlMeB_9C_2H_{10})_2$.

The 28·9 MHz $^{11}$B NMR spectra of $B_9X_9{}^{2-}$ ions show two resonances in the 1:2 ratio expected for a tricapped trigonal prismatic geometry. Chemical shift data are: $B_9Cl_9{}^{2-}$, 1·5 (1B), −5·5 (2B); $B_9Br_9{}^{2-}$, −0·8 (1B), −8·2 (2B); $B_9I_9{}^{2-}$, −3·1 (1B), −16·0 (2B). Interestingly, the chemical shift difference between the five- and six-coordinate boron increases in the order $I > Br > Cl$, a trend noted earlier in $B_{10}X_{10}{}^{2-}$.[63]

The 28·9 MHz $^{11}$B NMR spectra of $B_9Br_9$ and two alkylated derivatives have been reported. Chemical shift data are: $MeEtB_9Br_7$, −62·4; $B_9Br_9$, −60·4; $MeB_9Br_8$, −62·2 ppm. Again, the electron deficient, neutral clusters are very deshielded with respect to the dianion. Higher field and lower temperature spectra of $B_9Br_9$ would be of interest and might detect fluxional processes.[64]

## XII. DECABORANE DERIVATIVES

The temperature dependence of $^1$H and $^{11}$B longitudinal relaxation times $(T_1)$ of $B_{10}H_{14}$ in toluene-$d_8$ indicate that there is a transition between

anisotropic and essentially isotropic motion between ~−35 and 25 °C. Above ~25 °C, plots of $\ln[T_1(^1H)]$ and $\ln[T_1(^{11}B)]$ versus $1/T$ indicate isotropic motion. Between ~25 and −35 °C there is transitional behaviour. At <~−35 °C there appears to be increased solvent–solute interaction and an anisotropic tumbling which is probably associated with relatively free rotation about the $C_2$ axis.[65]

Cleavage of $Me_2SnB_{10}H_{12}$ with bromine provides $5,10-Br_2B_{10}H_{12}$ whose 70·6 MHz $^{11}B$ NMR spectrum contains resonances at −35·6 (d, B(2,4), 160), −4·3 (d, B(7,8), 165), 5·9 (s, B(5,10)), ~9·2 (d), and ~13 (d) ppm. The bromines are located by a single-crystal X-ray structure determination. The chemical shifts agree, where assignment is possible, with those calculated from earlier empirical relationships.[66]

Normal and partially relaxed (180°–$\tau$–90° pulse sequence) 32 MHz $^{11}B$ NMR spectra and $^{11}B$ spin–lattice relaxation times for $(6-B_{10}H_{13})_2O$ in chloroform and in benzene have been reported (Table 20). The overall spectral pattern is interpreted as being indicative of B(6) rather than B(2) substitution. A plot of $\delta(^{11}B)$ versus $\delta(^1H)$ is linear and has a slope of ~1·6. The effect on $^{11}B$ chemical shifts upon changing solvent from chloroform to benzene appears to be rather small but the effect on the proton shifts is much larger, up to 0·4 ppm for terminal protons.[67]

TABLE 20

$^{11}B$ chemical shift and relaxation time data for $(6-B_{10}H_{13})_2O$.

| Position | $\delta^{11}B$ in $CDCl_3$ | $\delta^{11}B$ in $C_6D_6$ | $J_{BH}$ (Hz)(±10 Hz) | $T_1$ (ms)(±15%) |
|---|---|---|---|---|
| B(6) | 21·8 | 22·1 | 0 | 6·8 |
| B(9) | 7·2 | 8·0 | 145 | 7·8 |
| B(1,3) | 5·6 | 5·6 | 145 | 17·1 |
| B(8,10) | 3·0 | 2·4 | 145 | 7·3 |
| B(5,7) | −10·7 | −10·9 | 150 | 10·2 |
| B(2) | −33·2 | −33·1 | 155 | 32·8 |
| B(4) | −42·5 | −42·4 | 155 | 11·3 |

The antipodal shielding effect, in which a substituent on a polyhedral boron framework causes a shift of the antipodal or opposite boron resonance[68] has been suggested to be analogous to the resonance effect observed in carbocyclic systems having delocalized $\pi$ electrons. Linear correlations are found for antipodal $^{11}B$ shieldings in $1-X-1,2-B_{10}C_2H_{11}$, $2-XB_{10}H_{13}$, $8-X-CpCo-1,2-B_9C_2H_{10}$, and the shieldings for the para $^{13}C$ in $1-XC_6H_5$, but not in 1-substituted bicyclo[2.2.2]octanes. Perturbations in ring currents may not be important since antipodal deshielding is observed in both 2- and 6-substituted decaboranes. The antipodal shift generally increases in

the order $RO > F > HS > Cl > Br > I$, i.e. with increasing electron donating capability of the substituent.[69]

## XIII. COUPLED BORANES AND CARBORANES

Mercury-sensitized gas-phase photolysis of pentaborane(9) and of 2,5-$B_5C_2H_7$ has yielded a wide variety of carboranes and boranes coupled by boron–boron bonds.[70] The 32 MHz $^{11}$B NMR data are given in Table 21.

TABLE 21

**NMR data for coupled boranes, carboranes, and metallocarboranes\*.**

| Compound | $\delta^{11}B\ (J_{BH})$ |
|---|---|
| $2,2'$-$(1$-$MeB_5H_7)_2$ | $-42\cdot2$ (2B), $-12\cdot0$ (d, 6, 113), $-10\cdot0$ (2B) |
| $3,3'$-$(2,4$-$B_5C_2H_6)_2$ | $-20\cdot9$ (d, 4, 183), $4\cdot9$ (d, 4, 176), $8\cdot9$ (2B) |
| $5,5'$-$(2,4$-$B_5C_2H_6)_2$ | $-20\cdot3$ (d, 4, 178), $6\cdot0$ (d, 2, 157), |
| | $7\cdot9$ (2B), $8\cdot4$ (d, 2, 183) |
| $1,1'$-$(2,4$-$B_5C_2H_6)_2$ | $-19\cdot1$ (2B), $-19\cdot1$ (d, 2B, 183), |
| | $5\cdot0$ (d, 4, 171), $7\cdot9$ (d, 2, 183) |
| $1,3'$-$(2,4$-$B_5C_2H_6)_2$ | $-20\cdot6$ (d, 2, 178), $-17\cdot6$ (d, 1, 181), |
| | $5\cdot2$ (d, 4, 167), $8\cdot1$ (d, 1, 157) |
| $1,5'$-$(2,4$-$B_5C_2H_6)_2$ | $-20\cdot2$ (d, 2, 181), $-17\cdot8$ (d, 1, 176), |
| | $-14\cdot4$ (br s, 1), $6\cdot2$ (d, 3, 174), |
| | $8\cdot7$ (d, 2, 196) |
| $3,5'$-$(2,4$-$B_5C_2H_6)_2$ | $-20\cdot2$ (d, 4, 181), $5\cdot4$ (d, 3, 183), |
| | $8\cdot6$ (d, 4, 176) |
| $2',2$-$(1',5'$-$B_3C_2H_4$-$1,6$-$B_4C_2H_5)$ | $-16\cdot6$ (d, 2, 189), $-11\cdot2$ (d, 1, 167), |
| | $2\cdot6$ (d, 2, 183) |
| $1',2$-$(1',5'$-$B_3C_2H_4$-$1,6$-$B_4C_2H_5)$ | $-22\cdot9$(d, 1, 178), $-16\cdot3$ (d, 2, 200), |
| | $-11\cdot1$ (1B), $5\cdot6$ (d, 3, 189) |
| $2$-$[1'$-$(2',4'$-$B_5C_2H_6)]$-$1,8,5,6$-$(CpCo)_2B_5C_2H_6$ | $114\cdot2$ (d, 1B, 152), $4\cdot9$ (5B), $-11\cdot5$ (3B), $-21\cdot5$ (d, 3B, 178) |
| $2$-$[3'$-$(2',4'$-$B_5C_2H_6)]$-$1,8,5,6$-$(CpCo)_2B_5C_2H_6$ | $114\cdot5$ (d, 1B, 134), $4\cdot3$ (5B), $-11\cdot8$ (2B), $-21\cdot5$ (d, 2B, 178) |
| $2$-$[5'$-$(2',4'$-$B_5C_2H_6)]$-$1,8,5,6$-$(CpCo)_2B_5C_2H_6$ | $116\cdot0$ (d, 1B, 160), $\sim4\cdot5$ (5B), $-11\cdot1$ (2B), $-21\cdot5$ (d, 2B, 174) |
| $3$-$[1'$-$(2',4'$-$B_5C_2H_6)]$-$1,8,5,6$-$(CpCo)_2B_5C_2H_6$ | $115\cdot6$ (d, 1B, 156), $4\cdot9$ (5B), $-10\cdot5$ (3B), $-20\cdot5$ (d, 1B, 183) |
| $3$-$[3'$-$(2',4'$-$B_5C_2H_6)]$-$1,8,5,6$-$(CpCo)_2B_5C_2H_6$ | $115\cdot2$ (d, 1B, 145), $\sim4\cdot7$ (5B), $-10\cdot5$ (2B), $-20\cdot8$ (d, 2B, 178) |
| $3$-$[5'$-$(2',4'$-$B_5C_2H_6)]$-$1,8,5,6$-$(CpCo)_2B_5C_2H_6$ | $115\cdot2$ (d, 1B, 145), $7\cdot6$ ($\sim$3B), $4\cdot6$ ($\sim$2B), $-10\cdot4$ (2B), $-20\cdot9$ (d, 2B, 178) |
| $4,5'$-$(2,3$-$Me_2$-$1,2,3$-$CpCoB_4C_2H_3)_2$ | $7\cdot3$ (br) |
| $5,5'$-$(2,3$-$Me_2B_4C_2H_5)_2$ | $-3\cdot3$ (dd, 3B, 151, 44), $-46\cdot3$ (d, 1B, 166) |

\* In some areas the integrals do not sum to give the expected number of boron atoms because of the presence of broad or overlapping resonances.

Spectra obtained at 115·5 MHz have been found to display $^{11}$B–$^{11}$B spin coupling involving the boron atoms linked by two-centre, two-electron single bonds. For example, the B(2') resonance in 1,5'-(2-$B_5H_8$)$_2$ shows quartet structure with a 106 Hz spacing which is attributed to coupling between B(1) and B(2'). The B(2') signal shows the required fine structure but is less well resolved. Similarly, in 1,5'-(2,4-$B_5C_2H_6$)$_2$, the B(1) resonance shows a 109 Hz splitting due to coupling with B(5').[71] These direct B–B couplings are quite large and consistent with the calculated results of Kroner and Wrackmeyer.[72]

Plotkin and Sneddon[73] have prepared metallocarboranes from the B–B coupled carboranes (2,4-$B_5C_2H_6$)$_2$ and (2,3-$Me_2$-2,3-$B_4C_2H_5$)$_2$. These compounds are characterized by 32 MHz FT $^{11}$B NMR spectroscopy. Data for compounds whose structures can be inferred from spectroscopic experiments are given in Table 21. In the case of the isomeric ($B_5C_2H_6$)· [($CpCo$)$_2B_5C_2H_6$] compounds, the doublet at ~115 ppm is indicative of a boron bonded to two cobalt atoms.[73]

Two isomers of bi(decaboranyl), formed by the photolysis or thermolysis of $B_{10}H_{14}$, have been carefully studied by $^{11}$B{$^1$H} and partially relaxed $^{11}$B NMR spectroscopy. In these materials, the two decaborane cages are connected by B–B $\sigma$ bonds, which has been confirmed by X-ray crystallography in the case of 2,2'-($B_{10}H_{13}$)$_2$.[74] $^{11}$B NMR data for 6,6'-($B_{10}H_{13}$)$_2$, recorded at 32 MHz in $C_6D_6$ at 25 °C, are given in Table 22. Comparison

TABLE 22

$^{11}$B NMR data for 6,6'-($B_{10}H_{13}$)$_2$.

| $\delta^{11}$B ($J_{BH}$) | $T_1$ (ms) |
| --- | --- |
| 15·0 (s, 1B) | 2·8 |
| 13·5 (d, 2B, 150) | 15·0 |
| 11·7 (d, 1B, 150) | 4·0 |
| 2·7 (d, 2B, 160) | 8·2 |
| 0·9 (d, 2B, 155) | 6·2 |
| −33·9 (d, 1B, 150) | 20·0 |
| −34·6 (d, 1B, 150) | 9·4 |

with the chemical shifts of pure $B_{10}H_{14}$ indicates that the two doublets with largest shieldings are due to B(2,2',4,4'). The fact that B(2) and B(4) are non-equivalent, when taken with the high symmetry indicated by the $^{11}$B spectrum, indicates that coupling involves the B(6,6') positions.[75]

The $^{11}$B NMR spectrum of 2,2'-($B_{10}H_{13}$)$_2$ is similar to that of $B_{10}H_{14}$. Positional assignments are made with the aid of partially relaxed 32 MHz

spectra obtained for benzene solutions at 23 °C. Apparently, increased resolution is achieved with toluene solutions at 88 °C which permit differentiation of the 6,9 positions. The results are given in Table 23. In this and the preceding table, the uncertainty in $T_1$ values is ±20%. It is interesting that the 2, 2', 9, and 9' boron nuclei have shorter longitudinal relaxation times than those in other positions. This effect is attributed to rotational anisotropy in rod-shaped $2,2'-(B_{10}H_{13})_2$ since the principal intramolecular rotation axes and molecular rotation axis should lie close to the 2,2' boron atoms. Nuclei on these axes will experience greater effective rotational correlation times and more effective relaxation than those residing in off-axis positions.

## TABLE 23

### $^{11}$B NMR data for $2,2'-(B_{10}H_{13})_2$.

| Position | $\delta^{11}$B $(J_{BH})$ | $T_1$ (ms) |
|---|---|---|
| 1, 3 | 14·0 (145) | 13·5 |
| 6 | 11·5 (~170) | 7·9 |
| 9 | 10·7 (~170) | 4·5 |
| 5, 7, 8, 10 | 0·9 (155) | ~5·5 |
| 2 | −31·6 (0) | 4·8 |
| 4 | −34·5 (155) | 21·0 |

The coupled carboranes $2,2'-(1,5-B_3C_2H_4)_2$ and $2,2'-3,2'-(1,5-B_3C_2H_4)_2$-$1,5-B_3C_2H_3$ have been comprehensively studied by quantum chemical calculations and ultraviolet photoelectron spectroscopy. There appears to be a substantial barrier to rotation about the B–B bonds connecting the cages, due to $\pi$ interaction between the carborane units. The $^{11}$B NMR spectra are indicative of averaging of the solution state conformers, however.[76]

Mercuri-boranes and -carboranes are less common than those, say, of iron, cobalt, and nickel because of the oxidizing properties of Hg(II), However, Hosmane and Grimes[77] have prepared $(B_5H_8)_2Hg$, $\delta^{11}$B −7·9 and −9·6 (overlapping d, 4B) and −43·9 (d, 1B, 176), and $(2,3-Me_2B_4C_2H_5)_2Hg$, $\delta^{11}$B −4·0 (d, 3B, 117) and −47·7 (d, 1B, 181). These compounds presumably feature boron cages connected by three-centre, two-electron B–Hg–B bridges, but no $^{199}$Hg–$^{11}$B spin coupling is reported. $(2,3-Me_2B_4C_2H_5)_2Hg$ undergoes a formal internal redox reaction on heating to generate the B–B coupled carborane $5,5'-(Me_2B_4C_2H_5)_2$, whilst oxidation in benzene proceeds by solvent attack to form $4-Ph-2,3-Me_2B_4C_2H_5$, $\delta^{11}$B 5·9 (s, 1B), −2·2 (d, 1B, 180), −4·9 (d, 1B, 180), −44·8 (d, 1B, 176).[77]

## XIV. MERCAPTO-SUBSTITUTED BORANES AND CARBORANES

Boranes and carboranes containing exopolyhedral sulphur substituents have received renewed attention on account of their potential for incorporation into pharmaceuticals and because of the potential scope of the

### TABLE 24

**$^{11}$B NMR data for mercapto-substituted boranes and carboranes.**

| Compound | $\delta^{11}$B ($J_{BH}$) |
|---|---|
| $B_{12}H_{11}SOSB_{12}H_{11}^{2-}$ | −5·0 (s, 1B), −8·1 (s, 1B), −16·9 (d, 22B, 131) |
| $B_{12}H_{11}S_2B_{12}H_{11}^{4-}$ | −6·7 (s, 2B), −15·6 (d, 10B, 138), <br> −17·2 (d, 10B, 131), −20·3 (d, 2B, 139) |
| $B_{12}H_{10}[S_2C_6H_3(NO_2)CO_2H]_2^{2-}$ | −6·9 (s, 2B), −15·8 (d, 10B, 120) |
| $B_{12}H_{11}S_2C_2H_4OH^{2-}$ | −7·1 (s, 1B), −16·6 (d, 11B, 125) |
| $B_{12}H_{12}S_2CH_2CO_2H^{2-}$ | −7·2 (s, 1B), −6·6 (d, 11B, 119) |
| $B_{12}H_{11}C_6H_3(NO_2)(CO_2H)^{2-}$ | −7·2 (s, 1B), −6·6 (d, 11B, 120) |
| $B_{12}H_{11}SC_6H_3(NO_2)_2^{2-}$ | −9·5 (s, 1B), −16·6 (d, 11B, 122) |
| $B_{12}H_{11}SH^{2-}$ | −10·4 (s, 1B), −14·8 (d, 5B, 125), <br> −17·0 (d, 5B, 112), −20·5 (d, 1B, 135) |
| $B_{12}H_{11}S_2OC_6H_4CH_3^{2-}$ | −11·0 (s, 1B), −16·8 (d, 11B, 131) |
| $B_{12}H_{10}(SH)_2^{2-}$ | −10·9 (s, 2B), −14·5, −17·5, −20·9 |
| $B_{12}H_{11}SCTh^{2-}$* | −14·3 |
| 2-HS-1,5-$B_3C_2H_4$ | 7·6 (d, 2B, 175), 6·0 (s, 1B) |
| 2-HS-1,6-$B_4C_2H_5$ | −12·2 (s, 1B), −16·8 (d, 2B, 191), <br> −22·6 (d, 1B, 186) |
| 1-HS-2,4-$B_5C_2H_6$ | 4·4 (d, 1B, 161), 1·2 (d, 2B, 170), −18·7 (s, 1B), <br> −31·0 (d, 1B, 180) |
| 3-HS-2,4-$B_5C_2H_6$ | 13·1 (s, 1B), 2·3 (d, 2B, 169), −18·4 (d, 2B, 180) |
| 5-HS-2,4-$B_5C_2H_6$ | 7·3 (s, 1B), 1·9 (d, 1B, 186), −3·5 (d, 1B, 161), <br> −23·3 (d, 2B, 185) |
| 5,5'-$S_2$-(2,4-$B_5C_2H_6)_2$ | 13·3 (s, 1B), 4·6 (d, 1B, 189), −0·7 (d, 1B, 145), <br> −19·6 (d, 2B, 183) |
| 1,1'-$S_2$-(2,4-$B_5C_2H_6)_2$ | 6·5 (d, 1B, 181), 2·9 (d, 2B, 153), −13·2 (s, 1B), <br> −27·9 (d, 1B, 188) |
| 3,3'-$S_2$-(2,4-$B_5C_2H_6)_2$ | 15·1 (s, 1B), −2·8 (d, 2B, 178), −18·1 (d, 2B, 185) |
| 9-HS-1,2-$B_{10}C_2H_{11}$ | 4·4 (B(9)), −1·5 (B(12)), −8·1 (B(8,10)), <br> −13·4 (B(4,5)), 14·1 (B(7,11), −16·5 (B(3,6)) |
| 9,9'-$S_2(1,2-B_{10}C_2H_{11})_2$ | 7·0 (B(9)), −2·1 (B(12)), −9·6 (B(8, 10)), <br> −13·4 (B(4,5)), −14·9 (B(7, 11), −17·1 (B(3,6)) |
| 8-HS-CpCo-3,1,2-$B_9C_2H_{10}$ | 13·1 (B(8)), −1·2 (B(10)), −4·9 (B(9,12)), <br> −6·8 (B(4,7)), −18·2 (B(5,11)), −27·5 (B(6)) |
| 9-HS-CpCo-3,1,2-$B_9C_2H_{10}$ | 5·6 (B(8)), 1·4 (B(10)), 0·2 (B(9)), <br> −5·4 (B(12)), −7·1 (B(4,7)), −17·6 (B(5,11)), <br> −23·5 (B(6)) |
| 8,8'-HS[($B_9C_2H_{10})_2$Co] | 2·4 (B(10)), −6·1, −7·2 (B(4,7,9,12)), <br> −14·1 (B(5,11)), 22·3 (B(6)) |

* SCTh = *N*-methylbenzothiazole-2-thione.

chemistry imparted by reactive mercapto groups. Tolpin and coworkers[78] have reported a large series of new polyhedral boranes based on $HSB_{12}H_{11}{}^{2-}$. The 28·9 MHz $^{11}B$ NMR data are collected in Table 24. The $^1H$ decoupled spectra of many of these compounds reveal unsymmetrical peaks with low-frequency shoulders. The shoulders may be due to the boron nucleus *para* to the substituents which experiences an antipodal shielding effect.

Mercapto derivatives of $1,5-B_3C_2H_5$, $1,6-B_4C_2H_6$, and $2,4-B_5C_2H_7$ are formed in reactions of the carboranes with atomic ($^1D$) sulphur. Their 32 MHz $^{11}B$ NMR spectra are also summarized in Table 24. Both boron atoms in $2-HS-1,5-B_3C_2H_4$ are deshielded relative to the parent carborane ($\delta$ −1·1). In $2-HS-1,6-B_4C_2H_5$, B(2) is deshielded by 6·8 ppm and the *trans*, or antipodal, boron atom is shielded by 3·6 ppm. Similarly, in $1-HS-2,4-B_5C_2H_6$, the antipodal B(7) is shielded by 10 ppm relative to the starting carborane but B(3) and B(5,6) shift by only 2·8 ppm. Photolytic decomposition of the *B*-mercapto derivatives of $2,4-B_5C_2H_7$ provides $5,5'-S_2-(2,4-B_5C_2H_6)_2$, $1,1'-S_2-(2,4-B_5C_2H_6)_2$, and $3,3'-S_2-(2,4-B_5C_2H_6)_2$ in which the carborane cages are linked by disulphide bonds. The $^{11}B$ resonances shift to slightly higher frequencies in disulphide compounds, but otherwise the spectra are quite similar to those of the *B*-mercapto analogues.[79]

Sulphydrylation of $1,7-B_{10}C_2H_{12}$, achieved with aluminium chloride and elemental sulphur, provides $9-HS-1,7-B_{10}C_2H_{11}$ along with a series of polysulphides $9,9'-(S)_x-(1,7-B_{10}C_2H_{11})_2$ ($x = 1, 2, 3$). The 9-mercaptocarborane is a useful starting point for the synthesis of carboranes containing such functional groups as $SO_2Cl$, $SO_2NMe_2$, $SMe_2{}^+$, SOMe, and $SO_2Me$. The 32 MHz $^{11}B$ NMR spectra of these compounds are fairly well resolved and have been assigned (see Table 25).[80] Electrophilic sulphydrylation of $1,2-B_{10}C_2H_{11}$ and $CpCo-3,1,2-B_9C_2H_{11}$ has also been reported. $^{11}B$ NMR data for the mercaptoboranes are in Table 24.[81]

## TABLE 25

### $^{11}B$ NMR data for $9-X-1,7-B_{10}C_2H_{11}$ compounds.

| X | B(9) | B(5,12) | B(10) | B(4,8; 6,11) | | B(3) | B(2) |
|---|---|---|---|---|---|---|---|
| −S− | −0·4 | −0·7 | −10·3 | −13·6 | −14·5 | −18·1 | −21·3 |
| −S$_2$− | | −5·8 | −9·5 | −12·6 | −13·2 | −17·0 | −19·6 |
| −S$_3$− | | −6·0 | −9·4 | −13·2 | | −17·0 | −19·4 |
| −SO$_2$Cl | 0·0 | −6·1 | −10·2 | −12·8 | | −16·6 | |
| −SO$_2$N(CH$_3$)$_2$ | −2·9 | −6·7 | −10·6 | −13·3 | | −17·0 | |
| −SCH$_3$ | | −6·4 | −9·6 | −13·3 | | −17·2 | −20·3 |
| −S$^+$(CH$_3$)$_2$ | | −7·3 | −11·0 | −13·9 | | −17·5 | −20·9 |
| −SOCH$_3$ | | −6·8 | −10·5 | −12·8 | | −16·5 | |
| −SO$_2$CH$_3$ | −2·2 | −6·4 | −10·4 | −12·6 | | −16·2 | |

## XV.  BERYLLABORANES

An unusual beryllium insertion into a pentaborane cage is achieved in
the reaction between 1-ClB$_5$H$_8$ and Be(BH$_4$)$_2$ to produce B$_5$H$_{10}$BeBH$_4$,
whose structure is shown in Fig. 10(A). The exopolyhedral boron, B(7),
appears as a quintet at $-33 \cdot 4$ ppm, $J$(B–H) 86 Hz, indicating that the bridge
and terminal hydrogens bonded to this boron undergo rapid intermolecular
exchange. The broad resonance at $-9 \cdot 8$ ppm is resolved by line narrowing



(A)                                                              (B)



(C)
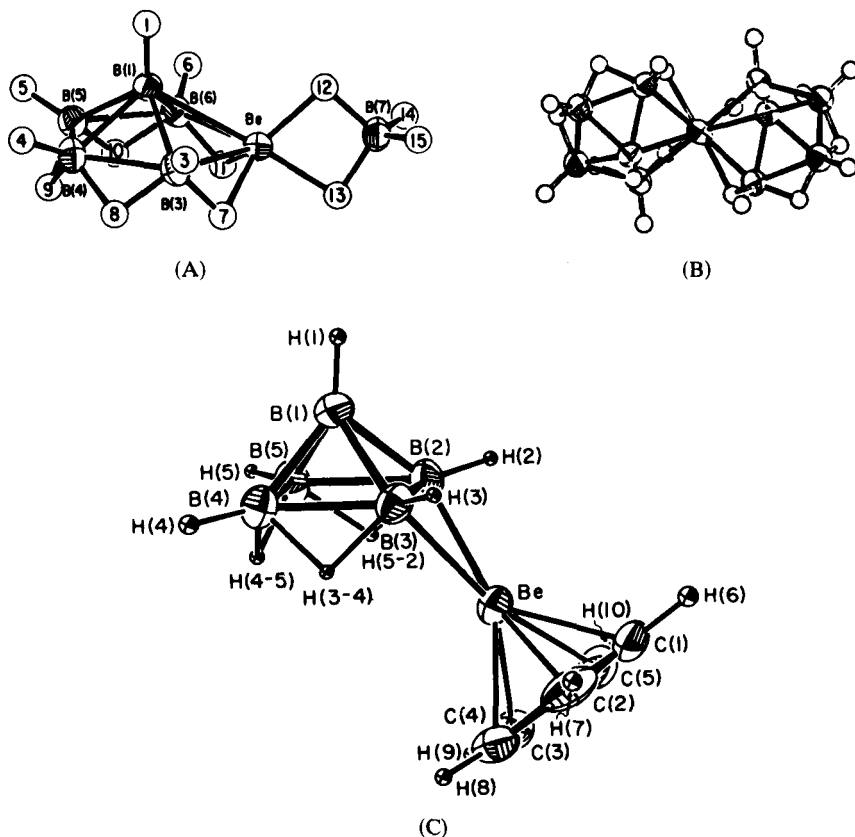
FIG. 10. Structures of (A) B$_5$H$_{10}$BeBH$_4$, (B) (B$_5$H$_{10}$)$_2$Be, (C) CpBeB$_5$H$_8$.

into a doublet of doublets whereupon it is seen that $J$(B–H) is 135 Hz and
$J$(B–Be) is 83 Hz. While the details of the structure and bonding in this
compound are not understood, it may be formally considered as a derivative
of B$_5$H$_{10}^-$. Consonant with this is the cleavage of B$_5$H$_{10}$BeBH$_4$ with HBr
to form the useful intermediate B$_5$H$_{10}$BeBr and, ultimately, B$_5$H$_{11}$. The

halogen atom in $B_5H_{10}BeBr$ may be displaced to afford $B_5H_{10}BeMe$ or $B_5H_{10}BeCp$, and a novel reaction with $CsB_3H_8$ yields $(B_5H_{10})_2Be$. The ^{11}B NMR spectra of this family of beryllaboranes are rather similar to each other (see Table 26), with the exception of $B_5H_{10}BeCp$ in which the B(3,6)

TABLE 26

^{11}B NMR data [$\delta^{11}$B ($J_{BH}$)] for beryllapentaboranes.

| Compound | B(1) | B(3,6) | B(4,5) | B(7) |
|---|---|---|---|---|
| $B_5H_{10}BeBH_4$ | −53·5 (146) | −9·8 (135, 83) | 8·2 (164) | −33·4 (86) |
| $(B_5H_{10})_2Be$ | −54·6 (139) | −8·1 (127, 98) | 5·3 (159) | |
| $B_5H_{10}BeBr$ | −54·0 (146) | −1·6 (138, 84) | 10·0 (161) | |
| $B_5H_{10}BeCl$ | −54·5 (146) | −2·9 (138, 84) | 9·2 (164) | |
| $B_5H_{10}BeCp$ | −64·0 (117) | −3·6 (117, 117) | −0·3 (156) | |
| $B_5H_{10}BeMe$ | −54·6 (146) | −2·0 (138, 83) | 9·6 (161) | |

resonance is a triplet, indicative of nearly equal coupling of boron with terminal and Be–H–B bridge hydrogens. The apical B(1) resonance in this compound occurs at lower frequency than in related compounds and $J$(B–H) is smaller.[82] The structures of $B_5H_{10}BeBH_4$ and $(B_5H_{10})_2Be$ inferred from NMR data have been confirmed by X-ray crystallography.[83] The former compound has a pentagonal pyramidal geometry with the beryllium atom in a basal position; B–B edges are bridged by hydrogen atoms and the $BH_4$ unit is attached to beryllium by two bridge hydrogens [see Fig. 10(B)]. The solid-state structure of $(B_5H_{10})_2Be$ reveals two pentagonal bipyramidal cages sharing a common beryllium atom; the compound crystallizes with one molecule of $m$-xylene.

Structurally different $CpBeB_5H_8$ is obtained from $KB_5H_8$ and $CpBeCl$. X-ray crystallography demonstrates a CpBe unit bridging one basal edge of a square pyramidal $B_5H_8$ ligand [Fig. 10(C)]. This architecture is similar to that found in other metal complexes of $\eta_2$-$B_5H_8$, but in the 86·7 MHz ^{11}B NMR spectrum the chemical shift difference between the two sets of basal boron nuclei is much larger: $\delta^{11}$B −13·4 (d, 2B, 161), −21·8 (d, 2B, 141), and −54·6 (d, 1B, 170).[84] NMR data for these beryllapentaboranes are summarized in Table 26.

At $\leqslant$−30 °C, $Be(B_3H_8)_2$ appears to be static on the NMR time scale. The 86·7 MHz ^{11}B NMR spectrum comprises a triplet at −11·8 ppm due to B(2) and a complex signal at −43·9 ppm due to B(1,3), the interpretation of which is not unambiguous even in the ^{1}H decoupled line narrowed spectrum. At 23 °C, the low-frequency resonance appears as a quartet with $J$(B–H) 74 Hz. At >60 °C, the [11]B signals broaden and begin to coalesce, indicating that all three boron atoms become equivalent and are
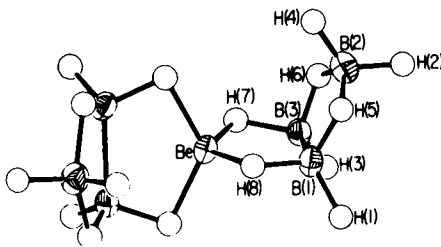
FIG. 11. Molecular structure and numbering scheme for Be(B₃H₈)₂.

equivalently coupled to all eight hydrogen atoms. The molecular structure of this beryllaborane and the numbering scheme used are shown in Fig. 11.

$^{11}$B NMR spectra for CpBeB₃H₈ and (MeBeB₃H₈)₂ are also reported. That of the former in CD₂Cl₂ at 23 °C consists of a nonet, $\delta$ −25·5, $J_{BH}$ 24 Hz; tautomerism is rapid even at −87 °C. The room temperature line narrowed $^{11}$B NMR spectrum of the methyl bridged dimer (which may be a mixture of geometric isomers) in benzene contains a triplet due to B(2) at −11·5 ppm, $J$(B–H) 116 Hz, and what appears to be a doublet of triplets centred at −42·2 ppm, $J$(B–H$_t$) 127 Hz and $J$(B–H$_b$) 56 Hz. At 37 °C, however, the B(1,3) resonance appears, under line narrowing conditions, as a quartet, $\delta$ −42·3, $J_{BH}$ 78 Hz.[85] It is a puzzle why the B₃H₈ ligand is fluxional in CpBeB₃H₈ and not in (MeBeB₃H₈)₂.

The gas-phase (saturated vapour) $^{11}$B NMR spectrum of Be(BH₄)₂ comprises a quintet with $J$(B–H) 87 Hz; similarly, a quintet, $\delta$ −35·8, $J$(B–H) 85 Hz, is observed for this compound in benzene solution. No evidence is seen of $^{11}$B or $^1$H spin coupling to $^9$Be ($I = 3/2$, 100% natural abundance). Beryllium borohydride in solution evidently contains a linear B⋯Be⋯B framework but the number of bridging hydrogen atoms cannot be specified on account of their rapid exchange with terminal hydrogen atoms. The $^{11}$B NMR spectrum of CpBeBH₄ exhibits a pentet of quartets at −56·3 ppm, which is an unusually low frequency for a borohydride compound, with $J$(B–H) 84 Hz and $J$(B–Be) 3·7 Hz. The lines for the BH₄ resonances are quite narrow; half-widths for the $^{11}$B and $^1$H signals are 1·5 and 1·2 Hz respectively.[85] A suggested mechanism for hydrogen interchange in solution phase Be(BH₄)₂ is depicted in Fig. 12.

## XVI. MANGANABORANES

The reaction of B₅H₉ with HMn(CO)₅ provides the novel manganaborane (CO)₃Mn-2-B₅H₁₀. Its suggested structure, shown in Fig. 13, comprises a pentagonal pyramid with a (CO)₃Mn unit in one of the basal positions.
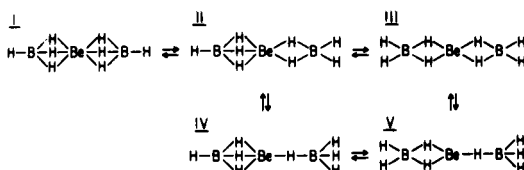
FIG. 12. Proposed mechanism for hydrogen interchange in $Be(BH_4)_2$.
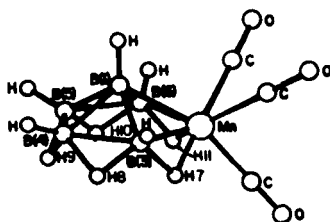


FIG. 13. Proposed structure of $(CO)_3MnB_5H_{10}$.

The compound is analogous to $(CO)_3FeB_5H_9$, $2\text{-}CpFeB_5H_{10}$, or $2\text{-}B_5CH_9$, and the gross structure follows from the normal 86·6 MHz $^{11}$B NMR spectrum, which shows three types of boron in a ratio of 2 : 2 : 1 (see Table 27). Upon line narrowing and selective proton decoupling, the B(3,6) resonance at 31·8 ppm is seen to be a doublet of doublets with couplings of 140 and 70 Hz. These splittings are due respectively to coupling of B(3,6) with the terminal and Mn–H–B protons. Similarly, the doublet at 11·3 ppm emerges to be a doublet of triplets with couplings of 156 and

## TABLE 27

$^{11}$B NMR data for $(CO)_3MnB_5H_{10}$ and related compounds.

| Compound | Solvent | B(3,6) | B(4,5) | B(1) |
|---|---|---|---|---|
| 2,2,2-(CO)$_3$-2-MnB$_5$H$_{10}$ | C$_6$D$_6$ | +31·84 b {140, 870}[2] | +11·27 (156) {156, 44 t}[2] | −53·70 (142)[1] |
| 2,2,2-(CO)$_3$-2-MnB$_5$H$_{10}$ | CD$_2$Cl$_2$ | +32·37 b {137, 72}[2] | +11·63 (161) {155, 48 t} | −53·45 (146)[1] |
| 1-Br-2,2,2-(CO)$_3$-2-MnB$_5$H$_9$ | C$_6$D$_6$ | +32·06 b {70 m}[2] | +11·05 (161) {161, estd. 41 t}[2] | −39·56 s[1] |
| Na[2,2,2-(CO)$_3$-2-MnB$_5$H$_9$] | (C$_2$D$_5$)$_2$O | +32·00 b {59 d}[2] | +17·57 b [2] | −43·85 (122)[1] |
| [(n-C$_4$H$_9$)$_4$N][2,2,2-(CO)$_3$-2-MnB$_5$H$_9$] | CD$_2$Cl$_2$ | +31·12 b [2] | +20·92 b [2] | −41·32 (119)[1] |

44 Hz. The large splitting is due to $^1J$(B–H), and the triplet structure to nearly equal coupling of B(4,5) to the two adjacent bridge protons.

Bromination of $(CO)_3MnB_5H_{10}$ produces $(CO)_3MnB_5H_9Br$. The $^{11}B$ NMR spectrum of this compound now contains a low-frequency singlet, indicating that substitution has occurred at the apical B(1) position. Deprotonation of the manganaborane gives $(CO)_3MnB_5H_9{}^-$, whose $^{11}B$ NMR spectrum still shows three resonances of relative areas $2:2:1$. Since the $^1H$ NMR spectrum shows equal numbers of B–H–B and Mn–H–B protons, and only one kind of the former, base removes the proton bridging B(4) and B(5).

Comparison of the $^{11}B$ NMR spectra of $(CO)_3MnB_5H_9$ with those of other pentagonal pyramidal molecules and with $B_6H_{10}$ is of interest. Substitution of a transition metal for a BH unit in $B_6H_{10}$ seems to have little effect on the shift of the apical boron but B(3,6) moves by 20–30 ppm to higher frequencies.[86]

## XVII. METALLO-BORANES AND -CARBORANES CONTAINING IRON AND RUTHENIUM

The metalloborane $K[\mu\text{-Fe(CO)}_4B_2H_2]$ is obtained from $K_2Fe(CO)_4$ and $THF·BH_3$. It appears to be an unusual example of a diborane(6) derivative with a bridging transition metal. The suggested structure, shown in Fig. 14, can be inferred from the $^{11}B$ NMR spectrum which comprises a triplet
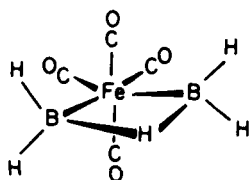


FIG. 14. Proposed structure of $[\mu\text{-Fe(CO)}_4B_2H_5]^-$.

of doublets, $\delta$ $-15\cdot4$. Coupling of the two equivalent boron nuclei to the terminal hydrogen atoms is 112 Hz and to the bridge hydrogen atoms 25 Hz.[87] A $Fe_2(CO)_6$ unit bridging hydrogen atoms in $B_2H_6$ is suggested to occur in $B_2H_6Fe_2(CO)_6$ (see Fig. 15). Its $^{11}B$ NMR spectrum contains a doublet at $-24\cdot0$ ppm, $J$(B–H) 90 Hz; coupling involving bridge hydrogens is not resolved.[88] A more complicated ferraborane, $B_3H_7Fe_2(CO)_6$, is prepared from $B_2H_6$, $Fe(CO)_5$, and $LiAlH_4$ in dimethoxyethane. Its structure is depicted in Fig. 16. Its $^{11}B$ NMR spectrum contains a doublet of relative area 2 at $4\cdot2$ ppm and a quartet of unit area at $12\cdot1$ ppm.[89] This
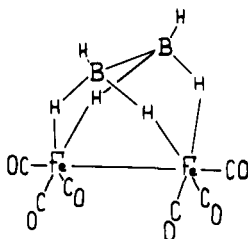
FIG. 15. Proposed structure of $B_2H_6Fe_2(CO)_6$
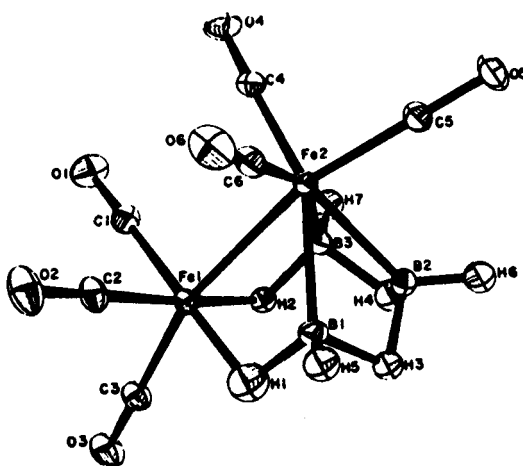


FIG. 16. Structure of $B_3H_7Fe_2(CO)_6$.

may be a case where coupling of B(2) to the bridge and terminal protons is nearly the same.

The five-boron cluster 2-CpFeB$_5$H$_{10}$ has been isolated in low yield from a reaction of FeCl$_2$ with NaCp and NaB$_5$H$_8$. The $^{11}$B NMR contains doublets at 44·4, 8·2, and −53·0 ppm in a 2:2:1 ratio, so the molecule is static at room temperature in toluene solution. On heating to 175 °C, rearrangement occurs to give 1-CpFeB$_5$H$_{10}$ whose $^{11}$B NMR spectrum exhibits only a doublet at 5·1 ppm. The suggested structures are shown in Fig. 17. A helpful view of these compounds is that they are analogues of B$_6$H$_{10}$ with a BH unit replaced by the isoelectronic CpFe group.[90]

A related ferraborane, (CO)$_3$FeB$_5$H$_9$, has been obtained by copyrolysis of B$_5$H$_9$ and Fe(CO)$_5$. The NMR data are consistent with a pentagonal pyramidal metalloborane having the Fe(CO)$_3$ unit in a basal position. Low temperature NMR spectra reveal that the bridging proton moves between
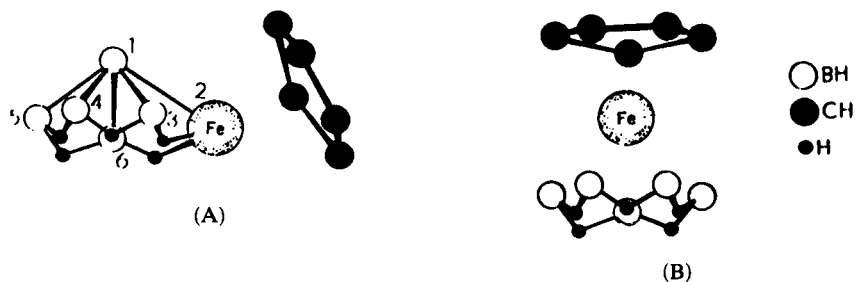
FIG. 17. Proposed structures of (A) 2-CpFeB$_5$H$_{10}$ and (B) 1-CpFeB$_5$H$_{10}$.

the two Fe–B polyhedron edges. This interconverts B(4) and B(5), B(3) and B(6) (see Fig. 18). $^{11}$B NMR data for (CO)$_3$FeB$_5$H$_9$ in CH$_2$Cl$_2$ at −80 and 25 °C are given in Table 28.[91]
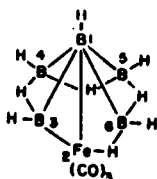


FIG. 18. Proposed structure of (CO)$_3$FeB$_5$H$_9$.

Maxwell, Wong and Grimes[93] have developed an extensive derivative chemistry of (2,3-Me$_2$-2,3-B$_4$C$_2$H$_4$)$_2$FeH$_2$. Irradiation of this material in presence of carbon monoxide affords 2,1,4-(CO)$_3$FeMe$_2$B$_7$C$_2$H$_7$. The suggested structure is that of a bicapped square antiprism with carbon atoms in the 1 and 4 positions and the iron atom in the 2 position. It can be deduced from the $2:2:2:1$ pattern of doublets in the $^{11}$B NMR spectrum and the observation of non-equivalent methyl groups. Deprotonation of

TABLE 28

Variable temperature $^{11}$B NMR data for (CO)$_3$FeB$_5$H$_9$.

| Position | $\delta^{11}$B (−80 °C) | $\delta^{11}$B ($J_{BH}$) (25 °C) |
|---|---|---|
| B(1) | −47·0 | −47·4 (140) |
| B(4) or B(5) | 2·3 | {8·2 (150)} |
| B(5) or B(4) | 13·5 | |
| B(6) | 37·7 | {46·0 (150)} |
| B(3) | 55·5 | |
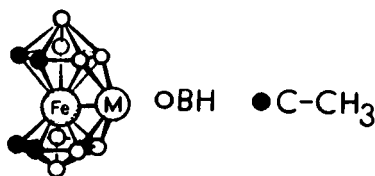
FIG. 19. Proposed structure of $MFeMe_4B_8C_4H_8$ (M = Sn, Ge).

$(2,3-Me_2B_4C_2H_4)_2FeH_2$ followed by reaction with $GeI_2$ or $SnCl_2$ leads to insertion of the Group IV element and formation of $MFeMe_4B_8C_4H_8$ (M = Sn, Ge). The suggested structures (Fig. 19) feature an iron atom $\pi$ bonded to pentagonal pyramidal $Me_2B_4C_2H_4$ cages; the Sn or Ge then occupies a wedge position between the carborane units. These molecules may be fluxional with tin or germanium alternating between two equivalent wedging positions involving the four $FeB_2$ faces. This would account for the chemically equivalent methyl groups and the 2:4:2 pattern of doublets in the $^{11}B$ NMR spectrum (Table 29). However, the $^1H$ NMR spectrum is unchanged at $-66$ °C. Reaction of $(2,3-Me_2B_4C_2H_4)_2FeH_2$ with ethanolic    KOH,    $CoCl_2$,    and    $C_5H_6$    produce    *inter    alia*   $(CpCoMe_2B_3C_2H_3)FeH_2(Me_2B_4C_2H_4)$ and $(CpCoMe_2B_3C_2H_3)Fe(H)Cp$. These compounds are considered to contain a $CoB_3C_2$ cage with cobalt in

TABLE 29

$^{11}B$ NMR data for metallo-boranes and -carboranes containing iron and ruthenium.

| Compound | $\delta^{11}B$ $(J_{BH})$ |
|---|---|
| $K[\mu\text{-}Fe(CO)_4B_2H_5]$ | $-15\cdot4$ (td, 112, 25) |
| $B_2H_6Fe_2(CO)_6$ | $-24\cdot0$ (d, 90) |
| $B_3H_7Fe_2(CO)_6$ | $12\cdot1$ (q, 1B, 170), $4\cdot2$ (d, 2B, 160) |
| $2\text{-}CpFeB_5H_{10}$ | $44\cdot4$ (d, 2B, 145), $8\cdot2$ (d, 2B, 146), $-53\cdot0$ (d, 1B, 145) |
| $1\text{-}CpFeB_5H_{10}$ | $5\cdot1$ (d, 145) |
| $2,1,4\text{-}(CO)_3FeMe_2B_7C_2H_7$ | $19\cdot1$ (d, 1B, 156), $6\cdot4$ (d, 2B, 156), $-13\cdot1$ (d, 2B, ~156), $-15\cdot9$ (d, 2B, ~156) |
| $GeFeMe_4B_8C_4H_8$ | $13\cdot8$ (d, 2B, 166), $3\cdot7$ (d, 4B, 156), $-9\cdot9$ (d, 2B, 126) |
| $SnFeMe_4B_8C_4H_8$ | $11\cdot4$ (d, 2B, 175), $2\cdot3$ (d, 4B, 170), $-10\cdot9$ (d, 2B, 160) |
| $(CpCoMe_2B_3C_2H_3)$ $FeH_2(Me_2B_4C_2H_4)$ | $10\cdot9, 7\cdot3$ |
| $(CpCoMe_2B_3C_2H_3)FeCp$ | $-355$ (W/2 ~1500), $-564$ (W/2 ~3000) |
| $(CpFe)EtOMe_2B_4C_2H_3$ | $6$ (W/2 ~1000), $-303$ (W/2 ~1300) |
| $4,5\text{-}(CpFe)_2\text{-}2,3\text{-}B_9C_2H_{11}$ | $-113\cdot1$ (d, 1B), $-42\cdot4$ (d, 2B), $-22\cdot4$ (d, 4B), $-5\cdot7$ (d, 2B) |

*(continued overleaf)*

## TABLE 29 (*cont.*)

| Compound | $\delta^{11}B$ ($J_{BH}$) |
|---|---|
| $Me_4N[(CpFe)B_9C_2H_{11}FeB_9C_2H_{11}]$ | $-110 \cdot 1$ (d, 1B), $-46 \cdot 1$ (d, 1B), $-39 \cdot 8$ (d, 1B), $-23 \cdot 9$ (d, 2B), $-22 \cdot 6$ (d, 2B), $-5 \cdot 8$ (d, 2B), $-7 \cdot 7$ (d, 1B), $0 \cdot 5$ (d, 1B), $4 \cdot 8$ (d, 4B), $17 \cdot 5$ (d, 2B) $20 \cdot 6$ (d, 1B) |
| $(CpFe)_2B_8C_2H_9(OH)$ | $-0 \cdot 8$ (d, 1B), $-3 \cdot 6$ (d, 1B), $-17 \cdot 3$ (d, 2B), $-19 \cdot 3$ (d, 2B), $-26 \cdot 4$ (d, 2B) |
| $(Ph_3P)_3Ru(H)-1,2,4-B_8C_2H_9$ | $35 \cdot 5$ (d, 1B, $J_{BP}$ 130), $6 \cdot 1$, $0 \cdot 6$, $-5 \cdot 2$, $-18 \cdot 5$, $-22 \cdot 7$, $-27 \cdot 1$, $-42 \cdot 0$ |
| $(Ph_3P)_2Ru-6,2,3-B_7C_2H_9$ | $108 \cdot 0$ (1B), $16 \cdot 4$ (1B), $-4 \cdot 2$ and $-5 \cdot 9$ (5B) |
| $(Et_3P)_2Ru-6,2,3-B_7C_2H_9$ | $105 \cdot 5$ (1B), $15 \cdot 4$ (1B), $-5 \cdot 7$ (2B), $7 \cdot 8$ (3B) |
| $(Et_3P)_2Ru(CO)-6,2,3-B_7C_2H_9$ | $14 \cdot 3$ (1B), $-4 \cdot 9$ (1B), $-10 \cdot 3$ (1B), $-21 \cdot 4$ (2B), $-24 \cdot 4$ (2B) |
| $(Et_3P)_3Ru-6,2,3-B_7C_2H_9$ | $-8 \cdot 1$ (4B), $-24 \cdot 2$ (3B) (at $-79\,°C$) |
| $(SP)Ru-6,2,3-B_7C_2H_9{}^a$ | $106 \cdot 8$ (1B), $18 \cdot 9$ (1B), $5 \cdot 6$ (1B), $-3 \cdot 8$ (1B), $-4 \cdot 6$ (1B), $-5 \cdot 9$ (1B), $-8 \cdot 8$ (1B) |
| $(AP)Ru-6,2,3-B_7C_2H_9{}^b$ | $108 \cdot 4$ (1B), $15 \cdot 0$ (1B), $4 \cdot 8$ (1B), $-5 \cdot 2$ (1B), $-7 \cdot 0$ (2B), $-10 \cdot 3$ (1B) |
| $(SP)Ru-6,2,3-Me_2B_7C_2H_7$ | $107 \cdot 6$ (1B), $17 \cdot 9$ (1B), $11 \cdot 9$ (1B), $-0 \cdot 1$ (1B), $-2 \cdot 2$ (2B), $-9 \cdot 6$ (1B) |
| $(SP)Ru-6,2,3-PhB_7C_2H_8$ | $106 \cdot 8$ (1B), $15 \cdot 2$ (1B), $9 \cdot 1$ (1B), $-4 \cdot 8$ (3B), $-10 \cdot 4$ (1B) |
| $(AP)Ru-6,2,3-Me_2B_7C_2H_7$ | $108 \cdot 0$ (1B), $19 \cdot 2$ (1B), $14 \cdot 6$ (1B), $-2 \cdot 1$ (3B), $-11 \cdot 0$ (1B) |
| $(MBP)Ru-6,2,3-Me_2B_7C_2H_7{}^c$ | $107 \cdot 5$ (1B), $17 \cdot 5$ (1B), $10 \cdot 6$ (1B), $0 \cdot 2$ (1B), $-2 \cdot 3$ (1B), $-3 \cdot 6$ (1B), $-9 \cdot 7$ (1B) |
| $(DBP)Ru-6,2,3-Me_2B_7C_2H_7{}^d$ | $106 \cdot 8$ (1B), $17 \cdot 2$ (1B), $9 \cdot 7$ (1B), $-0 \cdot 1$ (1B), $-2 \cdot 3$ (1B), $-4 \cdot 5$ (1B), $-9 \cdot 9$ (1B) |
| $(AP)Ru(CO)_2-6,2,3-B_7C_2H_9$ | $1 \cdot 4$ (2B), $-9 \cdot 3$ (1B), $-20 \cdot 4$ and $-23 \cdot 2$ (4B) |
| $(MBP)_2Ru-6,2,3-B_7C_2H$ | $107 \cdot 5$ (1B), $17 \cdot 3$ (1B), $2 \cdot 5$ (1B), $-5 \cdot 0$ (2B), $-6 \cdot 5$ (1B), $-8 \cdot 7$ (1B) (at $44\,°C$); $20 \cdot 4$ (2B), $-6 \cdot 0$ (2B), $-23 \cdot 2$ (3B) (at $-40\,°C$) |
| $(DBP)_2Ru-6,2,3-B_7C_2H_9$ | $2 \cdot 6$ (3B), $-15 \cdot 8$ (4B) (at $44\,°C$); $24 \cdot 9$ (2B), $-3 \cdot 4$ (2B), $-19 \cdot 9$ (3B) (at $-71\,°C$) |
| $(DBP)_2Ru(CO)-6,2,3-B_7C_2H_9$ | $0 \cdot 0$ (2B), $-9 \cdot 1$ (1B), $-23 \cdot 4$ (4B) |
| $(MBP)_2Ru(CO)-6,2,3-B_7C_2H_9$ | $0 \cdot 4$ (2B), $-8 \cdot 2$ (1B), $-22 \cdot 0$ (4B) |
| $(Ph_3P)_2RuH_2-2,1,7-B_9C_2H_{11}$ | $1 \cdot 2$ (1B), $-7 \cdot 6$ (3B), $13 \cdot 1$ (4B), $-18 \cdot 3$ (1B) |
| $(Ph_3P)_2RuH_2-3,1,2-B_9C_2H_{11}$ | $13 \cdot 9$ (2B), $4 \cdot 6$ (5B), $-5 \cdot 4$ (2B) |
| $(Ph_3P)_2Ru-2,1,7-B_9C_2H_{11}$ | $3 \cdot 0$ (1B), $0 \cdot 0$ (1B), $-5 \cdot 2$ (2B), $-10 \cdot 9$ (2B), $-22 \cdot 1$ (3B) |
| $(Ph_3P)_2RuH-7-C_5H_5N-$<br>$3,1,2-B_9C_2H_{10}$ | $5 \cdot 2$ (1B), $-11 \cdot 1$ (4B), $-13 \cdot 4$ (2B), $-23 \cdot 4$ (1B), $-29 \cdot 4$ (1B) |

---

$^a$ SP = (*o*-styryl)diphenylphosphine.
$^b$ AP = (*o*-allylphenyl)diphenylphosphine.
$^c$ MBP = (but-3-enyl)diphenylphosphine.
$^d$ DBP = di(but-3-enyl)phenylphosphine.

(A) (B)
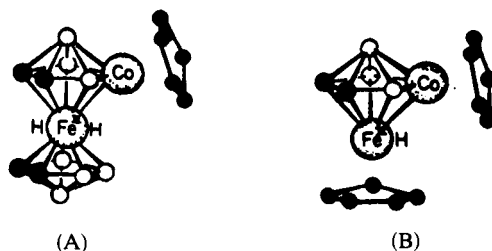
FIG. 20. (A) Proposed structure of $(CpCoMe_2B_3C_2H_3)FeH_2(Me_2B_4C_2H_4)$.
(B) Established structure of $(CpCoMe_2B_3C_2H_3)Fe(H)Cp$.

an equatorial position and an apical iron atom. This has been confirmed by an X-ray structure analysis of $(CpCoMe_2B_3C_2H_3)Fe(H)Cp$ (Fig. 20).[92] Amongst the major products of this complicated reaction are $(CpFe)Me_2B_4C_2H_4$ and its $B$-ethoxy derivative, $(CpFe)EtOMe_2B_4C_2H_3$. Both presumably have a pentagonal bipyramidal geometry with an apical iron atom and adjacent equatorial carbon atoms. The $^{11}B$ NMR spectra exhibit very broad signals (half-widths 1000–3000 Hz) and so do not reveal the position of the ethoxy group.[93]

Polyhedral expansion of $(CpFe)B_9C_2H_{11}$ leads to three new biferracarboranes: $4,5\text{-}(CpFe)_2\text{-}2,3\text{-}B_9C_2H_{11}$, $(CpFe)_2B_8C_2H_9(OH)$, and $Me_4N[(CpFe)B_9C_2H_{11}FeB_9C_2H_{11}]$. The first compound contains two paramagnetic centres and a preliminary X-ray study indicates that the Fe–Fe separation is about $3 \cdot 20$ Å. The $^{11}B$ NMR spectrum does not exhibit grossly broadened or contact shifted resonances, and the apparent diamagnetism may arise from spin pairing mediated by the carborane cage. A doublet at $-113 \cdot 1$ ppm is assigned to the low-coordinate boron atom adjacent to the two iron atoms. The thirteen-atom cage appears not to be fluxional and the $^{11}B$ NMR spectrum is unchanged at $-75\,°C$. A plane of symmetry is established by the $1:2:4:2$ pattern of doublets; placement of the iron atoms in the 4,5 positions and the carbon atoms in the 2,3 positions is reasonable (see Fig. 21). The $^{11}B$ NMR spectrum of
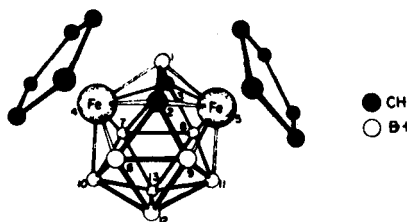


FIG. 21. Proposed structure of $4,5\text{-}(CpFe)_2\text{-}2,3\text{-}B_9C_2H_{11}$.

$Me_4N[(CpFe)B_9C_2H_{11}FeB_9C_2H_{11}]$ is interpretable as a superposition of resonances at $-110\cdot1$, $46\cdot1$, $-39\cdot8$, $-23\cdot9$, $-22\cdot6$, and $-5\cdot8$ ppm due to the $Fe_2B_9C_2H_{11}$ cage, and at $-7\cdot7$, $0\cdot5$, $4\cdot8$, $17\cdot5$, and $20\cdot6$ ppm due to the capping $B_9C_2H_{11}$ cage (see Table 29). It appears that insertion of a second iron atom causes an overall decrease in shielding of the cage boron atoms.[94]

Carboranes incorporating ruthenium as a heteroatom are currently of interest because of the potential of such materials as catalysts. Jung and Hawthorne[95] obtained $(Ph_3P)_3Ru(H)$-$1,2,4$-$RuB_8C_2H_9$ from $NaB_8C_2H_{11}$ and $(Ph_3P)_3RuHCl$. The NMR data are consistent with a *closo* eleven-atom cage structure. The $^{11}B\{^1H\}$ NMR spectrum reveals a high-frequency doublet, $\delta$ $35\cdot5$, assigned to a low-coordinate boron atom next to a ruthenium atom. The splitting is due to $^{31}P$–$^{11}B$ coupling and thus it appears that one of the triphenylphosphine groups is directly bonded to the cage.[95]

Metal insertion into $B_7C_2H_{12}^-$ (and its *C*-alkyl derivatives) generates $(Ph_3P)_2RuB_7C_2H_9$. Compounds of this type are referred to as *hyper-closo*, denoting an $n$ vertex cluster of less than $n+1$ skeletal electron pairs which is significantly distorted from the idealized *closo* polyhedral geometry. The $^{11}B\{^1H\}$ NMR spectrum of this ruthenacarborane is not well resolved but does indicate the presence of a plane of symmetry. A very high frequency resonance at $108\cdot0$ ppm appears to be characteristic of *hyper-closo* 10-vertex ruthenacarborane compounds, and such peaks are not observed in the $^{11}B$ NMR spectra of *closo*-metallocarboranes containing second- and third-row metals. The interesting solution phase chemistry of $(Et_3P)_3Ru$-$6,2,3$-$B_7C_2H_9$ has been probed by $^{11}B$ NMR spectroscopy. At $-80\,°C$, phosphine dissociation is slow. The 127 MHz $^{11}B\{^1H\}$ NMR spectrum at this temperature shows peaks at $-8\cdot1$ (4B) and $-24\cdot2$ (3B) ppm indicative of a fluxional process, which is probably restricted rotation of the $(Et_3P)_3Ru$ vertex. At higher temperatures, equilibrium loss of $Et_3P$ generates *hyper-closo* $(Et_3P)_2Ru$-$6,2,3$-$B_7C_2H_9$, with the formation of which a new resonance at $105\cdot6$ ppm is observed. This process is depicted in Fig. 22.[96] Ligand displacement by carbon monoxide is used to prepare $(CO)_2Ph_3PRu$-$6,2,3$-$B_7C_2H_9$ and $(CO)(Et_3P)_2Ru$-$6,2,3$-$B_7C_2H_9$. The $^{11}B\{^1H\}$ NMR spectrum of the latter compound is well resolved at 127 MHz and shows a $1:1:1:2:2$ pattern of resonances (see Table 29), indicating that the barrier to metal vertex rotation may be higher when phosphines are replaced by carbon monoxide.

Reaction of $(Ph_3P)_2Ru$-$6,2,3$-$B_7C_2H_9$ with styryl- and *o*-allylphenyldiphenylphosphine (L) produces *hyper-closo* $LRu$-$6,2,3$-$B_7C_2H_9$ in which the alkenyl group is coordinated to ruthenium. An X-ray structure analysis of (allylphenyldiphenylphosphine)$Ru$-$2,3$-$Me_2$-$2,3$-$B_7C_2H_7$ demonstrates this feature and an *arachno* $RuB_7C_2$ cage with boron and carbon atoms at the vertices of an 11-vertex polyhedron; the ruthenium atom is in a
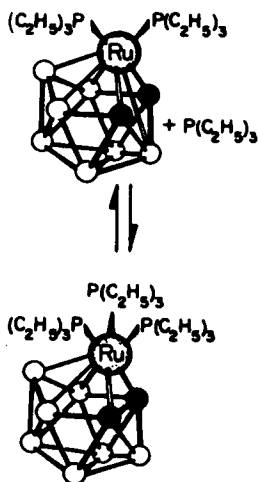
FIG. 22. Proposed equilibrium between $(Et_3P)_2RuB_7C_2H_9$ and $(Et_3P)_3RuB_7C_2H_9$.

non-vertex position but within bonding distance of all six atoms on the open face (Fig. 23). The most highly resolved $^{11}B$ NMR spectra of compounds of this class show seven doublets of unit area, and the resonance at 107 ppm is associated with B(1). The solid-state structure appears to
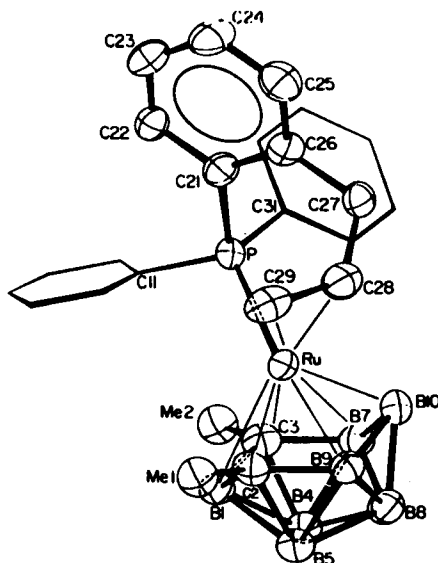


FIG. 23. Structure of [(o-allylphenyl)diphenylphosphine]Ru-2,3-Me$_2$-2,3-B$_7$C$_2$H$_7$.

persist in solution. The $^{11}$B NMR spectrum of $(CO)_2LRuB_7C_2H_9$ [L = (o-allylphenyl)diphenylphosphine] is quite similar to that of $(CO)_2Ph_3PRu$-6,2,3-$B_7C_2H_9$ (see above), indicating that the two Ru(II) compounds are isostructural and that the allyl group is not coordinated to ruthenium.[97]

Ruthenium complexes of $B_9C_2H_{11}{}^{2-}$ have also been reported. The 80·5 MHz spectrum of $(Ph_3P)_2Ru(H)_2$-2,1,7-$B_9C_2H_{11}$ in $CH_2Cl_2$ shows resonances at −1·2 (1B), 7·6 (3B), 13·1 (4B), and 18·3 (1B) ppm, which is similar to, for example, the rhodium analogue. This compound eliminates dihydrogen on heating. The $^{11}$B NMR spectrum of $(Ph_3P)_2Ru$-2,1,7-$B_9C_2H_{11}$ in THF contains peaks at −3·0 (1B), 0·0 (1B), 5·2 (2B), 10·9 (2B), and 22·1 (3B) ppm, and it appears that this rather drastic change at the metal centre has only a rather small effect on $^{11}$B shieldings.[98]

## XVIII. COBALTA-BORANES AND -CARBORANES

Condensation of $NaB_5H_8$, $NaC_5H_5$, and cobalt chloride leads to an almost bewildering variety of cobaltaboranes. They may be classified by electron counting rules into (a) *nido* or $2n + 4$ electron structures, (b) *closo* or $2n + 2$ electron structures, (c) capped polyhedral $2n$ electron systems. Structures of such molecules are elucidated in part by $^{11}$B NMR spectroscopy and representative examples are depicted in Fig. 24.[99]

The *nido* compound 5-$CpCoB_9H_{13}$ is a structural analogue of $B_{10}H_{14}$ and the B–B distances differ from those in the pure borane by an average of only 0·019 Å.[100] Indeed, considering the gross electronic changes attendant on replacing boron by cobalt, the $^{11}$B NMR spectra are rather similar.

Both $^{11}$B and $^1$H NMR data indicate that the dicobaltaborane $(CpCo)_2B_4H_6$ has $C_{2v}$ symmetry, so B(4,6) and B(3,5) form equivalent pairs. The location of the "extra" protons, i.e. those in excess of one per boron, is not precisely determined but some bonding interaction with boron seems probable. The B(4,6) positions, adjacent to only one cobalt atom, have $\delta$ 61·1, at high frequency with respect to B(3,5), $\delta$ 19·4, which are adjacent to two cobalt atoms. This assignment is reasonable in view of the single resonance at 62·7 ppm in $(CpCo)_3B_3H_5$ whose structure has been established by X-ray crystallography and in which all three boron atoms are each bonded to two cobalt atoms. The solid-state geometry is that of an octahedral $B_3Co_3$ cage. The two "extra" hydrogen atoms could not be refined but, from electron density maps, they appear to be associated with the triangular tricobalt face.[101] Therefore, in $(CpCo)_2B_4H_6$ an antipodal effect may operate so that B(4,6), which are antipodal to cobalt, appear at higher frequency. Usually, $^{11}$B signals of four-coordinate adjacent borons appear at very high frequencies. A crystal structure analysis of this compound confirms the octahedral $B_4Co_2$ cage inferred from the $^{11}$B NMR
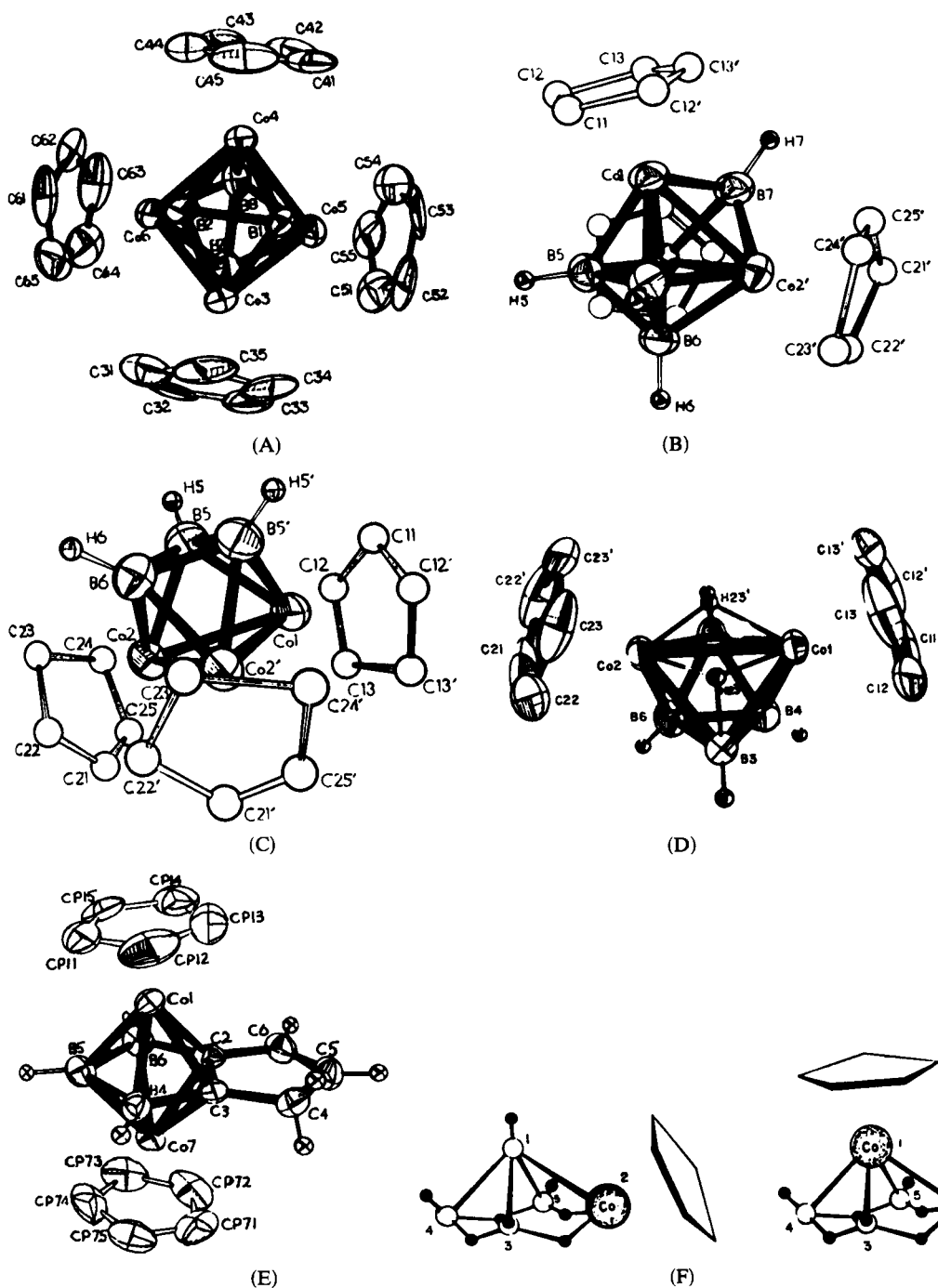
FIG. 24. Structures of (A) $(CpCo)_4B_4H_4$, (B) $(CpCo)_3B_4H_4$, (C) $(CpCo)_3B_3H_5$, (D) $(CpCo)_2B_4H_6$, (E) $\mu$-$(C_3H_4)$-1,7,2,3-$(CpCO)_2B_3C_2H_3$, and (F) 2- and 1-$CpCoB_4H_8$.

spectra. The metal atoms occupy adjacent vertices with the "extra" hydrogens in face bridging positions approximately over the centres of the two $BCo_2$ triangular faces.[102] Finally, $\mu$(2,3)-1,3-$C_3H_4$-1,7,2,3-$(CpCo)_2B_3C_2H_3$, also produced in the same reaction, possesses a seven-vertex pentagonal bipyramidal cage with the cage carbons bridged by an exopolyhedral propenylene group.[103]

The $^{11}B$ NMR spectrum of the cobaltaborane $(CpCo)_4B_4H_4$, which comprises a doublet at $121 \cdot 4$ ppm, conveys little structural information. An X-ray study reveals a *closo* eight-vertex $B_4Co_4$ cluster with nearly $D_{2d}$ symmetry; the cobalt atoms are in contiguous positions at the five-coordinate vertices and the boron atoms occupy four-coordinate vertices. It is a puzzle why this cage which has 16 skeletal valence electrons violates Wade's rules[104] and adopts a *closo* polyhedral geometry.[105] It is, of course, possible that a dynamic distortion occurs in solution which is not detected by $^{11}B$ NMR. In the same vein, it is possible that the bridging hydrogen atoms in $(CpCo)_3B_3H_5$ and $(CpCo)_2B_4H_6$ may be mobile and migrate between several polyhedral faces. High resolution, low temperature $^{11}B$ NMR studies of these molecules would be of interest.

The metalloborane $CpCoB_5H_8$ undergoes with acetylene an insertion reaction to produce the carborane derivative 1,2,3-$CpCoB_3C_2H_7$. In addition to insertion products, substituted alkynes, such as propyne, but-2-yne, and phenylacetylene, also yield products incorporating 1 equivalent of the acetylene. Extensive overlap of peaks in the 32 MHz $^{11}B$ NMR spectra hinders incisive structural characterization, but singlet resonances are observed which indicate that these products arise from hydroboration and that they are *B*-alkenyl derivatives of $CpCoB_4H_8$. Condensation of $CpCoB_4H_8$ with iron pentacarbonyl produces 1,2,3-$(CpCo)_2Fe(CO)_4B_3H_3$, whose suggested structure is shown in Fig. 25. In it there are two types of
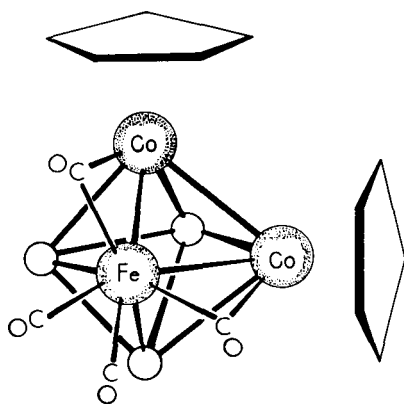


FIG. 25. Proposed structure of 1,2,3-$(CpCo)_2Fe(CO)_4B_3H_3$.

boron atoms, each bonded to two metal atoms. Such a structure should exhibit two very high frequency doublets, and these are observed at 87·5 and 73·0 ppm.[106]

Irradiation of $(2,3\text{-}Me_2\text{-}2,3\text{-}B_3C_2H_5)CoH(2,3\text{-}Me_2B_4C_2H_4)$ and CpCo-$(CO)_2$ in tetrahydrofuran yields $5\text{-}(CpCoC_5H_4)[2,3\text{-}Me_2B_4C_2H_3]\text{-}Co[2,3\text{-}Me_2B_3C_2H_5]$ and $\sigma\text{-}(THF)\text{-}[2,3\text{-}Me_2B_4C_2H_3]Co[2,3\text{-}Me_2B_3C_2H_5]$. These are zwitterionic compounds with exopolyhedral substituents. Unfortunately, the ^{11}B NMR spectra are not well resolved at 32 MHz. However, the X-ray crystal structure of the cobalticenium compound reveals a ring-like $2,3\text{-}Me_2B_3C_2H_5$ ligand with hydrogen atoms bridging the B–B edges and a pentagonal pyramidal $2,3\text{-}Me_2B_4C_2H_3$ ligand with the $CpCoC_5H_4$ unit bonded to the unique equatorial boron, B(5), as shown in Fig. 26.[107]
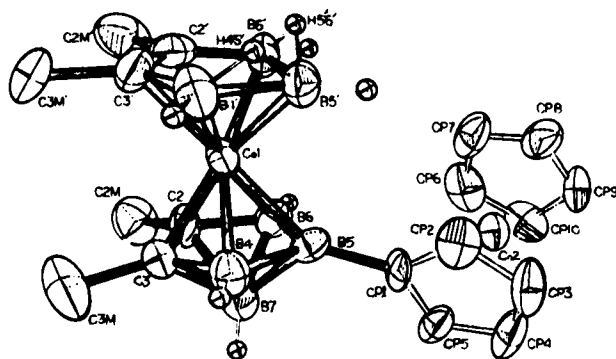


FIG. 26. Structure and numbering system of $5\text{-}[CpCoC_5H_4]\text{-}[2,3\text{-}Me_2B_4C_2H_3]Co[2,3\text{-}Me_2B_3C_2H_5]$.

Reaction of $(Et_3P)_4Co$ with $1,5\text{-}B_3C_2H_5$ results in insertion of the $(Et_3P)_2Co$ moiety to give paramagnetic $(Et_3P)_2Co\text{-}2,1,6\text{-}B_3C_2H_5$ whose ^{11}B NMR spectrum has not been reported; that of the hydrocobalt analogue $(Et_3P)_2Co(H)\text{-}2,1,6\text{-}B_3C_2H_5$ has doublets at 20·1 (1B) and −1·7 (2B) ppm. Similar insertion chemistry applied to $1,7\text{-}B_6C_2H_8$ yields $(Et_3P)_2Co(H)\text{-}2,1,8\text{-}B_6C_2H_8$. The ^{11}B NMR spectrum contains six doublets, consistent with the solid-state tricapped trigonal prismatic geometry with C(1), B(6), and B(8) in the capping sites (Fig. 27).[108]

The new cobaltacarborane $2,5\text{-}Me_2\text{-}(CpCo)_2\text{-}2,5,1,7\text{-}B_5C_2H_5$ is prepared from cobalt atoms, $B_5H_9$, $C_5H_6$, and but-2-yne. Its suggested structure is shown in Fig. 28. The ^{1}H and ^{11}B NMR spectra (Table 30) indicate the absence of a plane of symmetry. If it is assumed that the carbon cage atoms remain adjacent and that the cobalt atoms occupy five-coordinate positions,
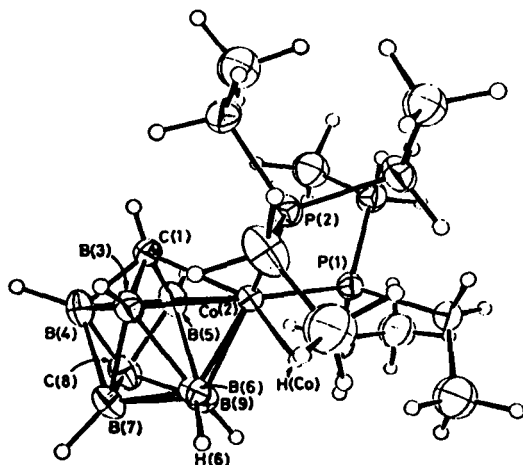
FIG. 27. Molecular structure and numbering system for $(Et_3P)_2Co(H)-2,1,8-B_6C_2H_8$.
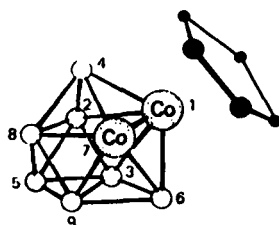


FIG. 28. Proposed structure of $2,5-Me_2-(CpCo)_2-2,5,1,7-B_5C_2H_5$.

then the doublets of area 1 at 73·2 and 55·4 ppm may be assigned to B(4) and B(6), the four-coordinate boron atoms adjacent to two cobalt atoms.[109]

2-CpCoB$_9$H$_{13}$, an analogue of decaborane with a CpCo unit replacing B(2) (see the isomeric 5-CpCoB$_9$H$_{13}$, above), is produced from pentaborane and CpCo(CO)$_3$. Also isolated from this rather energetic reaction is 1-CpCoB$_5$H$_9$. Its structure (Fig. 29) is suggested to contain a planar B$_5$H$_9^{2-}$ ring $\pi$-bonded to cobalt. The $^{11}$B{$^1$H} NMR spectrum at $-70\,°C$ shows two resonances at 15·2 (4B) and 4·8 (1B) ppm and a singlet at 25 °C. The borane ligand thus appears to be fluxional on the NMR time scale owing to rapid shifts of bridging hydrogens about the periphery of the B$_5$ ring.[110]

Metal atom chemistry has also led to the preparation of poly(cobalt)borane, (CpCo)$_3$B$_5$H$_5$, and the cyclopentenyl-substituted derivative (CpCo)$_3$B$_5$H$_4$(c-C$_5$H$_9$). Two possible structures for these compounds are shown in Fig. 30. The resonance at 12·8 ppm in (CpCo)$_3$B$_5$H$_5$ is attributable to B(8), the unique boron atom which is not bonded to

## TABLE 30

$^{11}$B NMR data for cobalta-boranes and -carboranes.

| Compound | $\delta^{11}B\ (J_{BH})$ |
|---|---|
| 1-CpCoB$_4$H$_8$ | $-4\cdot4$ (d, 162) |
| 2-CpCoB$_4$H$_8$ | $6\cdot2$ (d, 1B 154), $-15\cdot9$ (d, 3B, 136) |
| 5-CpCoB$_9$H$_{13}$ | $30\cdot2$ (d, 1B, 170), $25\cdot1$ (d, 1B, 200), $12\cdot3$ (d, 1B, 160), $8\cdot0$ (d, 2B, 160), $2\cdot2$ (d, 1B, 160), $-2\cdot9$ (d, 1B, 160), $-16\cdot0$ (d, 1B, 160), $-36\cdot4$ (d, 1B, 160) |
| 1,2-(CpCo)$_2$B$_4$H$_6$ | $61\cdot1$ (d, 2B, 151), $19\cdot4$ (d, 2B, 146) |
| 3-$\sigma$-C$_5$H$_9$-1,2-<br>(CpCo)$_2$B$_4$H$_5$ | $59\cdot3$ (d, 2B, 149), $39\cdot2$ (s, 1B), $18\cdot7$ (d, 1B, 122) |
| 4-$\sigma$-C$_5$H$_9$-1,2-<br>(CpCo)$_2$B$_4$H$_5$ | $76\cdot2$ (s, 1B), $55\cdot9$ (d, 1B, 142), $17\cdot7$ (d, 2B, 129) |
| 1,2,3-(CpCo)$_3$B$_3$H$_5$ | $62\cdot7$ (d, $\sim$112) |
| C$_5$H$_7$-(CpCo)$_3$B$_3$H$_4$ | $99\cdot8$ (d, 1B, 228), 63 (d, 1B, 225), 61 (s, 1B) |
| $\mu$-(2,3-C$_3$H$_4$)-1,7,2,3-<br>(CpCo)$_2$B$_3$C$_2$H$_3$ | $64\cdot4$ (d, 1B, 130), $4\cdot2$ (br, 2B) |
| (CpCo)$_3$B$_4$H$_4$ | $141\cdot4$ (br, 1B), $86\cdot6$ (d, 3B, 146) |
| (CpCo)$_4$B$_4$H$_4$ | $121\cdot4$ (d, 137) |
| 5-(CpCoC$_5$H$_4$)-<br>[2,3-Me$_2$B$_4$C$_2$H$_3$]-<br>Co[2,3-Me$_2$B$_3$C$_2$H$_5$] | $7\cdot0$ (3B), $-0\cdot1$ (br d, 6B, $\sim$156) |
| 1,2,3-CpCoB$_3$C$_2$H$_7$ | $\sim2\cdot7$ (d, 2B, 149), $\sim2\cdot0$ (d, 1B, 147) |
| 1,2,3-CpCoMeB$_3$C$_2$H$_6$ | $\sim-1\cdot8$ (asymm. d, 121) |
| 1,2,3-CpCoMe$_2$B$_3$C$_2$H$_5$ | $0\cdot9$ |
| 1,2,3-CpCoPhB$_3$C$_2$H$_5$ | $4\cdot4$ (d, 1B, 140), $1\cdot2$ (d, 2B, 140) |
| CpCoB$_4$H$_8\cdot$MeC$_2$H | $18\cdot9$ (s) |
| CpCoB$_4$H$_8\cdot$MeC$_2$Me | $21\cdot9$ (s) |
| CpCoB$_4$H$_8\cdot$PhC$_2$H | $18\cdot1$ (s) |
| 1,2,3-<br>(CpCo)$_2$Fe(CO)$_4$B$_3$H$_3$ | $87\cdot5$ (d, 1B, 166), $73\cdot0$ (d, 2B, 158) |
| (Et$_3$P)$_2$Co(H)-<br>2,1,6-B$_3$C$_2$H$_5$ | $20\cdot1$ (1B), $-1\cdot7$ (2B) |
| (Et$_3$P)$_2$Co(H)-<br>2,1,8-B$_6$C$_2$H$_8$ | $49\cdot6$ (1B), $-0\cdot2$ (1B), $-8\cdot2$ (1B), $-10\cdot1$ (1B), $-19\cdot6$ (1B), $-34\cdot8$ (1B) |
| (CpCo)$_2$-1,7,2,5-<br>Me$_2$B$_5$C$_2$H$_5$ | $73\cdot2$ (d, 1B, 156), $55\cdot4$ (d, 1B, 164), $1\cdot0$ (d, 1B, 133), $-1\cdot9$ (d, 1B, 129), $-13\cdot4$ (d, 1B, 164) |
| 1-CpCoB$_5$H$_9$ | $15\cdot2$ (4B), $4\cdot8$ (1B) (at $-70$ °C); $12\cdot8$ (at 25°) |
| 2-CpCoB$_9$H$_{13}$ | $17\cdot0$ (d, 2B, 133), $14\cdot6$ (d, 1B, 164), $9\cdot0$ (d, 1B, 173), $1\cdot7$ (d, 4B, 156), $-38\cdot2$ (d, 1B, 155) |
| (CpCo)$_3$B$_5$H$_5$ | $136\cdot8$ (d, 1B, 147), $124\cdot4$ (d, 1B, 141). $104\cdot0$ (d, 2B, 154), $-12\cdot8$ (d, 1B, 134) |
| (CpCo)$_3$(c-C$_5$H$_9$)B$_5$H$_4$ | $137\cdot4$ (d, 1B, 138), $123\cdot4$ (d, 1B, 137), $102\cdot1$ (d, 2B, 132), $3\cdot3$ (s, 1B) |
| (Me$_5$CpCo)Me$_2$B$_4$C$_2$H$_4$ | $14\cdot9$ (d, B(5), 146), $5\cdot5$ (d, B(4,6,7), 136) |
| 1,7,2,3-(Me$_5$CpCo)$_2$-<br>Me$_2$B$_3$C$_2$H$_3$ | $52\cdot0$ (d, B(5), 112), $12\cdot3$ (d, B(4,6), 115) |
| (Me$_5$CpCo)Me$_2$B$_3$C$_2$H$_5$ | $10\cdot5$ (d, B(5)), $4\cdot0$ (d, B(4,6)) |
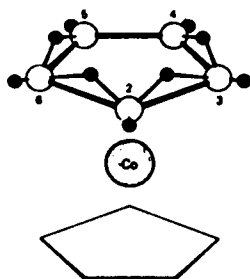
FIG. 29. Proposed static structure for 1-CpCoB$_5$H$_9$.
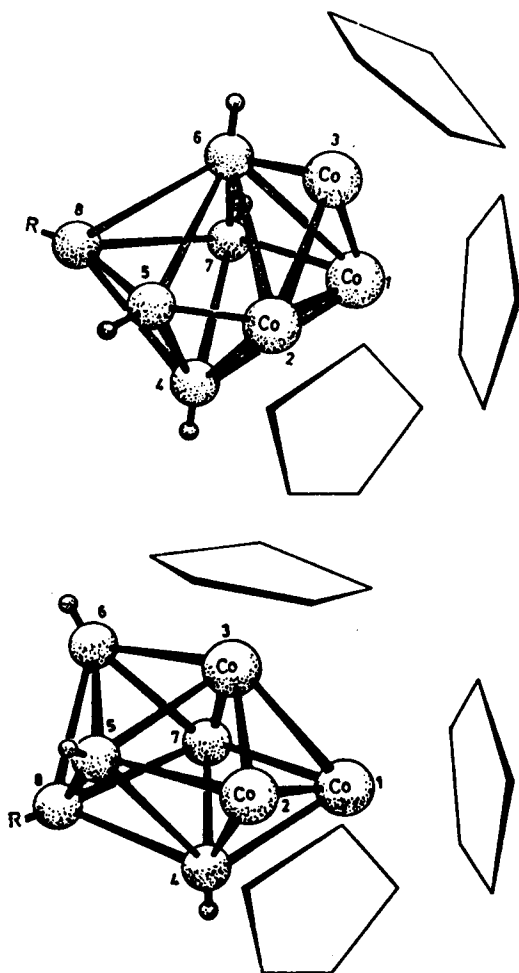


FIG. 30. Two possible structures for (CpCo)$_3$B$_5$H$_5$.

cobalt. This resonance collapses to a singlet and shifts to lower frequency in the cyclopentenyl compound, indicating that the assignment is correct.[111]

The pentamethylcyclopentadienylcobalt carboranes $(Me_5CpCo)$-$Me_2B_4C_2H_4$, $1,7,2,3$-$(Me_5CpCo)_2Me_2B_3C_2H_3$, and $(Me_5CpCo)$-$Me_2B_3C_2H_5$ have recently been reported. Their ^{11}B NMR spectra appear to parallel those of the corresponding cyclopentadienyl analogues.[112]

## XIX. RHODA- AND IRIDA-CARBORANES

Insertion of Rh(I) into $B_7C_2H_{12}^-$ gives $(Ph_3P)_2Rh(H)$-$6,2,3$-$B_7C_2H_9$. The proton decoupled ^{11}B NMR spectrum of this compound exhibits a $1:2:2:1:1$ pattern of resonances (see Table 31). Although no signal in

TABLE 31

^{11}B NMR data for rhodacarboranes.

| Compound | $\delta^{11}B$ ($J_{BH}$) |
|---|---|
| $(Ph_3P)_2Rh(H)$-$6,2,3$-$B_7C_2H_9$ | 23·6 (1B), −5·9 (2B), −19·5 (2B), −22·1 (1B), −33·6 (1B) |
| $[(p\text{-}tol)_3P]_2Rh(H)$-$6,2,3$-$B_7C_2H_9$ | 22·9 (1B), −7·3 (2B), −20·5 (3B), −34·0 (1B) |
| $(Ph_3P)_2Ir(H)$-$6,2,3$-$B_7C_2H_9$ | −8·5, −22·0, −22·4 |
| $(Ph_3P)_2Ir(H)$-$1,2,4$-$B_8C_2H_{10}$ | 55·2 (1B), 10·1 (1B), 2·7 (1B), −6·0 (1B), <br> −11·2 (1B), −24·8 (2B), −45·0 (1B) |
| $(PhPMe_2)_2Ir(H)$-$1,2,4$-$B_8C_2H_{10}$ | 53·6 (1B), 8·6 (1B), 1·4 (1B), −8·3 (1B), <br> −13·9 (1B), −22·8 (1B), −28·2 (1B), −46·5 (1B) |
| $(PhAsMe_2)_2Ir(H)$-$1,2,4$-$B_8C_2H_{10}$ | 51·9 (1B), 9·4 (1B), −0·4 (1B), −7·6 (1B), <br> −13·6 (1B), −23·7 (1B), −28·5 (1B), −47·8 (1B) |
| $(PhAsMe_2)_3Rh$-$9,7,8$-$B_8C_2H_{11}$ | 13·2 (2B), −3·3 (1B), −13·1 (2B), −18·4 (1B), <br> −22·6 (1B), −25·2 (1B) |
| $(PhPMe_2)_3Rh$-$9,7,8$-$B_8C_2H_{11}$ | 12·2 (2B), −3·9 (1B), −12·8 (2B), −18·5 (1B), <br> −22·4 (1B), −25·2 (1B) |
| $(Me_3P)_3Rh$-$9,7,8$-$B_8C_2H_{11}$ | 12·6 (1B), 9·3 (1B), 5·1 (1B), −13·4 (1B), <br> −15·2 (1B), −18·1 (1B), −22·2 (1B), −27·2 (1B) |
| $(Me_3As)_3Rh$-$9,7,8$-$B_8C_2H_{11}$ | 12·5 (1B), 10·2 (1B), −4·6 (1B), 14·6 (2B), <br> −18·6 (1B), −23·1 (1B), −27·7 (1B) |
| $(Me_3Sb)_3Rh$-$9,7,8$-$B_8C_2H_{11}$ | 10·7 (1B), 9·6 (1B), −6·3 (1B), −12·9 (1B), <br> −15·1 (1B), −18·7 (1B), −22·7 (1B), −26·5 (1B) |
| $(Ph_3P)_2Rh$-$9,7,8$-$B_8C_2H_{11}$ | 12·9, 1·4, −17·9, −20·5 |
| $[(p\text{-}tol)_3P]_2Rh$-$9,7,8$-$B_8C_2H_{11}$ | 13·3, 1·0, −18·3, −20·8 |
| $[(p\text{-}tol)_3P]_2Rh(CO)$-$9,7,8$-$B_8C_2H_{11}$ | 13·7 (2B), 0·8 (1B), −10·8 (2B), −18·1 (1B), <br> −21·3 (1B), −22·7 (1B) |
| $(Et_3P)_3Rh$-$9,7,8$-$B_8C_2H_{11}$ | 9·4 (2B), −7·3 (1B), −13·7 (1B), −18·5 (2B), <br> −22·6 (1B), −27·4 (1B) |
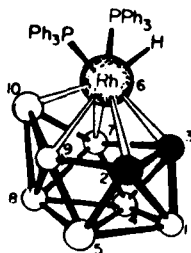
FIG. 31. Proposed structure of $(Ph_3P)_2Rh(H)$-6,2,3-$B_7C_2H_9$.

the 140–80 ppm region, which might be associated with a low-coordinate boron bonded to a first-row cage metal atom, is observed, the ten-vertex structure shown in Fig. 31 is suggested. Proton NMR studies indicate that the triphenylphosphine ligands dissociate in solution, so the spectrum observed may contain contributions from $(Ph_3P)Rh(H)$-6,2,3-$B_7C_2H_9$.[113]

Reaction of $NaB_8C_2H_{11}$ with $IrClL_2$ (L = $PhPMe_2$, $PhAsMe_2$) produces $L_2Ir(H)$-1,2,4-$B_8C_2H_{10}$ which can be regarded as a $B_8C_2H_{10}$ complex of octahedral Ir(III). In these compounds, the resonance at ~50 ppm is attributed to the low-coordinate boron atom next to iridium. A similar reaction with $RhClL_3$ yields instead $L_3$-9,7,8-$RhB_8C_2H_{11}$. Eight doublets are observed in the best resolved ^{11}B NMR spectra, those of the $PMe_3$ and $SbMe_3$ derivatives (Table 31). For steric reasons, only two triphenylphosphine ligands can be accommodated at the rhodium atom, and use of this ligand leads to $(Ph_3P)_2Rh$-9,7,8-$B_8C_2H_{11}$. Unfortunately, the ^{11}B NMR spectrum of this compound contains broad, poorly resolved peaks, so it is not possible to probe the effect of adding extra electron density to the cage rhodium atom. The solution chemistry of *nido*-$(Et_3P)_3Rh$-9,7,8-$B_8C_2H_{11}$ is complex and summarized in Fig. 32. In the tris(triethylphosphine) complex, the "extra" hydrogen is suggested to occupy a bridging position between B(10) and B(11). Dissociative loss of 1 equivalent leads to $(Et_3P)_2Rh$-9,7,8-$B_8C_2H_{11}$ which is *closo*-$(Et_3P)_2Rh(H)$-1,2,4-$B_8C_2H_{10}$. The rearrangement involves a shift of the "extra" hydrogen from a B–B edge to a terminal position on rhodium with concomitant cage closure. Variable temperature ^{11}B{^{1}H} and ^{31}P NMR data have been used to determine $\Delta H°$ for the process.[114]

Triphenylphosphine complexes of metallo-boranes and -carboranes frequently exhibit broad, structureless [11]B resonances. $(Et_3P)_2Rh(H)$-3,1,2-$B_9C_2H_{11}$ has been prepared by *in situ* phosphine exchange with the more easily prepared triphenylphosphine analogue. This greatly improves resolution in the ^{11}B NMR spectrum, possibly because of an increase in the rate of molecular tumbling and an increase in $T_1$. The decreased linewidths have facilitated an assignment of the 111·8 MHz ^{11}B NMR spectrum of
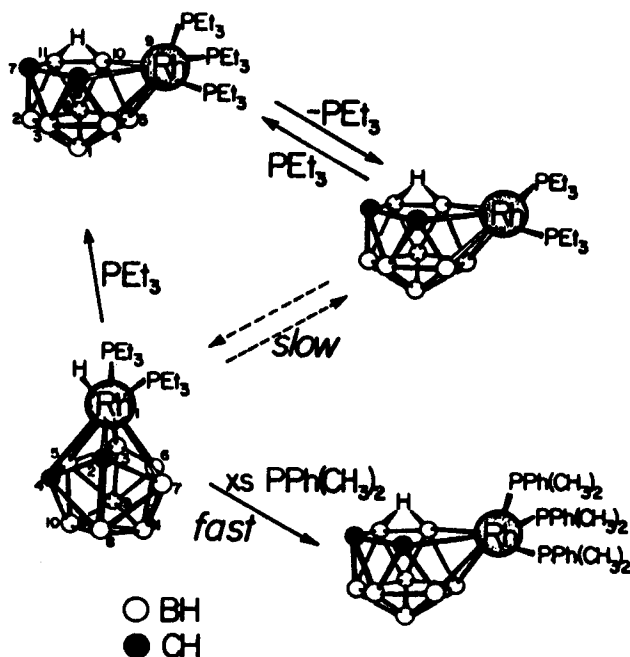
FIG. 32. Solution equilibria involving $(Et_3P)_3Ir\text{-}9,7,8\text{-}B_8C_2H_{11}$.

the rhodacarborane.[115] Its structure is probably very similar to that of the precursor, which features a regular icosahedron with the rhodium atom symmetrically bonded to the $B_3C_2$ pentagonal face.[116] The high resolution ^{11}B NMR contains five resonances of relative areas $1:1:2:2:3$. The implied increase in symmetry over that in the solid state is attributed to rapid rotation of the $(Et_3P)_2Rh$ vertex. Use of deuterium and bromine labelled derivatives leads to a complete assignment: $\delta$ −2·8 (d, B(10), 130), −3·9 (d, B(8), 115), −9·0 (d, B(9,12), 140), −10·9 (d, B(4,7), 100), and −21·1 (d, B(5,6,11), 150). The chemical shifts are, with the exception of that of B(6), to lower frequency than in $(B_9C_2H_{11})_2Co^-$. In the cobaltacarborane, the assignments, reading from high to low frequency, are B(8), B(10), B(9,12), B(4,7), B(5,11), and B(6); thus, the relative shifts of B(8) and B(10) are inverted.[117] Note that, for the sake of consistency, the numbering system used (Fig. 33) is that employed in the earlier literature and which is no longer fashionable.

Recently, the ^{11}B NMR spectrum of the rhodaborane catalyst $(Ph_3P)\text{-}(NO_3)Rh\text{-}3,1,2\text{-}B_9C_2H_{11}$ has been reported. In chloroform it has $\delta$ 11·8 (d, 2B), −3·1 (d, 4B), −9·2 (d, 2B), and −25·7 (d, 1B).[118] The spectrum of $(Ph_3P)_2Rh(HSO_4)\text{-}3,1,2\text{-}B_9C_2H_{11}$ contains two broad humps centred at −9 and +5 ppm.[119]
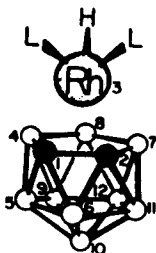
FIG. 33. Numbering system for $(Ph_3P)_2Rh(H)$-3,1,2-$B_9C_2H_{11}$.

## XX. NICKELABORANES

Reaction of $B_{11}H_{13}^-$ with sodium amalgam and $Cp_2Ni$ yields $CpNiB_{11}H_{11}^-$. The ^{11}B NMR spectrum of this ion contains three doublets at 19·9, 16·0, and −5·1 ppm in a 1:5:5 ratio, supporting the suggested structure, an icosahedral $B_{11}Ni$ cage. From $B_{10}H_{14}$ and $Cp_2Ni$ was obtained $CpNiB_{10}H_{13}$ which could be deprotonated to form $CpNiB_{10}H_{12}^-$. The ^{11}B NMR spectra of these nickelaboranes resemble that of $[(B_{10}H_{12})_2Ni]^{2-}$ and their suggested structure features a similar $\eta_2$-$B_{10}H_{12}$ cage bonded to CpNi. The bimetallic $Cp_2NiCoB_{10}H_{10}^-$ is produced by insertion of a CpCo unit into $CpNiB_{10}H_{12}^-$. It is believed to be the 1,2-isomer (i.e. the metal atoms are adjacent) on the basis of the 2:1:3:2:2 pattern of doublets in the 80·6 MHz ^{11}B NMR spectrum.

Metal insertion into $B_9H_{12}^-$ produces isomeric 1- and 2-$CpNiB_9H_9^-$. The 1:4:4 pattern of doublets in the ^{11}B NMR spectrum of the 1-isomer defines the cage geometry as a bicapped square antiprism with an apical CpNi unit. The other apical position is occupied by a boron atom and this position is strongly deshielded, $\delta$ 78·6, possibly owing to an antipodal effect of nickel. The antipodal boron in $CpNiB_{11}H_{11}^-$, however, has $\delta$ 19·9 and does not appear to be so strongly deshielded. In this regard it is curious that the antipodal boron positions in $Cp_2NiCoB_{10}H_{10}^-$ are not resolved; the highest frequency resonance appears at $\delta$ 45·7 (2B).

Nickel insertion into $B_{10}H_{10}^{2-}$ gives 1,2-$(CpNi)_2B_{10}H_{10}$. The placement of the nickel atoms in the adjacent 1 and 2 positions is indicated by the 1:1:2:1 pattern of doublets in the ^{11}B NMR spectrum in glyme and by the doublet of relative area 2 at 54·3 ppm. ^{11}B NMR data for these compounds are given in Table 32.[120]

Condensation of $B_5H_8^-$, $NiBr_2$, and $C_5H_5^-$ leads to a remarkable series of nickelaboranes. Icosahedral $(CpNi)_2B_{10}H_{10}$ could be either the 1,2- or the 1,7-isomer. 1,6-$(CpNi)_2B_8H_8$ presumably adopts a *closo* ten-vertex geometry [Fig. 34(A)]; placement of the metal atoms in the 1,6 positions

## TABLE 32

**$^{11}$B NMR data for nickelaboranes.**

| Compound | $\delta^{11}$B $(J_{BH})$ |
|---|---|
| $Me_4N(CpNiB_{11}H_{11})$ | 19·9 (1B), 16·0 (5B), −5·1 (5B) |
| $CpNiB_{10}H_{13}$ | 10·5 (3B), 4·8 (1B), 5·8 (1B), −6·7 (3B), −26·9 (2B) |
| $Me_4N(CpNiB_{10}H_{12})$ | 11·8 (3B), 6·4 (2B), −6·0 (3B), −26·9 (2B) |
| $Ph_4As(Cp_2NiCoB_{10}H_{10})$ | 45·7 (2B), 19·8 (1B), 10·7 (3B), 7·9 (2B), −5·2 (2B) |
| $1,2\text{-}(CpNi)_2B_{10}H_{10}$ | −4·3 (2B), 26·1 (2B), 21·3 (4B), 6·7 (2B) |
| $Me_4N(2\text{-}CpNiB_9H_9)$ | 59·0 (1B), 12·6 (1B), 6·9 (3B), −14·7 (2B), −21·8 (2B) |
| $Me_4N(1\text{-}CpNiB_9H_9)$ | 78·6 (1B), 29·0 (4B), −1·3 (4B) |
| $Me_4N(2\text{-}CpNiB_9Cl_9)$ | 60·5 (1B), 18·2 (1B), 12·4 (3B), −0·6 (2B), −11·1 (2B) |
| $Me_4N(1\text{-}CpNiB_9Cl_9)$ | 54·3 (1B), 38·5 (4B), 18·4 (4B) |
| $1,7\text{-}(CpNi)_2B_{10}H_{10}$ | 38·9 (d, 4B, 149), 20·3 (d, 4B, 149), −3·9 (d, 2B, 151) |
| $1,6\text{-}(CpNi)_2B_8H_8$ | 93·6 (d, 1B, 145), 47·5 (d, 2B, 147), 20·4 (d, 2B, 145), 12·2 (d, 1B, 140), 6·7 (d, 2B, 137) |
| $(CpNi)_4B_4H_4$ | 56·2 (d, 156) |
| $1,6,7,8\text{-}(CpNi)_4B_5H_5$ | 64·7 (d, 2B, 156), 55·0 (d, 1B, 157), 29·4 (d, 2B, 117) |
| $(CpNi)_2Me_2B_4C_2H_4$ | 24·6 (d, 2B, 166), 3·2 (d, 2B, 156) |
| $(CpNi)_2Me_2B_5C_2H_5$ | 30·1 (d, 1B, 146), 1·2 (d, 2B, 156), −2·8 (d, 2B, 127) |

is indicated by a doublet of unit area at 93·6 ppm, due to a four-coordinate boron atom adjacent to two nickel atoms.

$(CpNi)_4B_4H_4$ is an eight-vertex 20-electron system [Fig. 34(B)] but the X-ray structure reveals that the cage has nearly $D_{2d}$ dodecahedral geometry. The nickel atoms occupy the four low-coordinate positions and the compound shows one resonance at 56·2 ppm in its $^{11}$B NMR spectrum. In contrast, the cobalt atoms in $(CpCo)_4B_4H_4$ occupy the five-coordinate positions and the equivalent boron nuclei have $\delta$ 121·4 (d, 137). The
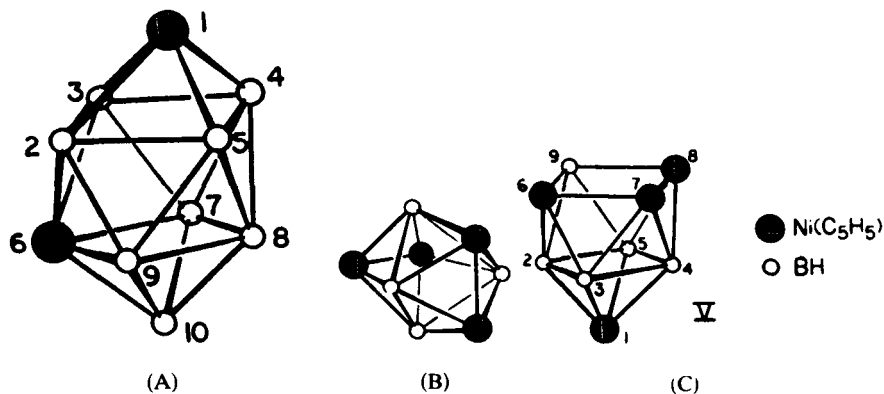


FIG. 34. (A) Proposed structure of $1,6\text{-}(CpNi)_2B_8H_8$. Established structures of (B) $(CpNi)_4B_4H_4$ and (C) $(CpNi)_4B_5H_5$.

tetrametallic $(CpNi)_4B_5H_5$ adopts a nine-vertex monocapped square antiprismatic *nido* structure [Fig. 34(C)], and the ^{11}B NMR spectrum contains three doublets at 64·7 (2B), 55·0 (1B), and 29·4 (2B) ppm in agreement with this. The nickelacarboranes $(CpNi)_2Me_2B_4C_2H_4$ and $(CpNi)_2Me_2B_5C_2H_5$ are also prepared by nickel insertion.[121]

## XXI. PLATINABORANES

Metal insertion into $2,3-B_4C_2H_8$ or $2-B_5CH_9$ using $Pt_2(cod)(PEt_3)_4$ (cod = cycloocta-1,5-diene) yields the *nido* platinaboranes $(Et_3P)_2Pt(H)-2,3-B_4C_2H_7$ and $(Et_3P)_2Pt(H)-2-B_5CH_8$ respectively, whose ^{11}B NMR spectra are summarized in Table 33. A crystal structure of the former compound demonstrates the essential preservation of the pyramidal pentagonal cage structure with the $(Et_3P)_2Pt(H)$ moiety bridging one of the B–B edges [Fig. 35(A)]. In the 32 MHz ^{11}B NMR spectra (Table 33) the basal boron resonances are broad, and only two signals for these positions are seen; the apical positions occur at much lower frequency, ~50 ppm.[122] Loss of dihydrogen occurs to give *closo*-1-$(Et_3P)_2Pt-2,3-Me_2-2,3-B_4C_2H_4$. The ^{11}B NMR data show that this compound, whose structure is depicted in Fig. 35(B), is not isostructural with $(Et_3P)_2PtB_4C_2H_6$ in which the equatorial carbon atoms are probably non-adjacent.[123] Similarly prepared from $5,6-B_8C_2H_{12}$ is $(Et_3P)_2Pt(H)-7,8,9-B_8C_2H_{11}$ which undergoes de-

## TABLE 33

### ^{11}B NMR data for some platinaboranes.

| Compound | $\delta^{11}B$ ($J_{BH}$) |
|---|---|
| $(Et_3P)_2Pt(H)-2,3-$ $B_4C_2H_7$ | 0·5 (br, 2 basal B), −9·2 (br, 1 basal B), −52·3 (d, 1B, 168) |
| $(Et_3P)_2Pt(H)-2,3-$ $Me_2-2,2-B_4C_2H_5$ | −1·5 (d, 2B), −10·9 (d, 1B), −45·6 (d, 1B, 159) |
| $(Et_3P)_2Pt(H)-2-B_5CH_8$ | 14·9 (d, 2 basal B), −5·6 (d, 2 basal B), −50·5 (d, apical B) |
| $(Et_3P)_2Pt-2,4-B_4C_2H_6$ | 7·4 (1B), −1·8 (3B) |
| $(Et_3P)_2Pt-2,3-$ $Me_2-2,3-B_4C_2H_4$ | 6·3 (3B), −50·3 (1B) |
| $(Et_3P)_2Pt(H)-$ $7,8,9-PtB_8C_2H_{11}$ | 8·9, −11·9, −22·2, −26·8 |
| $(Et_3P)_2Pt-7,8,9-$ $PtB_8C_2H_{10}$ | 8·8, 0·6, −13·7, −22·5 (100 °C in $C_6D_6$) |
| $(Ph_3P)_2PtB_8SH_{10}$ | 38 (d, 1B), 4·6 (d, 1B), −6·7 (d, 2B), −17 (d, 2B), −25·5 (d, 2B) |
| $(PhMe_2)_2PtB_8SH_{10}$* | 36·8 (d, 1B, 130), 3·7 (d, 1B, 130), −5·1 (d, 2B, 116), −21·6 (d, 2B, 113), −27·0 (d, 2B, 142) |
| $(Et_3P)_2PtSB_8H_{10}$ | 38 (d, 1B), 4·2 (d, 1B), −5·1 (d, 2B), −21·5 (d, 2B), 26 (d, 2B) |
| $(Ph_3P)_2Pt(8-EtOB_8SH_9)$ | 36·1 (1B), 7·7 (2B), −5·5 (2B), −13·3 (1B), 23 (1B), 26·1 (1B) |

* Recorded at 86·6 MHz.
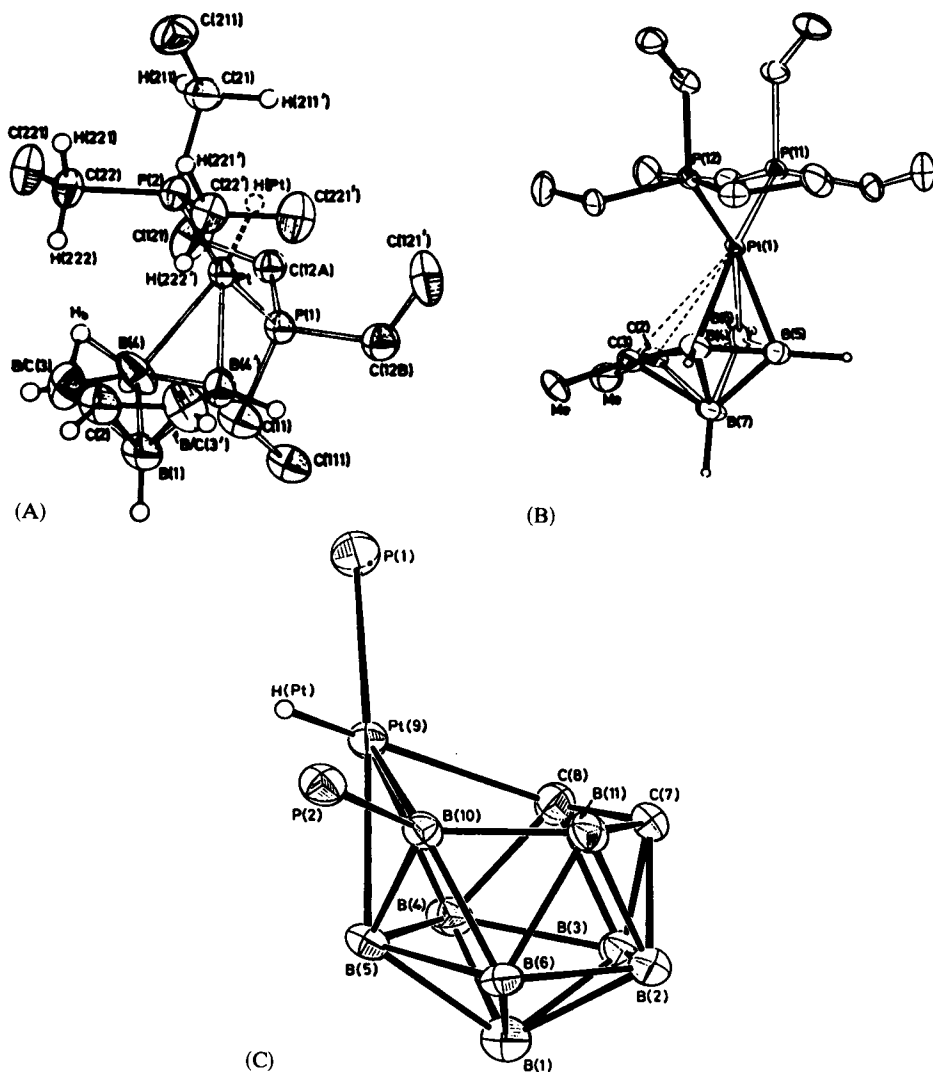
FIG. 35. Molecular structure of (A) nido-(Et₃P)₂Pt(H)-2,3-B₄C₂H₆, (B) closo-(Et₃P)₂Pt-2,3-Me₂-2,3-B₄C₂H₄, and (C) (Et₃P)₂Pt(H)-7,8,9-B₈C₂H₉.

hydrogenation and cage closure to yield $(Et_3P)_2Pt-7,8,9-B_8C_2H_9$; a singular feature of this reaction is the shift of one triethylphosphine from platinum to B(10), as indicated in Fig. 35(C). No P–B spin coupling has been reported.[124]

Reaction of $1-B_9SH_9$ with $(R_3P)_4Pt$ in refluxing ethanol leads to elision of one boron atom and the formation of nido platinathiaboranes of the type $(R_3P)_2PtB_8SH_{10}$, but use of $(Ph_3P)_2Pt(C_2H_4)$ affords $(Ph_3P)_2Pt(8-EtOB_8SH_9)$. An X-ray crystal structure (Fig. 36) determination of the
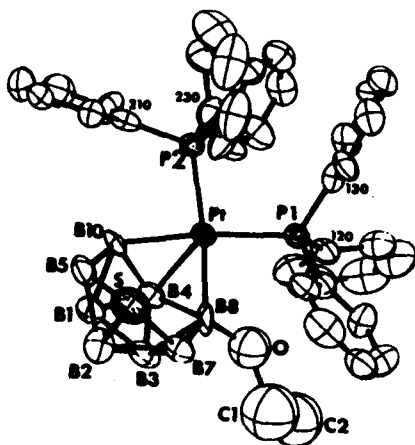
FIG. 36. Structure of $(Ph_3P)_2Pt(8\text{-}EtOB_8SH_9)$.

8-ethoxy substituted compound shows that the platinum is bonded to the cage boron atoms in a $\eta_3$ fashion. The bridge hydrogen atoms are not located but evidence for their presence is found in the $^1H$ NMR spectrum where they appear at $-1$ to $-2$ ppm. The boron resonances are broad, possibly complicated by $^{195}Pt\text{-}^{11}B$ coupling, and do not provide clear evidence for B–H–B units. The chemical shifts are listed in Table 33.[125]

## XXII. METALLOPENTABORANES

A large class of metallopentaboranes of the type $(ligand)_n MX(B_5H_8)$ containing Pd, Pt,[126] has been prepared from $B_5H_8^-$ and a metal halide complex. $^{11}B$ NMR data for these compounds are summarized in Table 34. In these metallopentaboranes, the metal is considered to bridge two adjacent basal boron atoms. This structural paradigm has been verified by X-ray crystallography in the case of $(B_5H_8)Cu(PPh_3)_2$ in which all borane hydrogens are located.[130] It should be noted that a structure featuring two metal–H–B bridges may exist in solution; movement of hydrogens from B–B to B–metal edges would not perturb the molecular symmetry, and it might be difficult to detect in low-resolution $^{11}B$ NMR spectra obtained at $\sim$27 °C. In the cadmium and silver $B_5H_8$ derivatives, the signals from the non-equivalent pairs of basal boron atoms are resolved in the 29 MHz spectra. Comparison with the chemical shift data for pure pentaborane(9) suggests that the higher frequency of the basal boron resonance is due to the boron atoms being bonded to the metal. In the transition metal series,

## TABLE 34

### $^{11}$B NMR data for metallopentaboranes.

| Compound | $\delta^{11}$B ($J_{BH}$) |
|---|---|
| $(B_5H_8)PdCl(Ph_2PC_2H_4PPh_2)$ | $-47\cdot6$ (d, 1B, 160), $-12\cdot5$ (br d, 4B) |
| $cis$-$(B_5H_8)PdCl(PPh_3)_2$ | $-46\cdot1$ (d, 1B, 165), $-13\cdot0$ (br d, 4B) |
| $cis$-$(B_5H_8)PdCl(PPh_2Me)_2$ | $-45\cdot7$ (d, 1B, 150), $-13\cdot2$ (br d, 4B) |
| $(B_5H_8)PtCl(Ph_2PC_2H_4PPh_2)$ | $-44\cdot1$ (d, 1B, 160), $-12\cdot1$ (br s, 4B) |
| $cis$-$(B_5H_8)PtCl(PPh_3)_2$ | $-46\cdot4$ (d, 1B, 160), $-12\cdot9$ (br s, 4B) |
| $cis$-$(B_5H_8)PtCl(PPh_2Me)_2$ | $-45\cdot1$ (d, 1B, 160), $-11\cdot6$ (br s, 4B) |
| $cis$-$(B_5H_8)PtCl(PMe_3)_2$ | $-51\cdot0$ (d, 1B, 155), $-15\cdot5$ (br s, 4B) |
| $(B_5H_8)PtBr(Ph_2PC_2H_4PPh_2)$ | $-46\cdot1$ (d, 1B, 160), $-13\cdot6$ (br s, 4B) |
| $cis$-$(B_5H_8)PtBr(PPh_3)_2$ | $-48\cdot3$ (d, 1B, 155), $-14\cdot3$ (br s, 4B) |
| $cis$-$(B_5H_8)PtBr(PPhMe_2)_2$ | $-49\cdot1$ (d, 1B, 155), $-15\cdot0$ (br s, 4B) |
| $(B_5H_8)PtI(Ph_2PC_2H_4PPh_2)$ | $-47\cdot8$ (d, 1B, 155), $-12\cdot6$ (br s, 4B) |
| $cis$-$(B_5H_8)PtI(PPh_3)_2$ | $-49\cdot0$ (d, 1B, 160), $-12\cdot3$ (br s, 4B) |
| $cis$-$(B_5H_8)PtI(PPhMe_2)_2$ | $-50\cdot0$ (d, 1B, 155), $-14\cdot7$ (br s, 4B) |
| $cis$-$(B_5H_8)PtMe(PPhMe_2)_2$ | $-48\cdot3$ (d, 1B, 150), $-14\cdot3$ (br s, 4B) |
| $cis$-$(B_5H_8)PtCl(AsPh_3)_2$ | $-46\cdot3$ (d, 1B, $\sim$140), $-13\cdot8$ (br s, 4B) |
| $trans$-$(B_5H_8)PtI(PPh_3)_2$ | $-47\cdot1$ (d, 1B, 150), $-14\cdot5$ (br s, 4B) |
| $trans$-$(B_5H_8)PtMe(PPhMe_2)_2$ | $-48\cdot8$ (d, 1B, 160), $-12\cdot8$ (br s, 4B) |
| $cis$-$[(B_5H_8)Pt(\mu\text{-}SMe)(PPhMe_2)]_2$ | $-49\cdot1$ (d, 1B, 160), $-15\cdot1$ (br s, 4B) |
| $(B_5H_8)Cu(PPh_3)_2$ | $-49\cdot1$ (d, 1B, 146), $-14\cdot3$ (br s, 4B) |
| $(1\text{-}BrB_5H_7)Cu(PPh_3)_2$ | $-42\cdot5$ (s, 1B), $-14\cdot6$ (br s, 4B) |
| $(B_5H_8)Cu(Ph_2PC_2H_4PPh_2)$ | $-46\cdot6$ (d, 1B, 145), $-13\cdot6$ (br s, 4B) |
| $(B_5H_8)Ag(PPh_3)_2$ | $-48\cdot0$ (d, 1B, 140), $-14\cdot0$ (d, 2B, $\sim$130), $-8\cdot0$ (d, 2B, $\sim$130) |
| $(B_5H_8)CdCl(PPh_3)_2$ | $-51\cdot5$ (d, 1B, 160), $-13\cdot8$ (d, 2B, $\sim$150), $-9\cdot4$ (d, 2B, $\sim$150) |
| $(1\text{-}BrB_5H_7)CdCl(PPh)_3$ | $-45\cdot2$ (s, 1B), $-14\cdot2$ (d, 2B, $\sim$145), $-9\cdot6$ (d, 2B, $\sim$145) |
| $(B_5H_8)NiCl(Ph_2PC_2H_4PPh_2)$ | $-44\cdot1$ (d, 1B, 150), $-12\cdot5$ (d, 4B, 160) |
| $(1\text{-}BrB_5H_7)NiCl(Ph_2PC_2H_4PPh_2)$ | $-38\cdot5$ (s, 1B), $-12\cdot6$ (d, 4B, 155) |
| $(B_5H_8)NiBr(Ph_2PC_2H_4PPh_2)$ | $-44\cdot4$ (d, 1B, 155), $-12\cdot6$ (d, 4B, 155) |
| $(1\text{-}BrB_5H_7)NiBr(Ph_2PC_2H_4PPh_2)$ | $-38\cdot1$ (s, 1B), $-12\cdot9$ (d, 4B, 158) |
| $(B_5H_8)NiI(Ph_2PC_2H_4PPh_2)$ | $-45\cdot0$ (d, 1B, 155), $-12\cdot0$ (d, 4B, 155) |
| $(1\text{-}BrB_5H_7)NiI(Ph_2PC_3H_4PPh_2)$ | $-37\cdot8$ (s, 1B), $-13\cdot0$ (d, 4B, 150) |
| $(B_5H_8)NiBr(Ph_2PC_3H_6PPh_2)$ | $-45\cdot6$ (d, 1B, 150), $-13\cdot0$ (d, 4B, 155) |

the linewidths of the high-frequency peaks increase in the order $Ni < Pd <$ Pt, and in the case of $cis$-$(B_5H_8)PtCl(PPh_3)_2$ it also increases on cooling. More recently, the 64 MHz $^{11}$B NMR$_n$ spectrum of $(B_5H_8)$-$PtCl(Ph_2PC_2H_4PPh_2)$ has been obtained. In it, the signals from the basal positions are resolved with $\delta^{11}$B $-11\cdot3$ and $-13\cdot7$ ($\pm1\cdot0$) ppm; $T_1$ values are short, $\sim$1 ms.[131]

Structurally different metallopentaboranes, $2\text{-}B_5H_8Fe(Cp)(CO)_2$ and $2,4\text{-}B_5H_8[Fe(Cp)(CO)_2]_2$, are obtained from $B_5H_9$ by successive

deprotonation and treatment with $CpFe(CO)_2I$. These compounds may be considered as derivatives of pentaborane(9) having exopolyhedral iron–boron $\sigma$ bonds. The $^{11}B$ NMR data are collected in Table 35.[132]

TABLE 35

$^{11}B$ NMR data for iron-substituted pentaboranes.

| 2-$B_5H_8F_e$(Cp)(CO)$_2$ | | 2,4-$B_5H_7$[Fe(Cp)(CO)$_2$]$_2$ | |
|---|---|---|---|
| Position | $\delta^{11}B(J_{BH})$ | Position | $\delta^{11}B(J_{BH})$ |
| 1 | −48·5 (170) | 1 | −45·0 (168) |
| 2 | 7·9 (0) | 2, 4 | 1·4 (0) |
| 3, 4 | −10·6 (150) | 3, 5 | −8·6 (127) |
| 5 | −14·3 (160) | | |

## XXIII. TETRACARBON CARBORANES AND METALLOCARBORANES

The tetracarbon carborane $Me_4B_8C_4H_8$ is derived from the air oxidation of $(Me_2B_4C_2H_4)_2Co$ [133] or $(Me_2B_4C_2H_4)_2FeH_2$,[134] and this unusual material is now fairly readily available. It has a distinct and substantive chemistry, primarily centred about metal insertion products. A critical feature of $C_4$ metallocarboranes is that, whilst electron counting rules predict gross geometries, they are silent about many subtle structural features which must be elucidated by X-ray diffraction studies. It is a long-range hope that $^{11}B$ NMR data obtained at very high fields can be correlated with X-ray data and be used to directly deduce solution phase structures.

Reduction of $Me_4B_8C_4H_8$ produces $Me_4B_8C_4H_8^{2-}$ into which one or two metal atoms can be inserted. $^{11}B$ NMR data for the dianion and related metallocarboranes are collected in Table 36. The $^{11}B$ NMR spectrum of $Na_2(Me_4B_8C_4H_8)$ in $CD_3CN$ contains signals at $\delta$ −1·7 (2B), −13·3 (2B), −22·9 (2B), and −38·6 (2B). Taken by itself, this spectrum could be interpreted in terms of a static structure having a mirror plane of symmetry. However, the distribution of metallocarboranes derived from $Me_4B_8C_4H_8^{2-}$ suggests that the dianion is actually a mixture of rapidly interconverting isomers; indeed, neutral $Me_4B_8C_4H_8$ itself is known to be fluxional. Unfortunately, low solubility of the sodium salt precludes determination of the low temperature $^{11}B$ NMR spectrum but such a study on another salt would be of great interest.

Iron insertion into $Me_4B_8C_4H_8$ produces $CpFeMe_4B_7C_4H_8$ and three isomers of $(CpFe)_2Me_4B_8C_4H_8$; nickel insertion yields three isomers of

## TABLE 36

$^{11}$B NMR data for tetracarbon carboranes and metallocarboranes.

| Compound | $\delta^{11}B$ ($J_{BH}$) |
|---|---|
| $Me_4B_8C_4H_8$ (isomer A) | 9·2 (2B), 8·4 (2B), −22·4 (2B), −29·5 (2B) |
| $Na_2Me_4B_8C_4H_8$ (CD$_3$CN) | −1·7 (2B), −13·3 (2B), −22·9 (2B), −38·6 (2B) |
| $(CpFe)_2Me_4B_8C_4H_8$ | |
|   isomer 1 | 38·5 (d, 1B, 156), ~26·6 (d, 1B, 127), <br> ~22·7 (d, 2B, 137), ~19·0 (d, 1B, 137), <br> 12·9 (d, 1B, 180), −3·8 (d, 1B, 157), <br> −18·7 (d, 1B, 136) |
|   isomer 2 | 9·3 (d, 2B, 160), 2·3 (d, 2B), −1·6 (d, 3B), <br> −12·5 (d, 1B) |
|   isomer 3 | 5·0 (d, 3B), −3·5 (d), −8·9 (d), −23·9 (d) |
|   isomer 4 | 24·1 (d, 1B, 137), 19·9 (d, 1B, 185), <br> 13·4 (d, 1B, 157), 9·2 (d, 1B, 127), <br> 5·5 (d, 2B, 136), 2·7 (d, 1B, 115), <br> −12·4 (d, 1B, 156) |
|   isomer 5 | −12·8 (d, 1B, 145), −17·5 (d, 2B, 146), <br> −19·7 (d, 1B, 186) |
|   isomer 6 | −18·0 (d, 152) |
| $CpFeMe_4B_7C_4H_8$ | 5·4 (d, 2B, 166), −0·1 (d, 1B, 168), <br> −6·2 (d, 1B, 175), −15·0 (d, 1B, 160), <br> −25·0 (d, 2B, 146) |
| $(Ph_2PC_2H_4PPh_2)NiMe_4B_7C_4H_7$ | |
|   isomer 1 | 17·3 (d, 2B), 4·2 (d, 1B), −16·8 (d, 3B), <br> −26·9 (d, 1B) |
|   isomer 2 | 1·8 (d, 3B), −13·8 (d, 3B), −36·0 (d, 1B, 156) |
| $(Ph_2PC_2H_4PPh_2)NiMe_4B_8C_4H_8$ | |
|   isomer 1 | 7·5 (d, 2B), −15·0 (d, 2B), −30·5 (d, 4B) |
|   isomer 2 | 5·2 (d, 2B), −2·7 (d, 4B, 165), −17·6 (d, 2B, 157) |
|   isomer 3 | 22·1 (d, 3B), 12·4 (d, 1B), −13·8 (d, 2B), <br> −21·7 (d, 2B) |
| $(CO)_3MoMe_4B_8C_4H_8$ | 50·9 (d, 3B, 156), 43·7 (d, 1B, 176), <br> 41·0 (d, 2B, 172), 29·5 (d, 2B, 168) |
| $CpCoB_7C_4H_{11}$ | 15·8 (d, 1B, 168), 8·9 (d, 1B, 160), <br> 2·5 (d, 2B, 168), −4·5 (d, 1B, 160), <br> −8·5 (d, 1B, 168), −11·5 (d, 1B, 136) |
| $(CpCo)_2B_6C_4H_{10}$ | |
|   isomer 1 | 34·8 (d, 2B, 145), −12·4 (d, 4B, 150) |
|   isomer 2 | 69·1 (d, 2B, 155), −15·8 (d, 4B, 135) |
|   isomer 3 | 30·6 (d, 1B, 130), 21·5 (d, 1B, ~165), <br> 15·4 (d, 1B, ~136), 12·5 (d, 1B, ~155), <br> 9·9 (d, 1B, 140), −7·8 (d, 1B, 170) |
| $(CpCo)_2Me_4B_6C_4H_6$ | 30·9 (d, 2B, 137), −12·8 (d, 4B, 122) |
| $CpCoMe_4B_7C_4H_7$ | |
|   isomer 1 | 16·6 (d, 1B, 144), ~2·0 (d, 2B, ~150), <br> −3·8 (d, 1B, 140), −8·7 (d, 1B, 112), <br> −12·9 (d, 1B, 136), −18·7 (d, 1B, 144) |

## TABLE 36 (cont.)

| Compound | $\delta^{11}B\ (J_{BH})$ |
|---|---|
| isomer 2 | 23·6 (d, 1B, 156), 11·7 (d, 1B, 147), −0·8 (d, ~136) and −2·8 (d, ~137) (3B total), −17·6 (d, 1B, 146), −29·1 (d, 1B, 146) |
| isomer 3 | 12·8 (d, 2B, ~140), 11·0 (d, 1B, ~140), 3·7 (d, 2B, 137), −8·2 (d, 1B, 156), −12·7 (d, 1B, 127) |
| $CpCoMe_4B_6C_4H_6$ | |
| isomer 1 | 4·9 (d, 3B, 156), −9·7 (d, 2B, 150), −23·4 (d, 1B, 140) |
| isomer 2 | −3·0 (d, 3B, 160), −10·3 (d, 2B, 150), −32·1 (d, 1B, 140) |
| $CpCoMe_4B_8C_4H_8$ | 12·7 (d, 1B, ~112), 9·5 (d, 1B, ~146), 2·3 (d, 1B, 166), −7·5 (d, 2B, 166), −11·5 (d, 1B, 120), −15·1 (d, 1B, ~136), −18·5 (d, 1B, 127) |
| $\sigma\text{-}(CpCoC_5H_4)Me_4B_8C_4H_8$ | 14·9 (d, 1B, 150), −6·0, −11·9, −13·4 (5B), −22·2 (s, 1B), −47·2 (d, 1B, 146) |
| $Me_4(EtO)_2B_8C_4H_6$ | 1·0 (s+d, 4B), −10·0 (d, 2B, 127), −12·7 (d, 1B, 112) |
| $CpCoMe_4EtOB_7C_4H_6$ | 11·1 (d, 1B, 136), 9·1 (s, 1B), 1·2 (d, 2B, 137), −7·9 (d, 2B, 127), −16·8 (d, 1B, 136) |
| $4\text{-}CpFeC_5H_4\text{-}2,3,7,8\text{-}Me_4B_8C_4H_7$ | 7·1 (s, 1B), −4·8 (d, 3B, 150), −9·4 (d, 2B, 140), 22·4 (d, 1B, 180),−28·8 (d, 1B, 180) |
| $Me_4B_4C_4H_4$ | −12·4 (d, 2B, 138), −14·0 (d, 2B, 170) |
| $(EtC)_4(BMe)_4$ | −6·3 |

$(Ph_2PC_2H_4PPh_2)NiMe_4B_8C_4H_8$, and from $Mo(CO)_6$ is obtained $(CO)_3MoMe_4B_8C_4H_8$.[135]

The geometry and isomerization reactions of the fourteen-vertex iron compounds are particularly complex and are summarized in Fig. 37. Crystal structures of isomers 1 and 2 of $(CpFe)_2Me_4B_8C_4H_8$ have been determined.[136] Both are open-sided (nido) cages. The former has a $B_3C_2$ open face and, in isomer 2, this face is comprised of one boron, one iron, and three carbon atoms. Both of these compounds rearrange at about 170 °C to provide isomer 4 in which the BH and CMe units at positions 3 and 11 are interchanged. Finally, isomer 4 is converted at 300 °C into isomers 5 and 6. The pattern of $^{11}B$ resonances in isomer 5 is suggestive of a bicapped hexagonal antiprism with capping CpFe units; placement of the cage carbon atoms in the 2, 4, 10, and 12 positions is preferred on the basis that the span of $^{11}B$ chemical shifts is small, 7 ppm. The $^{11}B$ NMR spectrum of isomer 6 comprises one doublet. This is indicative of a $D_{2d}$ hexagonal antiprismatic geometry with the two iron atoms at the antipodal, high-coordinate vertices and the cage carbon atoms in a staggered arrangement
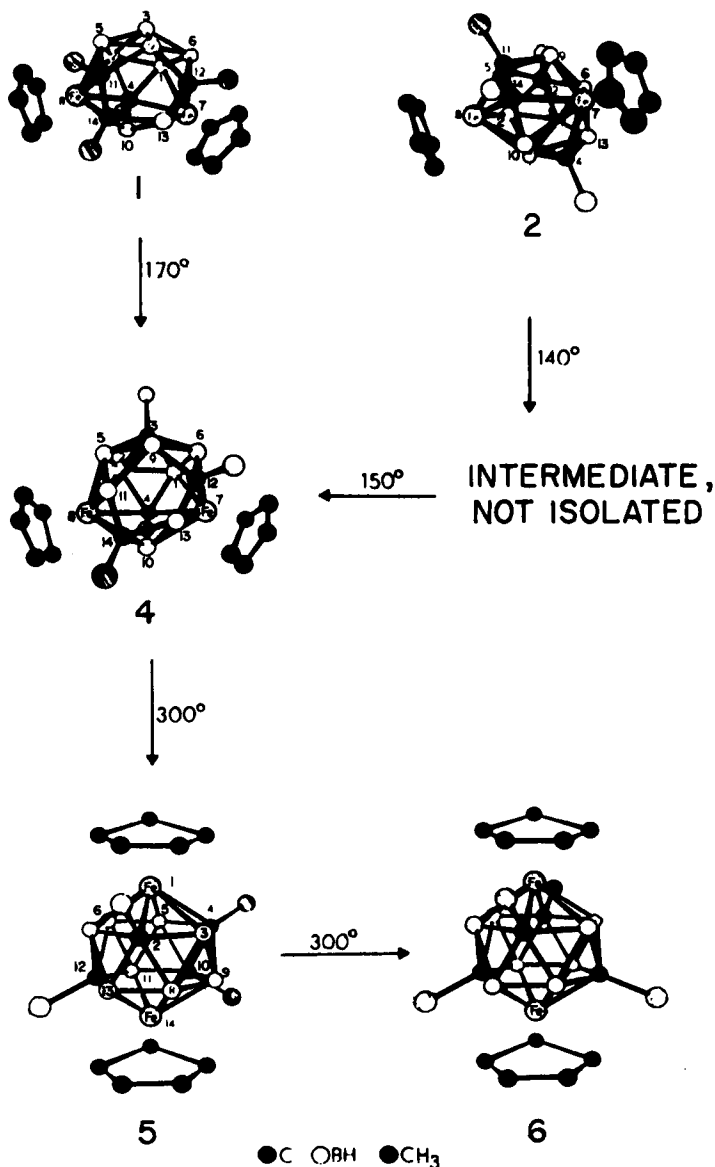
FIG. 37. Interconversion of $(CpFe)_2Me_4B_8C_4H_8$ isomers.

in the two equatorial rings. The structure suggested on the basis of NMR data has been confirmed by a single-crystal X-ray study.[137]

The structure of the nickelacarborane $(Ph_2PC_2H_4PPh_2)NiMe_4B_8C_4H_8$ has recently been described.[138] It is a thirteen-vertex *nido* cage derived

from a bicapped hexagonal antiprism with a nickel atom and a BH unit in the apical positions by removal of an equatorial vertex.

The structure of the twelve-vertex *nido* $CpFeMe_4B_7C_4H_8$ is shown in Fig. 38. The "extra" proton is located at a B–B edge in the $B_3C_3$ open face although the 32 MHz $^{11}$B NMR spectrum of the compound is not reported to show coupling between boron and the bridge proton. More highly resolved spectra and line narrowing would be helpful in assigning the facial boron atoms.
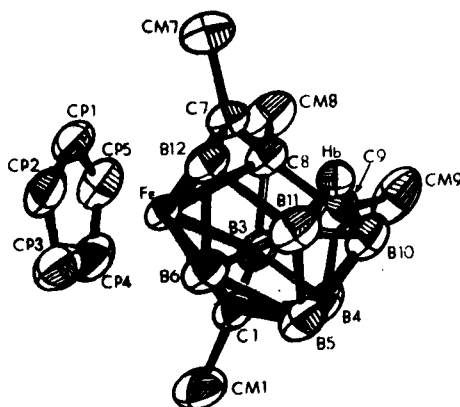


FIG. 38. Structure of $CpFeMe_4B_7C_4H_8$.

One isomer of $CpCoB_7C_4H_{11}$ and three isomers of $(CpCo)_2B_6C_4H_{10}$ are formed in an oxidative fusion reaction which takes place when *closo*-CpCo-1,2,3-$B_4C_2H_6$ or *nido*-CpCo-1,2,3-$B_3C_2H_7$ are treated with air and ethanolic potassium hydroxide, but only one isomer (see below) of $(CpCo)_2Me_4B_6C_4H_6$ is produced from the *C*-methylated starting materials. The geometry of isomer 3 of $(CpCo)_2B_6C_4H_{10}$ is approximated by a thirteen-vertex *closo* polyhedron with one vertex removed to generate a six-membered open face containing two boron atoms and four adjacent carbon atoms as shown in Fig. 39.[139] The *C*-methylated metallocarborane formed in this complex reaction is, based on examination of its $^{11}$B NMR spectrum, isostructural with isomer 1 of $(CpCo)_2B_6C_4H_{10}$, since it is likely that replacement of CH terminal hydrogen atoms by methyl groups should only slightly perturb the spectral pattern. An X-ray structure analysis of the methylated compound reveals two pentagonal pyramidal $CpCoMe_2B_3C_2H_3$ units partially fused along the $B_3C_2$ faces, so the molecule resembles a severely distorted icosahedron with a large opening on one side.[140] The $^{11}$B NMR spectrum of isomer 2 of $(CpCo)_2B_6C_4H_{10}$ contains doublets at 69·1 (2B) and −15·8 (4B) ppm, indicative of a molecule with
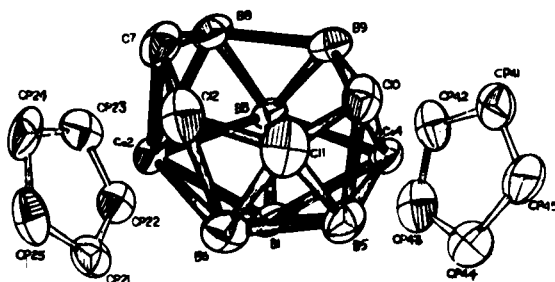
FIG. 39. Structure of $(CpCo)_2B_6C_4H_{10}$.

$C_{2v}$ symmetry and with two boron environments in a $2:4$ ratio. The resonance at $69 \cdot 1$ ppm suggests the presence of two four-coordinate B–H units adjacent to two cobalt nuclei and supports the suggested structure shown in Fig. 40.

Photochemical insertion of $CpCo(CO)_3$ into $Me_4B_8C_4H_8$ gives isomer 1 of $CpCoMe_4B_7C_4H_7$ and isomers 1 and 2 of $CpCoMe_4B_6C_4H_6$; isomer 3 is produced by rearrangement of isomer 1 at 140 °C. Cobalt insertion into $Me_4B_8C_4H_8$ affords *inter alia* $CpCoMe_4B_8C_4H_8$ and $\sigma$-$(CpCoC_5H_4)Me_4B_8C_4H_8$.[141] The latter compound is zwitterionic and it is
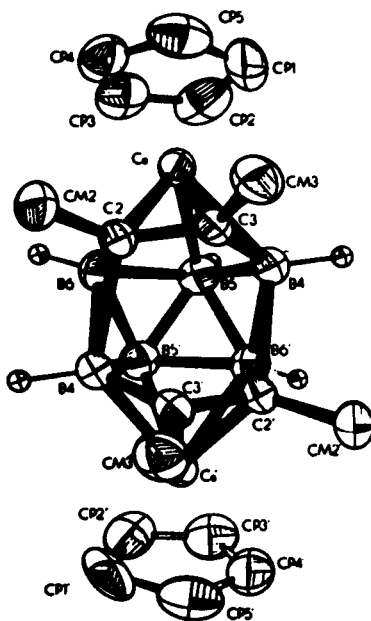


FIG. 40. Structure of $(CpCo)_2Me_4B_6C_4H_6$.

of interest because it can be regarded as a cobalticinium-substituted deriva-
tive of the unknown $Me_4B_8C_4H_9^-$ ion. The molecule has an open, basket-
like geometry in which the carbon atoms occupy contiguous positions on
the open face (Fig. 41). The "extra" hydrogen occupies an *endo* position
on the carbon next to the substituted boron atom. Removal of this proton
is thought to lead to a cage whose geometry is similar to that in one of the
(fluxional) isomers of $Me_4B_8C_4H_8^{2-}$.[142]
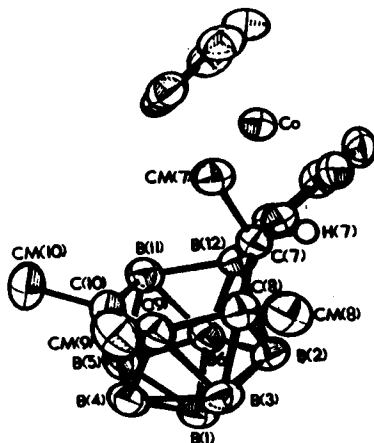


FIG. 41. Structure of $(CpCoC_5H_4)Me_4B_8C_4H_8$.

The tetracarbon carborane derivatives $(EtO)_2Me_4B_8C_4H_6$ and
$CpCoMe_4EtOB_7C_4H_6$ have been obtained from $(Me_2B_4C_2H_4)_2FeH_2$. The
^{11}B NMR spectra of both compounds show singlets due to the B–OEt
groups. The structure of the ethoxycobaltacarborane is that of a severely
distorted icosahedron the two halves of which have partly separated to
create a large opening on one side (Fig. 42).[143]

The unusual cobaltacarborane $(Me_5CpCo)_2CoMe_4B_8C_4H_7$ has been iso-
lated from the reaction of $LiMe_5Cp$, $NaMe_2B_4C_2H_5$, and $CoCl_2$. Its solid-
state structure (Fig. 43) is singular in that it contains a short bond between
B(8) and B(8'). This accounts for the broad singlet at 92·9 ppm in the [11]B
NMR spectrum. The position of the "extra" non-methyl hydrogen atom
is not established from electron density maps but detailed analysis of subtle
distortions in the heavy-atom framework suggests that it lies in a wedging
position [cf. $(Me_2B_4C_2H_4)_2FeH_2$] in the vicinity of Co(3), B(6,6'), and
B(8,8'). This proton is strongly deshielded with $\delta^1H$ 13·12 ppm. It is
suggested that in solution the B(8)–B(8') bond is cleaved and the "extra"
hydrogen atom tautomerizes between terminal positions on these two boron
atoms. If the rate is comparable to the reciprocal of the coupling constant,
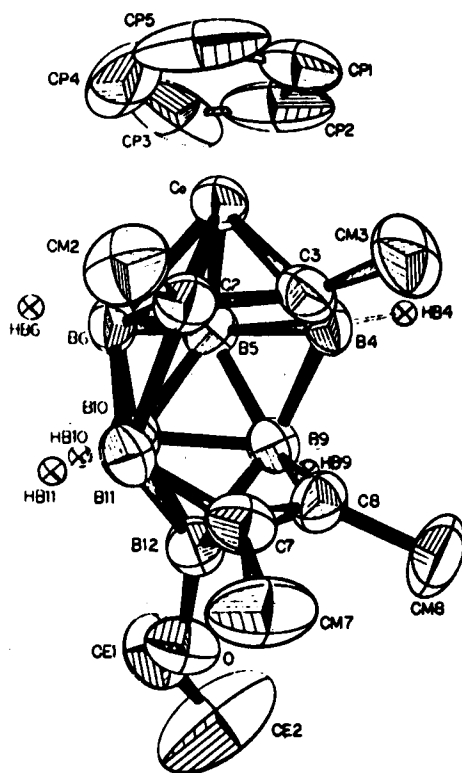
FIG. 42. Structure of CpCoMe$_4$EtOB$_7$C$_4$H$_6$.
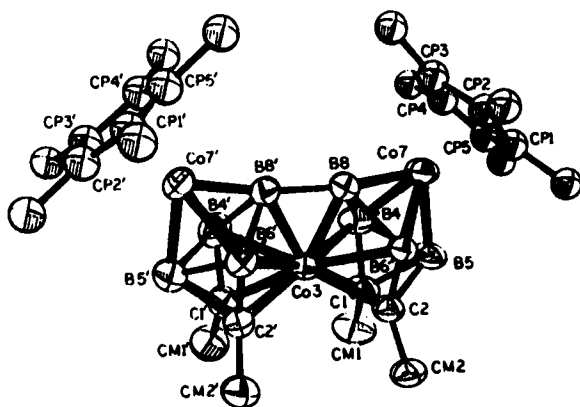


FIG. 43. Structure of (Me$_5$CpCo)$_2$CoMe$_4$B$_8$C$_4$H$_7$.

such a process would serve to reduce $J$(B–H). The $^{11}$B linewidths in ($Me_5CpCo)_2CoMe_4B_8C_4H_7$ are large, 260–290 Hz, owing to very fast relaxation of the $^{11}$B nuclei. The spin–lattice relaxation times are about 1 ms. This nearly obscures scalar coupling to terminal protons. An alternative possibility considered for the solution state structure features a static hydrogen bridge between B(8) and B(8′). This is consistent with the $4:2:2$ pattern of $^{11}$B resonances which are too broad to reveal coupling to the bridge proton. Low temperature NMR studies of this novel material, and of its conjugate base, would be of interest. The careful work already extant underscores the difficulty of precisely locating potentially mobile hydrogen atoms in metalloborane clusters.[144]

A derivative of $Me_4B_8C_4H_8$ with a ferrocenyl group substituted at the B(4) position has been prepared. The $1:3:2:1:1$ pattern of resonances in the $^{11}$B NMR spectrum of $4\text{-}CpFeC_5H_4\text{-}2,3,7,8\text{-}Me_4B_8C_4H_7$ indicates that the molecule is static on the NMR time scale, and the chemical shifts, with the exception of that of the $C$-substituted boron atom, 7·1 ppm, correspond to those of isomer A of the fluxional parent carborane $Me_4B_8C_4H_8$. An X-ray crystal structure determination shows that the 4-ferrocenyl substituent does not significantly affect the cage geometry.[145]

Photolysis of $B_4H_8Fe(CO)_3$ in the presence of but-2-yne affords $Me_4B_4C_4H_4$. The $^{11}$B NMR spectrum of this novel eight-vertex tetracarbon carborane shows two doublets at $-12·4$ (2B) and $-14·0$ (2B). The low-frequency signal is the broader of the two; the ratios of the peak widths are the same at 25·2 and 32·1 MHz and appear not to be temperature dependent over the range $-80$ to $80\,°C$. The NMR data do not define a structure; several *arachno* cage geometries are possible and the molecule may be fluxional. An intermediate in the synthesis reaction, $Me_4B_4C_4H_4Fe(CO)_3$, has been detected. Its $^{11}$B NMR spectrum comprises a multiplet centred at $-5$ ppm.[146] A possibly related tetracarbon carborane, $(EtC)_4(MeB)_4$, is obtained by desulphurization of 2,5-dimethyl-3,4-diphenyl-1,2,5-thiadiborol-2-ene. The $^{11}$B NMR spectrum shows a singlet at $-6·3$ ppm, and the $^1$H NMR spectrum indicates the presence of two non-equivalent ethyl groups. This suggests that alkyl groups may raise the energy barrier to fluxional processes or that this carborane has a cage structure different from $Me_4B_4C_4H_4$.[147] Precedent for the former explanation might be found in the behaviour of $4\text{-}CpFeC_5H_4\text{-}2,3,7,8\text{-}Me_4B_8C_4H_7$.


## XXIV. HETEROATOM BORANES

General methods have been developed for insertion of groups and heteroatoms such as $CH^-$, $CNMe_3$, AsR, As, S, Se, and Te into polyhedral boron cages, and the chemistry of the resulting heteroatom boranes now constitutes an important subset of boron chemistry.

A thorough 70·6 MHz $^{11}$B NMR study has been performed on eleven-vertex compounds of the type $B_{10}H_{12}E$ whose general structure is shown in Fig. 44. The NMR data are collected in Table 37. The spectra of these
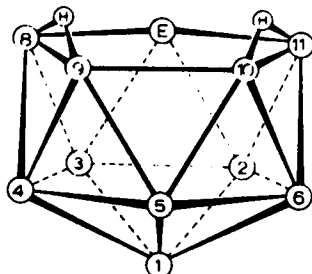


FIG. 44. Proposed general structure for $B_{10}H_{12}E$ compounds.

compounds generally exhibit a $1:2:2:2:1:2$ pattern of doublets. In particular, resonances in the spectrum of $B_{10}H_{12}CNMe_3$ are assigned (reading from high to low frequency) to B(5), B(2,3), B(8,11), B(9,10), B(1), and B(6). The B(8,11) peak is identified by use of a partially deuterated

## TABLE 37

$^{11}$B NMR data* for $B_{10}H_{12}E$ heteroatom boranes.

| Compound | Solvent | Shift | $J(^{11}B-^{1}H)$ | Area | Assignment | $T_1$ (ms) |
|---|---|---|---|---|---|---|
| CsNa[$B_{11}H_{13}$] | DMSO (with NaOH added) | −20·4 | 122 | 10 | B(2,3,4,5,6,7, 8,9,10,11) | 14 |
| | | −31·0 | 132 | 1 | B(1) | 24 |
| [(CH$_3$)$_4$N][$B_{10}H_{12}CH$] | acetone | 0·3 | 137 | 1 | B(5) | 62 |
| | | −11·2 | 139 | 4 | B(2,3) and B(8,11) | 34 |
| | | −22·4 | 141 | 2 | B(9,10) | 42 |
| | | −(24·8) | | 1 | B(1) | 69 |
| | | −30·4 | 136 | 2 | B(4,6) | 92 |
| $B_{10}H_{12}CNMe_3$ | acetone | 1·9 | 144 | 1 | B(5) | |
| | | −9·0 | 154 | 2 | B(2,3) | |
| | | −13·2 | 132 | 2 | B(8,11) | |
| | | −21·6 | 129 | 2 | B(9,10) | |
| | | −25·4 | 144 | 1 | B(1) | |
| | | −32·2 | 144 | 2 | B(4,6) | |
| $B_{10}H_{12}P(n\text{-propyl})$ | acetone | 3·2 | 144 | 1 | B(5) | |
| | | −8·3 | (181) | 2 | B(2,3) | |
| | | −12·4 | (154) | 2 | B(8,11) | |
| | | −17·2 | 149 | 2 | B(9,10) | |
| | | −(24·4) | | 1 | B(1) | |
| | | −25·0 | 147 | 2 | B(4,6) | |

TABLE 37 (*cont.*)

| Compound | Solvent | Shift | $J(^{11}B-^{1}H)$ | Area | Assignment | $T_1$ (ms) |
|---|---|---|---|---|---|---|
| [(CH₃)₄N]¹[B₁₀H₁₂As]⁻ | acetone | 7·8 | 142 | 1 | B(5) | 50· |
| | | −(6·9) | (137) | 2 | B(2,3) | 34 |
| | | −(8·7) | | 2 | B(8,11) | 27·5 |
| | | −14·5 | 137 | 2 | B(9,10) | 36 |
| | | −(21·6) | (149) | 1 | B(1) | 79 |
| | | −23·7 | 144 | 2 | B(4,6) | 93 |
| B₁₀H₁₂AsCH₃ | acetone | 4·4 | 141 | 1 | B(5) | 24·5 |
| | | −(2·5) | (120) | 2 | B(8,11) | 11·6 |
| | | −(4·4) | (139) | 2 | B(2,3) | 17·1 |
| | | −14·4 | 156 | 2 | B(9,10) | 20 |
| | | −18·1 | 151 | 1 | B(1) | 42 |
| | | −23·0 | 154 | 2 | B(4,6) | 42 |
| B₁₀H₁₂AsC₆H₅ | acetone | −4·4 | 137 | 1 | B(5) | |
| | | (2·5) | (188) | 2 | B(8,11) | |
| | | (4·9) | (159) | 2 | B(2,3) | |
| | | 14·2 | 144 | 2 | B(9,10) | |
| | | 18·2 | 149 | 1 | B(1) | |
| | | 22·9 | 154 | 2 | B(4,6) | |
| B₁₀H₁₂S | CHCl₃ | 16·4 | 151 | 1 | B(5) | 25 |
| | | −(1·7) | (171) | 2 | B(2,3) | 7 |
| | | −(4·0) | (151) | 2 | B(8,11) | 12 |
| | | −10·8 | 156 | 2 | B(9,10) | 20·5 |
| | | −17·7 | 156 | 1 | B(1) | 26·5 |
| | | −25·1 | 151 | 2 | B(4,6) | 39 |
| B₁₀H₁₂Se | acetone | 18·7 | 142 | 1 | B(5) | |
| | | (0·3) | | 2 | B(2,3) | |
| | | −(1·0) | | 2 | B(8,11) | |
| | | −9·1 | 149 | 2 | B(9,10) | |
| | | −16·1 | 151 | 1 | B(1) | |
| | | −24·6 | 151 | 2 | B(4,6) | |
| B₁₀H₁₂Te | acetone | 19·7 | 147 | 1 | B(5) | |
| | | −(3·3) | (174) | 4 | B(2,3) and B(8,11) | |
| | | −(5·9) | | 2 | B(9,10) | |
| | | −14·1 | 149 | 1 | B(1) | |
| | | −24·5 | 152 | 2 | B(4,6) | |
| (CH₃)₄N[4,6-Br₂B₁₀H₁₀CH] | DMF | 2·5 | 138 | 1 | B(5) | |
| | | −(11·1) | | 2 | B(2,3) | |
| | | −(13·1) | | 2 | B(8,11) | |
| | | −(21·0) | | 2 | B(9,10) | |
| | | −21·8 | | 2 | B(4,6) | |
| | | −(23·0) | | 1 | B(1) | |

\* Values in parentheses are approximate owing to overlap with other signals.

derivative, and the B(4) peak from the spectrum of 4-$BrB_{10}H_{11}CNMe$ obtained in turn from 2-$BrB_{10}H_{13}$. The B(9,10) signals are recognized from coupling to the static bridge protons. The peak of unit area at $-25\cdot4$ ppm is sharper than that at $1\cdot9$ ppm. This indicates that the former is associated with a boron nucleus in a more symmetrical electronic environment, and on this basis it is assigned to B(1). Similar sets of spectral assignments are probably valid for the other heteroatom boranes studied. The B(5) and B(9,10) positions, most remote from the heteroatom, are most shielded for Group IV derivatives and least shielded in the Group VI compounds.

$^{11}$B spin–lattice relaxation time data are reported for $B_{11}H_{13}^-$, $B_{10}H_{12}CH^-$, $B_{10}H_{12}As^-$, $B_{10}H_{12}AsMe$, and $B_{10}H_{12}S$. In these compounds, B(1), B(5), and B(4,6) are expected to have the most symmetrical electric field gradients, and the $^{11}$B signals assigned to these positions do indeed have the longest $T_1$ values. The authors make the cogent point that interpretation of $T_1$ data for different molecules in terms of field gradients may be invalid owing to differences in the details of molecular motion.[148]

The smaller heteroatom boranes $B_8Se_2H_{10}$, $B_9Se_2H_9$, and $B_7SeC_2H_{11}$ are obtained from sodium polyselenide and $B_9H_{13}SMe_2$, $B_9H_{14}^-$, and $B_7C_2H_{13}$ respectively.[149] $^{11}$B NMR data for these compounds are given in Table 38. The selenaborane $B_9Se_2H_9$ can be converted into other interesting selenaboranes. Treatment with ethanolic potassium hydroxide produces red $Me_4N(B_9Se_2H_{10})$. The $^{11}$B NMR spectrum displays six doublets of relative areas $2:1:2:2:1:1$; the absence of singlets suggests that the oxygen is attached to selenium. Subsequent treatment with base, $C_5H_6$, and $CoCl_2$ provides $CpCoB_9Se_2H_9$ and $(CpCo)_2B_9SeH_9$. The geometry of the former is that of a thirteen-vertex *closo* polyhedron with one vertex removed (Fig. 45). However, the $^{11}$B NMR spectrum contains six doublets in a $1:2:2:1:1:2$ ratio, which may be due to overlapping peaks or to fluxional processes. Treatment of $B_9SH_{12}^-$ with a mixture of potassium polysulphide and polyselenide affords both $B_9SSeH_9$ and $B_9S_2H_9$. The $^{11}$B NMR spectrum of $CpCoB_9SSeH_9$, produced by cobalt insertion, is very similar to that of $CpCoB_9Se_2H_9$, so it probably has a similar arrangement of boron and heteroatoms. Degradation of $B_9SSeH_9$ in methanolic potassium hydroxide yields $B_7SSeH_9$, whose 70·6 MHz $^{11}$B NMR spectrum shows seven doublets of unit area, indicative of the absence of symmetry.[150] The sharp doublet of unit area at $-1\cdot0$ ppm is most likely due to the boron atom on the open face of the cage bonded to both sulphur and selenium atoms.

Degradative insertion of sulphur into $B_9SH_{12}^-$ and the "reactive isomer" of $B_{10}C_2H_{13}^-$ provides 6,8-$B_7S_2H_9$ and 6,8-$B_7SCH_{11}$ respectively. $^{11}$B NMR spectroscopy has provided some insight into the electronic structure of these materials. Sulphur (or selenium) can in principle donate either four electrons (and three orbitals) or two electrons (and two orbitals) to
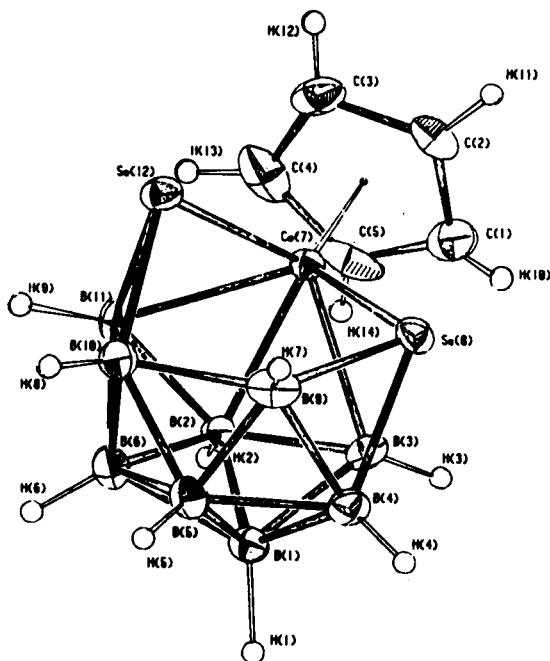
FIG. 45. Molecular structure of CpCoB$_9$Se$_2$H$_9$.

the bonding framework. In the second alternative, S is electronically similar to CH$_2$. The $^{11}$B spectra of both thiaboranes are similar to that of B$_7$C$_2$H$_{13}$ which is known to have CH$_2$ groups in the 6,8 positions (Fig. 46), and therefore sulphur in them functions as a two-electron donor. The sharp doublet at 4·0 ppm in B$_7$S$_2$H$_9$ and 0·7 ppm in B$_7$SCH$_{11}$ is assigned to B(7). This boron atom experiences a low symmetry field gradient about the B–H axis, is not connected to bridge hydrogen atoms, and is little broadened by $^{11}$B–$^{11}$B or $^{10}$B–$^{11}$B coupling. Narrow $^{11}$B signals may be a general feature of boron atoms located between two heteroatoms on the open face of a molecule.[151]
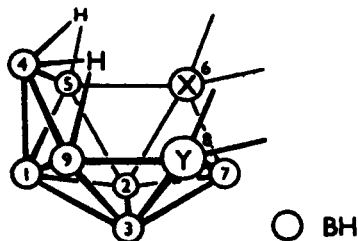


FIG. 46. Proposed structures of B$_7$S$_2$H$_9$ (X = Y = S) and B$_7$SCH$_{11}$ (X = S, Y = CH$_2$), and the established structure of B$_7$C$_2$H$_{13}$ (X = Y = CH$_2$).

Chalcogen insertion into $B_9H_{13}SMe_2$ with polyselenide or polytelluride salts gives $B_9SeH_{12}^-$ and $B_9TeH_{12}^-$. The chemistry of these anions is rather extensive and their $^{11}B$ NMR spectra, and those of related compounds, are given in Table 38.[152] Assignment of the various $^{11}B$ resonances in $B_9SeH_{12}^-$ and $B_9TeH_{12}^-$ presumably follows those deduced earlier for $B_9SH_{12}^-$,[153] and a decrease in shielding in the order $S > Se > Te$ is observed for B(4), B(9), and B(8,10). In the case of $B_9TeH_{12}^-$, B(2) and B(5,7), which are adjacent to the tellurium atom, show an increase in shielding.

Metal insertion into $B_{10}AsH_{12}^-$ provides $Co(B_{10}AsH_{10})_2^{3-}$, $Ni(B_{10}AsH_{10})_2^{2-}$, and $CpCo(B_{10}AsH_{10})^-$. From $B_9As_2H_{10}^-$ are obtained the metalloboranes $Co(B_9As_2H_9)_2^-$ and $CpCo(B_9As_2H_9)$. The 70·6 MHz $^{11}B$ NMR spectra of these compounds (Table 38) indicate $C_s$ cage symmetry.[154]

Decaborane(14) and $Na_2Se_4$ or $Na_2Te_4$ yield $B_{10}SeH_{11}^-$ and $B_{10}TeH_{11}^-$ which protonate to give $B_{10}SeH_{12}$ and $B_{10}TeH_{12}$ respectively. Metal insertion reactions afford $(B_{10}EH_{10})_2Co^-$, $CpCo(B_{10}EH_{10})$, and $(B_{10}EH_{10})_2Fe^{2-}$ (E = Se, Te). The $^{11}B$ NMR spectra of icosahedral heteroatom boranes of the type $(B_{10}EH_{10})Co(ligand)$ all show the expected $1:1:2:2:2:2$ patterns of doublets. The two highest frequency doublets of unit area are probably due to the boron atoms antipodal to cobalt and the heteroatom, and they exhibit the most variation in chemical shift.[155]

Insertion of antimony into $B_{10}AsH_{12}^-$ forms $1,2-B_{10}AsSbH_{10}$. The distibaborane, $1,2-B_{10}Sb_2H_{10}$ is prepared from decaborane, antimony trichloride, and zinc metal. The $^{11}B$ NMR spectrum of the arsastibaborane $B_{10}AsSbH_{10}$ contains two doublets of unit area at 14·2 and 12·3 ppm, while the highest frequency doublets of area 2 in the spectra of $1,2-B_{10}As_2H_{10}$ and $1,2-B_{10}Sb_2H_{10}$ occur at 15·5 and 13·9 ppm. Therefore, the 14·2 ppm signal is assigned to the boron nucleus antipodal to arsenic and that at 12·3 ppm to boron *para* to antimony. Similarly, the high-frequency doublet at 9·4 ppm in the $^{11}B$ NMR spectrum of $B_{11}SbH_{11}^-$ is assigned to boron *para* to the heteroatom.[156]

Treatment of $NaB_{11}H_{14}$ dioxanate with ammonium polyselenide affords $B_{11}Se_3H_9^{2-}$ which contains an exopolyhedral $Se_3$ chain bonded to adjacent boron atoms in the $B_{11}$ cage. The 70·6 MHz $^{11}B$ spectrum of the tetraethyl-ammonium salt in acetone contains a singlet of relative area 2 at $-6·9$ ppm due to the selenium-substituted boron atoms and a doublet of area 9 at $-14·2$ ppm. That the nine BH units appear equivalent suggests that, despite the presence of the $Se_3$ bridge, the boron cage may be fluxional.[157]

The reaction between $NaHSeO_3$ and $NaB_{11}H_{14}$ or $7,8-B_9C_2H_{12}^-$ leads to $B_{11}SeH_{11}$ and $B_8SeC_2H_{10}$; similarly, $B_{11}TeH_{11}$ is obtained from $NaB_{11}H_{14}$ and $TeO_2$. The $^{11}B$ NMR spectrum of $B_{11}SeH_{11}$ contains three doublets at 22·9 (1B), $\sim 3·5$ (5B), and $-4·4$ (5B) ppm; the 22·9 ppm peak is logically assigned to the boron atom *para* to selenium in the icosahedral

# TABLE 38

**$^{11}$B NMR data for heteroatom boranes.**

| Compound | $\delta^{11}$B $(J_{BH})$ |
|---|---|
| $B_8Se_2H_{10}$ | 14·9 (d, 2B, 178), −16·9 (dd, 4B, 160, 35) |
| $B_7SeC_2H_{11}$ | 5·2 (d, 1B, 166), −9·2 (br, 2B), −11·0 (d, 1B, 161), −18·2 (dd, 1B, 153, 47), −23·6 (d, 1B, 161), −48·1 (d, 1B, 151) |
| $Me_4N(B_9Se_2H_{10})$ | −0·9 (d, 2B, 150), −2·5 (d, 1B, 150), −3·5 (d, 2B, 145), −10·6 (d, 2B, 162), −44·5 (d, 1B, 140), −46·6 (d, 1B, 150) |
| $CpCoB_9SeH_9$ | 27·8 (d, 1B, 161), 14·0 (d, 2B, 166), ∼0·0 (2B), ∼2·1 (1B), ∼−4·5 (1B), −22·4 (d, 2B, 158) |
| $(CpCo)_2B_9SeH_9$ | 25·7 (d, 2B, 134), ∼13·4 (d, 3B, ∼150), ∼11·1 (1B), 0·1 (d, 2B, 149), −8·0 (d, 1B, 139) |
| $B_9S_2H_9$ | ∼−2·5 (7B), −11·4 (d, 1B, 176), −37·1 (d, 1B, 156) |
| $B_9SSeH_9$ | −1·1 (3B), −2·6 (4B), −10·5 (d, 1B, 176), −36·2 (d, 1B, 152) |
| $CpCoB_9SSeH_9$ | 25·4 (d, 1B, 176), 10·4 (d, 2B, 161), −1·3 (d, 3B, 146), −3·9 (d, 1B, 155), −20·3 (d, 1B, 163), −24·6 (d, 1B, 156) |
| $B_7SSeH_9$ | 5·8 (1B), 4·6 (1B), −1·0 (d, 1B, 166), −16·2 (d, 1B, 176), −21·7 (d, 1B, 185), −34·3 (d, 1B, 171), −48·9 (d, 1B, 152) |
| $6,8\text{-}B_7S_2H_9$ | 3·2 (d, 2B), −4·0 (d, 1B), −22·7 (d, 2B), −37·3 (dd, 1B), −48·4 (d, 1B) |
| $6,8\text{-}B_7SCH_{11}$ | 1·2, −0·7, −15·2, −26·9, −33·3 (dd), −49·9 |
| $Me_4N(B_9SeH_{12})$ | 5·5 (d, 1B, 137), ∼7·7 (unsymm. d, 3B), −13·6 (t, 1B, 115), −33·7 (d, 2B, 139), −36·3 (d, 2B, 141) |
| $B_8Se_2H_{10}$ | 14·9 (d, 2B, 178), −16·9 (dd, 4B, 160, 35), −30·7 (d, 2B, 155) |
| $Me_4N(B_9TeH_{12})$ | 7·3 (d, 1B, 137), ∼−10·8 (m, 4B), −25·3 (d, 2B, 137), −35·5 (d, 2B, 139) |
| $B_9SeH_{11}$ | 28·9 (d, 2B, 172), 16·7 (d, 1B, 161), 6·2 (d, 2B, 157), −9·6 (dd, 2B, 159, 37), −21·5 (d, 1B, 167), −29·9 (d, 1B, 174) |
| $B_9TeH_{11}$ | 31·3 (d, 2B, 170), 15·7 (d, 1B, 158), 7·5 (d, 2B, 146), −7·4 (d, 2B, 144), −21·4 (d, 1B, 149), −31·0 (d, 1B, 177) |
| $B_9SeH_{11}\cdot CH_3CN$ | 7·6 (d, 1B, 135), ∼−6·4 (d, 1B), −8·8 (d, 2B, 160), −19·5 (d, 1B, 130), −27·9 (dd, 2B, 142, 43), −36·9 (d, 2B, 149) |
| $B_9TeH_{11}\cdot CH_3CN$ | 8·7 (d, 1B, 137), −6·9 (d, 1B, 159), ∼−14·9 (unsymm. d, 3B), −23·3 (d, 2B, 129), −36·2 (d, 2B, 149) |
| $B_9SeH_{11}\cdot NEt_3$ | 2·6 (d, 1B, 130), −4·0 (d, 1B, 130), −8·8 (d, 3B), −29·8 (dd, 2B, 130, 40), −38·1 (d, 2B, 146) |
| $B_9SeH_9$ | 73·3 (d, 1B, 180), −5·4 (d, 4B, 176), −19·9 (d, 4B, 156) |
| $(Me_4N)_2[(B_{10}AsH_{10})_2Co]\cdot H_2O$ | 6·2 (d, 1B, 130), 4·3 (d, 2B, 130), 1·7 (d, 2B, ∼120), 0·0 (d, 1B, 120), −11·9 (d, 2B, 125), ∼−13·4 (d, 2B, ∼125) |
| $(Me_4N)_2[(B_{10}AsH_{10})_2Ni]$ | 20·9 (d, 1B, 130), 12·5 (d, 4B, 140), 8·3 (d, 1B, 145), −4·3 (d, 2B, 130), −6·1 (d, 2B, ∼130) |

**TABLE 38** (*cont.*)

| Compound | $\delta^{11}B$ ($J_{BH}$) |
|----------|---------------------------|
| $(Me_4N)CpCoB_{10}AsH_{10}$ | 8·0 (d, 2B, 125), ~6·7 (d, 1B, ~120), 5·0 (d, 1B, 120), 3·2 (d, 2B, 140), −7·3 (d, 2B, 135), −12·7 (d, 2B, 145) |
| $(Me_4N)_2[(B_9As_2H_9)_2Co]$ | 20·6 (d, 1B, 145), ~16·1 (d, 1B, ~140), 12·3 (d, 2B, 115), 11·5 (d, 2B, 130), ~−1·7 (d, 1B, ~140), −2·6 (d, 2B, 145) |
| $CpCoB_9As_2H_9$ | 17·1 (d, 1B, 145), 12·3 (d, 5B, 145), −4·7 (d, 2B, 155), −8·8 (d, 1B, 165) |
| $B_9Se_2H_9$ | −0·1 (d, 3B, 170), −2·6 (d, 4B, 175), −9·7 (d, 1B, 176), −36·3 (d, 1B, 158) |
| $B_{10}TeH_{12}$ | 21·4 (d, 1B, 149), −3·2 (d, 4B, 176), ~−5·6 (d, 2B), −14·0 (d, 1B, 151), −24·8 (d, 2B, 156) |
| $(Me_4N)B_{10}SeH_{11}$ | −6·0 (d, 2B, 138), −9·5 (d, 2B, 147), ~−15 (1B), −16·8 (d, 4B, 143), −35·9 (d, 1B, 139) |
| $(Me_4N)B_{10}TeH_{11}$ | −5·4 (d, 2B, 139), −12·4 (d, 3B, 139), ~−16·9 (2B), ~−18·3 (2B), −33·7 (d, 1B, 147) |
| $(Me_4N)_2[(B_{10}SeH_{10})_2Fe]$ | ~8·8 (d, 1B, ~145), 6·3 (d, 2B, 133), 0·9 (d, 3B, 130), −14·1 (d, 2B, 135), ~−17·3 (d, 2B, ~167) |
| $(Me_4N)_2[(B_{10}TeH_{10})_2Fe]$ | 12·4 (d, 1B, 134), 5·7 (d, 2B, 120), ~3·4 (d, 1B), ~−1·5 (d, 2B), −12·9 (d, 2B, 137), −19·5 (d, 2B, 142) |
| $(Me_4N)_2[(B_{10}SeH_{10})_2Co]$ | 16·3 (d, 1B, 149), 12·3 (d, 3B, 132), 6·1 (d, (d, 2B, 164), −7·0 (d, 2B, 144), −10·7 (d, 2B, 168) |
| $(Me_4N)_2[(B_{10}TeH_{10})_2Co]$ | 18·9 (d, 1B, 144), 15·2 (d, 1B, 143), 10·4 (d, 2B, 135), 5·9 (d, 2B, 157), −6·1 (d, 2B, 144), −10·9 (d, 2B, 152) |
| $CpCoB_{10}SeH_{10}SeH_{10}$ | 17·2 (d, 1B, 145), 12·4 (d, 2B, 140), 8·1 (d, 1B, 150), 4·5 (d, 2B, 170), −6·9 (d, 2B, 144), −12·5 (d, 2B, 161) |
| $CpCoB_{10}TeH_{10}$ | 19·9 (d, 1B, 140), 13·7 (d, 2B, 144), 9·1 (d, 1B, 145), 4·2 (2B, 160), −6·2 (d, 2B, 145), −13·6 (d, 2B, 162) |
| $1,2-B_{10}AsSbH_{10}$ | 14·2 (d, 1B, 140), 12·3 (d, 1B, 130), 3·0 (d, 2B, 160), −0·1 (d, 2B, 140), −2·0 (d, 2B, ~130), −3·5 (d, 2B, 130) |
| $1,2-B_{10}Sb_2H_{10}$ | 13·9 (d, 2B, 140), 3·9 (d, 2B, 155), −1·7 (d, 4B, 155), ~−4·6 (d, 2B, ~150) |
| $(Me_4N)B_{11}SbH_{11}$ | 9·4 (d, 1B, 135), −6·9 (d, 5B, 110), −9·3 (d, 5B, 120) |
| $CpCoB_9AsSbH_9$ | ~15·8 (d, 1B, ~130), 13·7 (d, 3B, 150), ~11·2 (d, 2B, ~140), ~−5·7 (d, 2B, ~130), −7·3 (d, 1B, 125) |
| $CpCoB_9Sb_2H_9$ | 15·7 (d, 2B, 140), 13·8 (d, 3B, 130), 9·5 (d, 1B, 145), −4·0 (d, 1B, 160), −7·5 (d, 2B, 145) |
| $(Et_4N)B_{11}Se_3H_{11}$ | −6·9 (s, 2B), −14·2 (d, 9B, 134) |
| $B_{11}SeH_{11}$ | 22·9 (d, 1B, 142), ~−3·5 (5B), −4·4 (d, 5B, 139) |
| $B_{11}TeH_{11}$ | 22·3 (d, 1B, 142), −4·3 (unsymm. d, 10B) |
| $B_8SeC_2H_{10}$ | 0·6 (d, 1B, 176), −5·3 (d, 2B, 173), −10·3 (d, 2B, 161), ~−12·5 (2B), −39·5 (d, 1B, 154) |
| $6,8,7,9-(CpCo)_2B_5S_2H_5$ | −11·7 (d, 4B, 169), −5·9 (d, 1B, 184) |
| $2,3,6-(CpCo)_2B_5SH_7$ | 100·9 (d, 1B, 158), 6·6 (d, 1B, 156), −4·0 (d, 1B, 145), −22·1 (d, 1B, 167), −32·1 (d, 1B, 154) |
| $7,6,8-CpCoB_6S_2H_8$ | 4·8 (d, 2B, 156), −9·8 (d, 2B, 166), −33·7 (d, 1B, 153), −40·2 (d, 1B, 143) |
| $B_9CH_{11}\cdot NMe_3$ | 31·8 (d, 1B, 142), −17·3 (d, 4B, 156), −26·0 (d, 4B, 142) |

cage. The spectra of $B_8SeC_2H_{10}$ and $B_8SC_2H_{10}$ are similar and both molecules probably have *nido* eleven-atom cage structures similar to $B_9C_2H_{11}$.[158]

Three novel cobaltathiaboranes have been synthesized in reactions of cobalt atoms, boron hydrides, and various sulphur-containing reagents. Their structures are shown in Fig. 47. The 115·5 MHz ^{11}B NMR spectrum
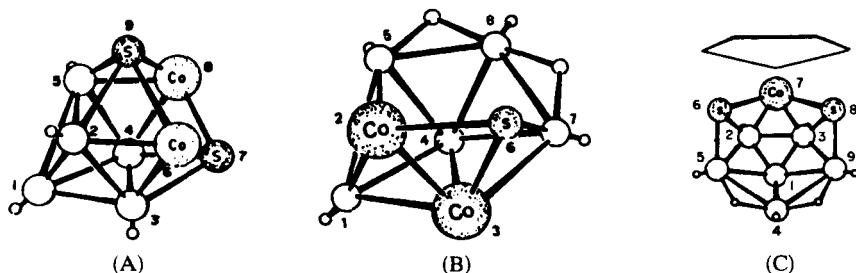


FIG. 47. Structure proposed for (A) $(CpCo)_2S_2B_5H_5$, and structures established for (B) $(CpCo)_2SB_5H_7$ and (C) $(CpCo)S_2B_6H_8$.

of $(CpCo)_2S_2B_5H_5$ comprises two overlapping doublets of relative area 4:1, indicating that the $B_5$ cage in the starting pentaborane(9) survives and that it incorporates two cobalt and two sulphur atoms into a *nido* monocapped square antiprism. Five doublets, each of unit area, are seen in the 32 MHz ^{11}B NMR spectrum of $(CpCo)_2SB_5H_7$, indicating the absence of a plane of symmetry. The 100·9 ppm resonance in this compound may be assigned to B(1), the four-coordinate boron atom next to two cobalt atoms. The peaks at −4·0 and −22·1 ppm are broadened, probably owing to coupling with the bridge protons. The 115·5 MHz spectrum of $CpCoS_2B_6H_8$ displays four resonances of relative areas 2:2:1:1. The doublet of unit area at 33·7 ppm shows evidence of structure due to spin coupling with the bridge protons and may be assigned on this basis to the unique atom, B(4).[159]

The derivative chemistry of $1-B_9SH_9$ and $B_{11}SH_{11}$ continues to expand. Sequential electrophilic halogenation of these thiaboranes has yielded a large number of substituted derivatives whose ^{11}B NMR spectra are summarized in Table 39. Knowledge of the crystal structure of 2,2'-(1-$B_9SH_8)_2$[160] allows assignment of the higher frequency doublet of area 4 at −4·8 ppm to the upper-belt B(2–5) positions (see Fig. 48) and the doublet at −17·6 (4B) ppm to the lower-belt B(6–9) borons. The axial B(10) resonance occurs at 74·5 ppm. From this assignment, the positions of substitution in the halogenated thiaboranes is deduced. For both axial and lower-belt boron atoms, a linear correlation between $\delta$[11]B and the Pauling
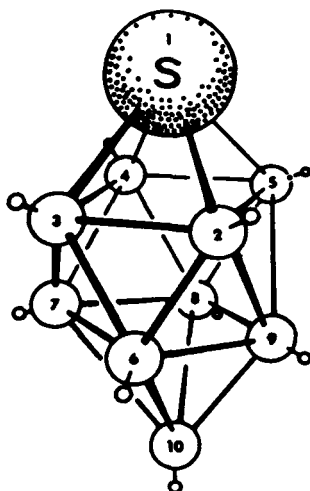
FIG. 48. Structure and numbering scheme for 1-$B_9SH_9$; positions B(2–5) are in the upper belt and B(6–9) are in the lower belt.

electronegativity of the halogen is found. As with alkylated thiaboranes, the principal chemical shift perturbations induced by lower-belt substitution are in the lower-belt resonances.[161]

A large number of alkyl derivatives of 1-$B_9SH_9$ have been prepared by Friedel–Crafts alkylation. ^{11}B NMR data for these compounds are included in Table 39. Several trends in the spectral data are noted. Substitution at B(10) causes a 5–10 ppm deshielding relative to the parent thiaborane. Lower-belt B(6–9) substitution has little effect on the shift of the axial boron nucleus but effects that propagate to other positions are more appreciable.[162]

Hydroboration by 6-$B_9SH_{11}$ of alkenes and alkynes occurs by addition of the *exo* B(9)–H bond to the C–C unsaturated linkage. ^{11}B NMR data for 9-R-6-$B_9SH_{10}$ compounds prepared in this manner are found in Table 40. B(9) is deshielded as a result of alkyl substitution. 32 MHz FT ^{11}B NMR spectroscopy was used to study the reactions of 6-$B_9SH_{11}$ with carbonyl compounds. Difference spectra, from which signals due to the starting material are subtracted, allow partial characterization of intermediates. In the reaction with acetaldehyde, peaks are observed at 32·1 (s, 1B), 23·1 (d, 2B), −4·4 (d, 2B), −22·1 (d, 1B), −28·6 (d, 2B), and −32·9 (d, 1B) ppm which are attributed to 9-EtO-6-$B_9SH_{10}$. Another product, possibly $(EtO)_2B_8SH_6$, is also found. Its [11]B difference spectrum contains peaks at 29 (s, ~2B), 4·8 (d, 1B), −1·6 (d, 2B), −13·4 (d, 2B), and 17·4 (d, 1B) ppm.[163]

## TABLE 39

**$^{11}$B NMR data for substituted thiaboranes.**

| Compound | $\delta^{11}$B ($J_{BH}$) |
|---|---|
| 1-B$_9$SH$_9$ | 74·5 (d, 1B, 180), −4·8 (d, 4B, 170), −17·6 (d, 4B, 150) |
| 6-I-1-B$_9$SH$_8$ | 71·2 (d, 1B, 175), −5·1 (d, 4B, 180), −16·8 (d, 2B, 135), −19·9 (d, 1B, 135), −24·1 (s, 1B) |
| 10-I-1-B$_9$SH$_8$ | 50·1 (s, 1B), −6·7 (d, 4B, 185), −16·2 (d, 4B, 165) |
| 6-Br-1-B$_9$SH$_8$ | 69·3 (d, 1B, 175), −3·0 (d, 2B, 175), −6·9 (d, 2B, 190), −10·0 (s, 1B), −15·4 (d, 2B, 180), −21·3 (d, 1B, 195) |
| 10-Br-1-B$_9$SH$_8$ | 65·6 (s, 1B), −8·3 (d, 4B, 175), −18·4 (d, 4B, 150) |
| 6-Cl-1-B$_9$SH$_8$ | 68·7 (d, 1B, 175), −2·0 (d, 2B, 194), −4·2 (s, 1B), −7·0 (d, 2B, 180), −14·6 (d, 2B, 170), −23·2 (d, 1B, 160) |
| 10-Cl-1-B$_9$SH$_8$ | 73·4 (s, 1B), −3·3 (d, 4B, 185), −17·3 (d, 4B, 160) |
| 6,10-I$_2$-B$_9$SH$_7$ | 48·4 (s, 1B), −5·5 (d, 4B, 180), −13·6 (d, 2B, 155), −15·7 (d, 1B, 180), −23·5 (s, 1B) |
| 6,10-Br$_2$-1-B$_9$SH$_7$ | 64 (s, 1B), −5·3 (d, 2B, 190), −7·6 (d, 2B, 175), −10·4 (s, 1B), −14·8 (d, 2B, 180), −20·6 (d, 1B, 185) |
| 6,7,8-Cl$_3$-1-B$_9$SH$_6$ | 61·9 (d,1B, 170), 1·5 (s, 1B), 0·6 (d, 2B, 180), −2·8 (d, 2B, 160), −3·5 (s, 2B), −13·9 (d, 1B, 165) |
| 1-B$_{11}$SH$_{11}$ | 19·2 (d, 1B, 145), −3·8 (d, 5B, 140), −5·8 (d, 5B, 160) |
| 12-I-1-B$_{11}$SH$_{10}$ | 0·8 (s, 1B), −1·8 (d, 5B, 160), −5·0 (d, 5B, 180) |
| 12-Br-1-B$_{11}$SH$_{10}$ | 16·8 (s, 1B), −2·8 (d, 5B, 140), −6·1 (d, 5B, 160) |
| 7-Cl-1-B$_{11}$SH$_{10}$ | 20·4 (d, 1B, 145), 8·1 (s, 1B), −3·6 (d, 4B, 150), −5·9 (d, 4B, 160), −11·7 (d, 1B, 170) |
| 10-CH$_3$-1-B$_9$SH$_8$ | 85 (s, 1B), −7·7 (4B, 176), −20·4 (4B, 161) |
| 6-CH$_3$-1-B$_9$SH$_8$ | 75·3 (1B, 171), −3·6 (2B, 176), −6·2 (2B, 195), −6·2 (s, 1B), −16·5 (2B, 146), −20·7 (d, 1B, 142) |
| 6,7,8-(CH$_3$)$_3$-1-B$_9$SH$_6$ | 74(1B, 156), 1·0 (2B, 150), −218 (2B, 150), −2·9 (s, 1B), −6·6 (s, 2B), −15·5 (1B, 151) |
| 6,7,8,9-(CH$_3$)$_4$-1-B$_9$SH$_5$ | 74·6 (1B, 151), −0·8 (4B, 166), −4·5 (s, 4B) |
| 6,7,8,10-(CH$_3$)$_4$-1-B$_9$SH$_5$ | 82·7 (s, 1B), −3·0 (2B, 150), −4·8 (2B, 150), −6·1 (s, 1B), −9·5 (s, 2B), −17·0 (1B, 146) |
| 6,7,8,9,10-(CH$_3$)$_5$-1-B$_9$SH$_5$ | 82·7 (s, 1B), −2·2 (4B, 166), −7·2 (4B) |
| 6-C$_2$H$_5$-1-B$_9$SH$_8$ | 73·2 (1B, 162), −3·3 (2B, 160), −5·7 (s, 1B), −6·4 (2B, 160), −16·6 (2B, 142), −21·0 (1B, 142) |
| 6,7,8,10-(C$_2$H$_5$)$_4$-1-B$_9$SH$_5$ | 84·1 (s, 1B), −3·2 (2B, 156), −4·3 (s, 1B), −6·9 (s, 2B), −18·2 (1B, 156) |
| 6,7,8,9,10-(C$_2$H$_5$)$_5$-1-B$_9$SH$_4$ | 79·9 (s, 1B), −5·0 (4B, 190), −5·9 (s, 4B) |

Cobalt insertion into B$_9$CH$_{11}$·NMe$_3$ affords the eleven-atom cluster CpCoB$_9$CH$_9$·NMe$_3$. This compound is clearly fluxional. The 70·6 MHz $^{11}$B NMR spectrum at −40 °C reveals nine overlapping resonances at 70·9 (br s), 3·9 (127), −1·7, −3·8, −6·8, −8·8, −16·2 (146), −21·2 (127), and −32·9 (137) ppm. At 16 °C, a doublet at 4·5 ppm and a broad hump at ∼−12 ppm

## TABLE 40

### $^{11}$B NMR data for alkyl and alkenyl derivatives of $B_9SH_{11}$.

| B(1,3) or B(5,7) | B(4) | B(2) | B(5,7) or B(1,3) | B(8,10) | B(9) |
|---|---|---|---|---|---|
| 3[9-(6-Thia-*nido*-decaboranyl)]hex-3-ene | | | | | |
| +3·4 (151) | −31·3 (181) | −16·4 (156) | +24 (161) | −16·4 (156) | −31·3 |
| 1-[9-(6-Thia-*nido*-decaboranyl)]cyclohexane | | | | | |
| +4·6 (146) | −31·7 (171) | −18·8 (151) | +24·1 (176) | −13·9 (161) | +34·2 |
| [9-(6-Thia-*nido*-decarboranyl)]ethane | | | | | |
| +4·6 (146) | −31·8 (177) | −18·5 (171) | +24 (171) | −13·3 (171) | +33·5 |
| 1-[9-(6Thia-*nido*-decaboranyl)]octane | | | | | |
| +4·4 (147) | −31·9 (191) | −18·6 (156) | +23·8 (176) | −13·7 (154) | +32·2 |
| 1-Methyl-2-[9-(6-thia-*nido*-decaboranyl)]cyclohexane | | | | | |
| +3·9 (149) | −31·7 (193) | −18·6 (144) | +24·3 (169) | −14 (144) | +34·8 |
| 1-[9-(6-Thia-*nido*-decaboranyl)]-*cis*-1,2-diphenylethane | | | | | |
| +3·7 (147) | −30·8 (201) | −16·6 (151) | +23·5 (156) | −16·6 (151) | +29·2 |
| 1,1-Bis-[9-(6-thia-*nido*-decaboranyl)]ethane | | | | | |
| +4·25 (152) | −31·8 (175) | −18·5 (123) | +24·6 (166) | −14·2 (142) | +33·8 |
| 1,3-Bis-[9-(6-thia-*nido*-decaboranyl)]cyclopentane | | | | | |
| +4·6 (146) | −30·1 (161) | −18·8 (156) | +24·4 (161) | −13·6 (177) | +34·1 |
| 6-Thia-*nido*-decaborane(11) | | | | | |
| +6·8 (150) | −30·7 (180) | −21·5 (160) | +24·9 (170) | −10·1 (145) | +17·3 (170) |

are observed. Owing to thermal lability, the limiting high-temperature spectrum was not attained but, at 70 °C, signals at 33·4 (br s, 2B), 5·1 (d, 1B, 127), −10·6 (d, 2B, 142), and −15·0 (d, 4B, 156) ppm are reported. The solid-state structure of $B_9CH_{11}\cdot NMe_3$ was established by an X-ray diffraction study, and the dynamic processes which occur in solution can be analysed in terms of a diamond–square–diamond rearrangement (see Fig. 49) of that structure. Cleavage of the bond between cobalt and B(1) generates an intermediate having a square face. Re-formation of a Co–B(4) bond reconstitutes the polyhedron. This mechanism would interconvert B(1, 4, 7, and 8), which boron atoms correspond to the doublet at −15·0 (4B) in the high-temperature spectrum. The belt of boron atoms including B(3, 5, 6, and 10) effectively rotates according to this mechanism. Therefore, two resonances would be expected, the pairs *ortho* and *meta* to the cobalt atom which are assigned to the broad resonance at 33·4 ppm and the doublet at −10·6 (2B) ppm respectively. The boron atom at position 9 does not participate in the rearrangement and is assigned to the 5·1 ppm
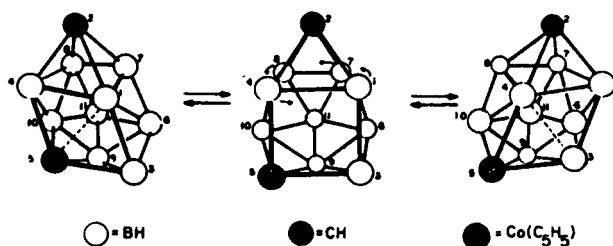
FIG. 49. Diamond–square–diamond rearrangement in $CpCoB_9CH_9 \cdot NMe_3$.

doublet; on cooling, it shifts to 3·9 ppm because of a small temperature effect. The doublet at 70·9 ppm is assigned to B(3), the low-coordinate boron atom next to cobalt. In the low-temperature spectrum, the doublets at −1·7 and −21·2 ppm are assigned to B(6,11) (*meta* to the cobalt atom).

Thermal degradation of $CpCoB_9CH_9 \cdot NMe_3$ results in extrusion of the CpCo unit and the formation of $B_9CH_9 \cdot NMe$. This compound is isoelectronic with $B_9CH_{10}^-$ and presumably has a similar bicapped square antiprismatic geometry with carbon in an apex position. In agreement with this, the 70·6 MHz ^{11}B NMR spectrum contains four doublets in a 1:4:4 ratio. Selenium insertion into $CpCoB_9CH_9 \cdot NMe_3$ using sodium polyselenide provides $B_9SeCH_9 \cdot NMe_3$, whose suggested structure is shown in Fig. 50. The
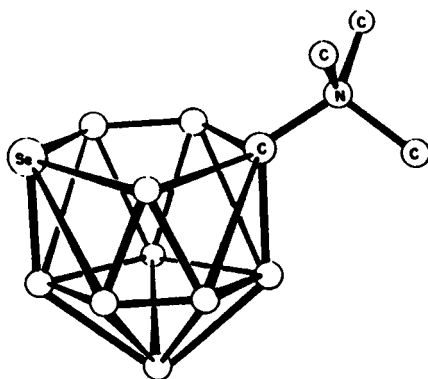


FIG. 50. Proposed structure of $B_9SeCH_9$.

^{11}B NMR spectrum of this compound is not well resolved at 70·6 MHz; doublets are observed at 5·3 (d, 1B, 151) and −40·9 (d, 1B, 149) ppm. In addition, there is an unusually sharp doublet at −17·0 ppm which is attributed to the boron atom on the open face of the cage, located between carbon and selenium.[164]

## XXV. BORATE GLASSES

Broad-line $^{10}$B and $^{11}$B NMR spectra have provided useful information about structural features in borate glasses which would have been difficult to obtain otherwise owing to the absence of long range order. Examination of $^{10}$B resonances in sodium borate glasses reveals the presence of five boron sites. There are two types of $BO_4$ units, those connected to all $BO_3$ units or to one $BO_4$ and three $BO_3$ units. Three-coordinate boron in $BO_3$ sites may be connected to all $BO_4$ units, to all $BO_3$ units, or to a combination of the two.[165] $^{11}$B NMR spectroscopy has been used to estimate the fraction of boron atoms contained in $BO_4$ units in glasses formed from the ternary system $K_2O-B_2O_3-P_2O_5$.[166] In view of the increasing technological interest in ceramics and in materials useful at high temperatures, these boron magnetic resonance techniques should assume greater importance in the future.

## REFERENCES

1. L. J. Todd and A. R. Siedle, *Progr. NMR Spectroscopy*, 1979, **13**, 87.
2. H. Nöth and B. Wrackmeyer, in *NMR Spectroscopy of Boron Compounds*, Springer Verlag, 1978.
3. R. N. Weiss and R. N. Grimes, *J. Amer. Chem. Soc.*, 1978, **100**, 1401.
4. R. N. Weiss and R. N. Grimes, *J. Amer. Chem. Soc.*, 1977, **99**, 1036.
5. C. R. Balulescu and P. C. Keller, *Inorg. Chem.*, 1978, **17**, 3707.
6. B. G. Cooksey, J. D. Gorham, J. H. Morris and L. Kane, *J. Chem. Soc. Dalton*, 1978, 141.
7. E. L. Hoel, M. Talebinasab-Savari and M. F. Hawthorne, *J. Amer. Chem. Soc.*, 1977, **99**, 4356.
8. D. F. Gaines and J. L. Walsh, *Inorg. Chem.*, 1978, **17**, 806.
9. H. Nöth and R. Rurlander, *Inorg. Chem.*, 1981, **20**, 1062.
10. G. E. Herberich, B. Buller, B. Hessner and W. Oschmann, *J. Organometal. Chem.*, 1980, **195**, 253.
11. G. Schmidt and J. Schultze, *Angew. Chem. Internat. Ed.*, 1977, **16**, 249.
12. G. E. Herberich, J. Hengesbach, U. Kolle and W. Oschmann, *Angew. Chem. Internat. Ed.*, 1977, **16**, 42.
13. J. Schultze and G. Schmid, *Angew. Chem. Internat. Ed.*, 1980, **19**, 54.
14. G. E. Herberich and M. Thonnessen, *J. Organometal. Chem.*, 1979, **177**, 357.
15. H. C. Brown and B. Singaram, *Inorg. Chem.*, 1980, **19**, 455.
16. H. C. Brown and S. U. Kulkarni, *Inorg. Chem.*, 1977, **16**, 3090.
17. J. M. Burtlich, J. H. Burk, M. E. Leonowicz and R. E. Hughes, *Inorg. Chem.*, 1979, **18**, 1702.
18. W. Biffer and H. Nöth, *Angew. Chem. Internat. Ed.*, 1980, **19**, 58.
19. N. M. D. Brown, F. Davidson, R. McMullen and J. W. Wilson, *J. Organometal. Chem.*, 1980, **193**, 271.

20. B. Wrackmeyer and H. Nöth, *Chem. Ber.*, 1977, **110**, 1086.
21. R. Goetze and H. Nöth, *J. Organometal. Chem.*, 1978, **145**, 151.
22. B. Wrackmeyer, *Z. Naturforsch.*, 1980, **35b**, 439.
23. J. D. Odom, T. F. Moore, R. Goetze, H. Nöth and B. Wrackmeyer, *J. Organometal. Chem.*, 1979, **173**, 15.
24. A. J. Zozulin, H. J. Jakobsen, T. F. Moore, A. R. Garber and J. D. Odom, *J. Magn. Resonance*, 1980, **41**, 458.
25. S. Brownstein, *J. Chem. Soc. Chem. Commun.*, 1980, 149.
26. J. B. Leach, M. A. Toft, F. L. Himpsl and S. G. Shore, *J. Amer. Chem. Soc.*, 1981, **103**, 988.
27. B. T. Pennington, M. A. Chiusano, D. J. Dye, E. D. Martin and D. R. Martin, *J. Inorg. Nucl. Chem.*, 1978, **40**, 389.
28. K. Schluter and A. Berndt, *Angew. Chem. Internat. Ed.*, 1980, **19**, 57.
29. W. Biffar, H. Nöth and H. Pommerening, *Angew. Chem. Internat. Ed.*, 1980, **19**, 56.
30. F. Bachman, H. Nöth, H. Pommerening, B. Wrackmeyer and T. Wirthlin, *J. Magn. Resonance*, 1979, **34**, 237.
31. W. Siebert and W. Rothermel, *Angew. Chem. Internat. Ed.*, 1977, **16**, 333.
32. C. A. Brown, *J. Organometal. Chem.*, 1978, **156**, C17.
33. D. F. Gaines and S. J. Hildebrandt, *Inorg. Chem.*, 1978, **17**, 794.
34. M. W. Chen, D. F. Gaines and L. G. Hoard, *Inorg. Chem.*, 1980, **19**, 2989.
35. R. K. Hertz, R. Goetze and S. G. Shore, *Inorg. Chem.*, 1979, **18**, 2813.
36. M. Kameda and G. Kodama, *Inorg. Chem.*, 1980, **19**, 2288.
37. M. Kameda and G. Kodama, *J. Amer. Chem. Soc.*, 1980, **102**, 3647.
38. W. Siebert and M. Bochmann, *Angew. Chem. Internat. Ed.*, 1977, **16**, 857.
39. A. R. Dodds and G. Kodama, *Inorg. Chem.*, 1979, **18**, 1465.
40. H. Kondo and G. Kodama, *Inorg. Chem.*, 1979, **18**, 1460.
41. J. D. Odom, T. F. Moore, W. H. Dawson, A. R. Garber and E. J. Stampf, *Inorg. Chem.*, 1979, **18**, 2179.
42. C. B. Ungerman and T. Onak, *Inorg. Chem.*, 1977, **16**, 1428.
43. K. E. Inkrott and S. G. Shore, *J. Chem. Soc. Chem. Commun.*, 1978, 866.
44. T. Davan and J. A. Morrison, *Inorg. Chem.*, 1979, **18**, 3194.
45. R. Wilczynski and L. G. Sneddon, *J. Amer. Chem. Soc.*, 1980, **102**, 2857.
46. D. F. Gaines and M. W. Jorgenson, *Inorg. Chem.*, 1980, **19**, 1398.
47. M. Kameda and G. Kodama, *Inorg. Chem.*, 1980, **19**, 2288.
48. J. Dubin, S. Hermanek and B. Stibr, *J. Chem. Soc. Chem. Commun.*, 1978, 287.
49. G. Siwapinyoyos and T. Onak, *J. Amer. Chem. Soc.*, 1980, **102**, 420.
50. J. B. Leach, G. Oates, J. B. Handley, A. P. Fung and T. Onak, *J. Chem. Soc. Dalton*, 1977, 819.
51. J. F. Ditter, E. B. Klusman, R. E. Williams and T. Onak, *Inorg. Chem.*, 1976, **15**, 1063.
52. T. Onak, A. P. Fung, G. Siwapinyoyos and J. B. Leach, *Inorg. Chem.*, 1979, **18**, 2878.
53. I. S. Jaworiwsky, J. R. Long, L. Barton and S. G. Shore, *Inorg. Chem.*, 1979, **18**, 56.
54. M. Kameda and G. Kodama, *Inorg. Chem.*, 1981, **20**, 1072.
55. R. J. Remmel, D. L. Denton, J. B. Leach, M. A. Toft and S. G. Shore, *Inorg. Chem.*, 1981, **20**, 1270.
56. P. J. Dolan, D. C. Moody and R. O. Schaeffer, *Inorg. Chem.*, 1981, **20**, 745.
57. H. Nöth and H. Pommerening, *Angew. Chem. Internat. Ed.*, 1980, **19**, 482.
58. K. Base, S. Hermanek and B. Stibr, *Chem. and Ind.*, 1977, 951.
59. F. R. Scholer, R. D. Brown, D. Gladkowski, W. F. Wright  and L. J. Todd, *Inorg. Chem.*, 1979, **18**, 921.
60. G. D. Mercer and F. R. Scholer, *Inorg. Chem.*, 1974, **13**, 2256.
61. L. J. Todd, A. R. Siedle, F. Sato, A. R. Garber, F. R. Scholer and G. D. Mercer, *Inorg. Chem.*, 1975, **14**, 1249.

62. J. Smith, G. Alexander and H. D. Smith, *Inorg. Chem.*, 1977, **16**, 1814.
63. E. H. Wong and R. M. Kabbani, *Inorg. Chem.*, 1980, **19**, 451.
64. D. Saulys and J. A. Morrison, *Inorg. Chem.*, 1980, **19**, 3057.
65. N. N. Greenwood and J. D. Kennedy, *J. Chem. Soc. Chem. Commun.*, 1979, 1099.
66. T. J. Dupont, R. E. Loffredo, R. C. Haltiwanger, C. A. Turner and A. D. Norman, *Inorg. Chem.*, 1978, **17**, 2062.
67. J. D. Kennedy and N. N. Greenwood, *Inorg. Chim. Acta*, 1980, **38**, 93.
68. A. R. Siedle, G. M. Bodner, A. R. Garber, D. C. Beer and L. J. Todd, *Inorg. Chem.*, 1974, **10**, 2321.
69. S. Hermanek, J. Plesek, V. Gregor and B. Stibr, *J. Chem. Soc. Chem. Commun.*, 1977, 561.
70. J. S. Plotkin, R. J. Astheimer and L. G. Sneddon, *J. Amer. Chem. Soc.*, 1979, **101**, 4155.
71. R. J. Astheimer, J. S. Plotkin and L. G. Sneddon, *J. Chem. Soc. Chem. Commun.*, 1979, 108.
72. J. Kroner and B. Wrackmeyer, *J. Chem. Soc. Faraday II*, 1976, **72**, 2283.
73. J. S. Plotkin and L. G. Sneddon, *Inorg. Chem.*, 1979, **18**, 2165.
74. N. N. Greenwood, J. D. Kennedy, W. S. McDonald, J. Staves and D. Taylorson, *J. Chem. Soc. Chem. Commun.*, 1979, 17.
75. S. K. Boocok, N. N. Greenwood, J. D. Kennedy and D. Taylorson, *J. Chem. Soc. Chem. Commun.*, 1979, 16.
76. E. L. Anderson, R. L. DeKock and T. P. Fehlner, *J. Amer. Chem. Soc.*, 1980, **102**, 2644.
77. N. S. Hosmane and R. N. Grimes, *Inorg. Chem.*, 1979, **18**, 2886.
78. E. I. Tolpin, G. R. Wellum and S. A. Berley, *Inorg. Chem.*, 1978, **17**, 2867.
79. J. S. Plotkin and L. G. Sneddon, *J. Amer. Chem. Soc.*, 1977, **99**, 3011.
80. J. Plesek, Z. Janousek and S. Hermanek, *Coll. Czech. Chem. Commun.*, 1978, **43**, 1332.
81. J. Plesek and S. Hermanek, *Coll. Czech. Chem. Commun.*, 1978, **43**, 1325.
82. D. F. Gaines and J. L. Walsh, *Inorg. Chem.*, 1978, **17**, 1238.
83. D. F. Gaines, J. L. Walsh and J. C. Calabrese, *Inorg. Chem.*, 1978 **17**, 1242.
84. D. F. Gaines, K. M. Coleson and J. C. Calabrese, *J. Amer. Chem. Soc.*, 1979, **101**, 3979.
85. D. F. Gaines, J. L. Walsh, J. H. Morris and D. F. Hillenbrand, *Inorg. Chem.*, 1978, **17**, 1516.
86. M. B. Fischer and D. F. Gaines, *Inorg. Chem.*, 1979, **18**, 3200.
87. G. Medford and S. G. Shore, *J. Amer. Chem. Soc.*, 1978, **100**, 3953.
88. E. L. Anderson and T. P. Fehlner, *J. Amer. Chem. Soc.*, 1978, **100**, 4606.
89. E. L. Anderson, K. J. Haller and T. P. Fehlner, *J. Amer. Chem. Soc.*, 1979, **101**, 4390.
90. R. Weiss and R. N. Grimes, *J. Amer. Chem. Soc.*, 1977, **99**, 8087.
91. S. G. Shore, J. D. Regaini, R. L. Smith, C. E. Cottrell and T. P. Fehlner, *Inorg. Chem.*, 1979, **18**, 670.
92. R. N. Grimes, E. Sinn and R. B. Maynard, *Inorg. Chem.*, 1980, **19**, 2384.
93. W. M. Maxwell, K. S. Wong and R. N. Grimes, *Inorg. Chem.*, 1977, **16**, 3094.
94. C. G. Salentine and M. F. Hawthorne, *Inorg. Chem.*, 1978, **17**, 1498.
95. C. W. Jung and M. F. Hawthorne, *J. Amer. Chem. Soc.*, 1980, **102**, 3024.
96. C. W. Jung, R. T. Baker and M. F. Hawthorne, *J. Amer. Chem. Soc.*, 1981, **103**, 810.
97. C. W. Jung, R. T. Baker, C. B. Knobler and M. F. Hawthorne, *J. Amer. Chem. Soc.*, 1980, **102**, 5782.
98. E. H. S. Wong and M. F. Hawthorne, *Inorg. Chem.*, 1978, **17**, 2863.
99. V. R. Miller, R. Weiss and R. N. Grimes, *J. Amer. Chem. Soc.*, 1977, **99**, 5646.
100. J. R. Pipal and R. N. Grimes, *Inorg. Chem.*, 1977, **16**, 3251.
101. J. R. Pipal and R. N. Grimes, *Inorg. Chem.*, 1977, **16**, 3255.
102. J. R. Pipal and R. N. Grimes, *Inorg. Chem.*, 1979, **18**, 252.
103. J. R. Pipal and R. N. Grimes, *Inorg. Chem.*, 1978, **17**, 10.

104. K. Wade, *Adv. Inorg. Chem. Radiochem.*, 1976, **18**, 1.
105. J. R. Pipal and R. N. Grimes, *Inorg. Chem.*, 1979, **18**, 257.
106. R. Weiss, J. R. Bowser and R. N. Grimes, *Inorg. Chem.*, 1978, **17**, 1522.
107. J. R. Pipal, W. M. Maxwell and R. N. Grimes, *Inorg. Chem.*, 1978, **17**, 1447.
108. G. K. Barker, M. Green, M. P. Garcia, F. G. A. Stone, J.-M. Bassett and A. J. Welch, *J. Chem. Soc. Chem. Commun.*, 1980, 1266.
109. G. Z. Zimmerman, R. Wilczynski and L. G. Sneddon, *J. Organometal. Chem.*, 1978, **154**, C29.
110. R. Wilczynski and L. G. Sneddon, *Inorg. Chem.*, 1979, **18**, 864.
111. L. W. Hall, G. J. Zimmerman and L. G. Sneddon, *J. Chem. Soc. Chem. Commun.*, 1977, 45.
112. D. Finster, E. Sinn and R. N. Grimes, *J. Amer. Chem. Soc.*, 1981, **103**, 1399.
113. C. W. Jung, R. T. Baker and M. F. Hawthorne, *J. Amer. Chem. Soc.*, 1981, **103**, 810.
114. C. W. Jung and M. F. Hawthorne, *J. Amer. Chem. Soc.*, 1980, **102**, 3024.
115. W. C. Kalb, C. W. Kriemendahl, D. C. Busby and M. F. Hawthorne, *Inorg. Chem.*, 1980, **19**, 1590.
116. G. E. Hardy, K. P. Callahan, C. E. Strouse and M. F. Hawthorne, *Acta Cryst.*, 1976, **32B**, 264.
117. A. R. Siedle, G. M. Bodner and L. J. Todd, *J. Organometal. Chem.*, 1971, **33**, 137.
118. Z. Demidowicz, R. G. Teller and M. F. Hawthorne, *J. Chem. Soc. Chem. Commun.*, 1979, 831.
119. W. C. Kalb, R. G. Teller and M. F. Hawthorne, *J. Amer. Chem. Soc.*, 1979, **101**, 5417.
120. R. N. Leyden, B. P. Sullivan, R. T. Baker and M. F. Hawthorne, *J. Amer. Chem. Soc.*, 1978, **100**, 3758.
121. J. R. Bowser, A. Bonny, J. R. Pipal and R. N. Grimes, *J. Amer. Chem. Soc.*, 1979, **101**, 6229.
122. G. K. Barker, M. Green, F. G. A. Stone, A. J. Welch, T. P. Onak and G. Siwapanyoyos, *J. Chem. Soc. Dalton*, 1979, 1687.
123. G. K. Barker, M. Green, T. P. Onak, F. G. A. Stone, C. B. Ungerman and A. J. Welch, *J. Chem. Soc. Chem. Commun.*, 1978, 169.
124. G. K. Barker, M. Green, F. G. A. Stone, A. J. Welch and W. C. Wolsey, *J. Chem. Soc. Chem. Commun.*, 1980, 627.
125. T. K. Hilty, D. A. Thompson, W. M. Butler and R. W. Rudolph, *Inorg. Chem.*, 1979, **18**, 2642.
126. N. N. Greenwood, J. D. Kennedy and J. Staves, *J. Chem. Soc. Dalton*, 1978, 1146.
127. N. N. Greenwood and J. Staves, *J. Chem. Soc. Dalton*, 1978, 1144.
128. N. N. Greenwood and J. Staves, *J. Chem. Soc. Dalton*, 1977, 1786.
129. N. N. Greenwood and J. Staves, *J. Chem. Soc. Dalton*, 1977, 1788.
130. N. N. Greenwood, J. A. Howard and W. S. McDonald, *J. Chem. Soc. Dalton*, 1977, 37.
131. J. D. Kennedy and J. Staves, *Z. Naturforsch.*, 1978, **34b**, 808.
132. N. N. Greenwood, J. D. Kennedy, C. G. Savory, J. Staves and K. R. Trigwell, *J. Chem. Soc. Dalton*, 1978, 237.
133. W. M. Maxwell, V. R. Miller and R. N. Grimes, *J. Amer. Chem. Soc.*, 1976, **98**, 4818.
134. W. M. Maxwell, V. R. Miller and R. N. Grimes, *Inorg. Chem.*, 1976, **15**, 1343.
135. W. M. Maxwell, R. F. Bryan and R. N. Grimes, *J. Amer. Chem. Soc.*, 1977, **99**, 4008.
136. W. M. Maxwell, R. Weiss, E. Sinn and R. N. Grimes, *J. Amer. Chem. Soc.*, 1977, **99**, 4016.
137. J. R. Pipal and R. N. Grimes, *Inorg. Chem.*, 1978, **17**, 6.
138. R. N. Grimes, E. Sinn and J. R. Pipal, *Inorg. Chem.*, 1980, **19**, 2087.
139. K.-S. Wong, J. R. Bowser, J. R. Pipal and R. N. Grimes, *J. Amer. Chem. Soc.*, 1978, **100**, 5045.

140. J. R. Pipal and R. N. Grimes, *Inorg. Chem.*, 1979, **18**, 1936.
141. W. M. Maxwell and R. N. Grimes, *Inorg. Chem.*, 1979, **18**, 2174.
142. R. N. Grimes, J. R. Pipal and E. Sinn, *J. Amer. Chem. Soc.*, 1979, **101**, 4172.
143. J. R. Pipal and R. N. Grimes, *J. Amer. Chem. Soc.*, 1978, **100**, 3083.
144. D. Finster, E. Sinn and R. N. Grimes, *J. Amer. Chem. Soc.*, 1981, **103**, 1399.
145. R. N. Grimes, W. M. Maxwell, R. B. Maynard and E. Sinn, *Inorg. Chem.*, 1980, **19**, 2981.
146. T. P. Fehlner, *J. Amer. Chem. Soc.*, 1980, **102**, 3424.
147. W. Siebert and M. E. M. El-Essawi, *Chem. Ber.*, 1979, **112**, 1480.
148. W. F. Wright, A. R. Garber and L. J. Todd, *J. Magn. Resonance*, 1978, **30**, 595.
149. G. D. Friesen, A. Barriola and L. J. Todd, *Chem. and Ind.*, 1978, 631.
150. G. D. Friesen, A. Barriola, P. Daluga, P. Ragatz, J. C. Huffman and L. J. Todd, *Inorg. Chem.*, 1980, **19**, 458.
151. J. Plesek, S. Hermanek and Z. Janousek, *Coll. Czech. Chem. Commun.*, 1977, **42**, 785.
152. D. Friesen, R. L. Kump and L. J. Todd, *Inorg. Chem.*, 1980, **19**, 1485.
153. A. R. Siedle, G. M. Bodner, A. R. Garber and L. J. Todd, *Inorg. Chem.*, 1980, **19**, 1485.
154. J. L. Little and S. S. Pao, *Inorg. Chem.*, 1978, **17**, 584.
155. J. L. Little, G. D. Friesen and L. J. Todd, *Inorg. Chem.*, 1977, **16**, 869.
156. J. L. Little, *Inorg. Chem.*, 1979, **18**, 1598.
157. G. D. Friesen, J. L. Little, J. C. Huffman and L. J. Todd, *Inorg. Chem.*, 1979, **18**, 755.
158. G. D. Friesen and L. J. Todd, *J. Chem. Soc. Chem. Commun.*, 1978, 349.
159. G. J. Zimmerman and L. G. Sneddon, *J. Amer. Chem. Soc.*, 1981, **103**, 1102.
160. W. R. Pretzer, T. K. Hilty and R. W. Rudolph, *Inorg. Chem.*, 1975, **14**, 2459.
161. W. L. Smith, B. J. Meneghelli, D. A. Thompson, P. Klymo, N. McClure, M. Bower and R. W. Rudolph, *Inorg. Chem.*, 1977, **16**, 3008.
162. R. J. Meneghelli and R. W. Rudolph, *J. Organometal. Chem.*, 1977, **133**, 139.
163. B. J. Meneghelli, M. Bower, N. Canter and R. W. Rudolph, *J. Amer. Chem. Soc.*, 1980, **102**, 4335.
164. R. V. Schultz, J. C. Huffman and L. J. Todd, *Inorg. Chem.*, 1979, **18**, 2883.
165. G. E. Jellison and P. J. Bray, *J. Non-Cryst. Solids*, 1978, **29**, 187.
166. Y. H. Yun and P. J. Bray, *J. Non-Cryst. Solids*, 1978, **30**, 45.
167. M. J. Park, K. S. Kim and P. J. Bray, *Phys. Chem. Glasses*, 1979, **20**, 31.

This Page Intentionally Left Blank

# Dynamic NMR Spectroscopy in Inorganic and Organometallic Chemistry

## B. E. MANN

*Department of Chemistry, University of Sheffield, Sheffield S3 7HF, U.K.*

## I. INTRODUCTION

The chemical aspects of dynamic NMR spectroscopy in inorganic and organometallic chemistry have been extensively reviewed,[1-4] and consequently the emphasis of this review is on the challenge offered to NMR spectroscopists by certain dynamic properties of inorganic and organometallic compounds. Well established areas are omitted.

Although, in principle, there are no differences in the applications of dynamic NMR spectroscopy to each branch of chemistry, differences exist in the types of problem available for study. In inorganic chemistry there are several classes of problem not commonly found in other areas.

(1) Multisite intramolecular exchange can occur, as shown for $Fe(\eta^4\text{-}C_8H_8)(CO)_3$ (1). The analysis of the four-site exchange problem is simple



(1)
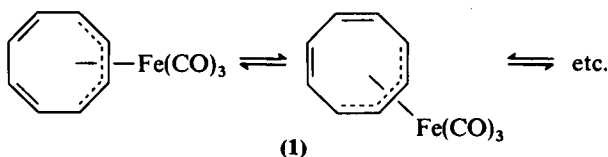
from the $^{13}$C NMR spectrum, but the analysis of the dynamic $^1$H NMR spectrum collapsing from [ABCD]$_2$ to a singlet is a far from trivial exercise.

(2) "Other nuclei" are frequently available, but their use in dynamic NMR studies is often avoided owing to sensitivity problems and the temperature dependence of the chemical shift and linewidth in the absence of exchange; for example, for $^{59}$Co in Co$_4$(CO)$_{12}$ (2), two signals in the intensity



(2)
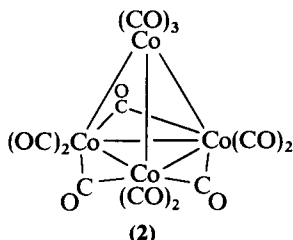
ratio 3 : 1 are observed at low temperature while at room temperature only one signal is observed.[5,6]

(3) Rapid exchange is commonly found in organometallic compounds requiring very low temperatures to obtain limiting spectra. Although, in principle, temperatures below −100 °C are available, suitable solvents are difficult to find. Thus Fe$_2$(CO)$_9$ (3) shows only one $^{13}$CO signal at room



(3)
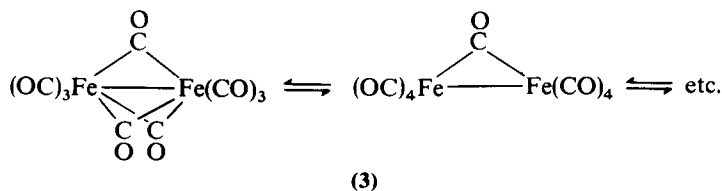
temperature where two are expected for a static structure.[7] Owing to limited solubility, limiting low temperature spectra have not been reported. In many cases, at the lowest achievable temperature, some broadening is observed but, in the absence of values for the limiting low temperature chemical shifts, rate data are not available; for example, the fluxional process shown for Pt($\eta^3$-CPh$_3$)(acac) (4) can be slowed enough at −90 °C



(4)
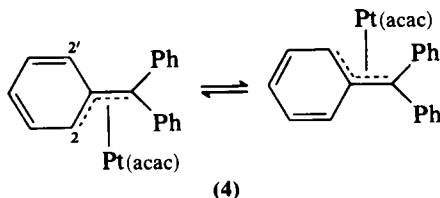
to cause a broadening of 10 Hz in the averaged 2,2′ $^{13}$C signal at 25·15 MHz.[8]

(4) Methyl group rotation in organic compounds has received consider-able attention. Similar problems exist in inorganic and organometallic chemistry, and a detailed investigation could yield interesting information on the balance of electronic compared with steric factors in the rotation of groups on metals, e.g. the rotation about metal–$NH_3$, –$OH_2$ (how significant is $\pi$ donation from the water to the metal?), and –$\eta^5$-$C_5H_5$ (is there any tendency of the $\eta^5$ ring to become $\eta^3$?).

In most cases the techniques to solve these problems already exist, but were developed using commercially available organic compounds. Many of these techniques are not readily available to the synthetic inorganic or organometallic chemist since they require specialist knowledge and/or equipment. It is hoped that this review will bring NMR spectroscopists and inorganic/organometallic chemists together, so a number of NMR tech-niques are examined, applications to inorganic/organometallic problems discussed, and further applications suggested. With a view to encouraging the application of advanced dynamic NMR spectroscopy to inorganic and organometallic problems, the approach is two-fold: techniques of potential value are discussed and then the mechanisms found in inorganic and organometallic chemistry are outlined.

## II. IDENTIFICATION OF NMR DIFFERENTIABLE REACTIONS

In the vast majority of dynamic processes in inorganic and organometallic compounds the derivation of the mechanism comes from the investigators drawing up a list of chemically feasible exchange processes and then using line shape analysis to test which mechanism(s) fit the observed spectra. Although this procedure is correct if all possible processes are identified, in complicated cases it is easy to omit some processes. This problem may be avoided by the use of a matrix representation of the exchange,[9] which has been discussed in detail elsewhere;[10] for example, for [Pd($\eta^3$-2-MeC$_3$H$_4$)(Ph$_2$PCH$_2$CH$_2$PPh$_2$)]$^+$ (5), possible mechanisms are given in



(5)
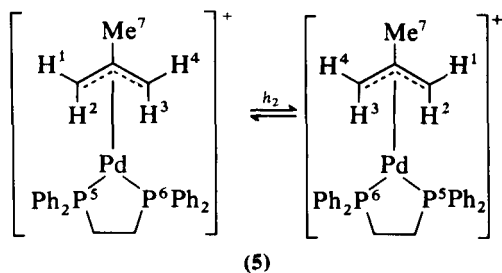
Table 1 as a matrix representation ($h_2$ is shown in the scheme). It is clear, from examination of the great variety of permutations in Table 1,

## TABLE 1

Exchange operations for $[Pd(2\text{-Me-allyl})(Ph_2PCH_2CH_2PPh_2)]^+$ (5); numbering as in the scheme.

| | | |
|---|---|---|
| $h_2 = (14)(23)(56)(7)$ | $h_7 = (12)(34)(56)(7)$ | $h_{12} = (1324)(56)(7)$ |
| $h_3 = (1)(2)(3)(4)(56)(7)$ | $h_8 = (13)(24)(5)(6)(7)$ | $h_{13} = (12)(3)(4)(56)(7)$ |
| $h_4 = (14)(23)(5)(6)(7)$ | $h_9 = (12)(3)(4)(5)(6)(7)$ | $h_{14} = (1)(2)(34)(56)(7)$ |
| $h_5 = (12)(35)(5)(6)(7)$ | $h_{10} = (1)(2)(34)(5)(6)(7)$ | $h_{15} = (1423)(5)(6)(7)$ |
| $h_6 = (13)(24)(56)(7)$ | $h_{11} = (1423)(56)(7)$ | $h_{16} = (1324)(5)(6)(7)$ |

that the usual approach of inspection frequently leads to omissions. For **5** a number of these mechanisms cannot be differentiated by NMR spectroscopy, but when these problems are realized it is possible to examine suitable derivatives to differentiate between mechanisms. Thus in **5** it is not possible to differentiate between $h_3$ and $h_4$, but if $[Pd(\eta^3\text{-}1\text{-}Pr^iC_3H_4)(Ph_2PCH_2CH_2PPh_2)]^+$ is used then the prochiral isopropyl methyl groups provide a method for differentiation.

Two mechanisms have been identified in related complexes. Thus allyl rotation ($h_3$) is observed in $Mo(\eta\text{-}C_3H_5)(\eta\text{-}C_5H_5)(CO)_2$ and a number of related compounds. The most common mechanism observed is $\pi \rightarrow \sigma$ conversion of the allyl, either intramolecularly (e.g. **6**) or intermolecularly (e.g. **7**), which can give rise to a number of rearrangements. Most of these

$$\text{[structure]} \quad \rightleftharpoons \quad \text{[structure]}-CH_2-Mo(\eta\text{-}C_5H_5)(CO)_2$$

Mo($\eta$-C$_5$H$_5$)(CO)$_2$

(6)

$$\left[\ \overset{Me}{\underset{Ph_2P\diagdown Pd \diagup PPh_2}{\bigtriangleup}}\ \right]^+ \quad \underset{}{\overset{\text{pyridine}}{\rightleftharpoons}} \quad \overset{Me}{\underset{Ph_2P}{N-Pd-PPh_2}}$$

(7)
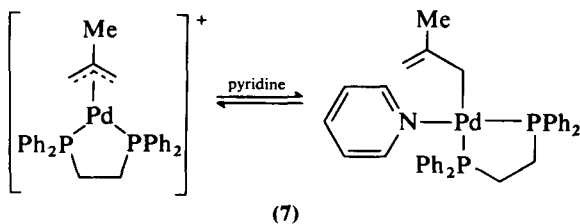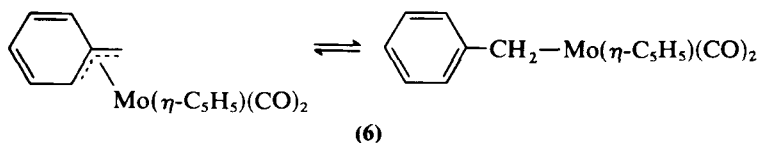
rearrangements should have different energies, but suitable investigations to differentiate between the mechanisms have not been performed. In order to do this the synthesis of carefully designed molecules is necessary, e.g. $[Pd(\eta^3\text{-}^{13}CH_2CPr^iCH_2)(Ph_2PCH_2CH_2PPh_2)]^+$ combined with detailed variable temperature multinuclear investigations.

## III. MULTISITE EXCHANGE IN COUPLED SYSTEMS

Although exchange between coupled sites is commonly observed in inorganic and organometallic chemistry, the coupled spectra are frequently analysed ignoring the coupling, or the problem is avoided by use of $^{13}C-\{^1H\}$ NMR spectroscopy. For example, the dynamic $^1H$ NMR spectrum of $Ru(\eta^4-C_8H_8)(CO)_3$ (8), a four-site exchange problem of $[ABCD]_2$ giving a singlet in the high temperature limit, was analysed as a simple four-site exchange problem with each site suitably broadened to represent the $^1H-^1H$ coupling (see Fig. 1). Subsequently the problem was reinvestigated using the more rigorous approach of $^{13}C-\{^1H\}$ NMR spectroscopy which is correctly analysed as a simple four-site exchange problem. Both approaches show that the mechanism is a 1,2 shift (see scheme), although the chemically



$$Ru(CO)_3 \qquad Ru(CO)_3$$

$$(8)$$
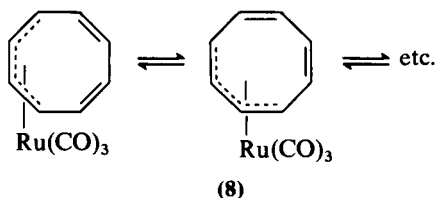
unlikely possibility of the metal moving from one face of the cyclo-octatetraene to the other was not considered. The agreement between the thermodynamic parameters derived using the two methods is remarkably good, with the $^1H$ NMR analysis yielding $E_a \approx 9.5$ kcal mol$^{-1}$ and log $A \approx$ 14, while the $^{13}C$ NMR analysis yields $E_a = 8.6 \pm 0.1$ kcal mol$^{-1}$ and log $A =$ $13.3 \pm 0.1$.[11,12] This agreement is in part attributable to the large chemical shift range permitting the dynamic process to be studied over a relatively large range of rates, 5–2100 s$^{-1}$, causing the inherent errors in the crude analysis of the $^1H$ NMR data to be small, but still significant.

One group has successfully analysed a large number of coupled systems, such as $[Rh\{P(OMe)_3\}_5]^+$, and used the coupling patterns to derive the mechanism.[13] Permutational analysis for a trigonal bipyramid shows that there are two groups of exchange processes which are differentiable by NMR spectroscopy. Mechanism (A) is better known as the Berry rearrangement; two mechanisms have been suggested that fit (B), the anti-Berry and



$$\text{(A)} \qquad \text{(B)}$$
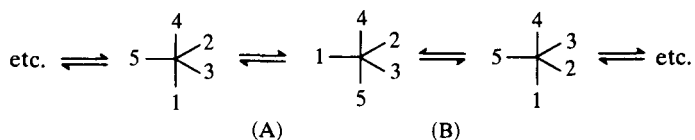
the turnstile mechanisms. For $[Rh\{P(OMe)_3\}_5]^+$, the $^{31}P-\{^1H\}$ spectrum is $A_2B_3X$ which is observed as the limiting low temperature spectrum at
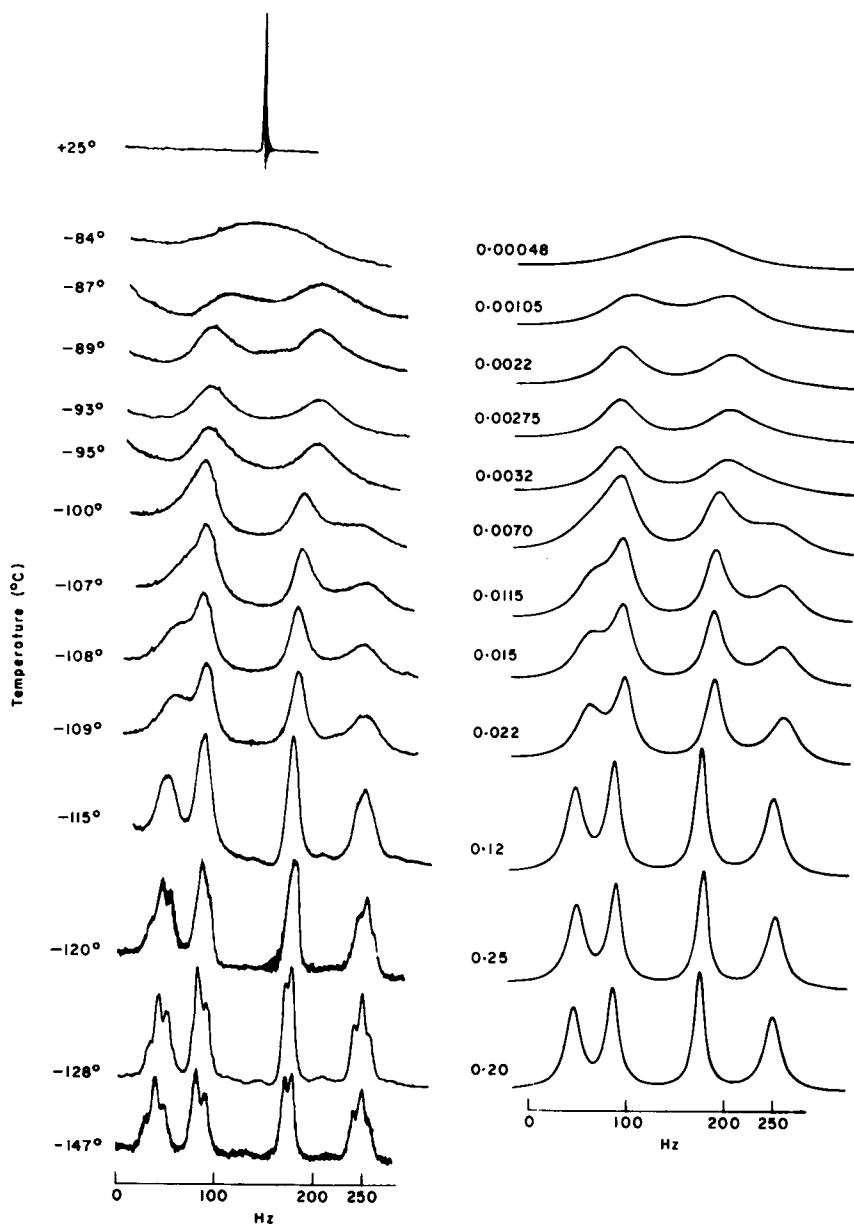
FIG. 1. Observed $^1$H NMR spectra (left) for Ru($\eta^4$-C$_8$H$_8$)(CO)$_3$ at various temperatures, and computed spectra (right) for various mean residence times based on 1,2 shifts. (Cotton, Davison, Marks and Musco[11])
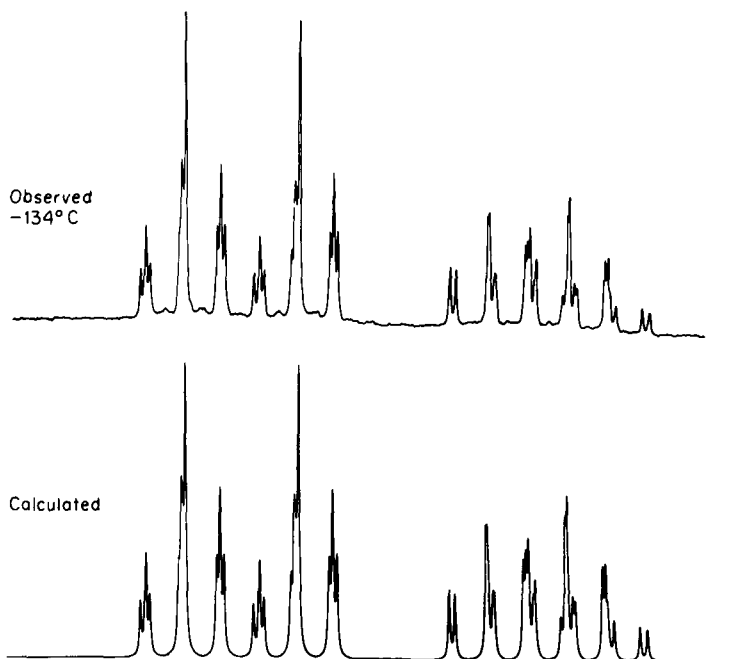
FIG. 2. Observed and simulated low-temperature (−134 °C) 36·43 MHz $^{31}$P–{$^{1}$H} NMR spectrum of [Rh{P(OMe)$_3$}$_5$]$^+$[BPh$_4$]$^-$ in 90% CHClF$_2$–10% CH$_2$Cl$_2$. (Jesson and Muetterties[13])

−134 °C (see Fig. 2). On warming to −114 °C exchange begins, and the observed $^{31}$P NMR spectrum is fitted on the basis of exchange processes (A) and (B) (see Fig. 3). Clearly exchange process (A) gives the better fit, but the differences are such that process (A) is not the proven mechanism. This is one of the rare examples where it has been possible to differentiate at all between the two mechanisms. In spite of this, it is the generally held dogma that the vast majority of trigonal bipyramidal molecules are fluxional by the Berry mechanism.

It is found that, the larger the ratio $J/\delta$ for the A$_2$B$_3$ or A$_2$B$_3$X spectrum in these complexes, the clearer the differences observed for the two dynamic processes, with no differences being observed when $J/\delta$ is small. Consequently this problem is best observed at low field. Thus the $^{19}$F NMR spectrum of SF$_4$ (9) was examined at 6·5 and 9·2 MHz in order to make



(9)
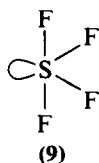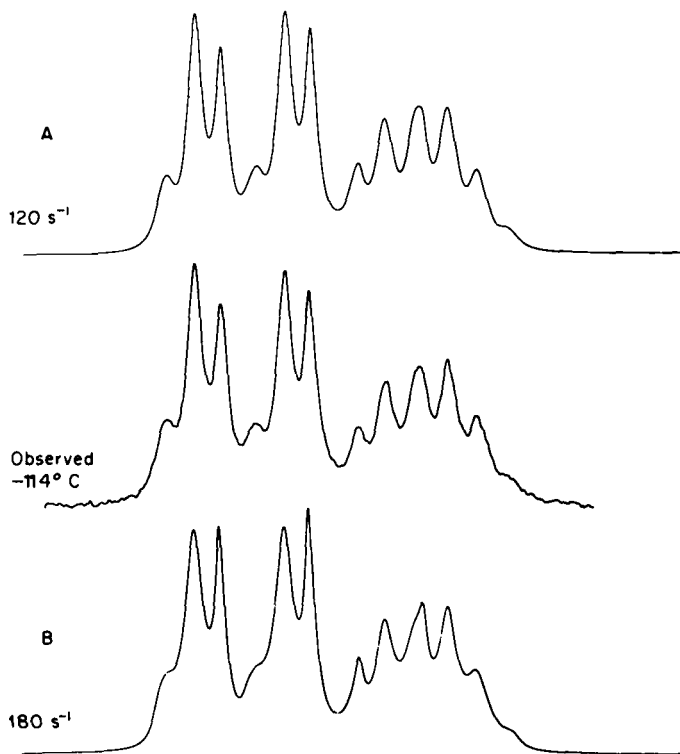
FIG. 3. Observed and calculated temperature-dependent $^{31}P-\{^1H\}$ NMR spectra for a solution of $[Rh\{P(OMe)_3\}_5]^+[BPh_4]^-$ in 90% $CHClF_2$–10% $CH_2Cl_2$ at $-114$ °C. The permutational mechanisms and exchange rates are given with the calculated spectra in the figure. Permutational mechanism A, which corresponds to simultaneous exchange of the axial ligands with two equatorial ligands, clearly gives the better fit. (Jesson and Muetterties[13])

the $^{19}F$ NMR spectrum strongly second-order.[14] After suitable precautions to avoid intermolecular exchange, it is shown that the dominant intramolecular fluorine exchange mechanism is process (A), i.e. the Berry mechanism.

It is clear that the use of coupling patterns yields additional mechanistic information which is normally ignored.

## IV. SPIN-SATURATION TRANSFER

Although spin-saturation transfer was first applied to exchange problems in 1963,[15] it has been rarely used in the area of inorganic/organometallic chemistry. This is surprising when it offers three advantages over other techniques:

(1) The accurate determination of exchange rates which are comparable with the $T_1$ of the nucleus being studied. When these measurements are combined with line shape analysis, two accurate regions of rate measurements are obtained in the Arrhenius/Eyring rate plot giving reliable activation parameters. When only one technique is used to determine rates, the activation parameters are subject to considerable errors due to inaccurate data at the two extremes of the plots.

(2) The study of slow processes where line shape analysis cannot be used on account of limitations due to available temperature ranges and/or sample decomposition. Thus Pd($\eta$-$C_7H_9$)(hfac) (**10**) is fluxional (see scheme). The



(**10**)
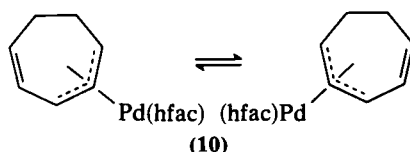
$^{13}$C NMR signals are broad at room temperature, but the sample decomposes, on warming, depositing palladium metal.[16] The exchanging carbon atoms are easily identified by use of spin-saturation transfer (see Fig. 4).
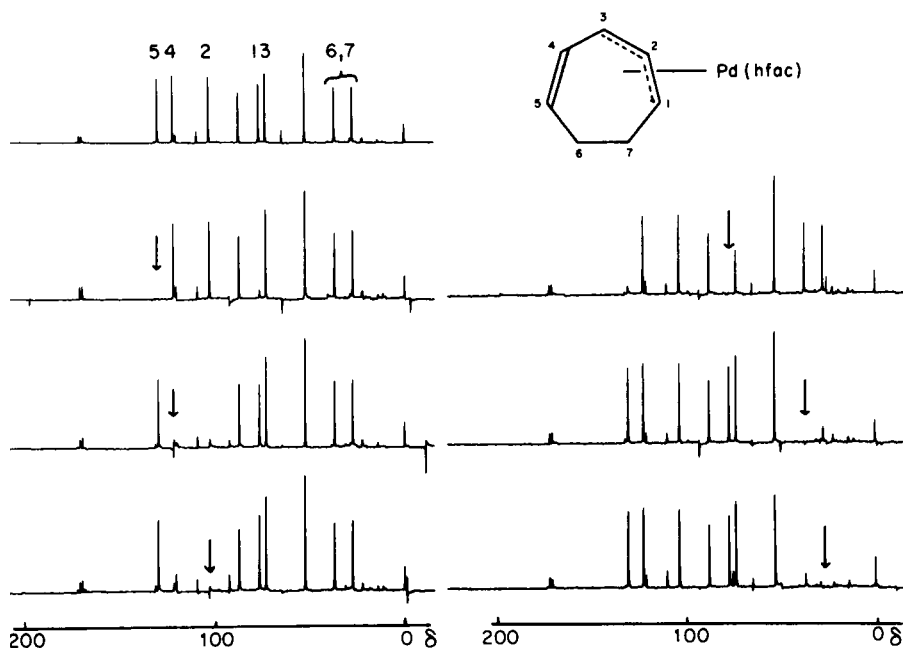


FIG. 4. The 25·15 MHz $^{13}$C NMR spectra of Pd($\eta^3$-$C_7H_9$)(hfac) showing saturation transfer from the saturated site (marked by arrow) to the exchanging site.

When site B is irradiated, the rate is determined by using the equation

$$k_A{}^{-1} = \frac{M_z{}^A(\infty)}{M_z{}^A(0) - M_z{}^A(\infty)} T_{1A} \qquad (1)$$

where $k_A{}^{-1}$ is the rate of exchange from site A, $T_{1A}$ is the spin–lattice relaxation time of site A, $M_z{}^A(0)$ is the magnetization at site A in the absence of irradiation at site B, and $M_z{}^A(\infty)$ is the equilibrium magnetization, i.e. at least $5(T_{1A}{}^{-1} + \tau_A{}^{-1})^{-1}$ s after the beginning of irradiation at site B.[17] Thus C(2) can be readily identified from its chemical shift and, as in Fig. 4, it exchanges with the signal at $\delta$ 128·4, thus C(4) is identified. Similar arguments permit the assignment of the other signals. This quantitative treatment is valid only if $T_{1A} = T_{1B}$, but a solution exists when $T_{1A} \neq T_{1B}$.[18]

A more elegant approach is to use a specific 180° pulse at site A. After a time $\tau$, a general 90° pulse is applied to observe both sites. The rate can be easily obtained from a plot of $\ln[M_z{}^A(t) - M_z{}^B(t)]$ against time, $t$, and the gradient is $-(T_1{}^{-1} + 2k_A)$; $M_z{}^A(t)$ is the magnetization (i.e. size) of
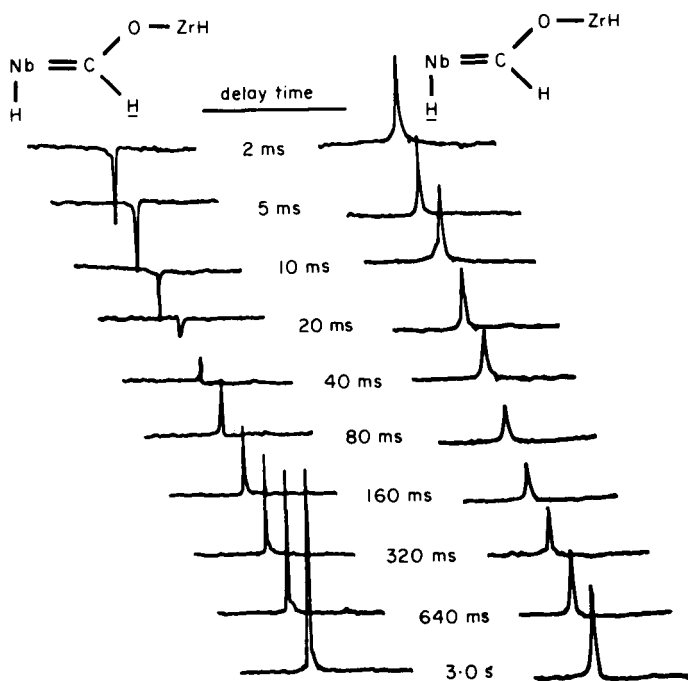


FIG. 5. Spin-saturation transfer experiments for $Cp_2(H)NbCHOZr(H)(C_5Me_5)_2$ in benzene-$d_6$ at 32·5 °C. The delay time is the interval between inversion of NbC$H$O and the observation pulse. (Threlkel and Bercaw[19])

the signal due to site A $t$ seconds after a specific 180° pulse has been applied to site A, and $k_A$ is the rate of leaving site A. In the derivation of equation (1) it is assumed that $T_1$ for both sites is the same. This method has been used to determine the rate of proton exchange in $Cp_2HNbCHOZrH(C_5Me_5)$ (see Fig. 5).[19]

(3) Line shape analysis gives the rate of leaving a site. For two-site problems it is usually possible to deduce to where the nucleus moves. However, for multisite exchange such a deduction is possible only in favourable cases. Spin-saturation labels the nuclei in one site with a non-equilibrium spin population. When these nuclei migrate to another site, they take their spin population information with them, thus labelling the site. For example, the $^{13}C$ NMR spectrum of $Cr(\eta^6\text{-}C_8H_8)(CO)_3$ shows equal line broadening for the four inequivalent cyclooctatetraene carbon atoms when exchange occurs.[20] Two mechanisms are consistent with this observation, a 1,3 shift mechanism (**11**) or a random shift mechanism (**12**).



(**11**)



(any consecutive six C atoms attached to the Cr atom)

(**12**)
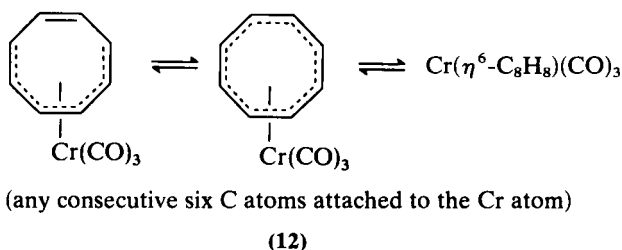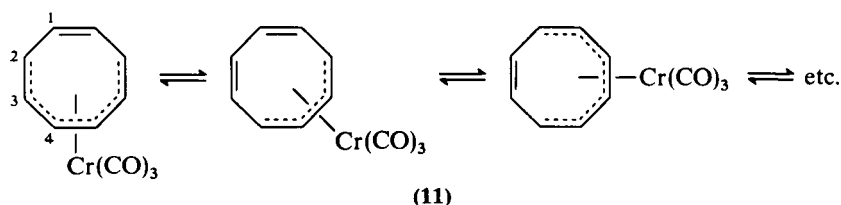
In the original report using line shape analysis, Cotton[47] favoured the latter mechanism while subsequently Whitesides[42] has argued in favour of the former mechanism. Some spin-saturation measurements are shown in Fig. 6. Simply, inspection of Fig. 6 shows that the spin-saturation transfer is non-uniform, and hence the mechanism must be the 1,3 shift. This is clearly shown by Fig. 6(b) where spin-saturation transfer has the greatest effect on the signals due to carbon atoms 2 and 3. The data were also treated quantitatively. After irradiating one site, the equation that applies for the Kth site[21] is

$$\frac{dM_z^K(t)}{dt} = \frac{M_z^K(0) - M_z^K(t)}{T_{1K}} - M_z^K(t) \sum_{\nu \neq K} \lambda_{K\nu} + \sum_{\nu \neq K} \lambda_{\nu K} M_z^\nu(t) \qquad (2)$$
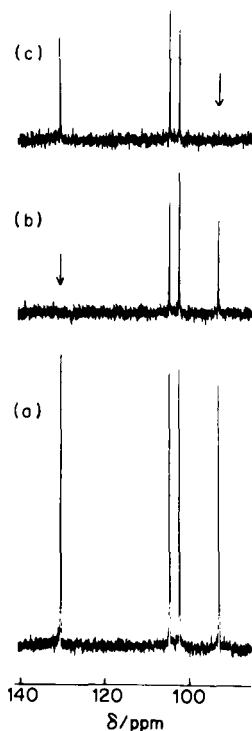
FIG. 6. Application of the Forsén–Hoffman spin-saturation method to the cyclo-octatetraene $^{13}$C resonances of $(\eta^6\text{-}C_8H_8)Cr(CO)_3$ in $CD_2Cl_2\text{-}CH_2Cl_2$ at $-15\,°C$: (a) normal spectrum; (b) irradiation at C(1); (c) irradiation at C(2). The places irradiated are indicated by arrows. (B. E. Mann, *J. Chem. Soc. Chem. Commun.*, 1977, 626)

where $\lambda_{K\nu}$ is the rate of exchange from site K to $\nu$. Solution of the series of simultaneous equations yields the separate exchange rates between each site. In the case of $Cr(\eta^6\text{-}C_8H_8)(CO)_3$ it is shown that, although the dominant mechanism is a 1,3 shift, 1,2 shifts also occur.

This technique is very powerful but has attracted very little attention. The greatest potential is in multiple site exchange problems, e.g. halogen exchange in mixtures of $SnCl_4$ and $SnBr_4$ or carbonyl scrambling in $Ir_4(CO)_{11}PMe_2Ph$.

## V. SPIN–LATTICE RELAXATION MEASUREMENTS

Extensive use has been made of spin–lattice relaxation time measurements to investigate intramolecular motion in organic molecules, but its application to inorganic and organometallic systems has been extremely limited. Several approaches have been used, and are illustrated here.

In a detailed study of $Sn(C^1H_3)_n(C^2H_3)_{4-n}$, $T_1(^1H)$, $T_1(^2H)$, $T_1(^{13}C)$, and $T_1(^{119}Sn)$ were measured as a function of temperature.[22] The internal rotation correlation time ($\tau_M$) and molecular correlation time ($\tau_\theta$) can be readily derived. For $T_1(^1H)$, the relaxation is purely intramolecular dipole–dipole and the relaxation rate is given by

$$T_{1dd}^{-1} = \frac{3\gamma_H^4 \hbar^2}{r_{HH}^6}\tau_c(H-H) \tag{3}$$

where $r_{HH}$ is the hydrogen–hydrogen distance. Additionally it is possible to show that

$$\tau_c(H-H) = \frac{1}{4}\tau_\theta + \frac{3}{4}\left(\frac{\tau_\theta\tau_M}{4\tau_\theta} + \tau_M\right) \tag{4}$$

Similarly for $T_1(^{13}C)$, the dipole–dipole component is derived from NOE measurements and the following equations apply

$$T_{1dd}^{-1} = \frac{3\gamma_H^2\gamma_c^2\hbar^2}{r_{CH}^6}\tau_c(C-H) \tag{5}$$

$$\tau(C-H) = \frac{1}{9}\tau_\theta + \frac{8}{27}\left(\frac{\tau_\theta\tau_M}{\tau_\theta} + \tau_M\right) + \frac{16}{27}\left(\frac{\tau_\theta\tau_M}{4\tau_\theta} + \tau_M\right) \tag{6}$$

Owing to the different coefficients in equations (4) and (6) it is possible to separate $\tau_M$ from $\tau_\theta$. From the temperature dependence of $\tau_M$ an activation of $0\cdot80$ kcal mol$^{-1}$ is determined. In this case the activation energy for molecular tumbling can be obtained from $T_1(^{119}Sn)$, and the agreement with the activation energy from $\tau_\theta$ is excellent.

This approach is good when there is a marked difference in angles between the rotation axis and the C–H vector, and the rotation axis and the H–H vector. This is the case for the rotation of a methyl group with $109°28'$ for the C–H vector and $90°$ for the H–H vector, but for the rotation of $\eta$-$C_5H_5$ groups the two angles are nearly the same. In this case an alternative approach is available. Provided that the molecule can be shown (or assumed) to be undergoing isotropic tumbling, the molecular tumbling time can be determined from $T_{1dd}$ for any C–H group within the rigid framework of the molecule. For a rotating group, $T_{1dd}$ will be longer owing to the additional motion due to rotation. The rotational correlation time is obtained by solving the equations

$$\frac{T_{1dd}(\text{rigid CH})}{T_{1dd}(\text{rotating CH})} = (1/4)(3\cos^2\theta - 1)^2 + 18(5+\chi)^{-1}\sin^2\theta\cos^2\theta$$

$$+ (9/4)(1+2\chi)^{-1}\sin^2\theta \tag{7}$$

$$\chi = (\tau_c + \tau_M)/\tau_M \tag{8}$$

where $\theta$ is the angle between the rotation axis and the C–H vector, $\tau_c$ is the rotation time, and $\tau_M$ is the molecular tumbling time. A temperature dependent study then yields the activation energy for rotation. This approach has recently been applied to a number of $\eta^5$-cyclopentadienyl groups and provides evidence for localization of bonding towards $\eta^3$-C$_5$H$_5$ in Pt($\eta$-2-Me-allyl)($\eta$-C$_5$H$_5$).[23]

An empirical approach has been used to estimate the barrier to methyl rotation, $V_0$. For organic molecules it has been shown[24] that the empirical equation

$$V_0 = (T_{1sr} - 25 \cdot 6)/9 \cdot 76 \tag{9}$$

relates the barrier to methyl rotation to the $^{13}$C spin–rotation relaxation time ($T_{1sr}$). This equation has subsequently been applied to organometallic compounds[25] and activation energies have been derived. Further work is necessary to test the validity of this approach.


## VI. SPIN–SPIN RELAXATION MEASUREMENTS

For the inorganic and organometallic chemist, the measurement of spin–spin relaxation times ($T_2$) has proved to have little attraction. This is understandable since most of the work is done on high-resolution spectrometers where the inherent magnetic field inhomogeneity is small. It is usually possible to cool the sample further to obtain additional broadening which is measurable in the extra linewidth. The attraction of this approach is that it can provide reliable rates near the high temperature limit. When this is combined with line shape analysis, which is quicker than $T_2$ measurements, and spin-saturation transfer measurements, highly accurate activation parameters should result.

For line shape analysis, the linewidth due to exchange ($\Delta\nu$) is normally determined directly from the spectrum, but it can also be calculated from $T_1$ and $T_2$ measurements. Only one inorganic/organometallic example appears to have been investigated, Fe(CO)$_5$.[26] It was shown that, at $-19 \cdot 5\,°$C, $T_1(^{13}$C) is predominantly controlled by chemical shielding anisotropy at 61 MHz with a small component due to spin–rotation. When $T_2(^{13}$C) is measured at $-19 \cdot 5\,°$C, it is found to be 6/7 of the value of $T_1(^{13}$C) as expected for chemical shielding anisotropy relaxation determined with no exchange broadening. This result leads to an upper limit for the exchange time for axial–equatorial exchange ($\tau_e$) as given by

$$(6/25)(\delta\omega)^2\tau_e \le 10^{-3}\,\text{s}^{-1} \tag{10}$$

where $\delta\omega$ is the chemical shift difference in rad s$^{-1}$ between axial and equatorial sites. In order to obtain an upper limit for $\tau_e$ it is necessary to

estimate $\delta\omega$ from a series of compounds $Fe(CO)_{5-n}(PF_3)_n$.[27] For these compounds the averaged $^{13}C$ chemical shift and $J(^{31}P-^{13}C)$ are measured as a function of temperature, and the isomeric composition is determined by IR spectroscopy. Analysis of the data yields $\delta\omega$ and an upper limit for $\tau_e$ of $9 \times 10^{-11}$ s.

## VII. SOLID-STATE NMR SPECTROSCOPY

Although solid-state NMR spectroscopy is potentially a very powerful tool, it has largely resided in the hands of specialists, and inorganic and organometallic compounds have rarely attracted much attention to date. Most compounds investigated appear to have been chosen on the basis of ease of synthesis or purchase rather than chemical interest. However, in one study, of metal migration around the cyclopentadienyl ring in $Hg(\sigma$-$C_5H_5)X$ (X=Cl, Br, I), considerable variation in the activation energy is found as a function of X.[28,29] Unfortunately the value of the activation energy is very dependent on the experimental method, showing inadequacies in the approach. There is great potential in this approach once all the problems of data analysis have been solved.

A more exciting development is the use of high-resolution $^{13}C$ NMR spectroscopy for solids. This technique is almost routine now at room temperature but, owing to the necessity to spin the sample fast at an angle of ~54° with respect to the magnetic field, the application to variable temperature work is very limited. There is considerable potential in these measurements. First, the measurement of limiting low temperature $^{13}C$ chemical shifts is valuable for solution studies where limiting low temperature spectra cannot be obtained, owing to restrictions imposed by solubility, solvents, and high-resolution NMR spectrometers. With this information the analysis of exchange broadened $^{13}C$ NMR spectra is possible. Secondly, it is feasible to carry out a high-resolution variable temperature NMR study on the solid state, such as for $Ru_3(CO)_4(C_8H_8)_2$.[30] Although in solution the cyclooctatetraene rings in this molecule are highly fluxional, they are rigid in the solid state. It is expected that this technique will prove to be very valuable for dynamic molecules with $\Delta G^{\ddagger}$ values less than 10 kcal mol$^{-1}$.

## VIII. PRINCIPAL MECHANISMS

### A. Coordination complexes

The principal mechanisms have previously been reviewed.[31,32] In this review emphasis is placed on intramolecular processes. For such processes, it is necessary to prove the intramolecular mechanism by: (1) the retention

of coupling constants; e.g. $PF_5$, a trigonal bipyramidal molecule, gives only one $^{19}F$ NMR signal, but $^1J(^{31}P-^{19}F)$ is observed, showing that the dynamic process is intramolecular; (2) concentration studies; (3) use of mixtures; e.g. the racemization of $Zn(Pr^iNCHCHCPhS)_2$ is fast compared with equilibration with $Zn(PhCH_2NCHCHCPhS)_2$.[33]

The established mechanisms for coordination complexes are based on interconversion of standard geometries, i.e.

| $ML_3$ | pyramidal | $\rightleftharpoons$ trigonal |
|---|---|---|
| $ML_4$ | tetrahedral | $\rightleftharpoons$ square planar |
| $ML_5$ | trigonal bipyramidal | $\rightleftharpoons$ square based pyramid |
| $ML_6$ | octahedral | $\rightleftharpoons$ trigonal prism |

The major problem is in devising molecules that can be investigated by NMR. The principal probe to these mechanisms is the introduction of prochiral groups, e.g. $Pr^i$, to act as a chiral probe to racemization in the pyramidal, tetrahedral, and octahedral cases.

For pyramidal molecules, it has only been possible to show that racemization occurs, presumably via a trigonal intermediate. For example, the $^1H$ spectrum of 1-$Pr^i$-2-Ph-5-Me-phosphole is shown in Fig. 7.[34] The limiting high temperature spectrum is a double doublet for the isopropyl methyl groups due to hydrogen and phosphorus coupling. The diastereotopic methyl groups become inequivalent on cooling.
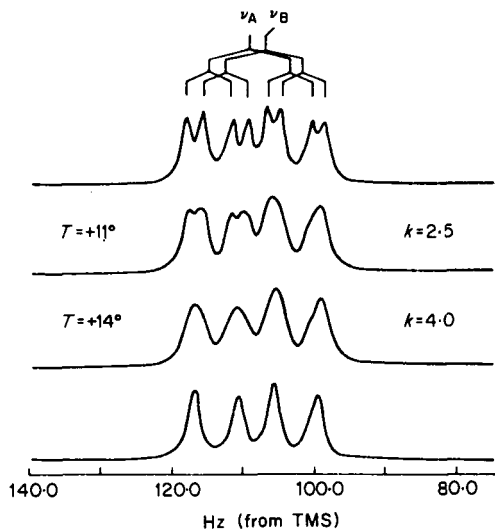


FIG. 7. Dynamic $^1H$ NMR spectra of 1-$Pr^i$-2-Ph-5-Me-phosphole showing only the diastereotopic methyl groups. (Egan, Tang, Zon and Mislow[34])

The demonstration of tetrahedral $\rightleftarrows$ square-planar exchange is clearest for nickel(II) complexes, where it is possible to observe in favourable cases both tetrahedral and square-planar isomers, e.g. in $Ni\{(p\text{-tol})_2MeP\}_2Br_2$ (see Fig. 8).[35] At $-64\,°C$, separate signals are observed for the square-planar and the paramagnetic tetrahedral complexes. Exchange occurs on warming.
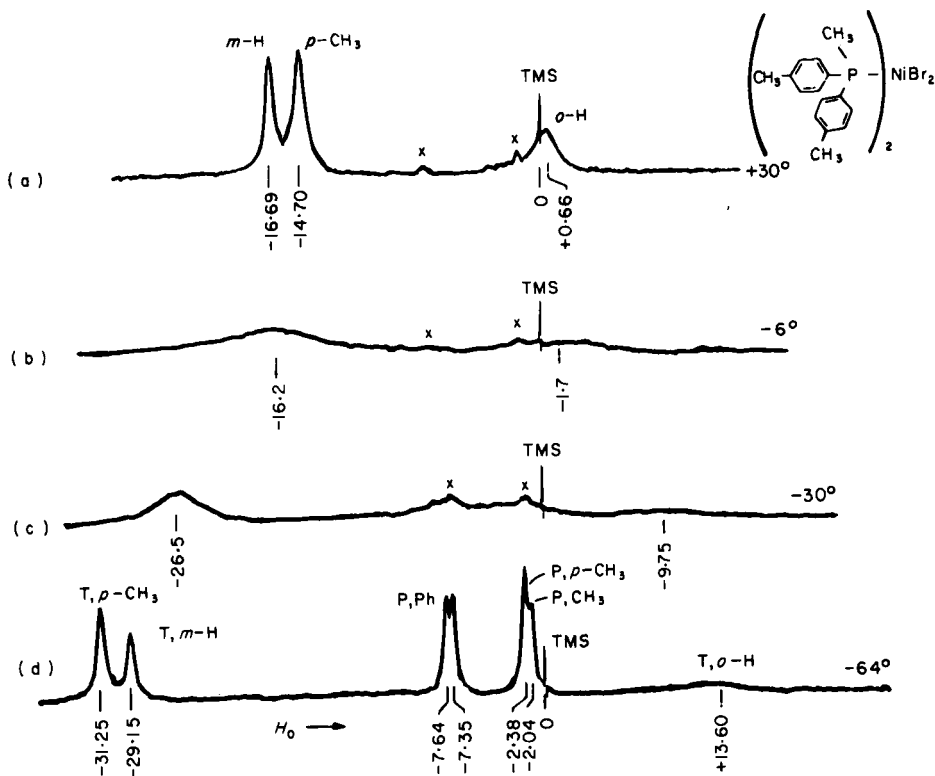


FIG. 8. 100 MHz $^1H$ NMR spectra of $Ni[(p\text{-tol})_2MeP]_2Br_2$ in $CDCl_3$ solution; × indicates an impurity, P = planar, T = tetrahedral. (Pignolet, Horrocks and Holm[35])

Exchange in the trigonal bipyramidal system is discussed in Section III. There are two possible mechanisms, the Berry mechanism and the anti-Berry or turnstile mechanism, which in very favourable circumstances can be resolved using NMR spectroscopy (Fig. 3), but usually no mechanistic information is available. It is generally believed that the Berry mechanism is the usual one.

The octahedral system offers a considerable challenge to the NMR spectroscopist. The tris-bidentate complexes have attracted the greatest

attention, e.g. Al(acetylacetonato)$_3$. Numerous mechanisms have been discussed, and it now appears that there are two basic ones, the trigonal twist and the trigonal bipyramidal mechanism. The complexity of the problem may be illustrated for Al(Pr$^i$COCHCOCH$_2$Ph)$_3$.[36] This molecule exists in two forms, the *fac* (13) and the *mer* (14). Both of these are optically active,



**(13)** *(fac)*                          **(14)** *(mer)*
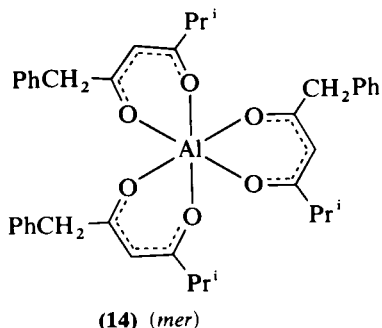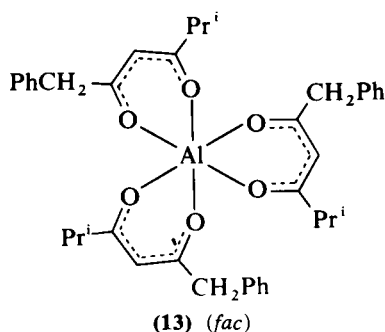
giving rise to four isomers. In the original work three mechanisms were considered. The trigonal twist mechanism can involve two types of trigonal prism intermediate, one with all three chelate ligands bridging the rectangular sides (15), the other with only one chelate ligand bridging the rectangular sides and the remaining two ligands bridging the triangular sides (16). Further complications are due to the inequivalent ends of the



**(15)**                          **(16)**
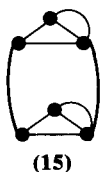
chelate ligand. The other two mechanisms (the square-planar primary process, SP-PRI, and the trigonal-bipyramidal-pyramid axial process, TBP-AXIAL) involve one end of the ligand dissociating to give a 5-coordinate intermediate. As a result of the complexity of this system, there are numerous possible rates to determine. Consequently no individual rate constants have been determined, but the spectra can be fitted on the basis of assumptions as to mechanism (see Fig. 9). Now, with higher-field instruments, $^{13}$C and $^{27}$Al NMR spectroscopy, and improved techniques, more information could be gleaned from this and related systems.

## B. Organometallic compounds

The greatest variety comes for the organometallic compounds. For polyenyl and polyene complexes there are two main mechanisms, the
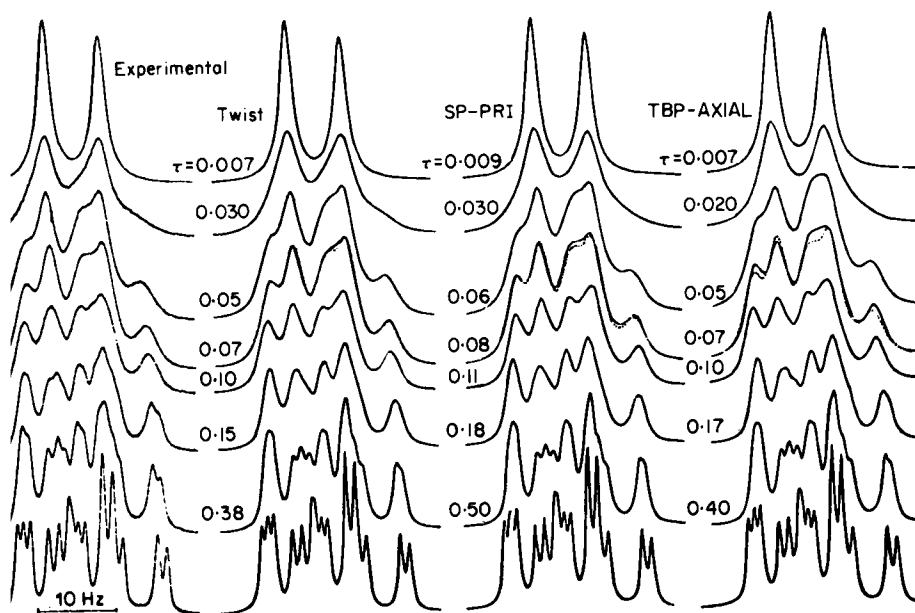
FIG. 9. Experimental methyl $^1$H NMR spectra (100 MHz) of Al(Pr$^i$COCHCOCH$_2$Ph)$_3$ in chlorobenzene, and spectra calculated for various rearrangement mechanisms; dotted lines indicate experimental spectra at 128 °C; $\tau$ values are in seconds. (Hutchison, Gordon and Holm[36])

Woodward–Hoffmann sigmatropic rearrangement and the interconversion of 18- and 16-electron complexes, with the Woodward–Hoffmann rearrangement being normally the lower energy process.

Woodward–Hoffmann sigmatropic rearrangement commonly occurs in $\sigma$-cyclopentadienyl derivatives, e.g. Fe($\sigma$-C$_5$H$_5$)($\eta$-C$_5$H$_5$)(CO)$_2$ (17).[37]



(17)
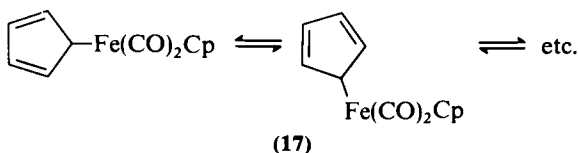
The iron migrates around the ring by 1,5 shifts. This 1,5 shift mechanism is demonstrated in the low temperature $^{13}$C NMR spectrum since the signal due to carbon atoms 1 and 4 broadens twice as fast as that due to carbon atoms 2 and 3 as fluxionality becomes significant (see Fig. 10). The only remaining problem is the assignment of the signals. This mechanism is found to be standard for all dienyl type derivatives studied to date, with
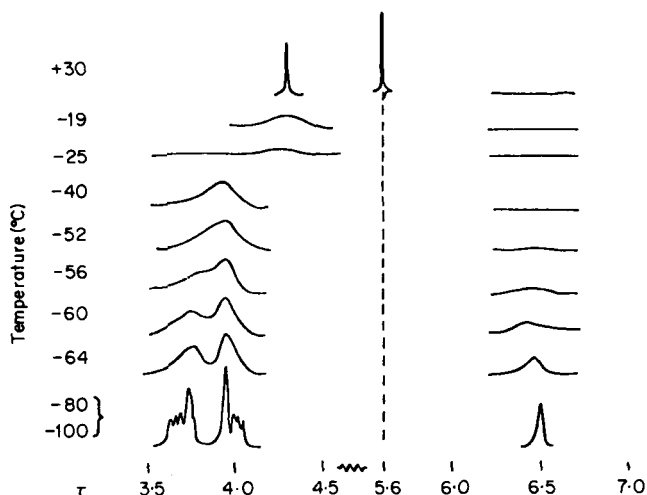
FIG. 10. The 60 MHz $^1$H NMR spectrum of CpFe(CO)$_2$($\sigma$-C$_5$H$_5$) in CS$_2$ at various temperatures; the $\eta^5$-C$_5$H$_5$ signal is shown only on the 30 °C spectrum, the amplitude of which is 0·1 times that of the others. (Bennett, Cotton, Davison, Faller, Lippard and Morehouse[37])

the one exception of Re($\sigma$-C$_7$H$_7$)(CO)$_5$ which undergoes a 1,7 shift.[38] The strength of this approach is that it also explains the fluxionality of $\pi$ systems, e.g. Ru($\eta^4$-C$_8$H$_8$)(CO)$_3$ (Fig. 1).[39] The structure can be represented in a valence bond form and the metal migration involves a 1,5 shift of a "$\sigma$ bond". NMR measurements have shown that the mechanism is as shown (18), since the 2 and 3 proton signals broaden twice as much as the 1 and



(18)
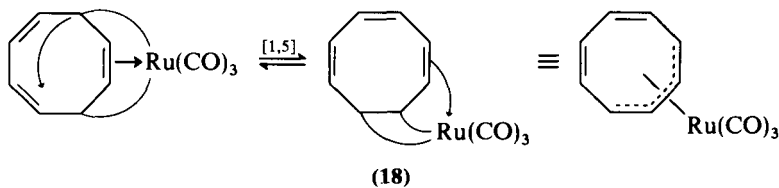
4 proton signals when exchange is relatively slow, e.g. 40 s$^{-1}$. The activation energy is low, 8·6 kcal mol$^{-1}$, as it is for the iron analogue, 8·1 kcal mol$^{-1}$. In contrast, for [Fe($\eta^2$-C$_8$H$_8$)(CO)$_2$($\eta$-C$_5$H$_5$)]$^+$ (19)[40] and [Fe($\eta^6$-C$_8$H$_8$)-($\eta$-C$_5$H$_5$)]$^+$ (20),[41] where Woodward–Hoffmann forbidden [1,7] and [1,3] suprafacial shifts are required, the molecules are static. For these forbidden shifts, the processes can occur, e.g. with Mn($\eta^5$-C$_7$H$_7$)(CO)$_3$,[42] but they are of considerably higher energy than the allowed process.

**(19)**



**(20)**
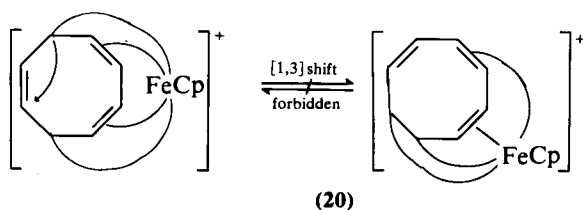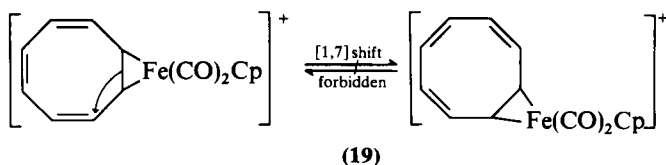
The alternative mechanism, involving changing the coordination at the metal, is normally high in energy but can occur[8,20,43,44] (e.g. **21–23**). These processes only appear to occur when the alternative shift of the metal is Woodward–Hoffmann forbidden or prevented by lack of $\pi$ conjugation;



18 valence electrons on Cr     16 valence electrons on Cr

**(21)**



**(22)**



16 valence electrons     18 valence electrons

**(23)**

(24)                                              (25)
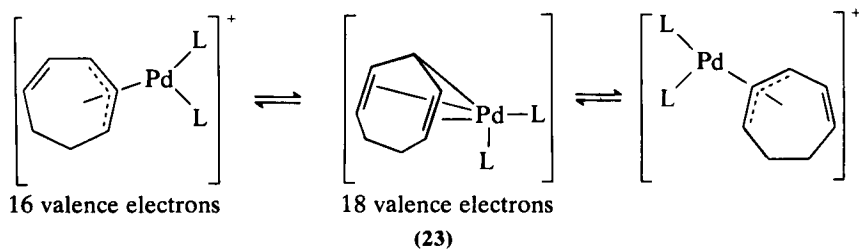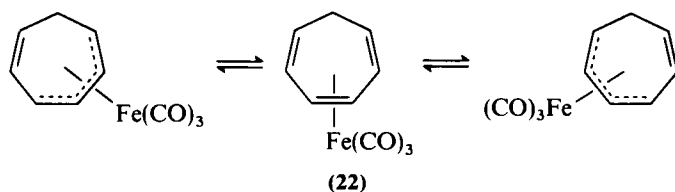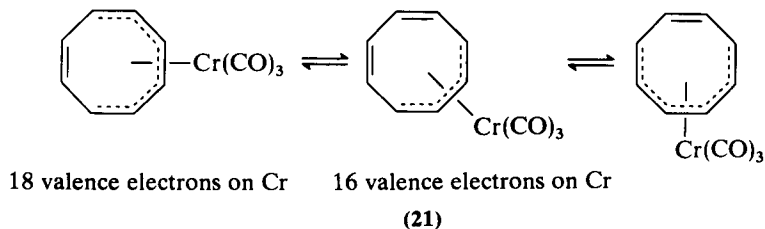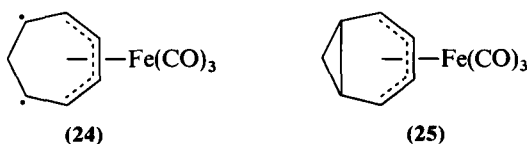
for example, the diradical intermediate **24** and the norcaradiene intermediate **25** are of high energy.

The rotation of groups on metals has only received detailed study when the process is of relatively high energy, e.g. olefin or acetylene rotation. In the case of $[Os(PPh_3)_2(CO)(NO)(\eta^2\text{-}C_2H_4)]^+$ (**26**) the $^{13}C$ NMR spectrum shows that both of the olefin carbon atoms become equivalent but still retain phosphorus coupling; hence the rotation occurs about the Os–ethylene axis rather than about the carbon–carbon axis or via olefin dissociation.[45] Little work has been done on the rapid processes such as methyl or $\eta^5$-cyclopentadienyl rotation.
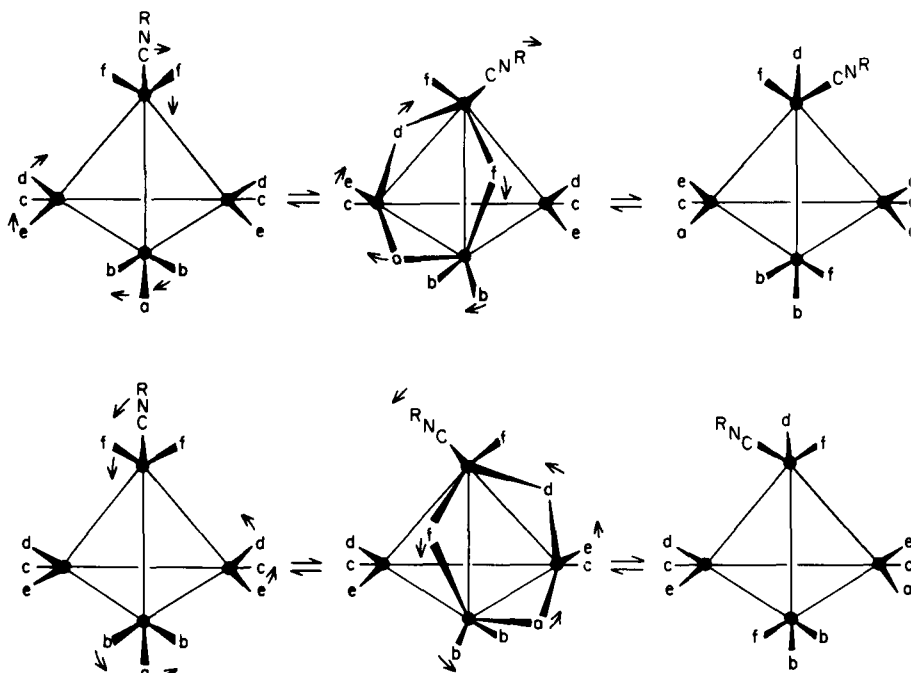


FIG. 11. Suggested "$T_d$" $\rightleftharpoons$ "$C_{3v}$" ligand migration process in $Ir_4(CO)_{11}(CNBu^t)$ involving movement of $NCBu^t$ and carbonyl "a". Note that the *trans* relationship of "a" to the isocyanide moiety is maintained, despite the site exchange; ligand migration about the remaining two tetrahedral faces does not alter this stereochemical relationship and hence carbonyl "a" remains magnetically distinct in this process. (Band and Muetterties[4])

(26)                                    (27)
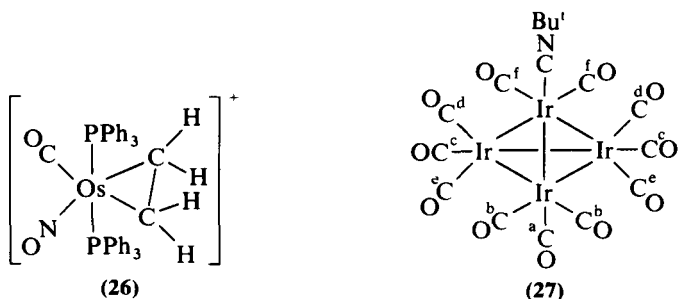
An area with considerable potential for the NMR spectroscopist is carbonyl scrambling in metal clusters. This area has been recently reviewed, but one example is mentioned to illustrate the challenge. At low temperature, $Ir_4(CO)_{11}CNBu^t$ (27) shows six different carbonyl signals, due to the different carbonyl environments labelled a–f.[46] On warming, exchange occurs to give two signals in the ratio 10:1, i.e. carbonyl "a" does not join in the exchange. At higher temperatures these two signals collapse to one. These observations can be fitted to a mechanism where carbonyls can bridge between the iridium atoms (see Fig. 11).

## REFERENCES

1. L. M. Jackman and F. A. Cotton (eds), *Dynamic Nuclear Magnetic Resonance Spectroscopy*, Academic Press, 1975.
2. B. E. Mann, in *Comprehensive Organometallic Chemistry* (ed. G. Wilkinson, F. G. A. Stone and E. W. Abel), Chapter 20, Pergamon, 1982.
3. S. Aime and L. Milone, *Progr. NMR Spectroscopy*, 1977, **11**, 183.
4. E. Band and E. L. Muetterties, *Chem. Rev.*, 1978, **78**, 639.
5. J. Evans, B. F. G. Johnson, J. Lewis and W. T. Matheson, *J. Amer. Chem. Soc.*, 1975, **97**, 1245.
6. M. A. Cohen, D. R. Kidd and T. L. Brown, *J. Amer. Chem. Soc.*, 1975, **97**, 4408.
7. F. A. Cotton and D. L. Hunter, *Inorg. Chim. Acta*, 1974, **11**, L9.
8. B. E. Mann, A. Keasey, A. Sonoda and P. M. Maitlis, *J. Chem. Soc. Dalton*, 1979, 338.
9. W. G. Klemperer, *J. Amer. Chem. Soc.*, 1973, **95**, 380, 2105.
10. W. G. Klemperer, in ref. 1, p. 23.
11. F. A. Cotton, A. Davison, T. J. Marks and A. Musco, *J. Amer. Chem. Soc.*, 1969, **91**, 6598.
12. F. A. Cotton and D. L. Hunter, *J. Amer. Chem. Soc.*, 1976, **98**, 1413.
13. For a review see J. P. Jesson and E. L. Muetterties, in ref. 1, p. 253.
14. W. G. Klemperer, J. K. Krieger, M. D. McCreary, E. L. Muetterties, D. D. Traficante and G. M. Whitesides, *J. Amer. Chem. Soc.*, 1975, **97**, 7023.
15. For a review see R. A. Hoffman and S. Forsén, *Progr. NMR Spectroscopy*, 1966, **1**, 173.
16. B. E. Mann and P. M. Maitlis, *J. Chem. Soc. Chem. Commun.*, 1976, 1058.
17. B. E. Mann, *J. Magn. Resonance*, 1976, **21**, 17.
18. B. E. Mann, *J. Magn. Resonance*, 1977, **25**, 91.
19. R. S. Threlkel and J. E. Bercaw, *J. Amer. Chem. Soc.*, 1981, **103**, 2650.
20. J. A. Gibson and B. E. Mann, *J. Chem. Soc. Dalton*, 1979, 1021.

21. M. M. Hunt, W. G. Kita, B. E. Mann and J. A. McCleverty, *J. Chem. Soc. Dalton*, 1978, 467.
22. C. R. Lassigne and E. J. Wells, *J. Magn. Resonance*, 1977, **26**, 55.
23. B. E. Mann and P. Yavari, unpublished results.
24. A. P. Zeno and P. D. Ellis, *J. Amer. Chem. Soc.*, 1975, **97**, 5685.
25. R. F. Jordan and J. R. Norton, *J. Amer. Chem. Soc.*, 1979, **101**, 4853.
26. H. W. Spiess and H. Mahnke, *Ber. Bunsenges. Phys. Chem.*, 1972, **76**, 990.
27. R. K. Sheline and H. Mahnke, *Angew. Chem. Internat. Ed.*, 1975, **14**, 314.
28. A. J. Campbell, C. A. Fyfe, R. G. Goel, E. Maslowsky and C. V. Senoff, *J. Amer. Chem. Soc.*, 1972, **94**, 8387.
29. A. J. Campbell, C. E. Cottrell, C. A. Fyfe and K. R. Jeffrey, *Inorg. Chem.*, 1976, **15**, 1326.
30. A. J. Campbell, C. E. Cottrell, C. A. Fyfe and K. R. Jeffrey, *Inorg. Chem.*, 1976, **15**, 1321; J. R. Lyerla, C. A. Fyfe and C. S. Yannoni, *J. Amer. Chem. Soc.*, 1979, **101**, 1351.
31. J. P. Jesson and E. L. Muetterties, in ref. 1, p. 253.
32. R. H. Holm, in ref. 1, p. 317.
33. S. S. Eaton and R. H. Holm, *Inorg. Chem.*, 1971, **10**, 1446.
34. W. Egan, R. Tang, G. Zon and K. Mislow, *J. Amer. Chem. Soc.*, 1971, **93**, 6205.
35. L. H. Pignolet, W. D. Horrocks and R. H. Holm, *J. Amer. Chem. Soc.*, 1970, **92**, 1855.
36. J. R. Hutchison, J. G. Gordon and R. H. Holm, *Inorg. Chem.*, 1971, **10**, 1004.
37. M. J. Bennett, F. A. Cotton, A. Davison, J. W. Faller, S. J. Lippard and S. M. Morehouse, *J. Amer. Chem. Soc.*, 1966, **88**, 4371.
38. D. M. Heinekey and W. A. G. Graham, *J. Amer. Chem. Soc.*, 1979, **101**, 6115.
39. F. A. Cotton, A. Davison, T. J. Marks and A. Musco, *J. Amer. Chem. Soc.*, 1969, **91**, 6598.
40. A. Cutler, D. Ehntholt, W. P. Giering, P. Lennon, S. Raghu, A. Rosan, M. Rosenblum, J. Tancrede and D. Wells, *J. Amer. Chem. Soc.*, 1976, **98**, 3495.
41. D. L. Reger and C. Coleman, *J. Organometal. Chem.*, 1977, **131**, 153.
42. T. H. Whitesides and R. A. Budnik, *Inorg. Chem.*, 1976, **15**, 874.
43. B. E. Mann, *J. Organometal. Chem.*, in the press.
44. K. J. Karel and M. Brookhart, *J. Amer. Chem. Soc.*, 1978, **100**, 1619.
45. J. A. Segal and B. F. Johnson, *J. Chem. Soc. Dalton*, 1975, 677.
46. J. R. Shapley, G. F. Stuntz, M. R. Churchill and J. P. Hutchinson, *J. Chem. Soc. Chem. Commun.*, 1979, 219.
47. F. A. Cotton, D. L. Hunter and P. Lahuerta, *J. Amer. Chem. Soc.*, 1974, **96**, 4723, 7926.

ADDENDUM

# High-resolution NMR of Solids

## R. E. WASYLISHEN AND C. A. FYFE

These further literature references, added at the proof stage, are a continuation of the list in the first review in this volume. Most of the important recent papers are included, grouped as follows: reviews (341–346); theory (347–353); experimental techniques (354–366); applications involving primarily carbon-13 (367–414), nitrogen-15/14 (415–421), silicon-29 (422–436), aluminium-27 (437–440), phosphorus-31 (441–445), other isotopes (446–457). The most important developments have been MASS studies of quadrupolar nuclei with non-integral spin (437–440, 449–453).

341. R. G. Griffin, *Methods in Enzymology*, 1981, **72**, 108; a comprehensive review of solid-state NMR of lipid bilayers.
342. T. M. Duncan and C. Dybowski, *Surface Science Reports*, 1981, **1**, 157; a comprehensive review of chemisorption and surface studies by NMR.
343. V. J. McBrierty and D. C. Douglas, *Macromol. Rev.*, 1981, **16**, 295; a comprehensive review of recent advances in the NMR of solid polymers.
344. R. K. Harris, K. J. Packer and B. J. Say, *Makromol. Chem.*, 1981, Suppl. 4, 117; a review summarizing recent advances in NMR techniques for the study of synthetic polymers.
345. J. R. Lyerla, in *Methods of Experimental Physics: Polymers, Part A, Molecular Structure and Dynamics* (ed. R. A. Fana), Vol. 16, p. 241, Academic Press, London, 1981; a comprehensive review covering solid-state NMR studies of polymers.
346. D. Brinkmann, *Solid State Ionics*, 1981, **5**, 53; a review summarizing applications of NMR in solid electrolyte studies.

347. S. Vega, T. W. Shattuck and A. Pines, *Phys. Rev. (A)*, 1980, **22**, 638.
348. S. Vega, *Phys. Rev. (A)*, 1981, **23**, 3152.
349. S. Vega and Y. Naor, *J. Chem. Phys.*, 1981, **75**, 75.
350. G. Bodenhausen. *Progr. NMR Spectroscopy*, 1981, **14**, 137.
351. E. Kundla, A. Samoson and E. Lippmaa, *Chem. Phys. Lett.*, 1981, **83**, 229.
352. E. M. Menger and W. S. Veeman, *J. Magn. Resonance*, 1982, **46**, 257.
353. V. V. Laiko and B. N. Provotorov, *Phys. Lett. (A)*, 1982, **88**, 51.

354. J. A. DiVerdi and S. J. Opella, *J. Chem. Phys.*, 1981, **75**, 5594.
355. G. Scheler, U. Haubenreisser and H. Rosenberger, *J. Magn. Resonance*, 1981, **44**, 134.
356. W. T. Dixon, *J. Magn. Resonance*, 1981, **44**, 220.
357. J. P. Bayle, J. Courtieu, J. Jullien and S. K. Kan, *Org. Magn. Resonance*, 1981, **16**, 85.
358. F. D. Doty and P. D. Ellis, *Rev. Sci. Instr.*, 1981, **52**, 1868.
359. F. D. Doty, R. R. Inners and P. D. Ellis, *J. Magn. Resonance*, 1981, **43**, 399.
360. R. R. Inners, F. D. Doty, A. R. Garber and P. D. Ellis, *J. Magn. Resonance*, 1981, **45**, 503.

361. (a) M. Bloom, J. H. Davis and M. I. Valic, *Canad. J. Phys.*, 1980, **58**, 1510.
     (b) M. Bloom, J. H. Davis and A. L. MacKay, *Chem. Phys. Lett.*, 1981, **80**, 198.
362. J. Courtieu, D. W. Alderman and D. M. Grant, *J. Amer. Chem. Soc.*, 1981, **103**, 6783.
363. T. Terao, H. Miura and A. Saika, *J. Chem. Phys.*, 1981, **75**, 1573.
364. C. A. Fyfe, C. G. Cobbi, S. J. Hartman, R. E. Lenkinski, J. H. O'Brien, E. R. Beange
     and M. A. R. Smith, *J. Magn. Resonance*, 1982, **47**, 168.
365. W. P. Aue, D. J. Ruben and R. G. Griffin, *J. Magn. Resonance*, 1981, **43**, 472.
366. W. P. Aue, D. J. Ruben and R. G. Griffen, *J. Magn. Resonance*, 1982, **46**, 354.

367. M. A. Wilson, *J. Soil Sci.*, 1981, **32**, 167.
368. K. W. Zilm, R. J. Pugmire, S. R. Larter, J. Allan and D. M. Grant, *Fuel*, 1981, **60**, 717.
369. G. E. Maciel, D. J. O'Donnell, J. J. H. Ackerman, B. H. Hawkins and V. J. Bartuska,
     *Makromol. Chem.*, 1981, **182**, 2297.
370. M. A. Wilson, R. J. Pugmire, K. W. Zilm, K. M. Goh, S. Heng and D. M. Grant,
     *Nature*, 1981, **294**, 648.
371. P. G. Hatcher, G. E. Maciel and L. W. Dennis, *Org. Geochem.*, 1981, **3**, 43.
372. P. G. Hatcher, I. A. Breger and W. L. Earl, *Org. Geochem.*, 1981, **3**, 49.
373. O. Jardetzky and N. G. Wade-Jardetzky, *FEBS Lett.*, 1980, **110**, 133.
374. C. M. Gall, T. A. Cross, J. A. DiVerdi and S. J. Opella, *Proc. Nat. Acad. Sci.*, 1982,
     **79**, 101.
375. S. Ganapathy, A. Naito and C. A. McDowell, *J. Amer. Chem. Soc.*, 1981, **103**, 6011.
376. K. W. Zilm and D. M. Grant, *J. Amer. Chem. Soc.*, 1981, **103**, 2913.
377. G. R. Hays, R. Huis, B. Coleman, D. Clague, J. W. Verhoeven and F. Rob, *J. Amer.
     Chem. Soc.*, 1981, **103**, 5140.
378. H. Saitô, R. Tabeta and T. Harada, *Chem. Lett.*, 1981, 571.
379. H. Saitô and R. Tabeta, *Chem. Lett.*, 1981, 713.
380. D. J. Iverson, G. Hunter, J. F. Blount, J. R. Damewood and K. Mislow, *J. Amer. Chem.
     Soc.*, 1981, **103**, 6073.
381. D. E. Leyden, D. S. Kendall and T. G. Waddell, *Analyt. Chim. Acta*, 1981, **126**, 207.
382. S. Nagaoka, T. Terao, F. Imasiro, A. Saika and N. Hirota, *Chem. Phys. Lett.*, 1981,
     **80**, 580.
383. H. W. Gibson, J. M. Pochan and S. Kaplan, *J. Amer. Chem. Soc.*, 1981, **103**, 4619.
384. W. H. Dawson, S. W. Kaiser, P. D. Ellis and R. R. Inners, *J. Amer. Chem. Soc.*, 1981,
     **103**, 6780.
385. M. Möller, H.-J. Cantow, J. K. Krüger and H. Höcker, *Polymer Bull.*, 1981, **5**, 125.
386. D. Michel, H. Pfeifer and J. Delmau. *J. Magn. Resonance*, 1981, **45**, 30.
387. D. E. Leyden, D. S. Kendall, L. W. Burggraf, F. J. Pern and M. DeBello, *Analyt.
     Chem.*, 1982, **54**, 101.
388. J. R. Havens, H. Ishida and J. L. Koenig, *Macromolecules*, 1981, **14**, 1327.
389. B. Schröter and A. Posern, *Makromol. Chem.*, 1981, **182**, 675.
390. T. Taki, S. Yamashita, M. Satoh, A. Shibata, T. Yamashita, R. Tabeta and H. Saitô,
     *Chem. Lett.*, 1981, 1803.
391. E. W. Hagaman and M. C. Woody, *Fuel*, 1982, **61**, 53.
392. H. Ueda and T. Nagai, *Chem. Pharm. Bull.*, 1981, **29**, 2710.
393. M. A. Hemminga, W. S. Veeman, H. W. M. Hilhorst and T. J. Schaafsma, *Biophys. J.*,
     1981, **35**, 463.
394. D. L. Van der Hart, *J. Magn. Resonance*, 1981, **44**, 117.
395. I. T. Ali and I. D. Gay, *J. Phys. Chem.*, 1981, **85**, 1251.
396. W. G. Blann, C. A. Fyfe, J. R. Lyerla and C. S. Yannoni, *J. Amer. Chem. Soc.*, 1981,
     **103**, 4030.
397. A. Naito, S. Ganapathy and C. A. McDowell, *J. Chem. Phys.*, 1981, **74**, 5393.

398. H. Dorn, B. E. Hanson and E. Motell, *Inorg. Chim. Acta*, 1981, **54**, L71.

399. K. W. Zilm, A. J. Beeler, D. M. Grant, J. Michl, T.-C. Chou and E. L. Allred, *J. Amer. Chem. Soc.*, 1981, **103**, 2119.

400. P. F. Barron, J. F. Stephens and M. A. Wilson, *Fuel*, 1981, **60**, 547.

401. W. L. Earl and D. L. Van der Hart, *Macromolecules*, 1981, **14**, 570.

402. C. S. Yannoni, V. Macho and P. C. Myhre, *J. Amer. Chem. Soc.*, 1982, **104**, 907.

403. J. Elguero, A. Fruchier and V. Pellegrin, *J. Chem. Soc., Chem. Commun.*, 1981, 1207.

404. L. G. Pease, M. H. Frey and S. J. Opella, *J. Amer. Chem. Soc.*, 1981, **103**, 467.

405. G. Boxhoorn, R. A. van Santen, W. A. VanErp, G. R. Hays, R. Huis and D. Clague, *J. Chem. Soc., Chem. Commun.*, 1982, 264.

406. T. Bernstein, L. Kitaev, D. Michel, H. Pfeifer and P. Fink, *J. Chem. Soc., Faraday I*, 1982, **78**, 761.

407. T. J. Sanford, R. D. Allenderfer, E. T. Kang, P. Ehrlich and J. Schaefer, *J. Polymer Sci., Polymer Phys.*, 1981, **19**, 1151.

408. N. Zumbulyadis and H. J. Gysling, *Inorg. Chem.*, 1982, **21**, 569.

409. W. Gronski, A. Hasenhindl, H. H. Limbach, M. Möller and H.-J. Cantow, *Polymer Bull.*, 1981, **6**, 93.

410. B. Schröter, H.-H. Hörhold and D. Raabe, *Makromol. Chem.*, 1981, **182**, 3185.

411. M. A. Markevich, P. A. Karavaikov, T. Valimae, I. Heinmaa, E. Lippmaa and N. S. Enikolopyan, *Dokl. Akad. Nauk SSSR*, 1981, **257**, 939.

412. D. J. O'Donnell, J. J. Ackerman and G. E. Maciel, *J. Agric. Food Chem.*, 1981, **29**, 514.

413. W. T. Dixon, J. Schaefer, M. D. Sefeik, E. O. Stejskal and R. A. McKay, *J. Magn. Resonance*, 1981, **45**, 173.

414. D. Igner and D. Fiat, *J. Magn. Resonance*, 1982, **46**, 233.


415. T. A. Cross, J. A. DiVerdi and S. J. Opella, *J. Amer. Chem. Soc.*, 1982, **104**, 1759.

416. J. A. DiVerdi and S. J. Opella, *J. Amer. Chem. Soc.*, 1982, **104**, 1761.

417. M. Munowitz, W. W. Bachovchim, J. Herzfeld, C. M. Dobson and R. G. Griffin, *J. Amer. Chem. Soc.*, 1982, **104**, 1192.

418. D. Michel, A. Germanus, D. Scheller and B. Thomas, *Z. Phys. Chem.*, 1981, **262**, 113.

419. T. A. Skokut, J. E. Varner, J. Schaefer, E. O. Stejskal and R. A. McKay, *Plant Physiol.*, 1982, **69**, 314.

420. D. J. Siminovitch and K. R. Jeffrey, *Biochim. Biophys. Acta*, 1981, **645**, 270.

421. T. M. Rothgeb and E. Oldfield, *J. Biol. Chem.*, 1981, **256**, 6004.


422. E. Lippmaa, M. Magi, A. Samoson, M. Tarmak and G. Engelhardt, *J. Amer. Chem. Soc.*, 1981, **103**, 4992.

423. J. M. Thomas, J. Klinowski, C. A. Fyfe, J. S. Hartman and L. A. Bursill, *J. Chem. Soc., Chem. Commun.*, 1981, 678.

424. G. Engelhardt, U. Lohse, E. Lippmaa, M. Tarmak and M. Magi, *Z. Anorg. Allg. Chem.*, 1981, **482**, 49.

425. G. Engelhardt, E. Lippmaa and M. Mägi, *J. Chem. Soc., Chem. Commun.*, 1981, 712.

426. J. Klinowski, J. M. Thomas, M. Audier, S. Vasudevan, C. A. Fyfe and J. S. Hartman, *J. Chem. Soc., Chem. Commun.*, 1981, 570.

427. J. M. Thomas, L. A. Bursill, E. A. Lodge, A. K. Cheetham and C. A. Fyfe, *J. Chem. Soc., Chem. Commun.*, 1981, 276.

428. G. Engelhardt, H. Jancke, E. Lippmaa and A. Samoson, *J. Organometal. Chem.*, 1981, **210**, 295.

429. D. W. Sindorf and G. E. Maciel, *J. Amer. Chem. Soc.*, 1981, **103**, 4263.

430. S. Ramdas, J. M. Thomas, J. Klinowski, C. A. Fyfe and J. S. Hartman, *Nature*, 1981, **292**, 228.
431. J. B. Nagy, J.-P. Gilson and E. G. Derouane, *J. Chem. Soc., Chem. Commun.*, 1981, 1129.
432. C. A. Fyfe, G. C. Gobbi, J. Klinowski, J. M. Thomas and S. Ramdas, *Nature*, 1982, **296**, 530.
433. J. Klinowski, J. M. Thomas, C. A. Fyfe and G. C. Gobbi, *Nature*, 1982, **296**, 533.
434. G. Engelhart, E. Lippmaa and M. Maegi, *J. Chem. Soc., Chem. Commun.*, 1981, 712.
435. E. Lippmaa, A. V. Samoson, V. V. Brei and Yu. I. Gorlov, *Dokl. Akad. Nauk SSSR*, 1981, **259**, 403.
436. G. E. Maciel, M. J. Sullivan and D. W. Sindorf, *Macromolecules*, 1981, **14**, 1607.

437. K. LeDang, P. Veillet, W. Nägele and K. Knorr, *J. Phys. (C) Solid State Phys.*, 1980, **13**, 6509.
438. D. Freude and H.-J. Behrens. *Crys. Res. and Techn.*, 1981, **16**, K36.
439. W. E. Dibble, B. H. W. S. De Jong and L. W. Cary, Proc. Intern. Symp. Water–Rock Interact., 3rd (ed. A. R. Campbell), p. 47, Alberta Research Council, 1980.
440. C. A. Fyfe, G. C. Gobbi, J. S. Hartman, J. Klinowski and J. M. Thomas. *J. Phys. Chem.*, 1982, **86**, 1247.

441. B. T. Nall, W. P. Rothwell, J. S. Waugh and A. Rupprecht, *Biochemistry*, 1981, **20**, 1881.
442. J. P. Yesinowski, *J. Amer. Chem. Soc.*, 1981, **103**, 6266.,
443. R. J. P. Williams, R. G. F. Giles and A. M. Posner, *J. Chem. Soc., Chem. Commun.*, 1981, 1051.
444. L. W. Dennis, V. J. Bartuska and G. E. Maciel. *J. Amer. Chem. Soc.*, 1982, **104**, 230.
445. J. B. Robert and L. Wiesenfeld, *Mol. Phys.*, 1981, **44**, 319.

446. B. Deloche and E. T. Samulski, *Macromolecules*, 1981, **14**, 575.
447. C. M. Gall, J. A. DiVerdi and S. J. Opella, *J. Amer. Chem. Soc.*, 1981, **103**, 5039.
448. H. Geib, B. Hisgen, U. Pschorn, H. Ringsdorf and H. W. Spiess, *J. Amer. Chem. Soc.*, 1982, **104**, 917.
449. M. D. Meadows, K. A. Smith, R. A. Kinsey, T. M. Rothgeb, R. P. Skarjune and E. Oldfield, *Proc. Nat. Acad. Sci.*, 1982, **79**, 1351.
450. E. Oldfield, S. Schramm, M. D. Meadows, K. A. Smith, R. A. Kinsey and J. Ackerman, *J. Amer. Chem. Soc.*, 1982, **104**, 919.
451. W. Basler, H. Lechert, K. Paulsen and D. Rehder, *J. Magn. Resonance*, 1981, **45**, 170.
452. E. Oldfield, R. A. Kinsey, B. Montez, T. Ray and K. A. Smith, *J. Chem. Soc., Chem. Commun.*, 1982, 244.
453. D. J. Burton and R. K. Harris, *J. Chem. Soc., Chem. Commun.*, 1982, 256.
454. P. DuBois Murphy, W. C. Stevens, T. T. P. Cheung, S. Lucelle, B. C. Gerstein and D. M. Kurtz, *J. Amer. Chem. Soc.*, 1981, **103**, 4400.
455. P. DuBois Murphy and B. C. Gerstein, *J. Amer. Chem. Soc.*, 1981, **103**, 3282.
456. P. F. Rodesiler and E. L. Amma, *J. Chem. Soc., Chem. Commun.* 1982, 182.
457. J. A. Ripmeester, *J. Amer. Chem. Soc.*, 1982, **104**, 289.

# SUBJECT INDEX

## A

Aceheptylene, carbon–proton couplings, calculations, 131

Acetic acid, phenyl-, carbon–carbon couplings, calculations, 145

Acetonitrile, carbon–nitrogen couplings, calculations, 147

Acetylene
carbon–carbon couplings, calculations, 141, 144
carbon–proton couplings, calculations, 126, 127

Adamantane
high resolution carbon-13 NMR of solids, 25–28
methyl-, carbon–carbon couplings, calculations, 144

Alane, proton–proton coupling, calculations, 109

Alcohols
carbon–proton coupling, calculations, 128
proton–proton coupling, calculations, 114

Alicyclic compounds, carbon–proton couplings, calculations, 130

Allenes, carbon–proton couplings, calculations, 130

Allyl rotation, NMR differentiable reactions and, 266

Allylic coupling, 118

Aluminium, tris(acetylacetonato)-, dynamic NMR spectroscopy, 280

Aluminium-27, high resolution NMR of solids, 70

Aluminosilicates, solid, high resolution silicon-29 NMR, 51

Amines, nitrogen–carbon couplings, calculations, 148

Amino acids, high resolution carbon-13 NMR of solids, 31

Ammonia
nitrogen–proton couplings, calculations, 133
proton–proton coupling, calculation, 108, 109

Anilines
carbon–nitrogen couplings, calculations, 150
nitrogen–proton couplings, calculations, 133
proton–proton coupling, long range, 119

Anilinium ions, carbon–nitrogen couplings, calculations, 150

Anisole, proton–proton coupling, long range, 119

Anisotropy in nuclear spin–spin coupling, 163–164

Anthracene, proton–proton coupling, calculations, 115

Arsastibaboranes, boron-11 NMR, 249

Aspartic acid, carbon–proton couplings, calculations, 129, 144

Azaadamantane, carbon–nitrogen couplings, calculations, 150

Azobenzene, 4-amino-
carbon–nitrogen couplings, calculations, 150
nitrogen–proton coupling, calculations, 133

Azulene, carbon–proton couplings, calculations, 131

## B

Benzene
carbon–carbon couplings, calculations, 145
carbon–proton couplings, calculations, 130

291

**D**

**E**